LAWRENCE TECHNOLOGICAL UNIVERSITY

USE OF UNBONDED CFCC FOR TRANSVERSE

POST-TENSIONING OF SIDE-BY-SIDE BOX-BEAM BRIDGES

Submitted to

MICHIGAN DEPARTMENT OF TRANSPORTATION

Testing and Research Section
Construction snd Technology Division
Contract No. 2004-0105

by

Dr. Nabil F. Grace, Project Investigator
and Dr. Elin Jensen, Co-Project Investigator

Department of Civil Engineering
Lawrence Technological University
Southfield, MI 48075-1058, USA.

February, 2008

Technical Report Documentation Page

1. Report No. Research Report RC-1509	2. Government Accession No.	3. MDOT Project Manager Roger Till
4. Title and Subtitle Use of Unbonded CFCC for Transverse Post-Tensioning of Side-by-Side Box-Beam Bridges		5. Report Date February 2008
7. Author(s) Dr. Nabil Grace, Dr. Elin Jensen, Dr. Vasant Matsagar, Mena Bebawy, Elsam Soliman, and Joseph Hanson		6. Performing Organization Code
9. Performing Organization Name and Address Center for Innovative Material Research (CIMR), Department of Civil Engineering, Lawrence Technological University, 21000 West Ten Mile Road, Southfield, MI-48075		8. Performing Org. Report No.
12. Sponsoring Agency Name and Address Michigan Department of Transportation (MDOT) Construction and Technology Division P.O. Box 30049 Lansing, MI-48909		10. Work Unit No. (TRAIS) 11. Contract Number: 2004-0105 11(a). Authorization Number:
15. Supplementary Notes		13. Type of Report & Period Covered Final Report, Sept. 2006-Feb. 2008 14. Sponsoring Agency Code

16. Abstract

An experimental and numerical research project was developed to addresss the effect of the level of transverse post-tensioning (TPT) and the number of the transverse diaphragms on the performance of side-by-side box-beam bridges using unbonded carbon fiber composite cables (CFCC). The experimental program included the construction, instrumentation, and testing of one half-scaled 30° skew bridge model. The numerical program investigated the sensitivity to longitudinal cracking for a wide range of side-by-side box-beam bridges with different spans and different widths. The experimental program consisted of load distribution tests conducted during three different deck slab conditions; uncracked, cracked, and repaired stage. The transverse strain distribution tests were conducted when the bridge deck was uncracked. The cracked stage involved the initiation of longitudinal cracks above the shear-key locations while the repaired stage involved the replacement of an assumed damaged exterior beam with a new one. The distribution of the transverse strain developed at the top surface of the deck slab and the deflection across the width of the bridge were examined by varying the number of transverse diaphragms (five, four, and three) and the levels of TPT forces (20, 40, and 80 kip) at each transverse diaphragm. An ultimate load test was performed to evaluate the performance of the unbonded CFCC used for TPT during failure.

Analysis of the experimental results shows that the application of TPT significantly improved load distribution among the side-by-side box-beams. Increasing the level of TPT forces generally improved the deflection response of the bridge model in all the three cases studied. Different arrangements of the TPT forces had insignificant influence on the transverse strains developed in the region between the diaphragms. From the ultimate load test results, it was noted that the TPT system coupled with the deck slab distributed the eccentric load in the transverse direction until the complete failure of the bridge model. The numerical study revealed that the influence of the live load alone is not the major cause of the longitudinal cracks. Combining the temperature gradient with the live load can lead to the development of longitudinal cracks between the adjacent beams. The adequate number of diaphragms is a function of the bridge span while the adequate TPT force level is a function of the bridge width. The developed recommendations are presented in design charts relating the number of diaphragms to the bridge span and the level of the TPT force to the bridge width. The onset of longitudinal cracks can be delayed using adequate TPT arrangements.

17. Key Words Box-beam bridges, transverse post-tensioning, longitudinal cracks, transverse diaphragms	18. Distribution Statement No Restrictions. This document is available to the public through the Michigan Department of Transportation (MDOT).

19. Security Classification (Report) Unclassified	20. Security Classification (Page) Unclassified	21. No. of Pages	19. Price

Keywords:

Carbon Fiber Composite Cable (CFCC)

Composite Materials

Finite Element Analysis

Flexure Strength

Load Distribution

Differential Camber

Prestressed Concrete

Shear-Key

Side-by-Side Box-Beam Bridge

Skew Alignment

Strain Distribution

Transfer Length

Transverse Post-Tensioning

Load Fraction

Center for Innovative Materials Research (CIMR)
Structural Testing Center
Department of Civil Engineering
Lawrence Technological University
21000 West Ten Mile Road
Southfield, MI 48075-1058, USA.
Tel: 1-248-204-2556
Fax: 1-248-204-2568
E-mails: Nabil@LTU.edu, Jensen@LTU.edu
Web pages: http://www.NabilGrace.com, http://qbx6.LTU.edu/Jensen

TABLE OF CONTENTS

LIST OF FIGURES

LIST OF TABLES

EXECUTIVE SUMMARY

Prestressed precast concrete box-beam bridges have numerous advantages over other types of bridges such as low life-cycle costs, quick and easy construction, and low depth-to-span ratio. Nevertheless, there are several problems associated with the performance of side-by-side box-beam bridges. One of the major distress types in the side-by-side box-beam bridges is the longitudinal cracks in the deck slab above the shear-keys between the adjacent box-beams. The crack development can cause secondary distresses associated with lack of transverse load distribution leakages, debonding, delamination, and corrosion of steel reinforcements. A frequent challenge in box-beam bridges is the misalignment of transverse post-tensioning (TPT) ducts, which arises as a result of differential camber between the adjacent box-beams. Furthermore, the replacement of a damaged beam is difficult with the use of bonded TPT steel strands in side-by-side box-beam bridges.

The use of transverse post-tensioning (TPT) force has been considered as a viable solution to the development of longitudinal cracks in the box-beam bridges (El-Remaily et al., 1996). To examine the influence of the level of TPT and the number of the transverse diaphragms on the performance of the bridge model in the transverse direction, experimental and numerical research program developed. The experimental program included the construction, instrumentation, and testing of one half-scale 30° skew side-by-side box-beam bridge model with effective span of 31 ft. The experimental bridge model consisted of four adjacent precast prestressed concrete box-beams interconnected using full-depth shear-keys, reinforced composite deck slab, and unbonded TPT carbon fiber reinforced polymer (CFRP). The numerical study included performing extensive finite element (FE) analysis using ABAQUS, which is a commercially available software package. A series of finite element models were generated to simulate a wide range of side-by-side box-beam bridges with different spans and different widths. Different loading cases were evaluated to establish the adequate number of diaphragms and the appropriate TPT forces, in order to prevent the development of longitudinal deck slab cracks. The experimental program consisted of load distribution test conducted during three different deck slab conditions of the bridge model. These conditions were uncracked, cracked, and the repaired deck slab. Transverse strain distribution test was conducted in the stage where the deck slab was uncracked. The cracked stage involved the

initiation of longitudinal cracks above the shear-key locations while the repaired stage involved the replacement of an assumed damaged exterior beam with a new one. The distribution of the transverse strain developed at the top surface of the deck slab and the deflection across the width of the bridge were examined for different combination of number of transverse diaphragms (five, four, and three) and the levels of TPT forces (20, 40, and 80 kip) at each transverse diaphragm. Once the load distribution test had been completed, the bridge model was loaded to failure to evaluate the response of the unbonded carbon fiber composite cables (CFCC) used for TPT strands and to assess the load-carrying capacity of the bridge model. The ultimate load test was conducted by applying an eccentric load using symmetrical two-point loading frame.

Analysis of the experimental results shows that the application of the TPT significantly improved load distribution among the side-by-side box-beams. Increasing the level of TPT forces generally improved the overall behavior of the bridge model in all the three cases studied. For this bridge model and load arrangements, the case of five diaphragms outperformed the three diaphragms case in terms of load distribution. Different arrangements of the TPT forces had insignificant influence on the transverse strains developed in the region between the diaphragms. From the ultimate load test results, it is noted that the TPT system coupled with the deck slab evenly distributed the eccentric load in the transverse direction until the complete failure of the bridge model. Furthermore, a close examination of the ten salvaged unbonded CFCC is clearly indicated that none of these strands experienced any rupture.

The numerical study revealed that the influence of the live load alone is not the major cause of the longitudinal cracks. However, combining the temperature gradient with the live load can lead to the development of longitudinal cracks between the adjacent beams. The adequate combination of number of diaphragms and TPT force level can delay the development of longitudinal cracks. The number of diaphragms is a function of the bridge span while the TPT force level is a function of the bridge width. Furthermore, using concrete of high strength in the deck slab can slightly reduce the amount of TPT forces required per diaphragm. The developed recommendations are summarized in design charts relating the number of the diaphragms to the bridge span and the TPT force level to the bridge width.

ACKNOWLEDGEMENTS

The authors would like to express their appreciation to the Michigan Department of Transportation (MDOT) in conjunction with the U.S. Federal Highway Administration (FHWA) for sponsoring this research project under Contract No. 2004-0105. The technical advice and directions provided by Roger Till, Steven Beck, and the members of the Research Advisory Panel of MDOT have been greatly helpful for the successful completion of this investigation. The staff of Center for Innovative Materials Research (CIMR), Lawrence Technological University, Charles Elder, Moheb Labib, Delali Noamesi, Prasadu Penjendra, Chenglin Wu, Charles Aziabor, Kapil Patki, Andrew Weller, Kendall Stevens, Lawrence Bukowski, and Tony Magnan extended their tremendous efforts and contributions. The carbon fiber composite cable (CFCC) for transverse post-tensioning were supplied by the Tokyo Rope Mfg. Co. Ltd., Japan. The opinions expressed in this project report are those of the authors and do not necessarily reflect the views of the sponsors.

CHAPTER 1: INTRODUCTION

1.1 Introduction

According to the United States Federal Highway Administration's 2005 National Bridge Inventory data, about 25% of the nation's 595,625 bridges are structurally deficient or functionally obsolete, as reported in the Better Roads Magazine, May 2007 issue. Such high number of structurally or functionally deficient bridges calls for weight limits, rehabilitation, or withdrawal and replacement. Corrosion of steel reinforcements, resulting from aggressive environmental conditions and the use of deicing salts, has been one of the major causes for deterioration of concrete bridge structures, as shown in Figures 1.1-1a and Figure 1.1-1b.

In Michigan State, the percentage is higher than the average 28% of Michigan's 10,825 bridges are structurally deficient or functionally obsolete. It has been reported that in Michigan, bridge deterioration is primarily the combined result of 1) use of deicing salts leading to corrosion of conventional steel reinforcement, 2) repeated freeze and thaw cycles, 3) development of longitudinal cracks between the side-by-side box-beams allowing ingress of water, which accelerates rate of corrosion, 4) uneven load distribution giving rise to dissimilar deterioration of beams, and 5) heavy traffic volume and axle loads (Better Roads Magazine, May, 2007).

Prestressed concrete bridges make up a major portion of the bridges constructed in Michigan and USA where the typical cross-sections used are I- or T-sections, and spread or side-by-side box-beams. Prestressed concrete box-beams are commonly used in bridge construction due to their many advantages as follows.

1. High torsional stiffness making the box-beam sections ideal for curved bridge alignments and for segmental bridge construction.
2. High span-to-depth ratios making a suitable choice for longer spans.
3. Structural stability and good aesthetic appearance due to monolithic construction.

(a) Deterioration and concrete spalling

(b) Deterioration and leakage

Figure 1.1-1 Deterioration of concrete due to leakage and corrosion.

However, side-by-side box-beam bridges are prone to the development of longitudinal cracks in the deck slabs where the cracks are observed above the longitudinal shear-key joints between adjacent box-beams. Currently, the side-by-side box-beam bridges are designed with transverse post-tensioning (TPT) arrangements to limit the development of longitudinal deck cracking as well as limit any differential movement between the adjacent box-beams, once the cracks have formed. However, the current design of the TPT arrangement is not adequate in preventing deck cracking. Typical results of deck cracking observed over side-by-side box-beam is seen in Figure 1.1-2. The presence of the longitudinal cracks above the longitudinal shear-key joint allows water and deicing solutions to saturate the concrete near the joints. It is well known that the presence of chloride leads to accelerated corrosion of the reinforcing and prestressing steel. Furthermore, the seepage of water through the shear-key during freezing conditions allows for the formation of icicles below the bridge surface. The unexpected falling of icicles can pose a high risk for vehicles moving under the bridges.

Figure 1.1-2 Deterioration due to lack of adequate post-tensioning in transverse direction.

Several issues are addressed in this report to improve the performance of prestressed concrete side-by-side box-beam bridges. These issues include: 1) replacement of

interior/exterior damaged bridge beams due to deterioration or high load impact (Figure 1.1-3), 2) longitudinal cracks in the deck slabs between the box-beams due to lack of TPT and joint detail (Figure 1.1-4), 3) unbonded TPT (Figure 1.1-5 and Figure 1.1-6), 4) deterioration of concrete and corrosion of steel strands resulting from leakage (Figure 1.1-7), and 5) misalignment of TPT ducts due to differential camber of box-beams of skew bridges.

Figure 1.1-3 Damaged exterior prestressed concrete box-beam due to impact.

Figure 1.1-4 Longitudinal cracks in deck slab along shear-keys between box-beams.

Figure 1.1-5 Close-up view of field application of transverse diaphragm for unbonded CFRP strand.

Figure 1.1-6 Details of seven transverse diaphragms for unbonded CFRP post-tensioning strands.

Figure 1.1-7 Corrosion of longitudinal prestressing strands.

1.2 Project Objectives

The main objective of this study is to determine the adequate TPT arrangement, which would delay and reduce the development of longitudinal deck cracking in side-by-side box-beam bridges. The results and recommendations of comprehensive numerical and experimental investigations would provide MDOT engineers guidance in developing revised design specifications for the TPT arrangement for side-by-side box-beam bridges. These design specifications would provide strategies for the construction and performance issues outlined in Section 1.1. The following tasks have been conducted to achieve the project objectives. The tasks were:

1. Conduct a numerical analysis to determine the adequate number of transverse diaphragms and the effective level of TPT forces applied with unbonded CFRP strands in order to avoid longitudinal cracking.
2. Construct, instrument, and test a one-half scale 30º skew box-beam bridge model with transverse diaphragms located at the two supports, quarter-span sections, and mid-span section.
3. Investigate the suitability and effectiveness of using unbonded CFCC for TPT.
4. Develop an adaptable construction approach to address the issue related to misalignment of transverse ducts due to differential camber experienced in skew box-beam bridges.
5. Recommend a suitable rehabilitation construction methodology to allow the replacement of a deteriorated/damaged box-beam within any part of the box-beam bridge.
6. Establish recommendations for revised construction and design specifications for side-by-side box-beam bridges.

1.3 Report Organization

This numerical and experimental research project on skewed prestressed concrete box-beam bridge models addresses the provision of adequate numbers of transverse diaphragms and their effective level of TPT forces. This report documents these efforts in the following chapters:

Chapter 2: This chapter presents a comprehensive review of the past research work conducted on variety of prestressed concrete bridges with particular focus on the performance of side-by-side box-beams with respect to longitudinal deck cracking.

Chapter 3 and 4: These chapters present the details of the finite element analysis of skewed prestressed concrete box-beam bridge. Furthermore, recommendations have been made for the TPT arrangement for side-by-side box-beam bridges with spans ranging from 50 ft to 120 ft and widths ranging from 24 ft to 72 ft. The TPT arrangement included the levels of TPT force, and the number of transverse diaphragms.

Chapter 5: This chapter presents the details of the experimental program for a 30° skewed prestressed concrete box-beam bridge model including details of the construction, instrumentation, test setup, and test procedures.

Chapter 6: This chapter presents the discussion of the experimental results.

Chapter 7: This chapter presents the project conclusions and recommendations.

CHAPTER 2: LITERATURE REVIEW

2.1 Introduction

This chapter presents a comprehensive literature review conducted on the use of transverse post-tensioning (TPT) in bridges with particular focus on side-by-side box-beam bridges. Precast prestressed concrete members are widely used in the construction of bridges due to their constructional, structural, and field advantages. The use of box-beam bridges in USA has increased gradually since the year 1955 due to distinctive advantages (Taly, 1998; and Aktan et al., 2004):

1. High span-to-depth ratio of box sections provide a slender and aesthetically pleasing appearance.
2. Monolithic construction imparts structural stability as well as enhanced appearance;
3. High torsional stiffness of box-beam sections make them ideal for curvilinear and segmental bridge construction.
4. High industry acceptance of box-beam bridges due to their simple design, rapid construction, and low life-cycle cost.

However, as discussed in Chapter 1, the performance issues and construction challenges associated with the current design details and construction practices of precast prestressed concrete box-beam bridges warrants an in-depth review of the factors that affect these issues and challenges. The service life performance of side-by-side box-beams is measured in terms of the load distribution between the girders when subjected to vehicle loading, the presence or absence of longitudinal deck cracking, and the deterioration of the concrete and reinforcing material. These measures are affected by TPT force level, number of transverse diaphragms, shear-key design, bonded versus unbonded post-tensioning strands, and skew angle.

Significant experimental, field, and numerical investigations have been performed over the last two decades, providing an improved understanding on the interaction between the measures and the factors. One of the key findings was that TPT could be used as a mitigating design feature to control deck and shear-key cracking. However, a significant portion of the research was directed towards bridge systems other than side-by-side box-beam bridges.

Therefore, this literature review synthesizes the general knowledge as it pertains to side-by-side box-beam bridges with TPT arrangements through the beam sections. Emphasis has been placed on features that overcome some of the prominent performance problems such as cracking in skewed side-by-side box-beam bridges.

Service life performance and the durability/longevity of bridges have been regarded as crucial factors in bridge management nationwide (Ramey and Wright, 1997a and 1997b). Premature and accelerated distress development in bridge decks, in particular, was often observed where aggressive weather and heavy traffic conditions prevailed. Hence, aspects associated with these loading and environmental conditions should be integral parts of a design and bridge management program (Ramey et al., 1997a and 1997b). Particular performance issues for box-beam bridges were reported by Aktan et al. (2004). Evaluation of 15 side-by-side prestressed concrete box-beam bridges with skew angles ≤ 30° indicated that the major distresses were related to beam moisture, shear-key moisture, beam cracking, spalling, shear-key cracking, and deck condition. The study recommended 1) inspecting the concrete cover of the prestressing tendon near the top of the bottom flange, and 2) developing detailed finite element models to represent the entire bridge system as a way to analyze shear-key cracking, movement between adjacent beams, and structural capacity. Furthermore, the study found a need to confirm the effectiveness of various employed maintenance and repair techniques.

In 1998, the Ohio Department of Transportation (ODOT) constructed a high performance concrete (HPC) side-by-side box-beam bridge (Greuel et al., 2000). In this bridge, an experimental shear-key was utilized at mid-depth of the cross-section whereas the beams were tightened together using non-prestressed threaded rods located transversely through diaphragms at the ends and quarter-spans of the bridge. After constructing the entire bridge, it was subjected to eccentric load using four ODOT trucks filled with gravel to record load of 30 kip for each truck. It was reported that while subjecting the bridge to eccentric load, the deflection was larger on the loaded side than the opposite side of the bridge width. However, the side-by-side placed beams acted in unison, sharing the applied truck load, as evident from the live load distribution test.

Badwan and Liang in 2007, reported an analysis method, based on grillage analogy (skeleton structure with transverse loads), for calculating the required TPT stress for a deck

built with precast concrete multi-beams. The researchers concluded that the effect of skew angle was significant when the skew angle was greater than 30°. Furthermore, it was found that the required post-tensioning stress for optimum design of a precast concrete multi-beam deck was decreased with increase in skew angle. The tests were conducted with maximum skew angle of 45°.

2.2 Transverse Post-Tensioning

For decades, TPT has been used as a mitigating design feature to control deck and shear-key cracking (Moll, 1984; Phipps et al., 1985; Poston et al., 1985 and 1989). Analytical and experimental investigations indicated overall improved bridge performance in terms of strength and serviceability when applying substantial TPT forces through the deck of a slab-girder bridge model. This placed the majority of the deck slab in compression counteracting any tensile forces developed through loading. Poston et al. (1985, 1989) also concluded that transverse prestressing of a slab-girder or box-girder bridge effectively developed compressive stresses.

Thoman et al. (1984) conducted load tests on a single-cell box girder bridge with cantilever deck. The bridge incorporated TPT in the bridge deck. The experimental results were in agreement with the analytical models used to predict the behavior of the structure through the case study on the transverse cantilever decks of the bridge. Lately, Csagoly (1997) showed experimentally that post-tensioning prevented the formation of transverse surface cracking and decreased the tendency for longitudinal surface cracking when applied in bridge decks. Roschke and Pruski (2000) constructed a large, two-span $^{3}/_{10}$ scale model of a post-tensioned slab bridge in a laboratory, where in addition to uniformly distributed longitudinal post-tensioning a band of transverse tendons was placed in a narrow region directly above the supporting columns. The transverse strain distribution due to prestressing in the transverse direction was compared with the finite element results. It was concluded that the experimental and finite element results matched closely.

2.3 Finite Element Modeling of Transverse Post-Tensioning Arrangements

A simple mechanical model was developed and verified by Kaneko et al. (1993a and 1993b) for the analysis and design of plain and fiber reinforced concrete shear-key joints. The basic feature of the study was to identify two main fracture mechanisms for shear-off failure of the key joints such as single curvilinear cracking and development of multiple diagonal cracks. An experimental investigation was also conducted and good agreement was obtained between the experimental and numerical analysis results.

In a finite element study carried out by Issa et al. (1998), the main objective was to determine the amount of longitudinal post-tensioning required to secure the tightness of the transverse joints between the precast concrete bridge deck panels, and keep them in compression. Two finite element models analyzed were simply supported model and three-span models. The models were subjected to the load of an AASHTO HS-20 truck as a live load. The analysis revealed that for simply supported spans, the required longitudinal post-tensioning should not be less than 200 psi to secure the tightness of the transverse joints between the precast concrete bridge deck panels for simply supported bridges. The longitudinal post-tensioning should not be less than 450 psi to maintain transverse joint integrity at interior negative moment regions over supports in compression.

Experimental tests and finite element analyses of different bridges conducted by Barr et al. (2001) revealed that the use of end diaphragms, increased skew angle, and load type (truck and lane) significantly affected the live load distribution factors. On the other hand, continuity and intermediate diaphragms had the least effect. Earlier work by Sithichaikasem and Gamble (1972) as well as Stanton and Mattock (1986) contradict these findings. For the exterior girders, the intermediate diaphragms slightly increased the live load distribution factor at low skew angles. At high skew angles (≥30°), the diaphragms were slightly beneficial. At larger skew angles, the live load distribution factor decreased with increasing skew.

2.4 Shear-Key Performance

The longitudinal grouted shear-key connection between side-by-side precast, prestressed concrete box-beams enables the shear load transfer between the adjacent elements. Different types of non-shrink grouts may be used to fill the keyways. The load distribution amongst the

adjacent girders is thus dependent on the performance of shear-keys. Moreover, failure of a shear-key leads to uneven live load distribution, stressing the individual girders excessively, which results in the formation of longitudinal cracks giving a path for water to seep through, thereby increases the risk of accelerated corrosion of the reinforcing steel. For determining transverse shear intensity in the shear-keys of multi-beam bridges due to design vehicle loads, a simplified method was presented by Bakht et al. (1983). It was shown that the behavior of multi-beam bridges could be characterized by a single, dimensionless parameter, without relying on any empirical approach. Later, connection response was modeled by linear and rotational springs resisting relative displacement between adjacent beams of a prestressed precast skewed multi-beam double-tee bridge by Jones and Boaz (1986).

2.4.1 Location of Shear-Key and Grout Material

Huckelbridge et al. (1995) and Huckelbridge (1996) investigated the in-situ performance of the grouted shear-keys, located at the longitudinal joints between adjacent girders of multi-beam prestressed box bridges. All the bridges tested, exhibited relative displacements across at least some of the joints, which indicated a fractured shear-key. The study proposed to locate the shear-key at the neutral axis level of the cross-section. With the use of such new shear-key design, El-Esnawi (1996) observed that the static shear load capacity was almost tripled from the current shear-key design with the same grouting material, and fatigue life of the new shear-key design was extended to over 8,000,000 cycles. Gulyas et al. (1995) made a comparative laboratory study on composite specimens for vertical shear, longitudinal shear, and direct tension, using two different grouting materials such as non-shrink grouts and mortars of magnesium ammonium phosphate. The results obtained indicated significant differences in performance between these two materials, which necessitate proper selection of grout material for constructing shear-keys.

Hlavacs et al. (1996) used a full-scale portion of a side-by-side box-beam bridge to test the performance of grouted shear-keys under environmental and cyclic loads. The shear-keys were grouted between the beams twice, first in the autumn season and second in the summer season. The beams were subjected to tests after each grouting in order to investigate the behavior of shear-keys. In the first test, shear-keys that were grouted in autumn cracked soon after casting, before any load had been applied. Data from instruments embedded in the beams and shear-

keys showed large discontinuities in strain caused by freezing temperatures in the following winter. Moreover, the strains caused by temperature were much larger than strains occurring under loads corresponding to the weight of an HS20-44 truck. The beams were subjected to 41,000 cycles of loading, simulating HS20-44 wheel loads. No new cracking occurred from the loading, but cracks caused by temperature propagated under loads. In the second test, high temperature caused by the sun heat on the top of the beams again caused large thermal strains, which cracked the shear-keys. These cracks were subjected to 10,000,000 cycles of the load corresponding to an HS20-44 wheel load. As in the first test, the load itself did not cause any cracks but the existing thermal cracks propagated under the load.

2.4.2 Thermal Stresses

The thermal cycles are believed to have significant influence on the load-carrying capacity of the joint formed at the shear-key locations. Not many studies have been conducted on the thermal effect owing to the difficulties in simulating it in an experimental setup. Miller et al.. (1999) had studied three different shear-key configurations under thermal effects. The three shear-keys differed in their locations within the section and in the materials used. It was concluded that the shear-keys located towards the deck surface cracked primarily due to the thermal stresses caused by daily heating and cooling. The shear-keys provided at mid-depth of the section were found less susceptible to the thermal stresses. The cracks developed due to the thermal stresses initiated the cracking process which was further propagated by the live load applied. Notably, the thermal cracks were found to be more pronounced at the support locations than at the mid-span locations.

2.4.3 Construction Practices

Lall et al. (1998) studied performance of full-depth shear-keys and transverse tendon systems in adjacent prestressed box-beam bridges. The researchers recommended providing higher TPT forces and two tendons over the depth of the beam at each post-tensioning location. Proper grouting during the shear-key installation was shown to be essential, emphasizing sandblasting, pre-wetting of keyway surfaces and maintaining proper water cement ratio in the grout. Miller et al. (1999) studied different shear-key configurations and tests were conducted on a full-scale, four-beam assembly that represented part of a bridge. The mid-depth shear-key was found less

susceptible to the stresses developed and was found to be more resistant to cracking. The epoxy shear-keys did not crack. However, it is evident that further studies are warranted in order to arrive at the appropriate shape of shear-key and its location by investigating the behavior of shear-keys in transmission of forces across the adjacent bridge girders.

Issa et al. (2003) studied the performance of transverse joint grout material in precast concrete bridge deck systems. The study was performed on 36 full-scale specimens fabricated and tested under vertical shear, direct tension, and flexural capacity. Different grout materials were examined for the shear-key connection such as Set 45, Set 45 HW, Set Grout, and polymer concrete. The connected surfaces were sandblasted, cleaned from dust, dried, treated chemically with hydrochloric acid, HCL (10% solution) to eliminate carbonation, and then washed by water. The researchers recommended high quality control during the construction for such joints. The study revealed that polymer concrete was the best material for the transverse joints in terms of strength, bond, and mode of failure as compared to the rest of the Set grouts. The Set grouts however facilitated ease of construction.

2.5 Transverse Diaphragms

As mentioned erstwhile, research supports the use of post-tensioning of transverse beams, also denoted as diaphragms, in addition to or replacement of the transverse prestressing of the deck slab (El-Remaily et al., 1996; Ebeido and Kennedy, 1996a, 1996b). The transverse diaphragms help improve integrity of the side-by-side box-beam bridges through the post-tensioning applied through it, i.e. it help increase live load distribution evenly amongst the beams. The MDOT Bridge Design Guide 6.65.13 (2006) recommends the locations of post-tensioning tendons to be provided in prestressed concrete box-beam bridges.

The influence of intermediate transverse diaphragms on the distribution of reaction on the pier supports was investigated by Ebeido and Kennedy (1996a, 1996b) experimentally and through finite element analyses. It was found that the presence of intermediate transverse diaphragms played an important role in the distribution of shear forces at the pier supports, making the shear distribution more uniform thereby avoiding localization of forces. Such even distribution of live loads amongst adjacently placed beam in a bridge avoids faster deterioration of a particular beam, thereby delaying the need for replacement of the deteriorated beam. The

connection achieved through the transverse diaphragms was observed to improve bridge stiffness, load distribution, and increase ultimate load-carrying capacity.

The effect of arrangement of internal transverse diaphragms and skew angle was also investigated by Khaloo and Mirzabozorg (2003) using finite element models. The variation of defined load distribution factor (DF) with different arrangements of transverse diaphragms is reproduced here in Figure 2.5-1, for bridges with skew angle, $\theta = 60°$ and three different I-girder spacing, *S*. Four different arrangements for internal transverse diaphragms of rectangular cross-sections were considered, designated with system type numbers 1 through 4. In system type number 1, the models did not include any internal transverse diaphragms. The internal transverse diaphragms, located at approximately each third point of the span length, were parallel to the supporting lines of the decks in system type number 2. The locations of the internal transverse diaphragms were based on AASHTO (1996) code and provided perpendicular to the longitudinal girders in system type number 3. Lastly, in system type number 4 the spacing between the internal transverse diaphragms was about 5 m, provided perpendicular to the longitudinal girders. Two standard trucks HS20-44 were used, placed side-by-side on the decks with $S = 1.8$ and 2.4 m, while for the decks with $S = 2.7$ m girder spacing, three trucks were used side-by-side. It was concluded that the effect of orientation of the internal diaphragms relative to the supporting lines and the girders on the load distribution was significant. Systems 3 and 4 showed significantly improved performance. In addition, the effect of spacing between internal transverse diaphragms perpendicular to the longitudinal girders might be neglected, such that the maximum difference between systems 3 and 4 is 7-10%.

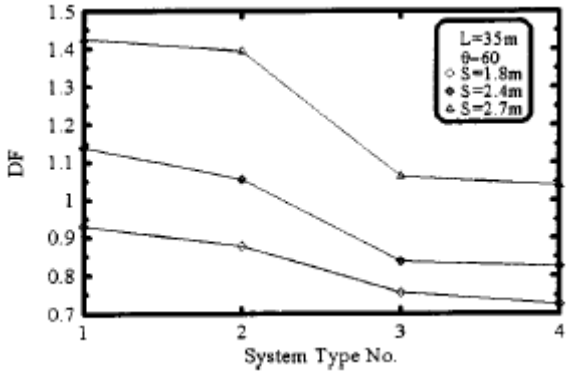

Figure 2.5-1 Effect of number of internal transverse diaphragms on the load distribution factor when skew angle is 60° (Khaloo and Mirzabozorg, 2003).

The contribution of intermediate diaphragms in enhancing precast bridge girder performance was investigated by Green et al. (2004) through modeling of the Florida Bulb Tee 78 precast concrete bridge girders. It was shown that the presence of intermediate diaphragms helped in stiffening of the precast bridge girders and thereby reduced maximum girder deflections. El-Remaily et al. (1996) reported an in-depth study on the design of TPT in adjacent precast prestressed concrete box girder bridges. They observed that post-tensioned transverse diaphragms serve as the primary mechanism for the distribution of wheel loads across the bridge. The amount of post-tensioning required at each diaphragm was shown to depend on the bridge geometry and loading, and a chart had been developed for the determination of the required amount of TPT (Figure 2.5-2). In general, it is observed that the level of post-tensioning recommended by the researchers is significantly higher than that suggested by the current MDOT Specifications. The researchers suggested use of a full-depth vertical shear-key at each diaphragm and the post-tensioning distributed equally between the top and bottom of the diaphragm. The authors recommended performing a detailed grid analysis for situations where large skew is present, and accurate results are needed.

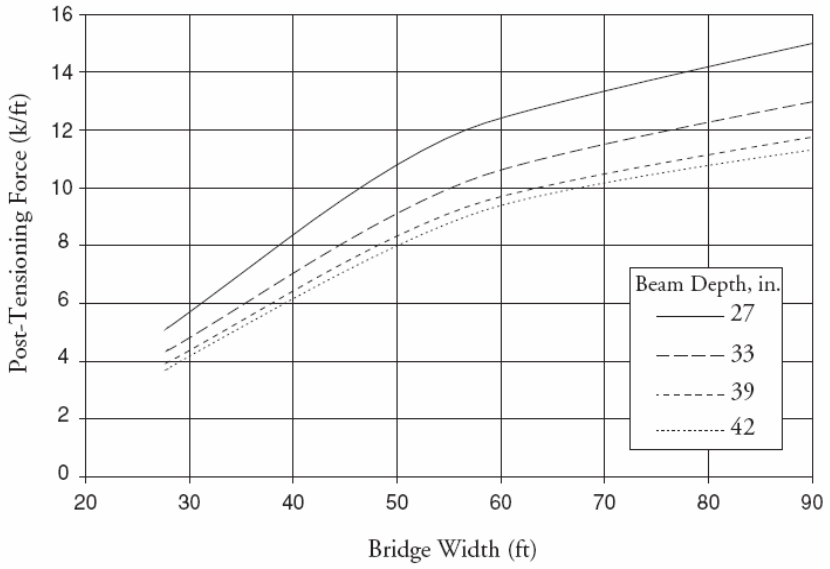

Figure 2.5-2 Design chart for effective post-tensioning force (El-Remaily et al., 1996).

Indented transverse pre-tensioning strands were shown to provide satisfactory prestress transfer by Yamane et al. (1998). In addition, the grouted post-tensioned transverse joints between precast panels were shown to exhibit satisfactory performance. For a deck replacement project, it was also advised to develop a scheme to maintain continuity at the existing-to-new deck joint to avoid edge loading when the deck remains temporarily open to the traffic.

2.6 Load Distribution

The provision of shear-key, transverse prestressing, and deck slab facilitates the distribution of live loads amongst the adjacently placed box-beams in bridges. The effective transmission of loads evenly across the entire width of bridge reduces chances of differential movement among the side-by-side placed beams and relative joint opening at the beam bottom, thereby hindering development of longitudinal cracks and hence ensures improved performance and durability. The distribution of truck wheel loads and performance of joints between the two adjoining members in multi-beam precast bridges were investigated by Stanton and Mattock (1986). The report presented different types of geometric shapes of keys, connection methods such as a grouted key, welded steel connectors etc. and calculated the shear forces transmitted between

the members. They concluded that the grouted keyway was much stiffer than the steel connectors.

Abendroth et al. (1989) and Ebeido and Kennedy (1996a) had emphasized the role of transverse diaphragms in live load distributions and bridge load-carrying capacities. Transverse diaphragms tie the beams together to facilitate construction, transfer lateral loads (such as wind load), and improve vertical load (such as traffic load) distributions. It was concluded that both the span and support girder moments were decreased significantly with increases in the skew angle of the bridge, especially for skew angles >30°. Moreover, the skew angle was shown to have more influence on the design of interior girders than the exterior girders. The presence of intermediate transverse diaphragms was shown to enhance load distribution characteristics of the bridge.

Service load tests were performed by Klaiber et al. (2001) on four deteriorated precast concrete deck bridge panels; two with shear-keys in place and two without. Based on the field results, it was determined that these bridges had sufficient lateral load distribution and adequate strength when shear-keys were properly installed between the adjacent panels. The measured lateral load distribution factors were larger than AASHTO values when the shear-keys were not installed. Since some of the reinforcement had hooks, deterioration of the reinforcement had a minimal effect on the service level performance of the bridges when there was minimal loss of cross-sectional area. Laboratory tests were performed on the precast concrete deck bridge panels obtained from three bridge replacement projects, as shown in Figure 2.6-1.

(a) Load distribution test (b) Ultimate load test

Figure 2.6-1 Reported experimental program by Klaiber et al. (2001).

Twelve deteriorated panels were loaded to failure in a four-point bending arrangement (Klaiber et al., 2001). Although the panels had significant deflections prior to failure, the experimental capacity of eleven panels exceeded the theoretical capacity. Experimental capacity of the twelfth panel, an extremely distressed panel, was only slightly below the theoretical capacity. Service tests and an ultimate strength test were performed on a laboratory bridge model consisting of four joined panels to determine the effect of various shear connection configurations. These data were used to validate a finite element model of the precast concrete deck bridge providing more accurate live load distribution factors for use in rating calculations.

Results of structural load tests were performed on the Bridge Street Bridge, the first prestressed concrete bridge in the United States, reinforced almost entirely with CFRP (Grace et al., 2005). Based on the results from load tests, it was concluded that the applied loads per lane were effectively distributed to all four beams of each bridge span; the three spans of the bridge exhibited similar load distribution behavior; the actual load distribution behavior was consistent with the distribution factors derived from the provisions of the AASHTO (2004) Specifications, and that the provisions of the AASHTO Standard or LRFD Specifications could be used to predict the load distribution behavior of bridge superstructure.

2.7 Level of Prestressing

The extent of prestressing provided in the transverse direction affects the stiffness of the bridge and governs the structural behavior, and importantly the development of cracks under service load conditions. Many State DOTs recommend the use of prestressed transverse diaphragms. A study by Cai and Sahawy (2004) demonstrated the effect of the transverse diaphragms on load distribution factor (LDF) and maximum strain for different skew angles (see Figure 2.7-1) in bridges with I-girders. The normalization is made with the case when no diaphragm was provided. From the Figure, it is observed that the diaphragms had significant effect on LDF and maximum strain developed. However, this effect diminished with the increased skew angle. Increasing the number of diaphragms did not have much effect on LDF and maximum strain. They concluded that an increase of the diaphragm stiffness could significantly reduce both the strains developed and the load distribution. A full stiffness can be achieved by

prestressing the diaphragms, which also can prevent cracking and ensure the continuity of the diaphragms across the beams. Later a formula was proposed by Cai (2005) to quantify the intermediate diaphragm effect on live load distribution, and the results were compared with AASHTO (American Association of State Highway and Transportation Officials) LRFD (Load and Resistance Factor Design) load distribution factors.

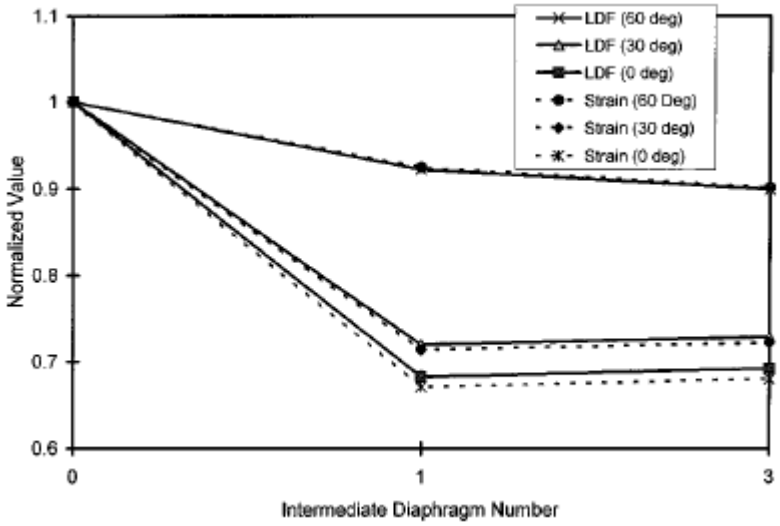

Figure 2.7-1 Diaphragm effects on load distribution factors (Cai and Sahawy, 2004).

Nevertheless, contradictory observations from the field studies of cracked bridge decks were reported by Chamberlain and Kreger (1999) - that the transverse post-tensioned strands were not successful in making the box girders act compositely. As the study was focused on field observations, no data is available to know if the increased level of TPT or increased number of transverse diaphragms would help the beams act in unison sharing the live load uniformly.

2.8 CFRP Bonded and Unbonded Transverse Prestressing

The use of fiber reinforced polymers (FRPs) in bridges has been started owing to its corrosion resistant properties and higher strength to weight ratio. A substantial amount of research work has been reported on the performance of FRPs when used for construction applications. A state-of-the-art paper by Bakis et al. (2002) presents a concise historical background, accomplishments of the investigations and research progress made so far on FRPs.

Furthermore, FRPs implemented successfully in real-life bridge construction projects were also reported by Grace et al. (2002).

Carbon fiber reinforced plastic tendons were used by Braimah et al. (1998) for transverse prestressing of a bridge model, and tested under simulated concentrated wheel loads. The test results showed that transverse prestressing considerably enhanced the punching failure loads of the deck slabs resting on steel I-beam girders. Grace and Abdel-Sayed (1998) discussed the comparative effectiveness of fully bonded and completely unbonded applications of the carbon fiber reinforced polymer (CFRP) tendons. The bridge models in this study consisted of CFRP rods grouted and ungrouted in the transverse direction. It was concluded that ductility of the bridges could be increased by keeping the transverse tendons unbonded.

Later, Marshe and Green (1999) described an experimental investigation on the punching behavior of composite bridge decks transversely prestressed with CFRP tendons. Their investigation provided information on the usefulness of transverse prestressing using CFRP, and the consequent effects. The transverse prestressing of the deck slab improves the compressive membrane action and allows a reduction in the slab thickness, however with a reduced thickness durability is a concern with steel prestressing tendons. By using FRP prestressing tendons, the durability of the bridge deck slab would be improved. The feasibility of using CFRP tendons to prestress the composite bridge decks in transverse direction was demonstrated by Marshe and Green (1999), and the CFRP prestressed bridge deck showed better overall structural performance than the steel prestressed deck.

2.9 Effect of Skew Angle on Load Distribution

In many bridge construction projects, due to the practical difficulties in providing a right-angled alignment of the bridges, skew alignments become inevitable. However, the load distribution amongst adjacent bridge girders is significantly influenced by the skew angle. El-Ali (1986); Bishara et al. (1993); and Khaloo and Mirzabozorg (2003) showed that the increase in skew angle reduced the ability of the bridge system to distribute the load between individual girders.

The ratio of distribution factor at any skew angle to the distribution factor at zero skew, illustrating the effect of skew, is shown in Figure 2.9-1 (Barr et al., 2001). Model 1 was a

simply supported, single-span model of span 80 ft with only the deck and girders modeled. This model did not account for lifts (the layer of concrete between the top of the girder and the bottom of the deck), intermediate diaphragms, end diaphragms, or span continuity. Model 2 was the same as model 1, but the lifts were included between the girders and deck. In model 3, intermediate diaphragms were added, and in model 4 end diaphragms were added. Model 5 was the same as model 4, but spans 80 ft were added and the three spans were made continuous. The skew angle of each model was varied between 0 and 60° to evaluate the effect of skew. It was concluded that skew had little effect for an angle of 20°, and for some models, the live load distribution factor actually increased slightly. However, at larger skew angles, the live load distribution factor decreased with increasing skew. In general, the interior girders were more affected by skew than were the exterior girders.

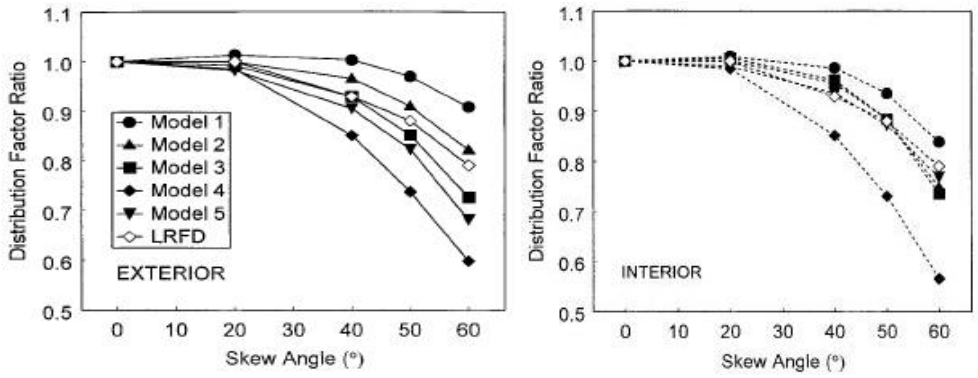

Figure 2.9-1 Effect of bridge skew angle on load distribution factor (Barr et al., 2001).

It was shown by Green et al. (2004) that the presence of intermediate diaphragms helped in reduction of the maximum girder deflections; however, such reductions were shown to decrease with the increased skew angles. The addition of intermediate diaphragms had an overall effect of reducing the deflections by about 19% for straight bridges, about 11% for 15-30° skew bridges, and about 6% for 60° skew bridges.

The paper by Huang et al. (2004) presented a study on the transverse load distribution in highly skewed (60°) bridges. Finite element analyses of the bridge were conducted to investigate the influence of model mesh, transverse stiffness, diaphragms, and modeling of the supports. The AASHTO (1998) formulas for transverse load distribution were shown to be

conservative for positive bending, and not conservative for negative bending for slab-on-steel girder bridges with skews as large as 60°. However, it is necessary to conduct similar investigations on precast prestressed bridges to verify the applicability of similar observations made on slab-on-steel girder bridges.

2.10 Summary

In summary, the above literature review brought about several interesting observations regarding the provision of transverse prestressing in precast prestressed bridges systems, and regarding performance of the shear-keys. Although providing transverse prestressing to the deck slab was recommended during earlier research, later it was shown more preferable to provide transverse prestressing to the transverse diaphragms. However, the extent of prestressing to be provided in the transverse direction was not suggested by any of the researchers. In their code recommendation, MDOT adopted post-tensioned transverse diaphragms to be provided in precast prestressed bridges. However, the number of diaphragms and prestressing force have not been optimized using experimental or numerical evidence. This calls for further research to be conducted so as to determine the most effective number of transverse diaphragms and prestressing force levels to be provided. Moreover, the severe problems associated with the development of premature longitudinal cracks on the deck slab along the joints between side-by-side box-beams could possibly be either reduced or delayed, if not eliminated altogether through adequate TPT arrangements. Load distribution studies for skewed precast prestressed bridges are also necessary because no particular study has been carried out for these types of bridges.

CHAPTER 3: NUMERICAL METHODOLOGY

3.1 Introduction

The development of the longitudinal cracks in side-by-side box-beam bridges was investigated through an in-depth finite element analysis (FEA) to determine the adequate transverse post-tensioning force level and number of diaphragms required to eliminate cracking. The FEA was conducted using the commercial software package ABAQUS 6.6.1. In this chapter, a detailed explanation of the modeling technique is presented first by defining: the finite element (FE) model components, material properties, elements types, boundary conditions, analysis steps, and all the assumptions that have been used through the process of modeling to simulate the response of side-by-side box-beam bridges under service loads. Then, the results of the numerical analysis are presented and discussed. Finally, recommendations are provided for MDOT engineers to formulate revised design Specifications for transverse post-tensioning (TPT) arrangements for typical side-by-side box-beam bridges.

According to MDOT Bridge Design Guide 6.65.13 (2006) for the transverse post-tensioning details, box-beam bridges are categorized by their spans. There are four categories: bridges with spans up to 50 ft, bridges with spans over 50 ft but not more than 62 ft, bridges with spans over 62 ft but not more than 100 ft, and bridges with spans over 100 ft. For each of these categories, the number of diaphragms is specified in the Bridge Design Manual. In this FE study, the results of the longest span of each category were used as a guideline for the entire category; four models of spans 50, 62, 100, and 124 ft were generated. The last span was an example for bridges with spans over 100 ft. The required box-beam depth and reinforcement details were justified based on flexural design specifications for each bridge performed according to the AASHTO LRFD (2004).

3.2 Components of the Bridge Model

The FE models simulated side-by-side box-beam bridges with superstructure composed of:

1. Box-beams reinforced with prestressing strands and reinforcing bars.

2. Unbonded transverse post-tensioning carbon fiber composite cables (CFCC) with end bearing nuts or plates.
3. Deck slab of 6 in. thick reinforced with one layer of reinforcement at the mid-thickness.
4. Elastomeric bearing pads (supports).
5. Non-shrink grout material in the shear-keys connecting the adjacent box-beams.

The following subsections provide the details of modeling each component.

3.2.1 Box-Beams

The cross-sections of the box-beams were selected from MDOT Bridge Analysis Guide (2005), as shown in Figure 3.2-1, Figure 3.2-2, and Figure 3.2-3. Box-beams are commonly manufactured in widths of 36 and 48 in., and depths ranging from 17 to 60 in. Beams with depths of 12 and 17 in. are manufactured only in a width of 36 in. Other shallow box-beams are manufactured in both widths. Beams deeper than 42 in. are manufactured only in a width of 48 in. The FE models were initially generated using beams of a width of 48 in. and depth satisfying the flexural requirement for the span (Table 3.2-1). Later on, the models were regenerated using box-beams of a width of 36 in. to make the results of the analysis more comprehensive.

In the transverse direction, each box-beam was provided initially with two end blocks of a width of 24 in. each, and interior diaphragms of a width of 14 in. each (MDOT Bridge Design Guide 6.65.13, 2006). The number and spacing of the interior diaphragms varied according to the span, as shown in Table 3.2-2 (MDOT Bridge Design Guide 6.65.13, 2006).

Box-beams and the transverse diaphragms were meshed using a brick element (C3D8R). This is a three dimensional element with eight nodes, as shown in Figure 3.2-4. Each node has three transitional degrees of freedom (U_x, U_y, U_z). A typical mesh for a single box-beam is shown in Figure 3.2-5 with a maximum element size less than 10 in.

Concrete properties for box-beams

A continuum, plasticity-based, damage model for concrete was used to model the material behavior. The concrete damaged plasticity model uses concepts of isotropic damaged elasticity in combination with isotropic tensile and compressive plasticity to represent the inelastic

behavior of concrete. It assumes that the two main failure mechanisms are tensile cracking and compressive crushing of the concrete material. Consequently, the concrete material was defined by its uniaxial compressive and tensile performance in addition to the elastic properties.

Table 3.2-1 Box-beam depths for the investigated spans.

Span (ft)	Box-beam depth (in.)
50	27
62	33
100	39
124	54

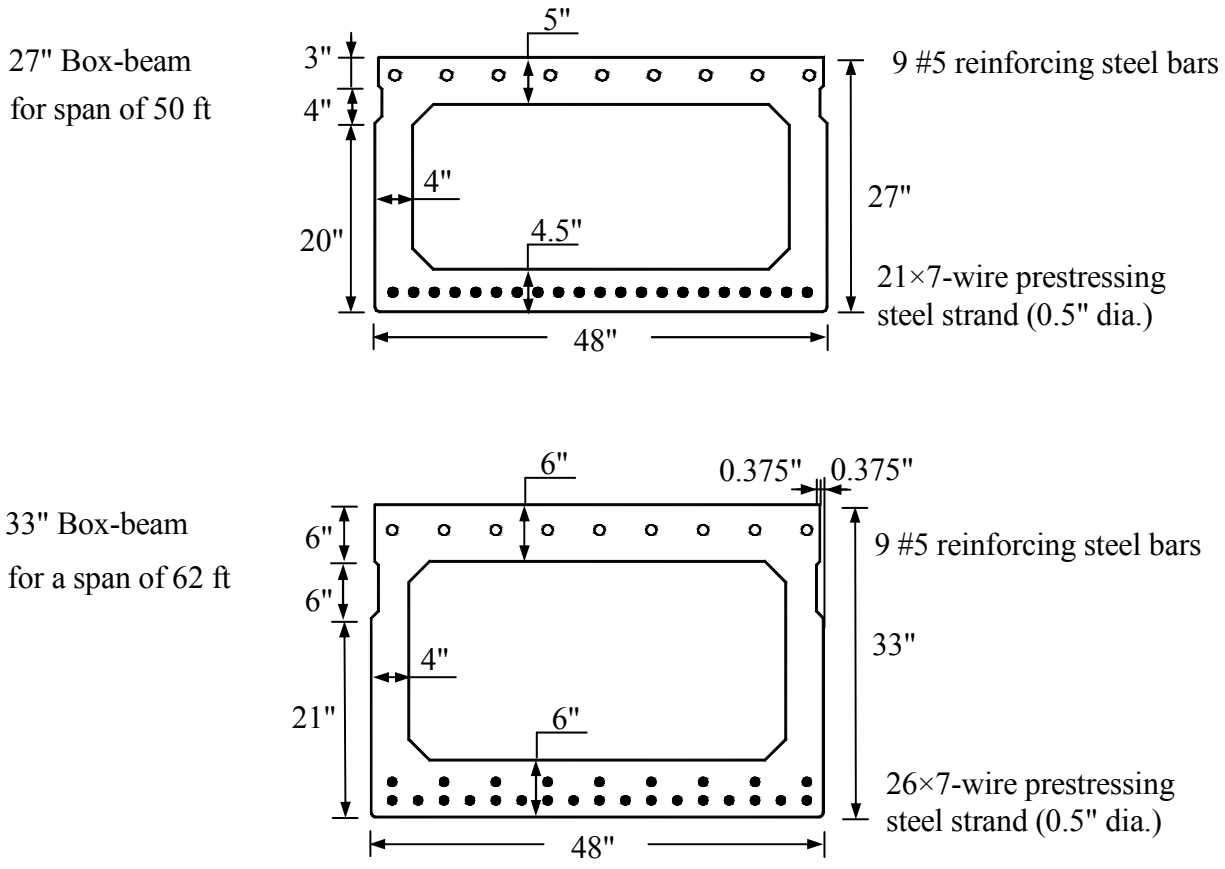

Figure 3.2-1 Cross-sectional details for box-beams.

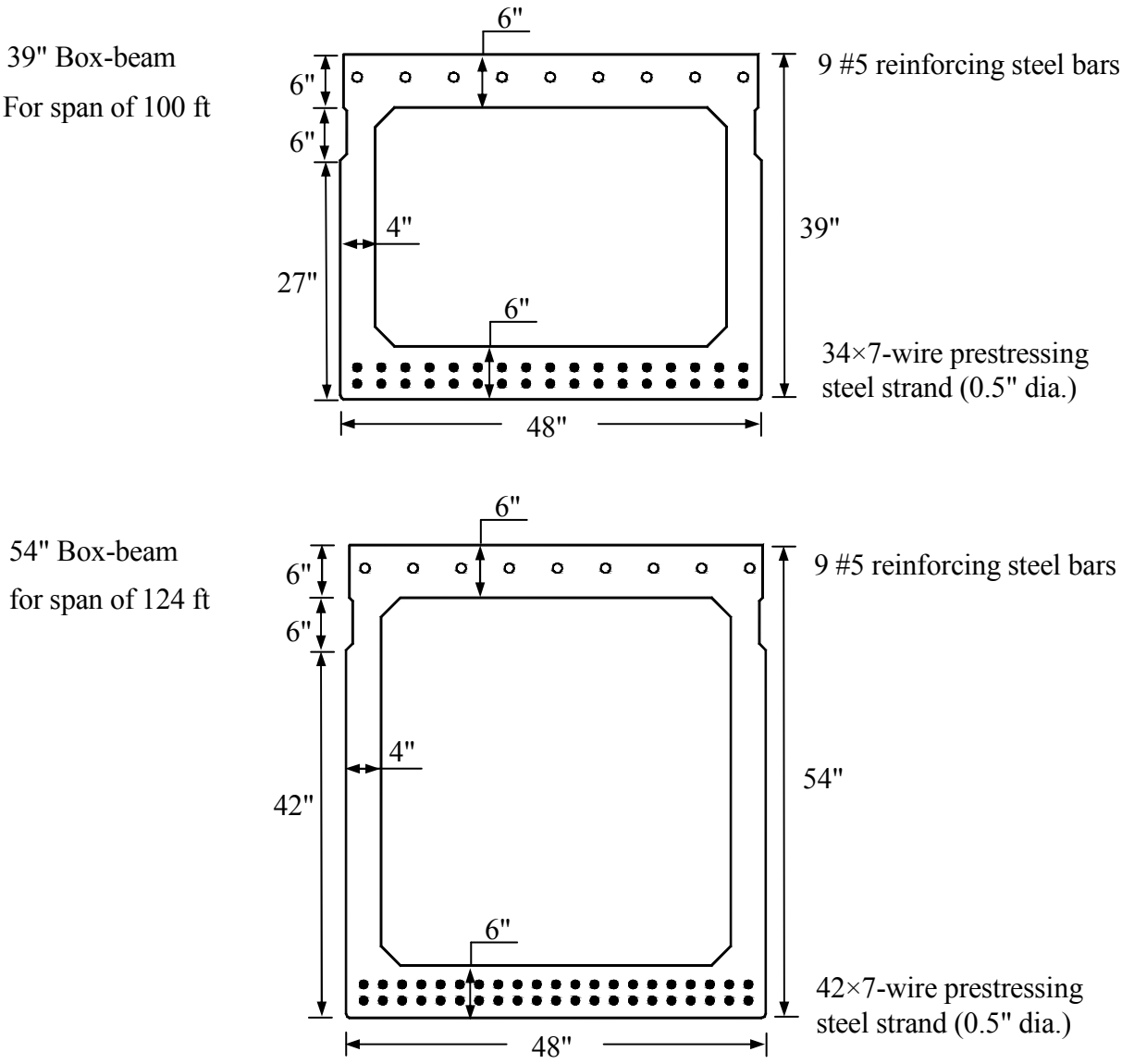

Figure 3.2-2 Cross-sectional details for box-beams (continued).

27" Box-beam
for a span of 50 ft

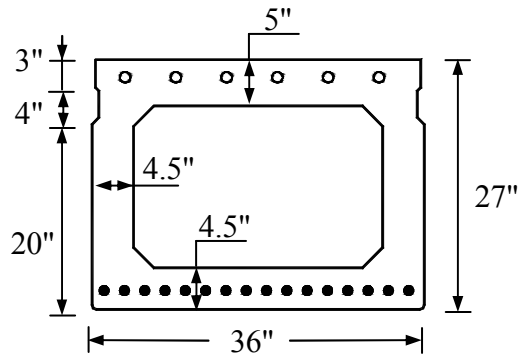

6 #5 reinforcing steel bars

16×7-wire prestressing
steel strand (0.5" dia.)

33" Box-beam
for a span of 62 ft

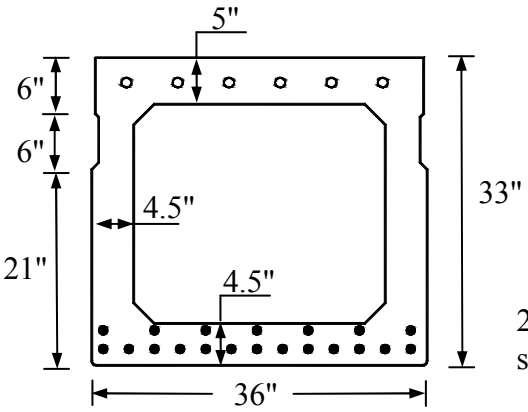

6 #5 reinforcing steel bars

20×7-wire prestressing
steel strand (0.5" dia.)

39" Box-beam
for a span of 100 ft

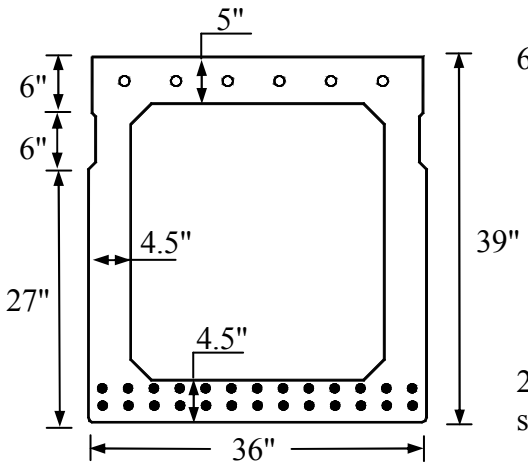

6 #5 reinforcing steel bars

26×7-wire prestressing
steel strand (0.5" dia.)

Figure 3.2-3 Cross-sectional details for box-beams (continued).

Table 3.2-2 Post-tensioning tendons location (MDOT Bridge Design Guide 6.65.13, 2006).

Span Length, ft	Locations
Up to 50	2 @ center of span (11 ft apart); 1 @ each end of beam
Over 50 to 62	1 @ each quarter point; 1 @ center of span; 1 @ each end of beam
Over 62 to 100	2 @ center of span (11 ft apart); 1 @ each quarter point; 1 @ each end of beam
Over 100	1 @ each end of beam with 5 equally spaced between

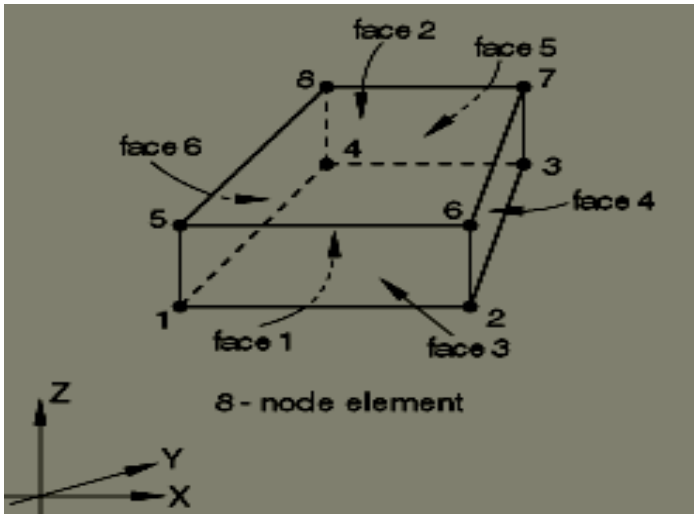

Figure 3.2-4 Brick element used in modeling box-beams (ABAQUS Manual, 2006).

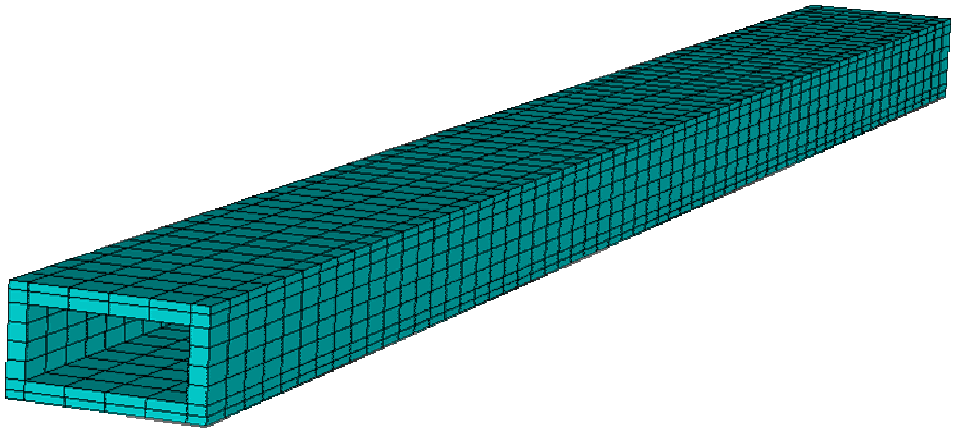

Figure 3.2-5 Three dimensional view for box-beam sides.

For the compressive stresses, as shown in Figure 3.2-6, the material model response is linear until the value of initial yield; the initial yield usually occurs at stress equal to 60% of the concrete ultimate strength and then the material begins the plastic response, which is typically characterized by stress hardening followed by strain softening beyond the ultimate stress.

For the tensile stresses, as shown in Figure 3.2-7, the stress-strain response follows a linear elastic relationship until reaching the value of the cracking stress, which corresponds to the onset of localized cracking in the concrete material. Beyond the cracking stress, the formation of cracks is represented macroscopically with a softening stress-strain response, which includes strain localization in the concrete structure. The stress-strain curves for the concrete were adapted from Nawy (2003) for concrete with compressive strength of 7,800 psi.

Based on available experimental results for tests performed in LTU using cylinders made of concrete with similar strength and having a maximum aggregate size of 3/8", the modulus of elasticity was taken equal to 4,270 ksi. The test was performed according to ASTM C469 up to stress equal to 40% of the ultimate strength. The points on the stress-strain curve and the experimentally determined modulus of elasticity were in good agreement. In addition, Poisson's ratio (υ) was obtained from experimental results as 0.15.

The modulus of rupture (f_r) was calculated as 530 psi [$0.19\sqrt{f'_c}$ for prestressed concrete, AASHTO LRFD (2004) Table 5.9.4.2.2.-1]. The term "modulus of rupture" in the finite

element analysis indicates the maximum allowable tensile strength in the concrete and not necessarily as defined by AASHTO LRFD (2004) 5.4.2.6.

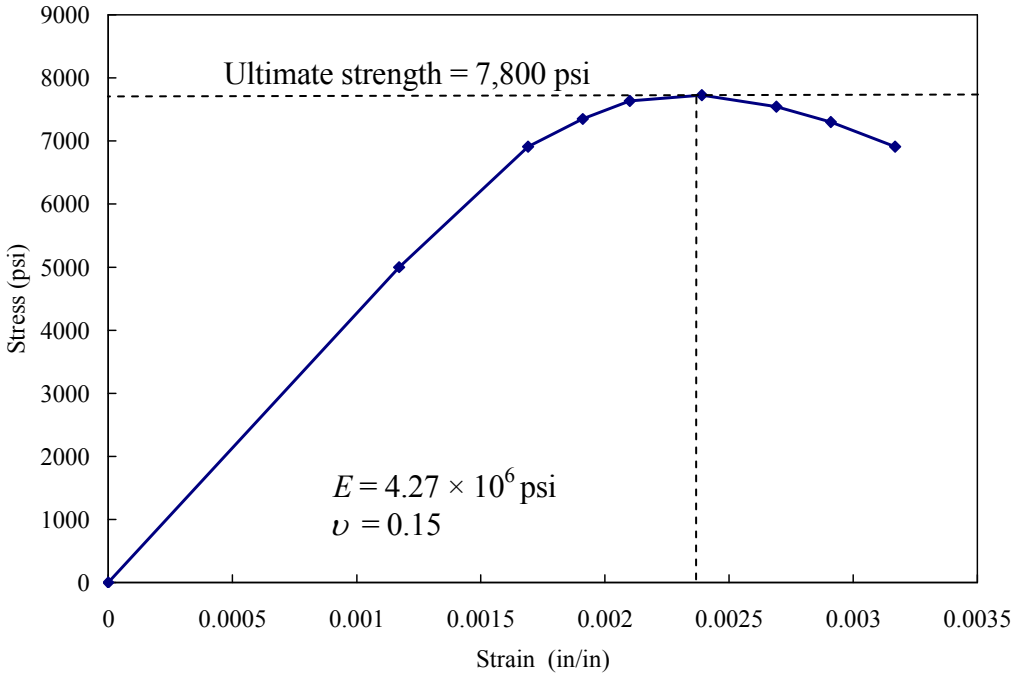

Figure 3.2-6 Compressive behavior for the concrete material in the box-beams (Nawy, 2003).

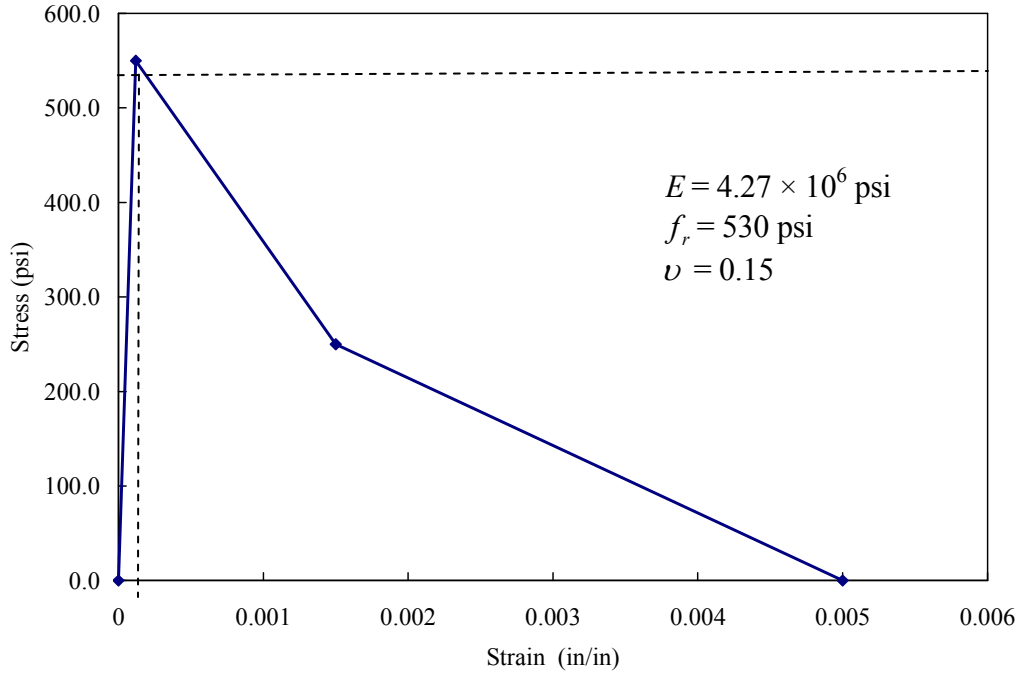

Figure 3.2-7 Tensile behavior for the concrete material in the box-beams (Nawy, 2003).

3.2.2 Box-Beam Reinforcement

Each box-beam was reinforced with bottom reinforcement composed of steel prestressing strands of a cross-sectional area of 0.153 in^2 each (seven-wire strand of 0.5 in. diameter). The number of strands per beam in the different bridge models varied according to the flexural design of each span (AASHTO LRFD, 2004). In addition, spans of 100 and 124 ft required some strands to be debonded for certain distances at the beam ends in order to prevent development of excessive tensile stresses in these end sections.Table 3.2-3 shows the number of strands for each beam and the number of debonded strands along with the debonded length as determined from the analysis. In addition, top flange reinforcement composed of nine reinforcing steel bars #5 (cross-sectional area of 0.3 in^2) was provided.

All the reinforcement was modeled with a two-node linear 3D truss element (T3D2) with each node having three degrees of freedom (Ux, Uy, Uz). Truss elements were embedded inside the host elements - concrete brick elements. The translational degrees of freedom of the embedded element nodes were constrained to the interpolated values of the corresponding degrees of freedom of the host element nodes.

Material properties for the longitudinal prestressing strands

The stress-strain curve for the strands shown in Figure 3.2-8 shows the stress-strain curve for the strands (Nawy, 2003). The material respondes linearly up to the yield stress, and then it behaves nonlinearly up to failure with an ultimate tensile strain of 5%. In addition, the material properties for prestressing steel strands are shown in Table 3.2-4. The input parameters to be used in ABAQUS are the stress and strain coordinates associated with the point of yielding and ultimate failure.

Table 3.2-3 Details of box-beam reinforcement for different spans.

Span (ft)	No. of Strands	No. of De-Bonded Strands	Length of De-Bonding (in.)
50	21	–	–
62	26	–	–
100	34	5	15
124	42	12	44

Table 3.2-4 Material properties for prestressing steel strands.

Ultimate tensile strength (psi)	270,000
Yield strength (psi)	230,000 (85% of the ultimate strength)
Modulus of elasticity (psi)	$27{,}500 \times 10^3$
Poisson's ratio	0.3

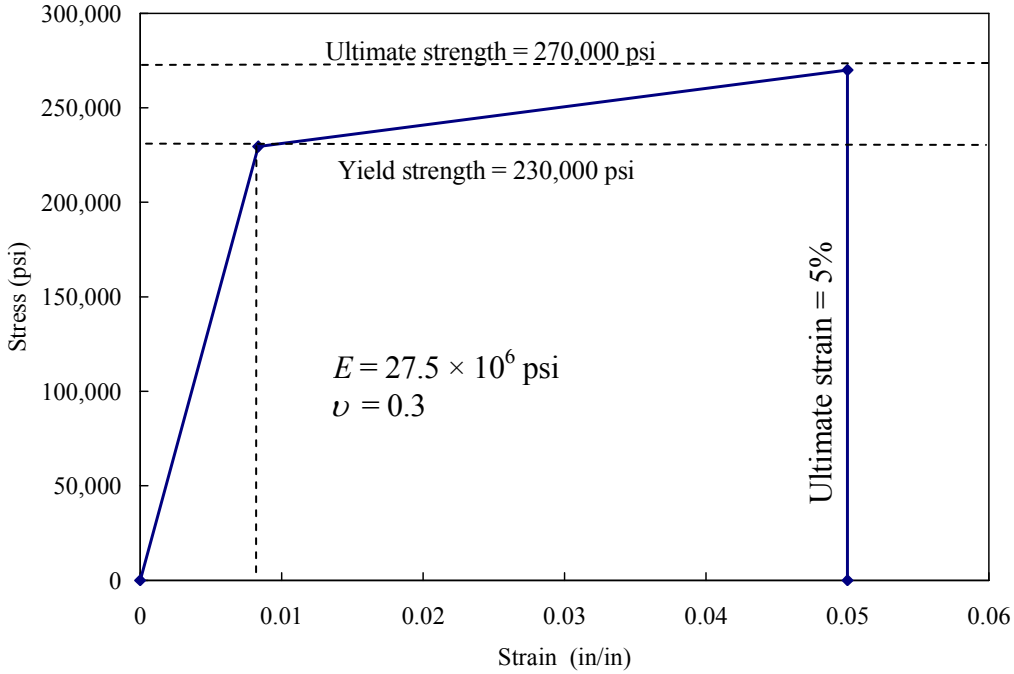

Figure 3.2-8 Stress-strain curve for prestressing steel strands (Nawy, 2003).

3.2.3 Transverse Post-Tensioning Strands (TPT Strands)

The same 2-node truss element (T3D2) was used to model the transverse unbonded post-tensioning strands, which functioned as ties confining the box-beams transversely. The end nodes of the transverse strand were tied to steel plates acting as end bearing plates. The steel plates were tied to the exterior sides of the external box-beams; however, the interior nodes of the post-tensioning strands were not tied to the surrounding objects. The steel plates in this connection were provided to distribute the post-tensioning force on the concrete surface and prevent any concrete crushing. Figure 3.2-9 shows the strands with their end bearing plates.

In the FE models, the unbonded transverse strands were modeled as cables made of carbon fiber composite cables (CFCC). The number of tendons per diaphragm was determined based on the depth of the box-beam; for box-beams of a depth of 12 in., one tendon should be placed 5.5 in. below the top of the beam. For beam depth: 17, 21, and 27 in., one tendon should be placed at the middle of the beam. For beam depths of 33 in. and over, two tendons should be placed at the third points of the beams depth. In addition, a TPT force of 104,500 lb per

diaphragm was provided initially based on the specifications provided by MDOT Bridge Design Guide (2006).

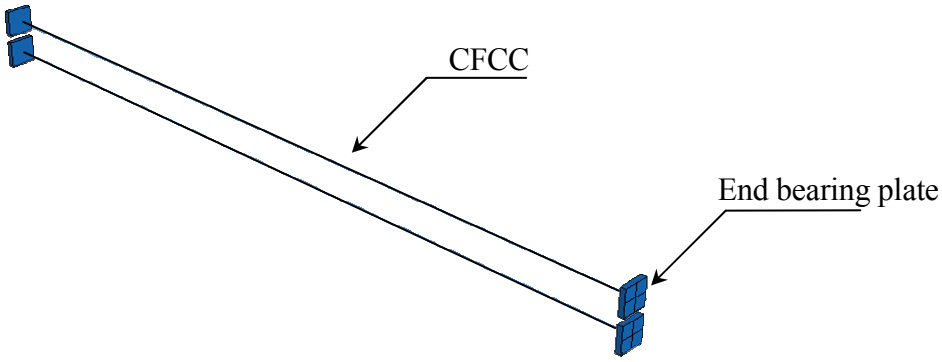

Figure 3.2-9 CFCC with end bearing plates.

Material properties of CFCC

The CFCC was defined in the model as an elastic-plastic material with its yield strength equal to its ultimate strength - the material behaved linearly up to failure. The CFCC was defined in the analysis with properties, as shown in Table 3.2-5.

Table 3.2-5 Material properties for CFCC.

Ultimate tensile strength (psi)	350,000
Modulus of elasticity (psi)	19.8×10^6
Ultimate strain (at failure)	1.62%

3.2.4 Deck Slab

The main study was performed using bridge models with 6 in. thick deck slabs as required by the current MDOT Specifications. The 8-node linear brick element (C3D8R) was used to mesh the slab with special attention; the slab thickness was 6 in.; yet, it was divided into three layers of elements (Figure 3.2-10). This meshing technique provided a good distribution for the stresses that were developed in the slab because of the relative movements between the box-beams.

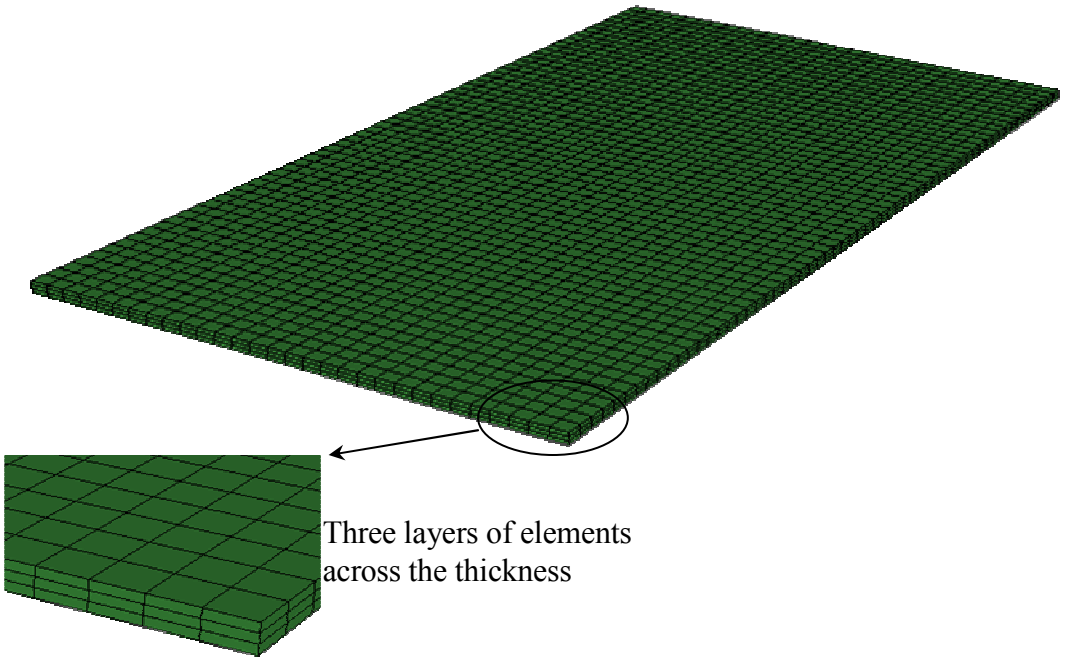

Figure 3.2-10 Deck slab FE mesh.

Being cast in place, the deck slab should not be influenced by the pre-tensioning force or the dead loads, which influence the box-beams only; however, it should be influenced along with the beams by the superimposed dead loads and service loads. Therefore, in the FE model, the connection between the deck slab bottom surface and the box-beams top surface was established in a later step of the model development. The deck slab was added as to simulate the construction sequence for this type of bridges. Figure 3.2-11 shows the procedure of integrating the deck slab to the whole model. This procedure can be summarized in the following steps:

1. The box-beams were analyzed first without the deck slab under the pre-tensioning forces, box-beams dead load, shear-key dead load, first stage of TPT force, and slab dead load.
2. Due to the aforementioned loads, the beams exhibited displacement (upward or downward). This deflection was deducted from the slab thickness in a separate computer analysis run. A modified deck slab of varying thickness resulted from the

analysis. The modification was only geometrical; the slab bottom surface exhibited artificially the same deflection of the beams without developing stresses in the slab.

3. The modified deck slab was added to the box-beams along with its reinforcement.
4. The complete model was then analyzed from the beginning starting from applying pre-tensioning force, box-beams dead load, shear-key dead load, first stage of TPT force, and slab dead load.
5. After applying the slab dead load, the beams exhibited the same deflection they exhibited before in Stage 2. As a result, the beams' top surface closely approached the artificially-deflected slab bottom surface. The virtual connecting elements - tie-elements were created between the top surface of the box-beams and the bottom surface of the slab and the model started to act as a one unit.
6. After establishing the contact between the slab and the beams, the whole model was subjected to time dependent losses, superimposed dead load, and service load.

By these steps of analysis, exact simulation of the sequence of construction for side-by-side box-beam bridges was possible.

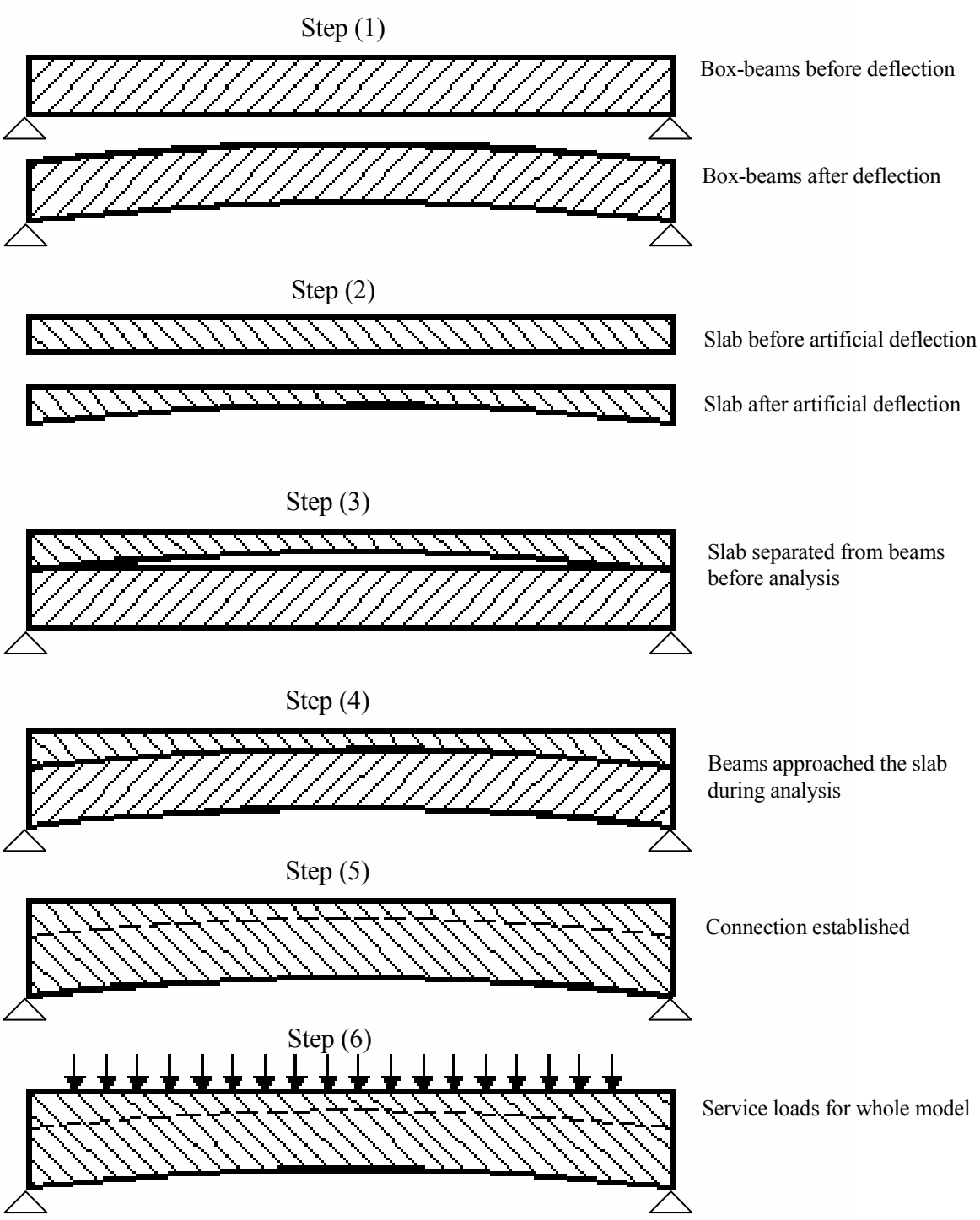

Figure 3.2-11 Deck slab connection with box-beams.

Properties of concrete in deck slab

A concrete with design compressive strength of 4,000 psi is usually used in the deck slabs (MDOT Bridge Design Guide 6.41.01, 2006); yet, replacing deck slabs is the most common rehabilitation task in bridge engineering because it is the major component exposed directly to the truck loading and the environmental conditions that can accelerate the concrete deterioration and reduce the strength and stiffness. Although there is no specific guide that can give an estimate for the strength loss in the deck slab over time, strength of 3,000 psi in this study was considered a fair estimation of the concrete ultimate strength in the deck slab towards the end of service life. The analysis was performed for three classes of deck slabs: deteriorated deck slab with concrete compressive strength of 3,000 psi, recently-constructed deck slab with concrete compressive strength of 4,000 psi, and special-quality deck slab with concrete compressive strength of 5,000 psi.

For concrete with strengths of 4,000 and 5,000 psi, the modulus of rupture was taken as $0.23\sqrt{f_c'}$ [AASHTO LRFD (2004) C5.4.2.7]. The maximum tensile strength of the concrete is required parameter in the finite element analysis and not the modulus of rupture. For deteriorated concrete, the value of the compressive strength (3,000 psi) was estimated based on available field tests for deteriorated decks (Kwasniewski et al., 2000). Note that the value of the compressive strength of the concrete is not of great influence on the analysis. The combination between the tensile strength of the concrete and the modulus of elasticity plays the key role in developing the cracks under the applied loads. The values of the modulus of elasticity and tensile strength of the deteriorated deck slab were selected after several trails to provide an upper limit for the required post-tensioning force.

Table 3.2-6 Material properties for the concrete in the deck slab.

Material Prop. / Class of Slab	Ultimate Strength f_c' (psi)	Modulus of Elasticity (psi)	Modulus of Rupture (psi)	Poisson's Ratio
Deteriorated	3,000	3.00×10^6	350	0.15
Recently-constructed	4,000	3.83×10^6	460	0.15
Special-quality	5,000	4.30×10^6	514	0.15

3.2.5 Deck Slab Reinforcement

To satisfy the minimum reinforcement required by AASHTO LRFD (2004) Section 5.10.8, the slab was provided with a single layer of reinforcement (Figure 3.2-12). The layer was composed of Grade 60 steel bars #5 @ 12 in. in both longitudinal and transverse directions. The stress-strain curve for the steel used is shown in Figure 3.2-13 with a modulus of elasticity of 29,000 ksi, yield strength of 60,000 psi, and ultimate strength of 90,000 psi. The 2-node truss element (T3D2) was also used to model the reinforcement layer.

It should be noted that While developing the finite element model, trials have been made to study the effect of changing the deck reinforcement on eliminating the longitudinal deck cracks but the finite element analysis showed that the deck reinforcement was of negligible influence on the longitudinal deck cracking when provided at the mid-depth of the deck slab. The final arrangement of the deck reinforcement in the finite element models was selected save some of the CPU memory for more important details.

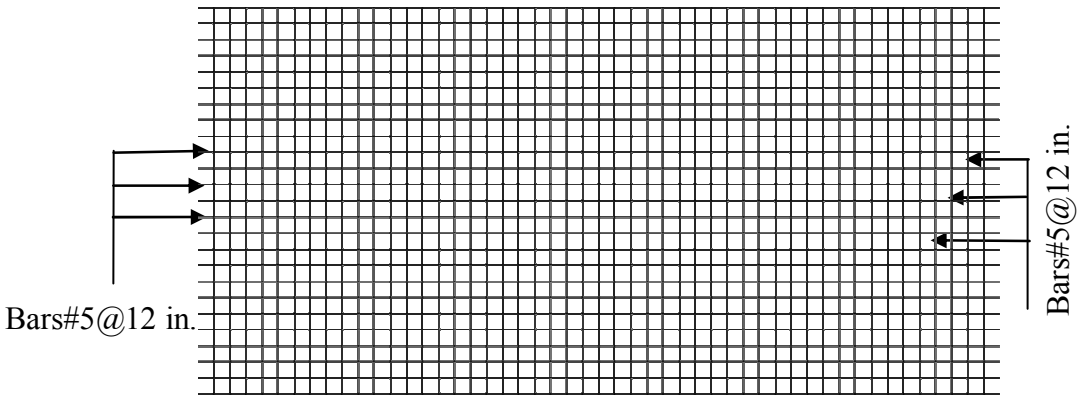

Figure 3.2-12 Deck slab reinforcement.

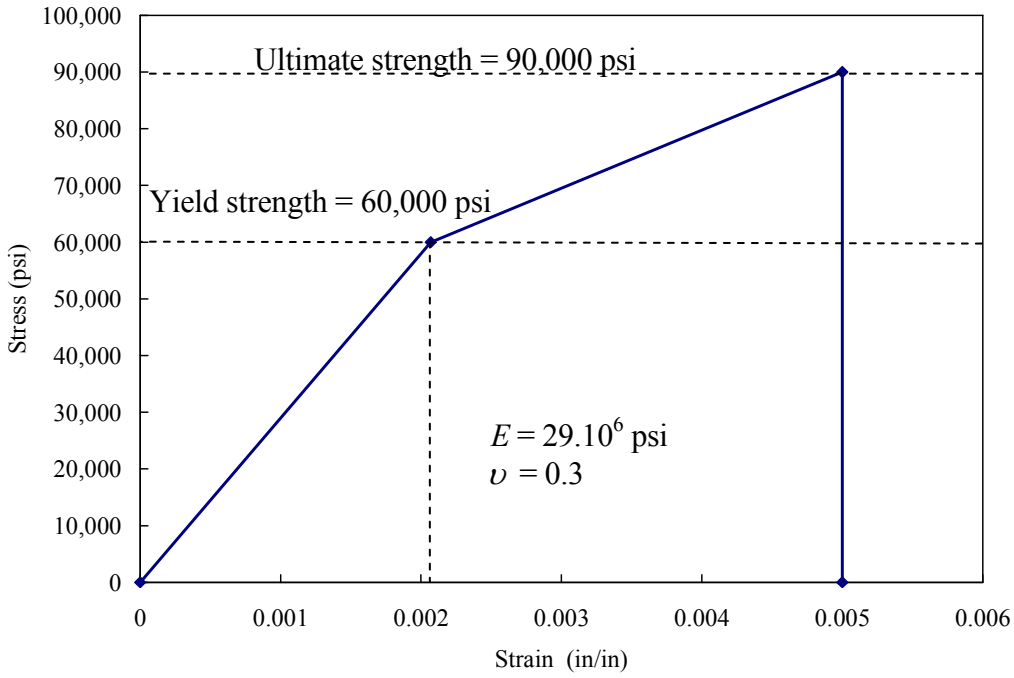

Figure 3.2-13 Idealized stress-strain curve for reinforcement bars.

3.2.6 Elastomeric Bearing Pads

The end supports were provided for the box-beams as steel-reinforced elastomeric bearings. The bearings were composed of alternate layers of steel reinforcement and elastomer bonded together, as shown in Figure 3.2-14. The elastomer - rubber -was defined in the FEA as a hyper-elastic material of ultimate uniaxial tensile stress of 2,500 psi and ultimate uniaxial tensile strain of 400% (complies with ASTM D412). Both of the reinforcement and the elastomer layers were modeled with 8 node linear brick elements (Figure 3.2-15) however the elements functioned differently during the FE analysis: the reinforcement layers were modeled with an element identified in ABAQUS library as C3D8R. This element is controlled by the reduced integration during the analysis (identified by the letter R at the end of the name). The elastomer layers, on the other hand, were modeled with an element identified as C3D8H. This element is controlled by hybrid formulations that can deal with the elastomer material behavior (identified by the letter H). The ABAQUS manual for element types provides a detailed description for both elements and their functions.

The length, width, and thickness of the bearing pads were calculated for the FEA according to AASHTO LRFD (2004) Section 14.7.6. The width of the bearing was fixed to 45 in. when used with 48 in. wide box-beams and to 33 in. when used with 36 in. wide box-beams. Furthermore, the length varied according to the bridge span. For the 50 ft span, the length was taken equal to 8 in. and for the 62, 100, and 124 ft spans, the length was taken equal to 10 in. In addition, the total thickness of the bearing was taken as 2.075 in. divided into:

1. Three steel layers of thickness 0.125 in. each.
2. Two interior elastomer layers of thickness 0.6 in. each.
3. Two exterior elastomer layers of thickness 0.25 in. each.

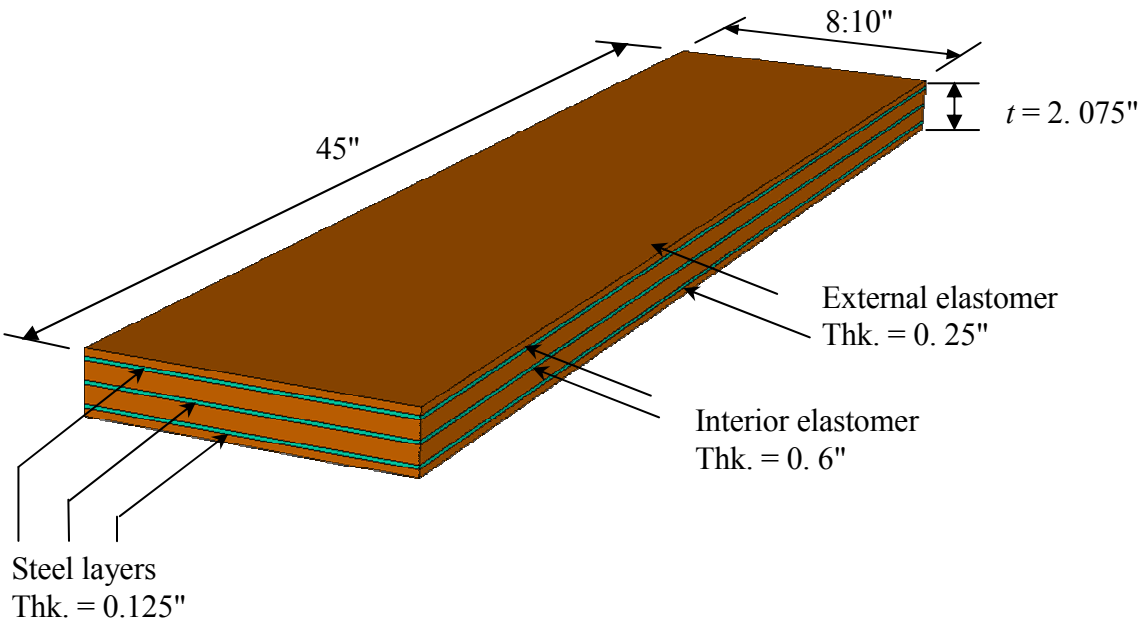

Figure 3.2-14 Elastomeric bearing pad for one beam.

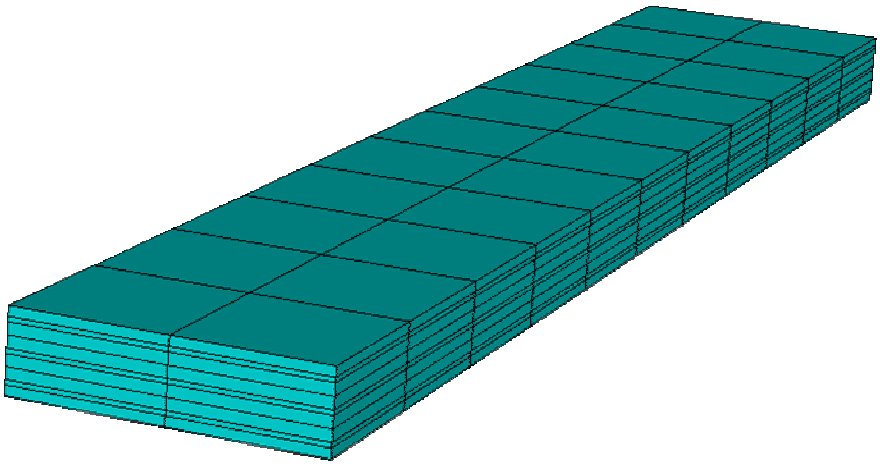

Figure 3.2-15 Meshing of the bearing pad.

3.2.7 Shear-Keys

Typically, shear-keys in side-by-side box-beams bridges serve as connectors between the box-beams to transfer the shear and prevent differential movement under service loads. In the transverse design of adjacent box-beam bridges, PCI Design Manual 8.9.3.6 (2003) refers to AASHTO LRFD (2004) Section 5.8.4, for checking the transfer shear in the vertical plane through the joints, and according to AASHTO LRFD (2004) Section 5.8.4, the interface shear transfer, in general, shall be considered across a given plane at:

1. An existing or potential crack,
2. An interface between dissimilar materials, or
3. An interface between two concretes cast at different times.

The second and third cases represent the interface plane between shear-keys and box-beams. Therefore, the nominal shear resistance of this interface plane shall be taken according to AASHTO LRFD (2004) Section 5.8.4.1-1 as:

$$V_n = cA_{cv} + \mu[A_{vf} f_y + P_c]$$

where

V_n = nominal shear resistance (kip)

A_{cv} = area of concrete engaged in shear transfer (in^2)

A_{vf} = area of shear reinforcement crossing the shear plane (in^2)

f_c' = specified 28-day compressive strength of the weaker concrete (ksi)

f_y = yield strength of reinforcement (ksi)

c = cohesion factor (ksi)

μ = friction factor

P_c = permanent net compressive force normal to the shear plane (kip)

The nominal shear resistance V_n used in the design shall not be greater than the lesser of "$V_n \le 0.2 f_c^{'} A_{cv}$" or "$V_n \le 0.8 A_{cv}$".

The equation provided in AASHTO LRFD (2004) primarily splits the nominal shear capacity into two separate components:

1. Cohesion between the two surfaces with a cohesion factor, c.
2. Friction between the two surfaces with a friction factor, μ.

These factors are determined in AASHTO LRFD (2004) Section 5.8.4.2.

1. For concrete placed against clean, hardened concrete with a surface intentionally roughened to an amplitude 0.25 in.: c = 0.1 ksi, μ = 1.0 λ (λ = 1.0 for normal weight concrete).
2. For concrete placed against clean hardened concrete and free of laitance but not intentionally roughened: c = 0.075 ksi, $\mu = 0.6\lambda$

However, shear-key connections are somewhere in between the aforementioned boundaries as the box-beam concrete surface is not intentionally roughened to an amplitude of 0.25 in. but at the same time, it has a groove of a depth of 0.25 in. in the box-beam side to be filled with the grout material. In addition, there is no reinforcement going through the connection; therefore, the friction component is a function only of P_c, which is the transverse post-tensioning force.

The coefficient of friction was taken as 0.7; however, the coefficient of cohesion, which represents the bond capacity between connected surfaces, was taken as 0.0 in the full-scale models, because:

1. In the PCI Design Manual 8.9.3.7 (2003), even though full-depth grouting of the shear-key was recommended, the shear-key is not considered a structural member transferring shear between the box-beams.
2. The transverse post-tensioning and the deck slab (reinforced structural overlay) are the available techniques that AASHTO LRFD (2004) Section C4.6.2.2.1 recommends to develop the interconnection between box-beams. It does not specify the bond capacity for the grout material.
3. Since it is a cold joint, the shear-key connection usually fails in bond between the surfaces unless special precautions are applied (Issa et al., 2003). Some of these precautions require higher quality control, which might not be available on the site while pouring the grout of the shear-keys.
4. To simulate the actual behavior for a cohesive connection, a very small element size must be used in meshing the connecting parts. Yet, a mesh that is too fine makes the analysis intractable. A coarser mesh leads to an overly high estimate for the joint capacity.

3.3 Construction Loads

Construction loads included the prestressing forces, dead loads, transverse post-tensioning force, and superimposed dead loads. Except for superimposed dead loads and time dependent losses in longitudinal prestressing strands, all construction loads were applied to the box-beams before integrating the deck slab into the model.

Prestressing forces were modeled as concentrated forces acting at the ends of the prestressing strands. Each strand was provided with an initial prestressing force of 28,500 lb, which dropped to 25,000 lb after deducting the time dependent losses. The time dependent losses were calculated according to Section 5.9.5.3 of AASHTO LRFD (2004), and applied at a later stage after integrating the deck slab to the model.

Dead loads of box-beams and deck slab were calculated assuming the concrete of unit weight of 150 lb/ft^3 and applied as a distributed load on the box-beams.

Transverse post-tensioning (TPT) force was applied as a bolt load (post-tensioning load from ABAQUS load library) through the post-tensioning CFCC which were tied to the beams exterior sides with steel bearing plates of dimensions of 10 in. × 10 in. × 2 in. each.

Superimposed dead loads included the weight of a wearing surface (25 lb/ft^2) and the weight of the barriers. Type 4 barriers with a weight of 475 lb/ft were provided at both sides of the bridge model. The superimposed dead loads were applied at the top surface of the deck slab after the deck slab was integrated to the FE model (recall Figure 3.2-11).

3.4 Load Combinations

According to AASHTO LRFD (2004) Section 3.4 for load factors and load combinations, the deck slab cracking was investigated by combining the loads according to Service I, which permits combining: dead loads (DC), wearing surface dead loads (DW), live loads (LL), impact allowance (IM), wind load (WS), wind on live load (WL), shrinkage (SH), creep (CR), uniform temperature (TU), temperature gradient (TG), and some additional types of loads not relevant to the current case of analysis.

Out of the aforementioned loads, TU does not create internal stresses in simply supported structures. It is primarily provided for the design of the support movement (AASHTO LRFD, 2004 Section 3.12.2). In addition, CR is not believed to develop cracks in the deck slab, which experiences compressive stresses most of the time. Furthermore, WS and WL would not be considered in analysis because it is not recommended to combine thermal gradient with high wind forces (AASHTO LRFD, 2004 Section C3.4.1). Finally, SH can not be blamed for the longitudinal cracks as the crack pattern due to shrinkage, regardless of the shrinkage value, is different from what is usually reported in the side-by-side box-beam bridges. In other words, TU, WS, WL, CR, and SH would not be included in the acknowledged load combination when checking deck slab longitudinal cracks.

The remaining loads -DC, DW, LL, IM, and TG -were combined together according to AASHTO LRFD (2004) to create the maximum influence on the deck slab. The AASHTO LRFD (2004) allows load factor of 1.00 for dead loads and superimposed dead loads when they are considered in Service I load combination. However, load factors for live loads, impact allowance, and temperature gradient need further consideration.

Section 3.6.1.2.1 of AASHTO LRFD (2004) provides new vehicular loading labeled as HL-93 and consists of a combination of a design truck or tandem in addition to a design lane load (Figure 3.4-1). Each design lane under consideration shall be occupied by either design

truck or tandem, along with the lane load. The load shall be assumed to occupy 10 ft transversely within a design lane (Figure 3.4-2). Furthermore, the maximum live load effect shall be determined by considering each possible load combination of number of loaded lanes multiplied by the corresponding multiple presence factor as provided by Section 3.6.1.1.2 of AASHTO LRFD (2004) (Table 3.4-1) to account for the probability of simultaneous lane occupation by the HL-93 live load. To account for the dynamic effect of the moving loads, AASHTO LRFD (2004) Section 3.6.2 specifies a percentage of the static load of the truck or the tandem, but not the lane load, to be added to the original load as a dynamic allowance. The limit shall be taken as 75% for the purpose of designing the deck slab joints and 33% for designing other bridge components. It is not specified clearly in Section 3.6.2 whether 75% is applicable for the design of the transverse deck joints only or it is applicable for the design of both transverse and longitudinal deck joints. In the FE analysis, the impact allowance was taken equal to 75% based on the calibration of a full-scale bridge model (Bebawy, 2007).

Table 3.4-1 Multiple presence factor, *m* (AASHTO LRFD 3.6.1.1.2, 2004).

Number of loaded lanes	Multiple presence factor (*m*)		
	ADTT[1] > 5,000	100 ≤ ADTT ≤ 1,000	ADTT < 100
1	1.20	1.14	1.08
2	1.00	0.95	0.90
3	0.85	0.81	0.73
> 3	0.65	0.62	0.59

[1] *ADTT: Average daily truck traffic*

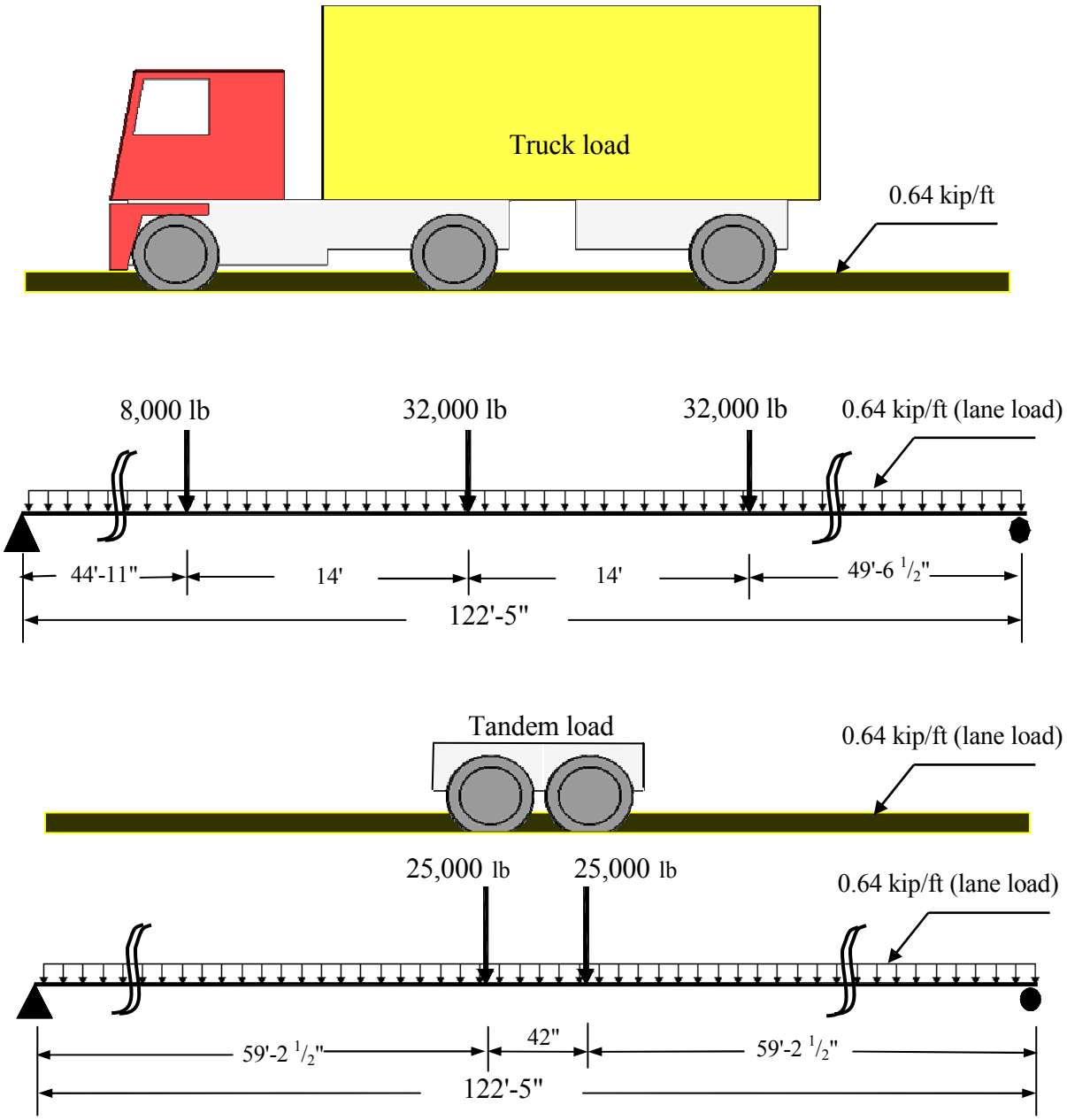

Figure 3.4-1 AASHTO LRFD HL-93 load (longitudinal direction).

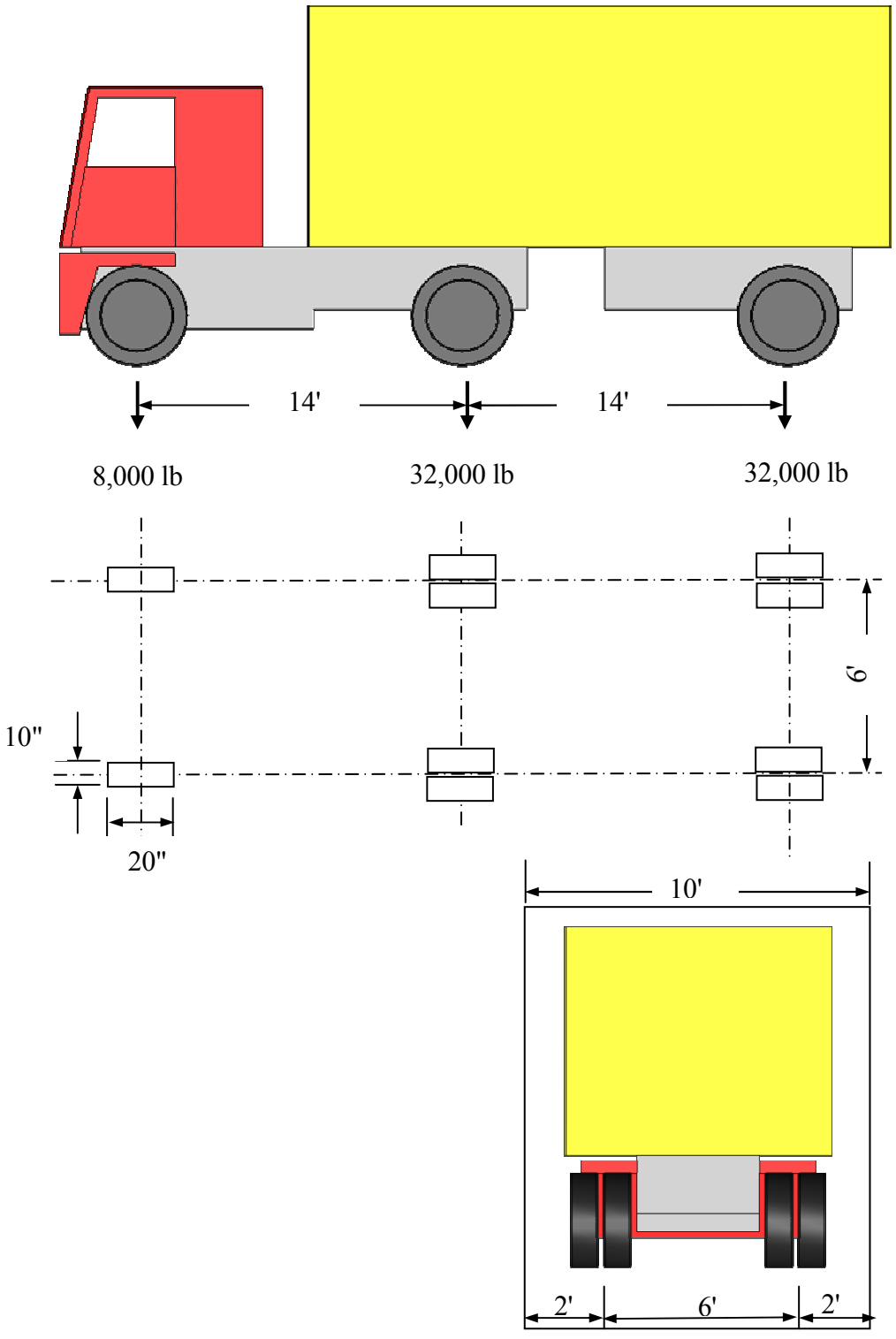

Figure 3.4-2 Truck in AASHTO load HL-93.

Temperature gradient

When exposed to sunlight during the daytime, the top fibers of the bridge experience higher temperatures than the bottom fibers, defined herein as positive gradient, and when the temperature drops down during the night, the top fibers experience lower temperatures than what the bottom fibers experience, defined herein as negative gradient. The variation of the temperature over the cross-section of the bridge is usually highly nonlinear. For simplicity, AASHTO LRFD (2004) Section 3.12.3 provides a general bi-linear configuration for the positive temperature gradient (Figure 3.4-3). The negative temperature gradient can be obtained from the same figure by multiplying the temperature values by -0.2 for decks with asphalt overlay and -0.3 for plain concrete.

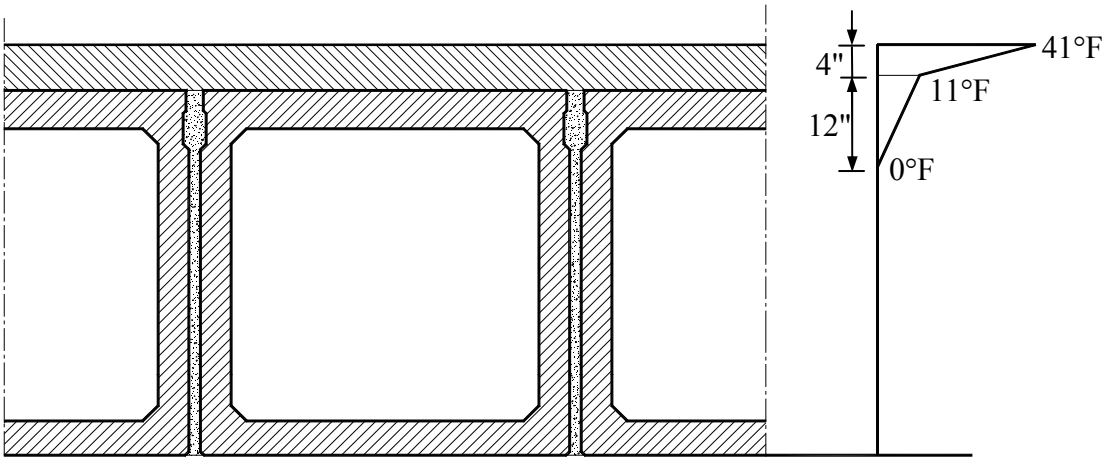

Figure 3.4-3 Typical positive temperature gradient over the bridge depth in Michigan.

3.5 Analysis Calibration

One essential step before conducting any of the study objective is to check the validity of the finite element analysis. This can be done by generating a numerical model for a small-scale experimental model or a full-scale prototype, and comparing the response of the FE model with that of the experimental/existing prototype. This finite element analysis has been verified for accuracy using two approaches:

1. By simulating an experimental half-scale bridge model built at Lawrence Technological University (Labib, 2007), and

2. By simulating an existing side-by-side box beam bridge built in south-east Michigan in 1999.

Simulating the existing bridge model can be found somewhere else (Bebawy, 2007 and Grace et al., 2007). In general, the analysis of this bridge yielded the following conclusions:

1. Traffic loads do not appear to be the key factor in developing longitudinal cracks in the slab. The positive temperature gradient is the major contributing factor in the initiation of the longitudinal cracks in the deck slabs in side-by-side box beam bridges.
2. To avoid the longitudinal deck cracking, the developed maximum principal stresses in the deck slab shall not exceed the cracking strength of the concrete when the bridge is subjected to positive temperature gradient with traffic loads and impact allowance.
3. AASHTO LRFD (2004) recommendation for 250 psi as minimum transverse prestress required to secure the longitudinal joints in side-by-side box beam bridges seems to be impractical and unreachable especially between the diaphragms location.
4. Impact allowance of 75% recommended by AASHTO LRFD (2004) for the design of the transverse deck joints is appropriate for the design of the longitudinal joints as well.
5. Since the combination of 100% of positive temperature gradient and traffic loads usually lasts for only a few hours during the day, it was determined that using presence factor corresponding to ADTT less than 1,000 is more appropriate than using presence factor corresponding to ADTT more than 5,000.

The experimental half-scale bridge model was composed of four simply supported side-by-side box-beams of cross-section 18 in. × 11 in. each, and a span of 20 ft. The bridge model had a 3 in. thick deck slab reinforced with one layer of reinforcement at the mid-thickness. The results of the experimental program were employed to validate the techniques of the finite element analysis -methods of applying loads and boundary conditions. In addition, the experimental results were used to evaluate the FE model input parameters such as the material properties and the element sizes to bring the numerical and experimental results into fair agreement.

Generating a FE model for the experimental half-scale bridge model provided confidence in the analysis and established the framework for the modeling approach. Yet, the experimental model analysis did not deal with numerous aspects that are essential for meeting all of the objectives of this study. For instance, the experimental model analysis did not include a simulation for AASHTO truck load; neither did it include applying environmental loads such as thermal cycles and temperature gradients. As mentioned earlier in the literature review, the formation of the longitudinal cracks between the box-beams is more likely attributed to the thermal stresses rather than to the moving live loads. Therefore, modeling a full-scale bridge was mandatory to simulate the live and thermal loads. One of the bridges that was built recently (1999) in Michigan experienced longitudinal cracks along the entire span between the box-beams. As this bridge reflects the problem of longitudinal cracks in fairly new bridges, it was selected for numerical simulation to examine the influence of each load type on the developments of the cracks. In this section, only the numerical simulation for the experimental half-scale bridge model has been presented.

3.5.1 Half-Scale Bridge Model

The experimental bridge model was constructed at Lawrence Technological University in 2006 to examine the influence of the TPT force on the development of the longitudinal cracks in the deck slab in side-by-side box-beam bridges (Labib, 2006). The bridge model was composed of four side-by-side box-beams with a cross-section and dimensions, as shown in Figure 3.5-1. The bridge model had a span of 19 ft (228 in.) and width of 75 in. The model included four transverse diaphragms: two at the ends with a width of 14 in. each and two at the mid-span (5.5 ft apart) with a width of 9 in. each. The bridge model included a 3 in. thick deck slab with one layer of reinforcement.

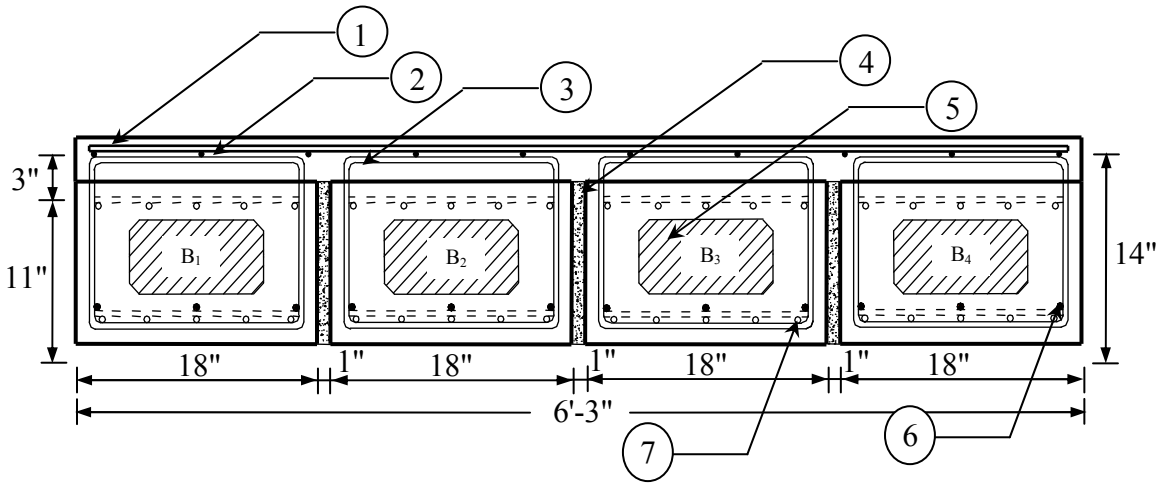

Cross-section

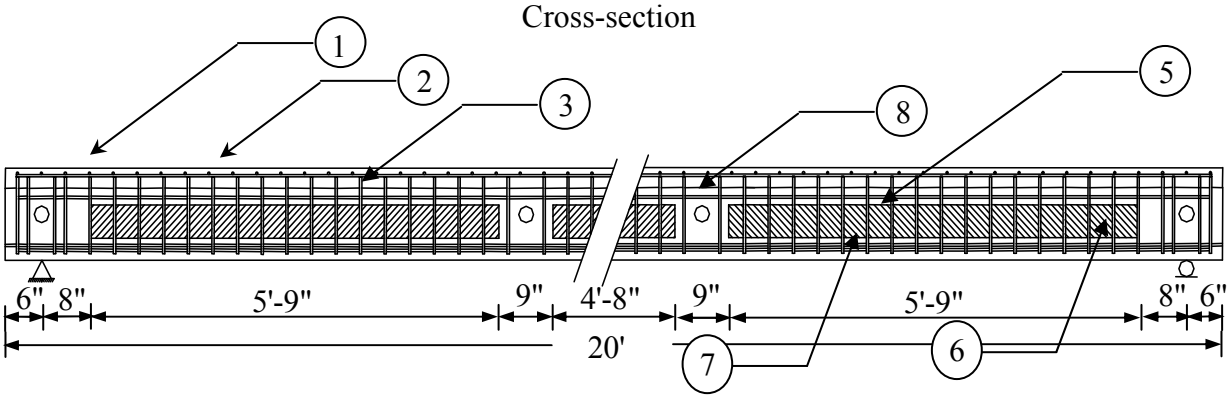

Longitudinal section

1- Slab transverse reinforcement
2- Slab longitudinal reinforcement
3- Steel stirrups #3 @ 4 in.
4- Shear-key
5- Hollow portion (10" wide and 5" deep)
6- Prestressing tendons ($\Phi = {}^{3}/_{8}$ in., A = 0.115 in^2)
7- Non-prestressing tendons ($\Phi = {}^{3}/_{8}$ in., A = 0.115 in^2)
8- Intermediate diaphragm with PVC duct for TPT strand

Figure 3.5-1 Half-scale experimental bridge model.

3.5.1.1 Bridge Model Components and Material Properties

The 28 day compressive strength of the concrete in the box-beams was 6,000 psi, while the 28 day compressive strength of the concrete in the slab was 5,700 psi. The box-beams were reinforced with:

1. Five bottom non-prestressing CFRP (DCI tendons, Diversified Composites, Inc.) tendons with a diameter of 0.375 in. and a cross-sectional area of 0.11 in^2.
2. Three bottom prestressing CFRP tendons with a cross-sectional area of 0.11 in^2. and each strand was pre-tensioned with a prestressing force of 12,000 lb.
3. Five top non-prestressing CFRP tendons with a cross-sectional area of 0.11 in^2.
4. Steel stirrups #3 @ 4 in.
5. Four CFRP tendons with a diameter of 0.375 in. and cross-sectional area of 0.11 in^2 in the transverse direction to apply transverse post-tensioning forces up to 30 kip.

The slab was reinforced with a single layer of reinforcement. This reinforcement layer was composed of longitudinal and transverse non-prestressing CFRP tendons with a diameter of 0.305 in., cross-sectional area of 0.073 in^2, and center-to-center spacing of 8 in. in both directions. The experimental bridge model was supported by steel roller and hinge supports.

In the finite element model, the concrete in the box-beams was modeled with an ultimate compressive strength of 6,000 psi, modulus of elasticity of 4.7×10^6 psi, and modulus of rupture of 562 psi as determined by AASHTO LRFD (2004). Likewise, the concrete in the deck slab was assumed to have a modulus of elasticity of 4.57×10^6 psi, and modulus of rupture of 550 psi. Furthermore, based on uniaxial test results, the CFRP tendons were modeled with an ultimate tensile strength of 340,000 psi, ultimate strain of 1.8%, and modulus of elasticity of 22.8×10^6 psi. The material of the tendons was assumed to behave linearly elastic until failure. The transverse tendons were modeled with the same material and provided with 6 in. × 6 in. × 1 in. steel bearing plate at both ends. The stirrups were not modeled in the finite element model as shear cracking was not expected. Steel bearing plates were used to simulate the supports. Each beam was provided with a 18" × 6" × 1" steel plate at each end. In addition, the vertical load was applied through two 15" × 6" × 2" steel plates with a center-to-

center spacing of 36 in. This modeling technique replicated the experimental setup Figure 3.5-2.

Several element sizes were examined in the FE model. It was found that an element size of 4 in. was the most appropriate element size to be used (Figure 3.5-3); the FE results closely matched the results of the experimental program when using this element size. All the concrete components and the steel plates were meshed using the 8-node linear brick element C3D8R; and the reinforcement was meshed using the 2-node linear 3D truss element T3D2.

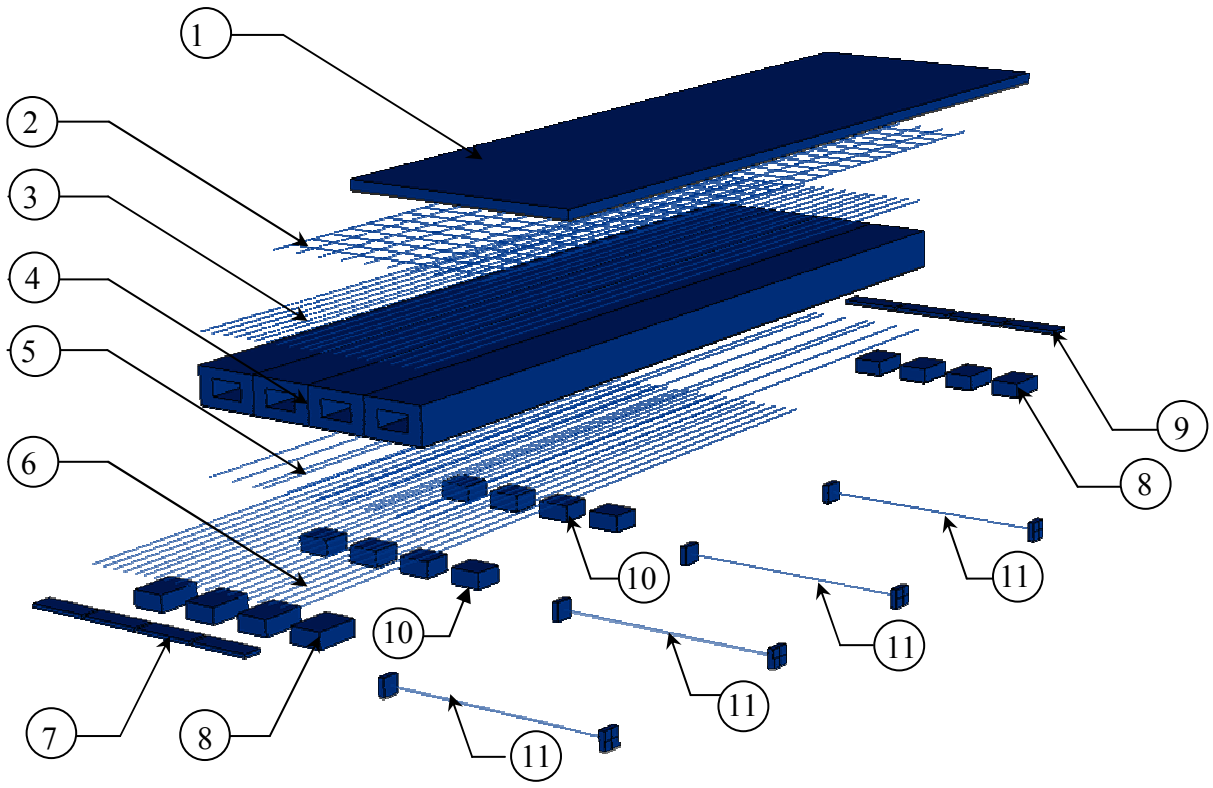

1- 3 in. thick deck slab
2- Deck slab reinforcement
3- Box-beams top reinforcement
4- 18" × 11" box-beams
5- Prestressing tendons
6- Non-prestressing tendons
7- Steel bearing plates (hinge support)
8- End diaphragm (width of 14 in.)
9- Steel bearing plates (roller support)
10- Interior diaphragm (width of 9 in.)
11- TPT tendon with end bearing plates

Figure 3.5-2 FE bridge model components.

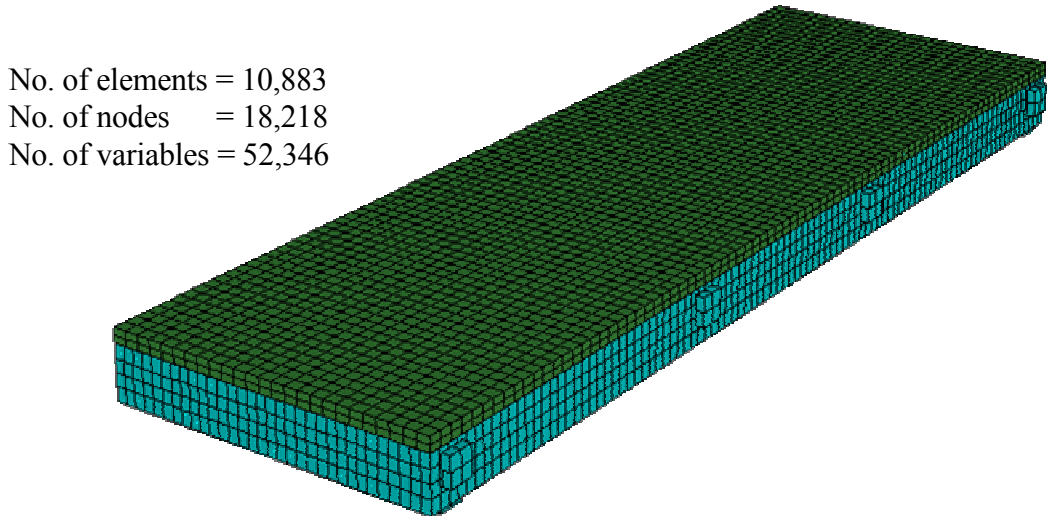

Figure 3.5-3 FE model meshing.

3.5.1.2 Loading Scheme

The loading set-up included loading beam B2, one of the interior beams (see Figure 3.5-1), with a four-point-load up to 80,000 lb with increasing increments of 10,000 lb (Figure 3.5-4 and

Figure 3.5-5). The load was then increased to failure (failure load was 130,000 lb). Loading tests up to 80,000 lb were repeated with TPT force of 0, 10, 20, and 30 kip while loading up to failure was performed with TPT force of 30 kip.

In the finite element model, loading tests without and with TPT force of 30 kip were simulated. The results presented in this section are those for loading test without TPT force. Another set of results were obtained for the case of loading with TPT force of 30 kip but was not provided to avoid repetition. The obtained results were used to evaluate the ability of the numerical models to predict the deflection and onset or locations of longitudinal cracks.

Figure 3.5-4 Load setup (experimental model).

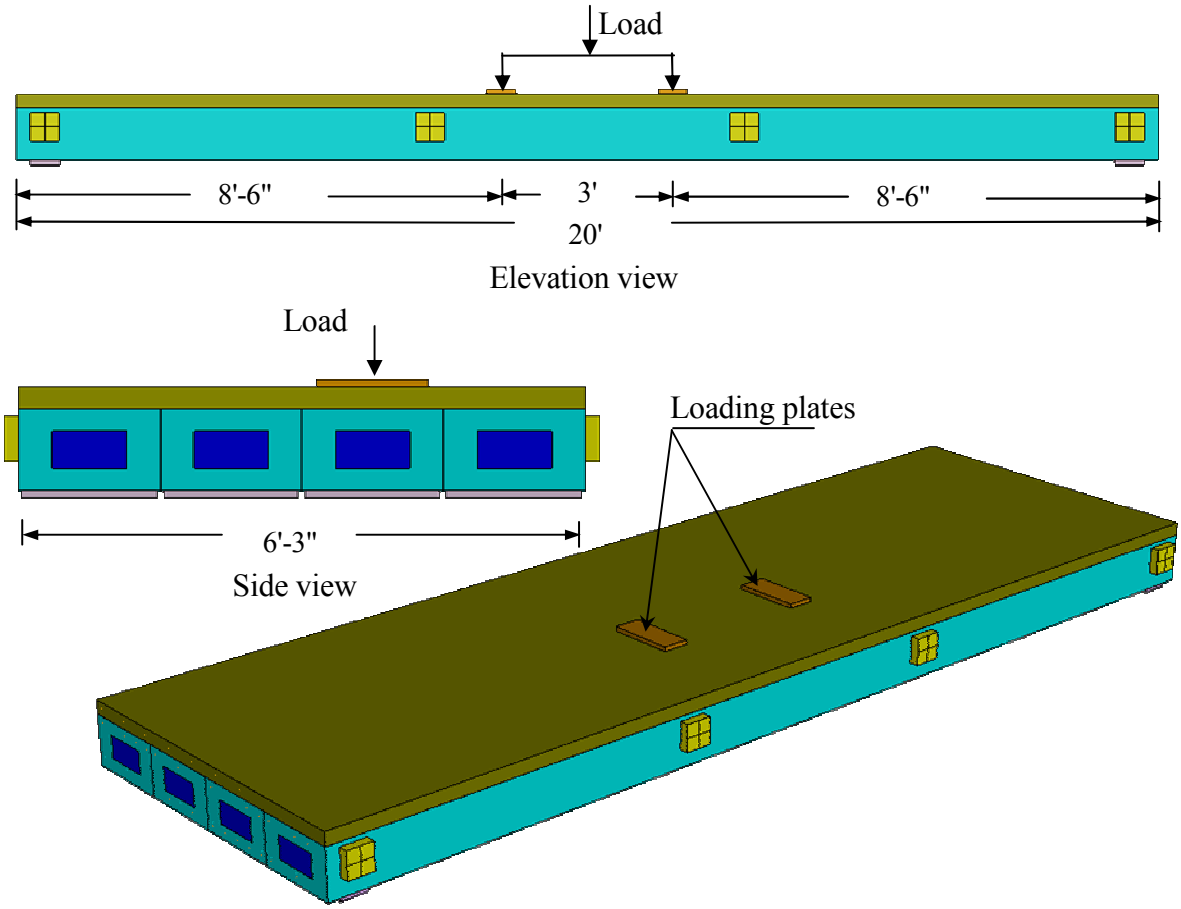

Figure 3.5-5 Load setup (numerical model).

3.5.1.3 Comparison Between Numerical and Experimental Results

The deflections of the experimental and numerical bridge models measured at the mid-span section under different vertical loads are shown in Figure 3.5-6 through Figure 3.5-11. In general, the FE results matched the experimental results. The difference between the numerical and the experimental results increased when the vertical load reached 50 kip (Figure 3.5-9). This can be attributed to the fact that after reaching a load of 50 kip, cracks started to develop in the experimental deck slab. The numerical model was able to predict the cracks location; however beyond the cracking stress, the formation of localized cracks was represented at the element level with a softening stress-strain response. Consequently, the crack size was not accurately represented in the FE model, which could be the reason for the difference between the experimental and numerical deflection results. In addition, the FE model was relatively stiffer than the experimental model. This is due to several approximation schemes used in the FE analysis, which assume ideal structures such as approximated displacement fields, integration schemes, etc.

Figure 3.5-12 through Figure 3.5-16 show the crack maps for the deck slab top and bottom surfaces under different levels of the vertical load. No cracks developed in the deck slab for vertical loads less than 50 kip. However, at a load of 50 kip, small longitudinal cracks developed at the slab bottom surface over the interior shear-key locations. The top surface, on the other hand, did not experience any cracks. The cracks propagated while increasing the vertical load to 70 kip, cracks started to appear in the slab top surface (
Figure 3.5-15). The cracks continued to propagate at both the top and bottom surfaces under a load of 80 kip as shown in Figure 3.5-16. These cracks matched the reported cracks in the experimental bridge model. The cracks in the experimental model were firstly observed in the slab top surface at a load of 70 kip and then propagated under a load of 80 kip as shown in Figure 3.5-17.

In summary, the deflection and the locations of the crack development obtained from the FE model closely matched with those of the experimental results. These results validated and confirmed the adequency of the developed numerical model and the various selected elements.

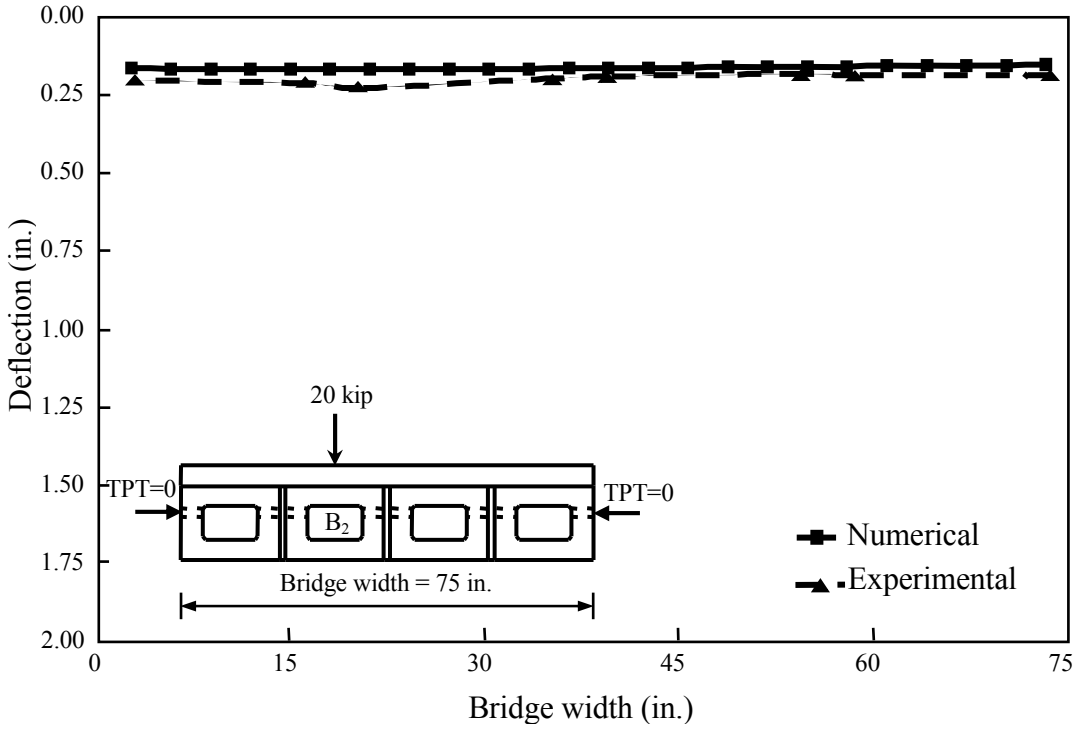

Figure 3.5-6 Deflection of the bridge model under vertical load of 20,000 lb.

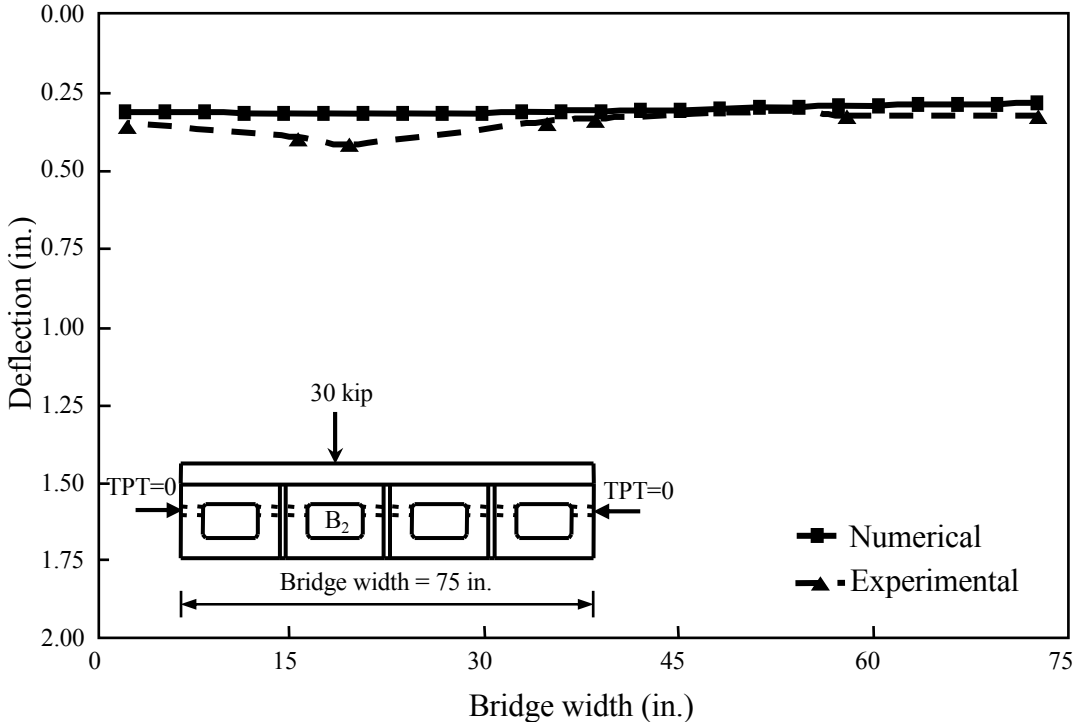

Figure 3.5-7 Deflection of the bridge model under vertical load of 30,000 lb.

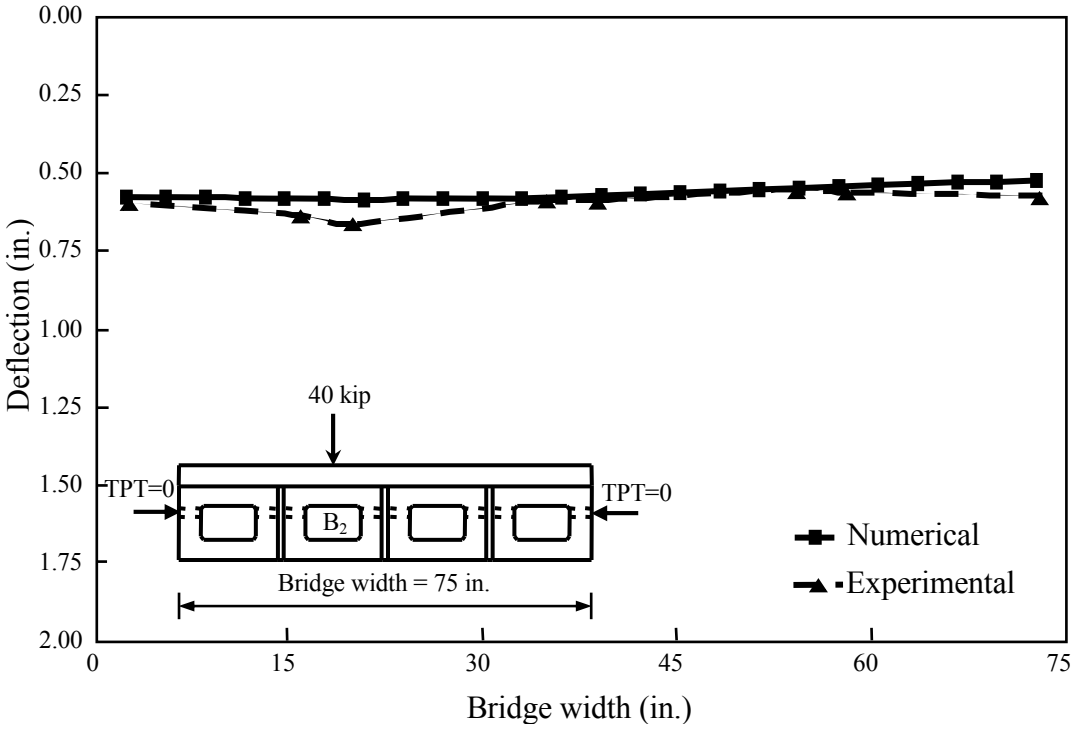

Figure 3.5-8 Deflection of the bridge model under vertical load of 40,000 lb.

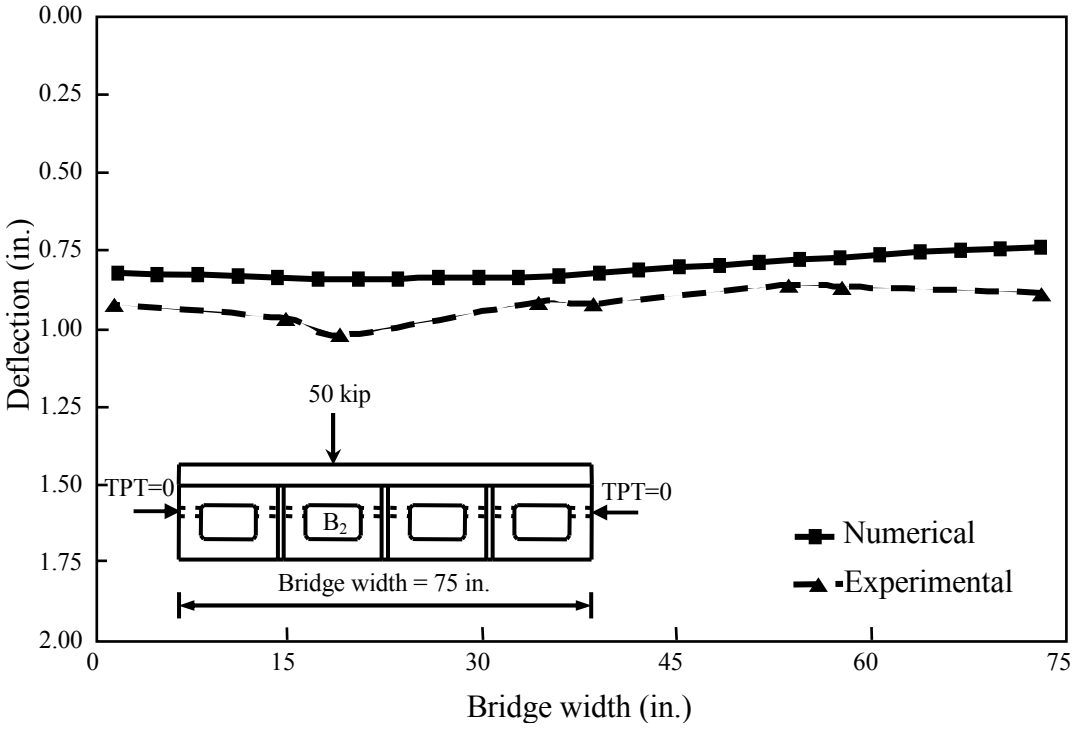

Figure 3.5-9 Deflection of the bridge model under vertical load of 50,000 lb.

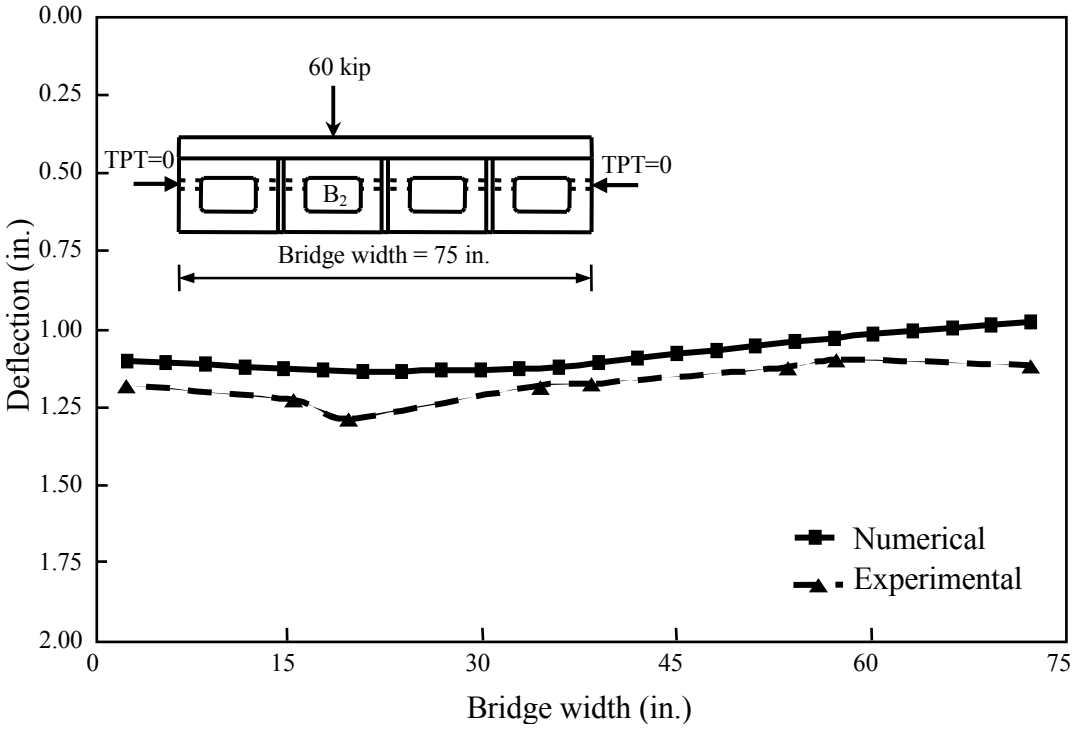

Figure 3.5-10 Deflection of the bridge model under vertical load of 60,000 lb.

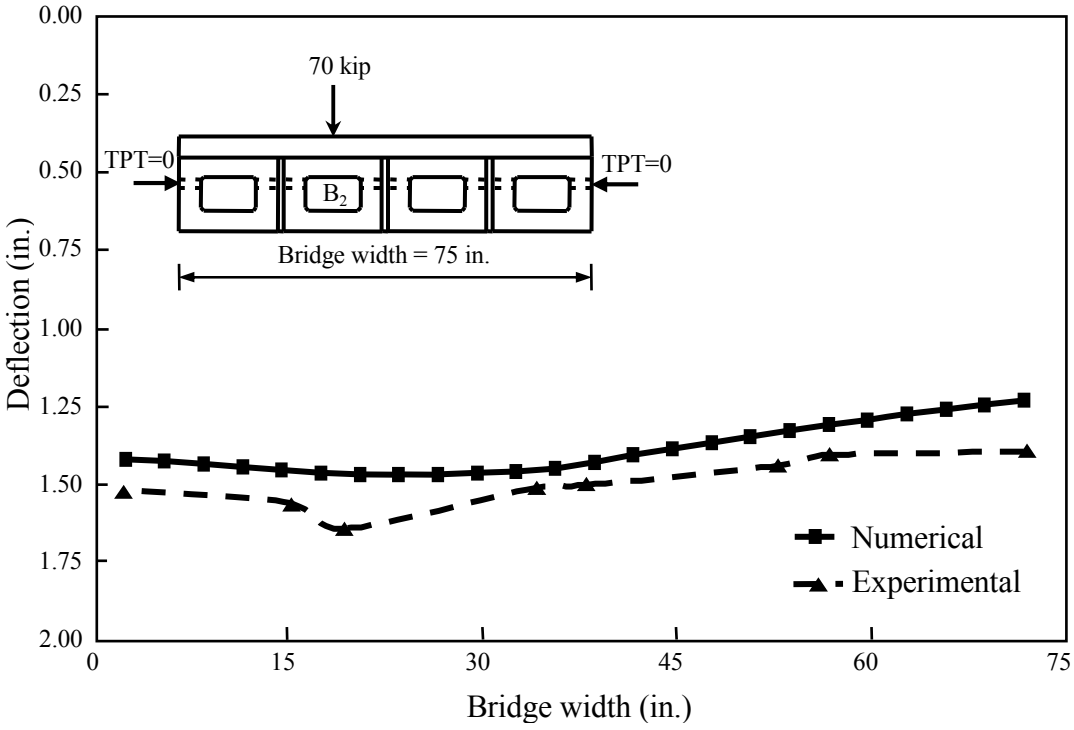

Figure 3.5-11 Deflection of the bridge model under vertical load of 70,000 lb.

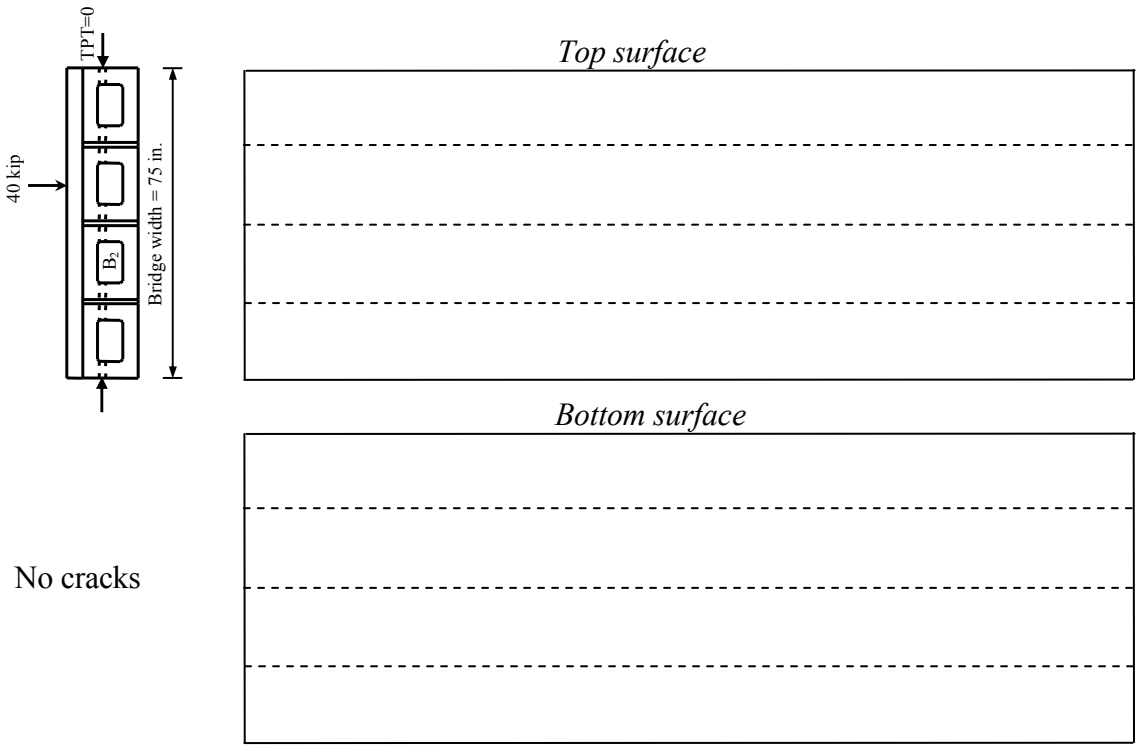

Figure 3.5-12 Crack development in the slab under vertical load up to 40,000 lb.

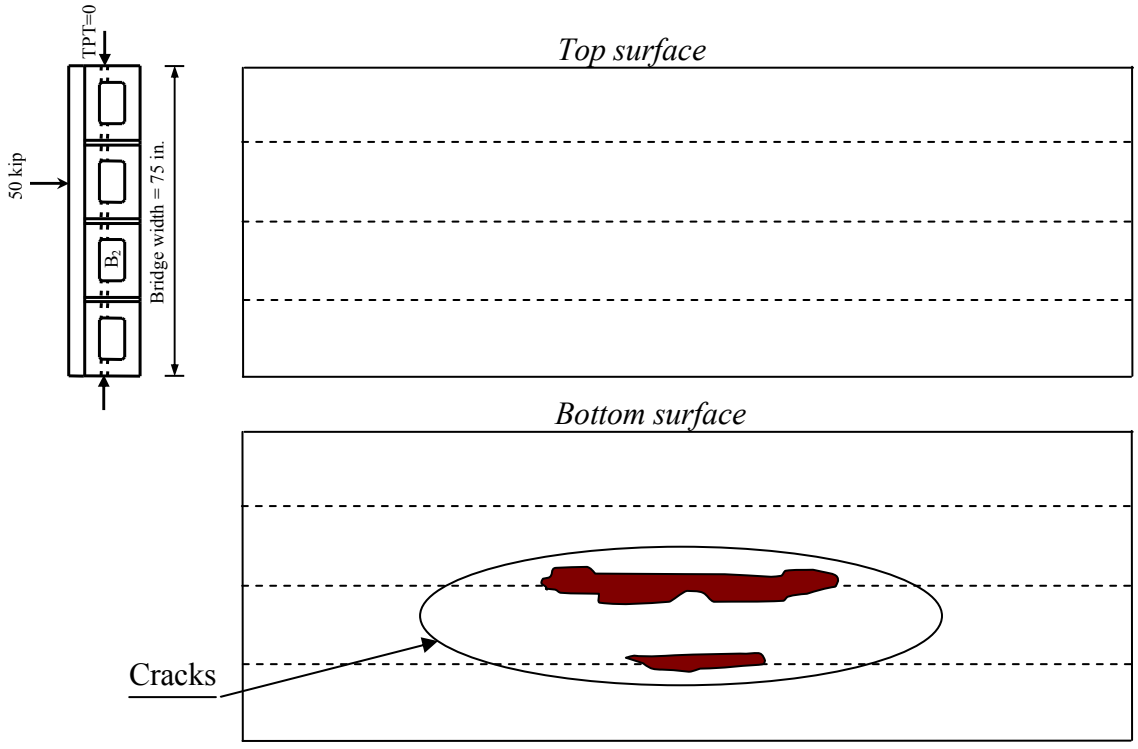

Figure 3.5-13 Crack development in the slab under vertical load of 50,000 lb.

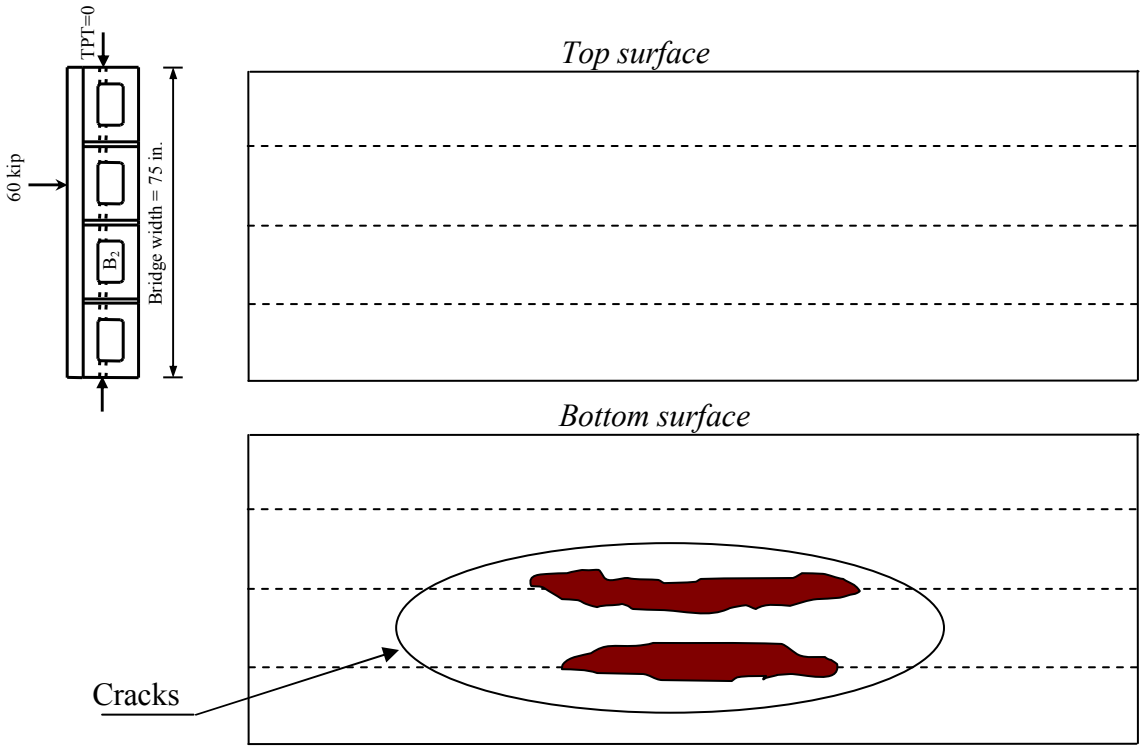

Figure 3.5-14 Crack development in the slab under vertical load of 60,000 lb.

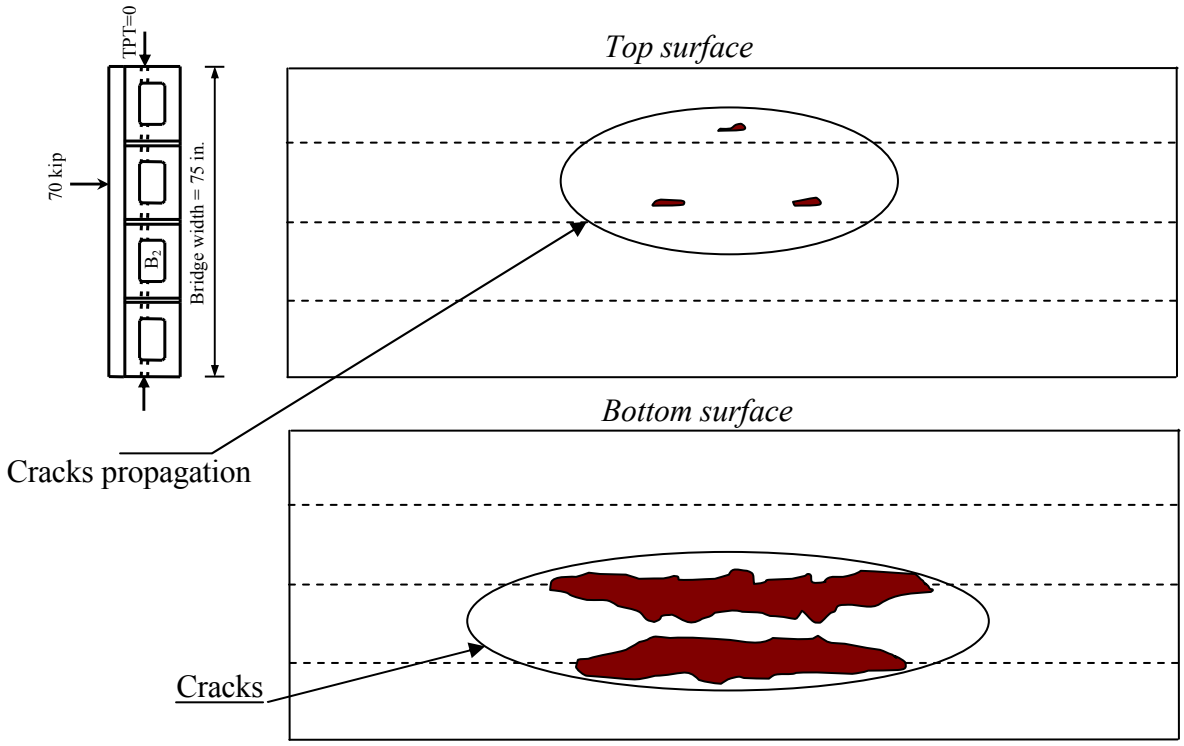

Figure 3.5-15 Crack development in the slab under vertical load of 70,000 lb.

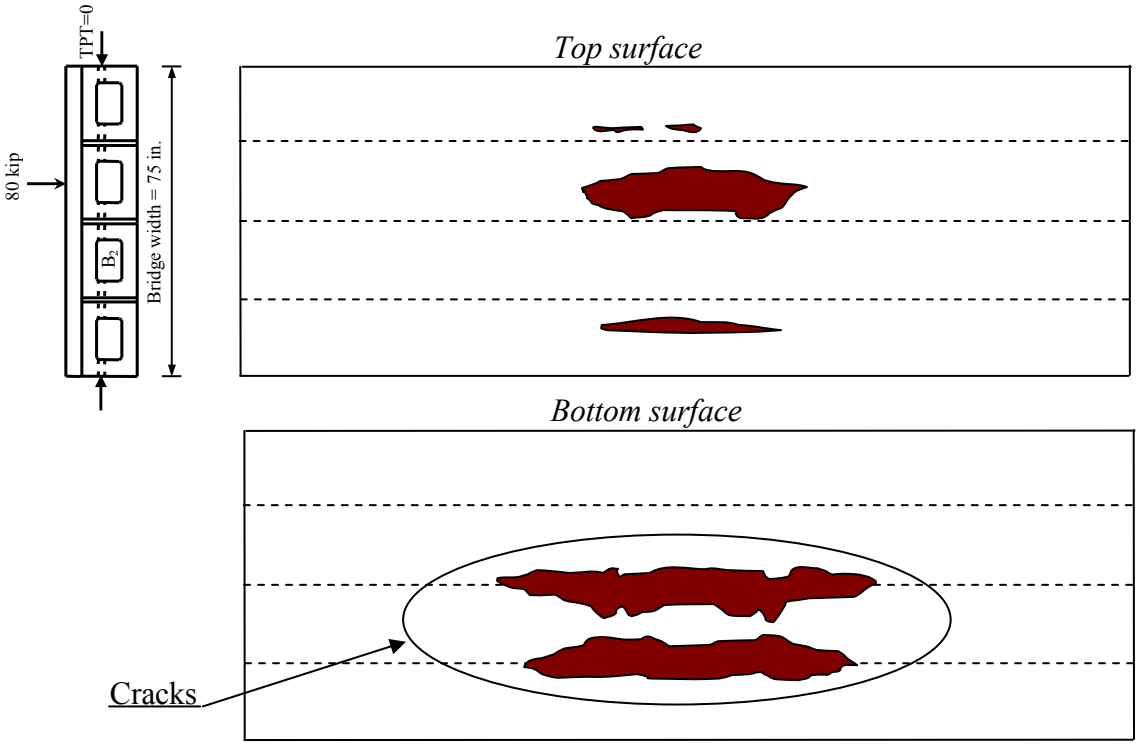

Figure 3.5-16 Crack development in the slab under vertical load of 80,000 lb.

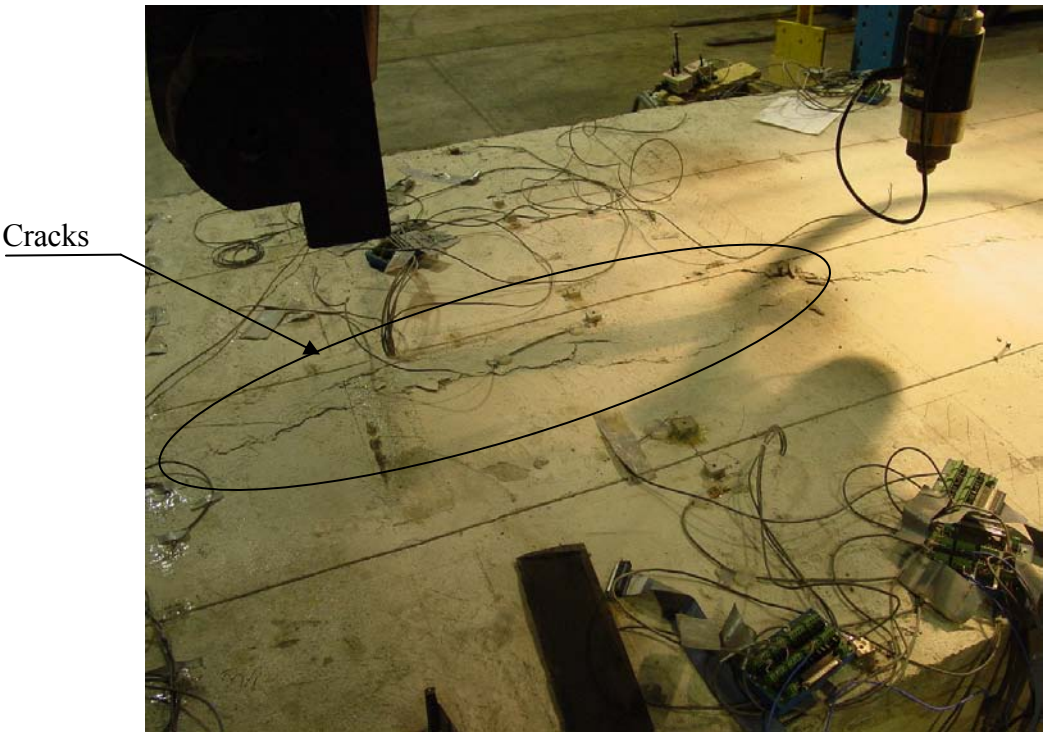

Figure 3.5-17 Crack development in the experimental bridge model under load of 80,000 lb.

CHAPTER 4: NUMERICAL INVESTIGATION OF TRANSVERSE POST-TENSIONING ARRANGEMENT

4.1 Introduction

The main objective of the finite element analysis was to eliminate the longitudinal deck cracking by establishing an adequate number of diaphragms and an appropriate TPT force level per diaphragm for wide range of bridges varying in span length and width as well. The analysis was conducted to relate the number of diaphragms to the bridge span and the TPT force level to the bridge width. Several bridge models with different spans were generated and analyzed with different numbers of diaphragms, and then wider bridge models were generated for the previous spans and analyzed with different TPT force levels. Finally, the results were summarized in charts showing the relationship between the bridge span and the number of diaphragms and the relationship between the bridge width and the TPT force level.

4.2 Adequate Number of Diaphragms

In order to establish the adequate number of diaphragms in side-by-side box-beam bridges, FE models for bridges with spans of 50, 62, 100, and 124 ft were generated. The width of the models was selected to be as small as practical in order to minimize the duration of the analysis. A width of 24 ft, which accommodates two traffic lanes without shoulders or one traffic lane with shoulders, was found to be the narrowest practical bridge width. Therefore, all the FE models in this part of the analysis were generated with a width of 24 ft. Eight side-by-side box-beams formed the bridge when 36 in. wide beams were used, and six box-beams formed the bridge when 48 in. wide beams were used.

4.2.1 Analysis Progression

The TPT arrangement is controlled by the number of diaphragms and TPT force level. An adequate transverse arrangement can be achieved by adjusting either the TPT level or the number of diaphragms. However, in some cases, increasing the TPT force level does not help in achieving an optimum TPT arrangement. Instead, the number of diaphragms has to be increased. Accordingly, the analysis to establish the adequate number of diaphragms was divided into five main steps:

1. Generating FE models following MDOT Specifications for transverse post-tensioning force and number of diaphragms.
2. Checking the development of the cracks in the deck slab under service loads.
3. Increasing the TPT level for the models that experienced cracks in the deck slab.
4. Increasing the number of diaphragms when increasing TPT level failed to eliminate crack development in the deck slab.

Repeating step 2 through 4 until eliminating the development of the cracks in the deck slab. The following sections present: first, a brief description of MDOT Specifications for TPT arrangement; second, a broad scheme for the loading and analysis steps; third, a discussion of the analysis and the results, and finally, charts showing the relationship between the number of diaphragms versus the bridge span for the 48 and 36 in. wide box-beams, respectively.

4.2.2 MDOT Specifications

Four bridge models were generated following MDOT Specifications for the TPT arrangement. The first model simulated a bridge with a span of 50 ft with four diaphragms. The second model simulated a bridge with a span of 62 ft with five diaphragms. The third model simulated a bridge with a span of 100 ft with six diaphragms; however, due to extensive details of this model, it was not feasible to model the full span. Instead, only half of the span was modeled and symmetry conditions were applied at the mid-span section. Finally, the fourth model was an example for spans over 100 ft where seven diaphragms were required. It simulated a bridge with a span of 124 ft; again, only half of the span was modeled. The following discussion offers detailed information on the behavior of each model under construction and service loads.

4.2.3 Loading Steps

Analysis and loading steps were identical throughout the entire study regardless of the model geometry or its TPT arrangement. The steps were organized as follows:

1. The pre-tensioning force was applied to the model through bottom reinforcement longitudinal steel strands. By using a force of 28,500 lb/strand, each strand was prestressed up to 70% of its ultimate strength.

2. The self-weight of the box-beams was calculated and applied as a distributed load over the top surface of the beams.
3. Virtual elements were created in between the box-beam sides in order to connect the beams together. The elements developed a friction interface between the adjacent surfaces with coefficient of friction equal to 0.7. This simulated the stage of pouring the shear-keys. As an approximation, the sides of the box-beams in the FE models were flat without the groove of the shear-key.
4. The first stage of transverse post-tensioning forces was simulated by applying a transverse force equal to 25,000 lb/location. It was assumed that the required transverse force would be applied in two stages: before and after pouring the deck slab. Subsequently, the slab could experience some compressive stresses that would contribute towards eliminating the development of the deck slab cracks. Applying the post-tensioning force in one or two stages (before and after casting the deck slab) has a little influence on the analysis as the post-tensioning force generates internal energy stored in the beams if the force is applied before casting the deck slab and in the beams and the slab if the force is applied after casting the deck slab. This level of internal energy will be used to connect the components of the superstructure and eliminate the deck cracking. In addition, the analysis were based on the assumption that un-bonded TPT strands will be used to enable future replacement for any deteriorated beam and reapplying the post-tensioning force. Subsequently, any future TPT force will be applied to the beams and the deck slab together.
5. The self-weight of the slab was applied to the model as a distributed load over the box-beams top surfaces.
6. A rigid connection was established between the deck slab bottom surface and the box-beams top surfaces. This type of connection prevented any slippage or sliding between the connected surfaces; consequently, the slab was integrated to the model.
7. The remaining TPT force was applied.
8. The weight of the wearing surface (25 lb/ft^2) was applied over the slab top surface and the weight of two Type 4 barriers (475 lb/ft each) was applied along the bridge edges.

In addition, the permanent losses were deducted from the longitudinal prestressing force in the same analysis step. Losses were calculated according to AASHTO LRFD (2004) lump-sum estimate of time dependent losses as provided in Section 5.9.5.3.

9. The service loads were applied as follows:

- 100% of positive temperature gradient was applied to the FE models according to AASHTO LRFD (2004) Section 3.12.3. The positive temperature gradient is the key for developing high tensile stresses in the deck slab, which subsequently leads to deck slab longitudinal cracking once applying the traffic loads (Bebawy, 2007 and Grace et al., 2007).
- A truck load was applied over one lane of the bridge model. Two types of live loads were investigated during the analysis. MDOT Specifications for TPT arrangement were based on using standard AASHTO trucks either HS-20 or HS-25; the bridge models were checked for both trucks; the heavier truck (HS-25) was selected to represent MDOT Specifications. The analysis was also performed using the AASHTO LRFD (2004) specifications because of the detailed explanation for the load types and the load factors. In AASHTO LRFD (2004) specifications, the standard trucks are no longer considered as live load; instead, a new type of loading identified as vehicular loading HL-93 is considered. The new loading is the standard HS-20 truck along with a lane load of 640 lb/ft distributed over 10 ft wide lane. Therefore, the models were checked for both HS-25 truck and HL-93 load though the difference in the response of models under both loads was not significant. The live loads were multiplied by presence factors corresponding to (Average Daily Truck Traffic) ADTT ranging between 100 and 1,000. The presence factor was taken as 0.95 in case of two lanes loaded and 1.14 in case of one lane loaded. In addition, an impact allowance of 75% was imposed in the entire analysis.

10. The analysis was completed when the deck slab was free of any cracks under the imposed loads.

4.2.4 Bridge Models Generated Using 48 in. Wide Box-Beams

4.2.4.1 50 ft Span Bridge Model

First, the 50 ft span bridge model had a TPT arrangement that conformed to current MDOT Specifications (Figure 4.2-1). Box-beams were set to a depth of 27 in. and a width of 48 in. One CFCC per diaphragm was provided at the middle of the transverse beam. Furthermore, as an AASHTO HS-25 truck was used as a design load, a transverse post-tensioning force of 104,500 lb was provided per diaphragm.

Analysis and discussion

The discussion herein addresses only the framework of the analysis and the results. The results are presented in detail for each loading case using stress contour maps in Bebawy (2007). The response of the FE bridge model under each loading step is summarized as follows:

1. The beams experienced a camber of 1.09 in. due to the longitudinal prestressing forces. The maximum stresses in the beams were less than the allowable stresses specified for prestressed concrete (AASHTO LRFD, 2004 Section 5.9.4).
2. After adding dead load of the box-beams, the camber decreased to 0.74 in. Longitudinal and transverse stress values remained within the allowable range for the stresses.
3. After applying the first stage of the TPT force, the transverse stresses in the beams did not change significantly as the TPT force was just 25,000 lb/diaphragm.
4. Adding the slab dead load reduced the camber in the beams to 0.58 in.
5. After casting the deck slab and before applying second stage of TPT force, the stresses in the deck slab in both directions were negligible because this stage simulated the deck slab just after casting and curing.
6. After applying the second stage of TPT force, the deck slab gained some compressive stresses in the transverse direction. However, the compressive stresses were localized near the diaphragms and the ends. The maximum developed transverse stress was 155 psi, concentrated at local areas near the supports. The majority of the slab experienced compressive stresses in the range of 7 to 31 psi, which were far less than the recommended limit of 250 psi that was specified by AASHTO LRFD (2004) Section

4.6.2.2. The longitudinal stress distribution was not affected significantly with the applied TPT force. At the same time, applying the remaining TPT force caused the compressive pressure on the box-beam sides to reach a value of 400 psi at the end diaphragms. However, the major contact areas experienced pressure levels below 10 psi. The poor distribution of the pressure indicated that AASHTO LRFD (2004) recommendations of obtaining uniform compressive prestress through the joint are not realizable unless the diaphragms are provided every few feet.

7. The last construction stage was to deduct time dependent losses from the longitudinal prestressing forces and to apply the superimposed dead loads (SDL) over the deck slab. The transverse stresses were not affected significantly; however, some longitudinal compressive stresses developed in the slab due to the flexural action of the loads in the longitudinal direction. By the end of this stage, the beams camber decreased to 0.40 in.

Model response under service loads

1. When applying 100% of the positive temperature gradient, the slab top and bottom surfaces experienced significant increase in the longitudinal compressive stresses. In the transverse direction, a sudden increase in the compressive stresses took place in the slab top surface; with the maximum value at the span ends (626 psi) while the major area experienced stresses in the range of 300 to 384 psi. At the same time, transverse tensile stresses of a value of 261 psi developed in the slab bottom surface. Consequently, the maximum principal stress reached 267 psi at the slab bottom surface, while the top surface experienced maximum principal stresses in the average of -22 psi (compression). The deformation in the slab before and after applying the temperature gradient is shown in Figure 4.2-2.

2. Applying AASHTO HS-25 truck load with impact or presence allowances caused the longitudinal compressive stresses in the loaded lane to reach 742 psi at the slab top surface; while small tensile stresses less than 55 psi developed at the bottom surface. The transverse stresses in the slab top surface remained compressive, while the transverse tensile stresses increased to about 300 psi at the bottom surface of the slab over some shear-key locations. Moreover, the maximum principal stresses in the slab

bottom surfaces reached a value of 311 psi at the same locations. However, the deck slab was able to sustain the applied loads without developing any tensile cracks.

3. By applying AASHTO HS-25 truck load (or HL-93 load) with the impact and presence allowances, some significant cracks developed in the deck slab, as shown in Figure 4.2-3 and Figure 4.2-4. The cracks initiated from the bottom surface and developed towards the top surface. Although they did not reach the top surface, repeated loads would likely cause the cracks to propagate throughout the full depth of the deck slab.

There are two possible solutions to avoid the propagation of the cracks. The first option is to increase the TPT force in each diaphragm. The other option is to increase the number of diaphragms. As mentioned earlier in this section, the first solution to be checked was always increasing the TPT; accordingly, in the subsequent analysis, the TPT force was increased up to 200,000 lb/diaphragm while maintaining the same number of diaphragms.

1. After applying a TPT force of 175,000 lb/diaphragm (25,000 lb/diaphragm was applied before casting the deck slab), localized transverse compressive stresses in the deck slab reached 362 psi at the span ends. Yet, the majority of the deck slab experienced compressive stresses in the range between 9 and 44 psi. In the longitudinal direction, small compressive stresses were seen in the deck slab, but they did not exceed 37 psi. Some longitudinal tensile stresses of a value of 114 psi developed at local areas in the slab ends. The pressure on the box-beams sides exceeded 500 psi at the diaphragms location. However, in the areas between the diaphragms locations, the compressive pressure did not exceed 10 psi.
2. Deducting time dependent losses and applying superimposed dead loads increased the longitudinal compressive stresses in the deck slab to 147 psi but did not affect the transverse stresses.
3. After applying positive temperature gradient, the slab top surface experienced longitudinal compressive stresses up to 551 psi while the stresses were negligible in the slab bottom surface. At the same time, the transverse compressive stresses in the slab top ranged between 300 and 395 psi. The bottom surface experienced tensile stresses up

to 240 psi over some shear-key locations. The maximum principal stresses in the slab bottom surface reached a value of 256 psi (tension).

4. After applying AASHTO HS-25 truck load without impact and presence allowances, the maximum principal stresses reached 285 psi (tension) at locations of the shear-key joints in the bottom surface.

5. Although the applied TPT force was nearly twice the TPT force in the first trial, the slab experienced small cracks in the bottom surface after applying AASHTO HS-25 truck load or HL-93 load with the impact and presence allowances (Figure 4.2-5 and Figure 4.2-6). It is obvious that the model performance was improved with the large TPT force; yet, the cracking problem was not controlled entirely.

As a parametric evaluation, the TPT force was increased to 300,000 lb/diaphragm to investigate the influence of high TPT level on the model. However, the transverse stresses in the slab did not reach the limit required by AASHTO LRFD (2004); neither did the pressure on the box-beams sides in the areas between the diaphragms. Moreover, some cracks developed immediately after applying the TPT force in the slab (Figure 4.2-7) and the box-beam sides as well (Figure 4.2-8) due to the stresses localization. So, even with high TPT level, the AASHTO LRFD (2004) requirement for transverse prestress was not reachable.

The second available solution to overcome the deck cracking was to increase the number of diaphragms; the number of diaphragms was increased to five instead of four; two at the ends and three equally spaced inbetween (Figure 4.2-9). The TPT force was set to 100,000 lb/diaphragm as a first trial.

1. The transverse compressive stresses reached 148 psi in the deck slab after applying the second TPT stage with a TPT force of 75,000 lb/diaphragm. The maximum stresses were concentrated near the support locations. However, the majority of the deck slab experienced compressive stresses in the range between 5 and 33 psi. In the longitudinal direction, small compressive stresses developed in the deck slab, but they did not exceed 15 psi. Likewise, some tensile stresses were generated at local areas near the supports and reached 44 psi. The pressure on the box-beams sides exceeded 400 psi at

the end regions. However, the regions between the diaphragms experienced pressure less than 10 psi.

2. After deducting time dependent losses and applying superimposed dead loads, the longitudinal compressive stresses reached 120 psi in the deck slab top surface at the mid-span. However, the transverse stresses were not affected by the applied loads.
3. After applying positive temperature gradient, the slab top surface experienced compressive stresses up to 565 psi and tensile stresses up to 53 psi in the longitudinal direction. On the other hand, the transverse stresses in the slab top surface experienced additional compressive stresses averaging 314 to 394 psi. The bottom surface experienced tensile stresses up to 244 psi at the shear-key locations. The same locations experienced maximum principal stresses up to 254 psi (tension).
4. After applying AASHTO HS-25 truck load without impact and presence allowances, the maximum principal stresses reached a value of 299 psi at the bottom surface; yet, the slab did not experience any cracks under the truck load. However, it experienced small cracks in the bottom surface after applying the truck load either HS-25 or HL-93 with the impact and presence allowances (Figure 4.2-10 and Figure 4.2-11).

Since the developed cracks were limited, some increase in the TPT level would assist in achieving an adequate TPT arrangement. A TPT force of 150,000 lb/diaphragm was applied to the modified system of diaphragms.

1. After applying TPT force of 125,000 lb/diaphragm in the second TPT stage, the deck slab experienced compressive stresses up to 227 psi. The uppermost values were concentrated at the slab ends and the rest of the slab areas experienced lower values; large areas of the slab experienced compressive stresses in the range between 11 and 54 psi. In the longitudinal direction, small longitudinal compressive stresses developed in the deck slab, but they did not exceed 22 psi. Similarly, some longitudinal tensile stresses developed at local areas near the supports and reached 83 psi. The pressure on the box-beams sides exceeded 475 psi. However, between the diaphragms, the compressive pressure was less than 10 psi.

2. After deducting time dependent losses and applying superimposed dead loads, the deck slab experienced longitudinal compressive stresses of an average of 130 psi; yet, the transverse stresses were not affected by the applied loads.
3. After applying a positive temperature gradient, the slab top surface experienced longitudinal compressive stresses of about 558 psi; yet, the average compressive stress was zero at the slab bottom surface. At the same time, the transverse stresses in the slab top surface increased to an average between 287 and 371 psi. The bottom surface experienced tensile stresses up to 219 psi. Some local areas over the shear-key joints in the slab bottom surface experienced maximum principal tensile stresses up to 229 psi.
4. After applying AASHTO HS-25 truck load without impact and presence allowances, the maximum principal stresses reached 254 psi at the bottom surface, and the slab did not experience any cracks.
5. The maximum principal stresses reached 299 psi at the slab bottom surface after applying AASHTO HS-25 truck load with the impact and presence allowances and they reached 286 psi after applying HL-93 load with the impact and presence allowances. The slab did not experience cracks in both cases (Figure 4.2-12 and Figure 4.2-13).
6. By applying post-tensioning force of 150,000 lb/diaphragm at five diaphragms, the model was capable of supporting 100% of positive temperature gradient and AASHTO HS-25 truck or HL-93 load without developing any longitudinal cracks in the deck slab. Therefore, this TPT arrangement was considered the optimum. Table 4.2-1 presents a summary for the aforementioned investigation. In addition, Figure 4.2-14 shows the contribution of each load type in the developed principal stresses in the deck slab. It is apparent that the temperature gradient was the greatest contributing factor to the tensile stresses in the deck slab.

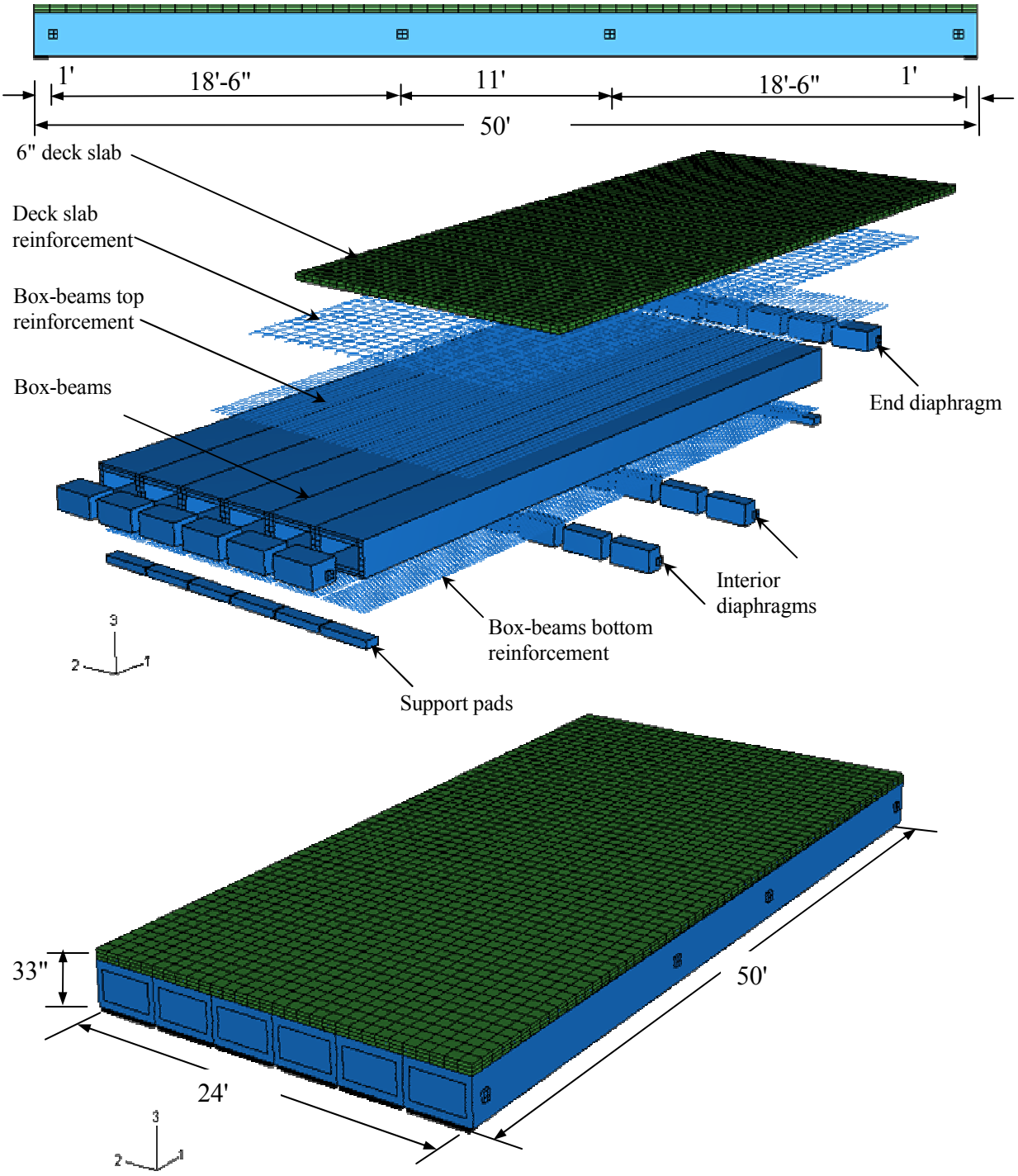

Figure 4.2-1 Assembly of 50 ft span bridge model.

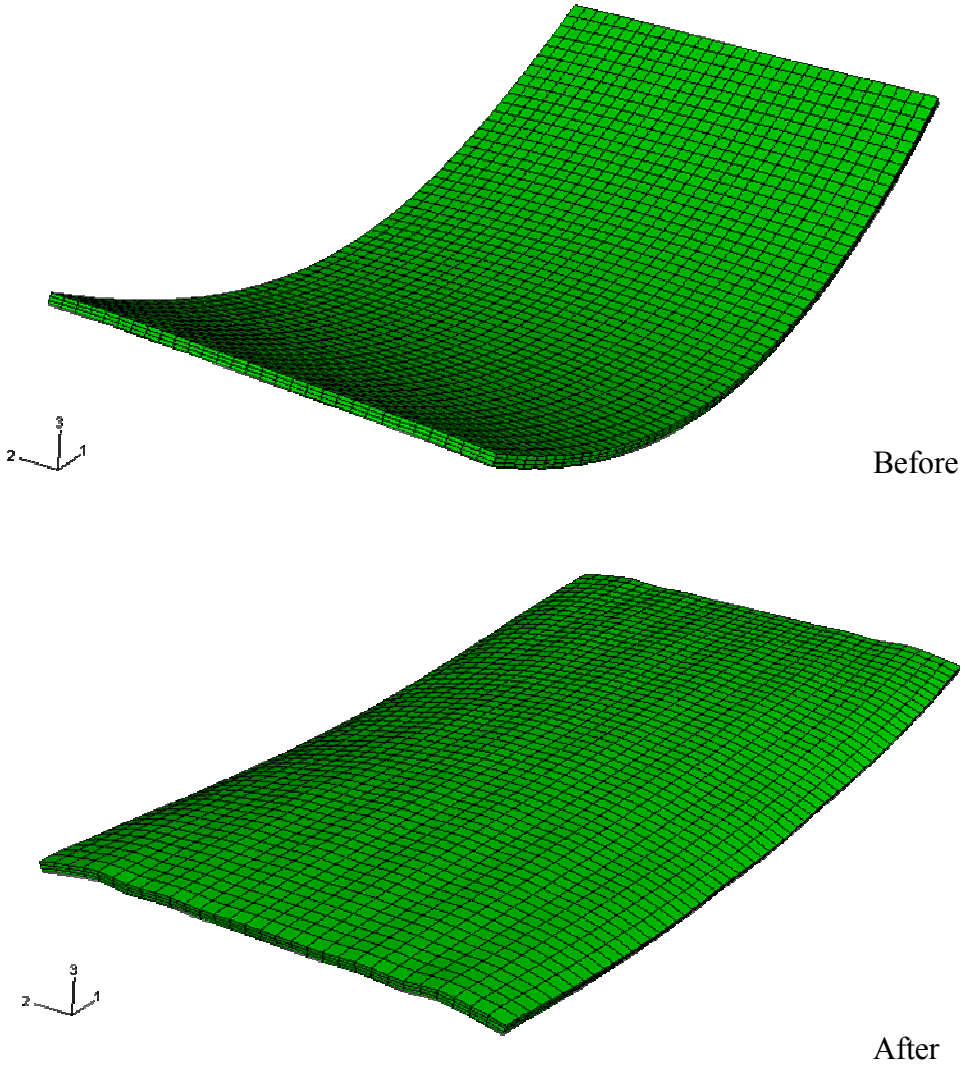

Figure 4.2-2 Exaggerated deformed shape of the slab before and after applying positive temperature gradient (Scale 1:500).

Diaphragms arrangement:

2 @ center of span (11" apart) TPT= 104,500 lb/diaphragm
1 @ each end of beam TPT= 104,500 lb/diaphragm

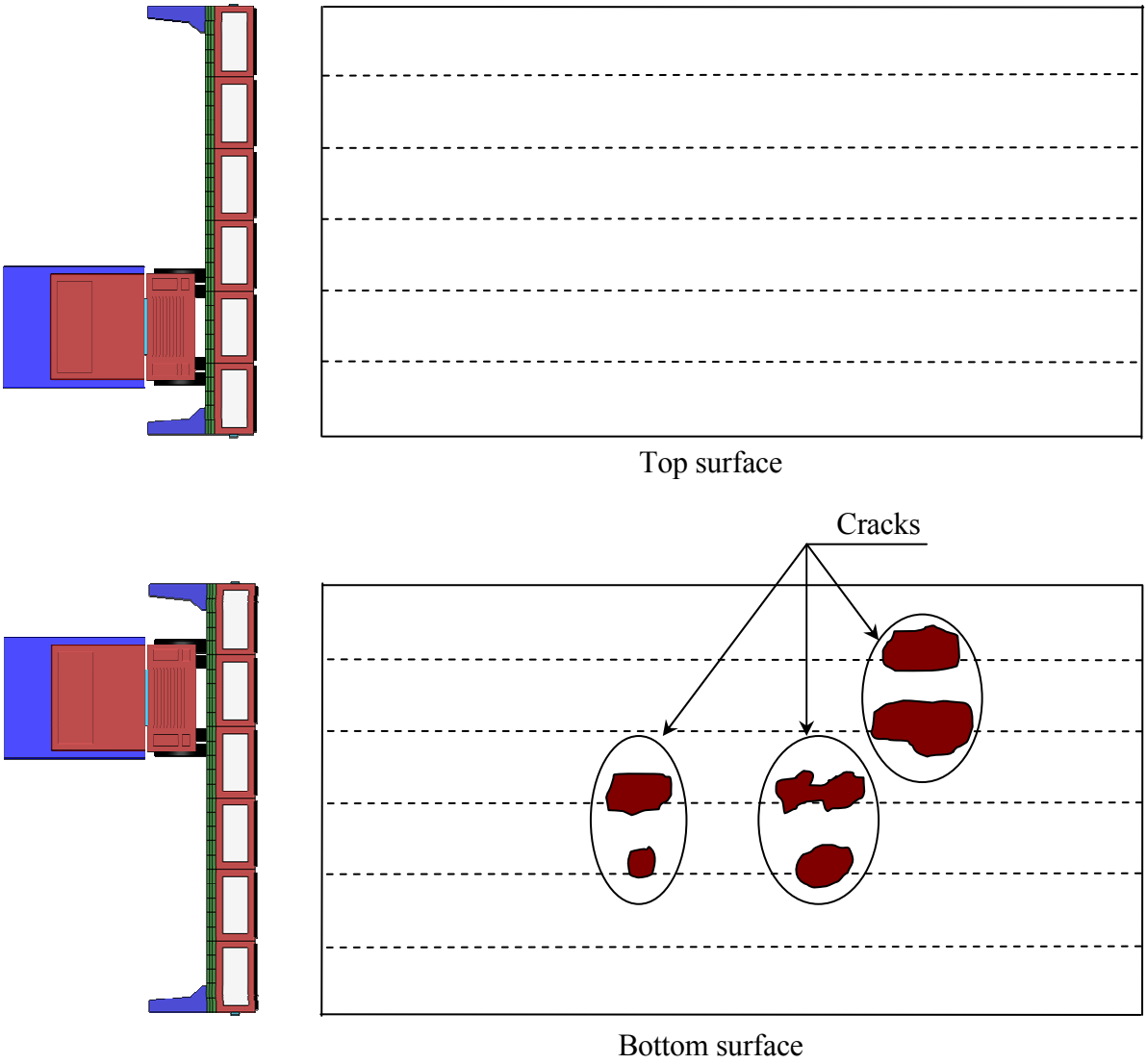

Figure 4.2-3 Crack development in the slab bottom surface after applying AASHTO HS-25 truck.

Diaphragms arrangement:

2 @ center of span (11" apart) TPT= 104,500 lb/diaphragm
1 @ each end of beam TPT= 104,500 lb/diaphragm

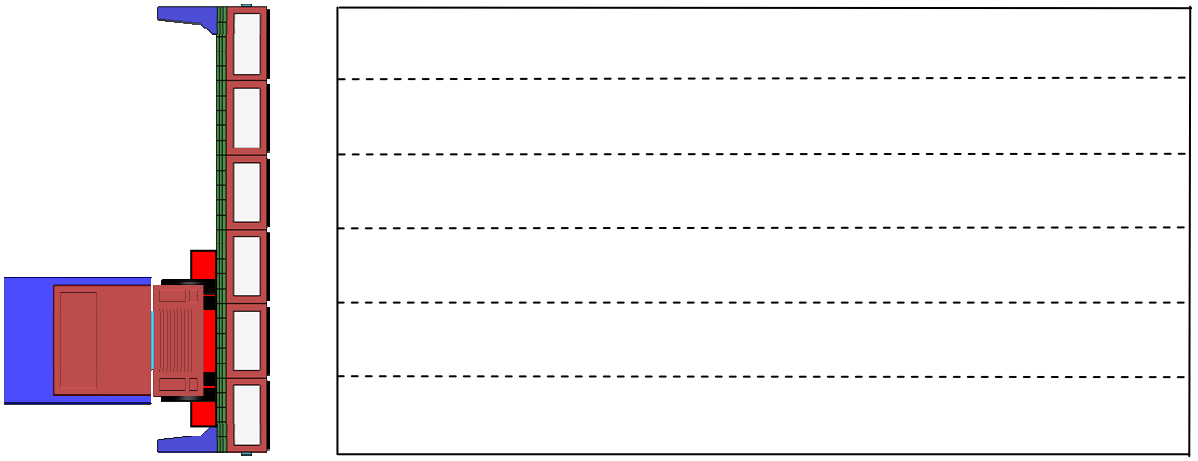

Top surface

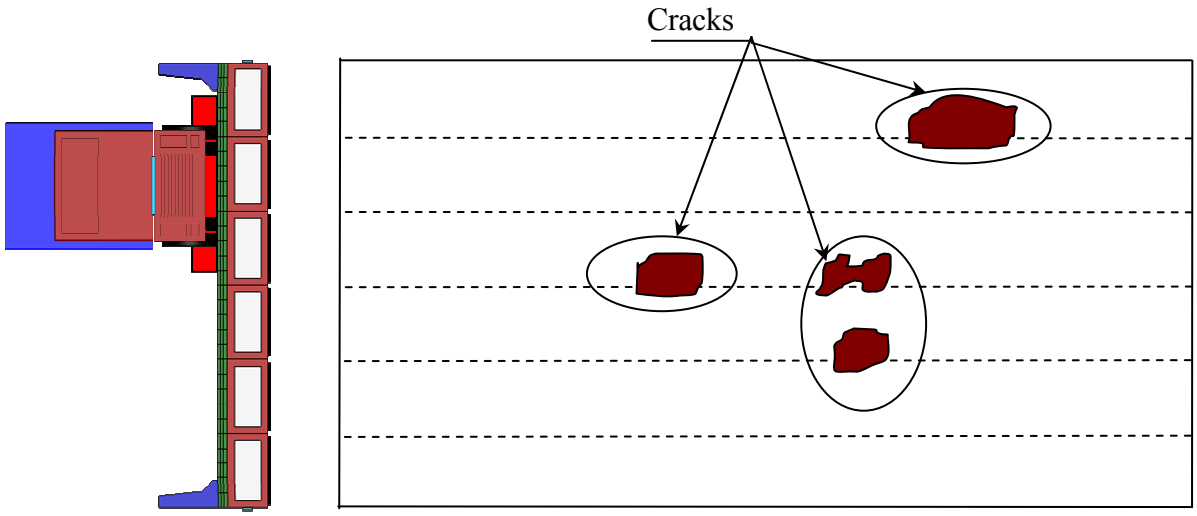

Bottom surface

Figure 4.2-4 Crack development in the slab after applying AASHTO HL-93 load.

Diaphragms arrangement:

2 @ center of span (11" apart) TPT= 200,000 lb/diaphragm
1 @ each end of beam TPT= 200,000 lb/diaphragm

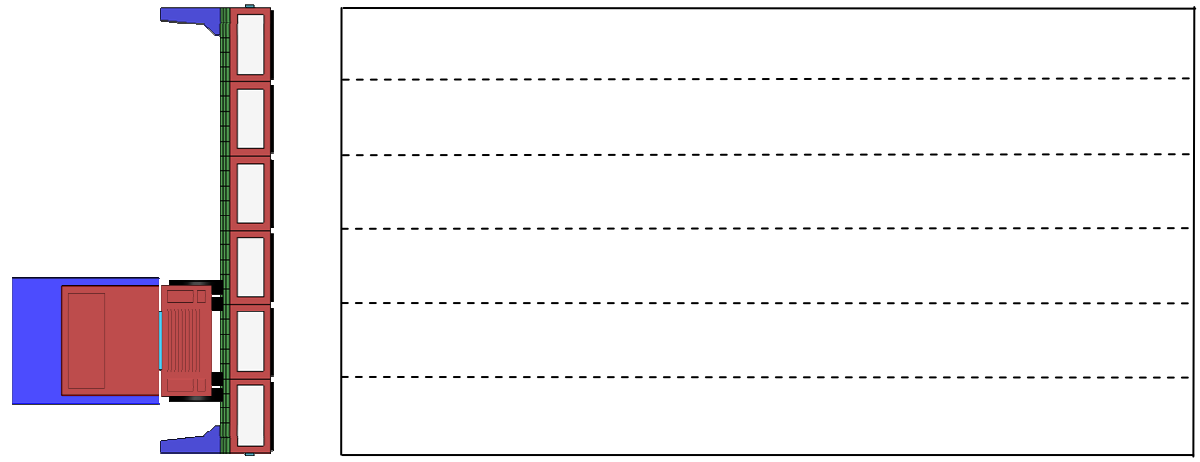

Top surface

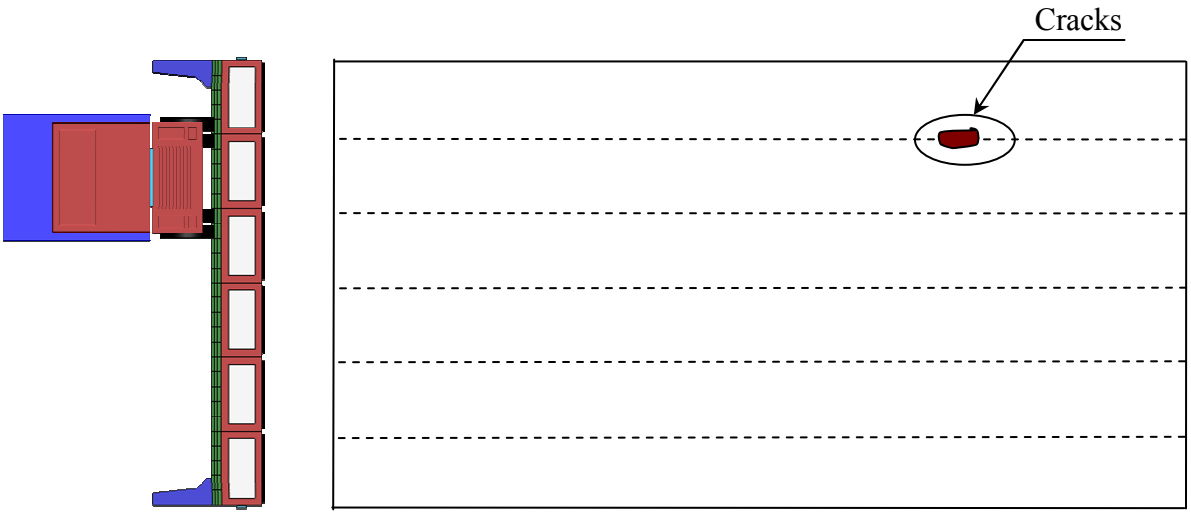

Bottom surface

Figure 4.2-5 Crack development in the slab after applying AASHTO HS-25 truck.

Diaphragms arrangement:

2 @ center of span (11" apart) TPT= 200,000 lb/diaphragm
1 @ each end of beam TPT= 200,000 lb/diaphragm

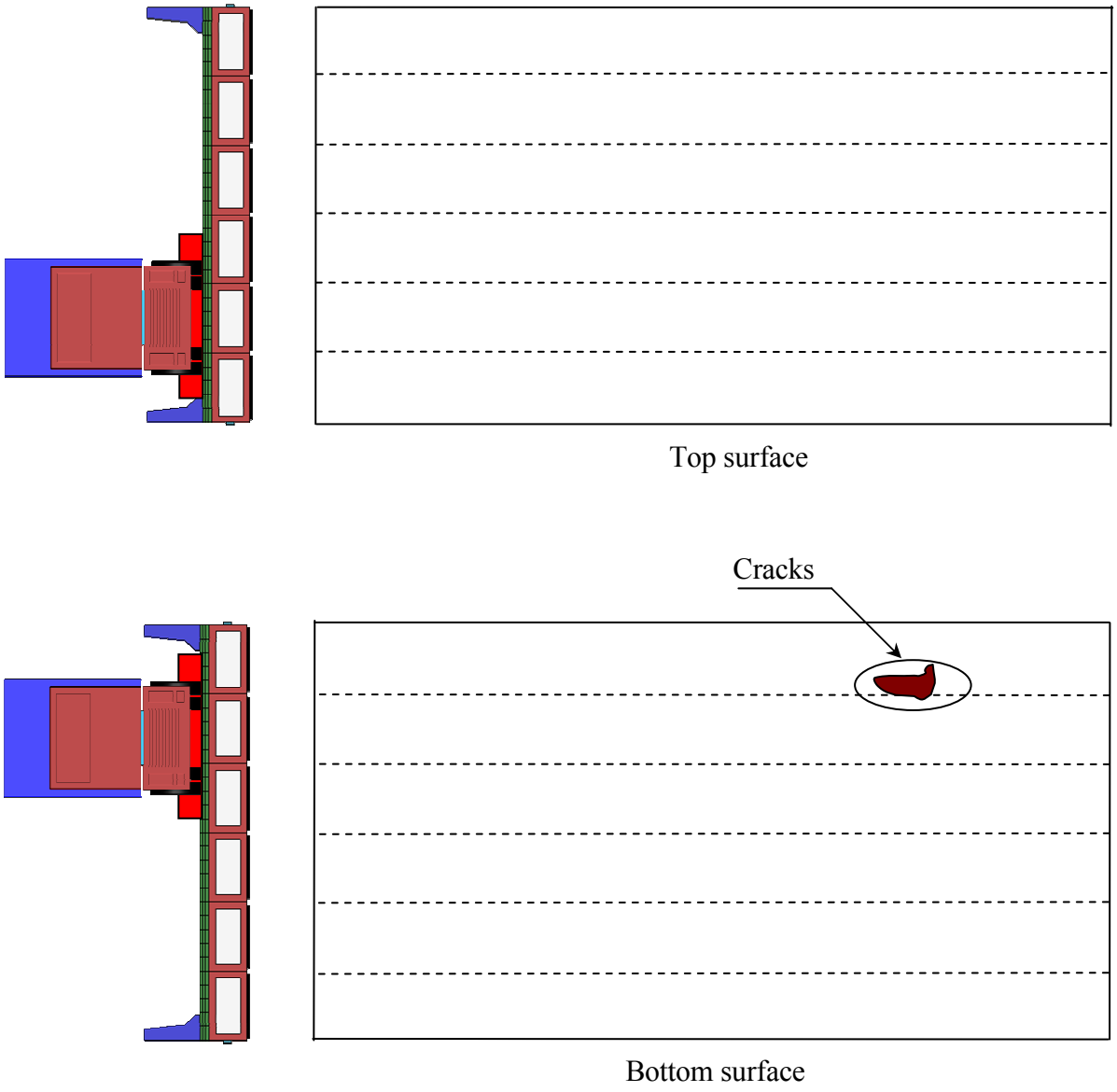

Figure 4.2-6 Crack development in the slab after applying AASHTO HS-93 truck.

Diaphragms arrangement:

2 @ center of span (11" apart)	TPT= 300,000 lb/diaphragm
1 @ each end of beam	TPT= 300,000 lb/diaphragm

Figure 4.2-7 Crack development in the slab bottom surface due to TPT force.

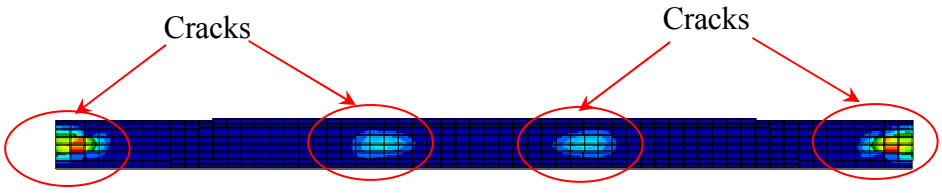

Figure 4.2-8 Crack development in box-beam sides due to TPT force.

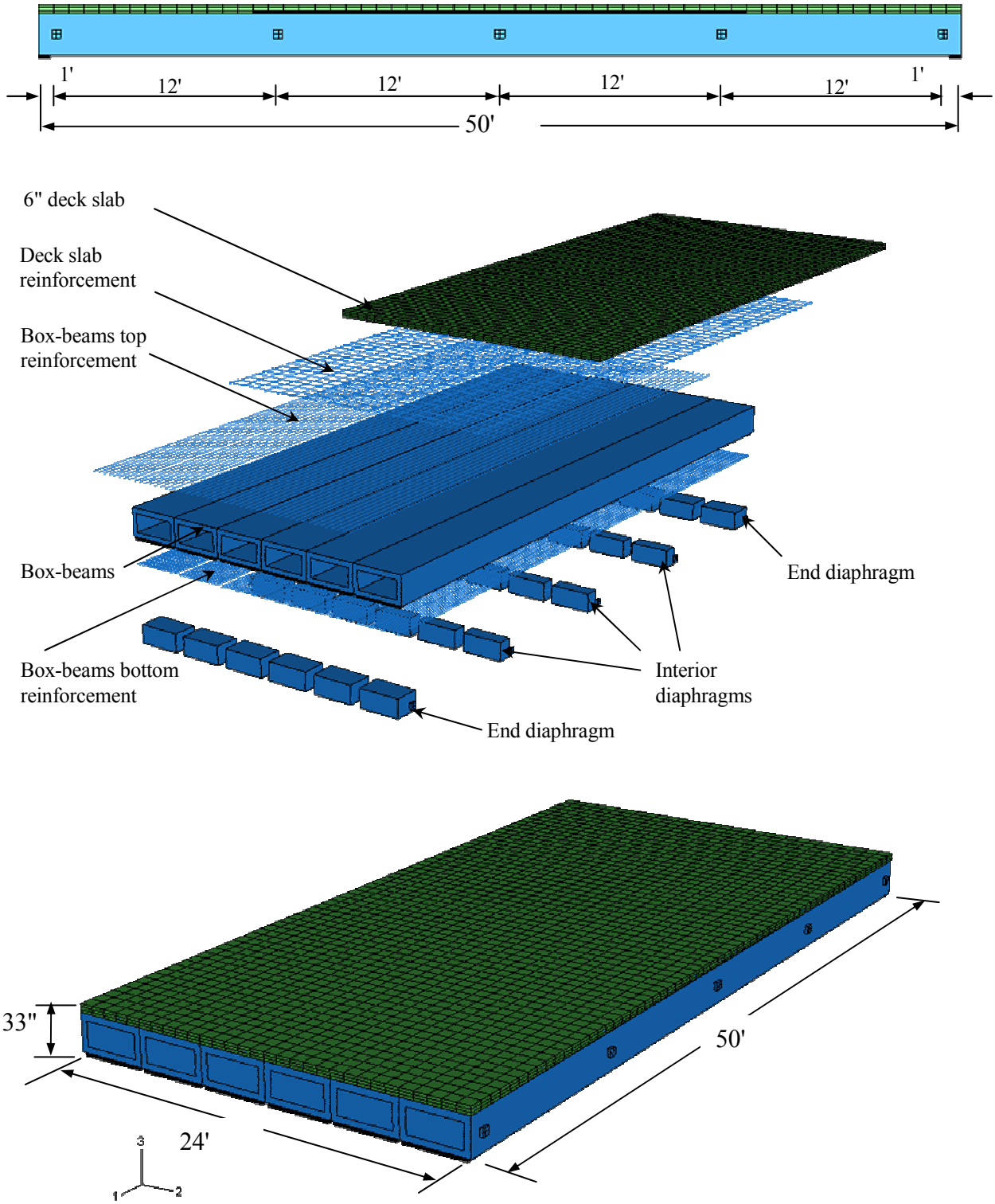

Figure 4.2-9 Modified assembly for 50 ft span bridge model.

Diaphragms arrangement:

1 @ each end of beam	TPT= 100,000 lb/diaphragm
3 equally spaced in-between	TPT= 100,000 lb/diaphragm

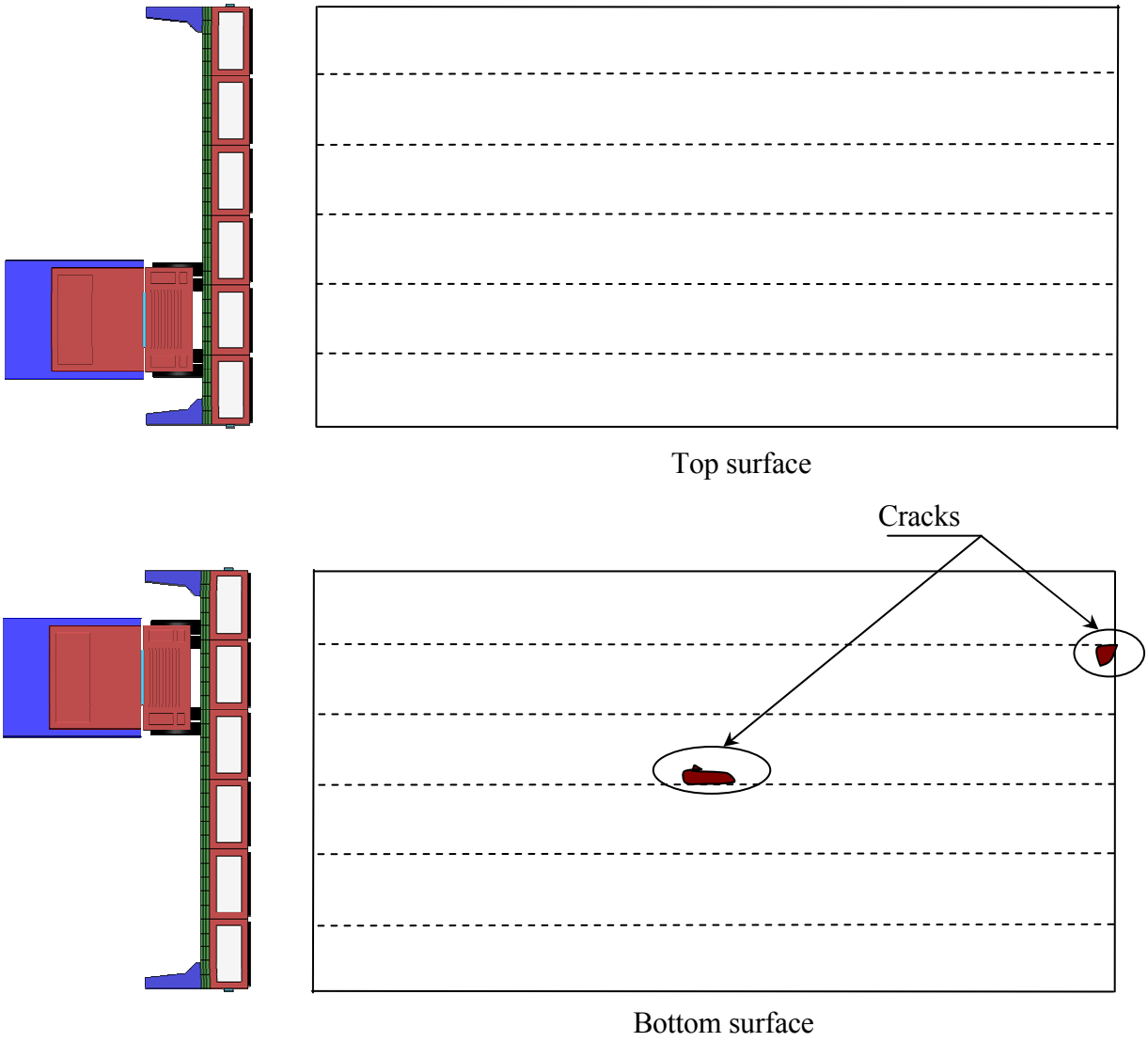

Figure 4.2-10 Crack development in the slab after applying AASHTO HS-25 truck.

Diaphragms arrangement:

1 @ each end of beam	TPT= 100,000 lb/diaphragm
3 equally spaced in-between	TPT= 100,000 lb/diaphragm

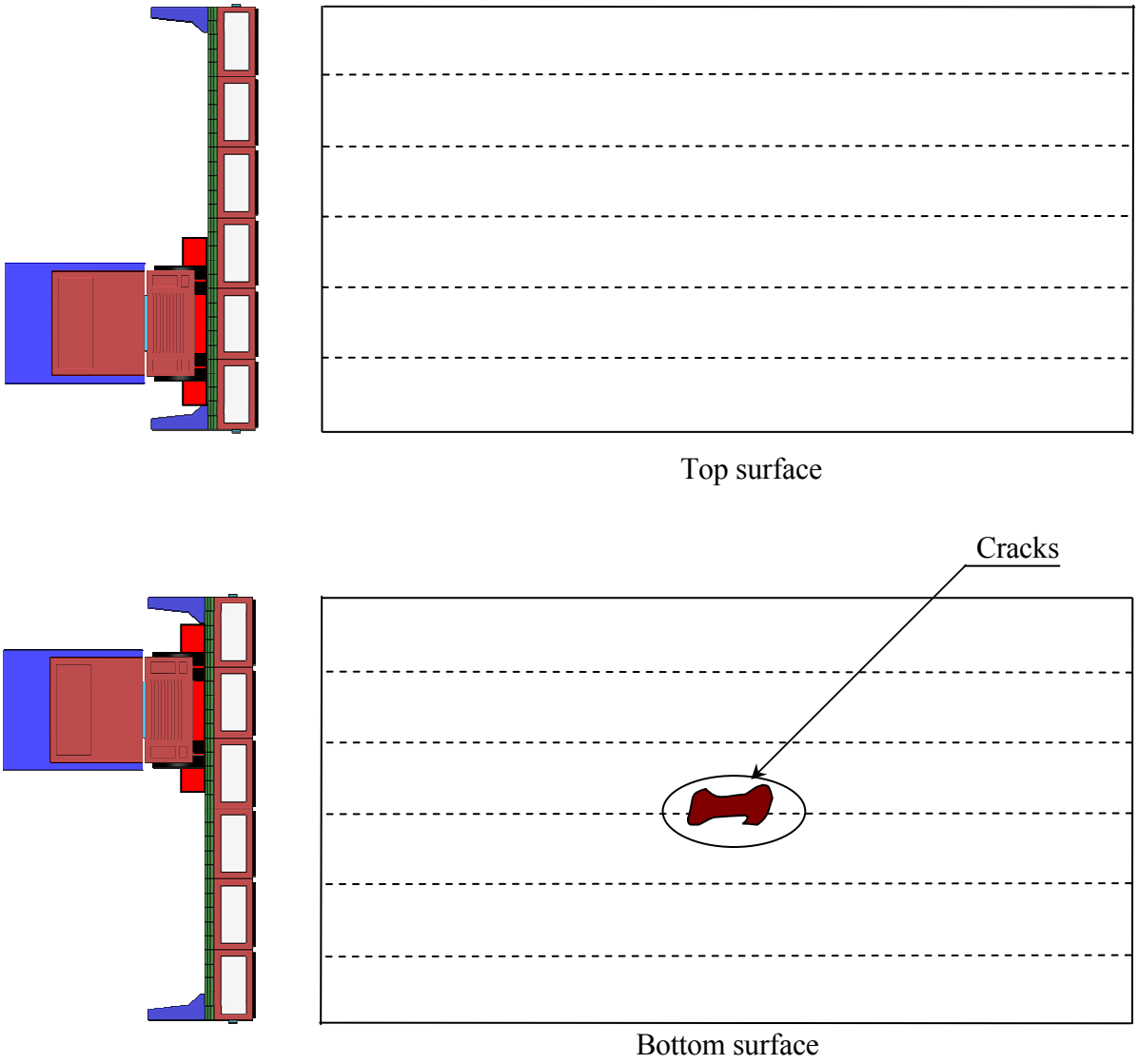

Figure 4.2-11 Crack development in the slab after applying AASHTO HL-93 load.

Diaphragms arrangement:

1 @ each end of beam	TPT= 150,000 lb/diaphragm
3 equally spaced in-between	TPT= 150,000 lb/diaphragm

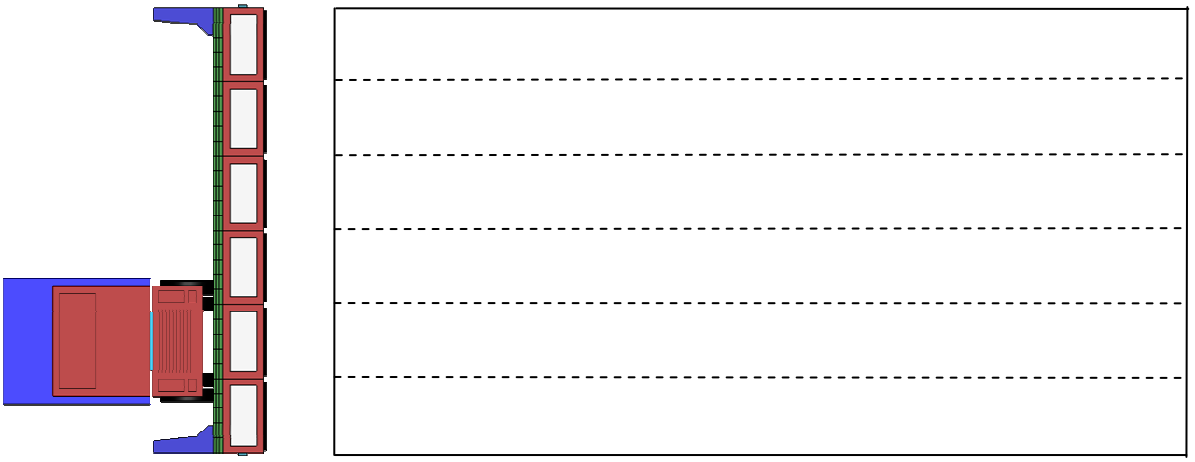

Top surface

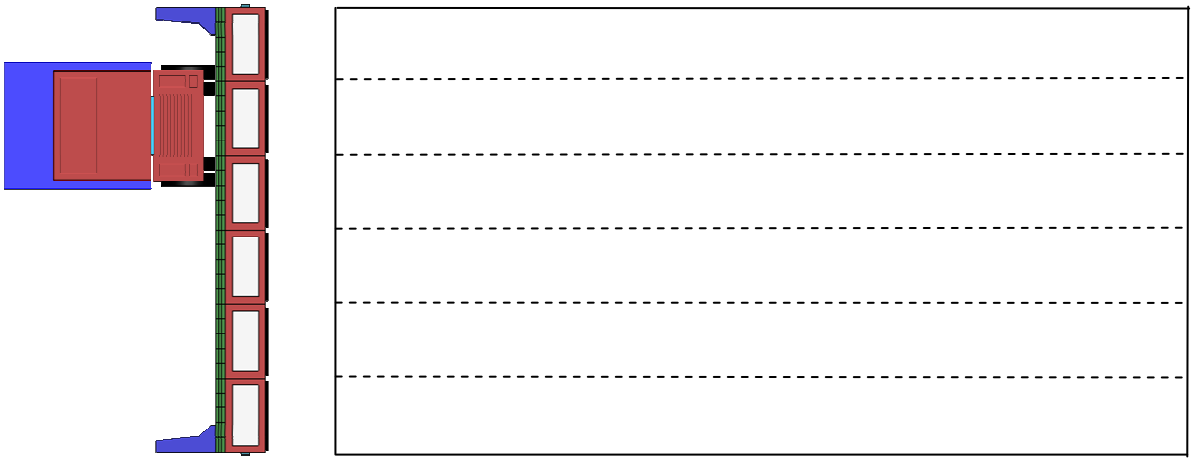

Bottom surface

Figure 4.2-12 Crack development in slab after applying AASHTO HS-25 truck.

Diaphragms arrangement:

1 @ each end of beam	TPT= 150,000 lb/diaphragm
3 equally spaced in-between	TPT= 150,000 lb/diaphragm

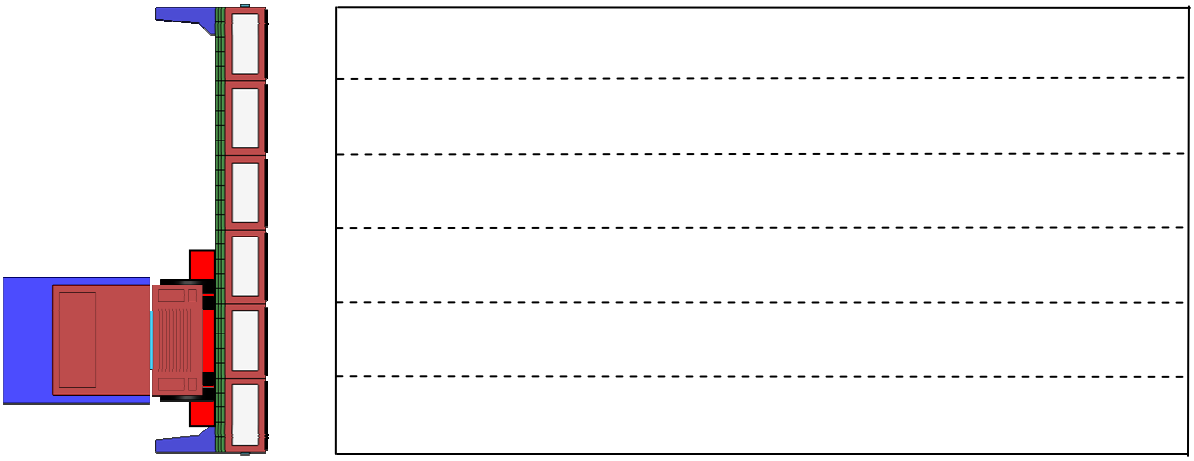

Top surface

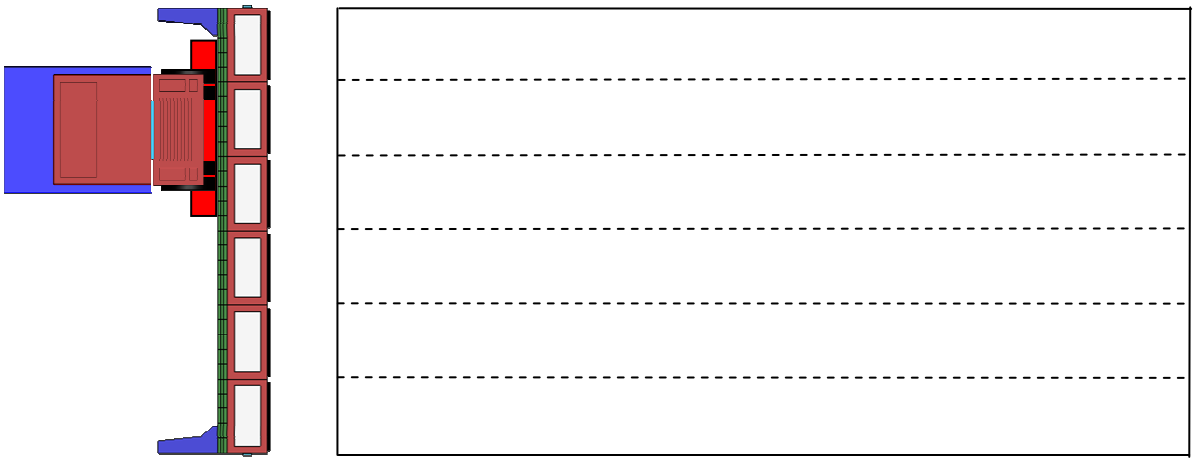

Bottom surface

Figure 4.2-13 Crack development in slab after applying AASHTO HL-93 load.

Table 4.2-1 Maximum principal stresses in the deck slab of 50 ft span bridge model under service loads.

Model	No. of Diaphragms	TPT Force lb/diaphragm	MP Positive Gradient (psi)	MP LL+ IM (psi)	
				HS-25 truck	HL-93 load
Span = 50 ft Width = 24 ft	4	104,000	267	N/A (cracks)	N/A (cracks)
	4	200,000	256	N/A (cracks)	N/A (cracks)
	4	300,000	N/A (cracks)	N/A (cracks)	N/A (cracks)
	5	100,000	254	N/A (cracks)	N/A (cracks)
	5	150,000	229	299	286

- MP: Maximum principal stresses
- LL: Live load
- IM: Impact allowances
- N/A: Not available

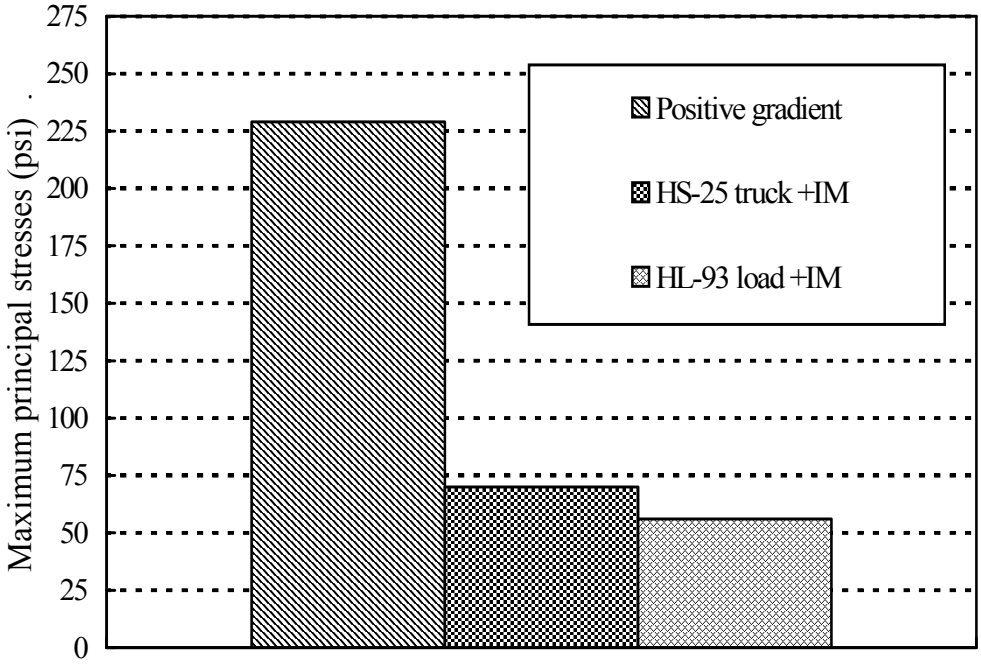

Figure 4.2-14 Service loads contribution in deck slab principal stresses (Case of five diaphragms, TPT = 150,000 lb/diaphragm).

4.2.4.2 62 ft Span Bridge Model

The second FE model was developed to simulate a 62 ft span bridge composed of six side-by-side box-beams of width 48 in. each, as shown in Figure 4.2-15. The model was provided with a TPT arrangement that conformed to current MDOT Specifications (2006), which require five diaphragms for this span; two diaphragms at the ends, two at the quarter points, and one at the mid-span. To satisfy the flexural requirements, a box-beam with a depth of 33 in. was used for this span. Two transverse strands were provided per diaphragm, with each transverse strand post-tensioned with a force equal to 52,250 lb (total of 104,500 lb/diaphragm).

Analysis and discussion

The current model was subjected to construction loads by: first, applying longitudinal prestressing forces; second, applying box-beams dead load; third, applying first stage of TPT force; fourth, adding slab dead load; fifth, applying second stage of TPT; and finally, deducting time dependent losses and applying the superimposed loads. Subsequently, service loads were applied by first applying positive temperature gradient and then applying AASHTO HS-25 truck or HL-93 load. By applying AASHTO HS-25 truck, or AASHTO HL-93 load, the deck slab developed cracks, as shown in Figure 4.2-16 and Figure 4.2-17. The cracks started developing from the bottom surface and propagated towards the top surface. Although they did not propagate to the top surface, repeated loads would likely cause the development of the full-depth cracks in the deck slab.

The first strategy used to eliminate the cracking problem was to increase the transverse post-tensioning force per diaphragm. The transverse post-tensioning force was increased to 150,000 lb/diaphragm while keeping the same number of diaphragms. The slab did not experience any cracks under the truck load without impact and presence allowances. However, it did experience small cracks in the bottom surface after adding the impact and presence allowances to the truck load. When applying AASHTO HL-93 load, the slab experienced similar cracks as well. The cracks were mainly concentrated at the mid-span over the intermediate diaphragm; so, increasing the TPT force in the intermediate diaphragm only appeared as a plausible solution; a TPT force equal to 200,000 lb/center-intermediate - diaphragm was applied while keeping the other diaphragms with TPT force equal to 150,000

lb/diaphragm. After applying AASHTO HS-25 truck load, the maximum principal stresses reached a value of 299 psi. The slab did not experience cracks.

By applying post-tensioning force 150,000 lb/diaphragm at four diaphragms and 200,000 lb/intermediate diaphragm, the model was able to support AASHTO HS-25 truck load as well as AASHTO HL-93 load with its impact and presence allowances without developing any longitudinal cracks in the deck slab. Therefore, this TPT arrangement was considered sufficient.

Instead of increasing the TPT force to 200,000 lb/intermediate-diaphragm, the cracks can be delayed by adding one more diaphragm and applying 150,000 lb in all the diaphragms. Increasing the diaphragms number has two benefits: first, high post-tensioning force can be avoided for a certain location; second, it allows better distribution for the pressure between the adjacent beams. Hence, the third trial was to examine the crack development when providing six equally-spaced diaphragms instead of five with TPT force equal to 150,000 lb/diaphragm (Figure 4.2-18).

After applying positive temperature gradient, the slab bottom surface experienced tensile stresses up to 233 psi. This value increased to 263 psi when adding AASHTO HS-25 truck load without impact and presence allowances, and then up to 306 psi when adding AASHTO HS-25 truck load with the impact and presence allowances. The slab did not experience any cracks under the AASHTO HS-25 truck or the ASHTO HL-93 load. In addition, a summary for the aforementioned investigation is presented in Table 4.2-2. Furthermore, the contribution of each load type to the principal stresses in the deck slab is shown in Figure 4.2-19.

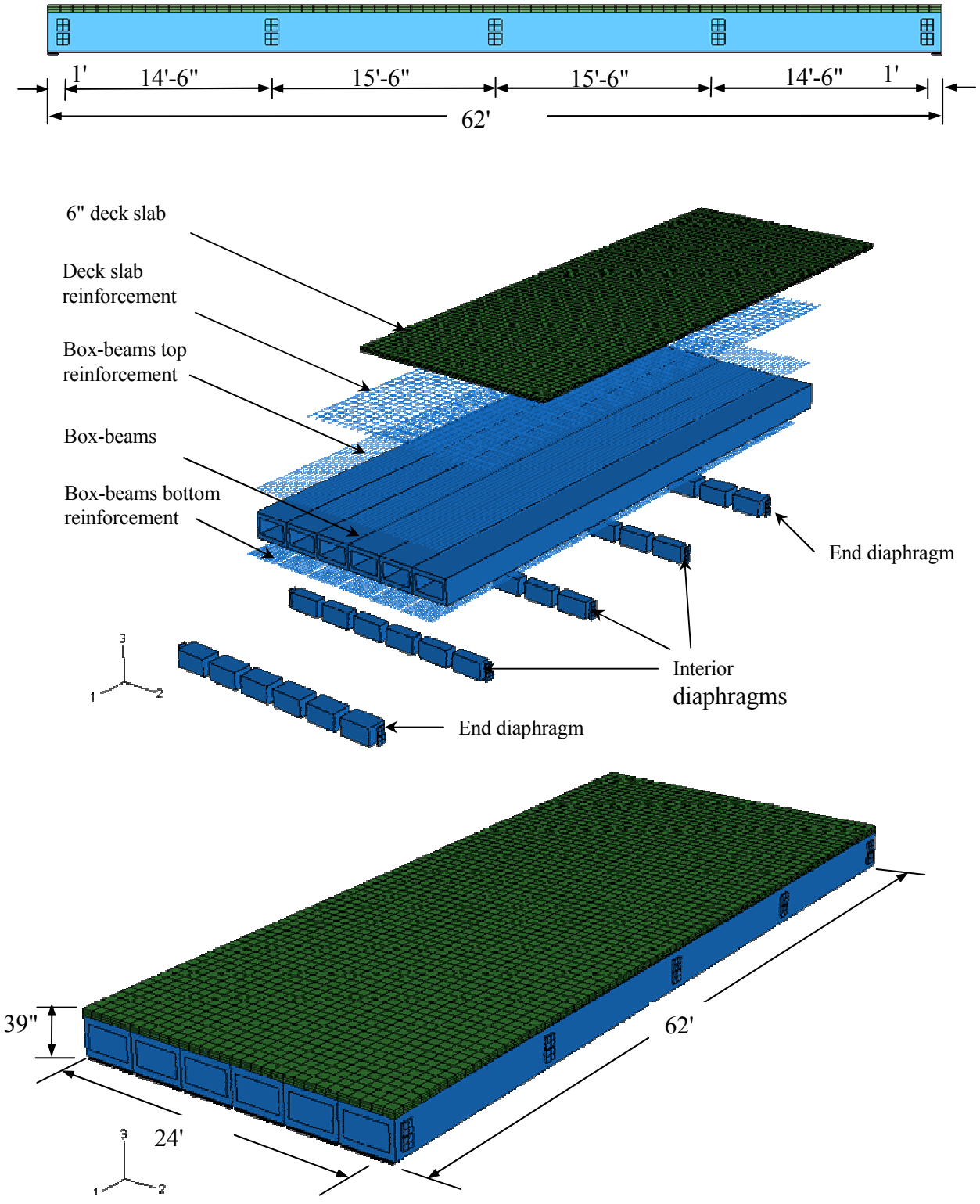

Figure 4.2-15 Assembly for 62 ft span bridge model.

Diaphragms arrangement:

1 @ each end of beam	TPT= 104,500 lb/diaphragm
2 @ quarter points	TPT= 104,500 lb/diaphragm
1 @ center of span	TPT= 104,500 lb/diaphragm

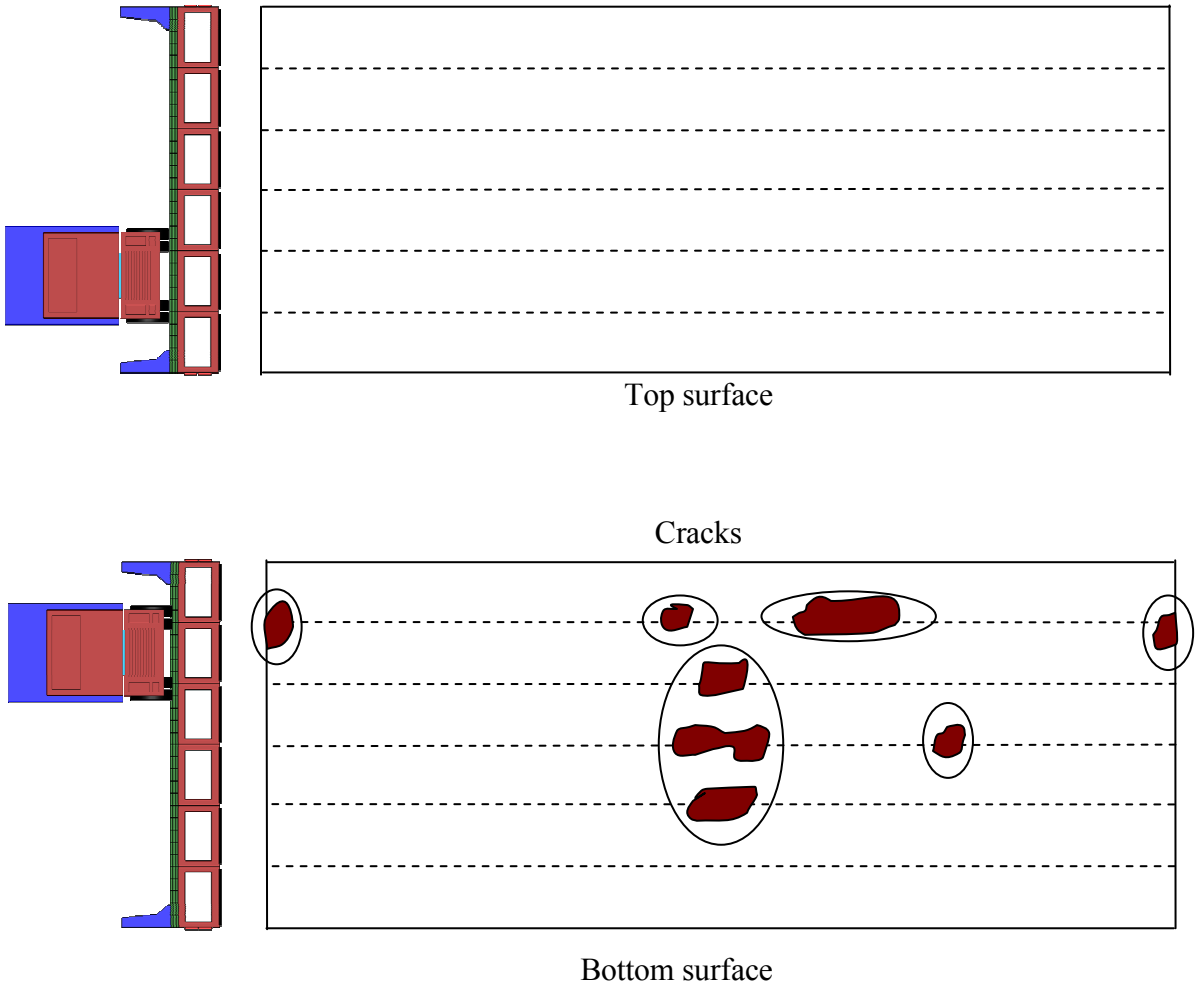

Figure 4.2-16 Crack development in slab after applying AASHTO-HS 25 truck.

Diaphragms arrangement:

1 @ each end of beam	TPT= 104,500 lb/diaphragm
2 @ quarter points	TPT= 104,500 lb/diaphragm
1 @ center of span	TPT= 104,500 lb/diaphragm

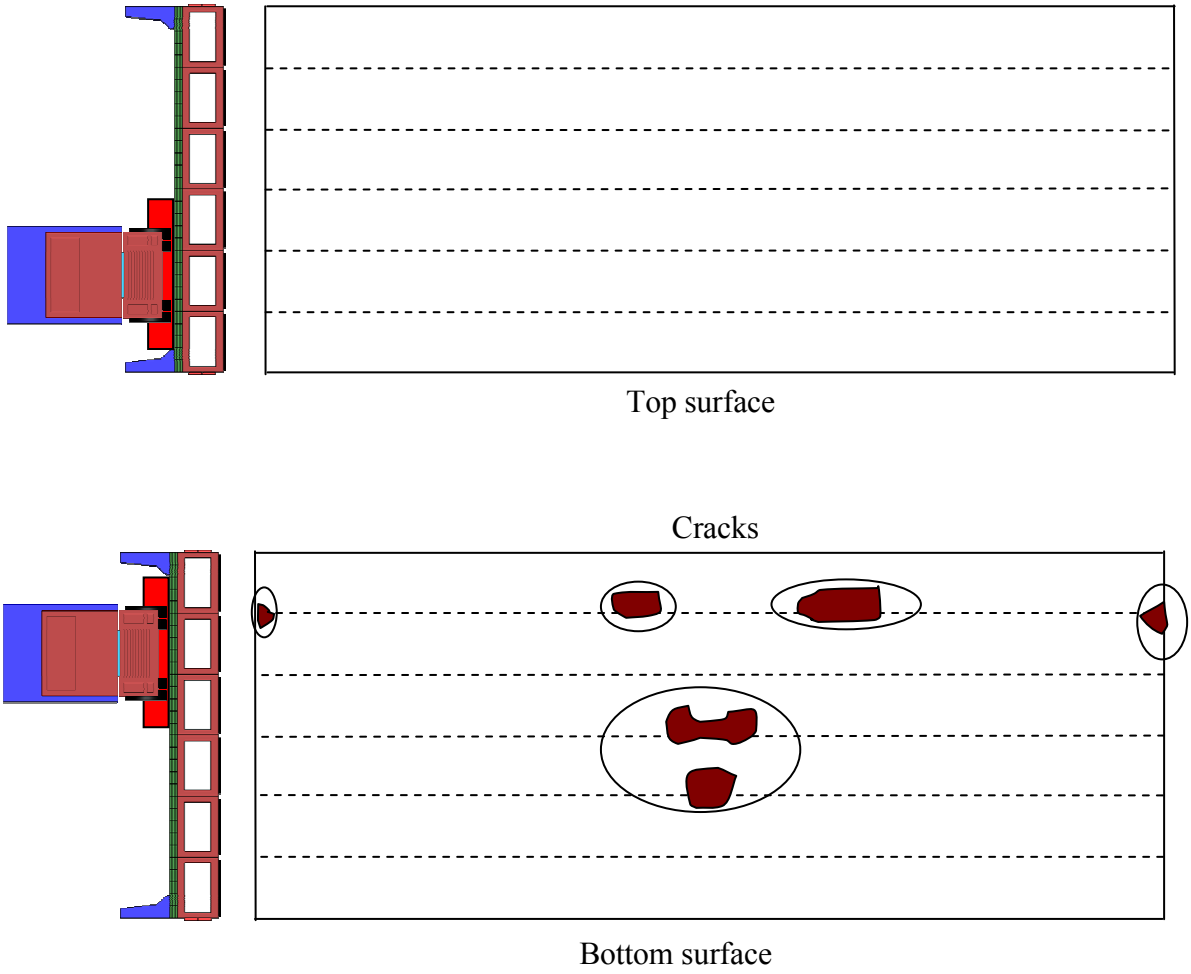

Figure 4.2-17 Crack development in slab after applying AASHTO HL-93 truck.

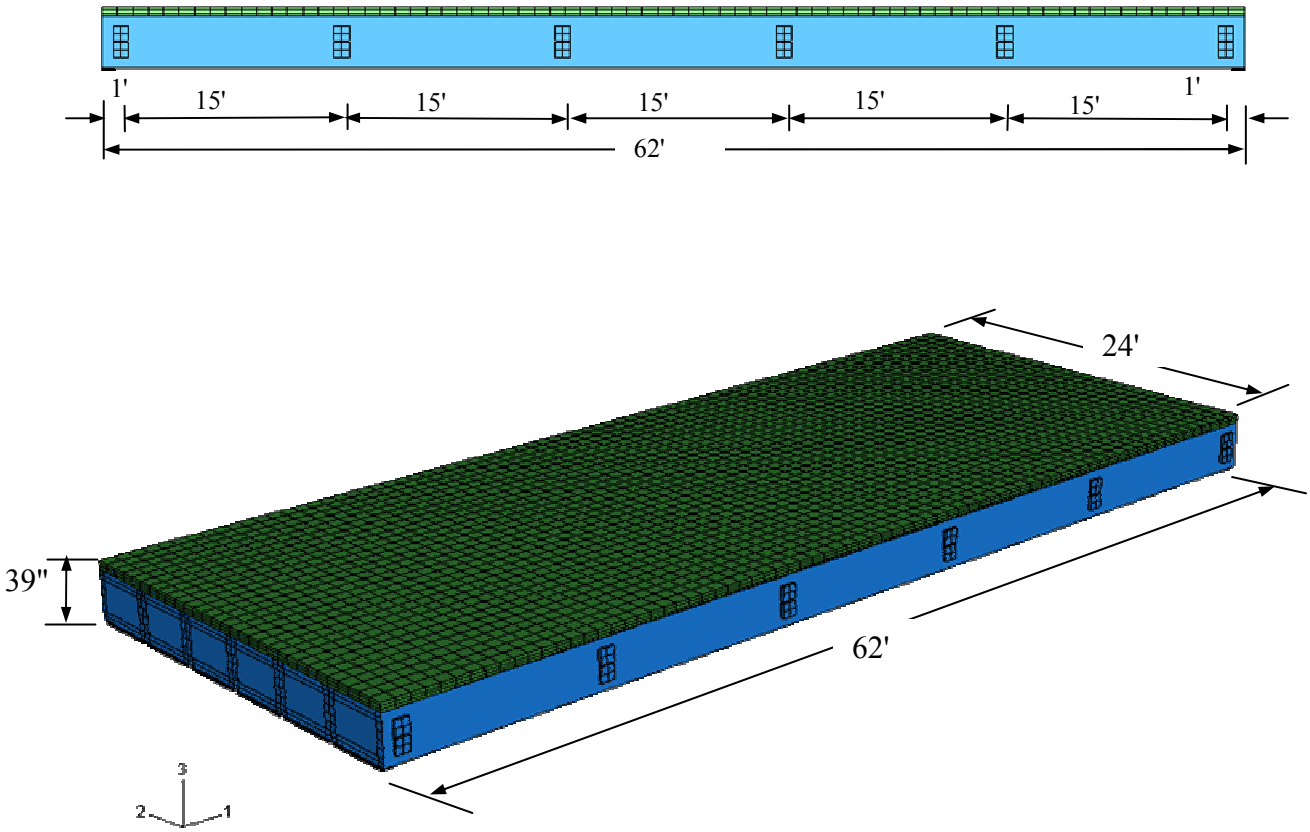

Figure 4.2-18 Assembly for modified 62 ft span bridge model.

Table 4.2-2 Maximum principal stress in the deck slab of 62 ft span bridge model under service loads.

Model	No. of Diaphragms	TPT Force lb/diaphragm	MP Positive Gradient (psi)	MP LL+ IM (psi)	
				HS-25 truck	HL-93 load
Span = 62 ft Width = 24 ft	5	104,000	265	N/A (cracks)	N/A (cracks)
	5	150,000	250	N/A (cracks)	N/A (cracks)
	5	150,000/200,000	241	299	291
	6	150,000	233	306	287

- MP: Maximum principal stresses
- LL: Live load
- IM: Impact allowances
- N/A: Not available

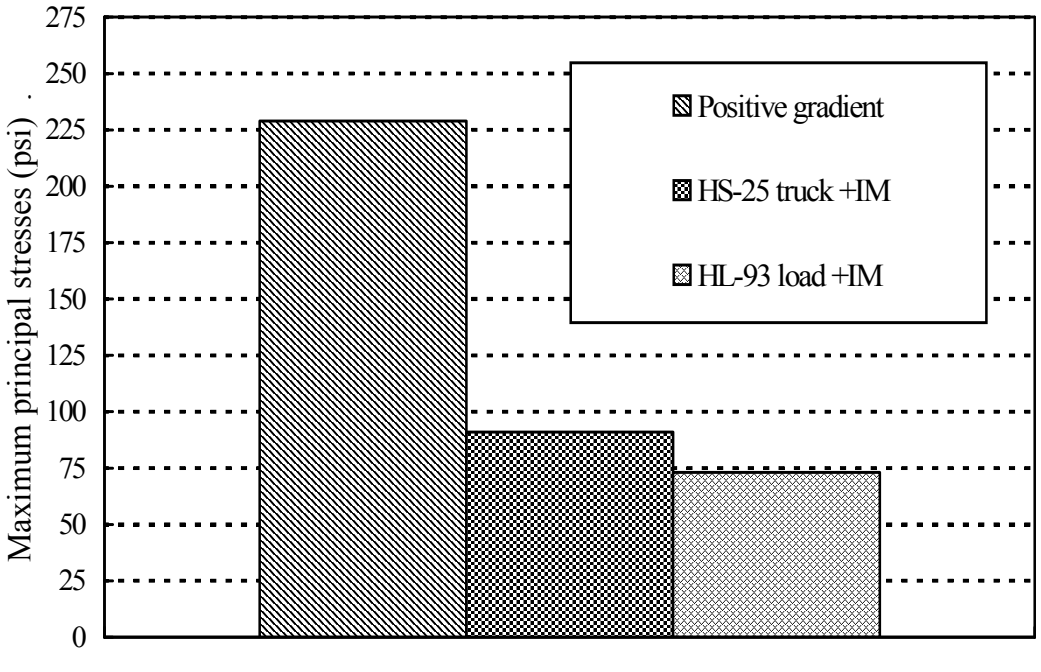

Figure 4.2-19 Service loads contribution in deck slab principal stresses (Case of six diaphragms, TPT = 150,000 lb/diaphragm).

4.2.4.3 100 ft Span Bridge Model

This FE model simulated a bridge with a span of 100 ft and width of 24 ft; yet, only half of the span was modeled and symmetry conditions were assumed across the mid-section of the span. Because of symmetry, it was not practical to apply AASHTO HS-25 truck load, non symmetric load, on a half model. Instead, an equivalent AASHTO HS-20 lane load, with concentrated load, was applied as a live load.

For 100 ft span, the truck load (not the lane load) governs the flexural design; so, a specific ratio was used to transform the lane load effect into its equivalent of the truck load. The ratio was the same as the ratio between the moment induced by AASHTO HS-25 truck load and that induced by AASHTO HS-20 lane load, which was found to be: ($M_{truck} = 1.5M_{lane}$).

For AASHTO HL-93 loading, the tandem load was used along with the lane load instead of using the truck load (because of the assumed symmetry conditions in the FE model). A transformation ratio was used to transform the tandem load effect into its equivalent of the HS-20 truck load; this ratio was found to be: ($M_{truck} = 1.27M_{tandem}$). By using these ratios, it was possible to keep the same analysis philosophy of establishing an appropriate TPT arrangement capable of connecting the box-beams to support AASHTO HS-25 truck or AASHTO HL-93 load without developing cracks in the deck slab.

The first model was provided with a TPT arrangement that conformed to MDOT Specifications (2006), which require six diaphragms for this span (Figure 4.2-20); two diaphragms at the ends, two at the quarter-spans, and two at the center (11 ft apart). To satisfy the flexural requirements, a box-beam of depth of 39 in. was used for this span; accordingly, two transverse strands were provided at each diaphragm. Each transverse strand was post-tensioned with a force of 52,250 lb (total of 104,500 lb/diaphragm).

Analysis and discussion

The analysis was performed according to the general sequence by applying: first, longitudinal prestressing forces and box-beams dead load; second, first stage of TPT force; third, slab dead load; fourth, second stage of TPT force; fifth, time dependent losses in addition to the superimposed dead loads; sixth, positive temperature gradient, and finally, equivalent AASHTO HS-25 truck load or AASHTO HL-93 load. By applying either the equivalent

AASHTO HS-25 truck load or equivalent AASHTO HL-93, the deck slab experienced longitudinal cracks between the box-beams (Figure 4.2-21 and Figure 4.2-22).

The first strategy applied to eliminate the longitudinal cracking was to increase the transverse post-tensioning force per diaphragm. The transverse post-tensioning force was first increased to 150,000 lb/diaphragm while maintaining the same number of diaphragms.

By applying equivalent AASHTO HS-25 truck load or equivalent AASHTO HL-93 load, the slab experienced small cracks in the bottom surface. The cracks were mainly concentrated at the mid-span over the intermediate diaphragm. Therefore, there were two options to eliminate the cracks, either increasing the TPT force per diaphragm or increasing the number of diaphragms. Generally, increasing number of diaphragms had more influence on crack control than increasing the TPT force. Therefore, the final trial was to increase the number of diaphragms from six to seven. The seven diaphragms were equally spaced, as shown in Figure 4.2-23.

After applying a positive temperature gradient, the slab experienced tensile stresses of 234 psi at the bottom surface. These tensile stresses increased to 353 psi when adding equivalent AASHTO HS-25 truck load, and to 351 psi when adding equivalent AASHTO HL-93. The slab finally did not exhibit any cracks under service loads. Table 4.2-3 presents a summary for the aforementioned investigation and Figure 4.2-24 shows the contribution of each load type to the principal stresses in the deck slab.

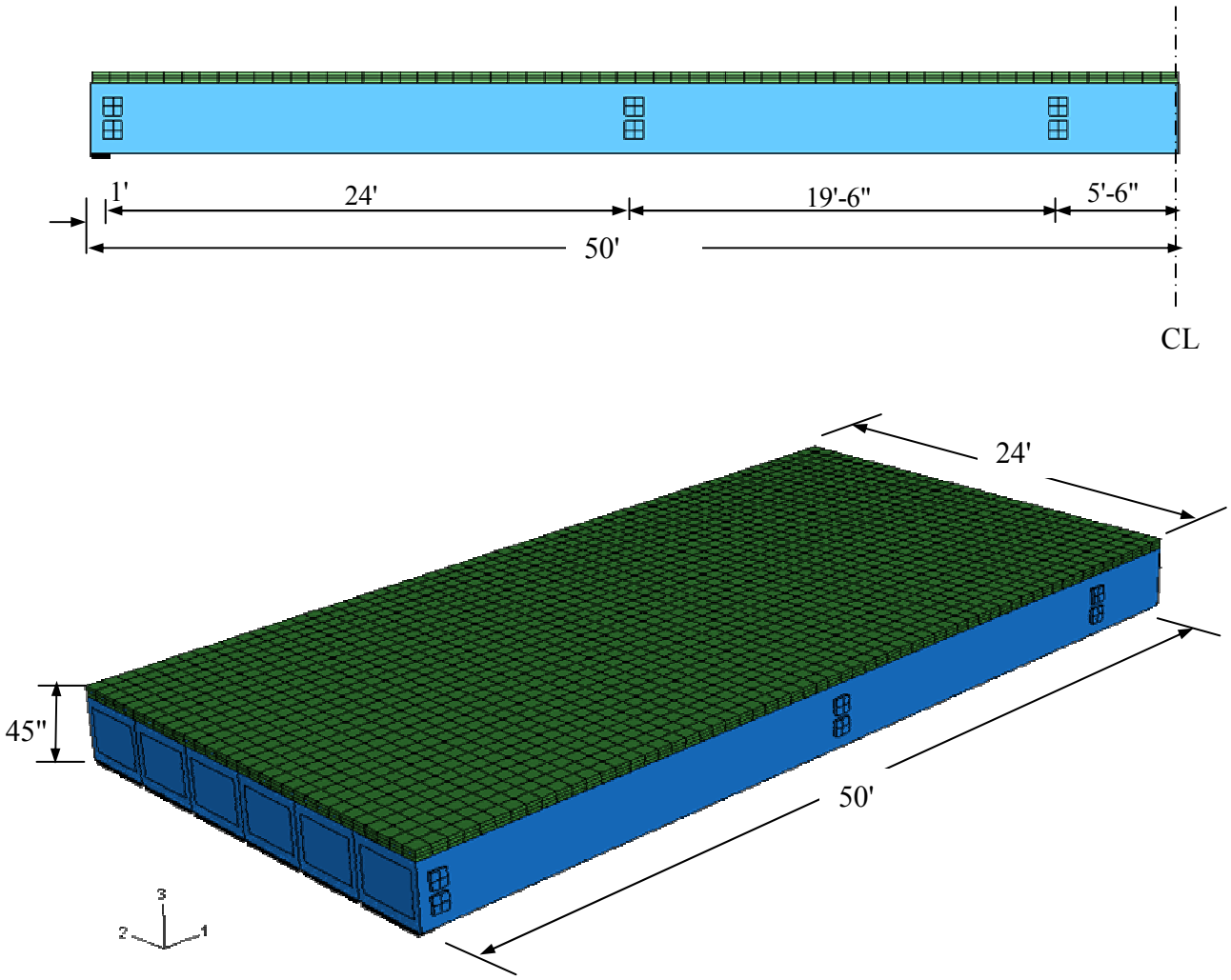

Figure 4.2-20 Assembly for 100 ft span bridge model.

Diaphragms arrangement:

1 @ each end of beam	TPT= 104,500 lb/diaphragm
2 @ quarter points	TPT= 104,500 lb/diaphragm
2 @ center of span (11 ft apart)	TPT= 104,500 lb/diaphragm

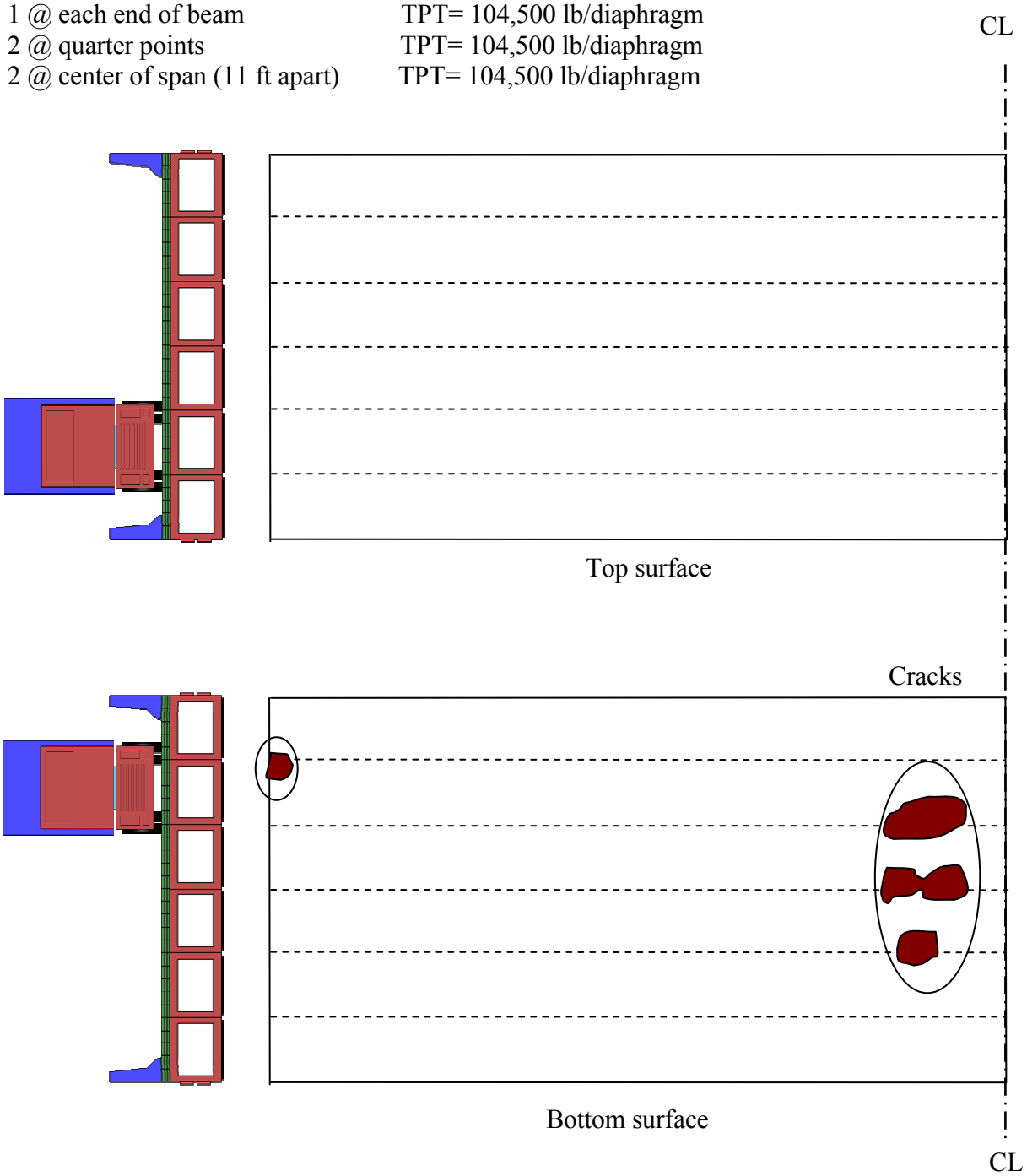

Figure 4.2-21 Crack development in the slab after applying equivalent AASHTO HS-25 truck.

Diaphragms arrangement:

1 @ each end of beam	TPT= 104,500 lb/diaphragm
2 @ quarter points	TPT= 104,500 lb/diaphragm
2 @ center of span (11 ft apart)	TPT= 104,500 lb/diaphragm

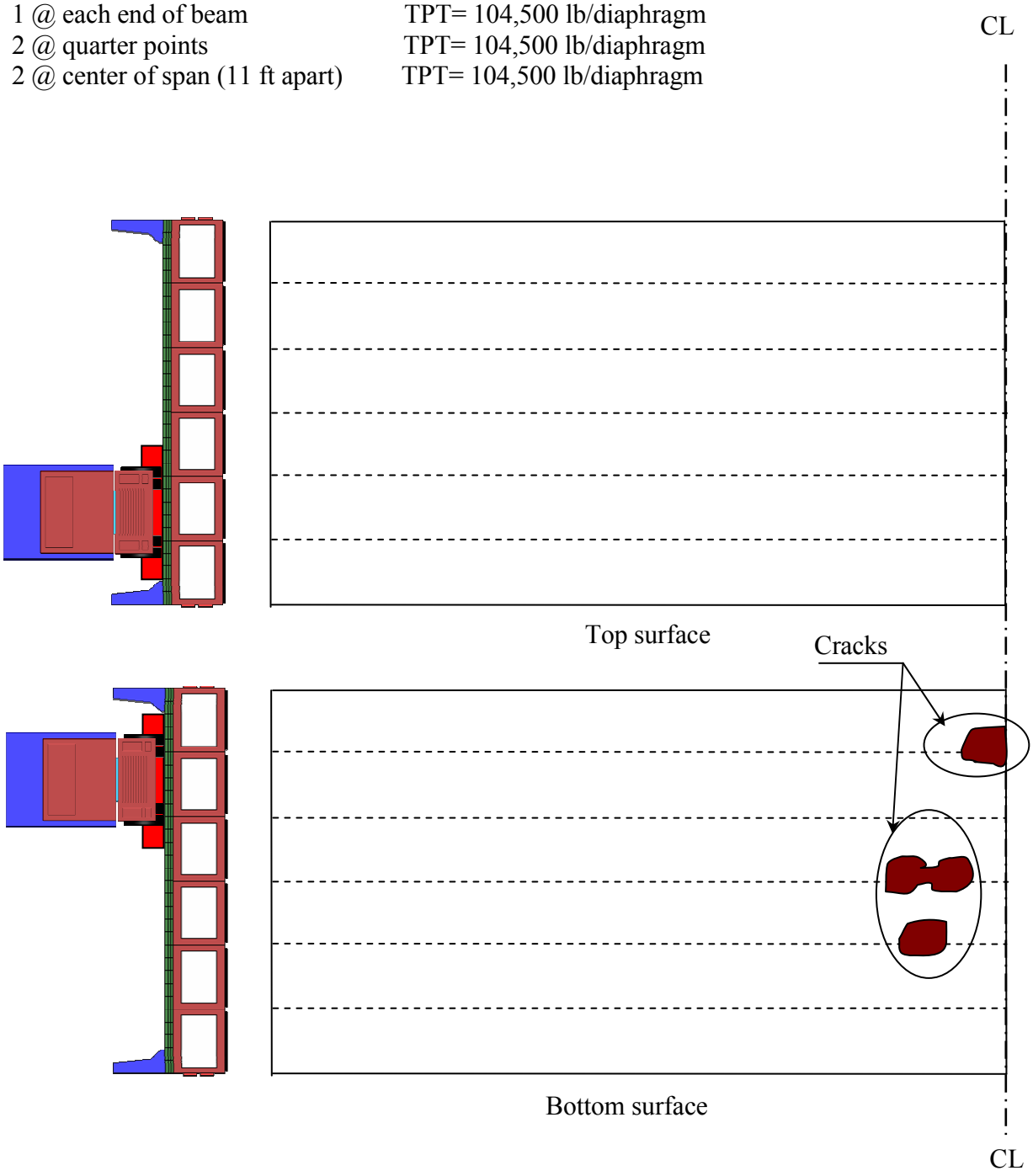

Figure 4.2-22 Crack development in the slab after applying equivalent AASHTO HL-93 load.

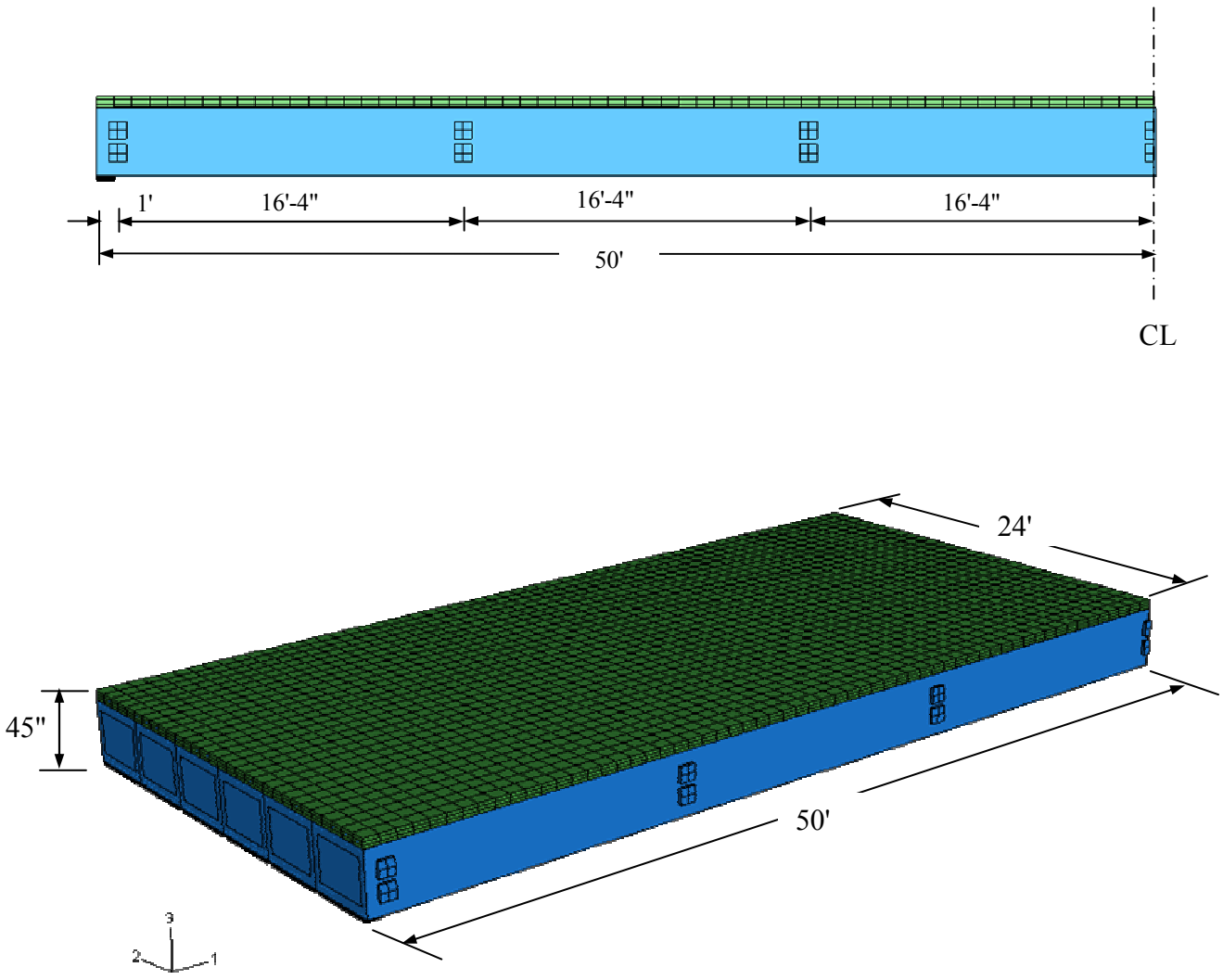

Figure 4.2-23 Assembly for modified 100 ft span bridge model.

Table 4.2-3 Maximum principal stress in the deck slab of 100 ft span bridge model under service loads.

Model	No. of Diaphragms	TPT Force lb/diaphragm	MP Positive Gradient (psi)	MP LL+ IM (psi)	
				HS-25 truck	HL-93 load
Span = 100 ft Width = 24 ft	6	104,000	254	N/A (cracks)	N/A (cracks)
	6	150,000	247	N/A (cracks)	N/A (cracks)
	7	150,000	234	353	351

- MP: Maximum principal stresses
- LL: Live load
- IM: Impact allowances
- N/A: Not available

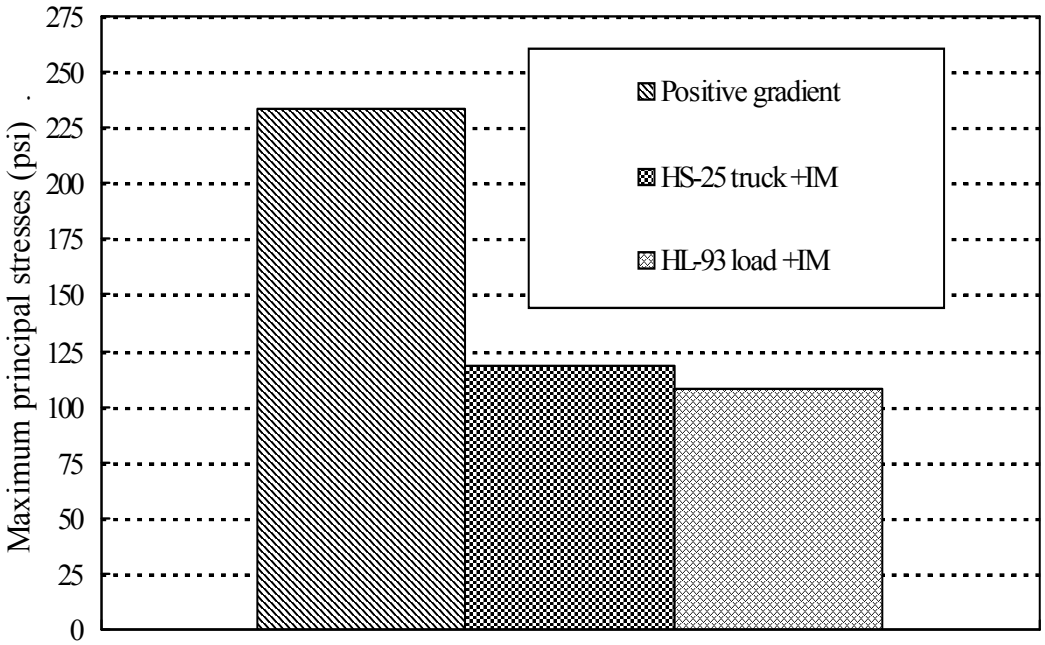

Figure 4.2-24 Service loads contribution in deck slab principal stresses (Case of seven diaphragms, TPT =150,000 lb/diaphragm).

4.2.4.4 124 ft Span Bridge Model

This FE model simulated a bridge with span of 124 ft and width of 24 ft. Half of the span was modeled, and equivalent loads were used to simulate the live loads. The ratio used to transfer the AASHTO HS-25 truck load effect to its equivalent of the lane load was $M_{truck} = 1.36 M_{lane}$. Similarly, the ratio used to transform the truck effect to the tandem effect in AASHTO HL-93 load was $M_{truck} = 1.30 M_{tadem}$.

The first model was provided with a TPT arrangement that conformed to the MDOT Specifications (2006), which require seven diaphragms for this span (Figure 4.2-25); two diaphragms at the ends and five equally spaced diaphragms in-between. To satisfy the flexural requirements, the box-beam depth was determined to be 54 in. Two transverse strands were provided per diaphragm, with each transverse strand prestressed with a force equal to 52,250 lb (total of 104,500 lb/diaphragm).

Applying the positive temperature gradient increased the longitudinal compressive stresses in the slab top and bottom surfaces. In the transverse direction, the compressive stresses increased to 610 psi at the slab ends, while the majority of the slab experienced compressive stresses in the range of 272 and 347 psi. At the same time, high transverse tensile stresses of about 251 psi developed in the slab bottom surface. Similarly, the maximum principal stresses increased to 285 psi (tension) at the slab bottom surface, while the top surface experienced maximum principal stresses averaging zero psi. The deck slab experienced cracks, as shown in Figure 4.2-26 and Figure 4.2-27 after applying equivalent AASHTO HS-25 truck load and equivalent AASHTO HL-93 load, respectively.

To prevent the crack development, the TPT force level was increased from 104,500 lb/diaphragm to 150,000 lb/diaphragm, without changing the number of diaphragms or their arrangement. No cracks developed after applying the positive temperature gradient; yet, the cracks developed when applying live loads.

Without changing the diaphragms number, a TPT force equal to 200,000 lb/diaphragm was applied. Increasing the TPT level did not eliminate the development of the deck cracks and it was considered impractical to apply TPT force larger than 200,000 lb/diaphragm. Therefore, the remaining option was to increase the number of diaphragms to nine instead of seven

(Figure 4.2-28); two at the ends and seven equally spaced in-between. The new arrangement was examined first with a TPT force equal to 100,000 lb/diaphragm.

When applying equivalent AASHTO HS-25 truck, few cracks developed in the slab bottom surface. Similar cracks developed also when applying AASHTO HL-93 load. However, from the stress distribution and the crack pattern, it was evident that some increase in the TPT force would eliminate the crack development. Therefore, the final trial was to apply TPT force of 150,000 lb/diaphragm.

By applying equivalent AASHTO HS-25 truck load, the maximum principal stresses reached 351, and the slab did not crack. The slab did not experience cracks under equivalent AASHTO HL-93 load either. Accordingly, by applying post-tensioning force of 150,000 lb/diaphragm at nine diaphragms, the model was able to support equivalent AASHTO HS-25 truck or AASHTO HL-93 loads along with 100% of positive temperature gradient without developing any longitudinal cracks in the deck slab. Hence, this TPT arrangement was considered sufficient. A summary for the aforementioned investigation is presented in Table 4.2-4. In addition, the contribution of each load type in the developed maximum principal stresses in the deck slab is shown in Figure 4.2-29.

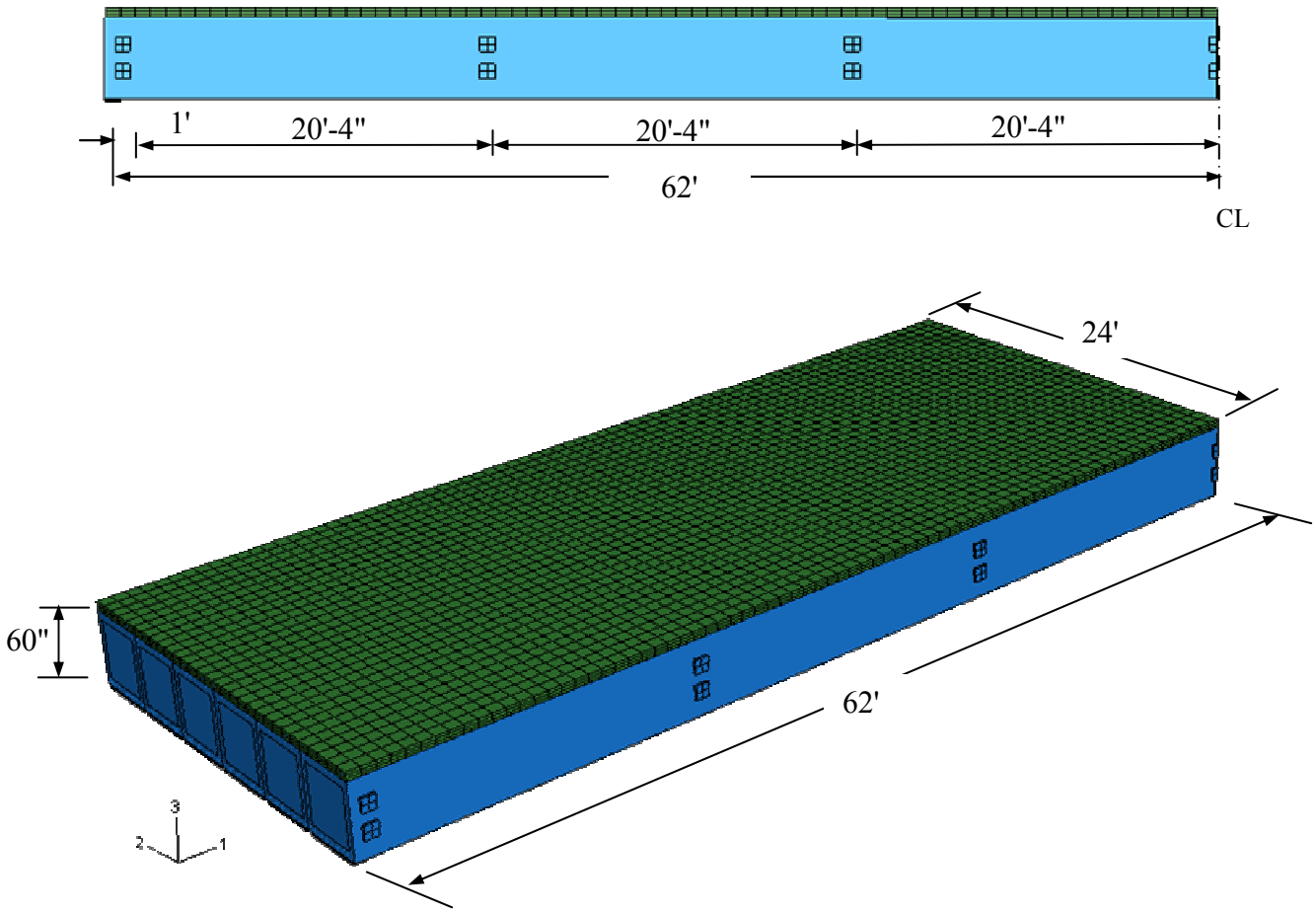

Figure 4.2-25 Assembly of 124 ft span bridge model.

Diaphragms arrangement:

1 @ each end of beam TPT= 104,500 lb/diaphragm
5 @ equally spaced in-between TPT= 104,500 lb/diaphragm

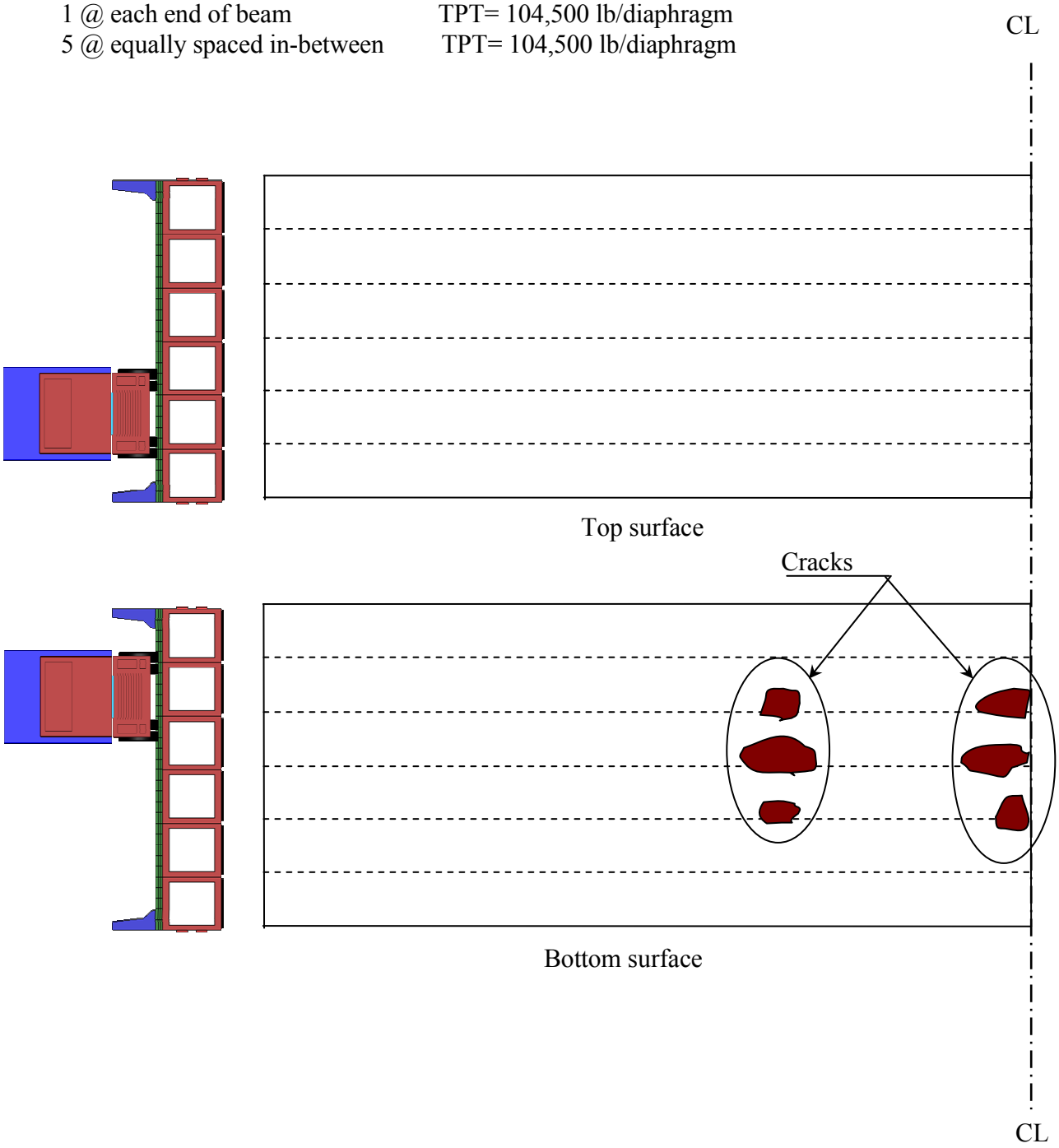

Figure 4.2-26 Crack development in the slab after applying equivalent AASHTO HS-25 truck.

Diaphragms arrangement:

1 @ each end of beam TPT= 104,500 lb/diaphragm
5 @ equally spaced in-between TPT= 104,500 lb/diaphragm

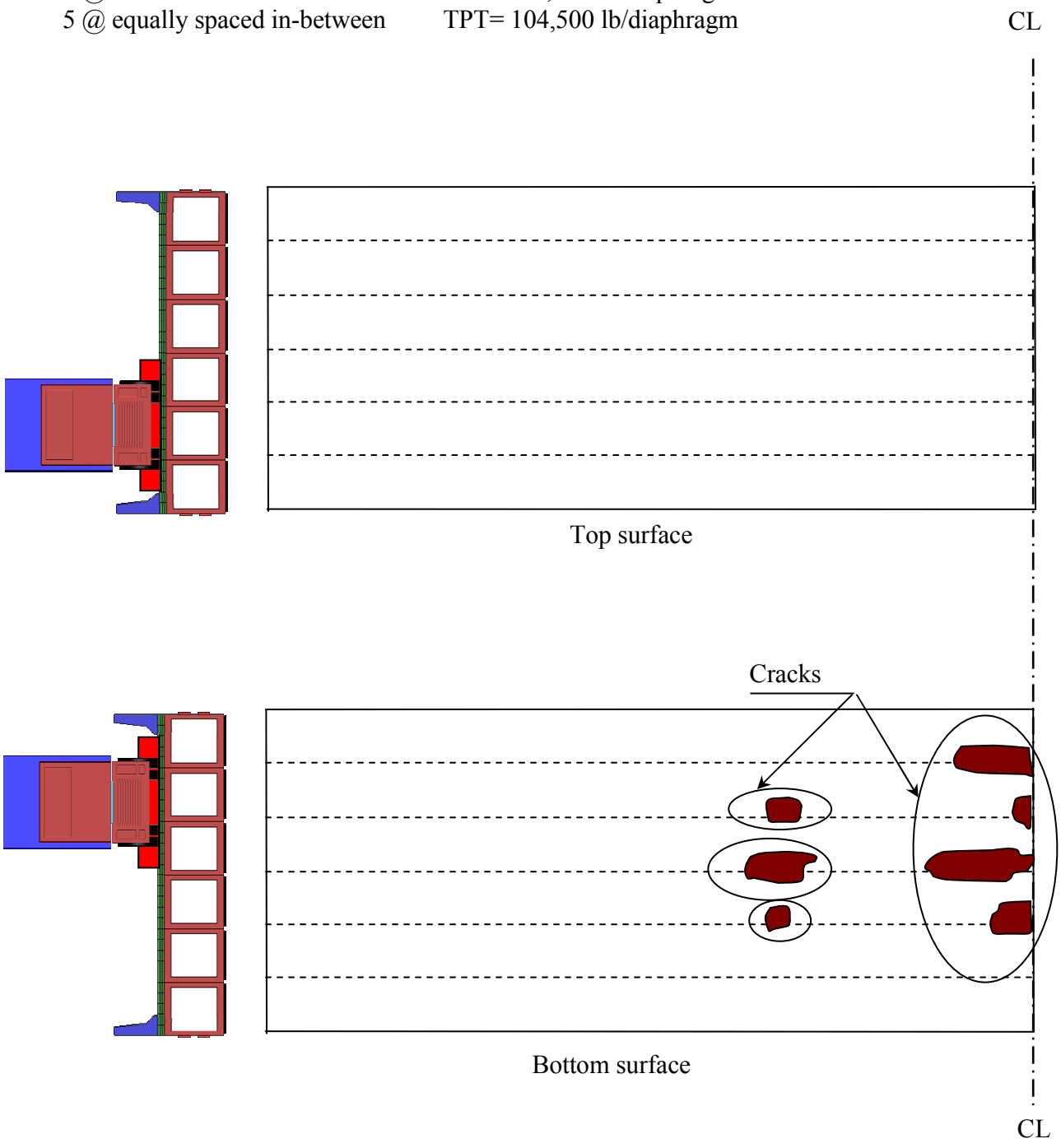

Figure 4.2-27 Crack development in the slab after applying equivalent AASHTO HL-93 load.

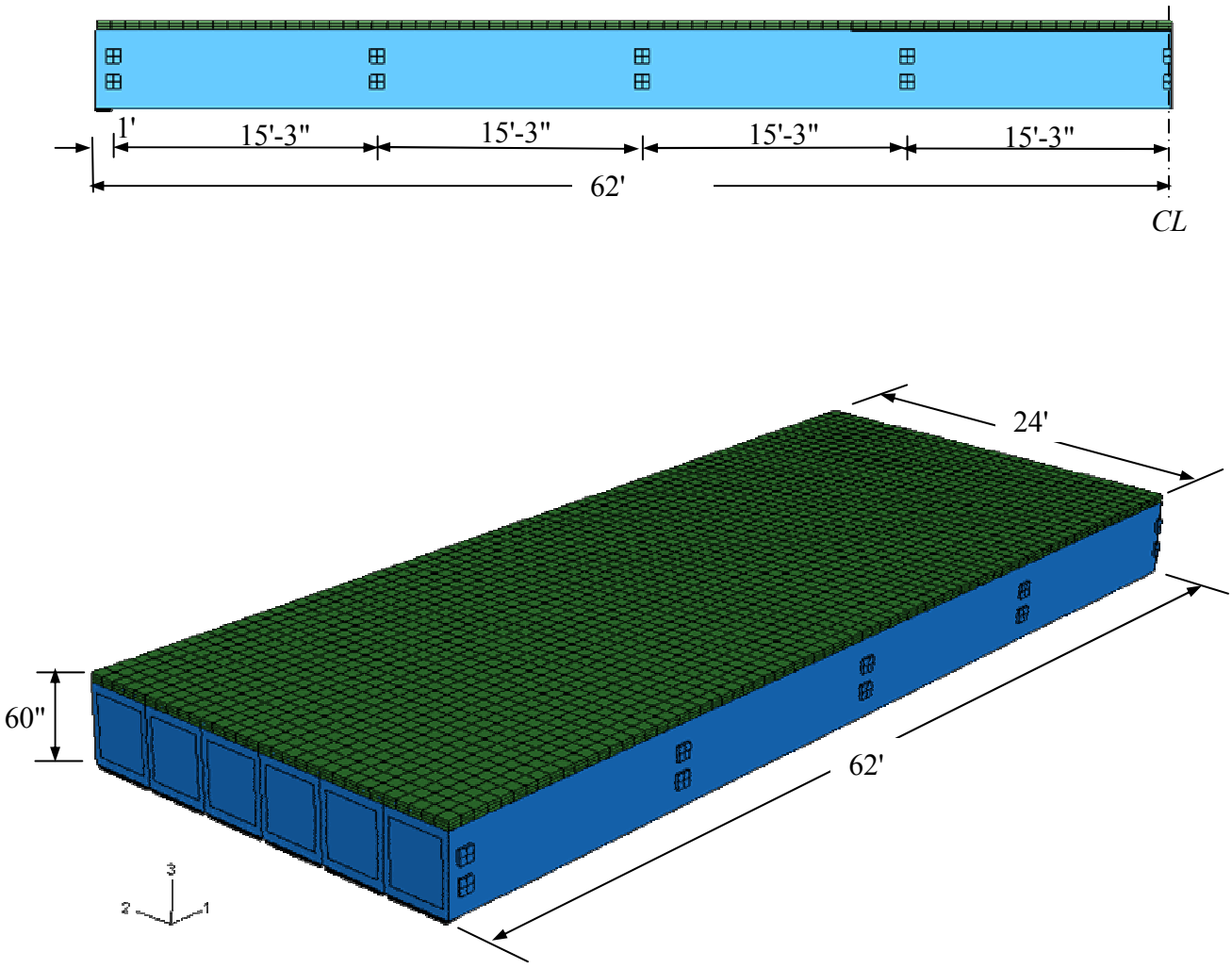

Figure 4.2-28 Modified assembly of 124 ft span bridge model.

Table 4.2-4 Maximum principal stresses in the deck slab of 124 ft span bridge model under service loads.

Model	No. of Diaphragms	TPT Force lb/diaphragm	MP Positive Gradient (psi)	MP LL+ IM (psi)	
				HS-25 truck	HL-93 load
Span = 124 ft Width = 24 ft	7	104,000	285	N/A (cracks)	N/A (cracks)
	7	150,000	277	N/A (cracks)	N/A (cracks)
	7	200,000	271	N/A (cracks)	N/A (cracks)
	9	100,000	270	N/A (cracks)	N/A (cracks)
	9	150,000	260	351	350

- MP: Maximum principal stresses
- LL: Live load
- IM: Impact allowances
- N/A: Not available

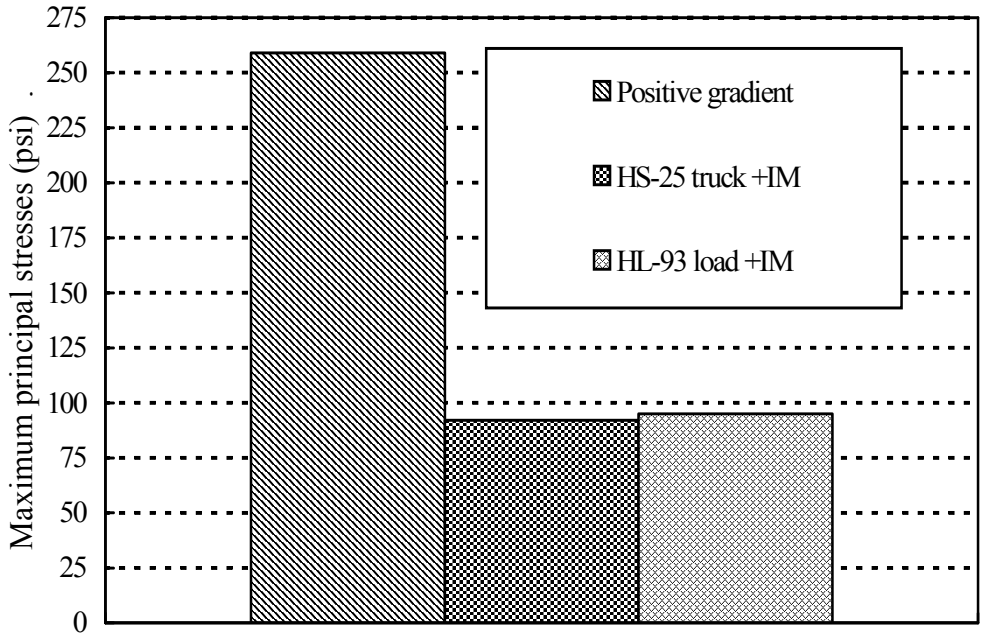

Figure 4.2-29 Service loads contribution in deck slab principal stresses (Case of seven diaphragms, TPT = 150,000 lb/diaphragm).

4.2.4.5 Effect of Deck Slab Concrete Strength on the TPT Arrangement

The previous analysis was performed assuming some deterioration in the concrete material in the deck slab and the concrete strength was reduced to 3,000 psi. However, the models were reanalyzed for concrete strength of 4,000 and 5,000 psi to establish the TPT arrangement for the cases of recently-constructed and special-quality deck slabs, respectively. The analysis revealed that the effect of the strength of the concrete in the deck slab on the adequate number of diaphragms is insignificant. On the other hand, the level of the TPT force can be reduced if higher concrete strength is reached in the deck slab. In summary, regardless of the span length:

- In case of using concrete of strength of 4,000 psi in the deck slab, the TPT force would be adjusted downward from 150,000 lb/diaphragm to 120,000 lb/diaphragm.
- In case of using concrete of strength of 5,000 psi in the deck slab, the TPT force would be adjusted downward to 100,000 lb/diaphragm.

The analysis and loading steps were the same as what was discussed earlier in this chapter; therefore, a detailed discussion is not provided, but the maximum principal stresses due to service loads in the deck slab are provided in Table 4.2-5. The detailed results for this case of analysis are provided in Bebawy (2007).

It should be noted that the analysis could have been performed with a reduced number of diaphragms rather than a reduced TPT force level to take into account the higher concrete strength in the deck slab. However, reducing the number of diaphragms resulted in developing some longitudinal deck cracks in some of the bridge models.

Table 4.2-5 Maximum principal stresses in the deck slab for bridge models with different deck slab concrete strengths.

Span (ft)	No.of Diaphragms	TPT Force lb/diaphragm	MP +ve TG (psi)	MP LL+ IM (psi)	
				HS-25 truck	HL-93 load
Concrete properties: $f'_c = 4{,}000$ psi, $f_r = 460$ psi, $E = 3.83 \times 10^6$ psi					
50	5	120,000	343	423	411
62	6	120,000	360	445	440
100	7	120,000	365	449	456
124	9	120,000	370	451	459
Concrete properties: $f'_c = 5{,}000$ psi, $f_r = 514$ psi, $E = 4.30 \times 10^6$ psi					
50	5	100,000	407	501	493
62	6	100,000	431	508	506
100	7	100,000	437	510	509
124	9	100,000	440	513	515

- MP: Maximum principal stresses
- LL: Live load
- IM: Impact allowances

4.2.5 Bridge Models Constructed Using 36 in. Wide Box-Beams

Using 36 in. wide box-beams, another set of FE models were generated for bridges of spans of 50, 62, and 100 ft and width of 24 ft. The fourth span, of 124 ft, could not be generated using 36 in. wide box-beams because spans greater than 100 ft require deep box-beams, which are not available in a width of 36 in. Eight box-beams were used to generate a bridge of a width of 24 ft, as shown in Figure 4.2-30. In addition, the concrete in the deck slab was assumed to have a strength of 4,000 psi, representative of a recently-constructed deck slab. As changing the box-beam width from 48 to 36 in. shall have the same influence on the analysis regardless of the strength of the concrete in the deck slab, the cases of deteriorated deck slab and special-quality deck slab were not simulated.

The analysis herein was performed by first generating FE bridge models with a number of diaphragms and TPT force similar to that recommended for bridges composed of 48 in. wide box-beams. Then, the number of diaphragms was readjusted without changing the TPT force for the models that experienced cracks in the deck slab.

4.2.5.1 50 ft Span Bridge Model

This model experienced no cracks in the deck slab under service loads when providing five diaphragms with each diaphragm post-tensioned with TPT force of 120,000 lb (Figure 4.2-30). The maximum principal stresses reached 358 psi after applying 100% of positive temperature gradient. The stresses then increased to 415 psi after applying AASHTO HL-93 load. Figure 4.2-31 shows the crack map in the deck slab bottom surface after applying AASHTO HL-93 load. Furthermore, Figure 4.2-32 shows the cracks expected if the bridge is overloaded by applying 120% of the load.

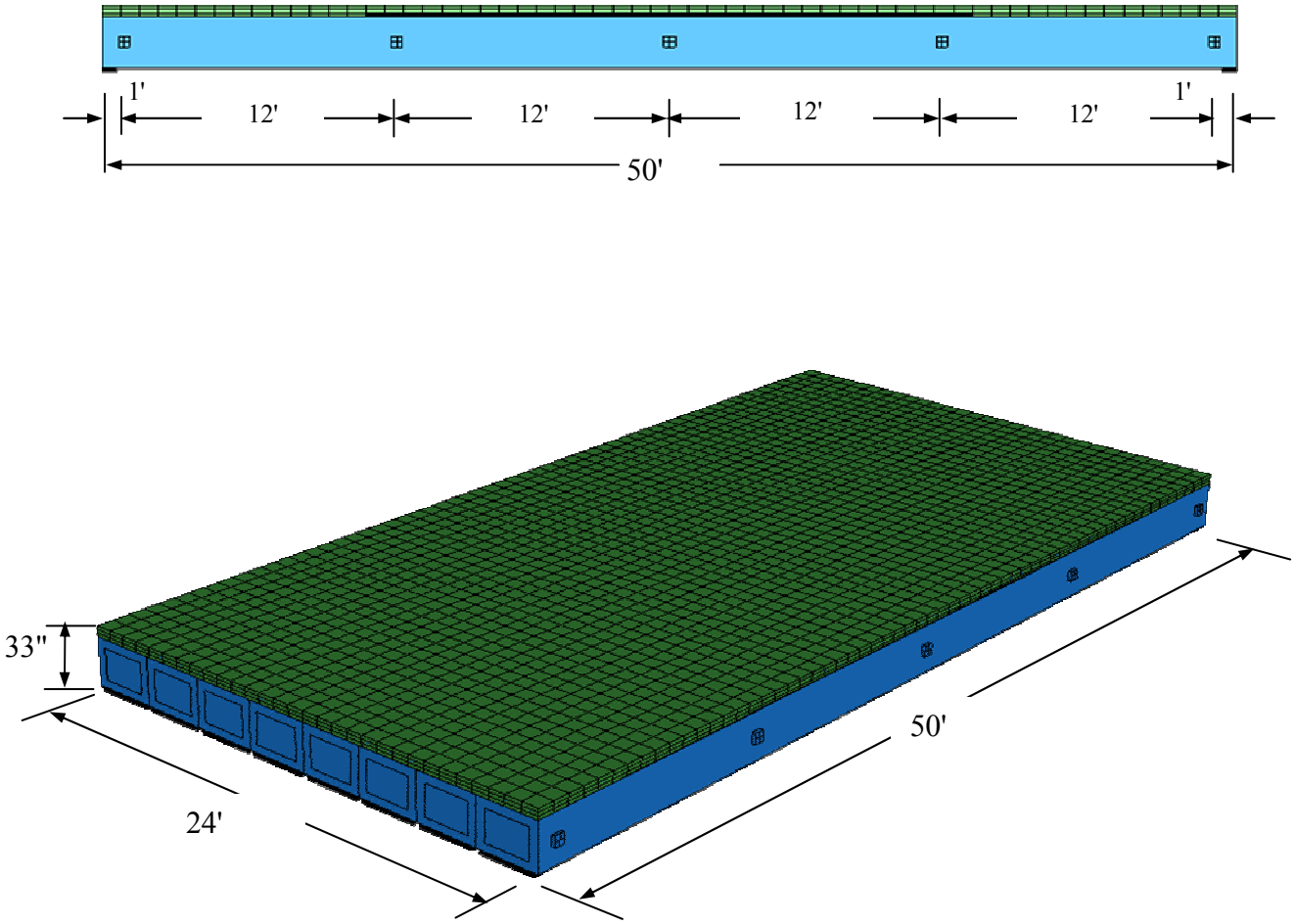

Figure 4.2-30 50 ft span bridge model constructed using 36 in. wide box-beams.

Diaphragms arrangement:

1 @ each end of beam	TPT= 120,000 lb/diaphragm
3 equally spaced in-between	TPT= 120,000 lb/diaphragm

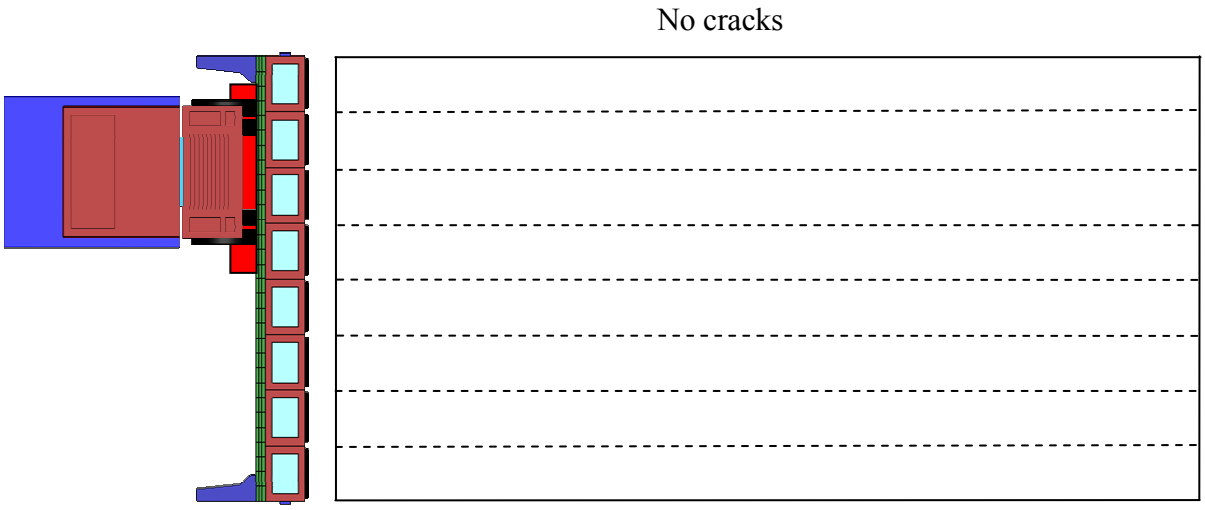

Figure 4.2-31 Crack development in the slab bottom surface after applying AASHTO HL-93 load.

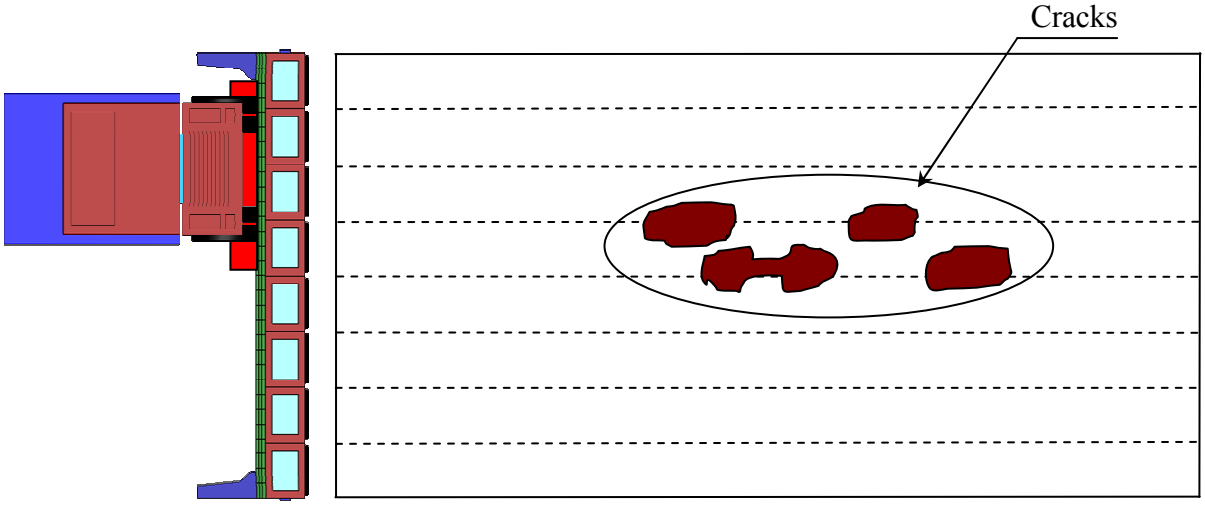

Figure 4.2-32 Crack development in the slab bottom surface after applying 120% of AASHTO HL-93 load.

4.2.5.2 62 ft Span Bridge Model

This bridge model was provided with six diaphragms with each diaphragm post-tensioned with TPT force of 120,000 lb (Figure 4.2-33). The deck slab did not experience any cracks after applying positive temperature gradient and AASHTO HL-93 load (Figure 4.2-34). The maximum principal stresses reached 410 psi when applying 100% of positive temperature gradient and 452 psi when applying AASHTO HL-93 load. However, when increasing the live load by 20% of the load, the deck slab experienced some cracks initiated from its bottom surface, as shown in Figure 4.2-35.

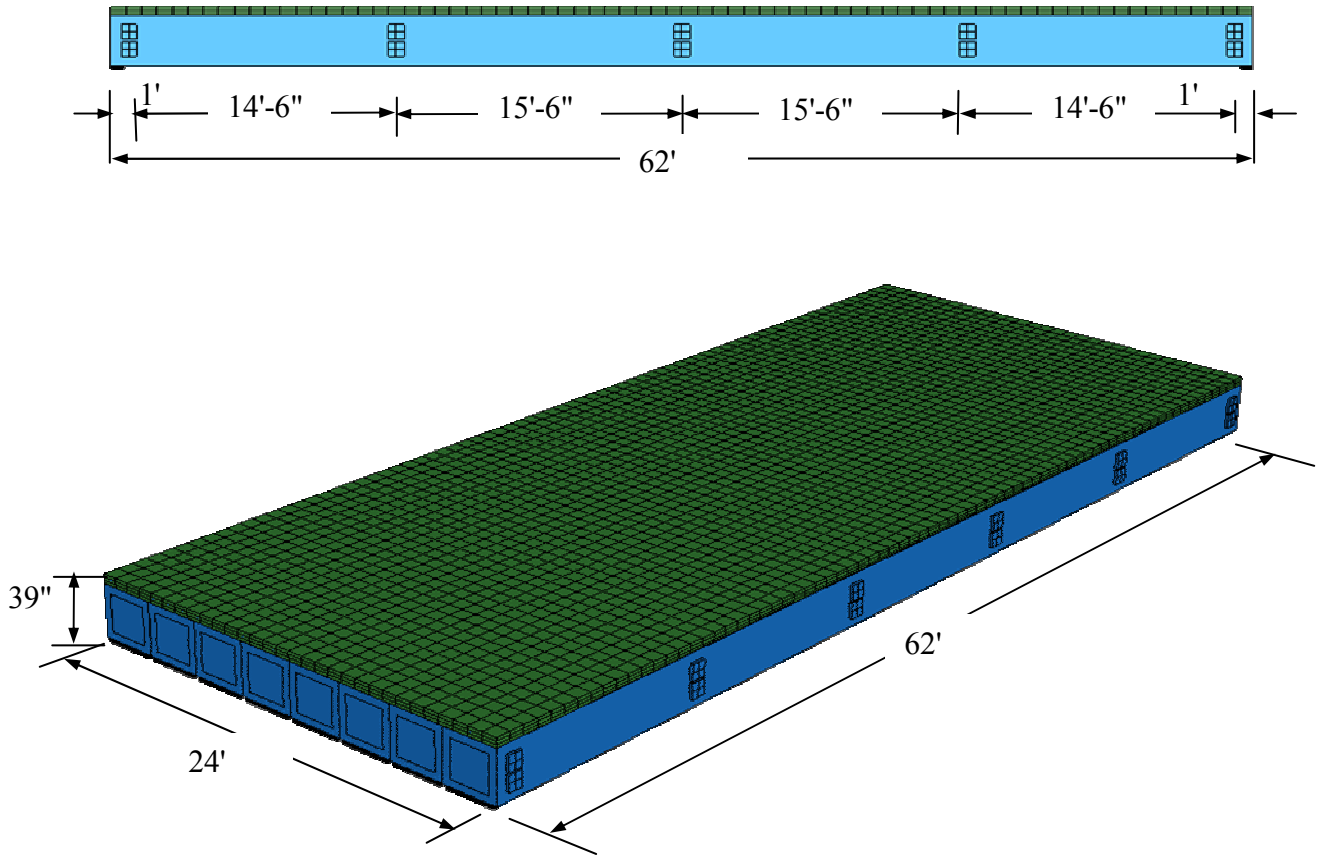

Figure 4.2-33 Assembly of 62 ft span bridge model constructed using 36 in. wide box-beams.

Diaphragms arrangement:

1 @ each end of beam	TPT= 120,000 lb/diaphragm
4 equally spaced in-between	TPT= 120,000 lb/diaphragm

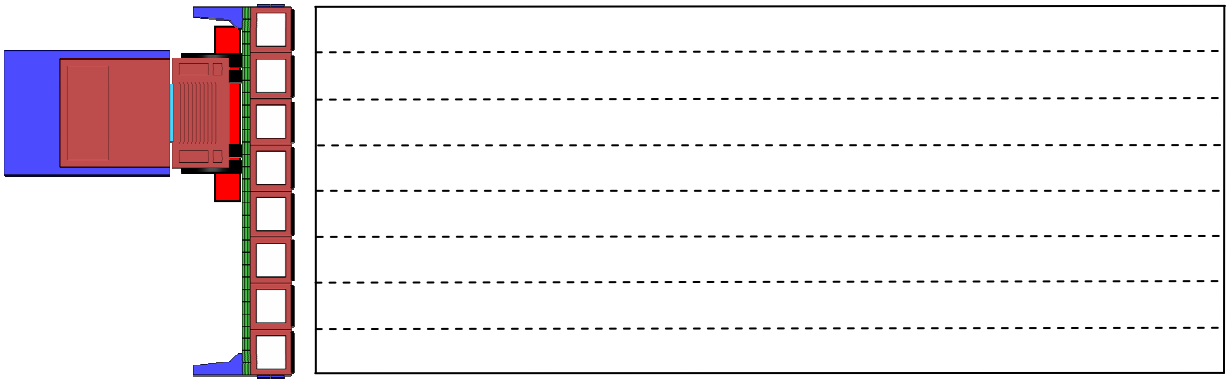

Figure 4.2-34 Crack development in the slab bottom surface after applying AASHTO HL-93 load.

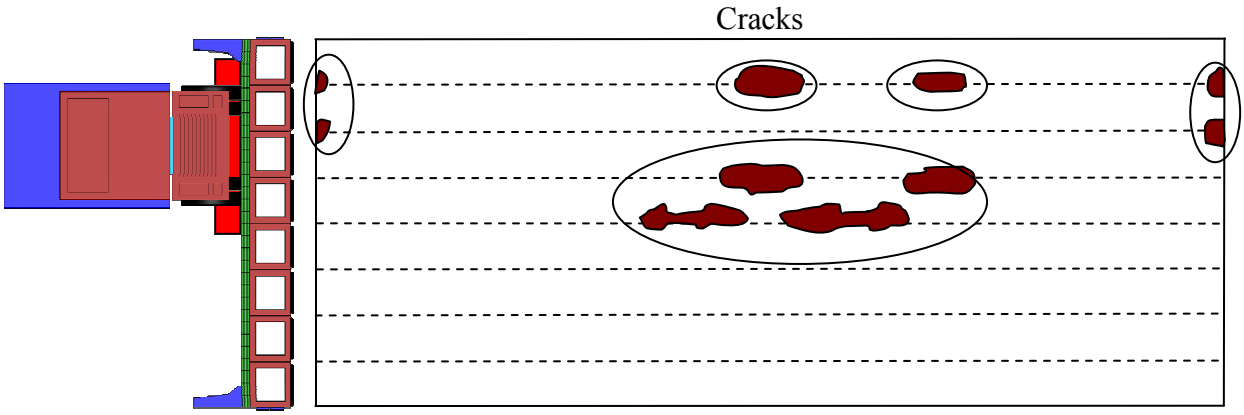

Figure 4.2-35 Crack development in the slab bottom surface after applying 120% of AASHTO HL-93 load.

4.2.5.3 100 ft Span Bridge Model

The analysis of 100 ft span bridge models constructed using 48 in. wide box-beams showed that this span required at least seven diaphragms. Therefore, the analysis herein was also conducted by providing seven diaphragms to the FE model (Figure 4.2-36). Each diaphragm was post-tensioned with a TPT force of 120,000 lb. After applying 100% of positive temperature gradient, the deck slab experienced tensile stresses up to 375 psi. However, the slab experienced longitudinal cracks over the shear-key locations, as shown in Figure 4.2-37 when adding the equivalent AASHTO HL-93 load. The bridge model, therefore, was provided with an additional diaphragm (Figure 4.2-38), and reanalyzed under the same loads. After applying 100% of positive temperature gradient, some areas in the deck slab bottom surface experienced tensile stresses of 355 psi. The stresses increased to 427 psi after applying AASHTO HL-93 load; the maximum stresses did not exceed the cracking strength of the concrete (460 psi); thus, the deck slab did not experience cracks, as shown in Figure 4.2-39. However, with additional 20% of the load, the slab would experience longitudinal cracks, as shown in Figure 4.2-40.

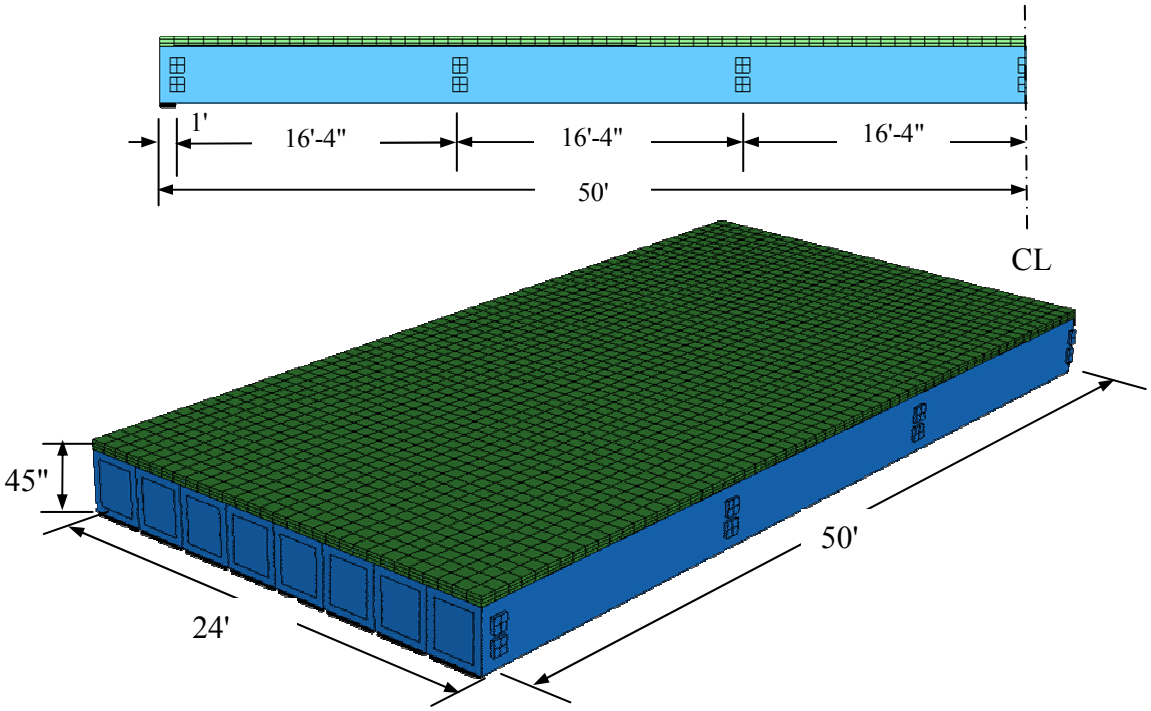

Figure 4.2-36 Assembly of 100 ft span bridge model constructed using 36 in. wide box-beams.

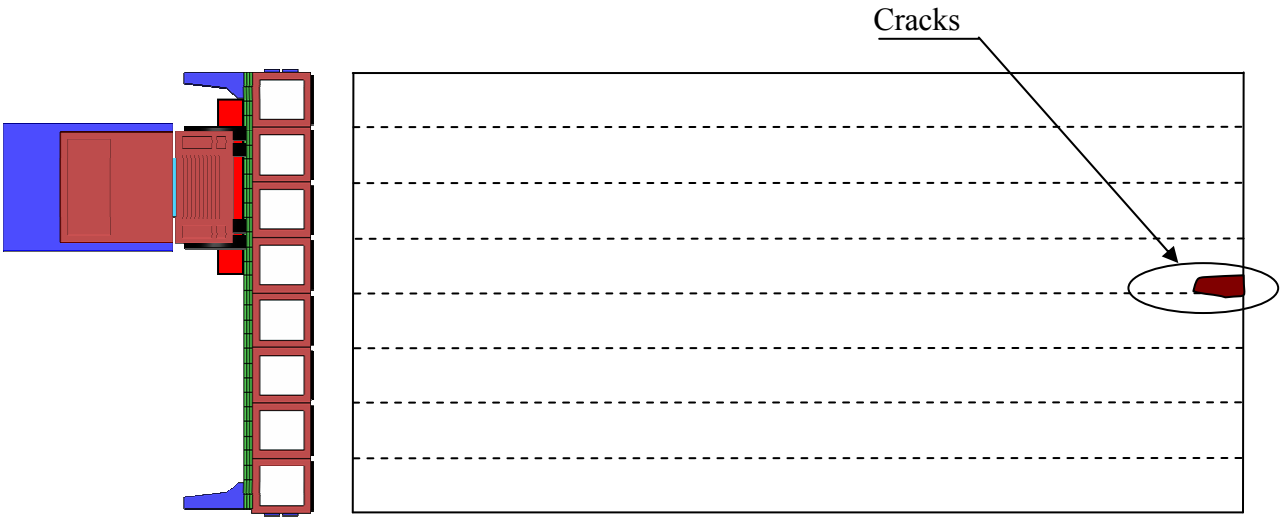

Figure 4.2-37 Crack development in the slab bottom surface after applying AASHTO HL-93 load.

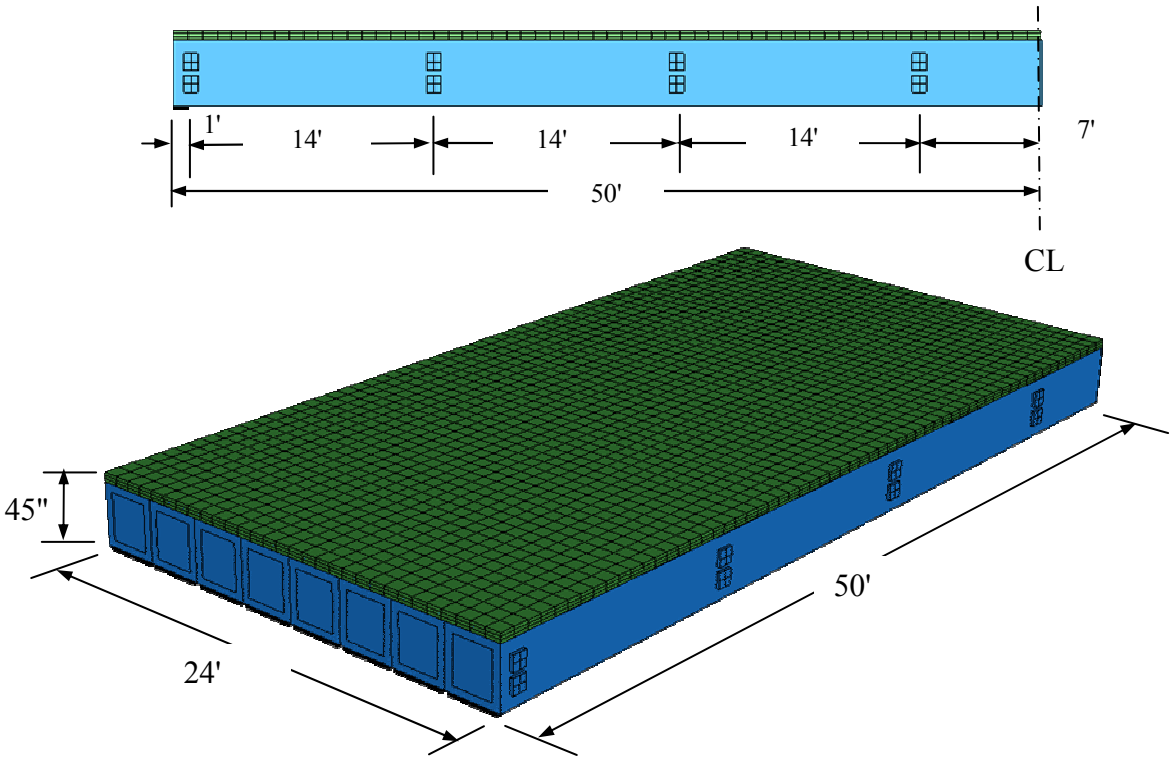

Figure 4.2-38 Modified assembly of 100 ft span bridge model constructed using 36 in. wide box-beams.

Diaphragms arrangement:

1 @ each end of beam	TPT= 120,000 lb/diaphragm
6 equally spaced in-between	TPT= 120,000 lb/diaphragm

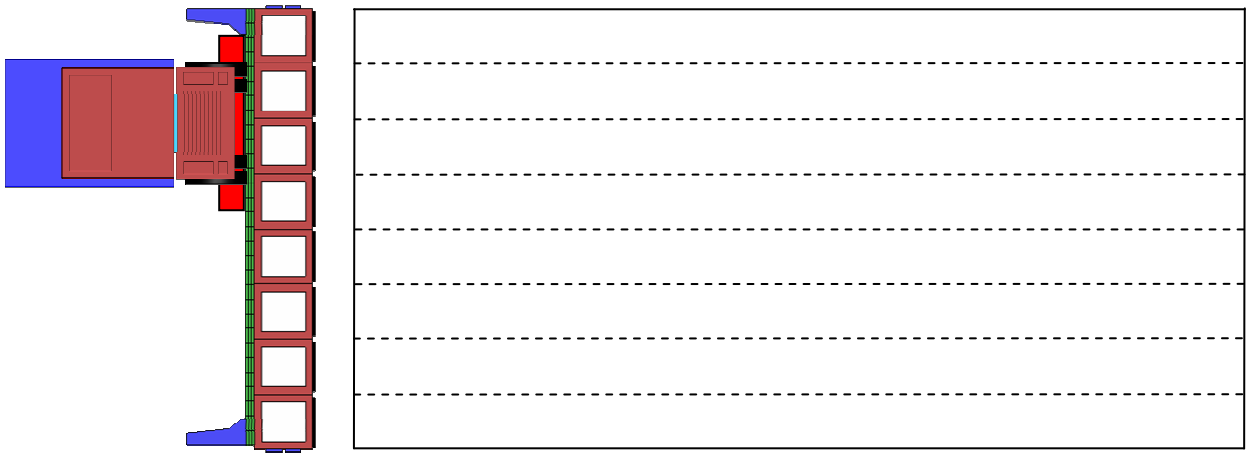

Figure 4.2-39 Crack development in the slab bottom surface after applying equivalent AASHTO HL-93 load.

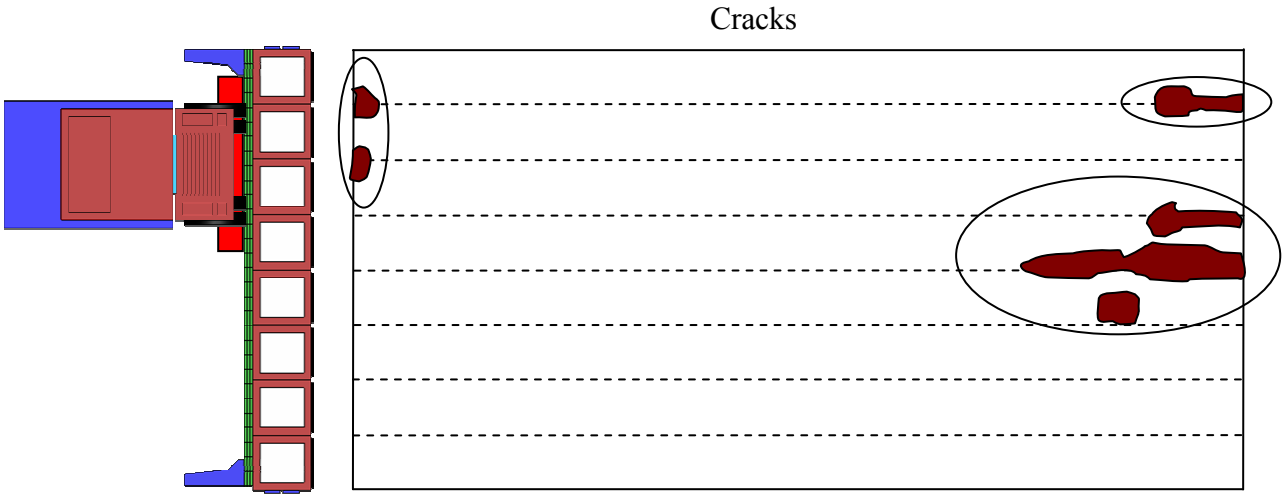

Figure 4.2-40 Crack development in the slab bottom surface after applying 120% of equivalent AASHTO HL-93 load.

4.2.6 Discussion of the Results

Based on the analysis of FE models for 24 ft wide side-by-side box-beam bridges with spans of 50, 62, 100, and 124 ft, using box-beams of widths of 36 and 48 in., the following findings were established:

1. The longitudinal deck cracks are expected to develop in side-by-side box-beam bridges when the current MDOT Specifications (2006) for TPT arrangement are followed.
2. In order to delay the development of the longitudinal deck slab cracks in bridges constructed using 48 in. wide side-by-side box-beams, the recommended number of diaphragms should be provided based on the bridge span, as shown in Figure 4.2-41. The Figure presents the minimum number of diaphragms required to prevent the longitudinal cracks. The diaphragms should be equally spaced along the entire bridge span.
3. The minimum number of diaphragms was selected to merely avoid the crack development in the deck slab; and the stresses in the deck slab in all cases of analysis were slightly less than the cracking strength of the concrete. Therefore, it may be beneficial to add more diaphragms over the minimum number as a safety factor to account for any unpredictable loads or concrete deterioration.
4. In case of 36 in. wide side-by-side box-beam bridges, the number of diaphragms should be provided according to Figure 4.2-42. This Figure presents the minimum number of diaphragms required to prevent longitudinal cracks along with the recommend number of diaphragms.
5. The number of diaphragms obtained from Figure 4.2-41 or Figure 4.2-42 is applicable for all bridges having the corresponding span regardless of their widths. However, the recommended TPT force per diaphragm depends on the concrete strength in the deck slab and the bridge width as well; the TPT force should be adjusted to counteract the effect of increasing the bridge width as presented in the following section. Finally, for 24 ft wide bridges, a TPT force of:

- 150,000 lb/diaphragm should be applied in the case of deteriorated slabs.

- 120,000 lb/diaphragm should be applied in the case of recently-constructed slabs.
- 100,000 lb/ diaphragm should be applied in the case of special-quality slabs.

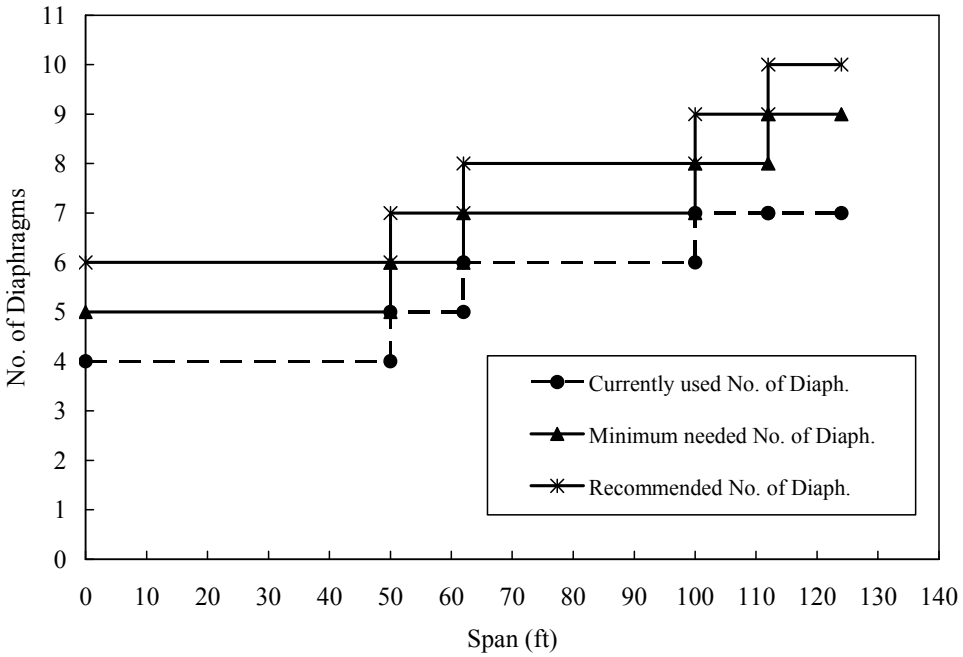

Figure 4.2-41 Adequate number of diaphragms for bridges constructed using 48 in. wide beams.

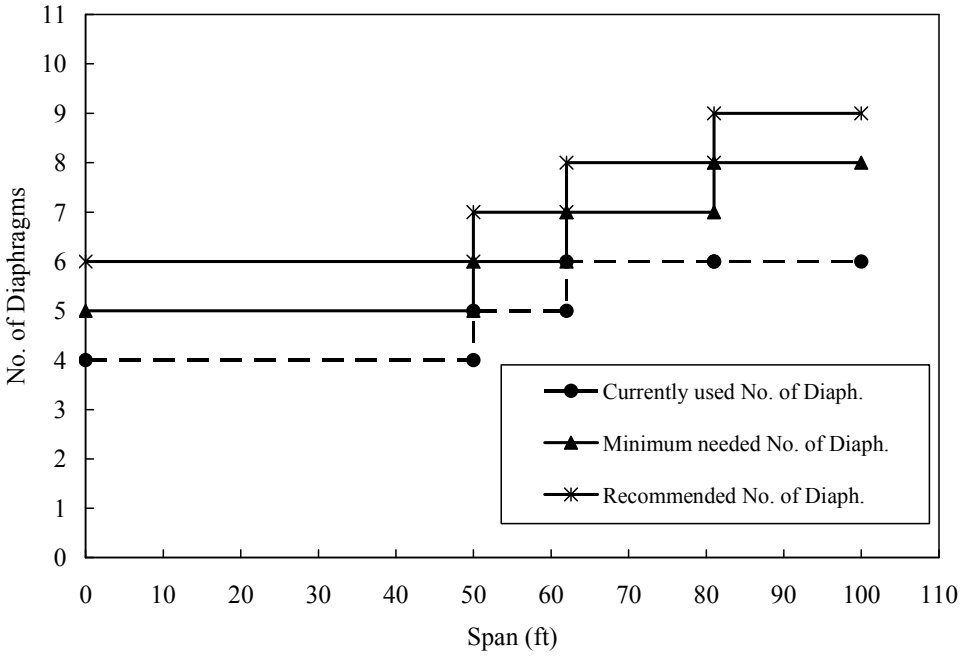

Figure 4.2-42 Adequate number of diaphragms for bridges constructed using 36 in. wide beams.

4.3 Appropriate Transverse Post-Tensioning Force

In the preceding section, the relationship between the bridge span and the adequate number of diaphragms was established for 24 ft wide bridge models. The transverse post-tensioning force per diaphragm was adjusted to 150,000 lb/diaphragm in the case of a deteriorated deck slab (concrete of strength of 3,000 psi) and to 120,000 and 100,000 lb/diaphragm for concrete of strength of 4,000 and 5,000 psi, respectively. In this section, the analysis is extended to establish the appropriate TPT force for wider bridges (Figure 4.3-1). The FE models for bridges of widths of 45, 58, 70, and 78 ft were generated, as shown in Figure 4.3-2 and provided with the minimum number of diaphragms as recommended from the previous section.

The models were subjected to the same analysis and loading steps discussed in the previous section; the service load included applying 100% of positive temperature gradient and then applying the vehicular load along with the presence and impact allowances. In the case of wide bridge models, the vehicular loads were applied at three different locations, as shown in Figure 4.3-3 and Figure 4.3-4. The load locations can be demonstrated as following:

1. One truck over one shoulder denoted as Location I.
2. Two trucks over both shoulders; one truck per shoulder -case of maximum transverse negative moment, denoted as Location II.
3. Two trucks adjacent to each other at the mid-width of the bridge model -case of maximum transverse positive moment, denoted as Location III.

In the longitudinal direction, the trucks were positioned to create the largest positive bending moment in simply supported spans. The spans of 50, 62, and 100 ft were investigated for the aforementioned bridge widths though changing span length does not affect the appropriate TPT force. Furthermore, the analysis was performed using AASHTO HS-25 truck load as well as AASHTO HL-93 load (placed at the same locations as AASHTO HS-25 truck) as vehicular loads although no significant difference was observed in the model response under both loads.

The analysis revealed that the appropriate TPT force should be increased when increasing the bridge width in order to delay the onset of cracking. Nevertheless, the required TPT force slightly decreases with increasing the strength of the concrete in the deck slab. The following subsection presents and discusses the results of the analysis.

4.3.1 Models Geometry

Two sets of models were generated, as shown in Figure 4.3-1; the first set of models was generated using 48 in. wide box-beams and the second set was generated using 36 in. wide box-beams. The geometry of the models in both sets is described below.

4.3.2 Bridge Models Generated Using 48 in. Wide Box-Beams

FE bridge models of spans of 50 and 100 ft and widths of 24, 45, 58, 70, and 78 ft were generated using 48 in. wide box-beams, as shown in Figure 4.3-2.

1. Six box-beams were used to form bridge models with a width of 24 ft; these models have been analyzed and discussed in the previous chapter.
2. Eleven box-beams were used to form bridge models with a width of 45 ft. Each bridge model accommodated two 12 ft wide traffic lanes, 8.5 and 9.75 ft wide shoulders, and two 1.5 ft wide barriers. The cross-section dimensions and reinforcement details of the beams were similar to those of the previous models.
3. Fourteen box-beams were used to form bridge models with a width of 58 ft. Each bridge model accommodated three 12 ft wide traffic lanes, 8.5 and 10.13 ft wide shoulders, and two 1.5 ft wide barriers.
4. Seventeen box-beams were used to form bridge models with a width of 70 ft. Each bridge model accommodated four 12 ft wide traffic lanes, two 9.5 ft wide shoulders, and two 1.5 ft wide barriers.
5. Nineteen box-beams were used to form bridge models with a width of 78 ft. Each bridge model accommodated five 12 ft wide traffic lanes, two 7.5 ft wide shoulders, and two 1.5 ft wide barriers. However, only half of the 78 ft wide bridge was modeled due to model size limitation.

Similar to the previous models, this set of models was analysed with deteriorated, recently constructed, and special-quality deck slabs (concrete of strength 3,000, 4,000, and 5,000 psi, respectively). Section 4.3.4 presents detailed results for the models constructed using 48 in. wide box-beams with a deteriorated deck slab (concrete of strength 3,000 psi, modulus of rupture 350 psi, and modulus of elasticity 3×10^6 psi). The results of analyzing models

constructed using concrete of strength of 4,000 or 5,000 psi are presented as a summary at the end of this section.

4.3.3 Bridge Models Generated Using 36 in. Wide Box-Beams

After analyzing the aforementioned bridge models and establishing the appropriate TPT force for each bridge width, the other set of models was generated using 36 in. wide box-beams. The models had spans of 50, 62, and 100 ft and widths of 24, 47, 59, 72, and 84 ft (Figure 4.3-1):

1. Eight box-beams were used to form bridge models with a width of 24 ft.
2. Fifteen box-beams were used to form bridge models with a width of 47 ft. Each bridge model accommodated two 12 ft wide traffic lanes, two 10 ft wide shoulders, and two 1.5 ft wide barriers. The cross-section dimensions and reinforcement details of the beams were similar to those of the previous models.
3. Nineteen box-beams were used to form bridge models with a width of 59.25 ft. Each bridge model accommodated three 12 ft wide traffic lanes, 10.0 and 10.25 ft wide shoulders, and two 1.5 ft wide barriers.
4. Twenty three box-beams were used to form bridge models with a width of 71.75 ft. Each bridge model accommodated four 12 ft wide traffic lanes, 10 ft and 10.75 ft wide shoulders, and two 1.5 ft wide barriers. Only half of the 72 ft wide bridge was modeled.
5. Twenty seven box-beams were used to form bridge models with a width of 84.25 ft. Each bridge model accommodated five 12 ft wide traffic lanes, 10 ft and 11.25 ft wide shoulders, and two 1.5 ft wide barriers. Only half of the 84 ft wide bridge was modeled.

The models were initially provided with TPT forces similar to those recommended for bridges constructed using 48 in. wide box-beams. The deck slab was considered recently constructed with concrete of strength of 4,000 psi, modulus of rupture of 460 psi, and modulus of elasticity of 3.83×10^6 psi. The results of analyzing models constructed using 36 in. wide box-beams are presented as a summary at the end of this section.

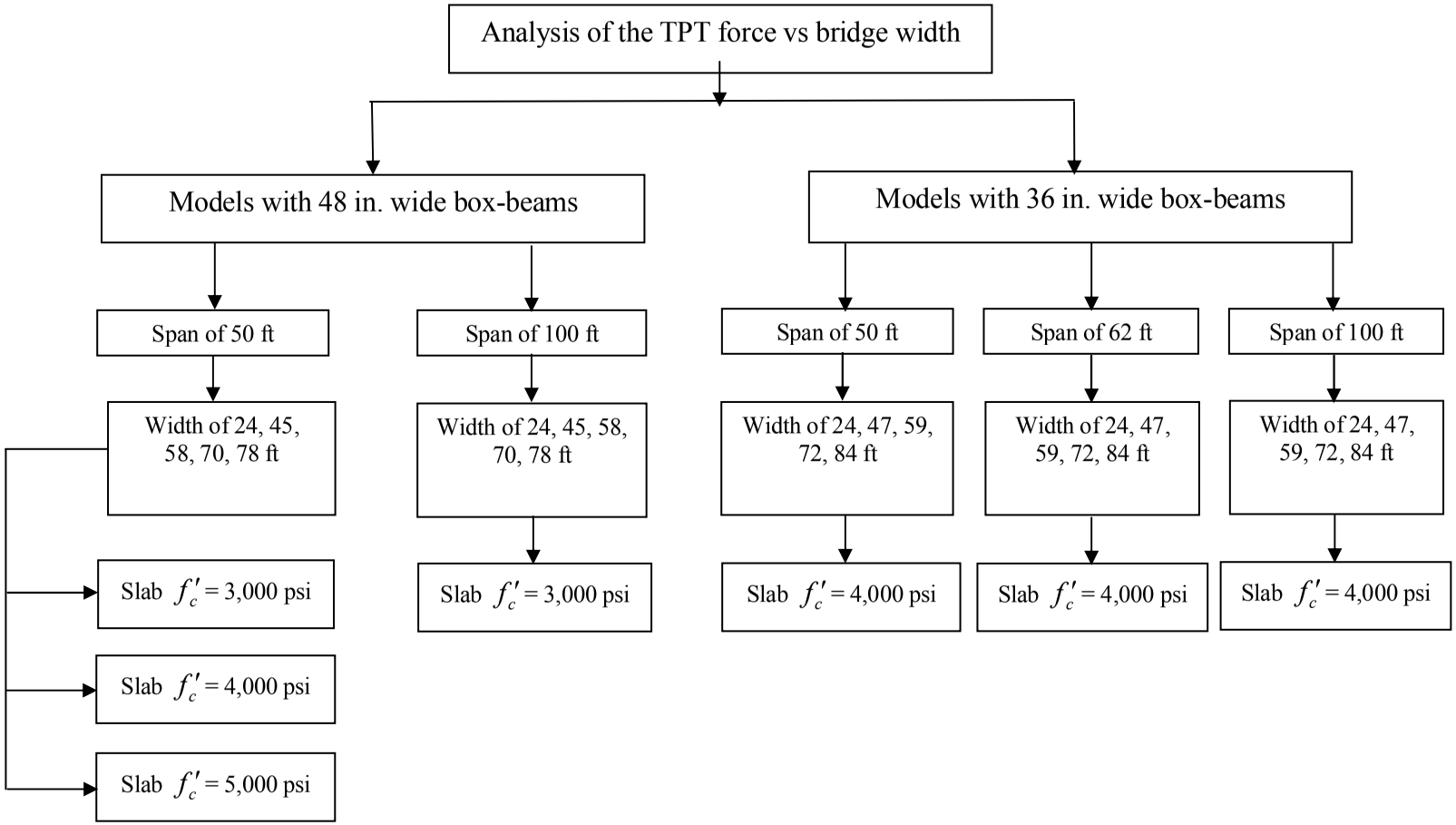

Figure 4.3-1 FE models to establish the appropriate TPT force.

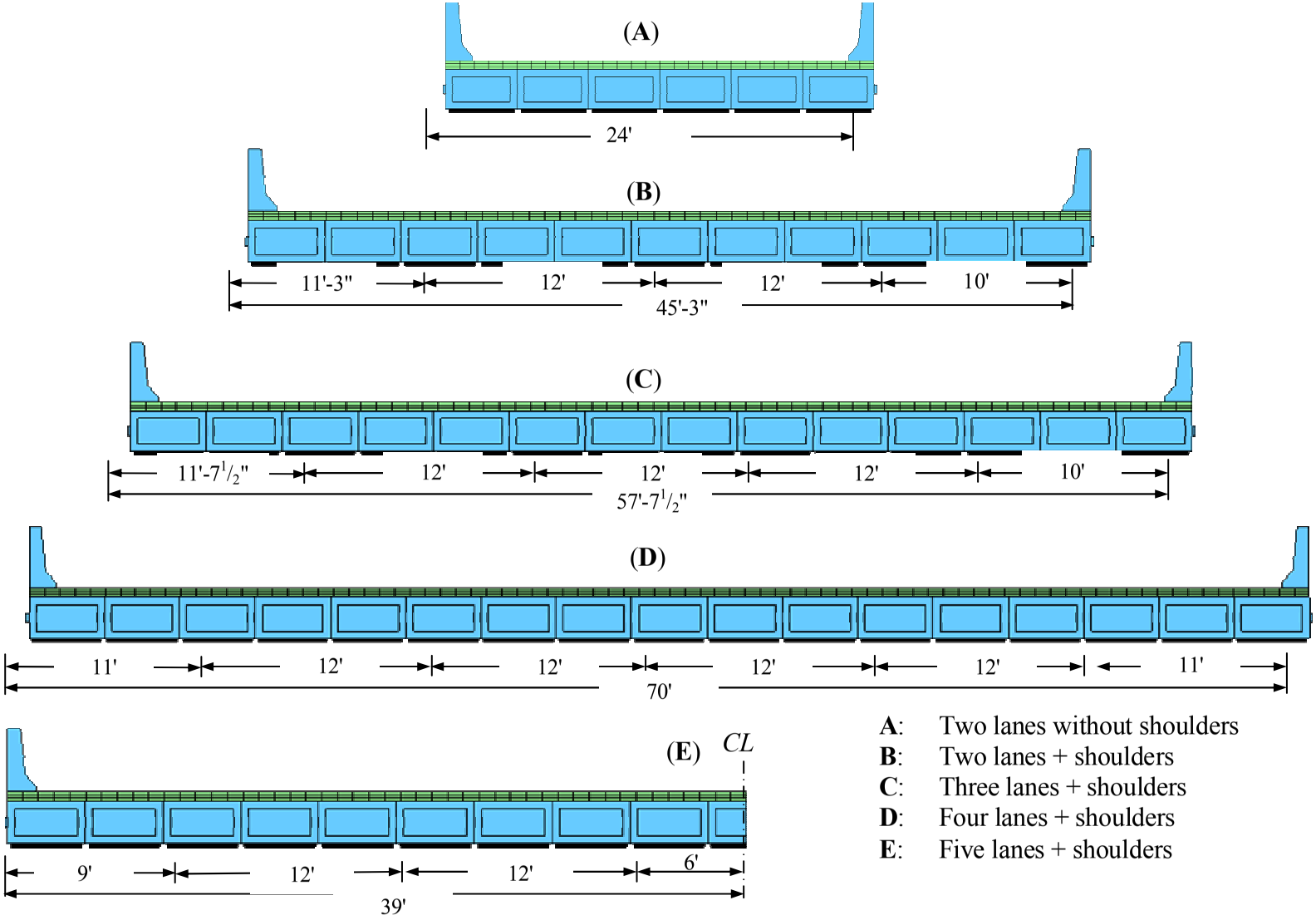

Figure 4.3-2 Bridge widths examined under different loading cases.

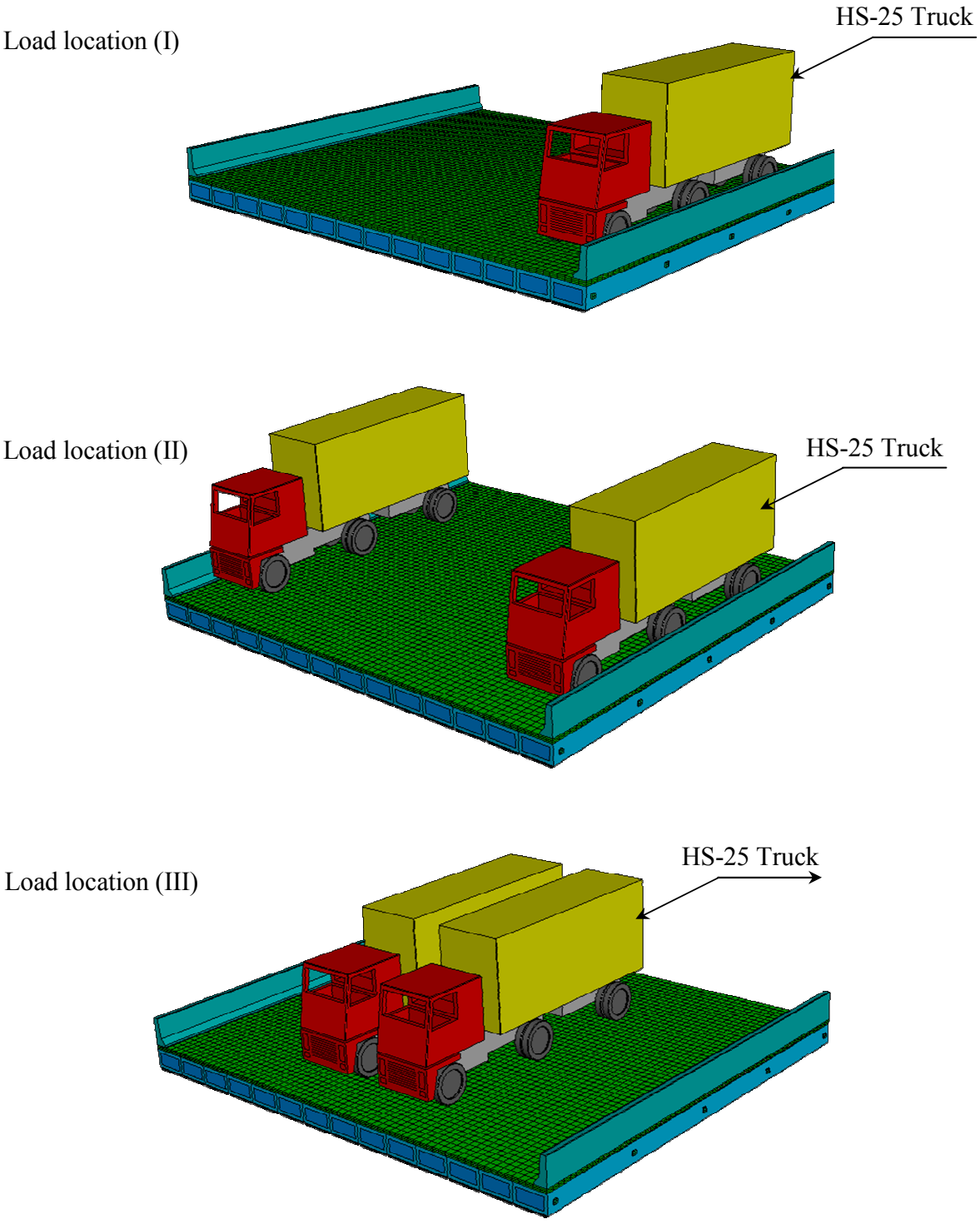

Figure 4.3-3 Load locations for live loads (3-lane model, isometric view).

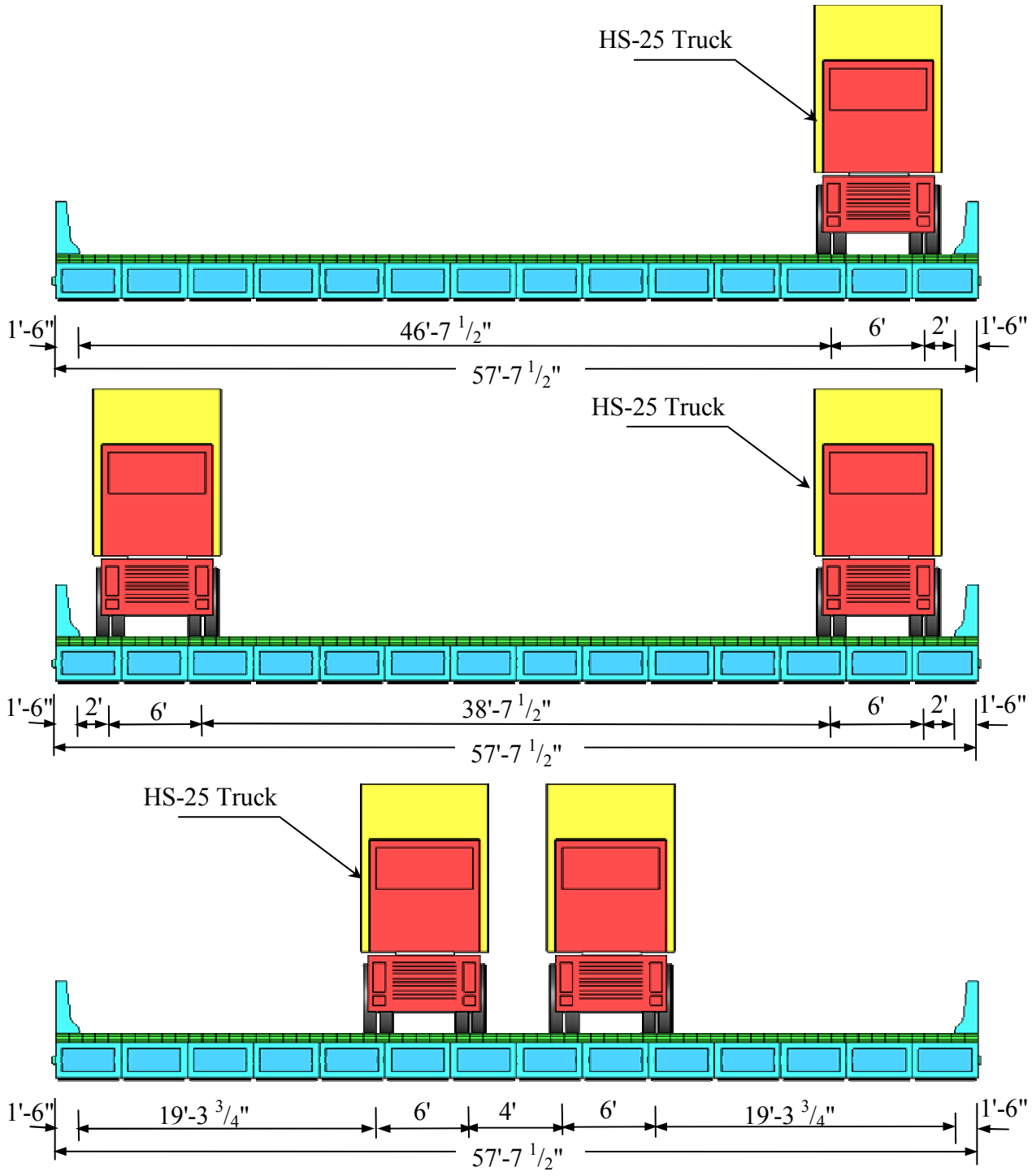

Figure 4.3-4 Load locations for live loads (3-lane model, front view).

4.3.4 Bridge Models Generated Using 48 in. Wide Box-Beams

4.3.4.1 Two-Lane Bridge Model (Span = 50 ft, Width = 45 ft)

The 45 ft wide bridge model was composed of eleven side-by-side box-beams of a depth of 27 in. and a width of 48 in. each. The reinforcement of the box-beams and the deck slab was similar to that described in the chapter 3 for 50 ft span bridge models. Five diaphragms were used to tie the beams together and the TPT force was set first to 125,000 lb/diaphragm. The force was applied through one strand at the beams mid-depth.

The construction stages before casting the deck slab were the same as what have been discussed in the previous section; thus, detailed discussion for the results from these stages is not presented. Most of the results in this section address the stresses developed after casting the deck slab.

Stress progressions in the deck slab ($f_c' = 3{,}000$ **psi)**

1. The stresses in the deck slab in both the longitudinal and transverse direction were negligible before applying the second stage of TPT force. However, after applying the second stage of TPT force (100,000 lb/diaphragm after casting deck slab), the stress distribution in the slab changed; the transverse stresses reached compressive stress level up to 182 psi at the slab ends. Conversely, the majority of the slab experienced compressive stresses in the range between 23 and 59 psi. In the longitudinal direction, the slab experienced negligible compressive and tensile stresses.
2. After deducting the time dependent losses and applying the superimposed dead loads, the slab experienced additional longitudinal compressive stresses. Some tensile stresses of value less than 66 psi developed at the slab ends near the outer shear-keys location at the fascia beams, most likely because of the barriers weight.
3. When applying positive temperature gradient, the slab bottom surface experienced maximum principal tensile stresses up to 272 psi concentrated at the shear-keys location.
4. **Live load Location I**: subsequent to applying the positive temperature gradient, applying one AASHTO HS-25 truck load over one of the shoulders (2 ft away from the barrier edge) increased the longitudinal stresses in the deck slab top surface up to 935

psi (compression). At the same time, additional tensile stresses developed in the transverse direction (220 psi), and caused the principal stresses to reach 348 psi. The slab did not experience any cracks under the applied load, as shown in Figure 4.3-5.. Furthermore, when the loads exceed the AASHTO HS-25 load by 20%, the cracks would be developed, as shown in Figure 4.3-6.

5. **Live load Location II**: subsequent to applying the positive temperature gradient, applying two AASHTO HS-25 trucks over both shoulders simultaneously after applying the temperature gradient (one AASHTO HS-25 truck per shoulder) increased the longitudinal stresses in the top surface to 971 psi (compression) and developed additional tensile stresses in the transverse direction (224 psi). The principal stresses increased to 344 psi. However, the slab did not yet experience cracks under the applied loads, as shown in Figure 4.3-7. If the loads exceed the AASHTO HS-25 truck by 20%, the cracks would be developed, as shown in Figure 4.3-8.
6. **Live load Location III**: subsequent to applying the positive temperature gradient, applying two AASHTO HS-25 trucks over the mid-width of the model after applying the temperature gradient caused the principal stresses to exceed the cracking strength of the concrete and the deck slab experienced cracks, as shown in Figure 4.3-9. By increasing the TPT level from 125,000 to 150,000 lb/diaphragm, the principal stresses reached a maximum of 351 psi and the slab did not experience any cracks, as shown in Figure 4.3-10.
7. With a TPT force of 150,000 lb/diaphragm and applying the positive temperature gradient in addition to AASHTO HL-93 load in locations I, II, and III, the deck slab experienced maximum principal stresses of 338, 297, and 306 psi, respectively. No cracks developed in the deck slab under any of the combined thermal and truck load conditions.

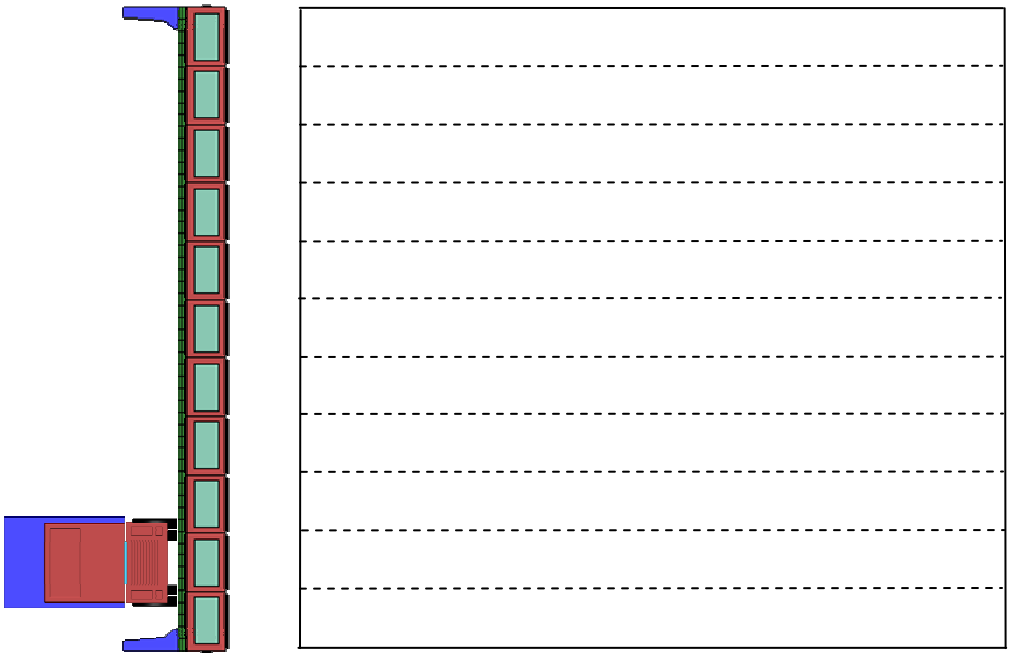

Figure 4.3-5 Crack development in the slab bottom surface after applying AASHTO HS-25 truck (Location I, TPT = 125,000 lb/diaphragm).

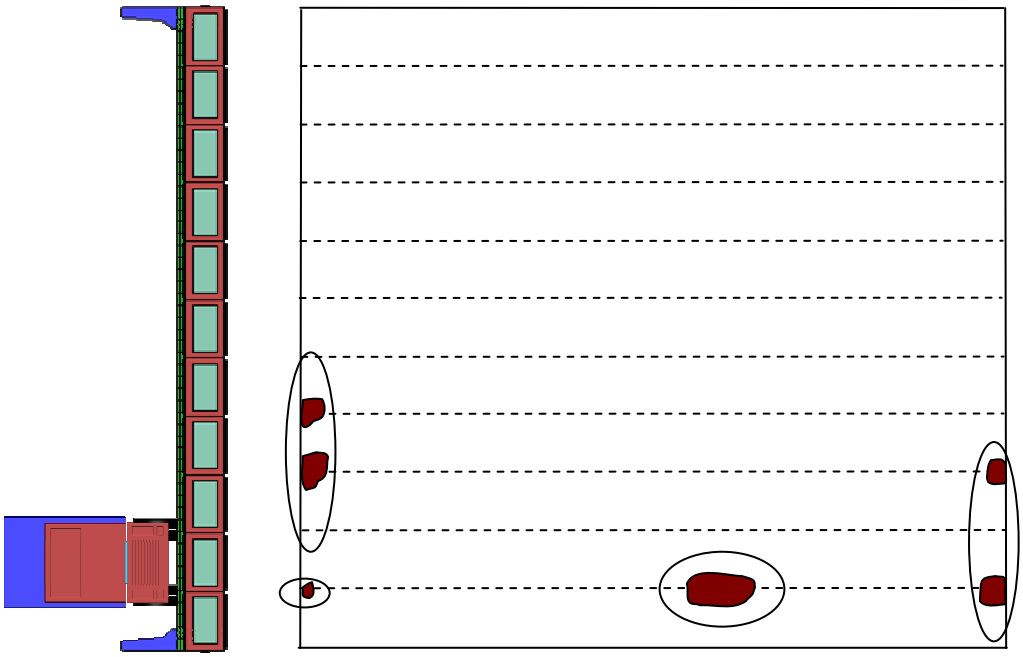

Figure 4.3-6 Crack development in the slab bottom surface after applying 120% of AASHTO HS-25 truck (Location I, TPT = 125,000 lb/diaphragm).

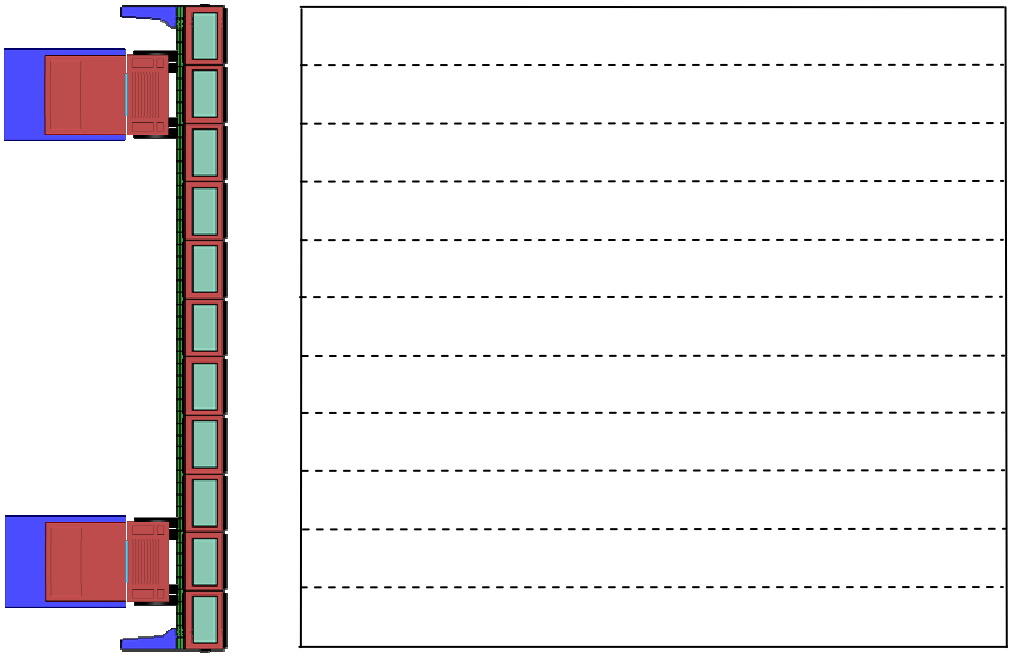

Figure 4.3-7 Crack development in the slab bottom surface after applying AASHTO HS-25 truck (Location II, TPT = 125,000 lb/diaphragm).

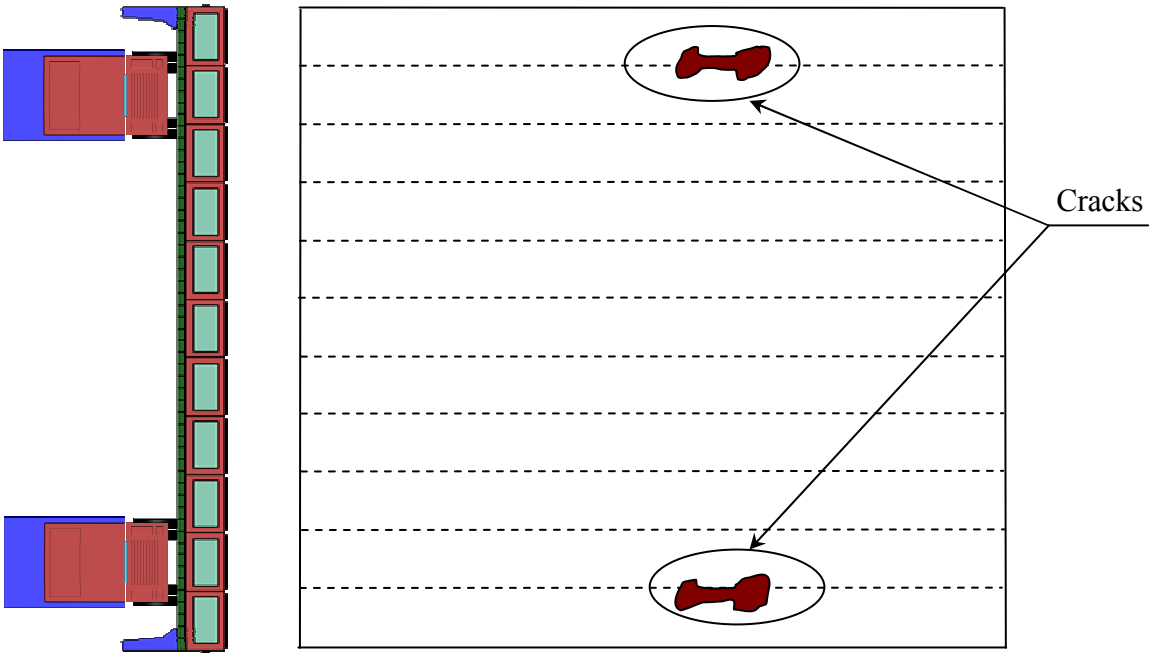

Figure 4.3-8 Crack development in the slab bottom surface after applying 120% of AASHTO HS-25 truck (Location II, TPT = 125,000 lb/diaphragm).

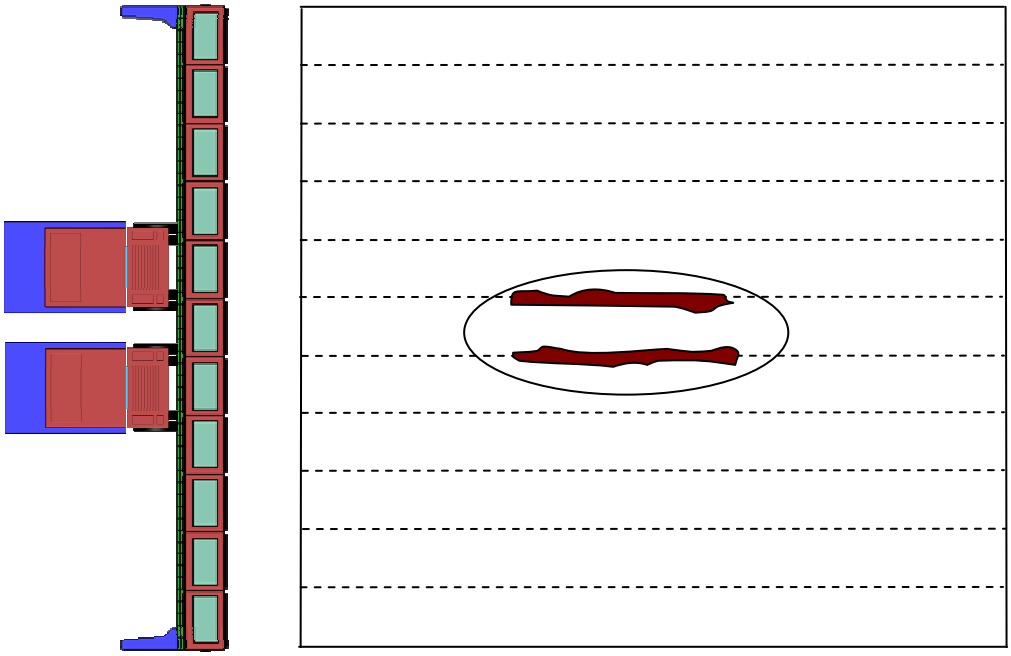

Figure 4.3-9 Crack development in the slab bottom surface after applying AASHTO HS-25 truck (Location III, TPT = 125,000 lb/diaphragm).

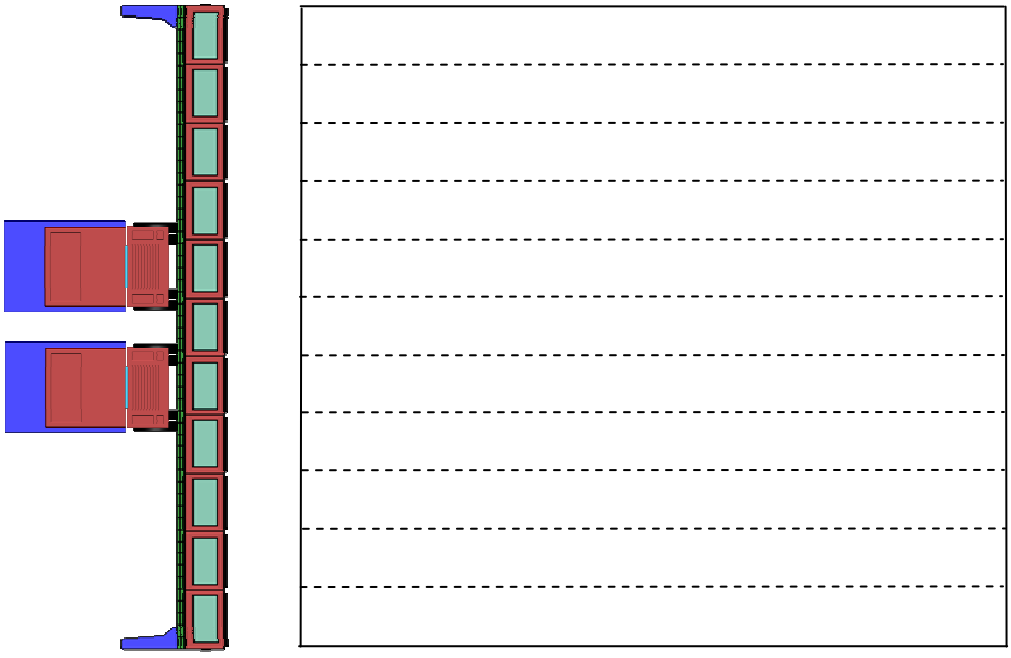

Figure 4.3-10 Crack development in the slab bottom surface after applying AASHTO HS-25 truck (Location III, TPT = 150,000 lb/diaphragm).

4.3.4.2 Three-Lane Bridge Model (Span = 50 ft, Width = 58 ft)

The 58 ft wide bridge model was composed of fourteen side-by-side box-beams of a width of 48 in. each. The initial TPT force was set to 150,000 lb/diaphragm applied through 5 diaphragms based on the final results for 45 ft wide bridge model.

Stresses and crack development in the deck slab (f_c' = 3,000 psi)

1. Both the longitudinal and transverse stresses in the deck slab were negligible before applying the second stage of TPT force.
2. After applying the second stage of TPT force (125,000 lb/diaphragm after casting the deck slab), the transverse compressive stresses reached 182 psi at the slab ends. Conversely, the majority of the slab experienced compressive stresses in the range of 23 to 59 psi. In the longitudinal direction, the slab experienced small stress values either in compression or in tension ranging from -20 to +98 psi. The stress on interior sides of the box-beam reached 471 psi at the diaphragms only.
3. When applying the positive temperature gradient, the slab bottom surface experienced localized tensile stresses up to 273 psi at the shear-key locations.
4. **Live load Location I**: subsequent to applying positive temperature gradient, applying one AASHTO HS-25 truck load over one of the shoulders (2 ft away from the barrier edge) increased the maximum principal stresses up to 351 psi. The slab experienced no cracks; however, the TPT force was considered just enough to prevent the cracks because if the load increases by 20% of the load, the cracks would develop.
5. **Live load Location II**: subsequent to applying positive temperature gradient, applying two AASHTO HS-25 trucks over the shoulders simultaneously (one truck per shoulder, 2 ft away from the barrier edge) increased the maximum principal stresses up to 341 psi. The slab did not experience cracks under the applied load.
6. **Live load Location III**: subsequent to applying positive temperature gradient, applying two AASHTO HS-25 trucks simultaneously over the mid-width of the model (4 ft apart from each other) caused maximum principal stresses to reach 185 psi at the slab bottom surface. The slab did not experience cracks under two AASHTO trucks, but when

applying 20% more than AASHTO HS-25 trucks, it experienced longitudinal cracks at the mid-width. In this particular loading case, the maximum principal stresses decreased with the application of the live loads because the response of the live load counteracted the response of the positive temperature gradient; the highest value of the principal stresses was reached at the slab edges when applying temperature gradient only and at the mid-width after the live loads were added.

7. By using TPT force of 150,000 lb/diaphragm, the deck slab experienced maximum principal stresses of 353, 330, and 186 psi when applying AASHTO HL-93 load in locations I, II, and III, respectively subsequent to applying positive temperature gradient. No cracks were developed in the deck slab under any of the load cases.

4.3.4.3 Four-Lane Bridge Model (Span = 50 ft, Width = 70 ft)

The 70 ft wide bridge model was composed of seventeen side-by-side box-beams of a width of 48 in. each. The initial TPT force level was 150,000 lb/diaphragm applied through five diaphragms.

Stress and crack development in the deck slab ($f_c' = 3{,}000$ psi**)**

1. After applying second stage of TPT force (125,000 lb/diaphragm after casting the deck slab), the transverse stress distribution reached compressive stresses of 220 psi at the slab ends. The majority of the slab experienced compressive stresses in the range of 49 to 92 psi. In the longitudinal direction, the slab experienced small stress values either in compression or in tension ranging between -19 and +83 psi.
2. After deducting time dependent losses and applying superimposed dead loads SDL, the tensile stresses reached a value of 102 psi at the slab ends.
3. When applying positive temperature gradient, the slab bottom surface experienced tensile stresses of 269 psi. These high tensile stresses were found at the shear-key locations near the supports of the fascia beams.
4. **Live load Location I**: subsequent to applying the positive temperature gradient, applying one AASHTO HS-25 truck over one of the shoulders (2 ft away from the

barrier edge) increased the maximum principal stresses to 353 psi and the slab experienced small cracks.

5. **Live load Location II**: subsequent to applying the positive temperature gradient, when applying two AASHTO HS-25 trucks over the shoulders simultaneously (one truck per shoulder, 2 ft away from the barrier edge), the slab experienced small cracks mainly at the locations of the shear-keys near the supports of the fascia beams.
6. **Live load Location III**: subsequent to applying the positive temperature gradient, when applying two AASHTO HS-25 trucks simultaneously over the mid-width of the model (4 ft apart from each other), the slab experienced cracking. The crack development implied that the applied TPT force was insufficient to eliminate the deck slab cracking in the four-lane bridge.
7. The TPT level was increased to 175,000 lb/diaphragm and the bridge model was reanalyzed. Increasing TPT level eliminated the crack development. However, the mid-region at the slab bottom surface remained the most likely region to develop cracks. By using a TPT force of 175,000 lb/diaphragm, the deck slab experienced maximum principal stresses up to 342, 327, and 267 psi when applying the positive temperature gradient with AASHTO HL-93 load in locations I, II, and III, respectively. No cracks were developed in the deck slab under these load cases.

4.3.4.4 Five-Lane Bridge Model (Span = 50 ft, Width = 78 ft)

The 78 ft wide bridge model was composed of nineteen side-by-side box-beams of a width of 48 in. each (total width of 78 ft). The entire bridge could not be modeled because of the required extensive FE elements. Instead, half of the width was modeled and symmetry conditions were provided along the longitudinal centerline. After a few trials, the TPT force was set to 180,000 lb/diaphragm applied through five diaphragms in order to eliminate the deck slab cracks.

Stresses and crack development in the deck slab ($f_c' = 3{,}000$ psi**)**

1. After applying the second stage of TPT force (155,000 lb/diaphragm after casting the deck slab), the transverse compressive stresses reached 265 psi at the slab ends. At the

same time, the majority of the slab experienced compressive stresses in the range of 61 to 112 psi.

2. After deducting time dependent losses and applying SDL, localized tensile stresses reached a value of 131 psi near the end supports.
3. When applying positive temperature gradient, the slab bottom surface experienced tensile stresses up to 262 psi. Again, the high tensile stresses were mainly observed above the outer shear-keys near the supports.
4. **Live load Location I**: as a result of modeling only half of the width of the bridge model, it was not possible to load one side only of the model with a truck; therefore, the first load case was not performed for the five-lane model.
5. **Live load Location II**: subsequent to applying the positive temperature gradient, applying two AASHTO HS-25 trucks over the shoulders simultaneously (one truck load per shoulder) increased the maximum principal stresses to 349 psi. The slab did not experience cracks under the applied load, but with an additional 20% of the loads applied, the slab experienced small cracks at the far ends.
6. **Live load Location III**: by applying two AASHTO HS-25 trucks simultaneously over the mid-width of the model after applying the positive temperature gradient, the maximum principal stresses increased to 324 psi. The slab did not experience cracks under the AASHTO HS-25 trucks. However, when applying an additional 20% of the load, the slab experienced cracks.
7. By using TPT force of 180,000 lb/diaphragm, the deck slab experienced maximum principal stresses up to 342 and 305 psi when applying the positive temperature gradient with AASHTO HL-93 loading in Location II and III, respectively. No cracks were developed in the deck slab under any of the load locations.

4.3.4.5 Two-Lane Bridge Model (Span = 100 ft, Width = 45 ft)

This bridge model was composed of eleven side-by-side box-beams of a width of 48 in. each (total width of 45 ft) and depth of 39 in. as specified earlier for bridge models with 100 ft span.

The TPT force was set to 150,000 lb/diaphragm, applied through two strands at the third points of the beam depth.

Only half of the span was modeled and symmetry conditions were applied at the mid-span section. Furthermore, because of the span symmetry, the response due to AASHTO HS-25 truck could not be replicated. Instead, AASHTO equivalent lane load was applied with a transformation ratio as explained earlier in Section 2.2.4.3. Also, AASHTO HL-93 load was applied as lane load and tandem load multiplied by the transformation ratio instead of the truck load.

Stress and crack development in the deck slab ($f_c' = 3{,}000$ psi**)**

1. After applying the second stage of TPT force (125,000 lb/diaphragm after casting deck slab), the transverse compressive stresses reached 223 psi at the slab ends. At the same time, the majority of the slab experienced compressive stresses in the range of 12 to 36 psi.
2. After deducting time dependent losses and applying SDL, the slab experienced additional compressive stresses. Some tensile stresses of about 86 psi developed at the slab ends near first and last shear-keys.
3. When applying positive temperature gradient, the slab bottom surface experienced localized tensile stresses of about 308 psi, mainly above the shear-keys.
4. **Live load Location I (after positive temperature gradient)**: subsequent to applying the positive temperature gradient, applying the equivalent AASHTO HS-25 truck load over one shoulder (2 ft away from the barrier edge) increased the maximum principal stresses to 340 psi. The slab did not experience cracks under the applied load.
5. **Live load Location II (after positive temperature gradient)**: subsequent to applying the positive temperature gradient, by applying load of two equivalent AASHTO HS-25 trucks over both the shoulders simultaneously (one truck per shoulder), the principal stresses reached 342 psi. The slab did not experience cracks under the applied load.
6. **Live load Location III (after positive temperature gradient)**: subsequent to applying the positive temperature gradient, by applying two equivalent AASHTO HS-25 trucks

at the mid-width of the model after applying the positive temperature gradient, the maximum principal stresses increased to 303 psi. The slab did not experience cracks. However the slab experienced cracks when the load exceeded the load by 20%.

7. By providing a TPT force of 150,000 lb/diaphragm and applying positive temperature gradient then equivalent AASHTO HL-93 loading in Location I, II, and III, the deck slab experienced maximum principal stresses up to 342, 323, and 311 psi, respectively. No cracks were developed in the deck slab under any of these load cases.

4.3.4.6 Three-Lane Bridge Model (Span = 100 ft, Width = 58 ft)

This bridge model was composed of fourteen side-by-side box-beams of a width of 48 in. each. The initial TPT force was set to 150,000 lb/diaphragm, applied through seven diaphragms.

Stress and crack development in the deck slab ($f_c' = 3{,}000$ psi)

1. After applying the second stage of TPT force (125,000 lb/diaphragm after casting the deck slab), the transverse compressive stresses reached 275 psi at the slab ends. At the same time, the majority of the slab experienced compressive stresses on the order of 16 to 45 psi.
2. When deducting the time dependent losses and applying SDL, the slab experienced some localized tensile stresses of about 107 psi near the supports.
3. When applying positive temperature gradient, the slab bottom surface experienced tensile stresses up to 291 psi at the shear-key locations.
4. **Live load Location I**: subsequent to applying the positive temperature gradient, applying the equivalent AASHTO HS-25 truck over one of the shoulders increased the maximum principal stresses to 352 psi. The slab experienced no cracks under the applied loads. However, the TPT force can be considered just enough to prevent the cracks because the maximum tensile stresses were very close to the concrete cracking strength. If the load exceeds the load by 20%, the cracks would develop.
5. **Live load Location II**: when applying two equivalent AASHTO HS-25 trucks over both the shoulders simultaneously after applying the positive temperature gradient, the

maximum principal stresses reached 319 psi. This load case did not result in longitudinal cracking in the deck slab.

6. **Live load Location III**: when applying two equivalent AASHTO HS-25 trucks simultaneously over the mid-width of the model after applying the positive temperature gradient, the maximum principal stresses in the deck slab bottom surface reached 316 psi; the slab experienced no cracks. However, the cracks developed at the mid-width under the trucks location when applying 120% of the load.
7. By providing TPT force of 150,000 lb/diaphragm and applying the positive temperature gradient then equivalent AASHTO HL-93 loading in locations I, II, and III, the deck slab experienced maximum principal stresses up to 351, 328, and 315 psi, respectively. No cracks were developed in the deck slab under any of the load cases.

4.3.4.7 Four-Lane Bridge Model (Span = 100 ft, Width = 70 ft)

The 70 ft wide bridge model was composed of seventeen side-by-side box-beams of a width of 48 in. each. The TPT force was set to 150,000 lb/diaphragm applied through seven diaphragms.

Stress and crack development in the deck slab ($f_c' = 3{,}000$ psi**)**

1. After applying the second stage of TPT force (125,000 lb/diaphragm after casting the deck slab), the transverse compressive stresses increased to 269 psi at the slab ends. At the same time, the majority of the slab experienced compressive stresses not exceeding 70 psi.
2. After deducting the time dependent losses and applying SDL, some tensile stresses of a value of about 131 psi developed locally in the slab bottom surface near the ends.
3. When applying positive temperature gradient, the slab bottom surface experienced tensile stresses up to 287 psi over the shear-keys of the fascia beams near the supports.
4. **Live load Location I**: when applying equivalent AASHTO HS-25 truck over one of the shoulders after applying the positive temperature gradient, the principal stresses in the deck slab bottom surface reached 350 psi; the slab experienced small cracks;

however, the TPT force can be considered just enough to prevent the cracks. The cracks propagated when increasing the load.

5. **Live load Location II**: subsequent to applying the positive temperature gradient, applying two equivalent AASHTO HS-25 trucks over both shoulders simultaneously (one truck per shoulder) increased the maximum principal stresses in the slab bottom surface to 352 psi. Small cracks developed near the edges and propagated when increasing the loads by 20%.
6. **Live load Location III**: when applying two equivalent AASHTO HS-25 trucks simultaneously over the mid-width of the model after applying the positive temperature gradient, the slab experienced longitudinal cracks. The crack sizes and propagation implied that the applied TPT force was not adequate for the four-lane bridge; therefore, a TPT force level of 175,000 lb/diaphragm was applied to the model.
7. Increasing the TPT level eliminated the development of the deck cracks. However, when applying an additional 20% of the load, the slab experienced longitudinal cracks.
8. By providing TPT force of 175,000 lb/diaphragm and applying the positive temperature gradient with equivalent AASHTO HL-93 load in Locations I, II, and III, the deck slab experienced maximum principal stresses of 310, 342, and 311 psi, respectively. No cracks were developed in the deck slab under any of these load cases.

4.3.4.8 Five-Lane Bridge Model (Span = 100 ft, Width = 78 ft)

This 78 ft wide bridge model was composed of nineteen side-by-side box-beams of a width of 48 in. each; however, it was not possible to model the entire bridge width. Instead, only one quarter of the bridge was modeled; symmetry conditions were applied through the mid-width section and the mid-span section. Considering the finding from the previous five-lane bridge model, a TPT force of 180,000 lb/diaphragm was applied through seven diaphragms.

Stress and crack development in the deck slab ($f_c' = 3{,}000$ psi**)**

1. After applying the second stage of TPT force (155,000 lb/diaphragm after casting the deck slab), the transverse compressive stresses increased to 309 psi at the slab ends. At

the same time, the majority of the slab experienced compressive stresses ranging between 17 and 82 psi.

2. Tensile stresses of about 152 psi developed locally at the slab ends after deducting the time dependent losses and applying SDL.
3. When applying the positive temperature gradient, the slab bottom surface experienced tensile stresses up to 282 psi at the outer shear-keys near the supports.
4. **Live load Location I**: the live load was not applied in Location I for the five-lane bridge model.
5. **Live load Location II**: when applying two equivalent AASHTO HS-25 trucks over the shoulders simultaneously after applying the positive temperature gradient, the maximum principal stresses increased to 352 psi in the slab bottom surface. The slab did not experience cracks under the applied load. With an extra 20% of the load, the slab experienced small cracks at the far ends.
6. **Live load Location III**: when applying two equivalent AASHTO HS-25 trucks simultaneously over the mid-width of the model after applying the positive temperature gradient, the maximum principal stresses increased to 325 psi, and the slab experienced no cracks under the loads. However, when applying additional 20% of the load, some longitudinal cracks developed near the mid-width.
7. By providing a TPT force of 180,000 lb/diaphragm, the deck slab experienced maximum principal stresses up to 349 and 344 psi when applying the positive temperature gradient and an equivalent AASHTO HL-93 loading in Locations II and III, respectively. No cracks were developed in the deck slab under any of the load cases.

Table 4.3-1 Stress development in the deck slab due to surface loads in FE bridge models generated using 48 in. wide box-beams.

Span (ft)	Width (ft)	No. of Diaph.	TPT Force lb/diaph.	Transverse Stresses* (psi)	MP +ve TG (psi)	MP Live load (HL-93 load) IM = 75% (psi)		
						Location I m= 1.14	Location II m= 0.95	Location III m= 0.95
Concrete properties: f_c'=3,000 psi, f_r = 350 psi, $E = 3 \times 10^6$ psi								
50	24	5	150,000	11-54	229	286	N/A	N/A
50	45	5	150,000	29-59	259	338	375	306
50	58	5	150,000	23-59	273	353	383	186
50	70	5	175,500	36-112	259	342	379	267
50	78	5	180,000	61-112	262	N/A	386	305
100	24	7	150,000	15-72	234	351	N/A	N/A
100	45	7	150,000	12-36	308	342	323	311
100	58	7	150,000	16-45	291	351	328	315
100	70	7	175,500	15-81	285	310	342	311
100	78	7	180,000	17-82	282	N/A	349	344
Concrete properties: f_c'=4,000 psi, f_r = 460 psi, $E = 3.83 \times 10^6$ psi								
50	24	5	120,000	5-80	343	411	N/A	N/A
50	45	5	140,000	29-95	366	434	426	450
50	58	5	140,000	28-93	367	427	421	436
50	70	5	160,000	30-106	346	441	424	448
50	78	5	165,000	32-110	348	N/A	441	447
Concrete properties: f_c'=5,000 psi, f_r = 514 psi, $E = 4.3 \times 10^6$ psi								
50	24	5	100,000	3-66	407	493	N/A	N/A
50	45	5	130,000	28-97	423	491	480	511
50	58	5	130,000	29-98	420	476	482	510
50	70	5	150,000	29-105	397	511	501	513
50	78	5	155,000	29-107	399	N/A	510	511

* = Range of compressive transverse stresses developed in the deck slab due to TPT force
MP = Maximum principal stresses in the deck slab (tension)
TG = Temperature gradient
IM = Impact allowances
m = Presence factor
N/A= Not available

4.3.5 Bridge Models Generated Using 36 in. Wide Box-Beams

The previous models simulated bridges constructed using 48 in. wide box-beams. The results in terms of adequate TPT force were also verified for bridges constructed using the 36 in. wide box-beams. FE models for bridges with spans of 50, 62, and 100 ft (Figure 4.3-11) and widths of 24, 47, 59, 72, and 84 ft Figure 4.3-12 were generated using 36 in. wide box-beams. The same technique of analysis was employed, and the results were compared with those of the previous models. The analysis revealed that adequate TPT force level to prevent the deck slab cracking is independent of the box-beams width.

The entire analysis in this section was performed assuming recently constructed deck slab with concrete ultimate compressive strength of 4,000 psi, modulus of rupture of 460 psi, and modulus of elasticity of 3.83×10^6 psi. No analysis was performed for the cases of deteriorated and special-quality deck slabs since the influence of the concrete strength on the adequate TPT force shall be similar to what was observed in the case of 48 in. wide box-beams. Table 4.3-2 shows the stress values that were achieved in the deck slab after applying service loads. Except for the stress values due to applying the TPT force, all the presented stresses are tensile and compared with a value of 460 psi (the cracking strength of the concrete in the deck slab).

Table 4.3-2 Stress development in the deck slab due to surface loads in FE bridge models generated using 36 in. wide box-beams.

Span (ft)	Width (ft)	No. of Diaph.	TPT Force lb/Diaph.	Transverse Stresses* (psi)	MP +ve TG (psi)	MP Live load (HL-93 load) IM = 75% (psi)		
						Location I *m*= 1.14	Location II *m*= 0.95	Location III *m*= 0.95
50	24	5	120,000	16-71	358	415	N/A	N/A
50	47	5	140,000	49-111	328	400	375	427
50	59	5	140,000	36-109	334	434	383	396
50	72	5	161,500	44-111	323	N/A	379	398
50	84	5	169,000	49-121	317	N/A	386	376
62	24	6	120,000	3-52	410	452	N/A	N/A
62	47	6	140,000	21-74	383	462	406	413
62	59	6	140,000	40-94	379	447	414	430
62	72	6	161,500	41-101	368	N/A	446	447
62	84	6	169,000	46-107	361	N/A	451	433
100	24	8	120,000	18-56	355	427	N/A	N/A
100	47	8	140,000	21-66	384	459	451	391
100	59	8	140,000	21-66	426	460	457	404
100	72	8	161,500	26-104	419	N/A	458	433
100	84	8	169,000	27-108	417	N/A	459	444

* = Range of compressive transverse stresses developed in the Deck slab due to TPT force
MP = Maximum principal stresses in the deck slab (tension)
TG = Temperature gradient
IM = Impact allowances
m = presence factor
N/A= Not available

50 ft span bridge model (8, 15, 19, 23, 27 box-beams)

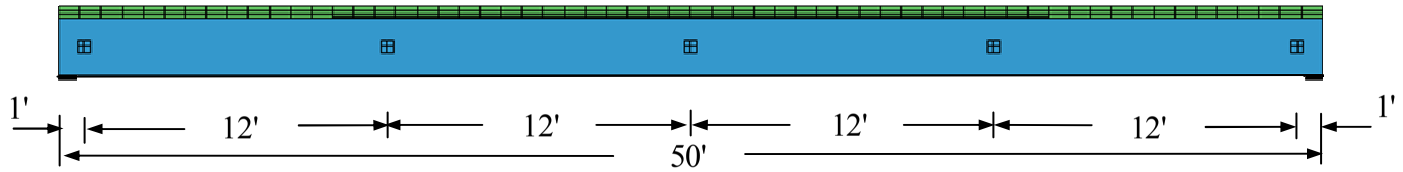

62 ft span bridge model (8, 15, 19, 23, 27 box-beams)

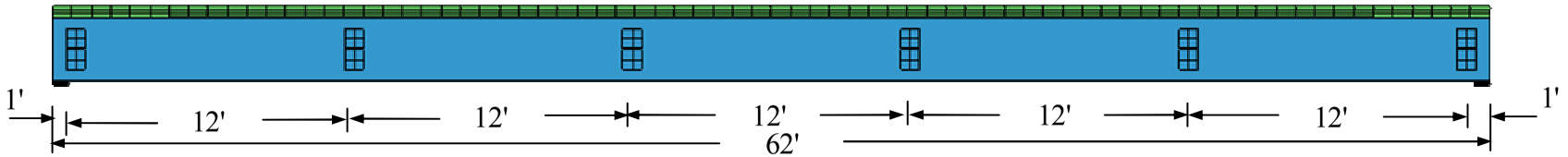

100 ft span bridge model (8, 15, 19, 23, 27 box-beams)

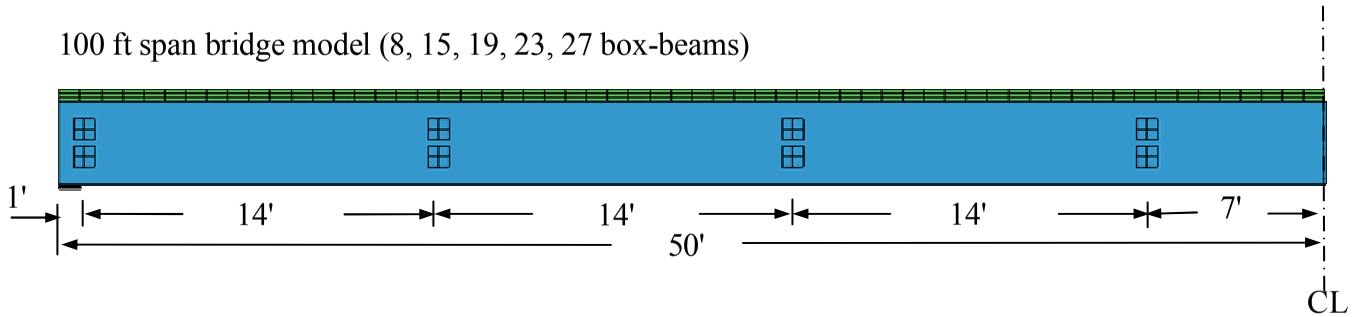

Figure 4.3-11 Bridge models generated using 36 in. wide box-beams (spans).

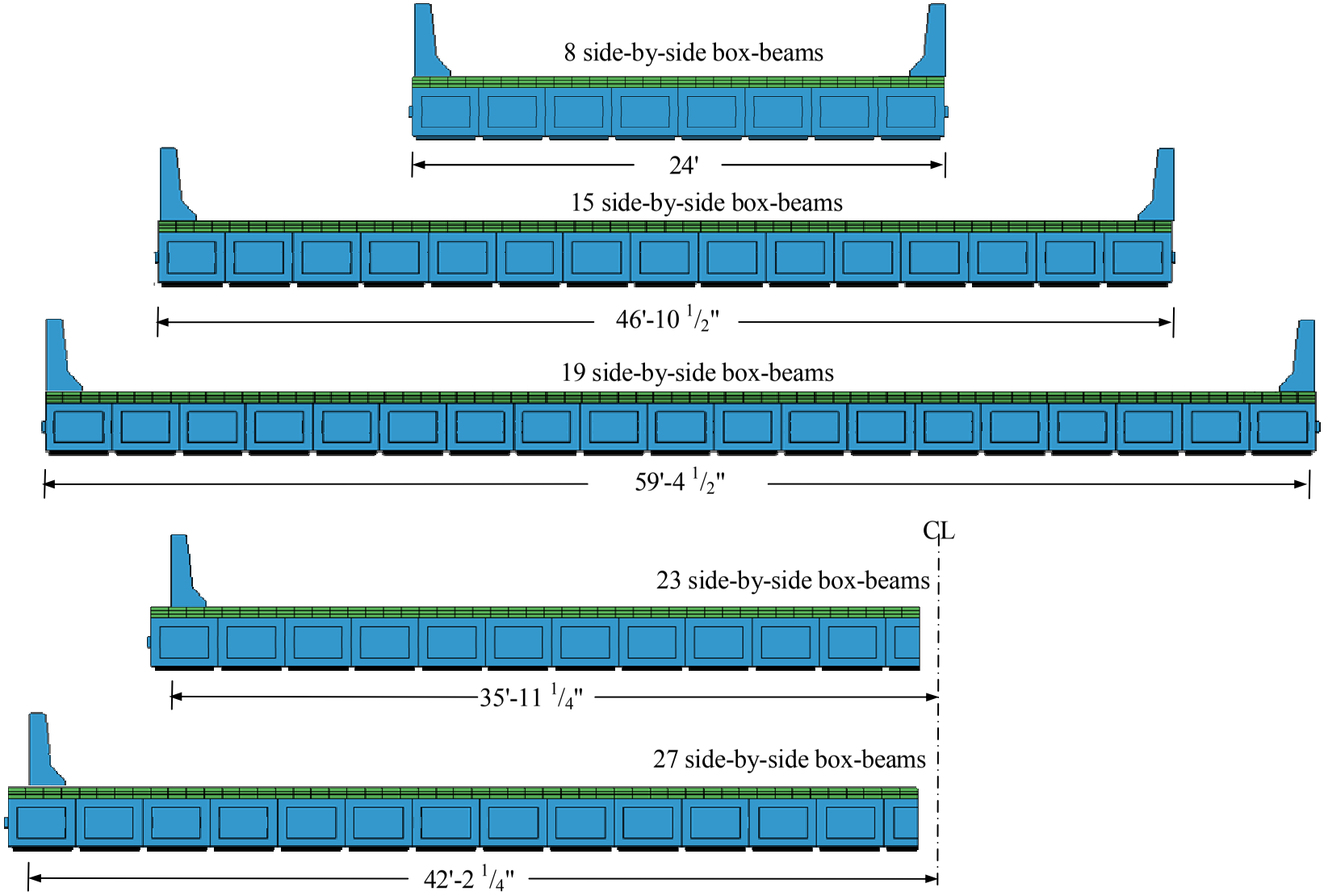

Figure 4.3-12 Bridge models generated using 36 in. wide box-beams (widths).

4.3.6 Discussion of the Results

Based on the analysis presented in this section for wide bridge models, the following findings were obtained:

1. The current TPT force recommended in the MDOT Bridge Design Guide (2006) is not adequate in preventing the development of longitudinal deck slab cracking in side-by-side box-beam bridges.
2. The AASHTO LRFD (2004) limit of 250 psi as a minimum uniform prestress in the longitudinal joints between the box-beams is not achievable regardless of the applied TPT force.
3. The adequate number of diaphragms was established for various bridge spans while keeping the TPT force level as close as possible to current recommended levels. Therefore, the TPT force required per diaphragm was independent of bridge span.
4. The analysis of the models generated using 48 in. wide box-beams and those generated using 36 in. wide box-beams yielded the same results for the adequate level of the TPT force to prevent longitudinal deck cracking. In other words, the required TPT force level for a given bridge width is independent of the width of the individual box-beams.
5. The appropriate level of the TPT force increases with increasing the bridge width and slightly decreases with increasing the concrete strength of the deck slab, as shown in Figure 4.3-13.
6. It is recommended to consider future slab deterioration when applying TPT force during construction to reduce any future repair labor.

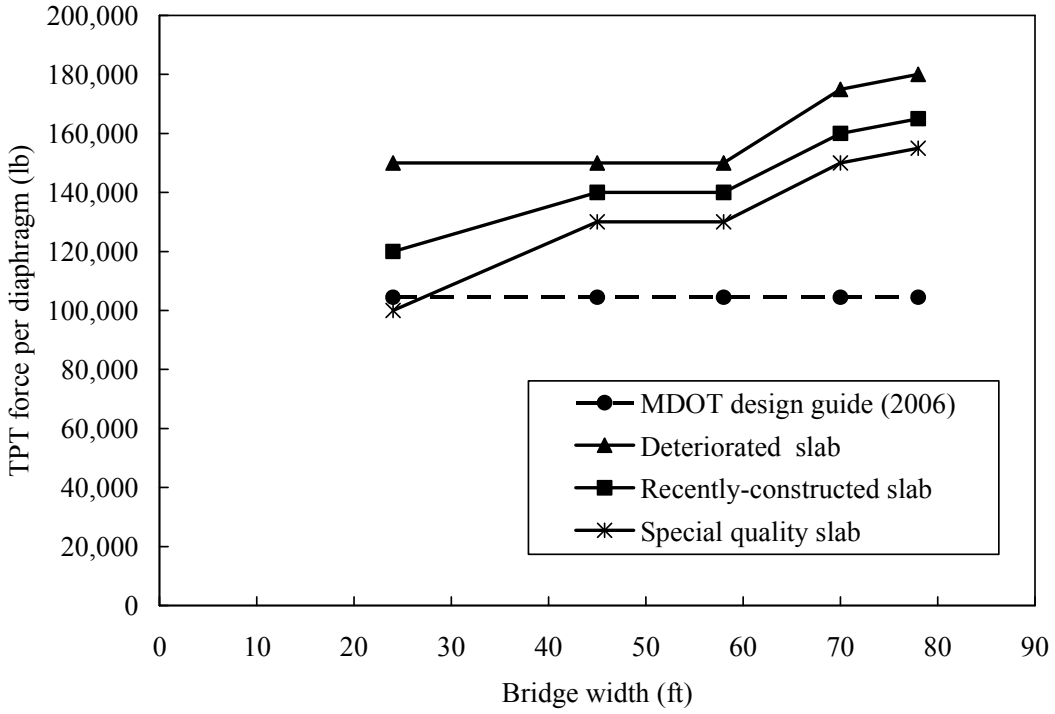

Figure 4.3-13 Appropriate TPT force vs. bridge width (valid for bridges constructed using 36 or 48 in wide box-beams).

CHAPTER 5: EXPERIMENTAL INVESTIGATION

5.1 Introduction

A 30° skewed precast prestressed box-beam bridge model was constructed to study its behavior in the transverse direction. The bridge model consisted of four adjacent precast prestressed concrete box-beams with a total span of 31 ft, as shown in Figure 5.1-1. The four box-beams were designated as B-1, B-2, B-3, and B-4.

Figure 5.1-1 General view of precast prestressed box-beam bridge model.

The construction of the formwork of the box-beams and the steel cages was completed in the casting yard located in the Center for Innovative Materials Research (CIMR) at the Lawrence Technological University (LTU). The precast prestressed concrete box-beams were pre-tensioned using seven-wire steel strands and constructed from high strength concrete. When the beams had gained adequate strength, the prestressing forces were released and subsequently, the beams were transported to the Structural Testing Center (STC) at the LTU. The bridge model was assembled using the four box-beams, steel reinforced deck slab, shear-

keys, and unbonded transverse post-tensioning (TPT) strands using carbon fiber composite cables (CFCC).

After the bridge deck slab had gained adequate strength, the experimental investigation was launched to study the transverse behavior of the bridge model under three different service life conditions. The first condition (uncracked deck slab) simulated a highway bridge, which was newly constructed and has not experienced any major cracks on the bridge deck. The second condition (cracked deck slab) simulated a highway bridge, which had experienced longitudinal deck cracking over the shear-key locations. The third condition (beam replacement stage), where an individual box-beam of the bridge was assumed damaged and replaced.

The bridge model behavior under these three conditions was evaluated using the strain and the load distribution tests. The purpose of the strain distribution test was to monitor the transverse strains developed in the deck slab due to the application of different levels of TPT force with different number of diaphragms. The purpose of the load distribution test was to investigate the deflection behavior of the individual box-beams and the deflection based load distribution when applying eccentric loads. In addition, the ultimate load test was conducted on the bridge model to study the efficiency of the TPT system and to determine the ultimate load-carrying capacity.

The chapter is divided into two major sections:

1. Construction program of the bridge model containing the description of all the materials used and a detailed description of the formwork and the steel cage construction.
2. Test program including the instrumentation of the bridge model and a detailed description of all the tests conducted in the study.

5.2 Bridge Model Construction Phase

5.2.1 Materials

The bridge model consisted of box-beams, shear-keys, deck slab, and TPT strands. These components were constructed from high strength concrete, steel reinforcements, non-shrink grout, and CFCC. Details of these materials are provided in the following sections.

5.2.1.1 Concrete

The precast prestressed concrete box-beams were made of high strength concrete, with steel prestressing strands and non-prestressing steel rebars as flexural reinforcements. Steel stirrups were also provided as shear reinforcement. The box-beams were constructed from a high strength concrete mix. The concrete mix design and the quantities as delivered are shown in Table 5.2-1. In order to ensure that the concrete mix had the appropriate workability before casting the beams, two slump tests were conducted. The designed slump was 8 in., which was close to the measured slump. Electrical vibrators as well as mechanical rods were used during the casting of the beams to ensure a uniform compaction of the concrete. The uniaxial compressive strength was determined according to the American Society for Testing and Materials (ASTM) C39 at 7, 21, and 28 days. The average 28 day compressive strength was 6,268 psi, as shown in Figure 5.2-1. The uniaxial compression test apparatus is shown in Figure 5.2-2. The mechanical properties of concrete mix are tabulated in Table 5.2-2.

Table 5.2-1 Concrete mix proportions for beams.

Material	Design Quantity per Cubic Yard, lb	Total Quantity, lb
Fine aggregates	1,287	7,915
Coarse aggregates	1,760	10,560
Cement (Type 1)	534	3,204
Cementitious material	288	1,728
Water reducing admixture	2.05	12.33
High range water-reducer	6.17	37
Water	265	1,590

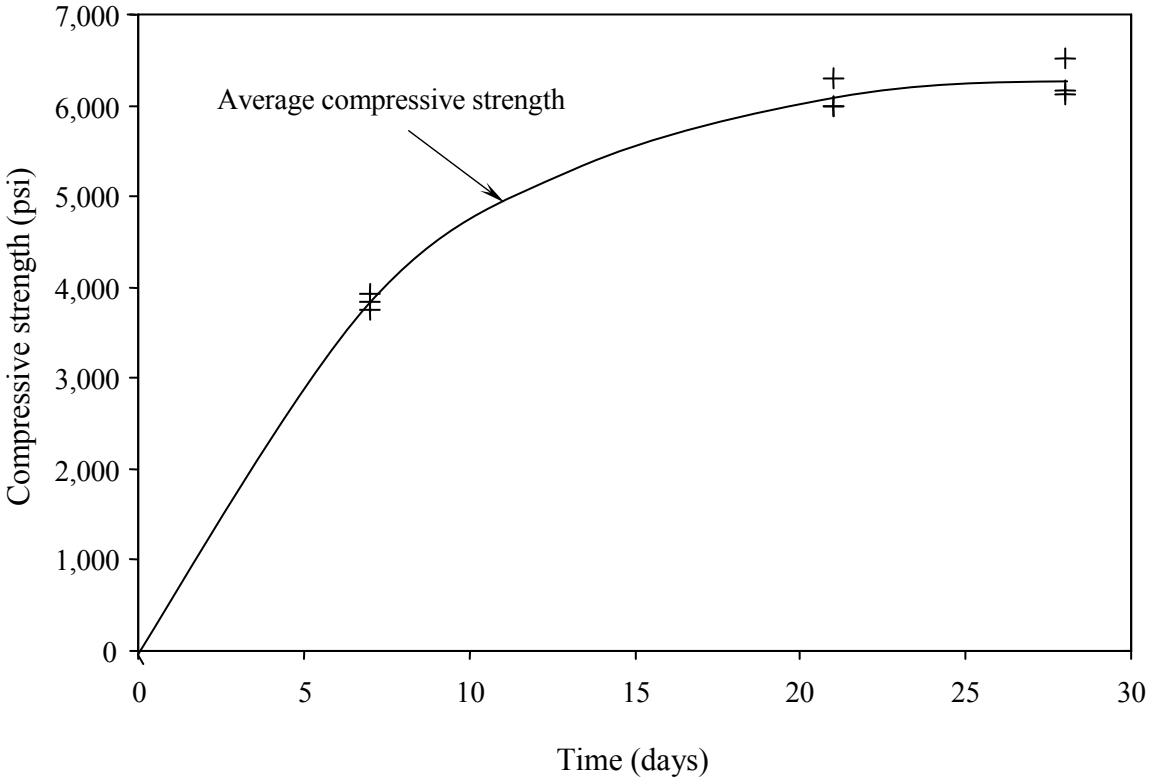

Figure 5.2-1 Compressive strength of concrete with time.

Table 5.2-2 Mechanical properties of the concrete mix.

Time, Days	Compressive Strength, psi	Average Compressive Strength, psi	Modulus of Elasticity, ksi
7	3,749	3,837	N/A*
	3,836		
	3,926		
21	6,287	6,086	N/A
	5,990		
	5,981		
28	6,130	6,268	4,450
	6,510		
	6,164		

N/A*: Not Applicable

(a) Concrete cylinder being tested (b) Failure of concrete cylinder

Figure 5.2-2 Typical uniaxial compression test setup for concrete cylinders.

5.2.1.2 Steel Reinforcement

The box-beams were constructed from steel reinforcement cages as mentioned earlier. The flexural reinforcement consisted of non-prestressing rebars and seven-wire prestressing strands. Details of the various reinforcements are presented in the following sections.

Prestressing strands

The longitudinal prestressing reinforcement used was 0.5 in. high strength low-relaxation seven-wire steel strands of Grade 270 supplied by the Victory Re-Steel, Inc. Three strands were provided in each box-beam at the bottom level resulting in an eccentricity of 5 in. from the centroid of the cross-section of the box-beam. Typical mechanical properties of the steel strands used are shown in Table 5.2-3 (Nawy, 2003).

Non-prestressing bars

Conventional normal-strength #4 steel bars of Grade 60 were used as the longitudinal non-prestressing reinforcements. Typical characteristics and mechanical properties of the #4 bars are shown in Table 5.4 (Macgregor and Wight, 2004). Each box-beam consisted of four bottom and four top non-prestressing reinforcements.

Shear reinforcements

The shear reinforcements were stirrups made of conventional #3 steel bars of Grade 60, and its characteristics and mechanical properties are shown in Table 5.2-4 (Macgregor and Wight, 2004). The non-prestressing reinforcements were tied to the stirrups using commercially available Weather Resistant Nylon Wire Ties (plastic zip-ties) supplied by the Industrial Products, Inc.

Table 5.2-3 Characteristics and mechanical properties of a typical seven-wire steel strand.

Property of Strand	Seven-Wire Prestressing Steel Strands
Grade	270
Nominal diameter, in.	0.5
Nominal weight, lb/ft	0.52
Cross-sectional area, in^2	0.153
Perimeter, in.	1.571
Min. breaking strength, lb	41,300
Specified minimum yield strength, ksi	229.5
Minimum tensile strength, ksi	250
Modulus of elasticity, ksi	27,000
Minimum load at 1% extension, lb	35,100
Yield strain, %	1

5.2.1.3 Carbon Fiber Reinforced Polymers (CFRP) Reinforcement

Conventional steel strands used as TPT system for side-by-side box-beam bridges are usually vulnerable to corrosion when exposed to harsh environmental conditions and deicing salt. The detrimental effect of this phenomenon is the reduction of the strength of the steel strands, which leads to a reduction in the load-carrying capacity of the bridge. To avoid this problem, the concept of using CFRP strands was introduced as an alternative material. The CFRP used for this project was CFCC manufactured by the Tokyo Rope Mfg. Co., Ltd., Japan. A total of

ten 1×7 0.67 in. diameter CFCC were used during the test program to apply the TPT forces at the transverse diaphragms. Table 5.2-.5 and Figure 5.2-3 show the mechanical properties and dimensions of the CFCC, respectively.

Table 5.2-4 Mechanical properties of the non-pretsressing bars and stirrups.

Property of Reinforcements	Non-Prestressing Bars	Stirrups
Designation	#4 bars	#3 bars
Grade	60	60
Diameter, in.	0.5	0.375
Weight, lb/ft	0.668	0.376
Cross-sectional area, in^2	0.20	0.11
Perimeter, in.	1.571	1.178
Yield load, kip	12	6.6
Minimum yield strength, psi	60,000	60,000
Breaking strength, kip	18	9.9
Minimum tensile strength, psi	90,000	90,000
Modulus of elasticity, ksi	29,000	29,000
Minimum elongation, %	9	9

Table 5.2-5 CFCC Quality Report (Tokyo Rope Mfg. Co., Ltd., 2007).

Item	Specifications		Test Results				
	Nominal	Tolerance					
Lot No.	_	_		N346	_	_	_
Diameter, in.	0.67		Ave.	0.68	_	_	_
Effective cross- sectional area, in^2	0.23		_	_	_	_	_
Pitch, in.	_		Ave.	9.53	_	_	_
Linear density, lb/in.	16.2		Ave.	15.98	_	_	_
Breaking load, kip	78.4	78.4 or above	Ave.	92.29 95.42 84.90	_	_	_
Tensile strength, ksi	0.34	0.34 or above	Ave.	0.39	_	_	_
Tensile rigidity, kip	_	_	Ave.	5,279.7	_	_	_
Tensile modulus, ksi	22,330	_	Ave.	22,620	_	_	_
Elongation at break, %	1.5	_	Ave.	1.8	_	_	_

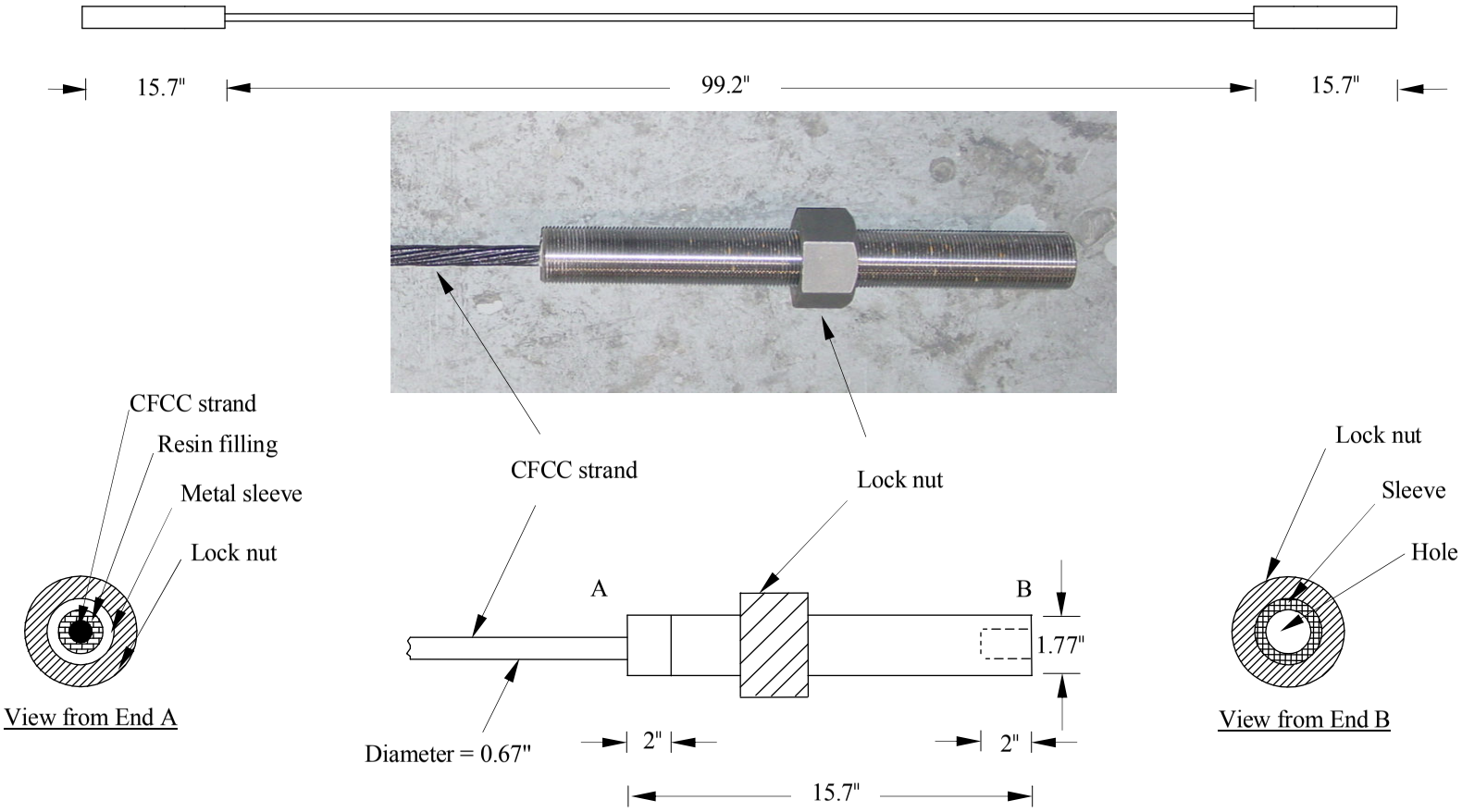

Figure 5.2-3 Dimensions of 1×7, 0.67 in. diameter CFCC for TPT.

5.2.2 Formwork

The formwork was designed to facilitate easy construction and disassembling. The formwork, constructed mainly from plywood, consisted of chairs, base plates, center plate and side plates. The formwork was supported on chairs with two vertical stiffeners at a spacing of 3 ft beneath the base plates to prevent the base plate from sagging when subjected to the weight of the concrete. Horizontal and vertical stiffeners were also provided to support the side plates and to ensure straight alignment of the edges of the box-beams. The cross-sections of the formwork for the interior and exterior beams are shown in Figure 5.2-4.

The formwork of the two exterior beams (B-1 and B-4) was constructed next to each other, likewise the two interior beams (B-2 and B-3). The major difference between the exterior box-beams and the interior box-beams was the presence of the protruded steel notches provided at the transverse diaphragm locations of the exterior beams, as shown in Figure 5.2-5. Steel plates of 0.08 in. thick were used as metal forms for the exterior beams notches. The inner faces of the exterior box-beams and both the inner and the outer faces of interior box-beams were designed geometrically to form full-depth keyways when placed side-by-side. Steel tie rods of 0.5 in. diameter were also provided to hold the center plate and the side plates in place, which ensured that the designed width of the box-beams was maintained while the concrete cured. More details of the formwork are shown in Figures 5.2-6 through Figure 5.2-1.

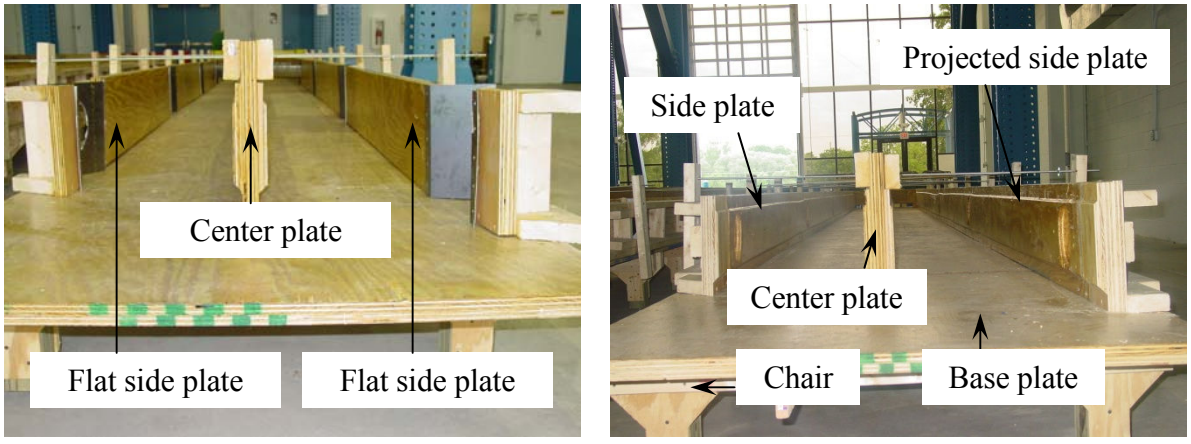

(a) Exterior box-beams (b) Interior box-beams

Figure 5.2-4 Cross-section of formwork.

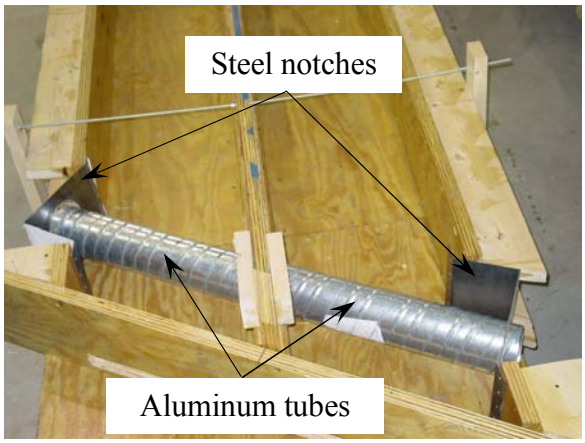

(a) Plan view for steel notches

(b) Side view for steel notches

Figure 5.2-5 Details of the steel notches.

(a) Side view of formwork

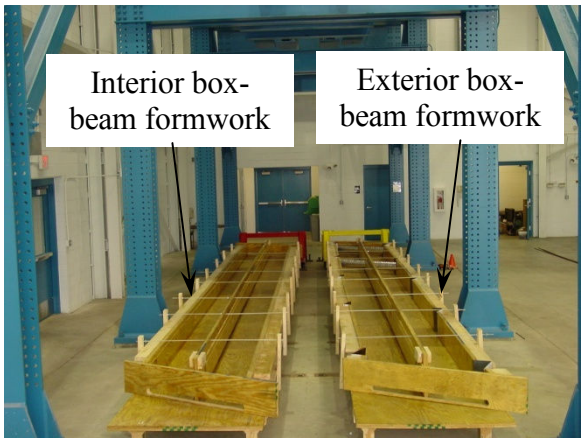

(b) General view of formwork

Figure 5.2-6 Formwork prepared for box-beams.

In order to accommodate the TPT strands and to avoid potential misalignment problems due to differential camber, oval-shape ducts were created by inserting aluminum tubes at the appropriate transverse diaphragm locations, as shown in Figure 5.2-5(a). The major vertical axis and the minor horizontal axis of the tube were 5.75 in. and 4.5 in., respectively.

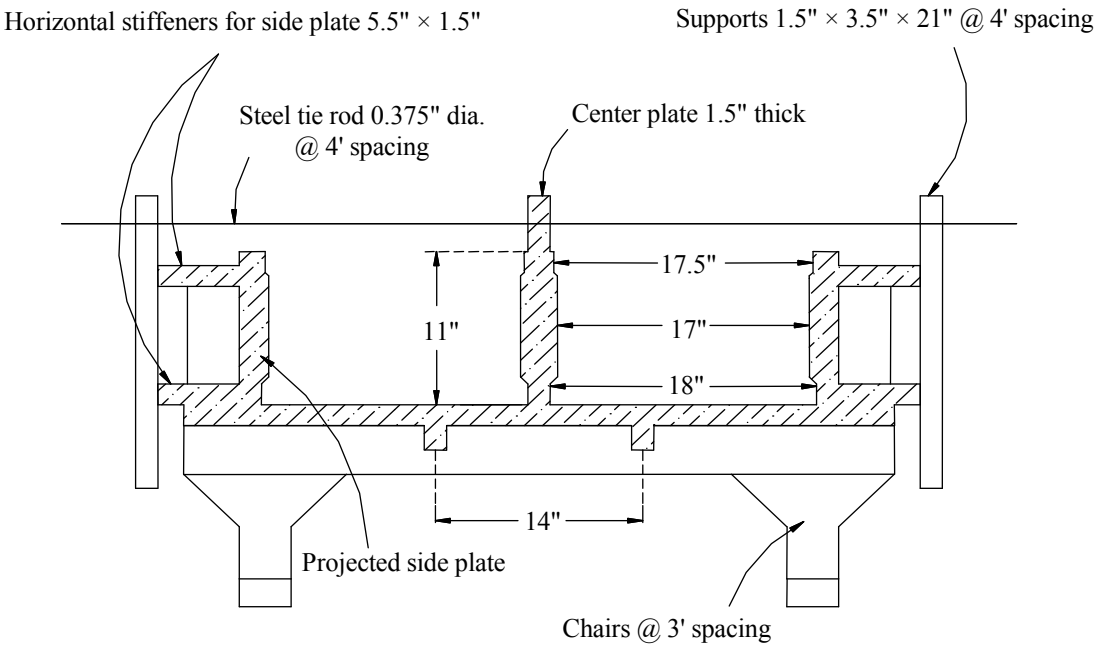

Figure 5.2-7 Cross-section of the formwork for the interior box-beams.

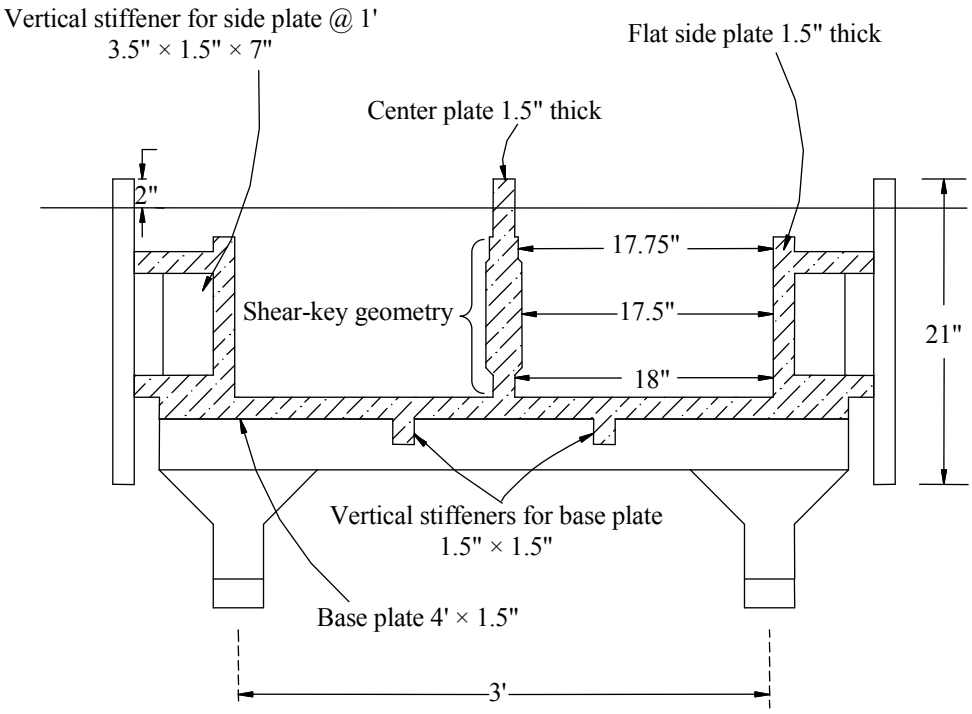

Figure 5.2-8 Cross-section of the formwork for the exterior box-beams.

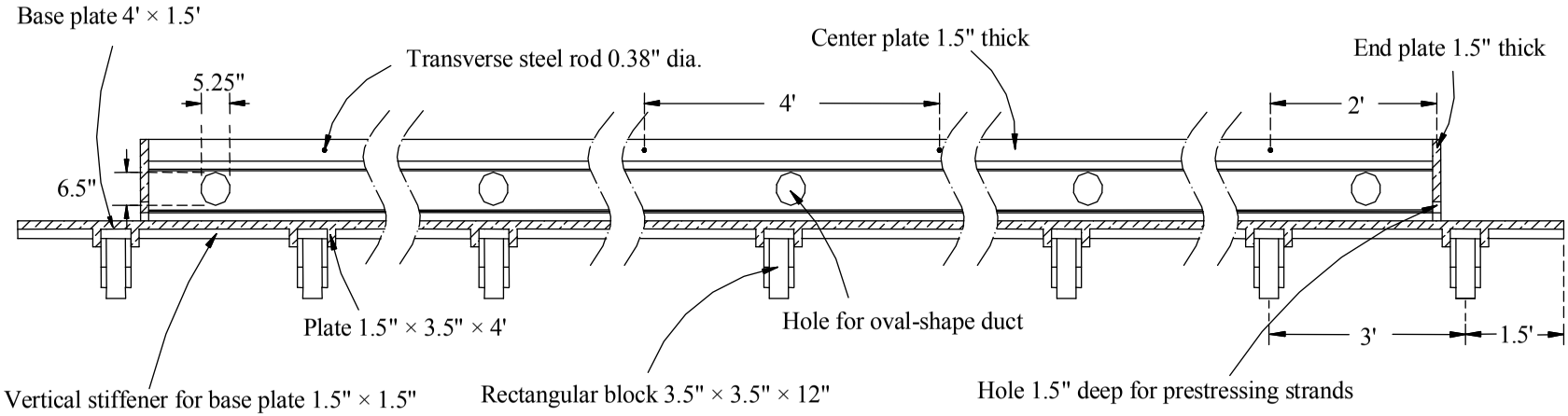

Figure 5.2-9 Longitudinal section of the formwork.

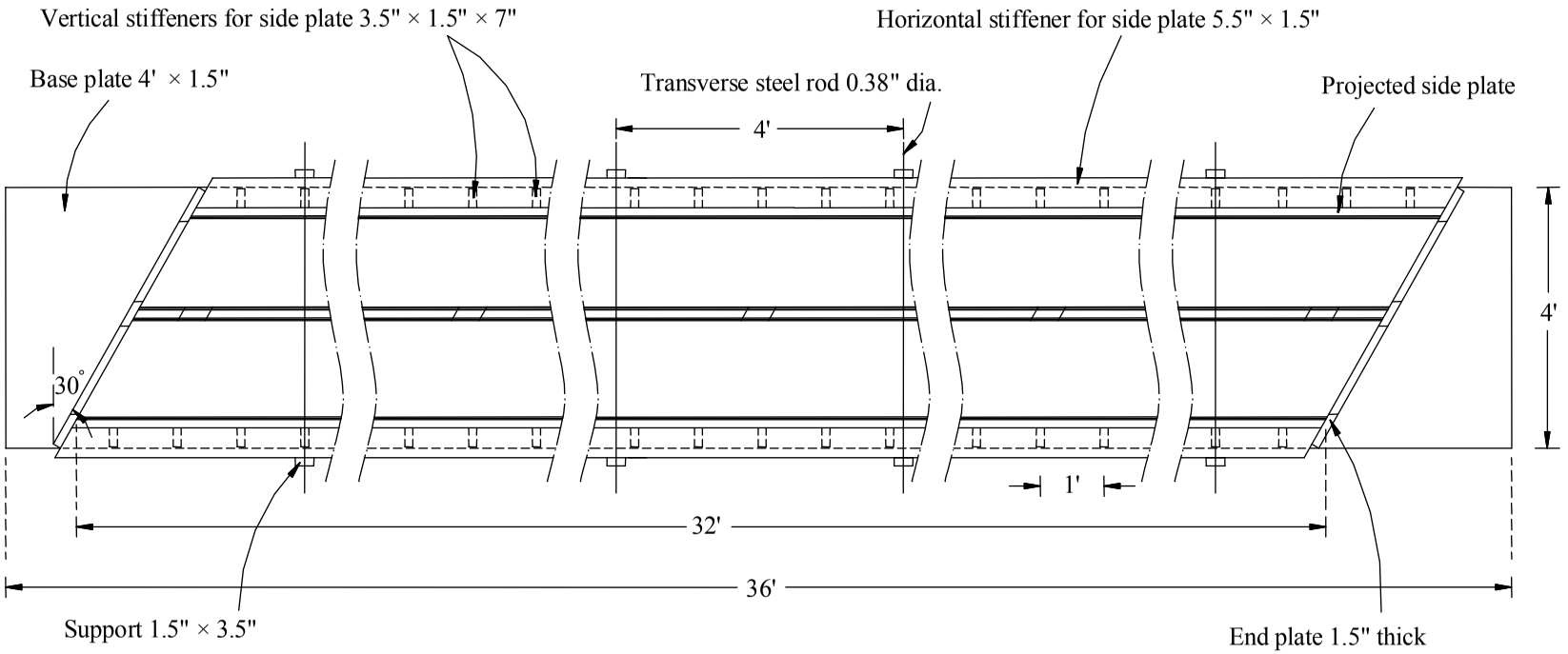

Figure 5.2-10 Plan view of the formwork for box-beams.

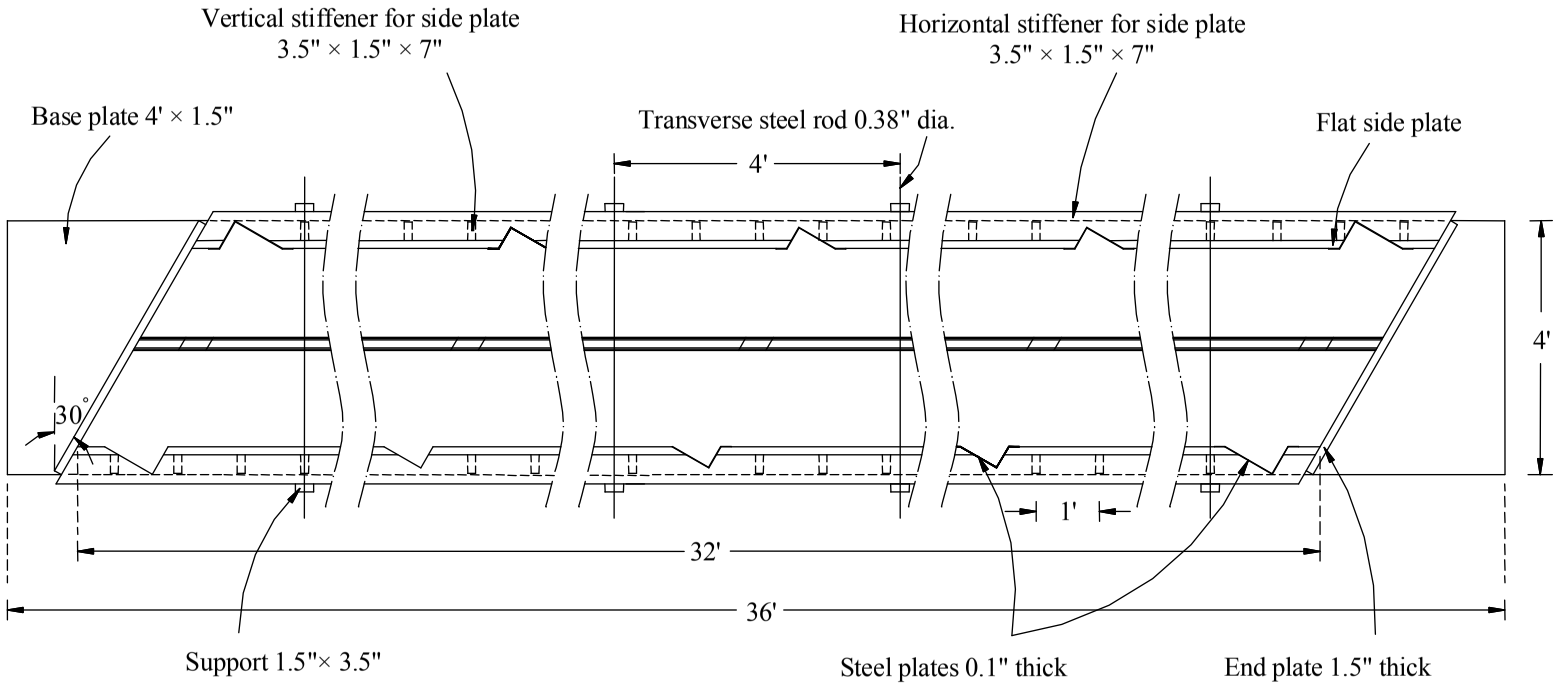

Figure 5.2-11 Plan view of the formwork for box-beams with projected side plates.

5.2.3 Reinforcement Cages

As mentioned earlier, each box-beam consisted of four #4 non-prestressing bars provided as top and bottom reinforcements. In addition, three 0.5 in. seven-wire steel strands were provided as prestressing strands and were located 2 in. from the bottom surface of the box-beams. The top reinforcements were located at 1.5 in. from the top surface of the box-beams and were held in position using #4 hanger bars placed at successive spacing of 4 ft. The stirrups were 11 in. deep and 15 in. wide from center-to-center and were placed at equal spacing of 5 in. The stirrups protruded 1.5 in. from the top surface of beams to achieve composite action between the box-beams and deck slab. Styrofoam of depth 5 in. and width of 10 in. was used to create the hollow portion within the cross-section of the box-beams and was placed at the mid-height of the box-beam cross-section. The box-beam cross-section is shown in Figure 5.2-12. The cross-section of the box-beams at the locations of the transverse diaphragms was modified to accommodate the Styrofoam gasket in order to ensure continuity of the aluminum tube in each beam and to also facilitate grouting of the shear-keys. The modified box-beam cross-section at diaphragm locations is shown in Figure 5.2-13.

Galvanized aircraft lifting cables were attached to the reinforcement cages at five equally spaced locations along the span to facilitate transportation and handling of the box-beams from the casting yard in the CIMR to the STC. The cables were made out of high strength strands with diameter of 0.25 in. and axial ultimate capacity of 7 kip as specified by the supplier, National Tool Grinding, Inc. Figure 5.2-14 and Figure 5.2-15 show the longitudinal section of the box-beam and steel reinforcement cages, respectively.

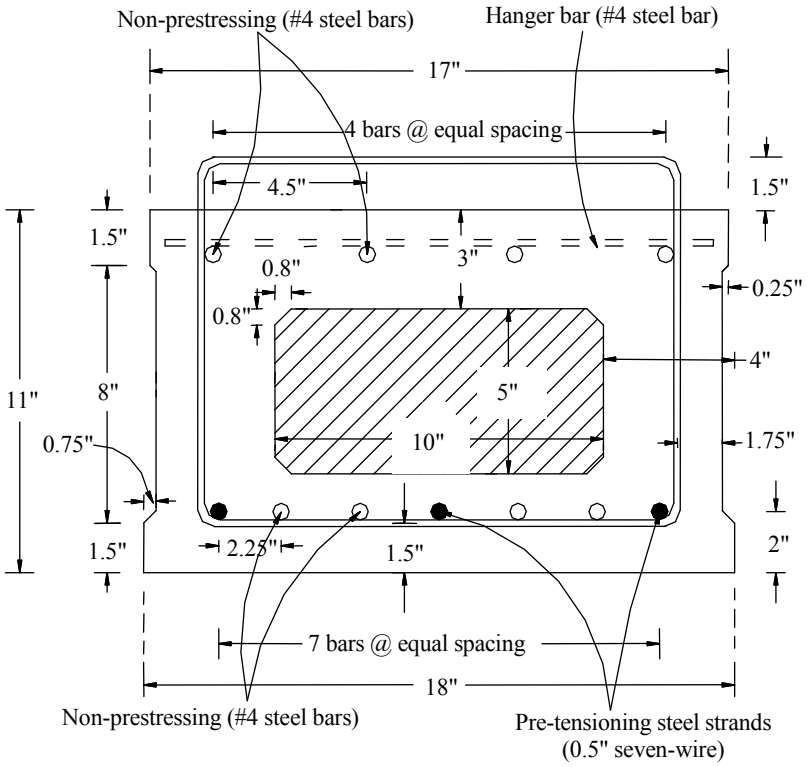

Figure 5.2-12 Cross-sectional details of the box-beams.

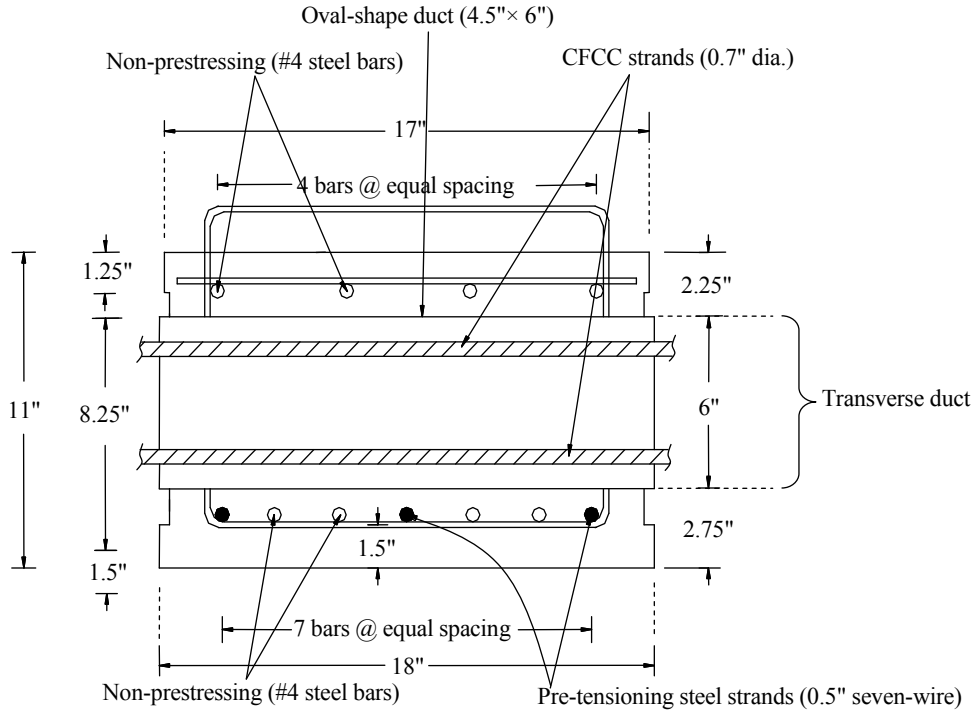

Figure 5.2-13 Cross-sectional details of the box-beams at diaphragms.

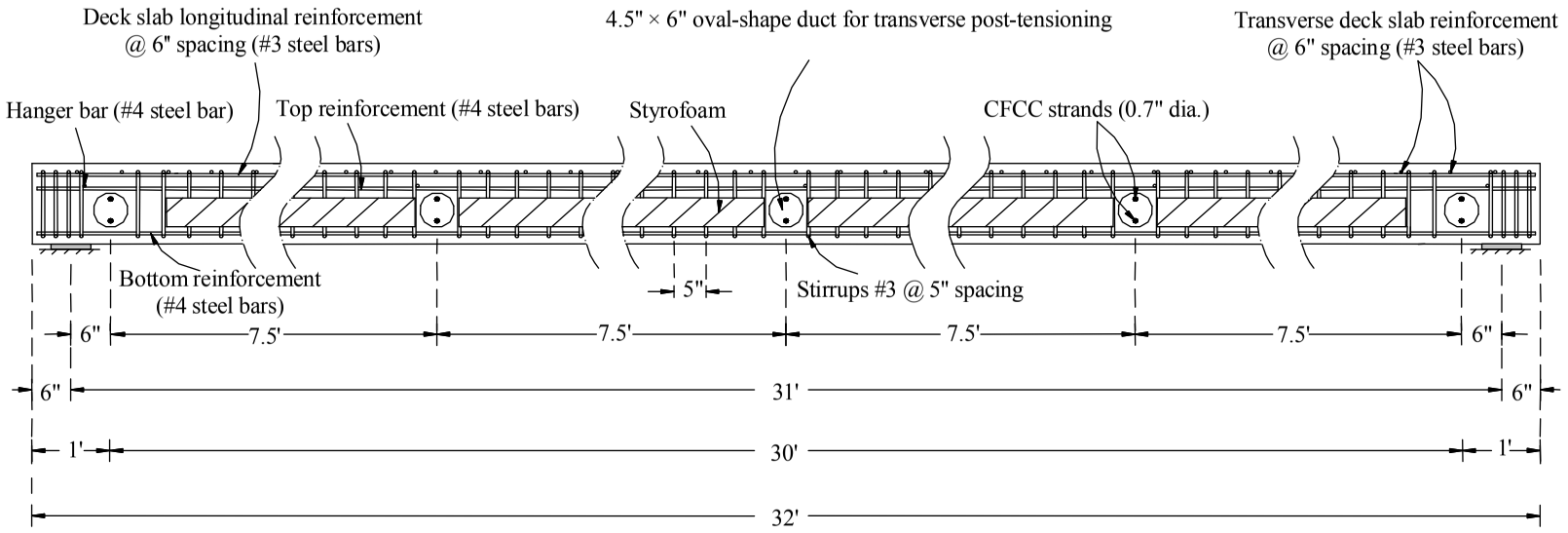

Figure 5.2-14 Longitudinal section details of box-beams.

(a) Reinforcement cages for the box-beams (b) Diaphragm reinforcement details

Figure 5.2-15 Steel reinforcement cages containing Styrofoam within.

5.2.4 End-Blocks

The end-blocks were designed to accommodate the localized stresses due to the pre-tensioning forces applied to the box-beams. Different levels of pre-tensioning forces were applied in order to develop the differential camber between the adjacent box-beams such as observed in the field. The reduced spacing between the stirrups at the end-blocks were employed to provide confinement for the concrete in order to resist the localized stresses that would be developed due to the pre-tensioning forces. The strength of the concrete was designed to resist the developed localized stresses at the end-blocks. The arrangements of the stirrups provided at the end-blocks and the end diaphragms are shown in Figures 5.2-16 through 5.2-18.

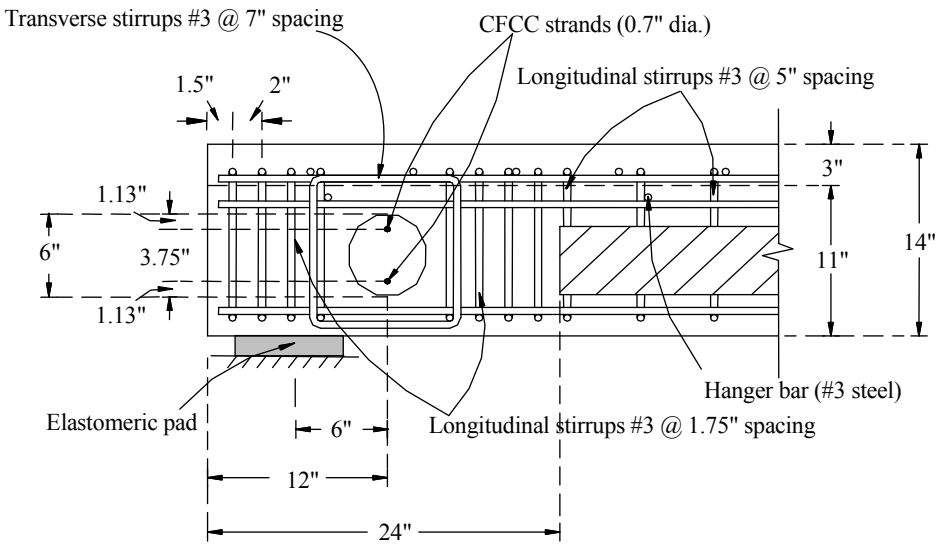

Figure 5.2-16 Cross-sectional details of the end diaphragm.

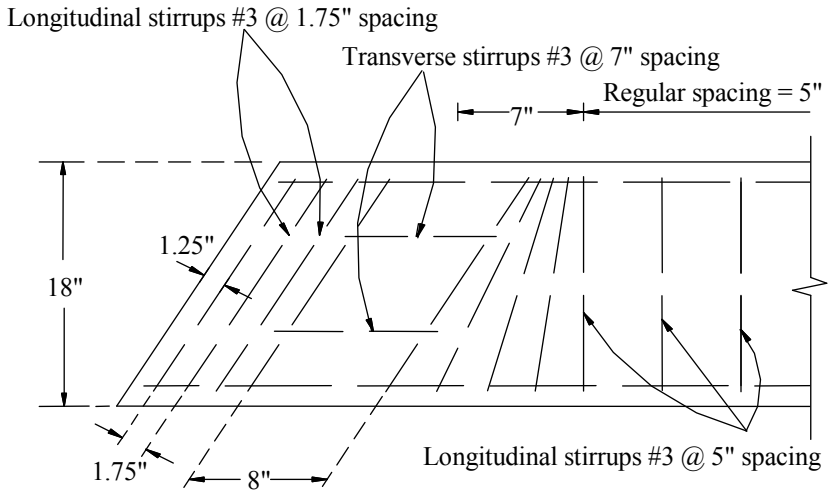

Figure 5.2-17 Reinforcement of interior box-beams at the end diaphragm.

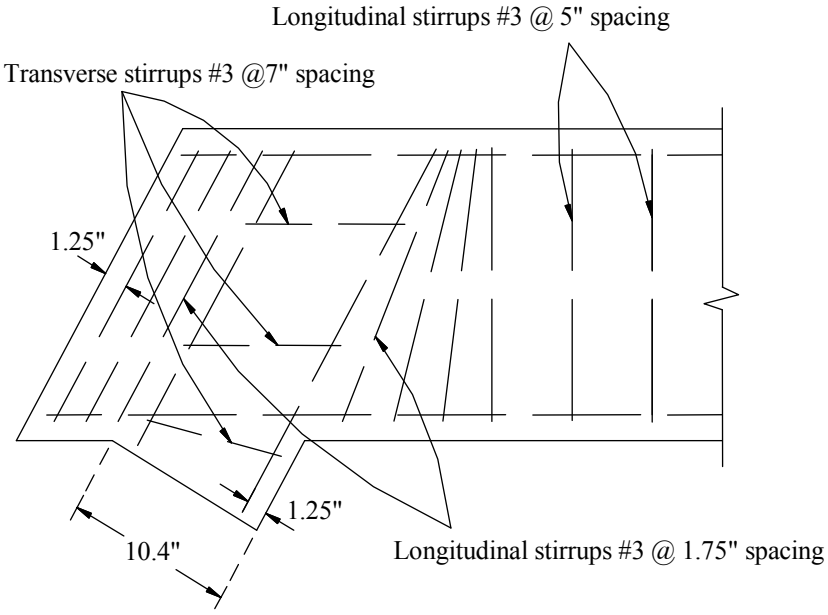

Figure 5.2-18 Reinforcement of exterior box-beams at the end diaphragm.

5.2.5 Transverse Diaphragms

As mentioned earlier, each box-beam contained five transverse diaphragms located at the ends, quarter-span, and the mid-span locations. The width of the intermediate diaphragms was 8 in. while that of the end/support diaphragms was 10.4 in. Because the bridge model had 30° skewed alignment, the centerlines of the diaphragms were made parallel to the support lines (i.e. making an angle of 60° with the longitudinal axis of the bridge model). The stirrups provided between the locations of the diaphragms were placed perpendicular to the longitudinal axes of the box-beams. However, the stirrups near the diaphragms locations were placed at gradually varying angles to ensure uniformity with the alignment of the transverse diaphragm. In addition, transverse stirrups were also provided within the diaphragms and placed at 7 in. spacing in order to resist localized stresses developed due to TPT forces as stipulated in the (MDOT Bridge Design Guide 6.65.12 and 6.65.13). The reinforcements provided in the transverse intermediate diaphragms for the interior and exterior box-beams are shown in Figure 5.2-19 through Figure 5.2-21. The details of the steel cages and the transverse ducts located at the transverse diaphragms locations are also shown in Figure 5.2-22.

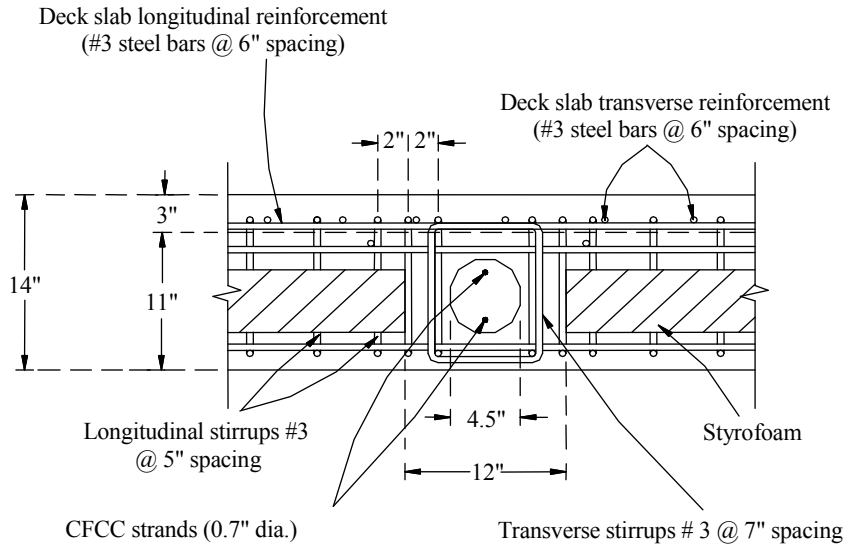

Figure 5.2-19 Cross-sectional details of intermediate diaphragm.

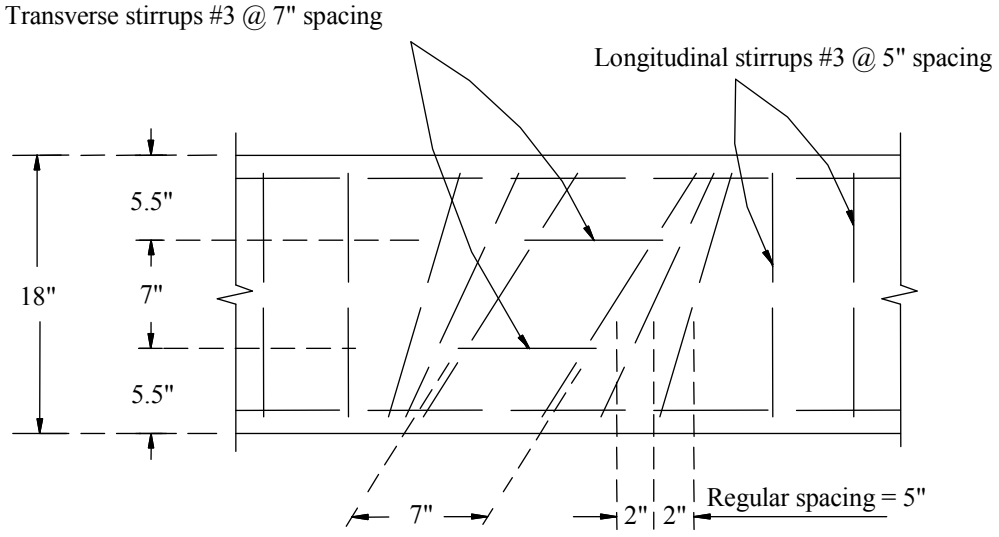

Figure 5.2-20 Reinforcement of interior box-beams at the intermediate diaphragm.

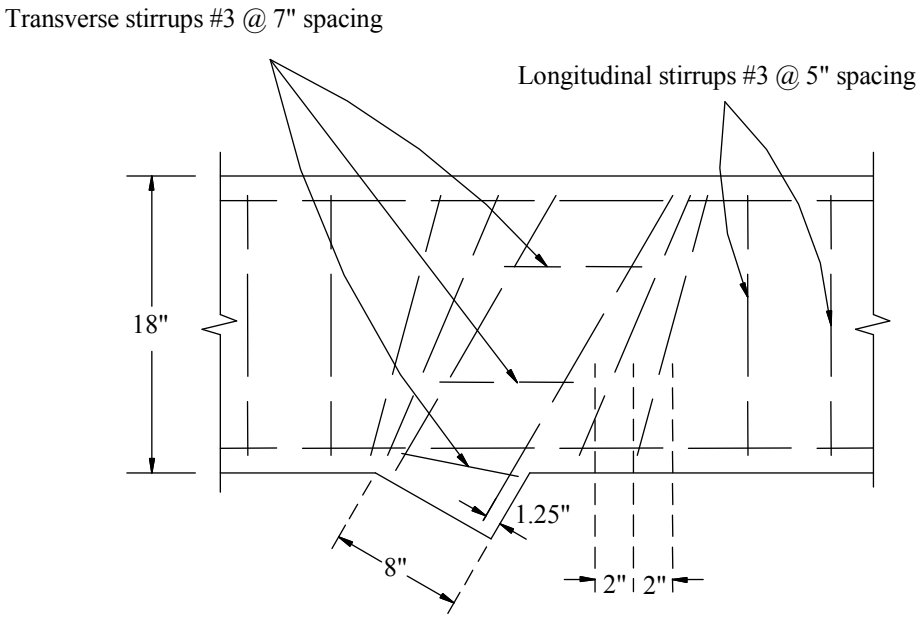

Figure 5.2-21 Reinforcement of exterior box-beams at the intermediate diaphragm.

5.2.6 Prestressing of Steel Strands

After the construction of the steel cages and the formwork were completed, the steel cages were placed inside the formwork. Plastic chairs with effective height of 1.25 in. were attached to the underside cages to create the bottom concrete cover, subsequently, another set of chairs with effective height of 0.75 in. were also attached to either side of the cages to create the concrete cover along the sides.

Bulkheads, needed for prestressing, were placed at both ends of the formwork, one set for the interior beams and one set for the exterior beams. Each bulkhead was anchored to the ground with six 1 in. diameter high strength bolts in order to transfer the pre-tensioning forces of the steel strands to the foundation. The steel strands were inserted through the holes of bulkheads along the length of box-beams. Conventional steel chucks were used as anchorage systems for the steel strands and attached at both the live and the dead-ends of the steel strands, as shown in Figure 5.2-23.

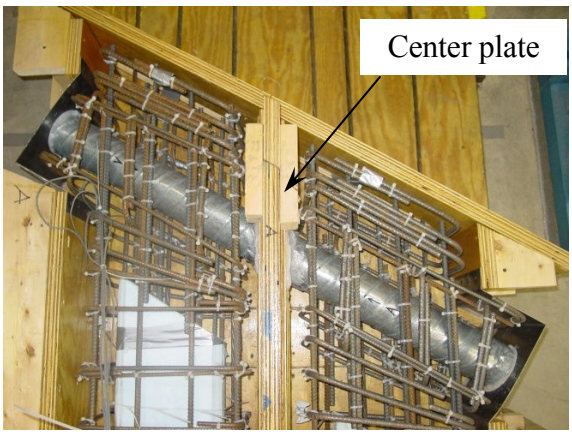

(a) End diaphragm for exterior beams

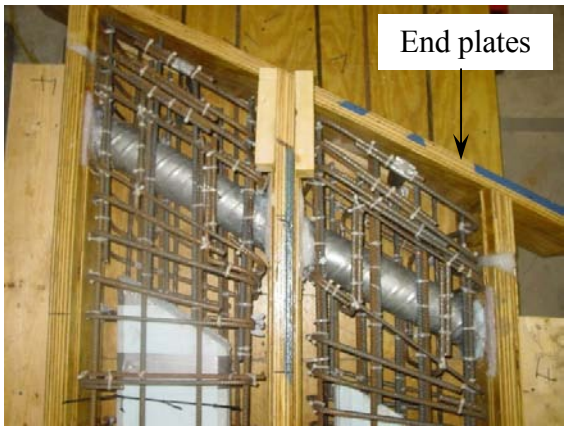

(b) End diaphragm for interior beams

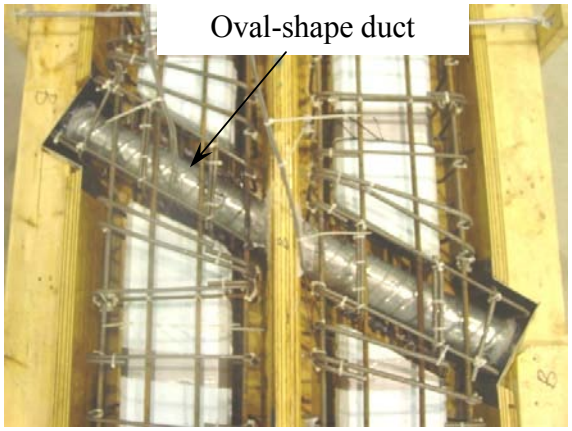

(c) Intermediate diaphragm for exterior beams

(d) Intermediate diaphragm for interior beams

Figure 5.2-22 Reinforcements and oval-shape ducts at the transverse diaphragms locations.

The live-end is the end of the box-beam where the strands are pulled while the other end is the dead-end. Center-hole load cell was attached to the dead-end of each strand to monitor the pre-tensioning forces applied to the steel strands during the pre-tensioning operation, as shown in Figure 5.2-23. The pre-tensioning sequence was designed to prevent the rotation of the bulkheads due to a possible eccentric reaction of the pre-tensioning force applied in the strands. Elongations of the steel strands were also measured to confirm the stresses developed due to pre-tensioning, as presented in Table 5.2-6. The pre-tensioning of the steel strands is shown in Figure 5.2-24.

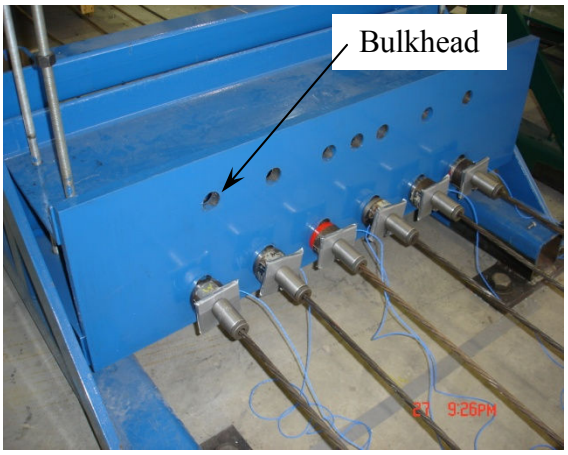

(a) Bulkhead placed at the dead-end

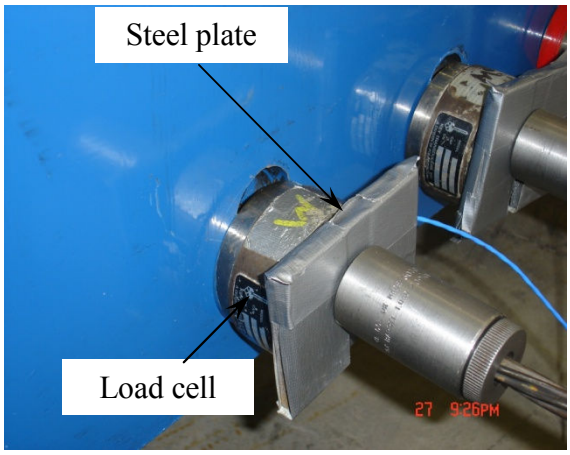

(b) Details of the dead-end for steel strands

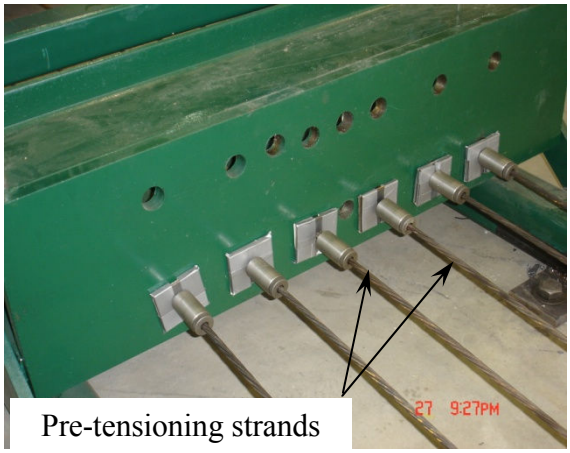

(c) Bulkhead placed at the live-end

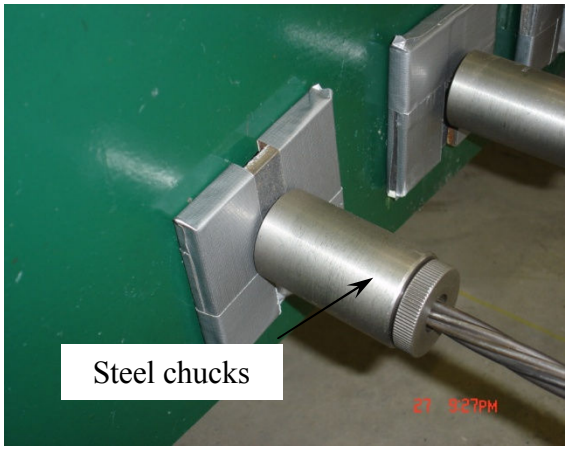

(b) Details of the live-end for steel strands

Figure 5.2-23 Instrumentation of the pre-tensioning steel strands.

In order to simulate differential camber observed in the field, the two exterior beams were prestressed with an average force of 20 kip/strand, i.e. 60 kip/box-beam, while the interior beams were prestressed with an average force of 25 kip/strand, i.e. 75 kip/box-beam. As a result, different levels of cambers were anticipated to occur at the mid-span of the exterior and the interior box-beams. The levels of prestressing measured during the casting of the concrete are shown in Table 5.2-6.

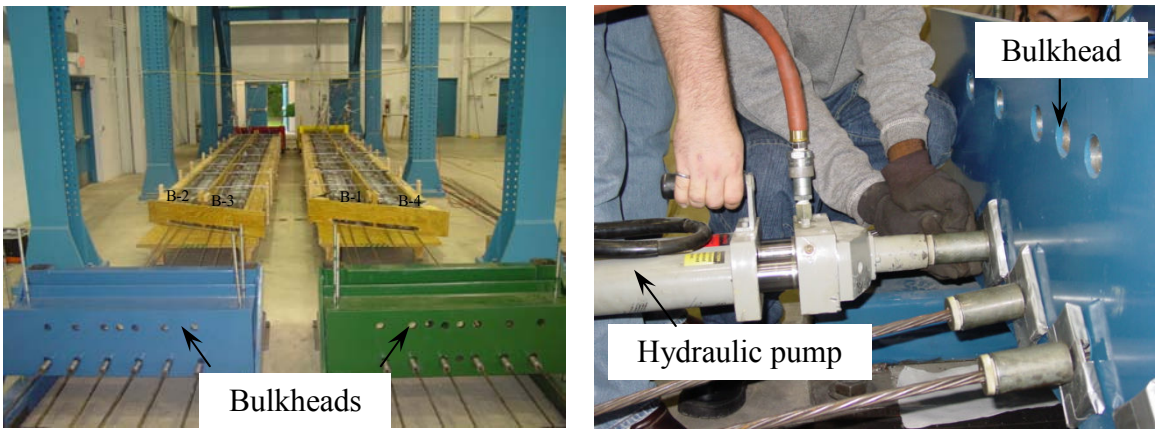

(a) Live-end for box-beams (b) Prestressing of steel strands

Figure 5.2-24 Pre-tensioning operation at the live-end of the box-beam.

5.2.7 Concrete Placement

A ready-mix concrete was used to cast the four box-beams. As mentioned earlier, the concrete mix was designed to achieve the required strength and the proper workability. Two slump tests were conducted according to ASTM C143/C143 to confirm the required workability of the concrete during the casting process. One test was conducted just before casting of the box-beams and the other was conducted immediately after casting two box-beams. The designed slump was 8 in. The first measured slump was 9 in. and the second slump was 8 in.

In order to ensure uniform compaction, three electrical pencil vibrators were used, simultaneously. Moreover, mechanical rods were used around the diaphragm locations and the end-block locations where the steel reinforcements were closely spaced. The box-beams were cast in succession (one after the other) in order to avoid premature setting of a concrete. Twenty test cylinders, 6 in. diameter and 12 in. in height were cast. Ten of them were cast at the beginning of placing the concrete in the box-beams and the remaining ten were cast immediately after casting the first two box-beams. The total duration of the concrete placement was approximately two hours. Figure 5.2-25 shows slump test in progress and cylinders been formed. Figure 5.2-26 shows the casting and curing of the box-beams.

Table 5.2-6 Pre-tensioning forces and the corresponding elongations of steel strands.

Box-Beam	Strand	Pre-Tensioning Force, kip	Average Force per Strand, kip	Elongation, in.
B-1 (exterior)	1	21.79	20.90	3.52
	2	20.67		3.40
	3	20.25		3.75
B-2 (interior)	1	25.73	25.14	4.80
	2	24.6		4.63
	3	25.08		4.10
B-3 (interior)	1	24.83	24.87	4.85
	2	24.58		4.45
	3	25.20		4.30
B-4 (exterior)	1	19.19	20.3	3.25
	2	20.36		3.86
	3	21.40		3.38

The load cells were connected to the data acquisition system and the forces in the prestressing strands were monitored continuously for one week after casting the box-beams. The box-beams and test cylinders were cured using wet burlap covered with plastic sheets to prevent water from evaporation during the hydration process. The side plates of the box-beams were removed the following day to ensure proper curing by increasing the surface area exposed to moisture.

(a) Compaction of concrete during slump test

(b) Measuring of concrete slump

(c) Compaction of concrete cylinders

(b) Smoothening of concrete cylinders

Figure 5.2-25 Conducting concrete slump test and casting the cylinders.

5.2.8 Release of Pre-Tensioning Forces

The steel strands were cut from the bulkheads in order to transfer the compressive stresses to the concrete after it had attained adequate strength. As described earlier, compression tests were conducted on three test cylinders after 7, 21, and 28 days of casting of the box-beams to monitor the compressive strength of the concrete with time. Based on the results from the compressive strength test, it was determined that the concrete had gained the required strength after 21 days and hence the steel strands were cut. The sequence of cutting the strands followed the same as that of applying the pre-tensioning forces to avoid any rotation of the bulkheads. The steel pre-tensioning strands were cut using the standard shock de-tensioning method, in

which a hot, oxy-acetylene flame was used to melt the strands, as shown in Figure 5.2-27(a) and (b). The cutting operation was done simultaneously at both ends of the box-beam for each strand. No cracks were observed at the ends of the box-beams after cutting the prestressing strands.

(a) Vibration of concrete for exterior beam

(b) Casted box-beams

(c) Wetting of burlap for curing

(d) Covered box-beams

Figure 5.2-26 Placement of concrete and curing process.

One linear motion transducer was attached at the mid-span of each box-beam to measure the camber developed due to the release of pre-tensioning forces, as shown in Figure 5.2-27(c). The cambers recorded at this stage were 0.11 in. and 0.09 in. for the interior box-beams corresponding to the pre-tensioning force of 25 kip/strand. The cambers for the exterior box-beams were 0.02 in. and 0.05 in. corresponding to the pre-tensioning force of 20 kip/strand.

Demountable Mechanical (DEMEC) points were attached at both ends of the interior box-beams at the level of the prestressing strands to measure the compressive strains for the determination of the transfer length. The DEMEC points were not attached to the exterior beams because of presence of the protruded notches. Figure 5.27(d) shows the arrangement of the DEMEC points attached to the interior box-beams.

5.2.9 Transporting Precast Beams from Casting Yard to Test Frame

After cutting the steel strands, the four box-beams were removed from the formwork and transported from the casting yard at the CIMR to the STC, where they were tested. Each box-beam was lifted up from the four designed lifting points using crane which has a maximum capacity of 50 kip. At the STC, steel supports were arranged at 60° with respect to the longitudinal axis to simulate the skew angle of support lines of the bridge model. The steel supports were 14 in. wide, 54 in. long, and 30 in. high. Elastometric bearing pads, supplied by the Seismic Energy Products, L.P. Athens, Texas, with dimensions of 6 in. wide, 16 in. long and 1 in. thick, were placed between the box-beams and the steel supports. Figure 5.2-28 and Figure 5.2-29 show the transportation operation and alignment of the box-beams for the final arrangements of the bridge model.

5.2.10 Addition of Superimposed Dead Load

Figure 5.2-30 and Figure 5.2-31(a) show the box-beams aligned on the supports. In order to increase the differential camber developed between the interior and exterior box-beams, two superimposed dead loads each weighing 1,000 lb were placed on the exterior box-beams, as shown in Figure 5.2-31(b). The dead load was achieved by adding two tin containers, with diameter of 2 ft and depth of 3 ft, containing dry sand. The applied superimposed dead loads were placed at the mid-span of the box-beams in order to reduce the levels of camber of the exterior box-beam, and hence increase the differential camber between the interior and exterior box-beams to the order of 0.38 in. The superimposed dead loads were removed after a week. The cambers in all the four box-beams were continuously monitored for a period of three weeks and the results are discussed in the following chapter.

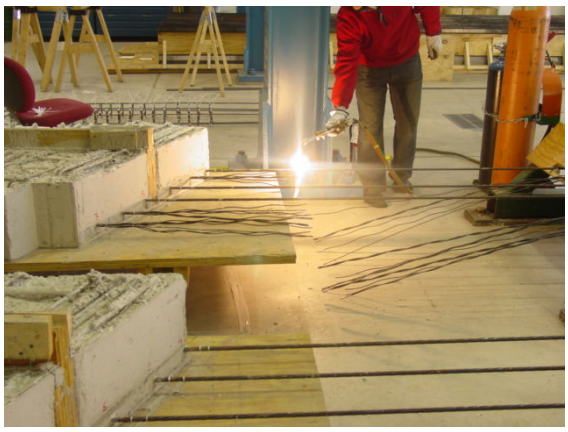

(a) Cutting of steel strands at live-end

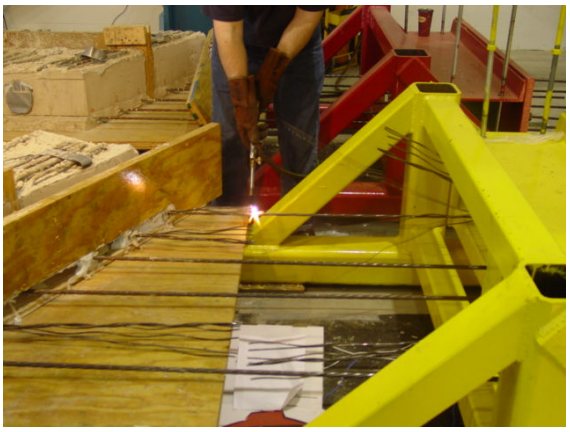

(b) Cutting of steel strands at dead-end

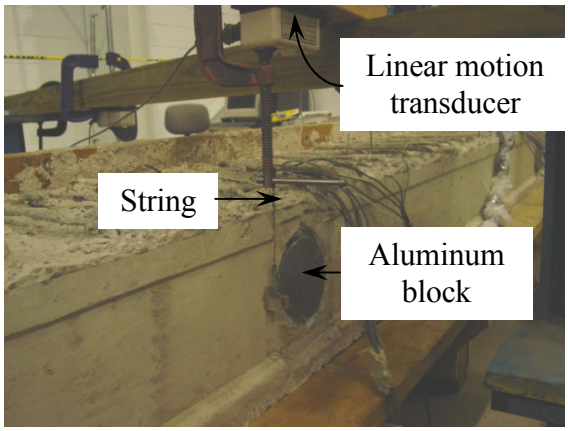

(c) Linear motion transducer at mid-span

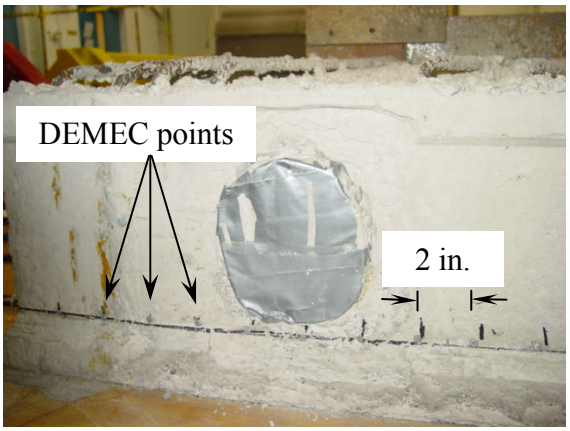

(d) DEMEC points at the end of box-beam

Figure 5.2-27 Instrumentation on box-beams and shock de-tensioning of steel strands.

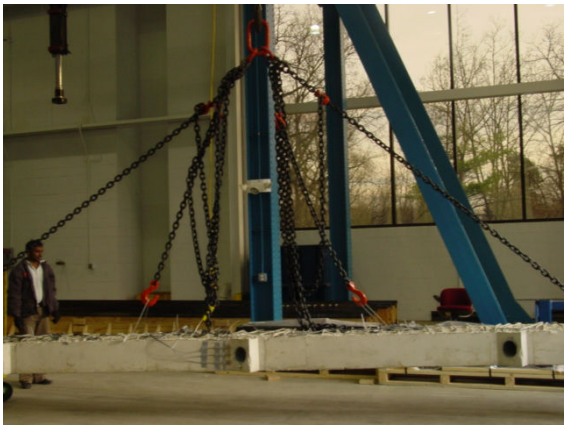

(a) Box-beam lifted using crane

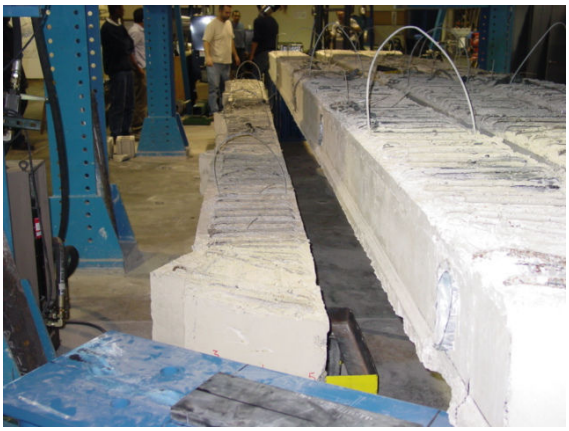

(b) Placing box-beam on supports

Figure 5.2-28 Transportation of precast box-beams to the STC.

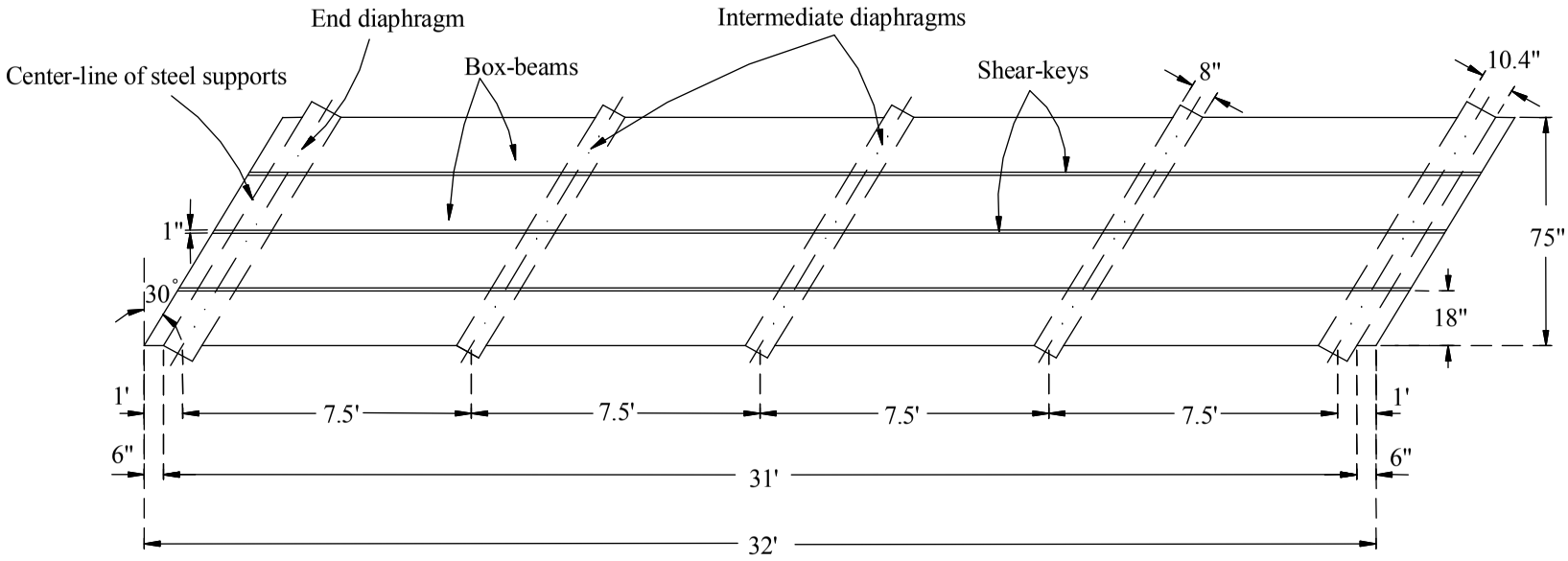

Figure 5.2-29 Plan view of the box-beams.

Figure 5.2-30 Aerial view of the four box-beams.

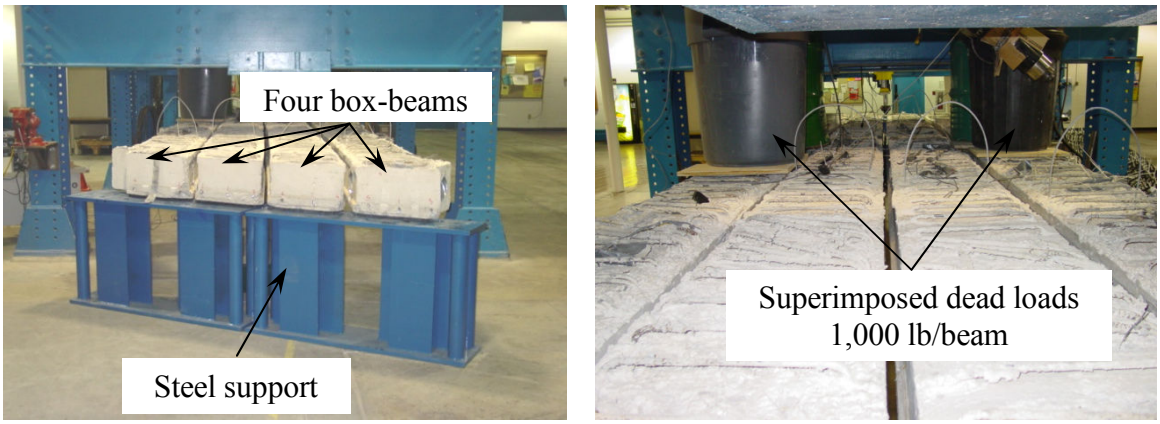

(a) Four box-beams on supports (b) Dead loads placed on exterior beams

Figure 5.2-31 Box-beams placed side-by-side and adding superimposed dead loads.

5.2.11 Deck Slab Construction

5.2.11.1 Formwork Construction

After the superimposed dead loads were removed, the keyways were formed between the beams with top and bottom widths of 2 in. and 1 in., respectively. Styrofoam gaskets were attached at the ends of each transverse duct opening between adjacent beams, as shown in Figure 5.2-32, to avoid the possible leakage of the shear-key grout into the ducts and to ensure the continuity of the ducts.

5.2.11.2 Shear-Key Casting

The shear-keys were constructed using Five Star Structural Concrete 300® (FSSC), manufactured by Five Stars Products Inc. The shear-keys were cured with wet burlap and plastic sheets. A bag of FSSC weighed 150 lb yielding 0.42 ft^3 at maximum water content of 0.1 ft^3. The construction and curing processes are shown in Figure 5.2-33. The properties of the FSSC as provided by the manufacturer are listed in the Table 5.2-7 and the gain of compressive strength of the shear-key grout is shown in Table 4.2-8.

Table 5.2-7 Mechanical properties of FSSC.

Compressive strength, psi	7,000 after 7 days 8,000 after 28 days
Bond strength, ASTM C882, psi	2,500 after 7 days
Linear length change, ASTM C157	+0.03% after 28 days (wet) -0.05% after 28 days (dry)
Thermal co-efficient of expansion, ASTM C531, in./in./°F	5×10^{-6}
Chloride ion permeability, ASTM C1202	< 1,000 Coulombs

The initial TPT forces were then applied on the box-beams after five days of curing of the shear-keys. The purpose of the initial TPT was to prevent any relative movement between the adjacent beams prior to casting the slab. An average force of 6 kip was applied to each steel strand, as shown Figure 5.2-34(a).

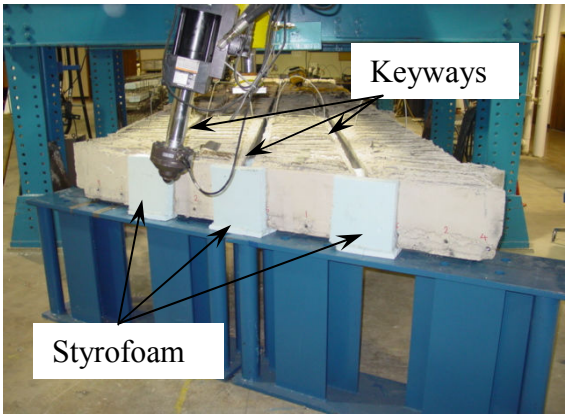

(a) Sealed keyways ends

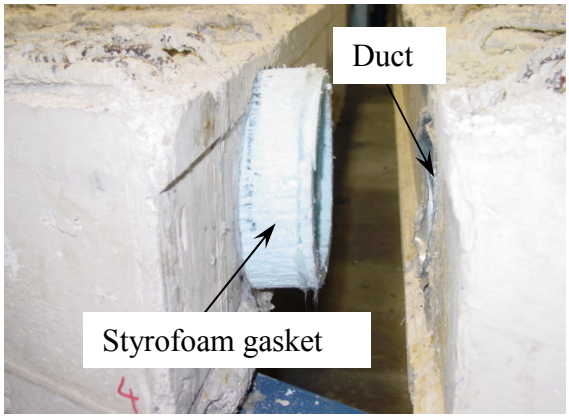

(b) Styrofoam gaskets attached to the ducts

Figure 5.2-32 Preparation of keyways before casting of shear-key.

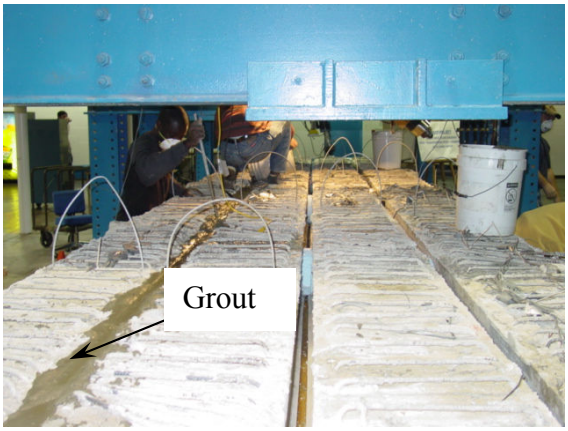

(a) FSSC placed inside keyways

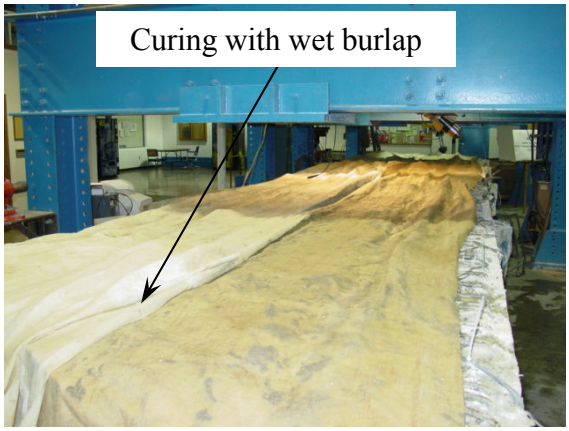

(b) Curing of shear-keys

Figure 5.2-33 Construction of shear-key using FSSC grout.

5.2.11.3 Deck Slab Reinforcement

The formwork for the deck slab was prepared. The reinforcement grid for the deck slab contained conventional #3 deformed steel bars spaced 6 in. center-to-center in the longitudinal and transverse directions of the bridge model. The deck slab reinforcement was attached to the protruded stirrups using zip-ties, as shown in Figure 5.2-34(b).

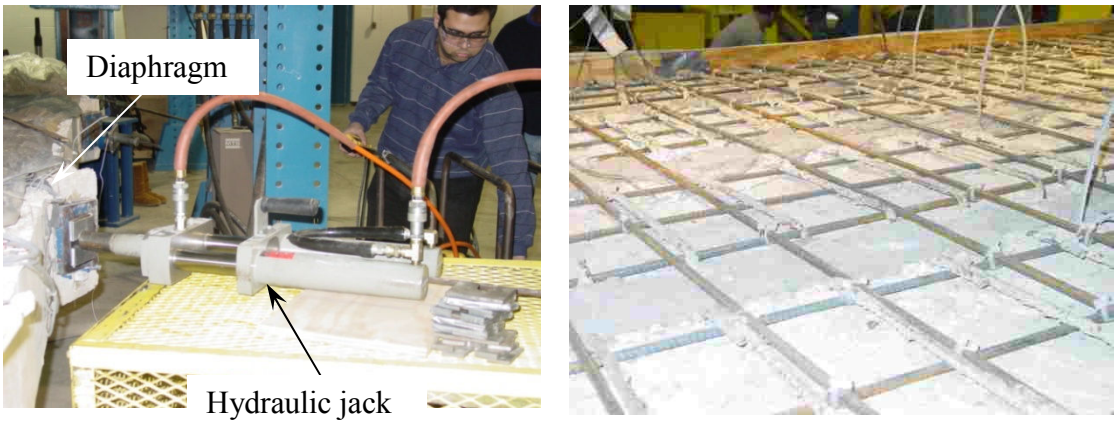

(a) Applying initial TPT forces (b) Deck slab reinforcements grid

Figure 5.2-34 Application of initial TPT forces and casting of deck slab.

5.2.11.4 Placing of Concrete

The cast-in-place deck slab was 3 in. thick constructed using MDOT recommended ready-mix concrete supplied by the McCoig Concrete Products [Figure 5.2-35(a)]. This mix design was approved by Michigan Department of Transportation (MDOT) project manager. The proportion of the concrete mix used is shown in Table 5.2-9. The deck slab was then allowed to cure under wet burlaps covered with plastic sheets, as shown in Figure 5.2-35(b). The average compressive strength of the concrete used in casting of the deck slab after 28 days was 4,600 psi. Figure 5.2-36 shows the details of the bridge model cross-section after completing the deck.

5.2.12 Construction of Additional Exterior Box-Beam

An additional exterior box-beam was constructed and used as a replacement for the "assumed-damaged" exterior box-beam from the bridge model. The main objective was to study the process of replacing a damaged exterior box-beam of the bridge on the distribution of the applied vertical load in the transverse direction. The procedures used during the construction of the former box-beams were also followed to construct the new exterior box-beam (see Figure 5.2-37).

Table 5.2-8 Compressive strength of shear-key grout.

Time, Days	3	7	14	28
Average compressive strength of grout, psi	4,350	6,200	7,250	7,750

Table 5.2-9 Concrete mix proportions for deck slab.

Material	Design Quantity per Cubic Yard, lb	Total Quantity, lb
Fine aggregates	1,390	2,840
Coarse aggregates	1,741	3,564
Cement (Type 1)	342	680
Cementitious material	184	400
Water reducing admixture	1	16
High range water-reducer	8	84

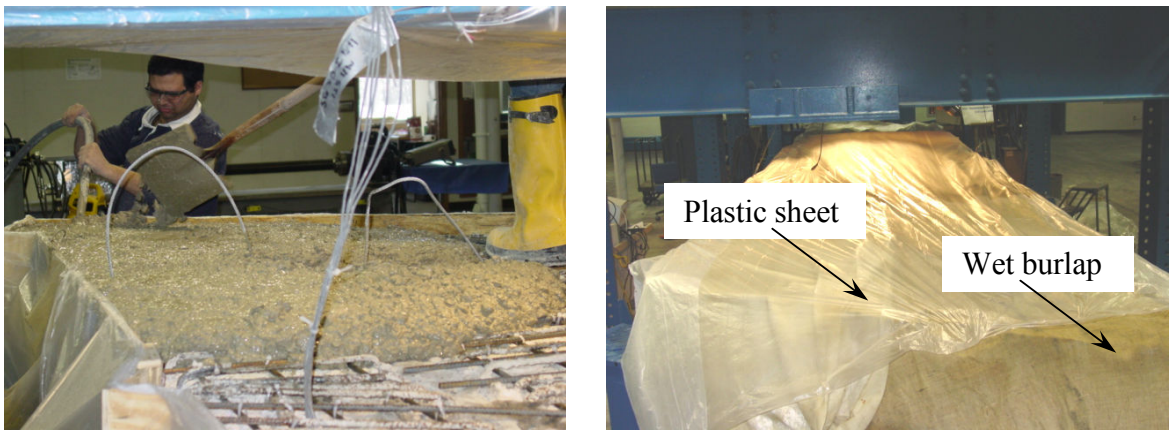

(a) Casting of deck slab for the bridge model (b) Curing of deck slab

Figure 5.2-35 Casting of deck slab concrete and curing proccess.

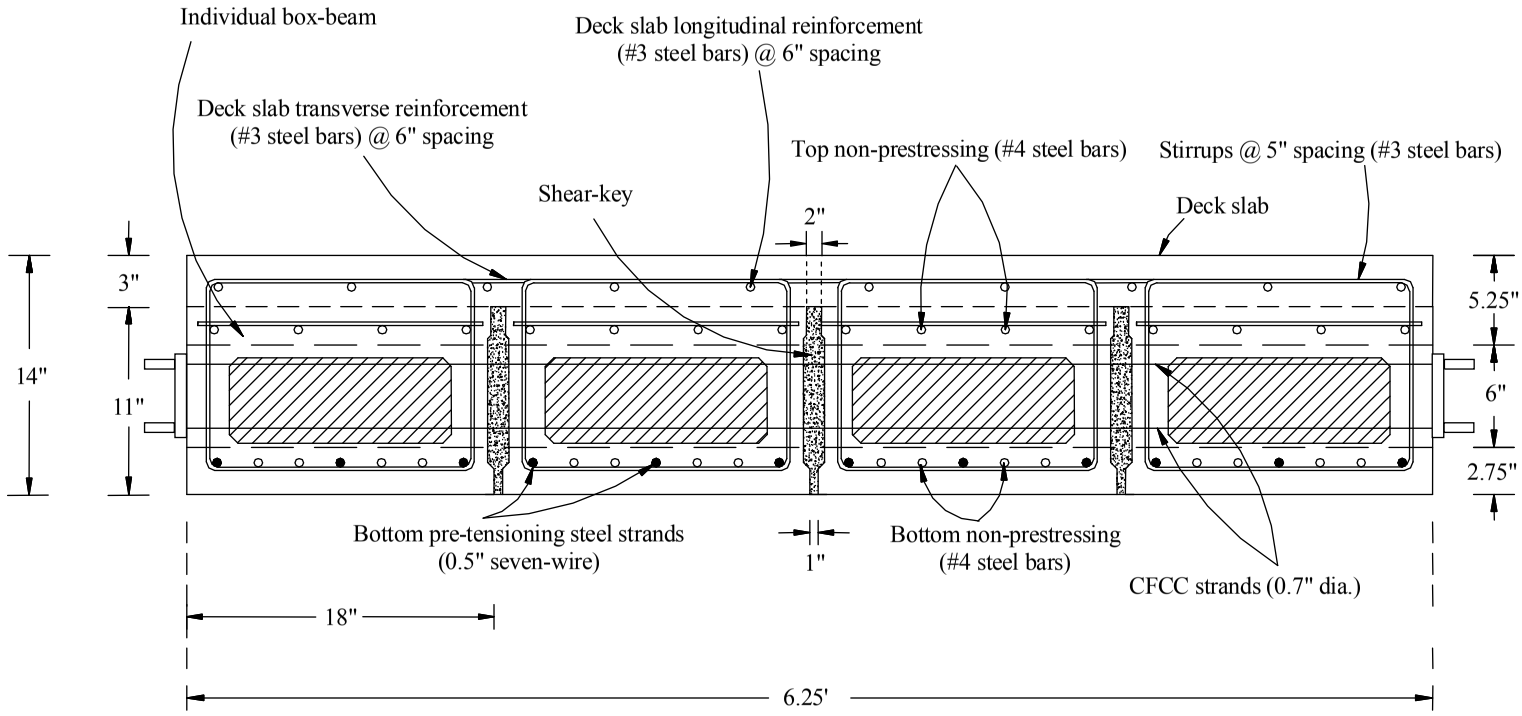

Figure 5.2-36 Cross-section of the completed box-beam bridge model.

(a) Construction of steel cages

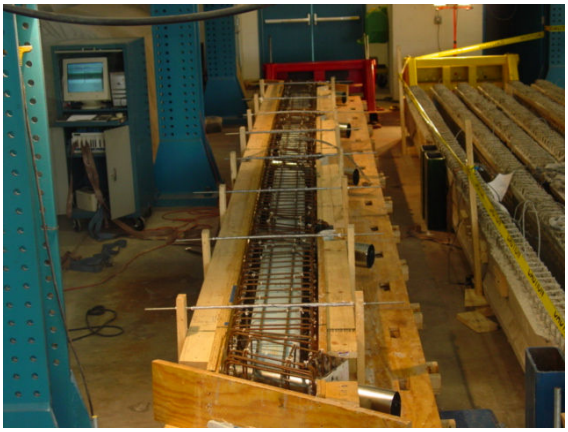

(b) Steel cages inside formwork

(c) Pre-tensioning of steel strands

(d) Casting of box-beam

(e) Curing of box-beam

(f) Cutting of pre-tensioning steel strands

Figure 5.2-37 Construction of additional exterior box-beam.

5.3 Test Program Phase

The strain and the load distribution tests conducted during the test program are described in this section. The data acquisition system and the different types of sensors employed in this study are also presented herein.

5.3.1 Data Acquisition System

The bridge model was instrumented with a range of sensors connected to a commercially available data acquisition system "P8048" supplied by the PROSIG Company (see Figure 5.3-1). The data acquisition system was connected to a Central Processing Unit (CPU) and subsequently linked to a monitor. The software used to run the data acquisition system was Dats for Windows 6.1, Data Acquisition V4.03.12c. This test setup was designed for forty-eight channels. The sensors were connected to terminal blocks, which were subsequently connected the data acquisition system.

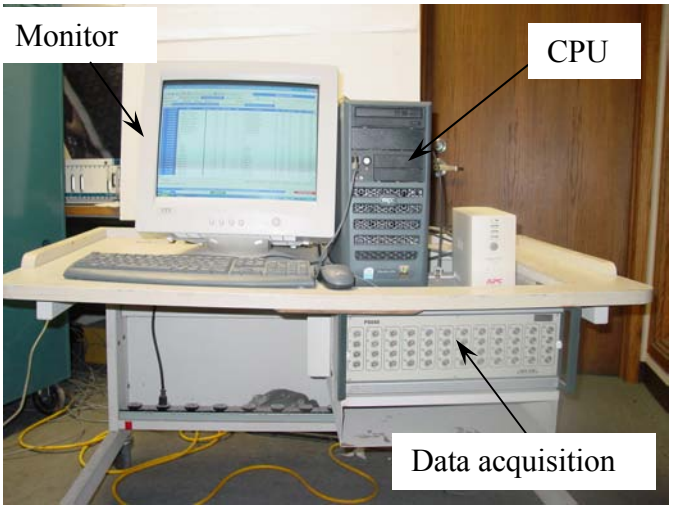

Figure 5.3-1 Data acquisition system.

5.3.2 Instrumentation of the Bridge Model

The three main types of sensors used in this study were strain gages, linear motion transducers, and load cells. The type of strain gages used for the test program was N2A-06-20CBW-350, supplied by the Vishay Micro-Measurements, Inc., and were installed on the top surface of the deck slab in the transverse direction. A total of twenty seven strain gages were installed on one-

half of the deck slab along the shear-key locations, where the longitudinal cracks usually develop as observed in the field, as shown in Figure 5.3-2. The length of the strain gage used was 2 in., similar to the designed top width of the grouted shear-keys. Four linear motion transducers were attached at the mid-span to the underside of each beam to measure the vertical deflection of each box-beam during loading, as shown in Figure 5.3-2. Load cells were attached to the unbonded TPT CFCC to monitor the applied TPT forces.

The transverse strain gages were labeled by creating a skew grid from three axes parallel to the longitudinal direction, from "A-A" to "C-C", and nine axes parallel to supports lines, from "1-1" to "9-9". A typical transverse strain gage was labeled as "A-1", when the strain gage was on the intersection between longitudinal axis "A-A" and transverse axis "1-1". As shown in Figure 5.3-3, the direction of the transverse strain gages was made perpendicular to the longitudinal axes of the box-beams to measure the effective transverse strains developed due to the application of the TPT forces. Before installing the strain gages, the area was ground and subsequently smoothed using sand paper. M-Prep Conditioner "A" was used as a degreaser to clean the surface of the gage area and moderate amount of M-Prep Neutralizer 5A was also added to naturalize the acidic content of the concrete surface. The strain gages were placed on a chemically cleaned board using PCT-2M 310009 gage installation tape and partially placed on deck slab. M-Bond AE-10 Adhesive was prepared and placed on both the strain gages locations on the deck slab and the bonding side of the strain gages. After the strain gages were attached to the top surface of deck slab, a dead weight was used to provide uniform pressure of 5 psi on the installed strain gage for a period not less than 24 hours as recommended by the supplier.

5.3.3 Tests Conducted on the Bridge Model

The test program was conducted to study the effect of number of transverse diaphragms and the level of TPT forces on the behavior of the bridge model in the transverse direction. As mentioned earlier, the two main tests conducted throughout the test programs were the strain and load distribution tests. Details of these tests are presented in the following sections.

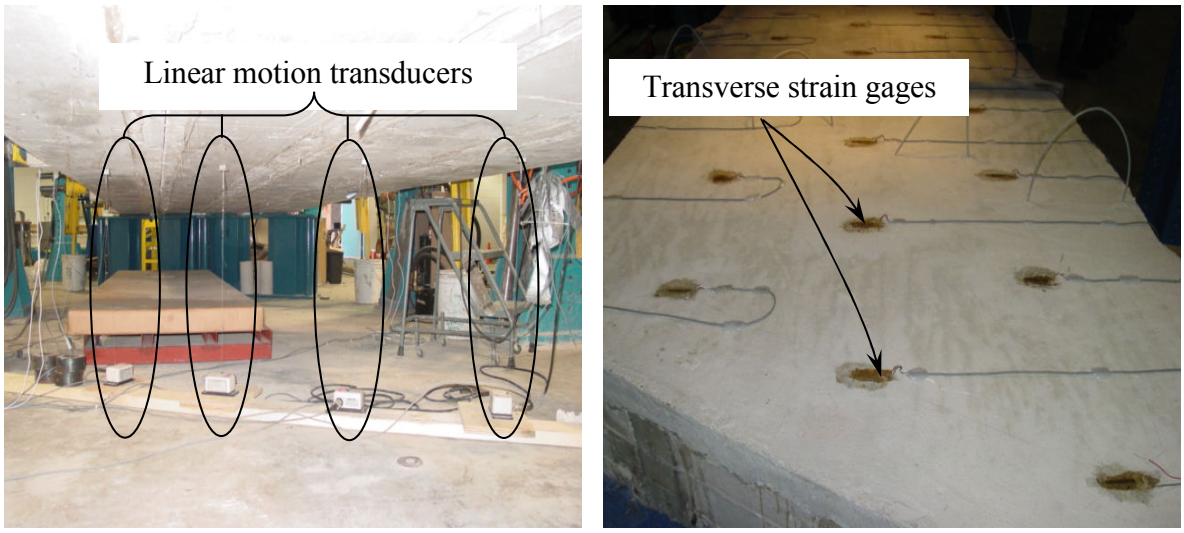

(a) Installed linear motion transducers (b) Installed strain gages on deck slab

Figure 5.3-2 Instrumentation of the bridge model before the test setup.

5.3.3.1 Strain Distribution Test

A parametric study was conducted by applying different levels of TPT forces at different number of diaphragms (different arrangements of TPT) and the corresponding transverse strains developed at the top surface of the deck slab were measured. The CFCC used for applying TPT forces are shown in Figure 5.3-4(a). The dead and live-ends for the TPT system are also shown in Figure 5.3-4(b) and Figure 5.3-4(c), respectively. The TPT forces were applied using a center-hole hydraulic cylinder, manufactured by the ENERPAC. The hydraulic cylinder has a maximum capacity of 132 kip and a maximum stroke of 12 in., as shown in Figure 5.3-4(d). The elongations of the CFCC were measured at three arbitrary levels of the TPT force; 10.8, 22.9 and 35 kip. The determination of the elongation was based on the numerical difference between the final and the initial measured readings of the elongation of the CFCC, as shown in Table 5.3-1. The initial reading corresponds to the elongation at a TPT force of 0.2 kip while the final reading corresponds to the elongation at the respective level of the TPT force. Steel spacers were used at the live-end to compensate for the expected elongation in the CFCC.

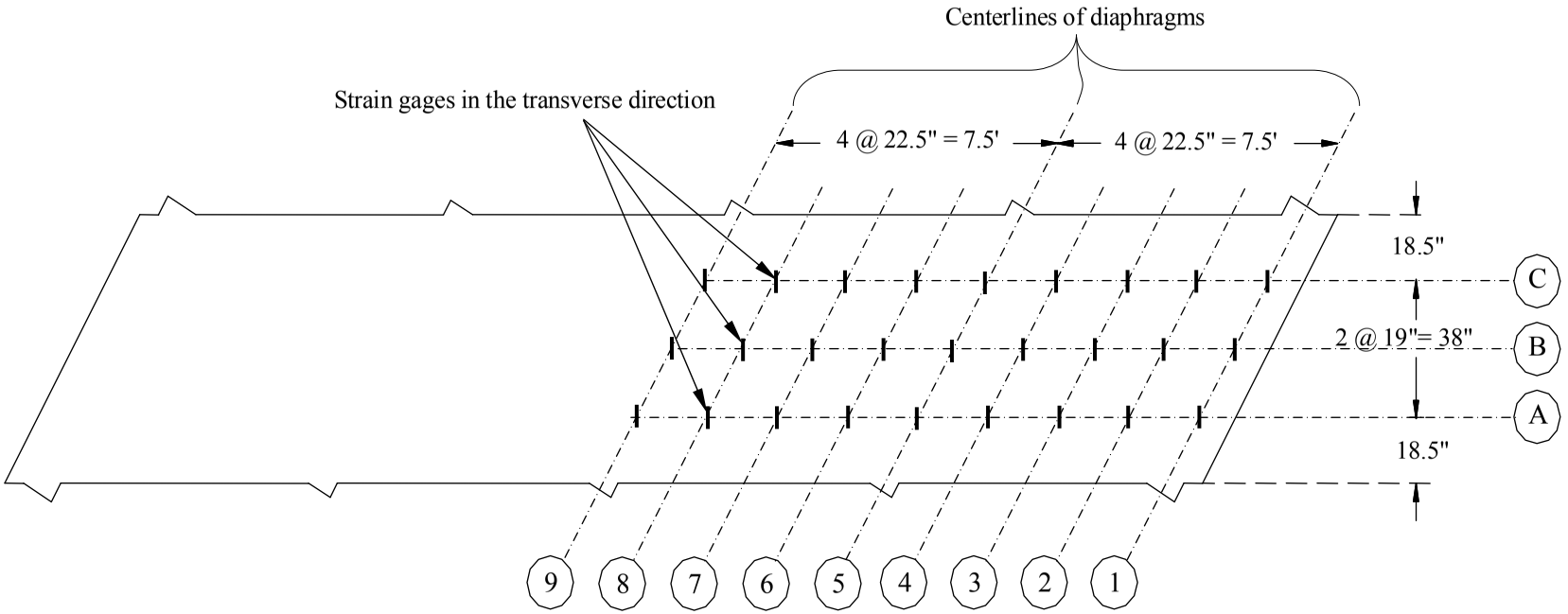

Figure 5.3-3 Layout of the strain gages installed on the deck slab.

One center-hole load cell, with a maximum capacity of 70 kip, was attached at the dead end of each CFCC to monitor the levels of the TPT force, as shown in Figure 5.3-4. Details of a typical dead-end for TPT system showing the load cells and the position of the CFCC are shown in Figure 5.3-5. In order to avoid possible local crushing of concrete due to the TPT forces, steel bearing plates, 7 in. wide, 8 in. high and 1.5 in. thick, were attached to all ends of the transverse diaphragms (ten plates). Rubber sheets of 0.25 in. thick were provided with the same width and height as the steel plates and attached to the bearing surface of the steel plates to ensure uniform distribution of the TPT forces on the bearing surfaces. The different arrangements of the strain distribution test are shown in Figure 5.3-6. The strain distribution test was intended to study the effect of different number of diaphragms and different levels of the TPT forces on the transverse strains as follows. The sequence of the strain distribution test is outlined as follows.

Case of all diaphragms:

The TPT forces were applied to all diaphragms at three different levels of 80, 40, and 20 kip/diaphragm.

Case of four diaphragms:

The TPT forces were applied to all diaphragms except the mid-span diaphragm at three different levels of 80, 40, and 20 kip/diaphragm.

Case of three diaphragms:

The TPT forces were applied to the end and the mid-span diaphragms only at three different levels of 80, 40, and 20 kip/diaphragm.

Case of no diaphragms:

In this case, no TPT force was applied to the bridge model. This case was used as the reference case throughout the test program.

Table 5.3-1 Elongation of CFCC at three different levels of TPT force.

TPT Force, kip	Initial Reading, in.	Final Reading, in.	Elongation, in.
10.8	5.44	5.69	0.25
22.9	5.44	6.00	0.56
35	5.44	6.31	0.87

(a) CFCC strands

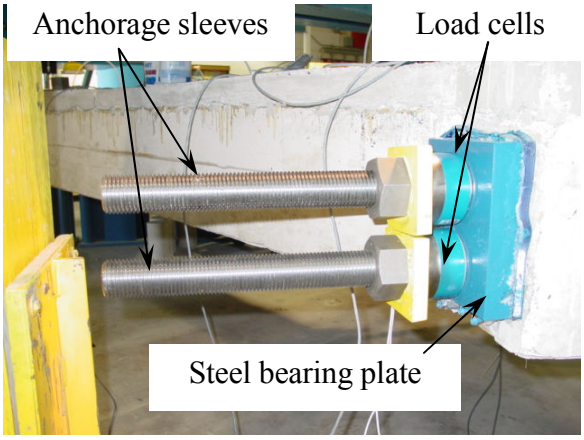

(b) Dead-end details for TPT

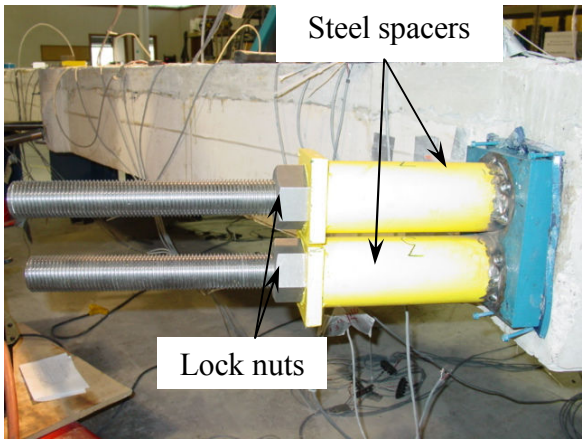

(c) Live-end details for TPT

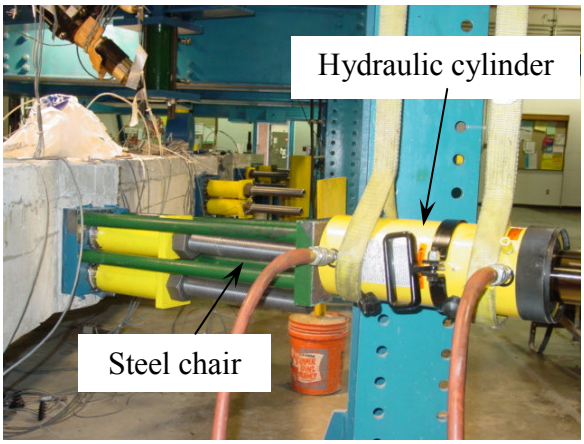

(d) TPT setup

Figure 5.3-4 Details of the unbonded TPT system.

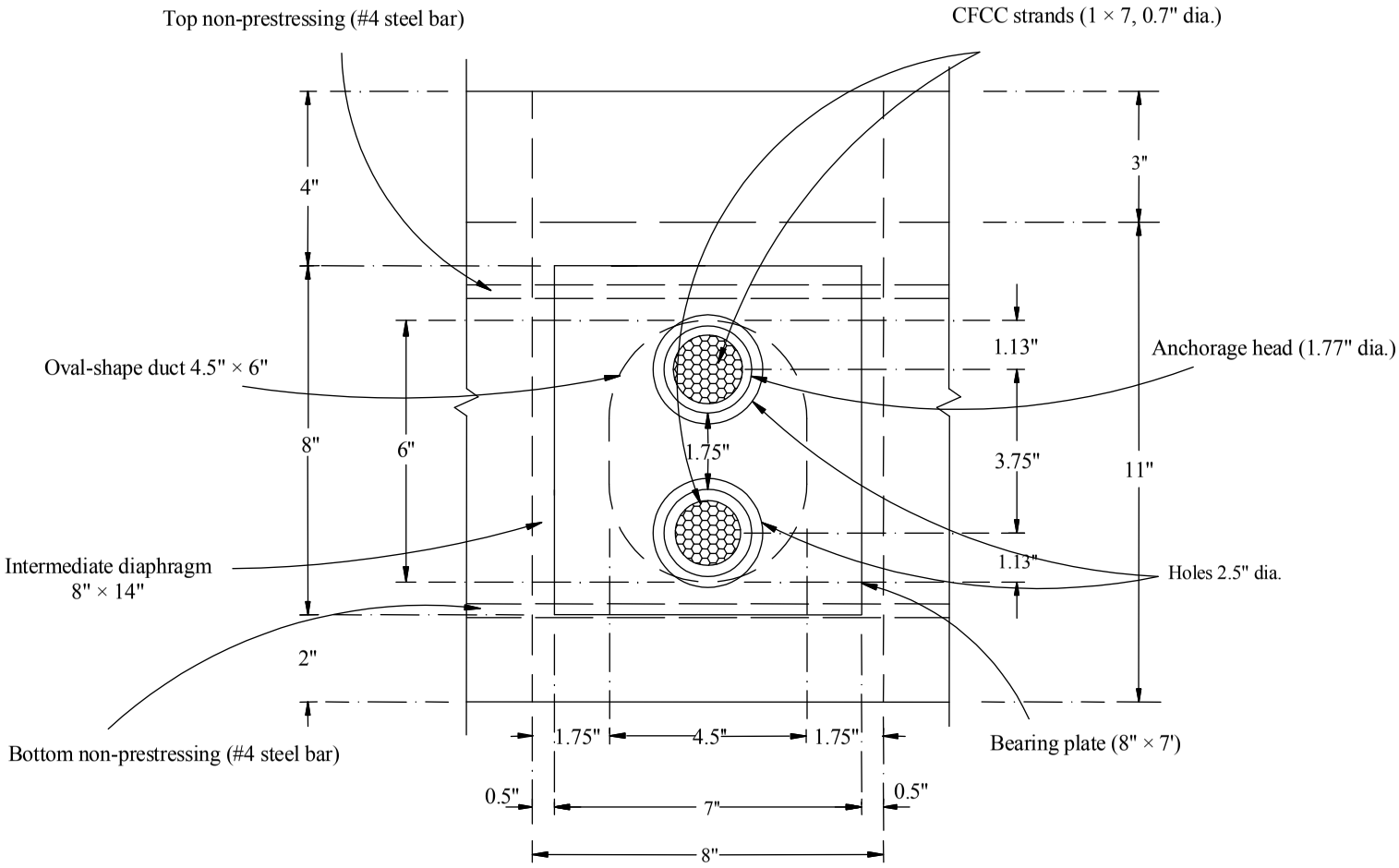

Figure 5.3-5 Typical dead-end of TPT system.

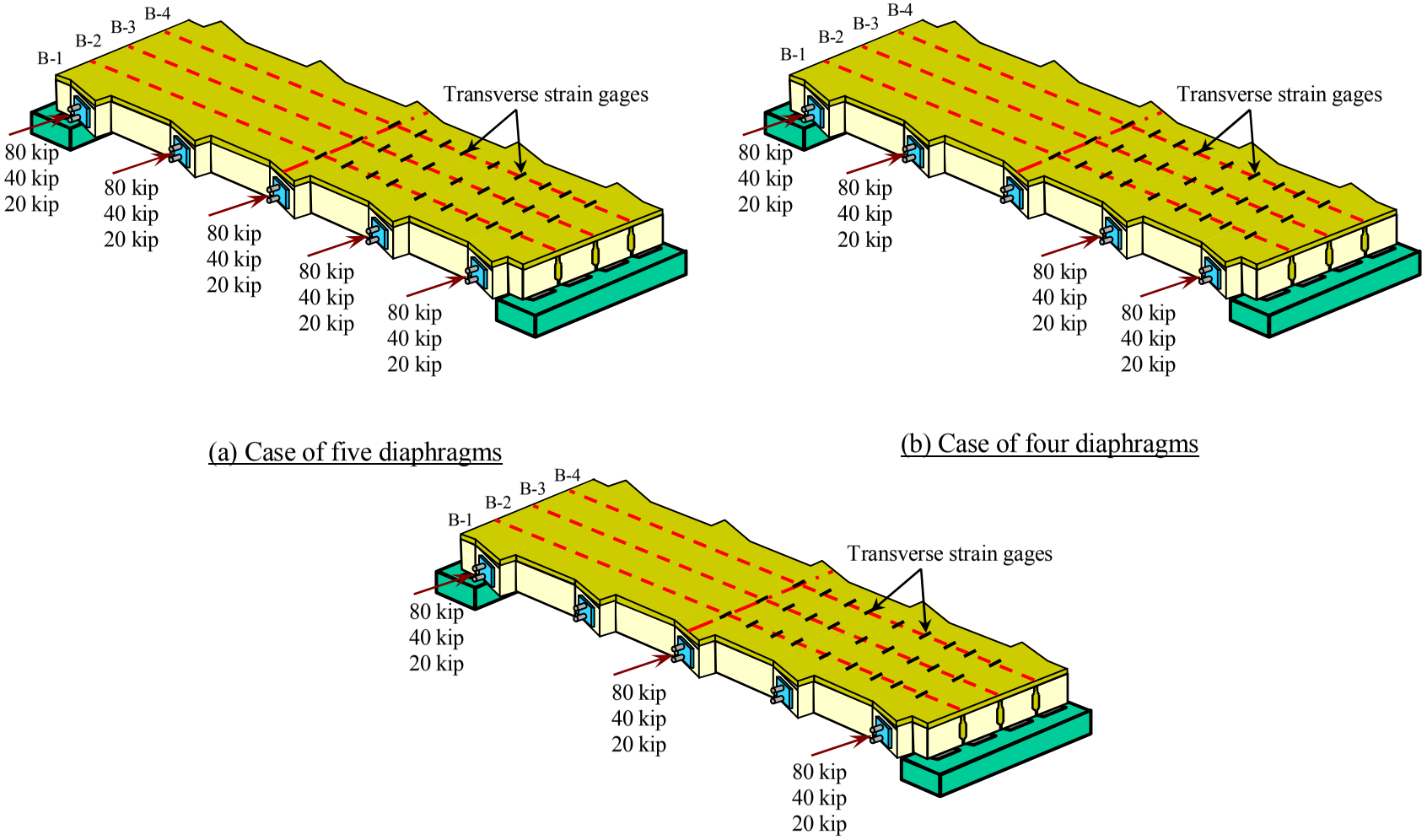

(a) Case of five diaphragms

(b) Case of four diaphragms

(c) Case of three diaphragms

Figure 5.3-6 Arrangements for strain distribution test.

5.3.4 Load Distribution Test

The load distribution test was conducted by applying a single point load at the mid-span of each box-beam one box-beam at a time and the corresponding deflections were measured using linear motion transducers. In order to avoid a possible premature cracking of the bridge beams, a service load of 15 kip was selected below the calculated cracking load of 16 kip for the entire bridge model. The vertical load of 15 kip was applied on each box-beam with different arrangements of the TPT forces, similar to the arrangements used for conducting the strain distribution test. The vertical load was applied by using a hydraulic cylinder, manufactured by the Templeton Kenly & Company, Inc., which has a maximum capacity of 220 kip and a maximum stroke length of 6 in. The hydraulic cylinder was attached to the bottom flange of an overhead transverse steel I-beam by four wheels to ensure easy movement from one location to the other, as shown in Figure 5.3-7. The single point load was applied using a steel cylinder with a diameter of 10 in. and height of 5 in. The 10 in. diameter was chosen to avoid the punching shear failure of the oval-shape ducts at mid-span underneath the loading locations. Figure 5.3-8 through Figure 5.3-11 show the load distribution test sequence.

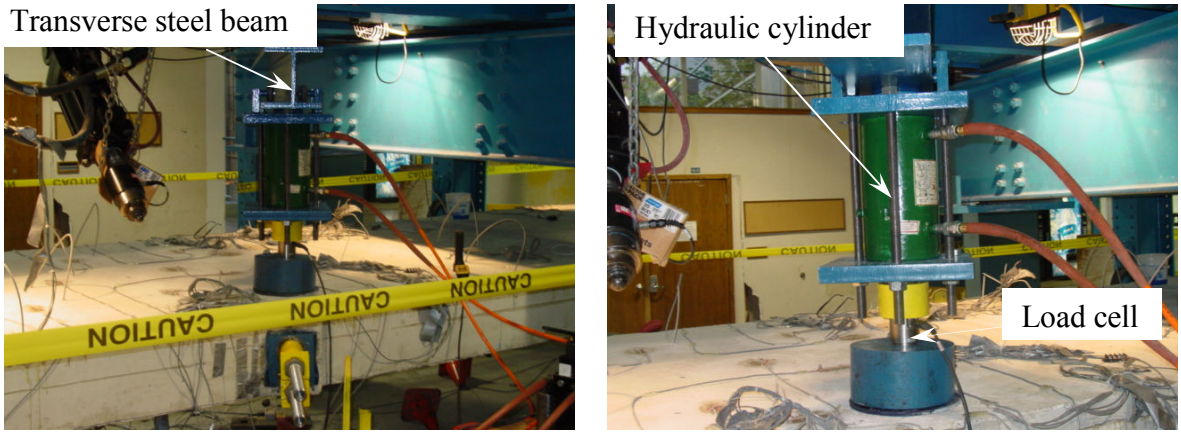

(a) Application of vertical load at mid-span (b) Details of load distribution test setup

Figure 5.3-7 Load distribution test setup.

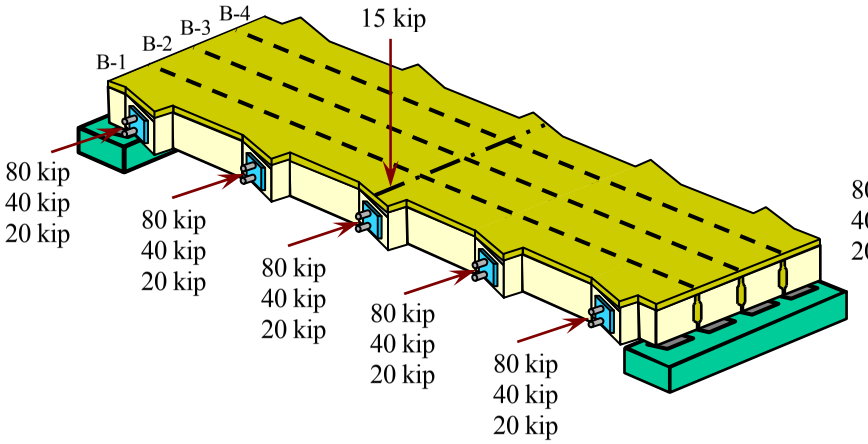

(a) Loading beam B-1

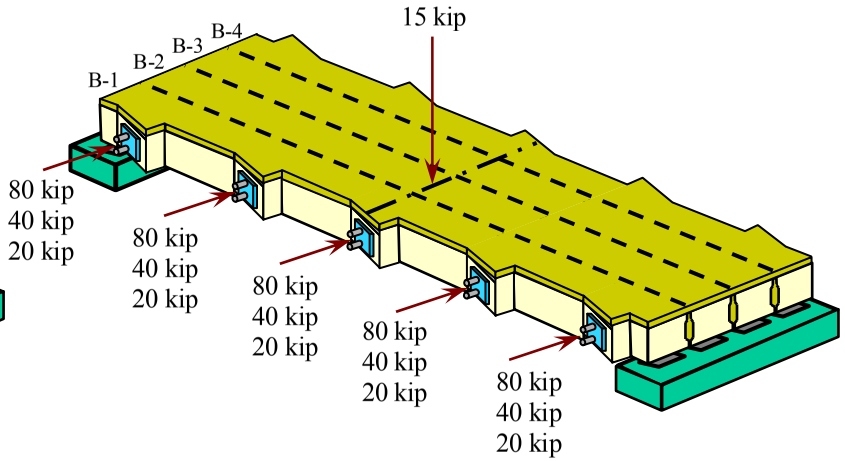

(b) Loading beam B-2

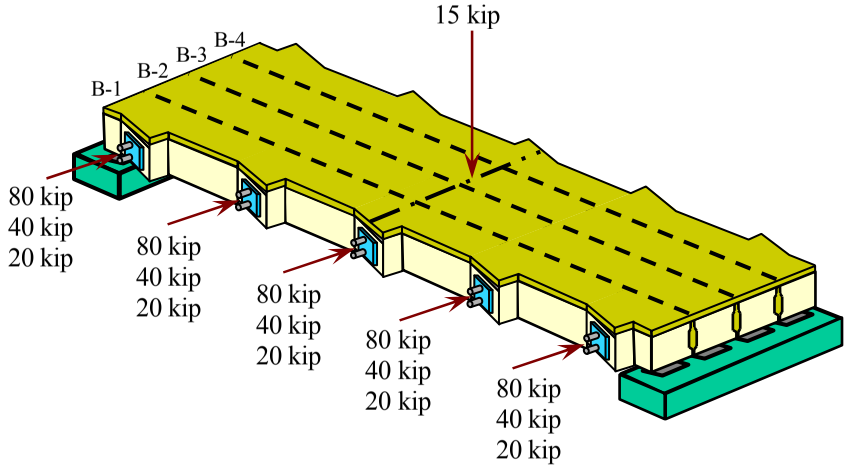

(c) Loading beam B-3

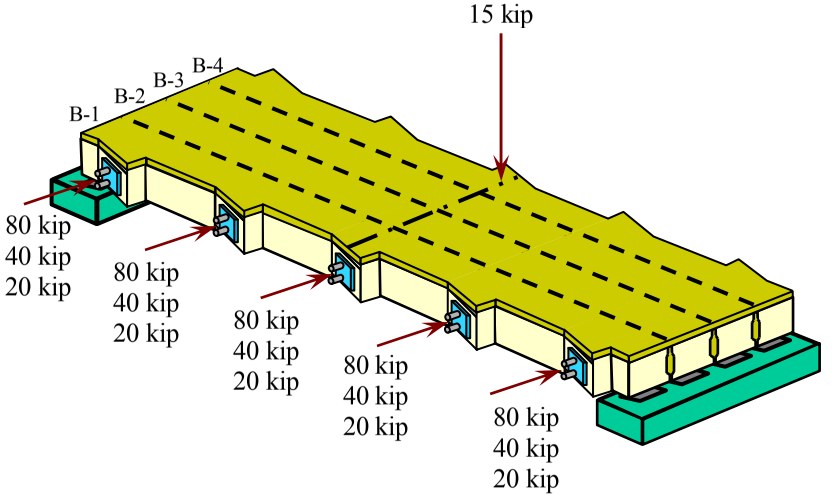

(d) Loading beam B-4

Figure 5.3-8 Load distribution test with the application of TPT forces at five diaphragms.

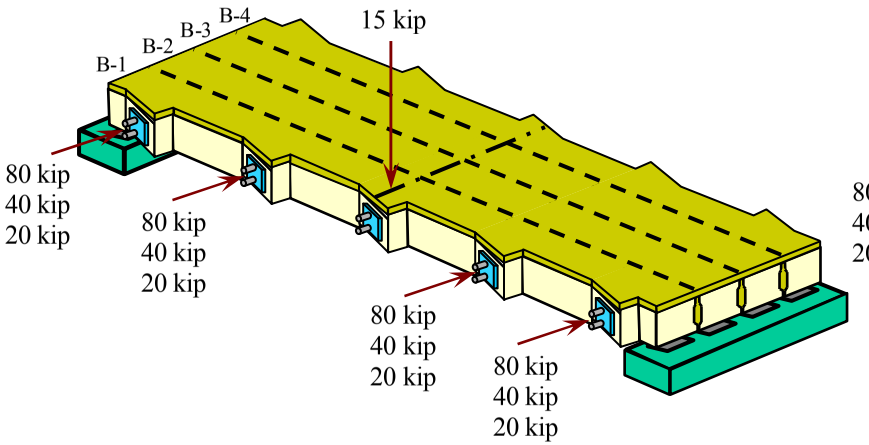

(a) Loading beam B-1

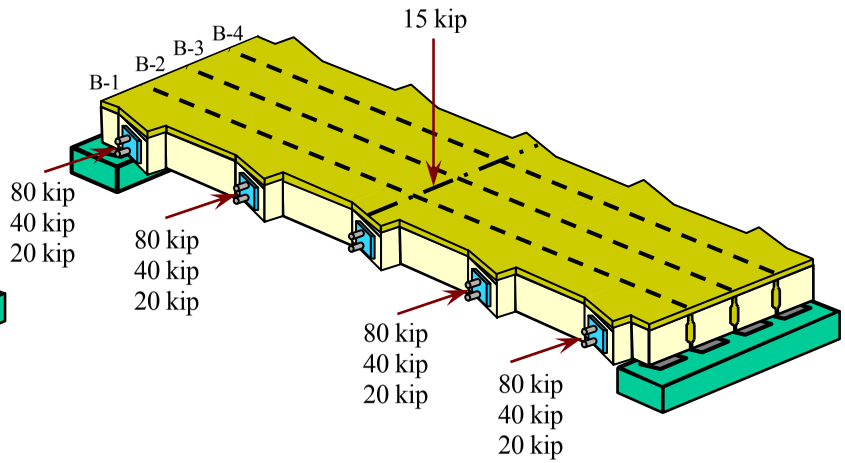

(b) Loading beam B-2

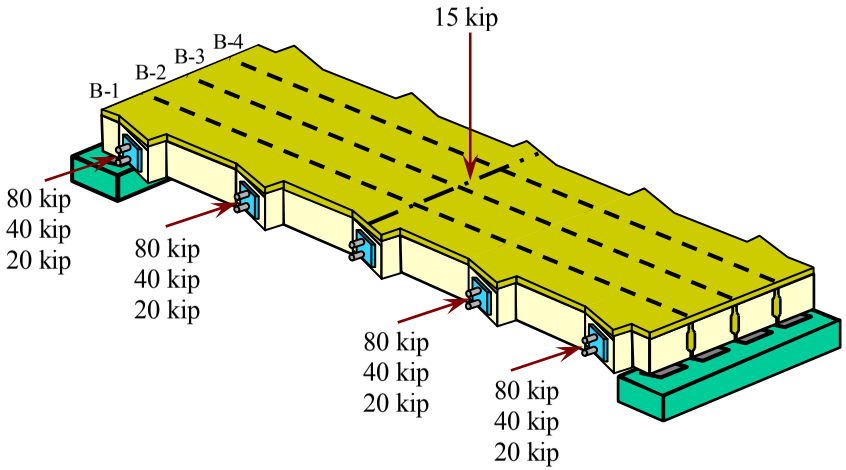

(c) Loading beam B-3

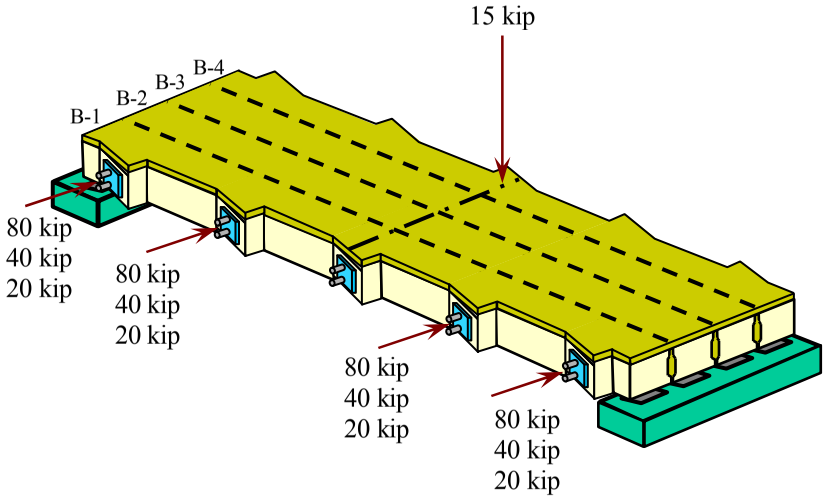

(d) Loading beam B-4

Figure 5.3-9 Load distribution test with the application of TPT forces at four diaphragms.

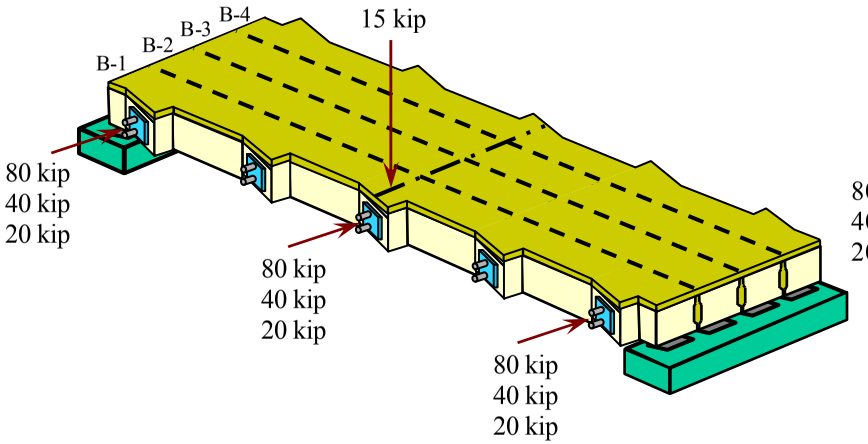

(a) Loading beam B-1

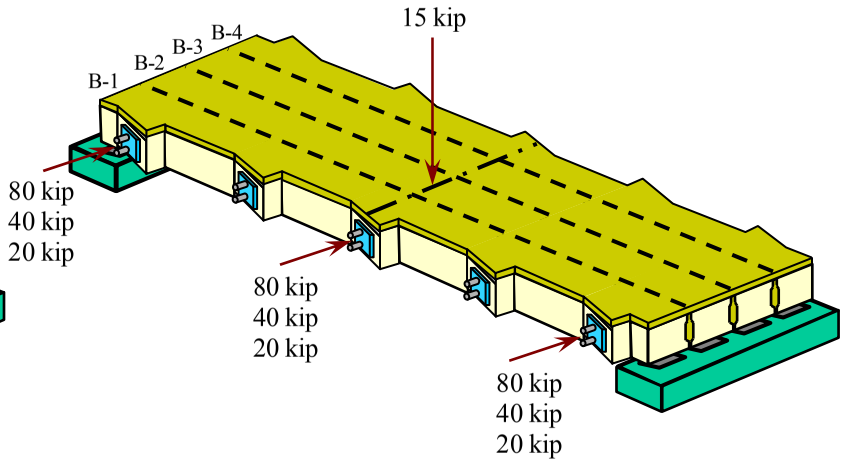

(b) Loading beam B-2

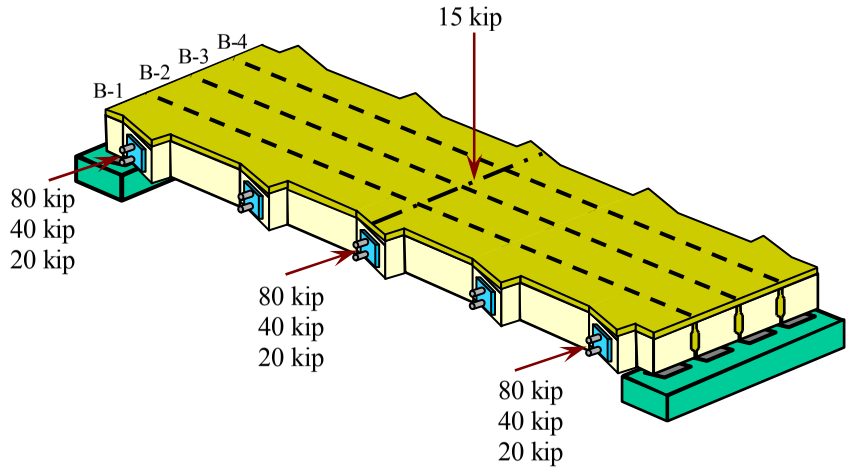

(c) Loading beam B-3

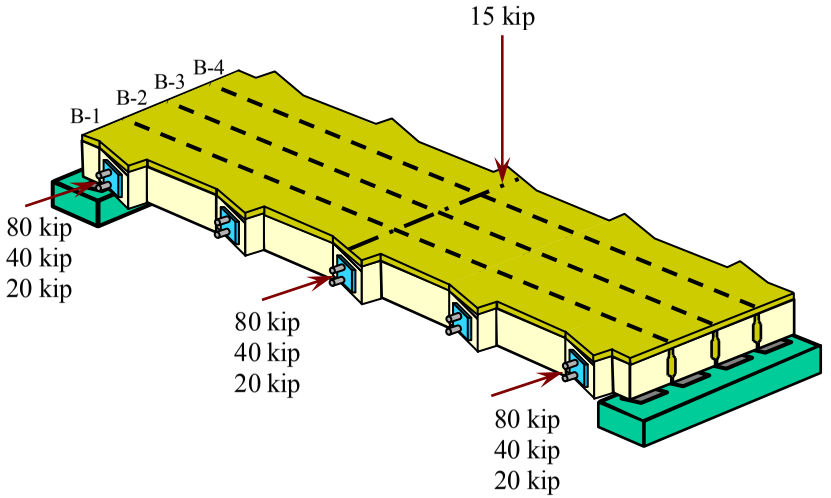

(d) Loading beam B-4

Figure 5.3-10 Load distribution test with the application of TPT forces at three diaphragms.

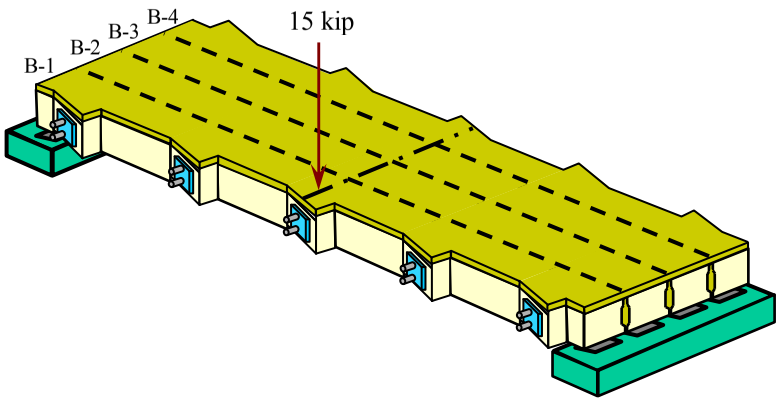

(a) Loading beam B-1

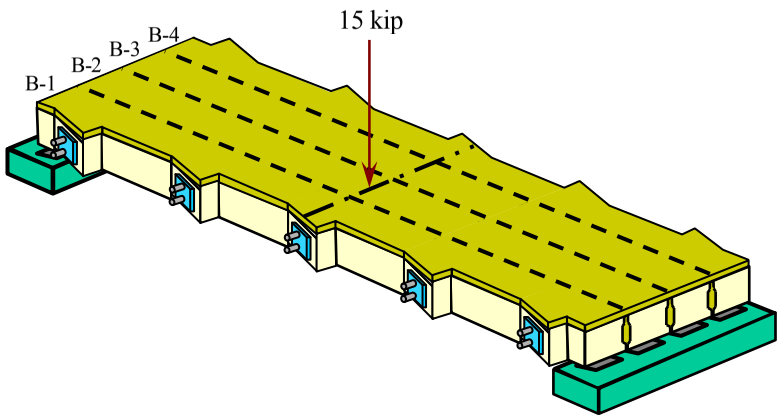

(b) Loading beam B-2

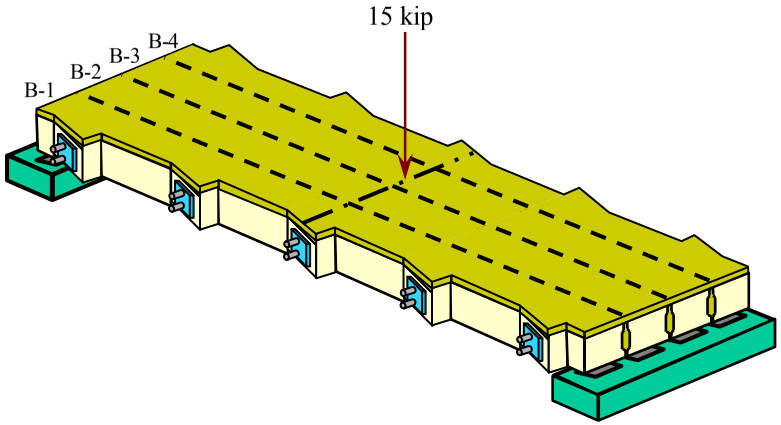

(c) Loading beam B-3

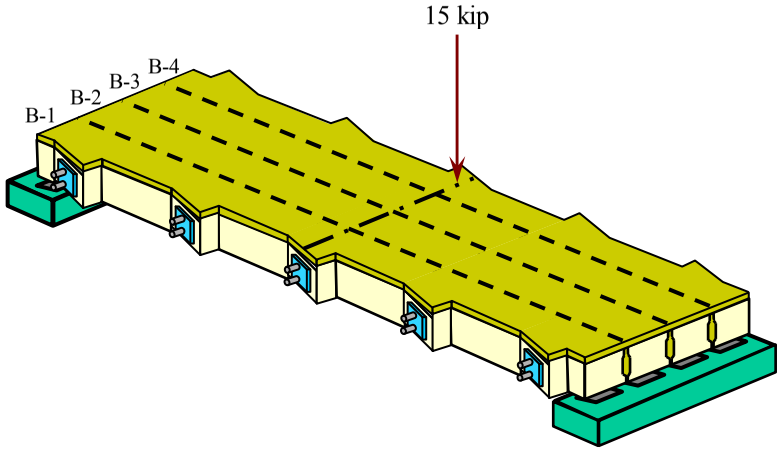

(d) Loading beam B-4

Figure 5.3-11 Load distribution test without applying TPT forces at any diaphragm.

5.3.5 Stages of Test Program

5.3.5.1 Uncracked Deck Slab

The reference point for the investigation was the condition before longitudinal cracks occur. This stage simulated a typical newly constructed highway bridge as stated earlier. The load and strain distribution tests were both conducted at this stage of the bridge model.

5.3.5.2 Cracked Deck Slab

At this stage, the cracked deck slab and the shear-keys were partially cracked. The purpose was to simulate the longitudinal cracks developed between the box-beams over the shear-keys due to a combination of vertical loads and thermal effects. The creation of longitudinal cracks was made in three steps. The vertical load was applied to one box-beam while partially restraining the other three box-beams from the top and the bottom to prevent the entire bridge from rotating as it tends to act as a one unit.

In order to crack the exterior shear-key on axis C-C, the load was applied at the mid-span of beam B-4 and beams B-1, B-2, and B-3 were partially restrained at the top and the bottom using steel supports, as shown in Figure 5.3-12. A reversed arrangement was adopted to crack the other exterior shear-key on axis A-A by applying the load at beam B-1 and partially restraining beams B-2, B-3, and B-4 from rotation and translation. However, in order to crack the interior shear-key on axis B-B, the load was applied to beam B-3 and beams B-1, B-2, and B-4 were restrained at the top and the bottom, as shown in Figure 5.3-13. The crack widths were measured using the crack comparator and compared with the cracks pattern provided by the Michigan Department of Transportation (MDOT) for the box-beam bridge number S03-63022 built in 1999. The bridge carries South Hill Road over I-96. The strain distribution test was not conducted at this stage because of the discontinuity of the deck slab in the transverse direction as a result of the longitudinal cracks. The load distribution test was the only test conducted after cracking the deck slab and the results were compared to the stage of uncracked deck slab. Details of the cracks pattern developed in the deck slab are shown in Chapter 6.

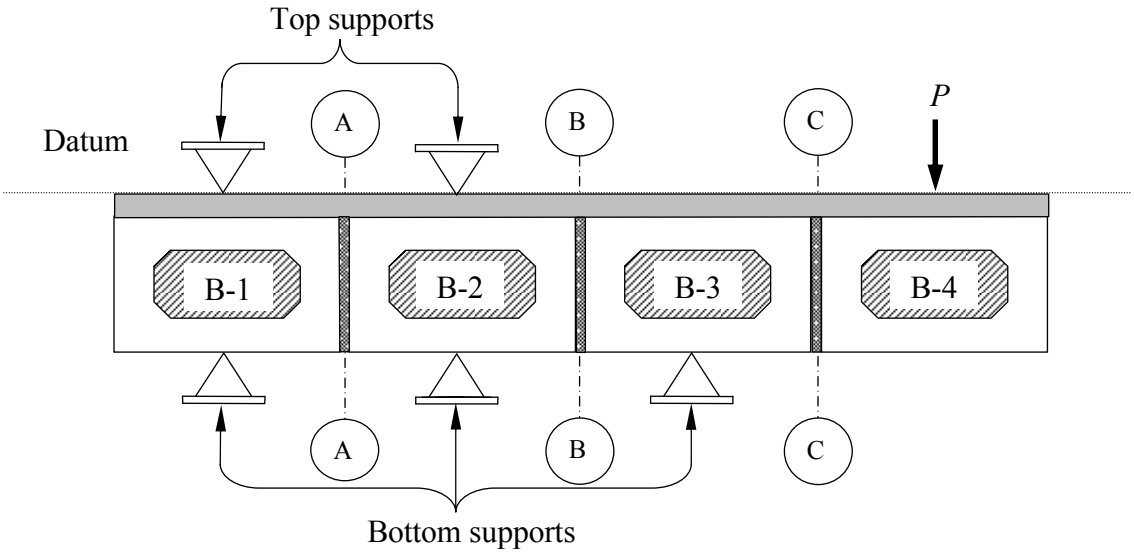

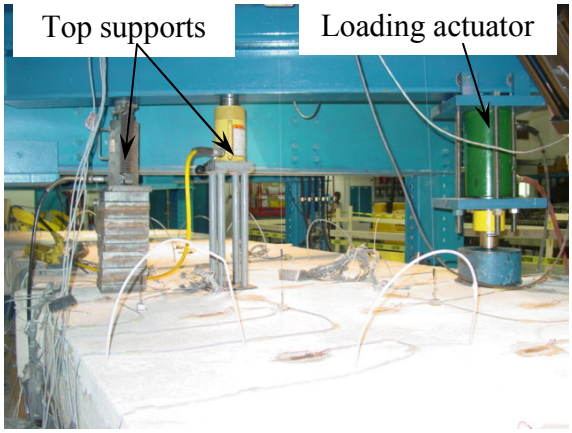

(a) Bottom view (b) Top view

Figure 5.3-12 Setup for cracking exterior shear-key C-C.

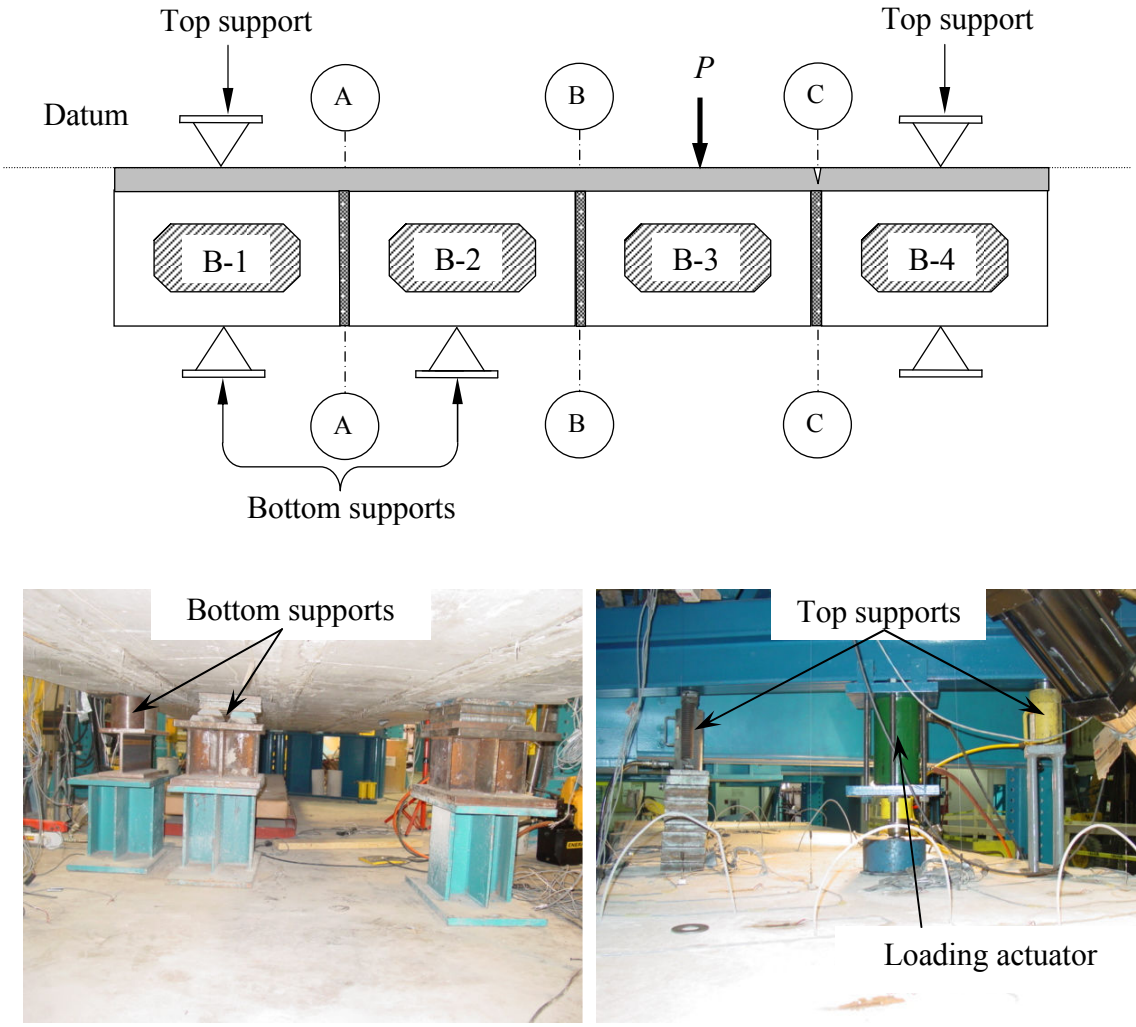

(a) Bottom view (b) Top view

Figure 5.3-13 Setup for cracking interior shear-key B-B.

5.3.5.3 Damaged Beam Replacement

This stage was developed also to demonstrate the merits of the use of unbonded TPT CFCC instead of bonded TPT steel strands in the construction of side-by-side box-beam bridges. It is a well known fact that replacing a damaged beam in a highway bridge, when bonded TPT steel strands is used, is challenging. Therefore, studying the effect of the replacement of a damaged beam on the behavior of the bridge model in the transverse direction can quantify the efficiency of the replacement process. In this project, the effect is evaluated under the eccentric loading

with the application of different TPT arrangements. Emphasis was also placed on the development of a more practical and simple approach for replacing the damaged box-beam. Only the load distribution test was conducted at this stage of the test program. The experimental work of this stage consisted of three major phases as follows.

Phase (I): Saw cutting of the damaged exterior beam.

1. The unbonded TPT CFCC were removed from the oval-shape ducts. This was followed by the removal of all the steel bearing plates from the bridge model.
2. The surface of the shear-key was cleaned. The cutting line was marked with a straight line along the entire span at the mid-width of the exterior shear-key C-C, which connected beam B-3 and beam B-4.
3. A full-depth cut of the shear-key was made over the marked line by using a circular saw provided by Fmg® Concrete Cutting, Inc. to separate the assumed damaged beam B-4 from the remaining portion of the bridge model (Figure 5.3-14).

Phase (II): Placement of the new exterior beam.

1. The first task undertaken at this phase was to remove the remaining FSSC grout from the shear-key C-C, as shown in Figure 5.3-15.
2. Horizontal holes of 0.75 in. diameter and 12 in. deep were drilled into the deck slab using electric hammer drill to accommodate the new transverse reinforcement bars, as shown in Figure 5.3-16(a). The spacing of the holes was uniformly maintained at 6 in. The holes were drilled at the mid-depth of the deck slab 1.5 in. from the top surface of the deck slab.
3. Styrofoam gaskets were then attached to the face of beam B-3 around the oval-shape ducts, as shown in Figure 5.3-16(b). This was to ensure continuity of the diaphragms when the new beam B-5 was placed and to prevent possible leakage of the shear-key grout inside the ducts.
4. The new box-beam was placed on the elastomeric bearing pads on the steel supports.
5. The formwork for the new shear-key was constructed by sealing the underside of the shear-key with plywood and the ends of the shear-key with a Styrofoam.

6. The shear-key was cleaned and the FSSC grout was placed in the keyway, as shown in Figure 5.3-17.
7. The newly constructed shear-key was cured under wet burlap and plastic sheets.

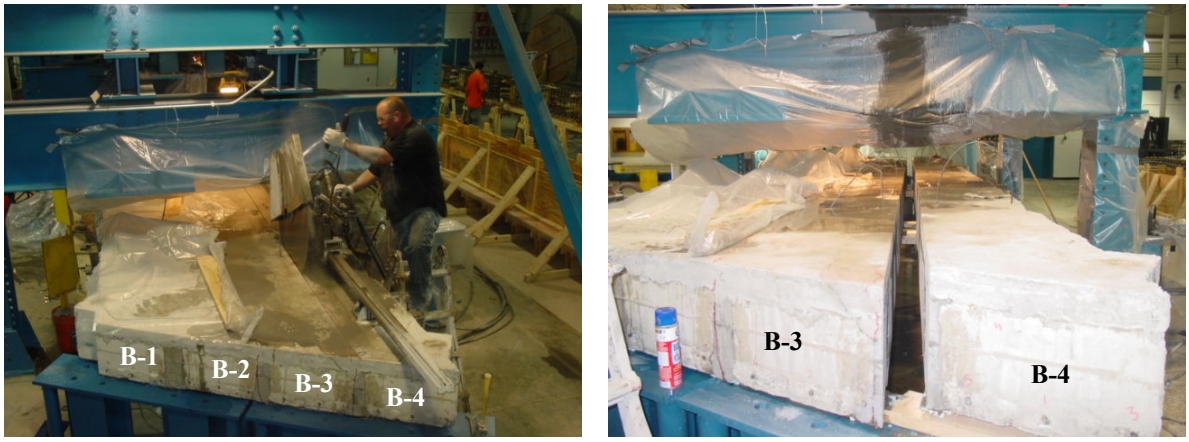

(a) Saw cutting of beam B-4 (b) Separation of beam B-4

Figure 5.3-14 Separation of exterior beam B-4 by saw cutting through shear-key C-C.

(a) Remained portion of shear-key (b) Grout removed from shear-key

Figure 5.3-15 Removal of the remaining grout from the bridge model.

(a) Drilling of horizontal holes (b) Instattaltion of styrofoam gasket

Figure 5.3-16 Drilling of horizontal holes and attachment of Styrofoam gasket.

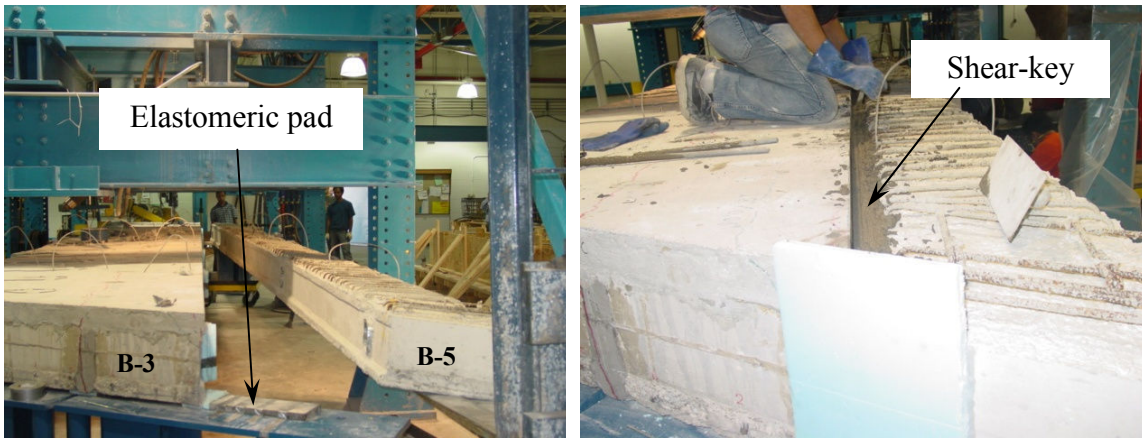

(a) Placement of new beam (b) Grouting of new shear-key

Figure 5.3-17 Placement of new beam and grouting the keyway.

Phase (III): Reinforcement and casting of the deck slab.

1. The longitudinal reinforcements were placed and tied at equal spacing of 6 in.
2. The transverse reinforcements were also placed by using a high performance epoxy resin called Sikadur Injection Gel/AnchorFix-4 listed in the MDOT's "Material Source Guide" Specification Number 603.02B. The procedures followed are as stated below:

a. The drilled holes were cleaned by blowing air through them using air-jet and water-jet accordingly to ensure that all dust particles are cleared to ensure bond between the bars and the concrete.
b. The nozzle of the dispensing gun was inserted into the drilled holes and the epoxy resin was pumped to fill the hole completely, as shown in Figure 5.3-18.
c. The reinforcement bars #3 were inserted gradually while rotating them to ensure that the rebar was coated in the epoxy.
d. The reinforcement bars #3 were left undisturbed for a duration of 24 hours until the epoxy resin cured and attained the required bond strength.
e. The deck slab formwork was then constructed. This was followed by casting of the deck slab with the same concrete mix design used for casting the old deck slab, as shown in Figure 5.3-19. The deck slab was cured under wet burlap and plastic sheets.

(a) Epoxy resin kit

(b) Insertion of epoxy into holes

Figure 5.3-18 Materials used and insertion of epoxy into the drilled holes.

(a) Reinforcing of new deck slab (b) Casted new deck slab

Figure 5.3-19 Construction of formwork and casting of deck slab.

5.3.5.4 Ultimate Load Test

The objectives of the ultimate load test were to determine the ultimate load-carrying capacity of the bridge model and to evaluate the efficiency of using two unbonded CFCC through the oval-shape duct at each diaphragm as a TPT system. The bridge model was loaded eccentrically at the mid-span of beam B-2 using a two-point loading frame (spreader), as shown in Figure 5.3-20. The two-point loading frame consisted of a 10 × 10 in. structural square steel tube with a total span of 7.5 ft. A TPT force of 80 kip was applied to all five diaphragms prior to testing. The TPT forces were monitored during the test using load cells attached to the dead-end of the CFCC. Four linear motion transducers were also installed at the mid-span of each of the beams to monitor the corresponding deflections of the four beams, as shown in Figure 5.3-21. In order to monitor the strains developed on the deck slab, two strain gages were installed in the longitudinal direction at the mid-span of beams B-2 and B-5. Five loading and unloading cycles were conducted before failing the bridge model in order to separate the elastic and inelastic energies. Each loading and unloading cycle was conducted by increasing and releasing the applied load at a rate of 15 kip/minute. The maximum applied loads in the five cycles were 20, 40, 60, 80, and 100 kip.

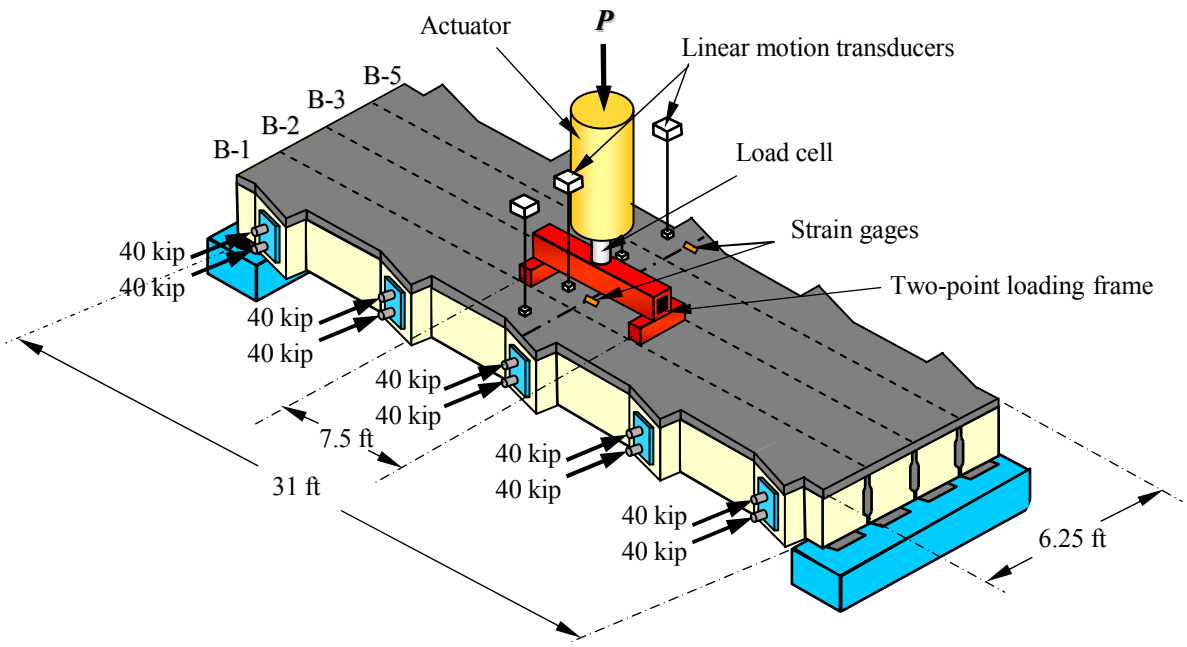

Figure 5.3-20 Experimental setup and instrumentation of the bridge model.

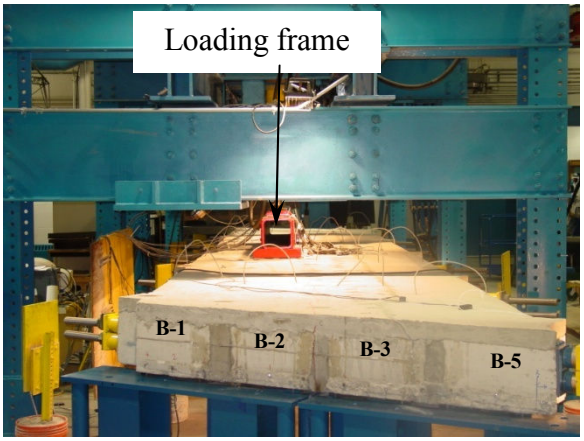

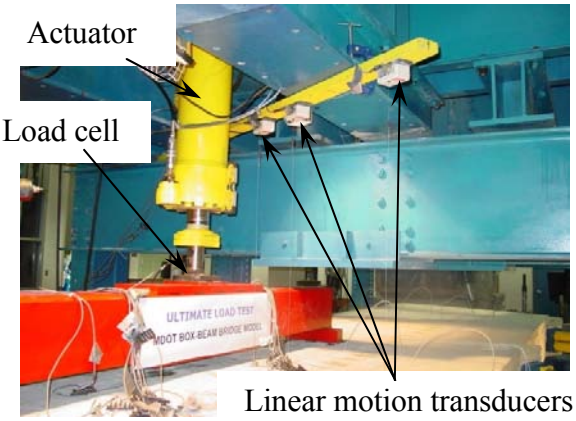

Figure 5.3-21 Ultimate load test setup.

CHAPTER 6: EXPERIMENTAL RESULTS AND DISCUSSIONS

6.1 Introduction

This chapter provides a comprehensive report and discussion of the results obtained during the experimental phases of this research project. The first section discusses the transverse strains induced on the deck slab due to varied levels of TPT forces applied to different number of diaphragms. The load distribution results obtained at different stages of deck slab condition are discussed in the second section. In the final section, the ultimate response of TPT system is evaluated using the ultimate load test.

The results related to the construction phase are presented in Appendix A. The appendix contains information on 1) the pre-tensioning forces during the curing period of the concrete, 2) continuous monitoring of the camber for the four individual box-beams, and 3) transfer length of the pre-tensioning forces.

6.2 Transverse Strain Distribution

6.2.1 Introduction

The transverse strain distribution test was conducted on the bridge model by varying the number of transverse diaphragms and the levels of TPT forces. Three different levels of TPT forces were applied to each diaphragm. These levels were 20, 40, and 80 kip. The forces were applied using two unbonded CFCC located at each diaphragm. Each CFCC was post-tensioned by half of the TPT force provided at each diaphragm. A total of five transverse diaphragms were employed for the application of TPT forces. Three different numbers of diaphragms were selected for the parametric study. These were three, four, and five diaphragms. The transverse strains were measured perpendicular to the longitudinal axis of the bridge model using twenty seven transverse strain gages mounted on the top surface of the deck slab directly above the shear-keys.

This section is divided into three sub-sections. The first sub-section presents the variation of the transverse strains as a result of different arrangement of TPT (different number of diaphragm and different levels of TPT force) along the span of the bridge model. The effect of the level of TPT forces and the number of diaphragms on the transverse strain at various

locations are presented in the second and the third sub-sections, respectively. In addition, American Association of State Highway and Transportation Officials Load and Resistance Factor Design (AASHTO LRFD, 2004) transverse prestress recommendation was evaluated. In this study, the transverse diaphragms with TPT forces are denoted post-tensioned diaphragms and the transverse diaphragms without any TPT force are denoted none post-tensioned diaphragms.

6.2.2 Longitudinal Variation of Transverse Strains

In order to investigate the effect of different arrangements of TPT on the transverse strains developed on the surface of the deck slab, the transverse strains were plotted against the distance from the bridge end for one-half of the bridge span, as shown in Figure 6.2-1 through Figure 6.2-9. Three data series are plotted in each figure indicating the strains measured over the shear-keys. Figure 6.2-1 through Figure 6.2-3 show the variation of the transverse strains when applying different levels of TPT forces to all five diaphragms. Figure 6.2-4 through Figure 6.2-6 show the variation when applying different levels of TPT forces to four diaphragms. Figure 6.2-7 through Figure 6.2-9 show the variation when applying different levels of TPT forces to three diaphragms.

The deck slab experienced the highest transverse strains at the locations aligned with the post-tensioned diaphragms. It is clear that the strains decrease towards zero in the areas between the post-tensioned diaphragms. For instance, as shown in Figure 6.2-2, point C-5, located over quarter-span diaphragm, experienced transverse strain of -98 με due to TPT force of 80 kip applied to four diaphragms. At the same time, point C-7, located between the quarter-span and mid-span diaphragms, experienced transverse strain of -29 με. In the case of applying TPT force of 40 kip to three diaphragms, the transverse strain developed at point A-9, located over the post-tensioned mid-span diaphragm, was -69 με, compared to the the transverse strain of 20 με at point A-5 located over the none post-tensioned quarter-span diaphragm. This is shown in Figure 6.2-8.

The variation of the transverse strains along the longitudinal axis defined by the shear-keys demonstrates that the effect of post-tensioning is localized and indicates uneven distribution of the TPT forces to the deck slab and shear-keys. Furthermore, the transverse strain distribution variations along the shear-keys are similar, yet reduced, when the TPT force is reduced from 80

kip to 40 or 20 kip. This observation is common for the different investigated arrangements of post-tensioned diaphragms. While the majority of the cases demonstrate localized strain levels below the recommended levels by AASHTO LRFD (2004), only the case of five diaphragms with 80 kip TPT force was able to maintain the recommended strain level along most of the length of the bridge model.

The effect of the skew angle of the bridge on the transverse strain distribution led to a concentration of the transverse strains near the acute corner of the bridge model. For the same arrangement of TPT forces, the points located near the acute corner (shear-key C-C) experienced higher transverse strains than those points located near the obtuse corner (shear-key A-A) for the same transverse axis. In addition, the points located at the mid-width of the bridge model (shear-key B-B) experienced transverse strains lower than those developed at the points located near the acute corner and higher than those developed at the points located near the obtuse corner. For example, the transverse strains developed due to TPT force of 80 kip applied to three diaphragms for points A-1, B-1, and C-1, located on the same transverse axis "1", were -34, -82, and -113 με, respectively, as shown in Figure 6.2-7. However, the difference in the transverse strains between the points located at the same transverse axis reduced towards mid-span. For example, the transverse strains developed due to TPT force of 80 kip applied to three diaphragms for points A-9, B-9, and C-9, located on the same transverse axis "9", were -95, -102, and -112 με, respectively, as shown in Figure 6.2-7.

The results also show a systematic difference in the transverse strains developed at the end-diaphragm and the mid-span diaphragm. The transverse strains developed near the end of the bridge model were lower than the strains near the mid-span. The lower strain levels at the end span are likely due to the increased volume of concrete of the end-blocks, which reduced the strains. As an example, the transverse strains, due to TPT force of 40 kip applied to five diaphragms for points C-9 and C-1, which are located at mid-span and end-diaphragms, were -143 and -90 με, respectively (see Figure 6.2-2). Similar behavior was observed when TPT force of 20 kip was applied to three diaphragms where the transverse strains for points A-9 and A-1 located at mid-span and end-diaphragms were -44 and -21 με, respectively (see Figure 6.2-9).

AASHTO LRFD Bridge Design Specification (2004) recommends that the minimum transverse prestress developed due to TPT forces should not be less than 250 psi. However, the

AASHTO LRFD (2004) did not provide any additional information about this limit. It did not clearly specify the region or area at which the limit should be maintained. By assuming full integrity on the behavior of the bridge model in the transverse direction, it is expected that the lowest transverse compressive strains due to the application of the TPT forces at diaphragms locations should develop at the top surface of the deck slab (extreme top fiber). This is because of the eccentric resultant of TPT force with respect to the total depth of the entire bridge model (box-beams and deck slab). In addition, the bearing plate is placed directly on the side face of the box-beams and there was no direct contact between the bearing plate and the deck slab. Therefore, the effect of the TPT forces would transfer from the box-beams to the deck slab only through the composite action. Since the longitudinal cracks in side-by-side box-beam bridges are usually observed on the deck slab between the adjacent box-beams, the strain gages mounted on the deck slab of the bridge model above the shear-keys were used to evaluate the AASHTO LRFD (2004) limit.

In order to compare the measured transverse strains with the AASHTO LRFD (2004) limit, the AASHTO LRFD (2004) limit was converted to an equivalent limit in micro-strains. The determination of the equivalent strains was based on the compressive strength of deck slab concrete during the test (5,000 psi), the American Concrete Institute (ACI 318-05) equation for predicting the modulus of elasticity of concrete, and the elasticity theory (Hooke's Law) as follows.

AASHTO LRFD (2004) minimum prestress limit (*f*)

$f = -0.25$ ksi

Compressive strength of deck slab concrete during the test (f_c')

$f_c' = 5{,}000$ psi

ACI 318-05 equation for determining the modulus of elasticity for concrete (E_c) [Section 8.5.1]

$$E_c = 57{,}000\sqrt{f_c'} = 57{,}000\sqrt{5{,}000} = 4{,}030 \times 10^3 \text{ psi} = 4{,}030 \text{ ksi} \quad (6.1)$$

Using the elastic theory for determining the equivalent strains (ε)

$$\varepsilon = \frac{f}{E_c} = \frac{-0.25}{4{,}030} = -62 \ \mu\varepsilon \quad (6.2)$$

The aformantioned strain limit presents the equivalent strain of the AASHTO LRFD (2004) prestress limit. The equivalent limit was superimposed on all the transverse strain distribution curves (Figure 6.2-1 through Figure 6.2-20). Figure 6.2-1 through Figure 6.2-9 show that at least eight points experienced transverse strains below the equivalent AASHTO LRFD (2004) limit for each arrangement of TPT forces. Furthermore, all the twenty seven points experienced transverse strains less than that of the equivalent AASHTO LRFD (2004) limit in some arrangements of TPT forces, such as applying TPT force of 20 kip at five, four, and three diaphragms (Figures 6.2-7, 6.2-8, and 6.2-9, respectively).

6.2.3 Effect of Number of Diaphragms

The effects of the number of diaphragms on the transverse strain distributions are evaluated in this section. Different number of diaphragms resulted in different spacing between the transverse diaphragms. Nevertheless, in all cases TPT forces were applied to the end-diaphragms. In the case of three diaphragms, the spacing between the three diaphragms was 15 ft. In the case of four diaphragms, two different spacings were introduced; 7.5 ft between the end and the intermediate-diaphrams and 15 ft between the intermediate-diaphragms. In the case of five diaphragms, the spacing was 7.5 ft. Furthermore, the bridge systems are not physically identical when the number of diaphragms is changed. Therefore, these results are compared using histograms.

The rate of increase in the transverse strains due to the corresponding increase in the TPT forces reflects the sensitivity of the transverse strains developed at any point to the applied TPT forces. It is based on the assumed linear relation between the TPT forces and the corresponding transverse strains for a given bridge system. Table 6.2-1 shows the rate of increase in the transverse strains due to different number of diaphragms.

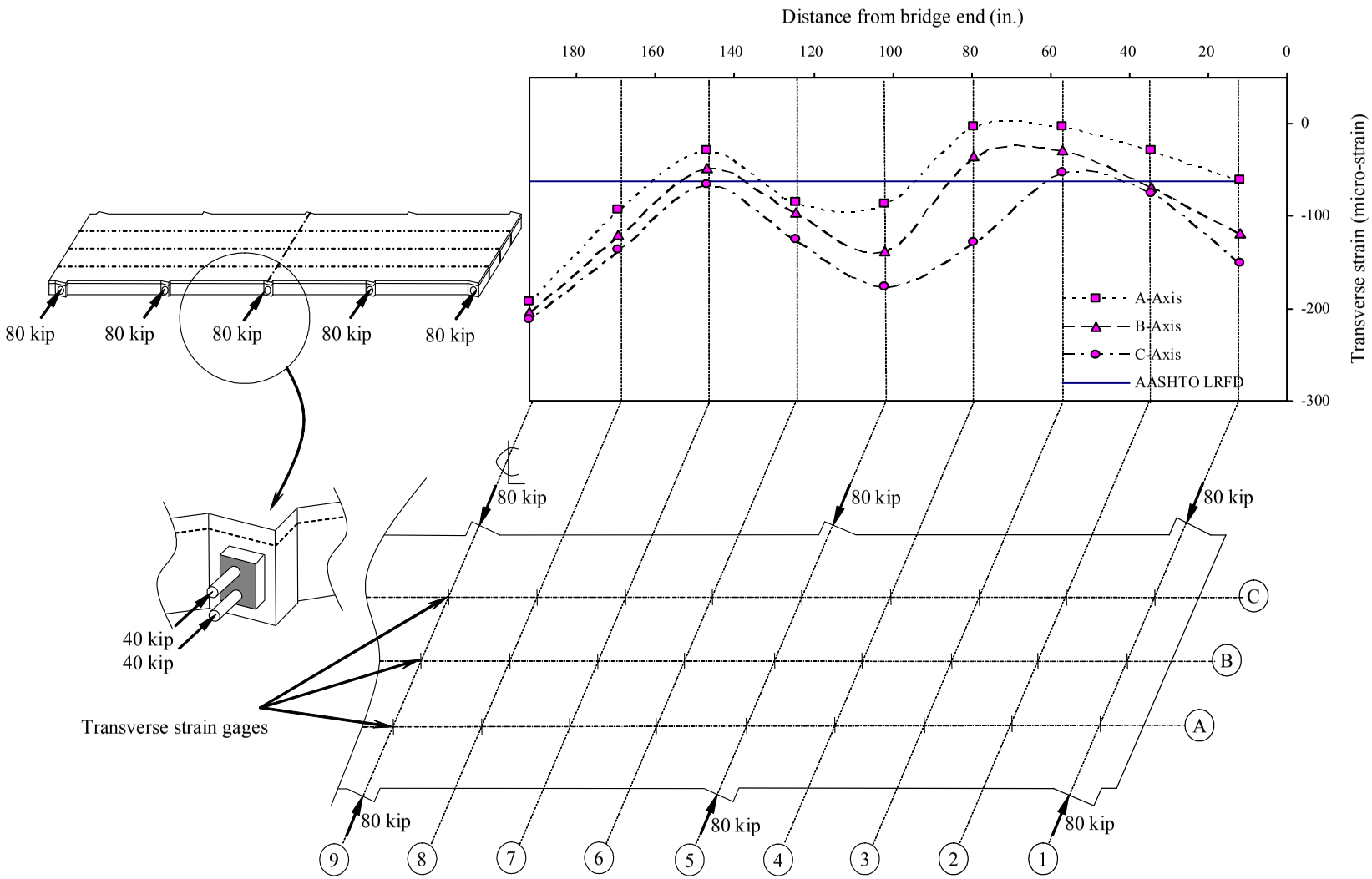

Figure 6.2-1 Transverse strain distribution due to applying 80 kip at five diaphragms.

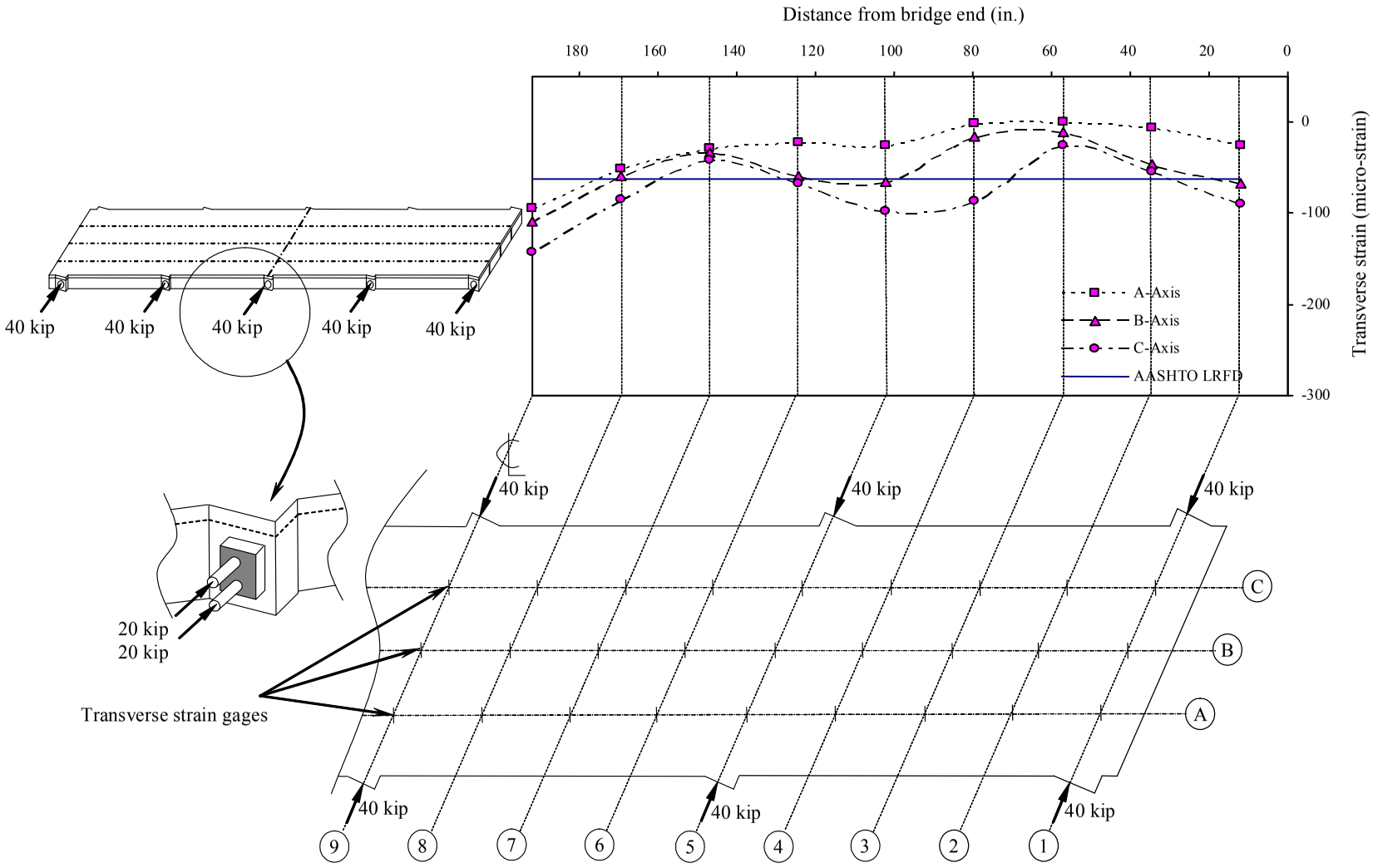

Figure 6.2-2 Transverse strain distribution due to applying 40 kip at five diaphragms.

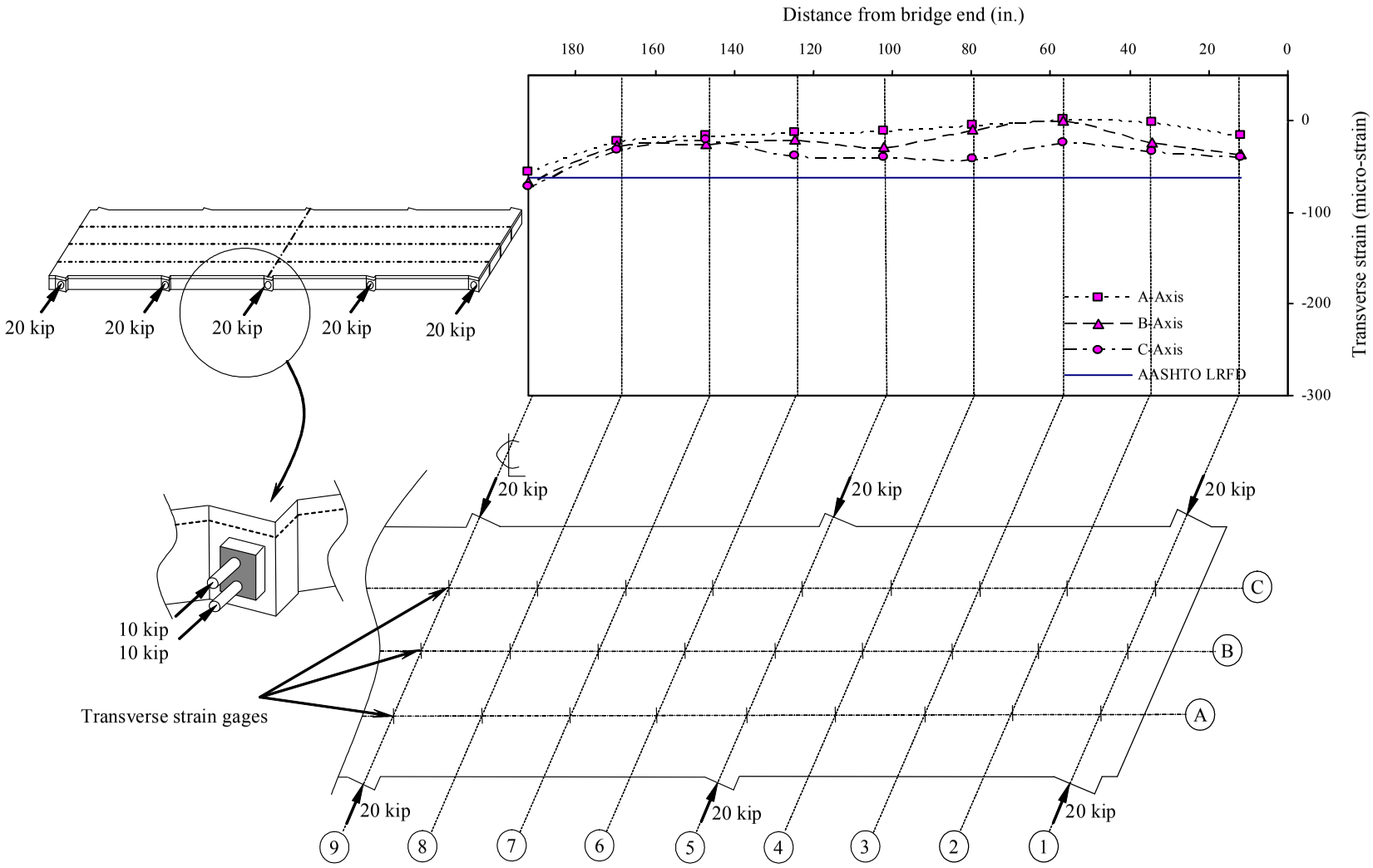

Figure 6.2-3 Transverse strain distribution due to applying 20 kip at five diaphragms.

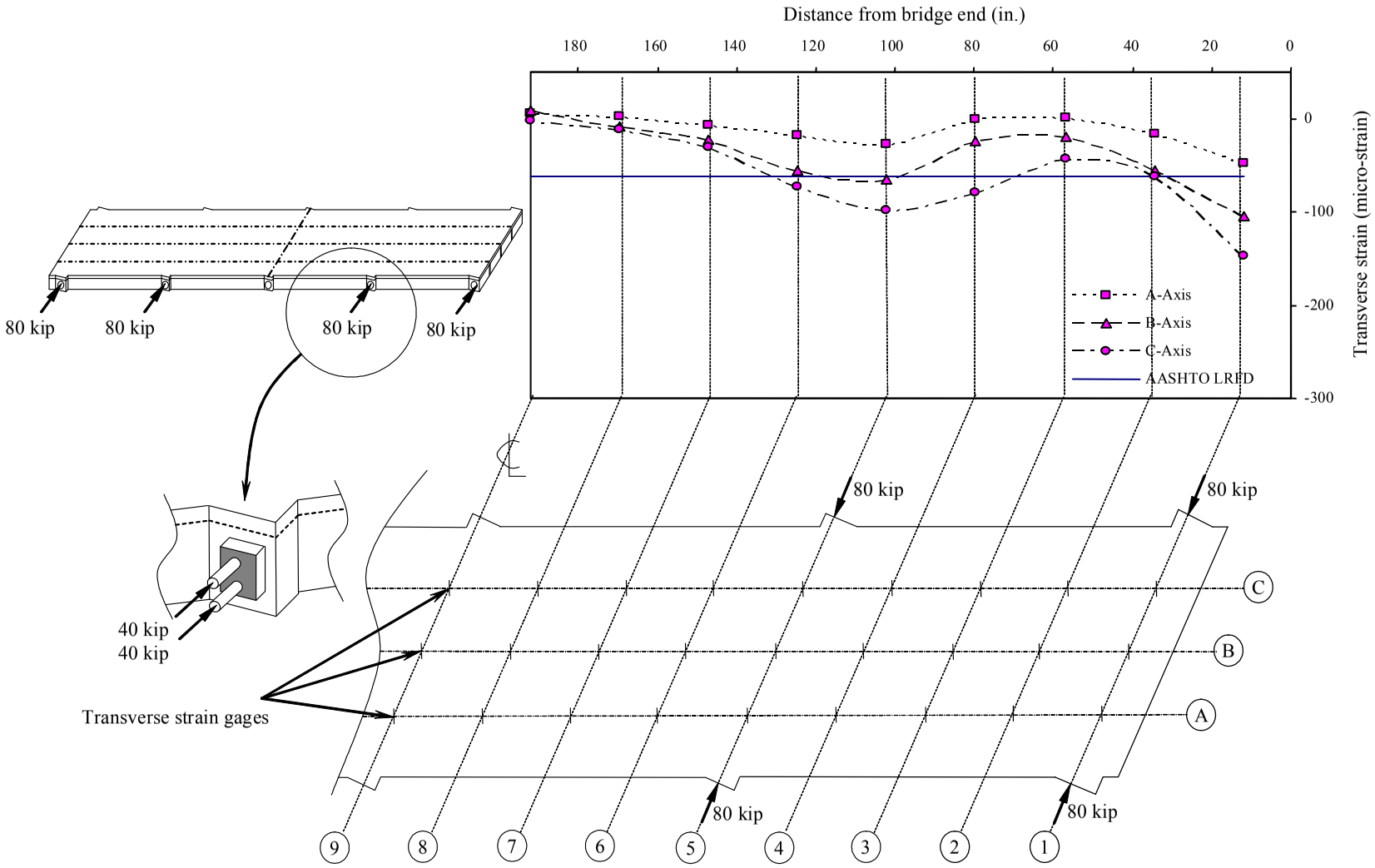

Figure 6.2-4 Transverse strain distribution due to applying 80 kip at four diaphragms.

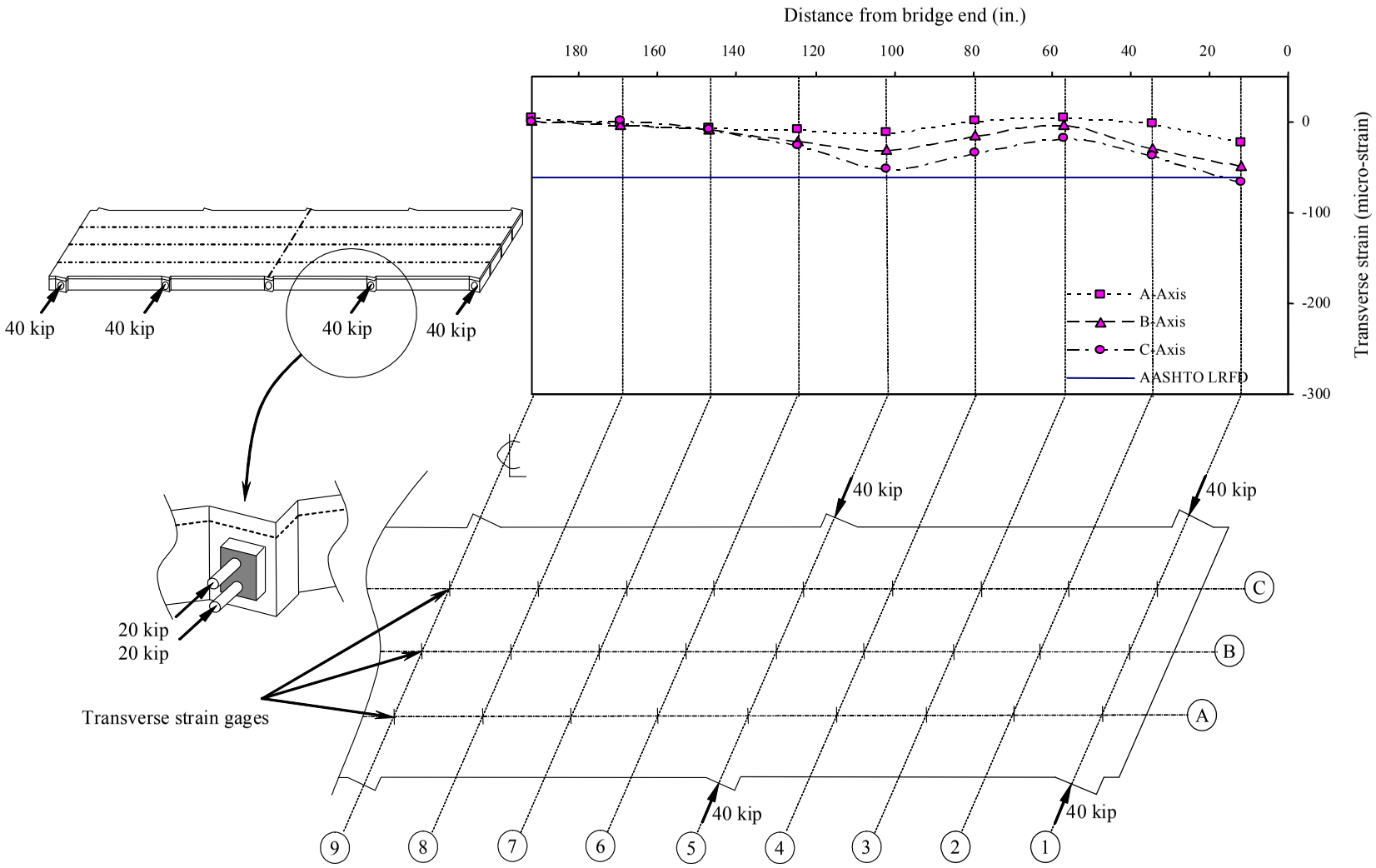

Figure 6.2-5 Transverse strain distribution due to applying 40 kip at four diaphragms.

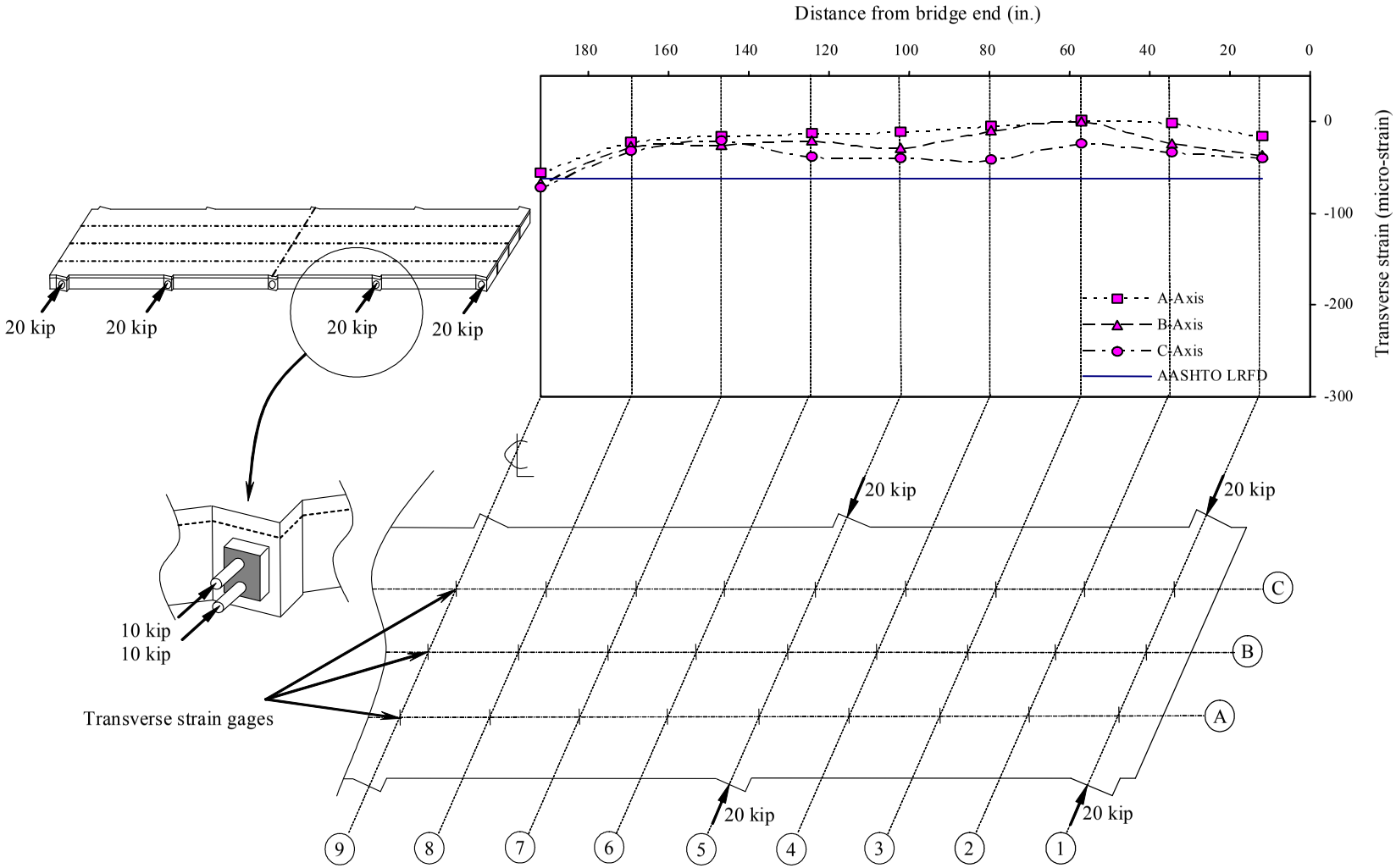

Figure 6.2-6 Transverse strain distribution due to applying 20 kip at four diaphragms.

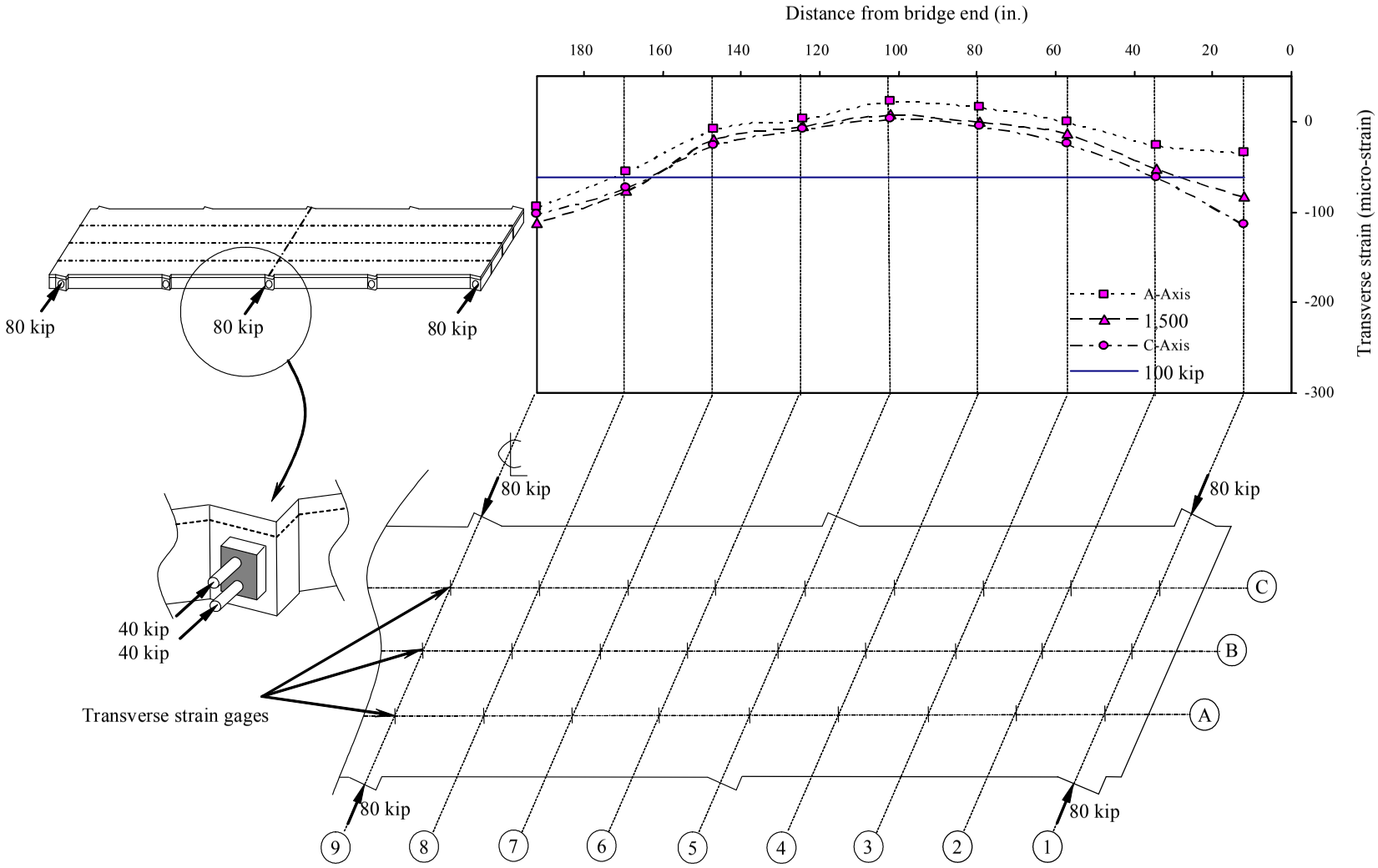

Figure 6.2-7 Transverse strain distribution due to applying 80 kip at three diaphragms.

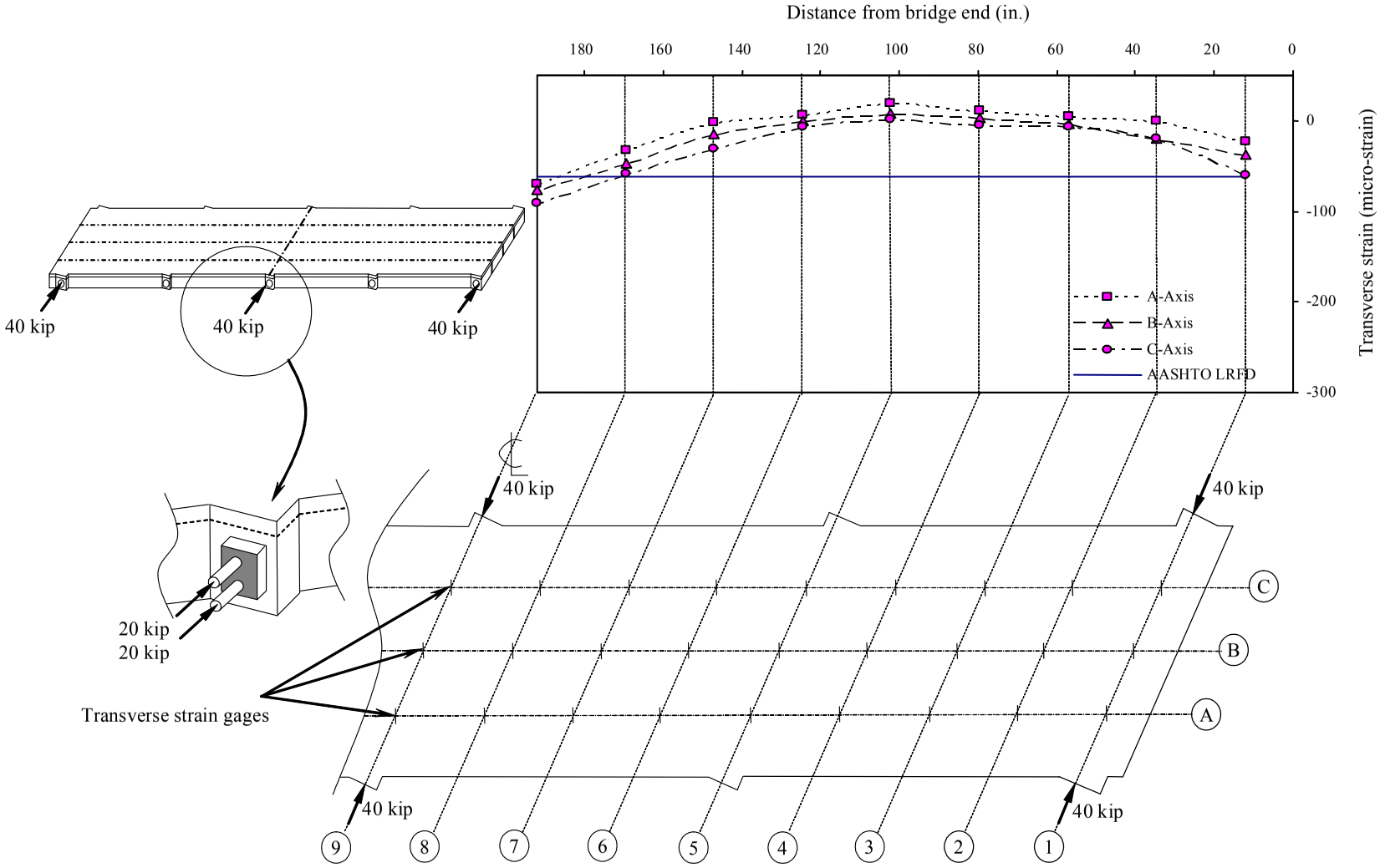

Figure 6.2-8 Transverse strain distribution due to applying 40 kip at three diaphragms.

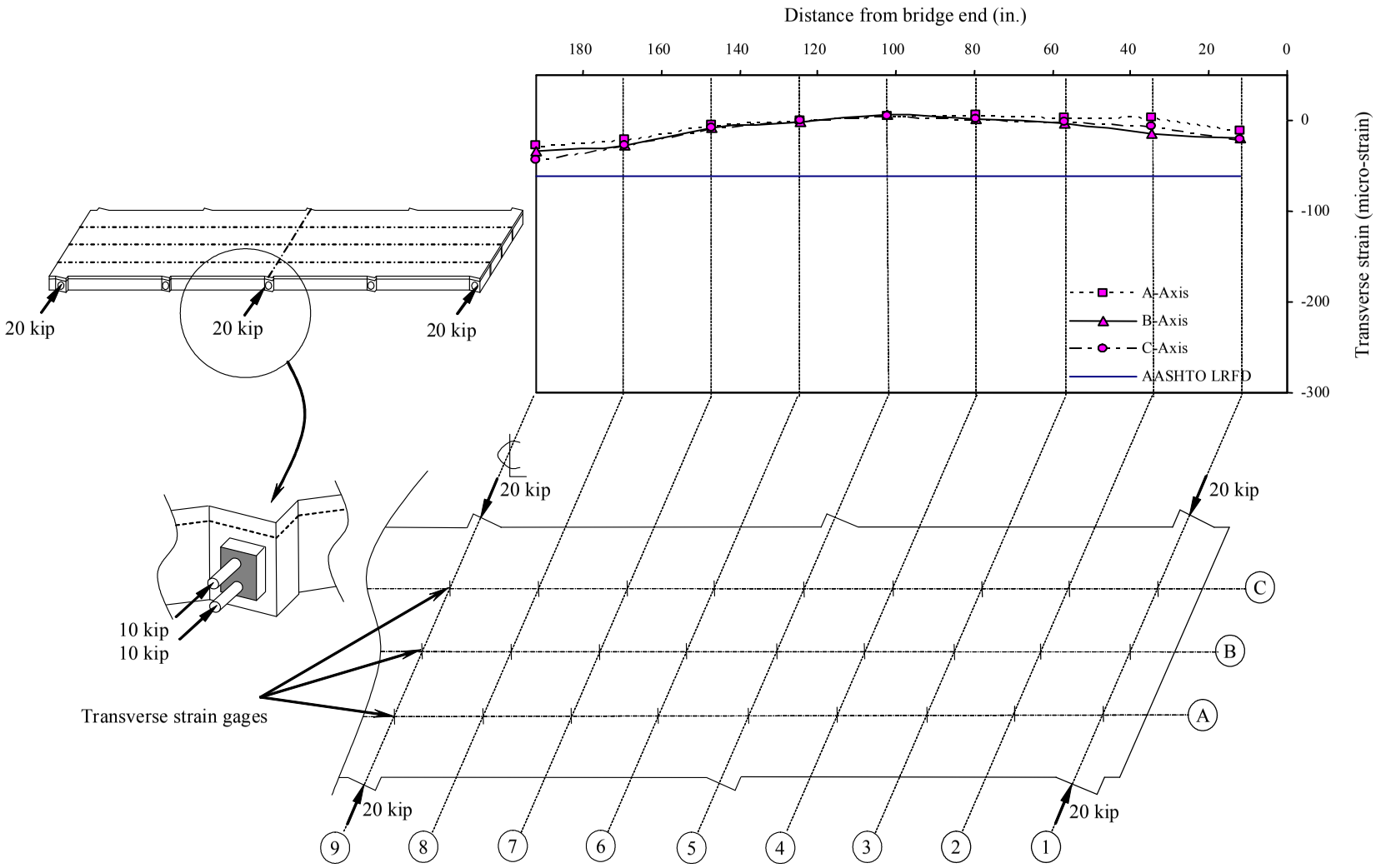

Figure 6.2-9 Transverse strain distribution due to applying 20 kip at three diaphragms.

The transverse strain is evaluated along the longitudinal axis and the results along shear-key A-A is presented in Figure 6.2-10 through Figure 6.2-12. Figure 6.2-10 shows the histogram of the transverse strains at five points (A-1, A-3, A-5, A-7, and A-9), located above the same shear-key A-A, due to TPT forces of 80 kip applied to different numbers of diaphragms. The horizontal axis represents different number of diaphragms and the vertical axis represents the corresponding transverse strains. As discussed in Section 6.2.1, the transverse strain decreases as the distance from the post-tensioned diaphragm increases. Point A-9, located at the mid-span diaphragm, experienced high transverse strains of -95 με due to TPT force of 80 kip at three diaphragms as the mid-span diaphragm was post-tentioned. This strain increased to -192 με for the bridge system with five diaphragms. However, as the mid-span diaphragm was not post-tensioned in the case of four diaphragms a low tensile transverse strain of 6 με was observed.

The results also show that as the distance from the point evaluated to the post-tensioned diaphragms increases, the transverse strains decreases towards zero and consequently, transverse tensile strains may indeed develop in the deck slab. Point A-5, located at the quarter-span diaphragm, experienced low transverse tensile strains of 23 με due to TPT force of 80 kip applied to three diaphragms and transverse compressive strains of -27 and -87 με when the same TPT force was applied at four and five diaphragms, as shown in Figure 6.2-10.

Point A-1, located at the end-diaphragm, experienced high transverse strains of -34, -48, and -61 με due to TPT force of 80 kip applied to three, four, and five diaphragms, respectively. It is observed that increasing the number of diaphragms increases proportionally the transverse strains as the total TPT forces acting on the bridge model increases. The results in Figure 6.2-10 also show that points A-3 and A-7 located between the post-tensioned diaphragms only experience small compressive stresses in all cases of number of post-tensioned diaphragms and level of TPT forces. Strain levels at these points ranged from 1 to about 29 με. The variation of transverse strains on the deck slab along shear-key A-A was also observed for the other two shear-keys defined as B-B and C-C.

In general, it could be noted that the rate of increase of transverse strains depends on the location of the point with respect to the post-tensioned diaphragms. The points located on the post-tensioned diaphragms experienced higher rates of increase in the transverse strains than the points located between the diaphragms or on the none post-tensioned diaphragms. Furthermore, points located 22.5 in. away from the centerline of the diaphragms (on the

transverse axes “2”, “4”, “6”, and “8”) experienced higher rates of increase than those points located at the mid-distance between the diaphragms on the transverse axes “3” and “7” (45 in. away from the centerline of the diaphragms). Therefore, it could be concluded that closer the point to the diaphragm, the more sensitive the transverse strain would be to any change of force at the diaphragm.

For example, the rates of increase in the transverse strain at points A-9, A-5, and A-1 due to TPT forces applied to five diaphragms were -2.4, -1.08, and -0.76 με/kip, respectively. However, the rates of increase at points A-7 and A-3 were -0.36 and -0.03 με/kip, respectively for the same number of diaphragms. The rates of increase for points A-9, A-5, and A-1 were higher than those for points A-7 and A-3 because of the location of the points with respect to the post-tensioned diaphragms. Points A-9, A-5, and A-1 were located directly over the post-tensioned diaphragms, while points A-7 and A-3 were located at the mid-distance between the post-tensioned diaphragms. In addition, point A-8 experienced higher rate of increase in the transverse strains (-0.69 με/kip) due to different levels of TPT forces at three diaphragms than point A-7, which experienced rate of increase in the transverse strains of -0.11 με/kip due to different levels of TPT forces at the same number of diaphragms.

In the case of four diaphragms, points A-5 and A-1 experienced high rates of increase in the transverse strains (-0.34 and -0.61 με/kip, respectively) compared to point A-9 (0.07 με/kip) since points A-5 and A-1 were located over post-tensioned diaphragms, while point A-9 was located over the mid-span diaphragm (none post-tensioned diaphragm). The close to zero positive rate of increase at point A-9 indicates the insignificant effect of TPT forces at that location. Similar behavior was observed at the shear-keys B-B and C-C.

Table 6.2-1 Rate of increase in the transverse strains in με/kip.

Number of Diaphragms	Longitudinal Axis	Transverse Axis								
		1	2	3	4	5	6	7	8	9
Five	A	-0.76	-0.36	-0.03	-0.04	-1.08	-1.05	-0.36	-1.16	-2.40
	B	-1.49	-0.86	-0.35	-0.43	-1.73	-1.20	-0.61	-1.50	-2.55
	C	-1.88	-0.9	-0.66	-1.59	-2.21	-1.57	-0.82	-1.69	-2.65
Four	A	-0.61	-0.21	0.02	-0.01	-0.34	-0.22	-0.09	0.03	0.07
	B	-1.31	-0.70	-0.23	-0.31	-0.82	-0.69	-0.28	-0.11	0.12
	C	-1.84	-0.77	-0.53	-0.99	-1.23	-0.92	-0.37	-0.14	-0.03
Three	A	-0.43	-0.33	0.00	0.20	0.28	0.04	-0.11	-0.69	-1.19
	B	-1.03	-0.64	-0.17	-0.01	0.11	-0.07	-0.24	-0.95	-1.40
	C	-1.41	-0.78	-0.31	-0.06	0.04	-0.10	-0.32	-0.91	-1.28

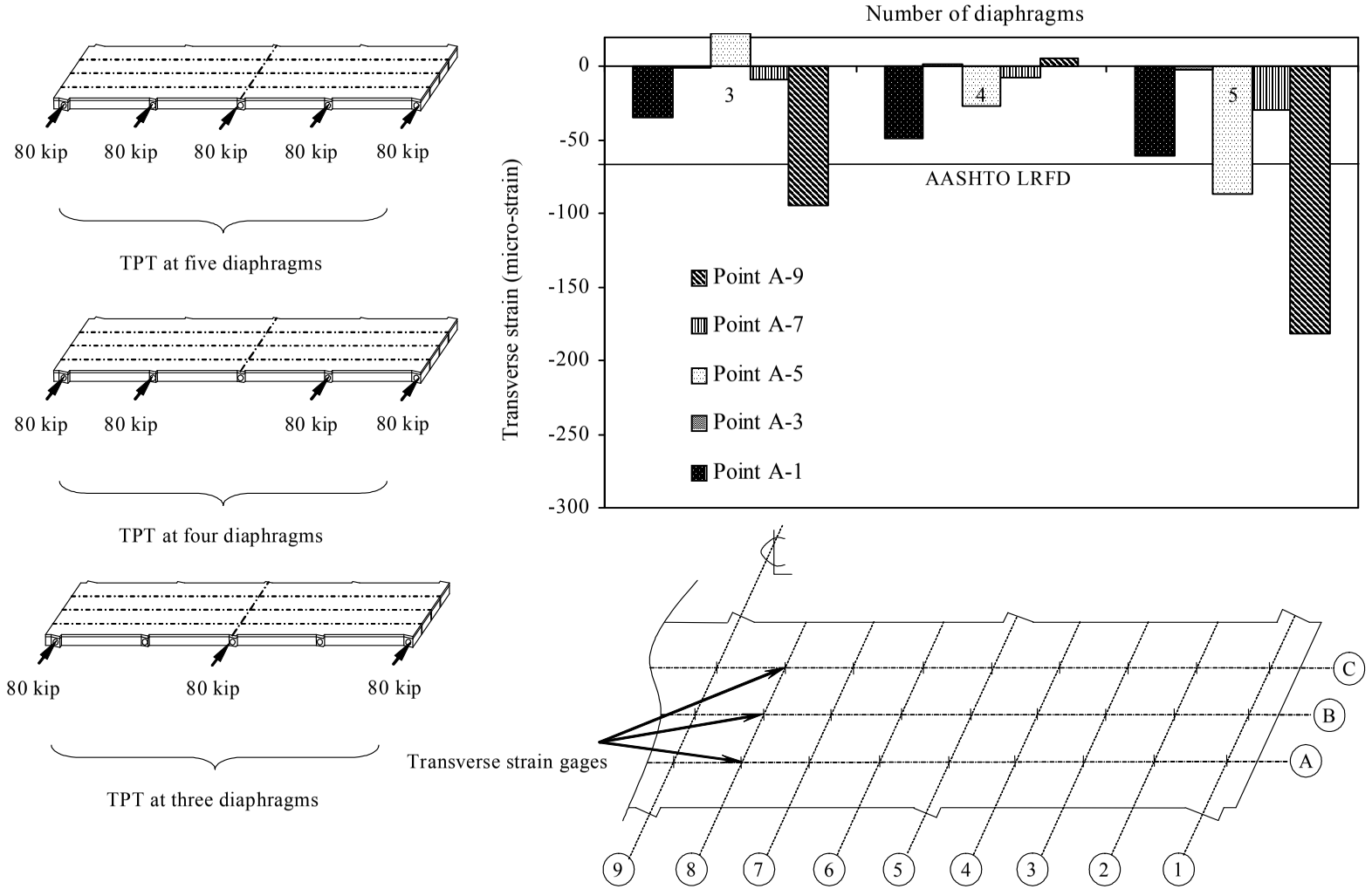

Figure 6.2-10 Transverse strains for shear-key A-A due to TPT force of 80 kip at different number of diaphragms.

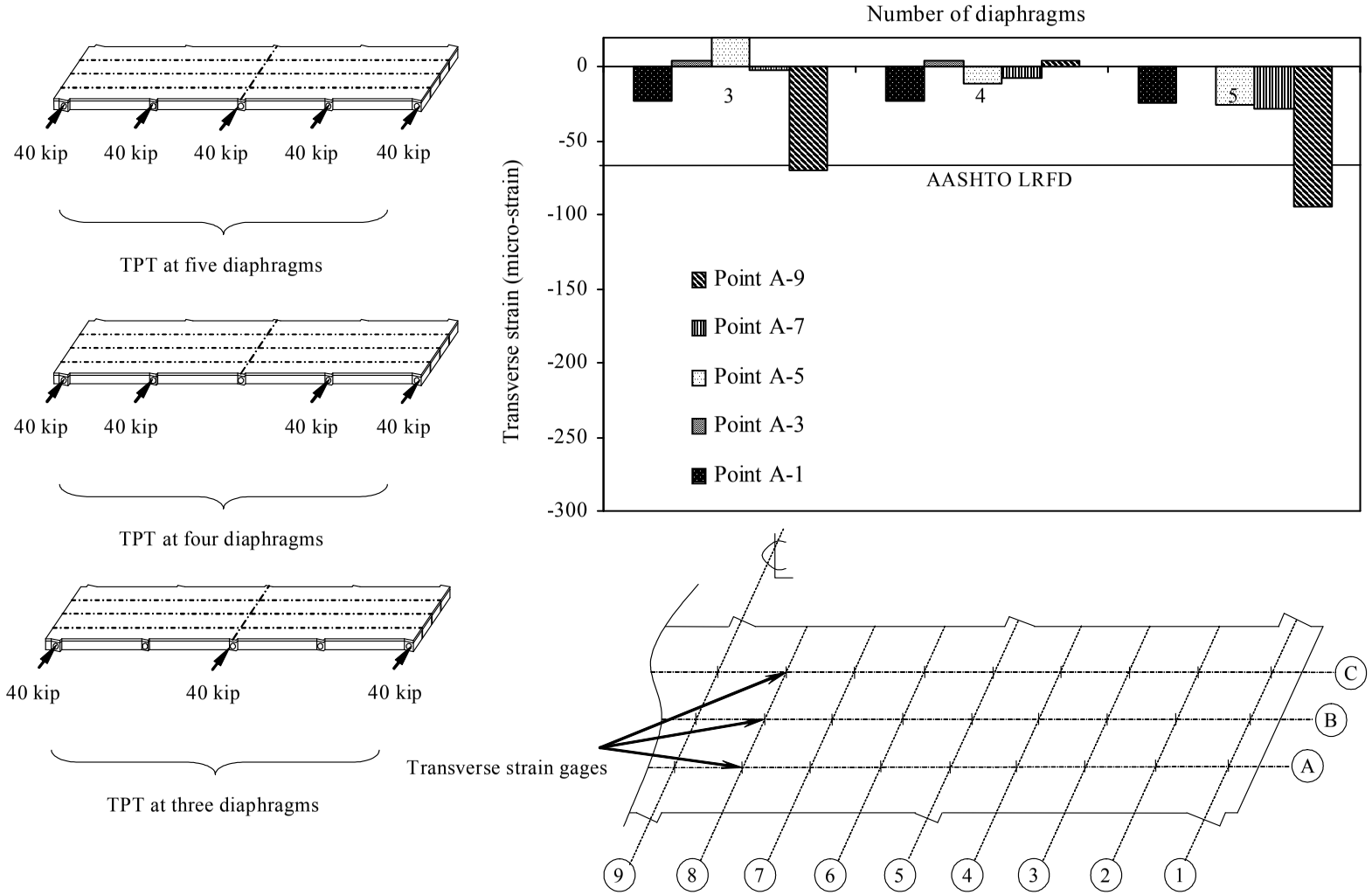

Figure 6.2-11 Transverse strains for shear-key A-A due to TPT force of 40 kip at different number of diaphragms.

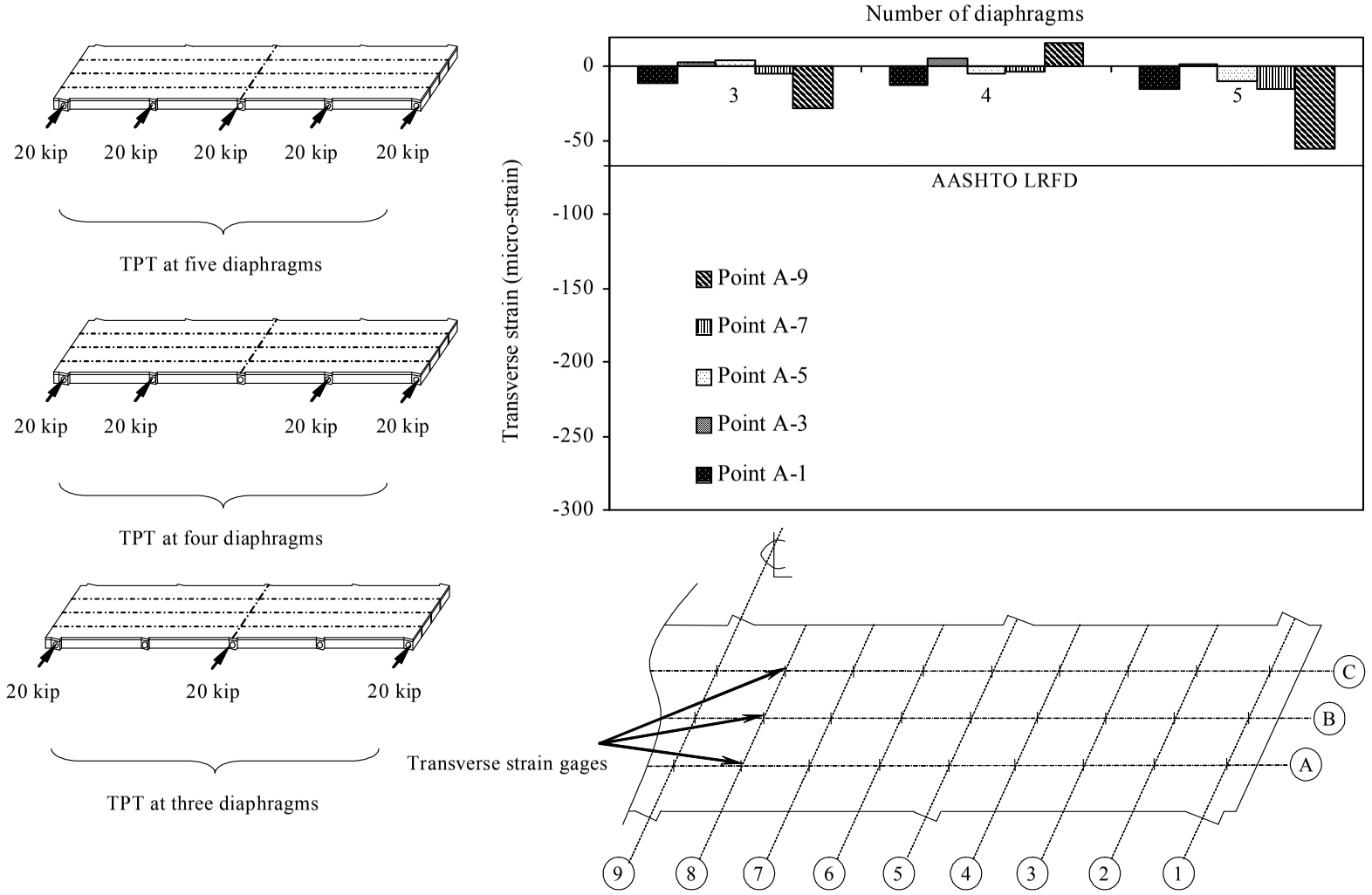

Figure 6.2-12 Transverse strains for shear-key A-A due to TPT force of 20 kip at different number of diaphragms.

6.2.4 Effect of Levels of TPT Forces

The effect of TPT forces on the transverse strains along the same longitudinal axis as well as locally is demonstrated in Figure 6.2-13 through Figure 6.2-15 and Figure 6.2-16 through Figure 6.2-20, respectively. Figure 6.10 shows the transverse strains developed at five points (A-1, A-3, A-5, A-7, and A-9), located at the same shear-key A-A, due to different levels of TPT forces applied to five diaphragms. Points A-1, A-5, and A-9 were located directly over the mid-span, quarter-span, and end-diaphragms, respectively. Points A-3 and A-7 were located at the mid-distance between the diaphragms. It was observed that by increasing the TPT forces, the transverse strains increased proportionally at all points located at the post-tensioned diaphragms. For example, point A-9 experienced transverse strains of -192, -94, and -56 με due to TPT forces of 80, 40, and 20 kip, respectively.

Similar behavior was observed at point A-5, which experienced transverse strains of -87, -25, and -10 με as a result of applying TPT forces of 80, 40, and 20 kip at five diaphragms, respectively. Similar behavior was observed at the cases of four and three diaphragms for the shear-key A-A as well as the points located at the shear-keys B-B and C-C. For example, point B-1 experienced transverse strains of -105, -48, and -27 με due to TPT forces of 80, 40, and 20 kip applied to four diaphragms, respectively. Also, point C-9 experienced transverse strains of -102, -91, and -44 με due to TPT forces of 80, 40, and 20 kip applied to three diaphragms, respectively.

On the other hand, the points located at the mid-distance between the diaphragms, such as those belong to the transverse axes “3” and “7”, experienced insignificant change in the transverse strains due to different levels of TPT forces. As shown in Figure 6.2-13, point A-3 experienced transverse strains of -2, 0.2, and 2 με due to TPT forces of 80, 40, and 20 kip applied to five diaphragms. Also, point A-7 experienced transverse strains of -29, -28, and -15 με due to TPT forces of 80, 40, and 20 kip applied to five diaphragms. Figures 6.2-14 and 6.2-15 indicate similar behavior for points A-3 and A-7 with four and three diaphragms cases. In addition, the same behavior was observed at the points located between the diaphragms in the other shear-keys B-B and C-C. The low transverse strains at these points located between the diaphragms confirmed the uneven distribution of the transverse stresses and that these strains were lower than the recommended levels as set by AASHTO LRFD (2004).

Figure 6.2-16 through Figure 6.2-20 show the levels of TPT force on the vertical axis and the corresponding transverse strains on the horizontal axis for points B-1, B-3, B-5, B-7, and B-9, which are located on the same shear-key B-B. Each plot presents three lines corresponding to three different numbers of diaphragms. It is observed that the relation between the TPT forces and the corresponding transverse strains is linear for any selected number of diaphragms. The linear relation between the level of the TPT forces and the corresponding transverse strains reflects the elastic behavior of the concrete when TPT forces were applied.

The average transverse strains and the standard deviation were calculated for each arrangement of TPT forces based on the average of the twenty seven strain readings. The results are as shown in Table 6.2-2. It is expected that increasing the level of TPT will increase the average transverse strains. However, the results also demonstrated that increasing the level of TPT also increased the variation of strains along the top of the deck slab at the shear-key locations. The effect of different levels of TPT on the average transverse strains as well as the standard deviation was evaluated for each number of diaphragms. From Table 6.2-2, it is evident that for the same number of diaphragms, increasing the level of TPT force resulted in a corresponding increase in the average transverse strain. In the case of five diaphragms, the average transverse strains were -95, -52, and -26 με due to TPT forces of 80, 40, and 20 kip, respectively. Same behavior was noted in the case of four and three diaphragms. In addition, increasing the TPT forces resulted in corresponding increase in the standard deviation for each number of diaphragm case. For instance, the standard deviations in five diaphragm case are 60, 36, and 19 due to TPT forces of 80, 40, and 20 kip, respectively. Similar behavior was observed at the four and three diaphragm cases.

It was observed that only the case of applying 80 kip at five diaphragms resulted in average transverse strain of -95 με that is higher than the equivalent AASHTO LRFD (2004) limit of -62 με. All the other TPT arrangements resulted in average transverse strains lower than the equivalent AASHTO LRFD (2004) limit. In other words, providing adequate spacing between the diaphragms, together with the application of 80 kip/diaphragm, could lead to a better distribution of the TPT forces along the longitudinal direction, and consequently satisfies the equivalent AASHTO LRFD (2004) limit.

Table 6.2-2 Average transverse strains.

Number of Diaphragms	Level of TPT Force, kip	Average Transverse Strains, με	Standard Deviation
Five	80	-95	60
	40	-52	36
	20	-26	19
Four	80	-37	39
	40	-16	19
	20	-7	11
Three	80	-35	41
	40	-20	30
	20	-9	14

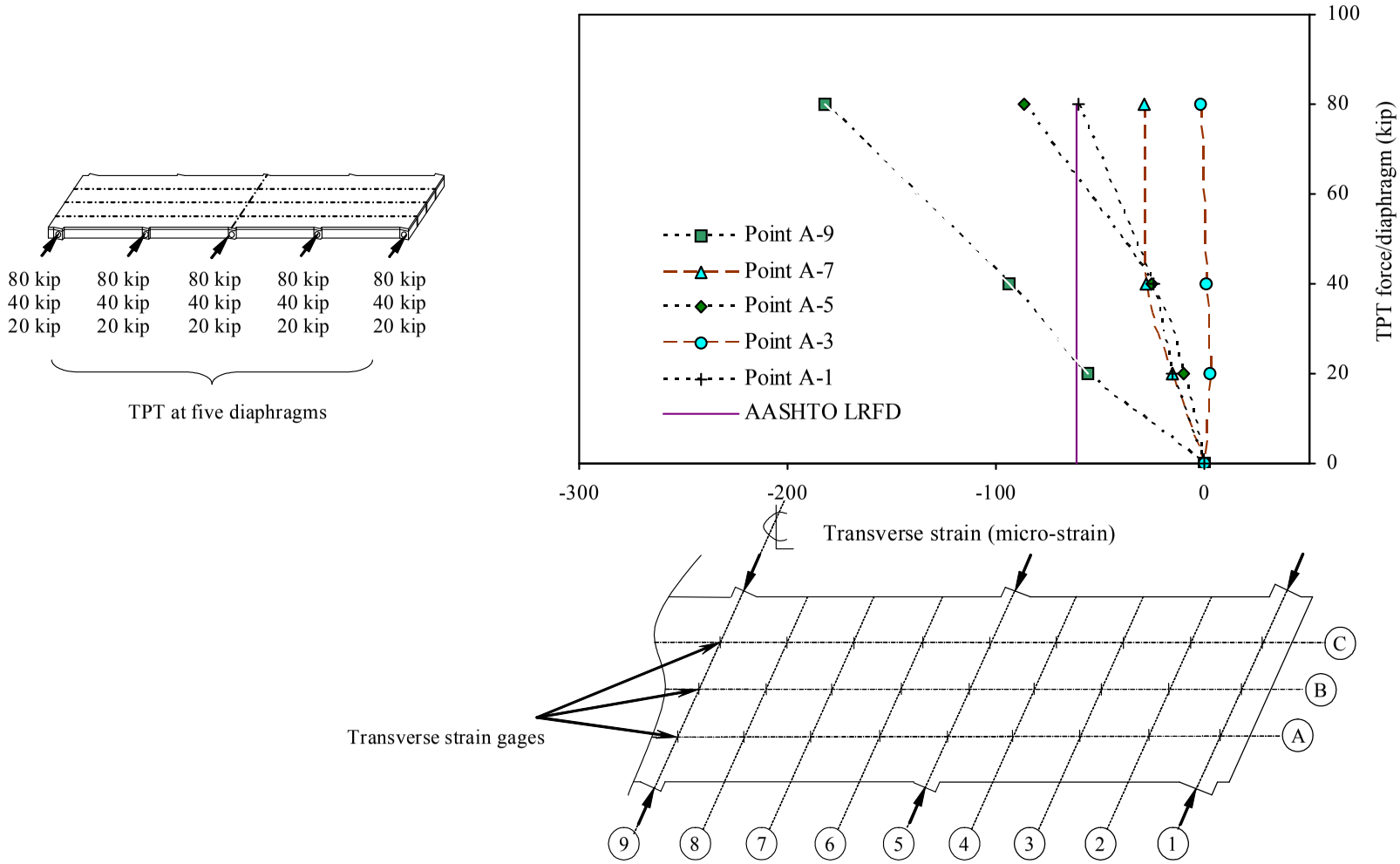

Figure 6.2-13 Transverse strains for shear-key A-A due to applying different levels of TPT force at five diaphragms.

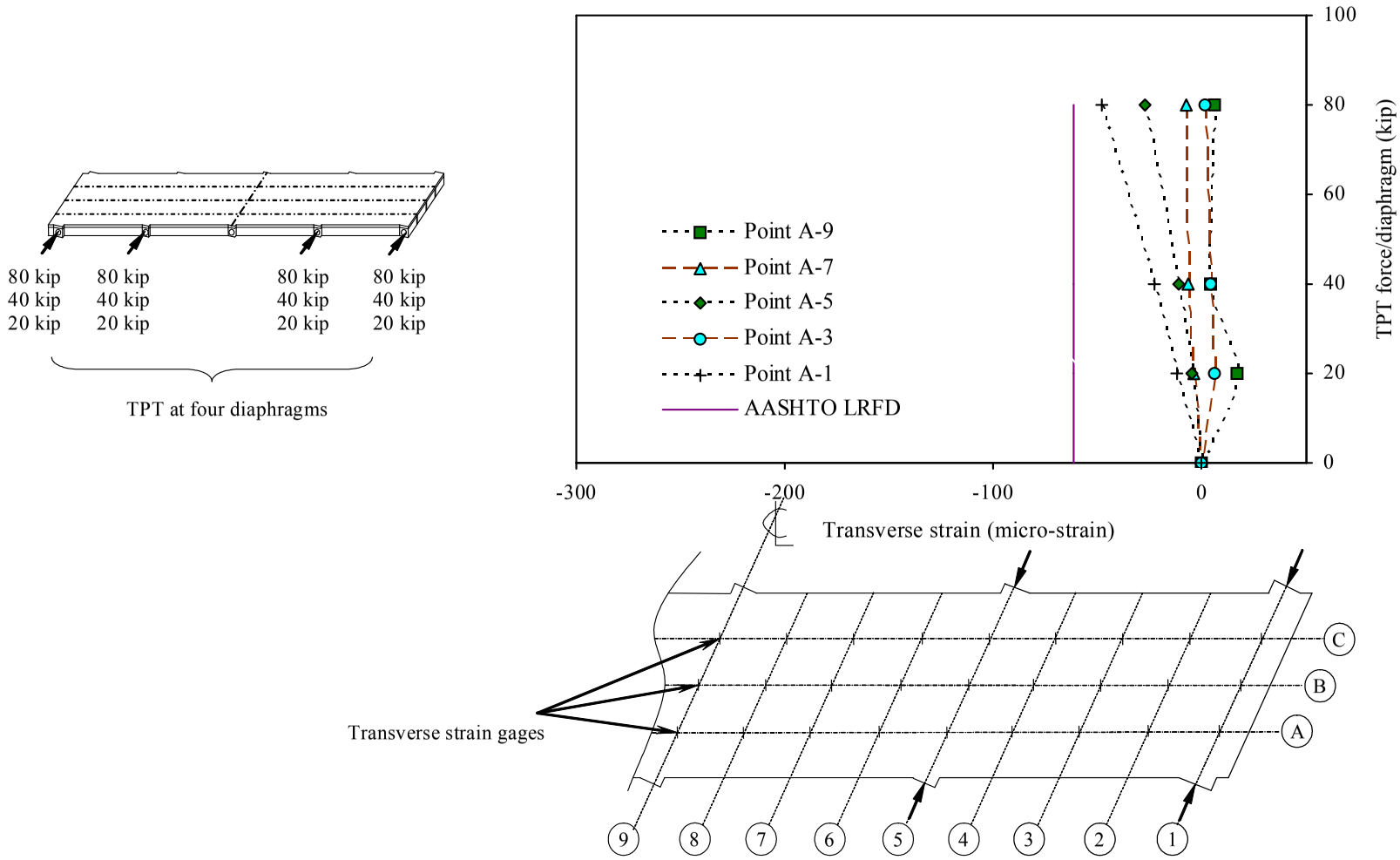

Figure 6.2-14 Transverse strains for shear-key A-A due to applying different levels of TPT force at four diaphragms.

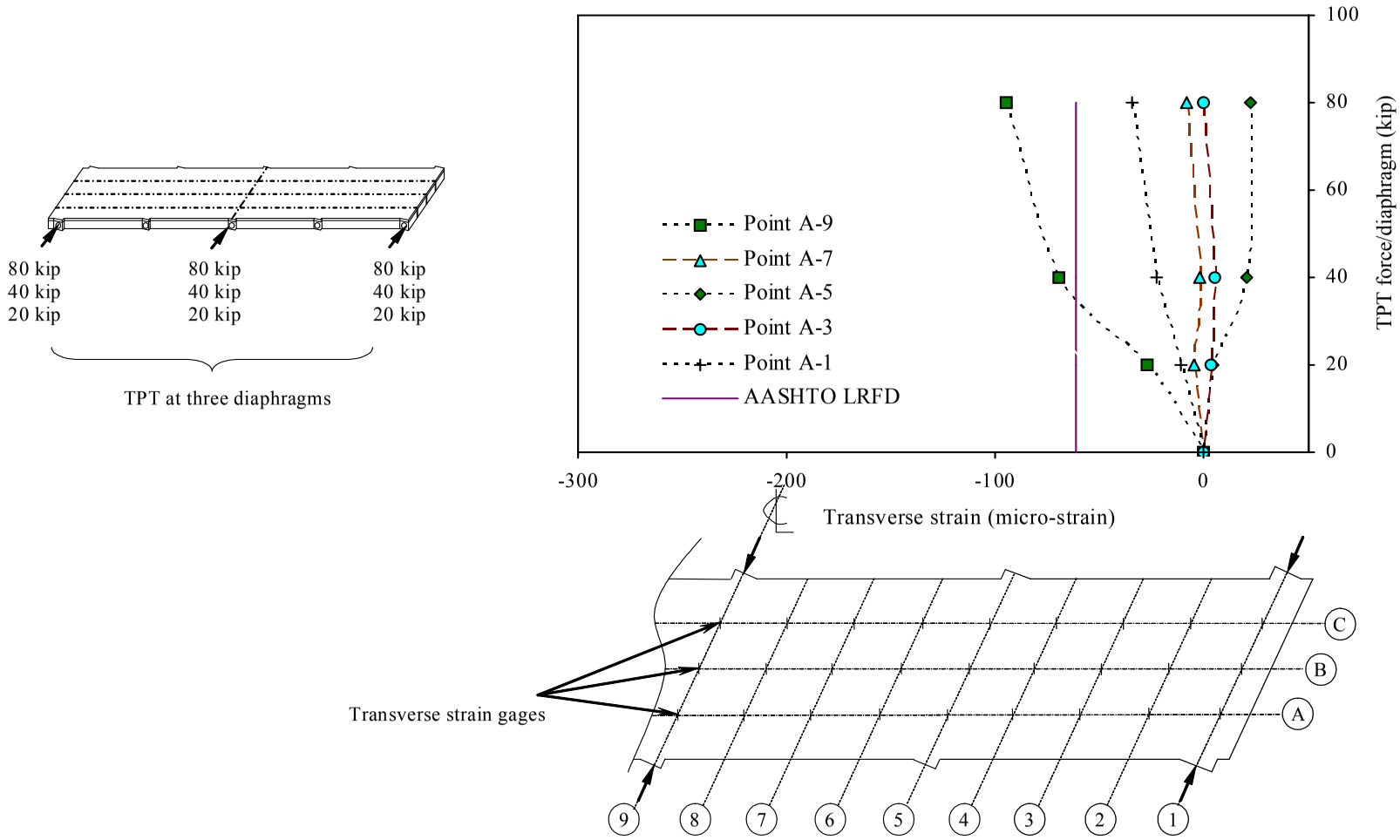

Figure 6.2-15 Transverse strains for shear-key A-A due to applying different levels of TPT force at three diaphragms.

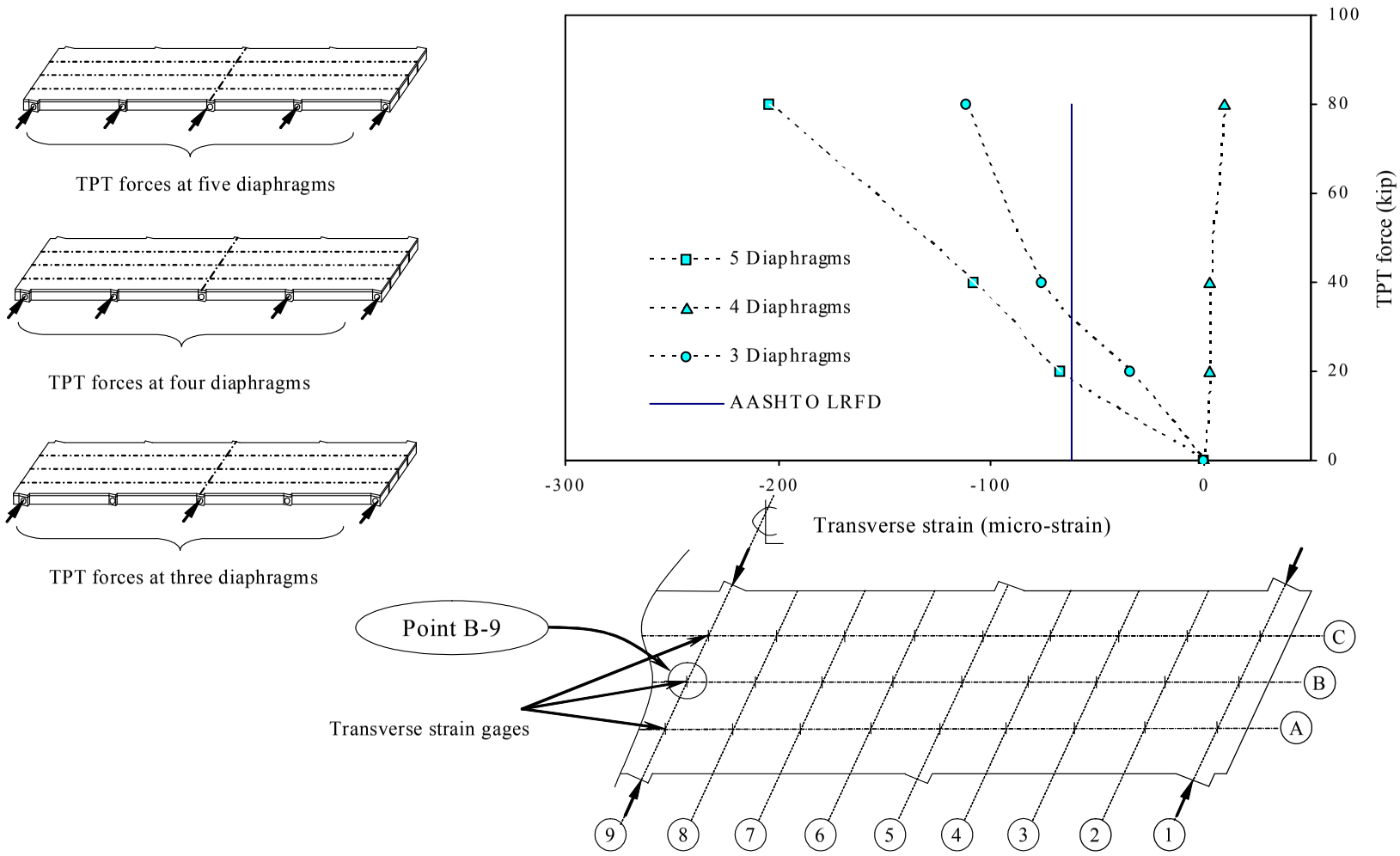

Figure 6.2-16 Transverse strains at point B-9 due to different levels of TPT force.

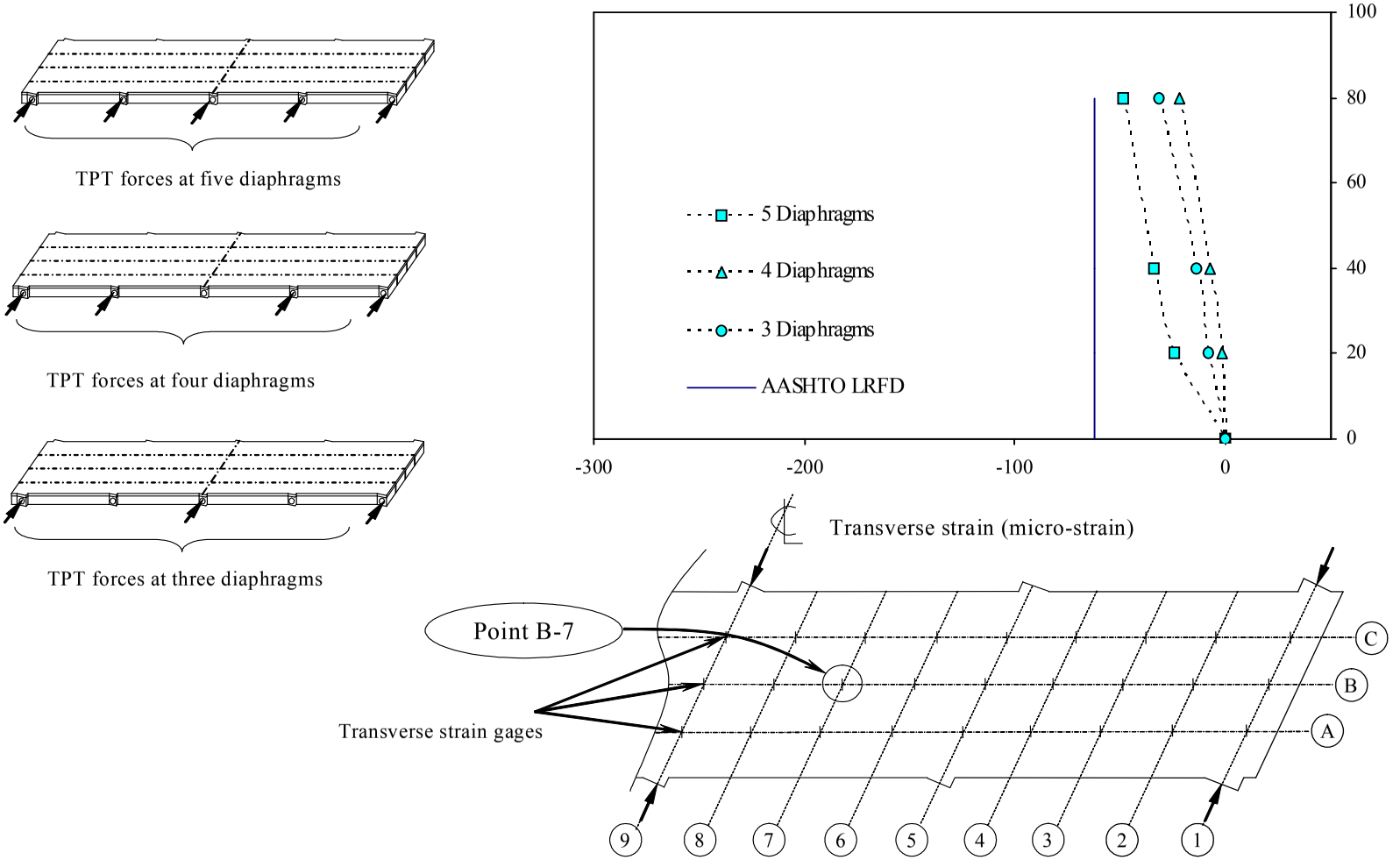

Figure 6.2-17 Transverse strains at point B-7 due to different levels of TPT force.

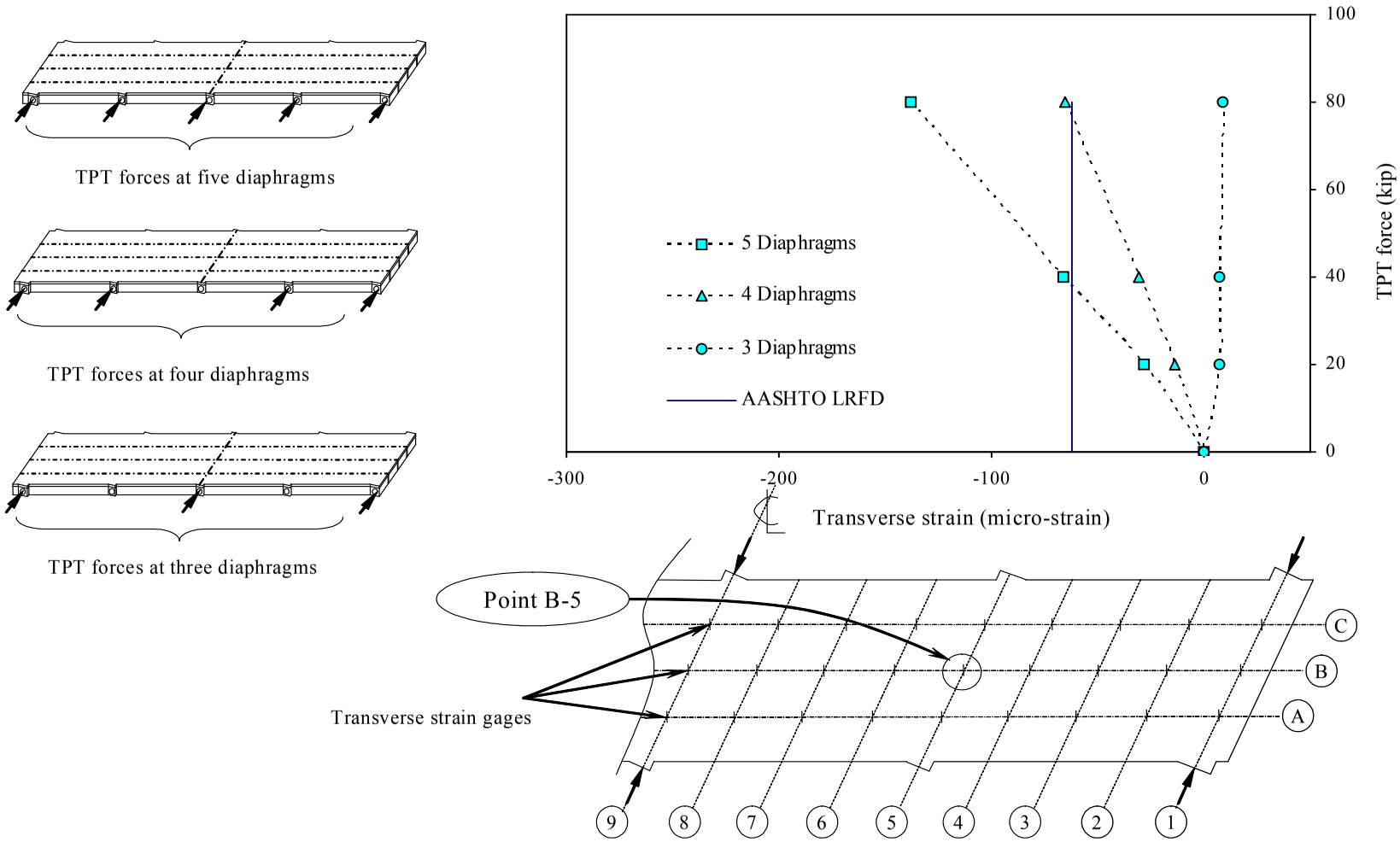

Figure 6.2-18 Transverse strains at point B-5 due to different levels of TPT force.

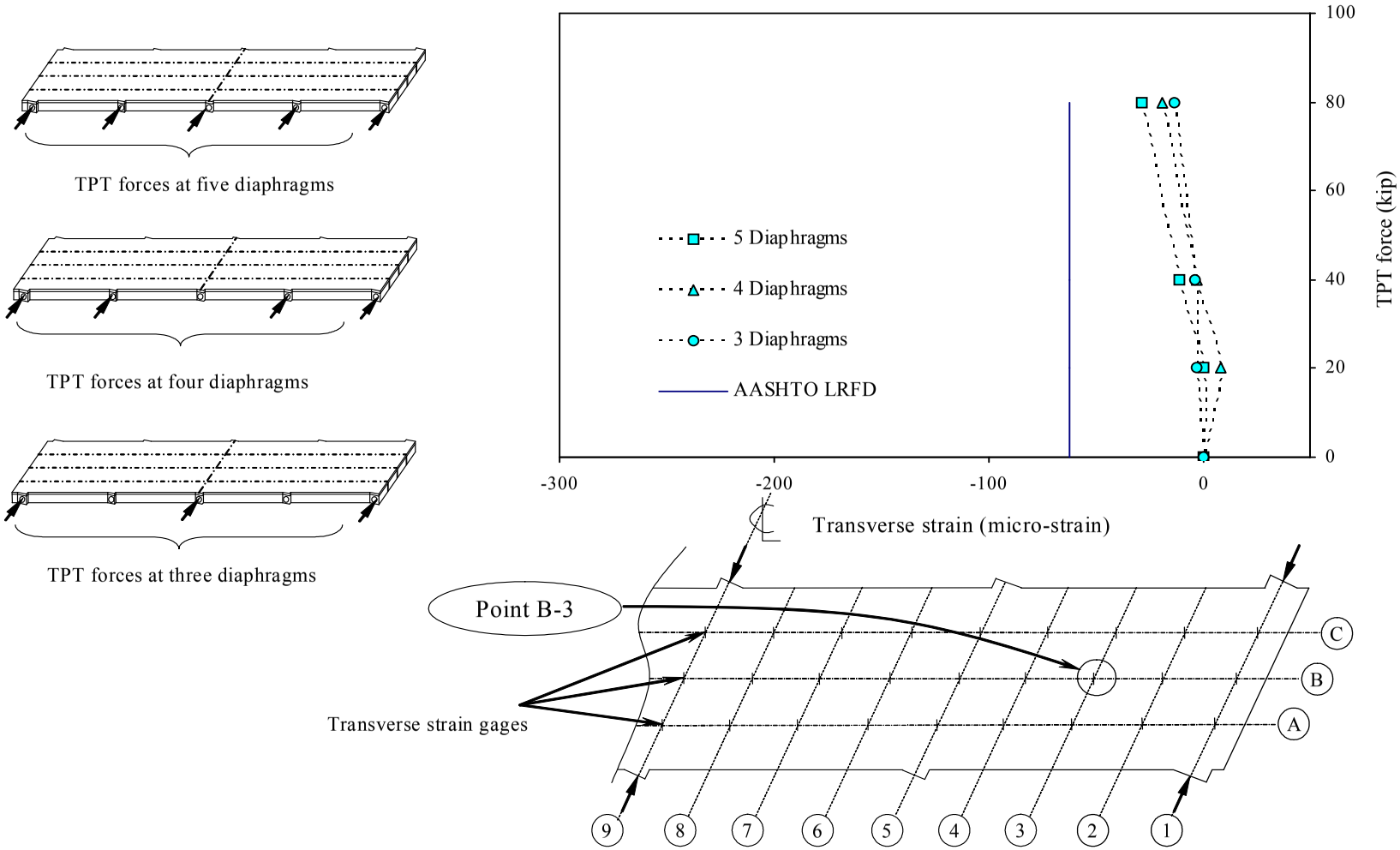

Figure 6.2-19 Transverse strains at point B-3 due to different levels of TPT force.

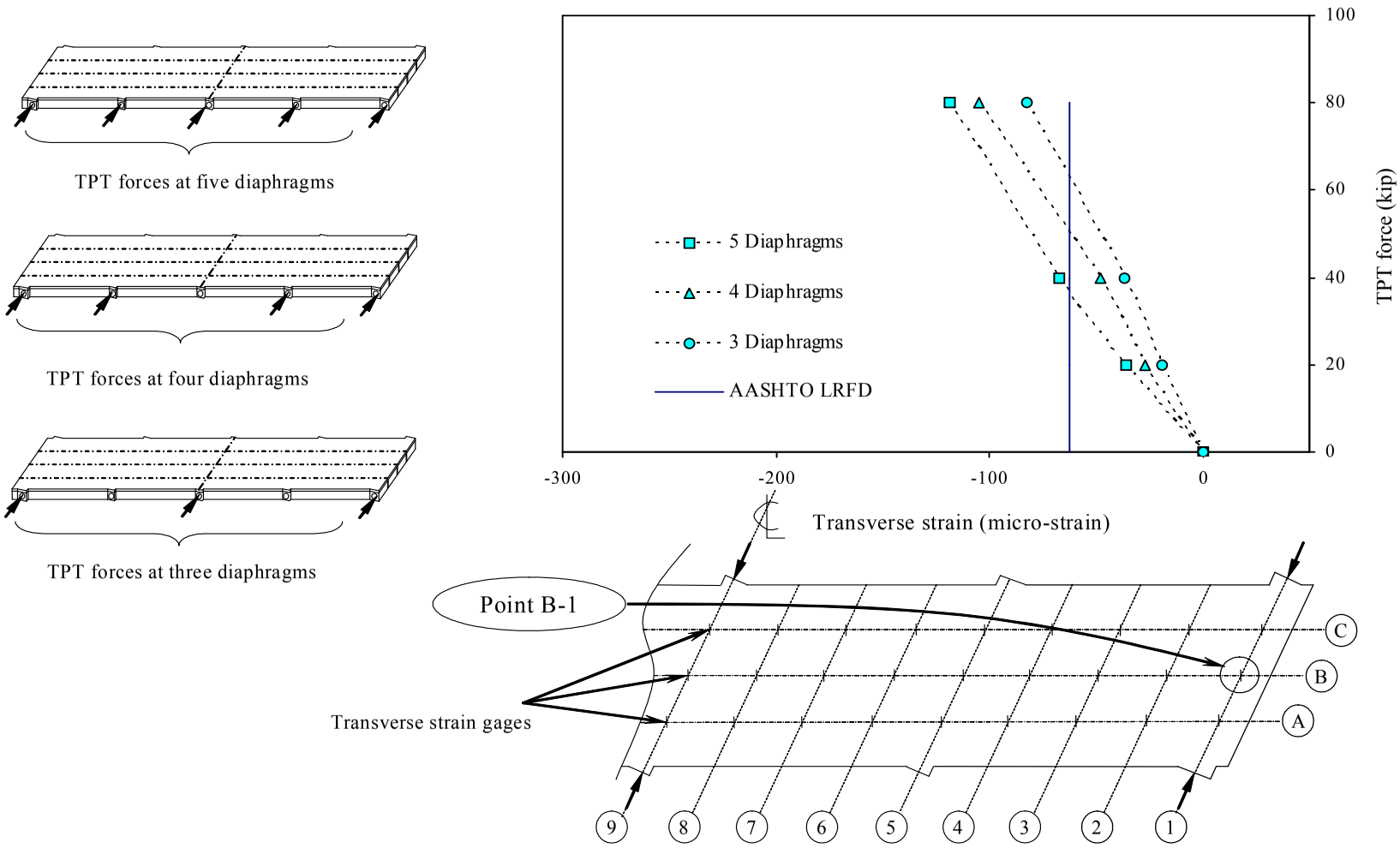

Figure 6.2-20 Transverse strains at point B-1 due to different levels of TPT force.

6.3 Load Distribution

6.3.1 Introduction

The fundamental function of the TPT system in side-by-side box-beam bridges is to tie the beams together to act as one unit, which when functioning properly provides the mechanism for the uniform distribution of service loads across the width of the bridge model. The behavior of the box-beam bridge model was investigated using the vertical deflections of the box-beams across the width of the bridge model. The deflections as described in Chapter 5 were measured by linear motion transducers installed at the mid-width of each individual box-beam. The load distribution test was based on the deflections induced by the application of a single point load of 15 kip subjected to the four individual beams. The single point load was applied over a cylindrical steel block of diameter, 10 in., which resulted in a contact stress of 191 psi on each loaded beam. The selection of the 15 kip single point load was to avoid major flexural cracking, as the theoretical first cracking load was 16 kip.

The load distribution test was conducted first in the presence of TPT force of 80 kip applied to all five diaphragms. Subsequently, the TPT forces per diaphragm were decreased to 40 and 20 kip. Similarly, the number of diaphragms were also reduced to four, three, and finally to the case of "*No TPT*" (where no TPT force was applied to any diaphragm). The corresponding deflections for all box-beams were recorded for each loading case investigated. The load distribution test was conducted in the three stages of the bridge model. These stages represent 1) uncracked deck slab, 2) cracked deck slab and shear-keys, and 3) repaired deck slab and shear-key due to the replacement of exterior box-beam. In this section, the results are presented and discussed from the three stages of the bridge model in terms of the load-deflection response of the bridge model and the load fraction (*LF*) across the width of the bridge model. Furthermore, the percentage improvement (*PI*) in the load distribution due to the investigated TPT arrangements is also presented. Definitions of the *PI* as well as the *LF* are also provided.

6.3.2 Derivation of Load Fraction and Percentage Improvement

The percentage of the applied load carried by each box-beam in the bridge model was evaluated using a deflection-based load fraction (*LF*) as defined by Grace et al. (2000) and Klaiber et al. (2001). It quantifies the ability of the bridge model to distribute an externally applied load across the width of the bridge model. The *LF* presented herein was based on the

deflection experienced by the loaded box-beam relative to the summation of deflections of all four box-beams, as shown by equation 6.3. A smaller difference in *LF* of the loaded box-beam relative to the unloaded box-beams confirms effective distribution of the applied load across the bridge width. Figure 6.3-1 shows a typical bridge model with no initial deflection prior to the application of any external load. However, the deflection between the loaded box-beam and the far exterior box-beam increased during loading as illustrated in Figure 6.3-2.

The *PI* was introduced to determine the effect of the TPT arrangement on the bridge model's ability to respond as a monolithic structural unit. The effect of the TPT arrangements is expected to have only minor influence on the bridge model behavior as long as the bridge deck and shear-keys remained uncracked. Whereas the TPT arrangement is expected to have significant effect on the bridge model behavior in the case of cracked deck slab and shear-keys.

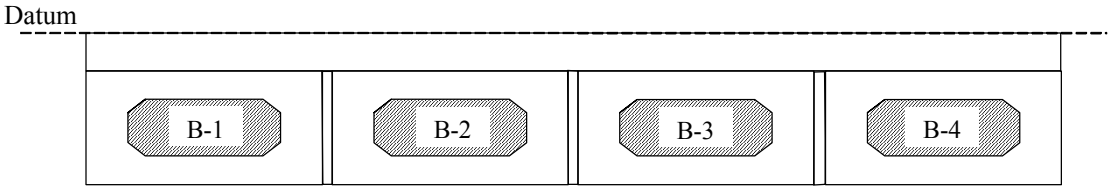

Figure 6.3-1 Bridge model in the uncracked stage with no external Load.

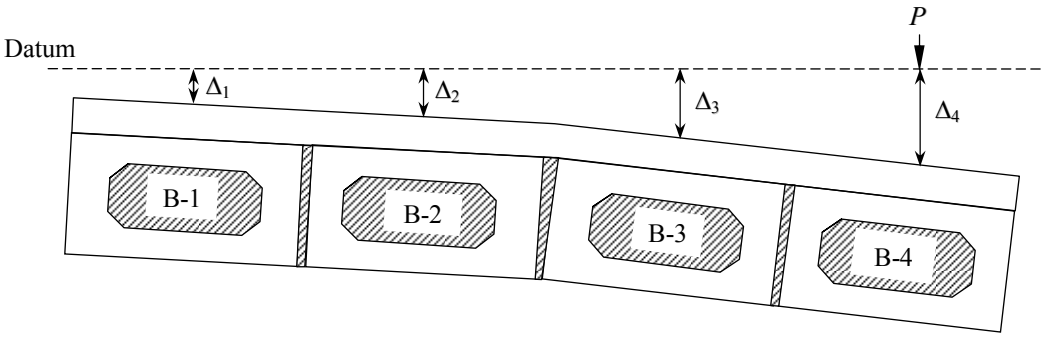

Figure 6.3-2 Deflection of the bridge model when loaded.

The load fraction is defined as follows.

$$LF = \frac{\Delta_i}{\sum_{i=1}^{4} \Delta_i} \times 100 \tag{6.3}$$

where i is the box-beam for which the load fraction is calculated, and Δ_i is the deflection of the i^{th} beam. From the LF, the PI is evaluated as follows.

$$PI = \frac{(LF_w - LF_{TPT})}{(LF_w)} \times 100 \tag{6.4}$$

where LF_w = the load fraction of the loaded beam in the absence of TPT force (i.e. no TPT force applied to any diaphragm), LF_{TPT} = the load fraction of the loaded beam when TPT arrangement is present.

6.3.3 Cracking of Deck Slab

After conducting the strain and load distribution tests on the uncracked bridge model, the bridge model was partially cracked at the shear-key joints between the adjacent box-beams, as mentioned earlier in Chapter 5. In general, the cracking of the shear-keys and deck slab was conducted by applying a vertical load at the mid-span of a single box-beam while partially restraining the other three box-beams from possible displacement and transverse rotation. Two types of cracks were initiated at this stage: shear-key cracks and other cracks. The shear-key cracks propagated as longitudinal cracks over the three shear-key locations, while the other cracks developed on the top surface of deck slab between the shear-keys especially at the locations of the applied load. In addition, cracking of the deck slab led to the development of transverse flexural cracks at the mid-span for the individual box-beams. The methodology for developing the longitudinal cracks is described in details in Appendix B. Figures 6.3-3 and Figure 6.3-4 show the shear-key cracks and other cracks developed on the top surface of the deck slab.

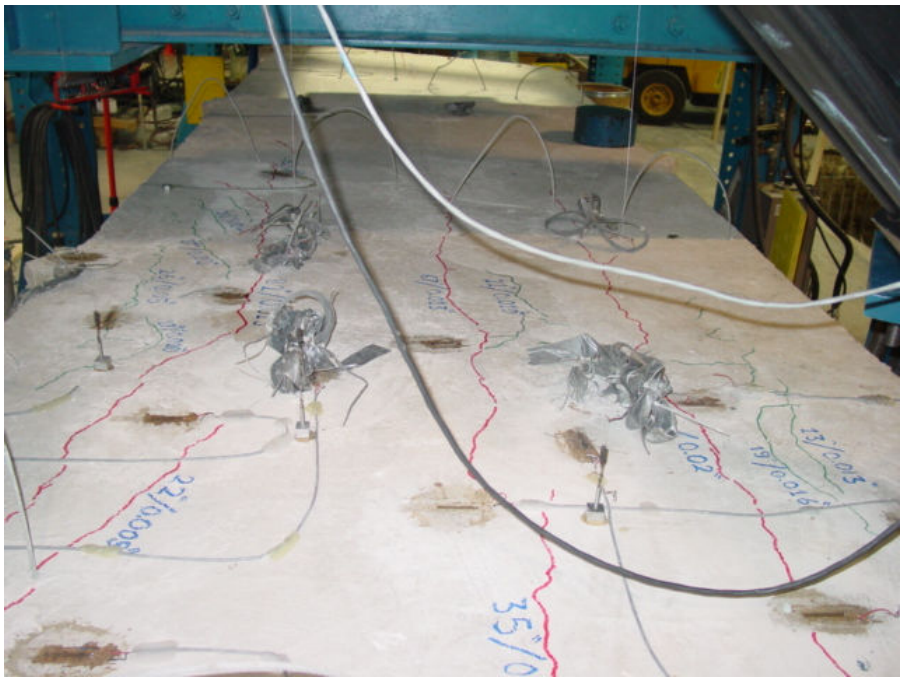

Figure 6.3-3 Cracks of deck slab at mid-span.

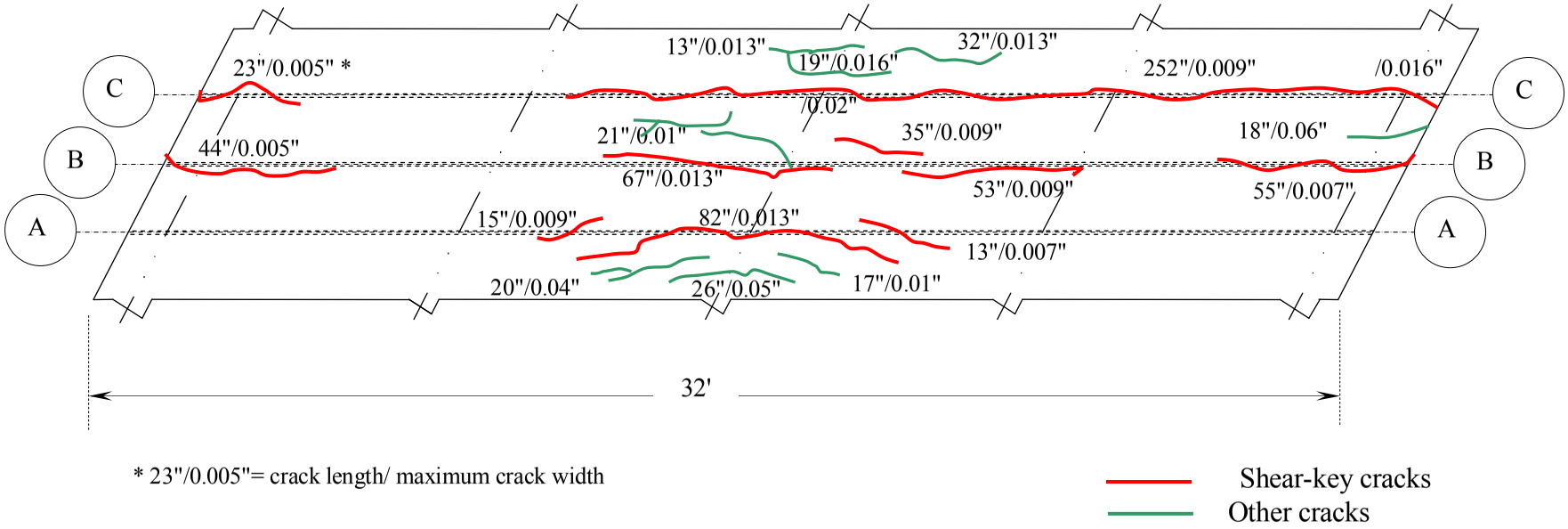

Figure 6.3-4 Cracks pattern of deck slab.

6.3.4 Effect of Number of Diaphragms

6.3.4.1 Introduction

In this section, the effect of the number of transverse diaphragms on the behavior of the bridge model in terms of load distribution is evaluated through three different stages: uncracked, cracked, and repaired stage. The cases of three, four, and five diaphragms were investigated. For simplicity, the uncracked stage of the bridge model is designated as *UC*, while the cracked and the repaired stages are denoted as *C* and *R*, respectively. Comparative analyses are conducted on how different number of transverse diaphragms influenced the deflection, load fraction, and percentage improvement of the bridge model.

6.3.4.2 Deflection and Load Fraction of the Bridge Model

As expected, the loaded beam experienced the largest deflection among the four beams in all cases of loading. In addition, the loaded exterior box-beams experienced larger deflections than the loaded interior box-beams. For instance, in the cracked stage, when the exterior beam B-1 was loaded with the application of TPT force of 80 kip to all five diaphragms, the deflections for the box-beams B-1, B-2, B-3, and B-4 were 0.30, 0.29, 0.28, and 0.26 in., respectively. On the other hand, when the interior beam B-2 was loaded under the same conditions, the deflections recorded were 0.29, 0.29, 0.28, and 0.27 in., respectively.

In the uncracked stage, the differential deflection between the adjacent box-beams were insignificant regardless of the number of diaphragms, as shown in Figure 6.3-5 through Figure 6.3-8. For example, the deflections of the beams, when a TPT force of 80 kip was applied to three transverse diaphragms and beam B-1 was loaded, were 0.26, 0.24, 0.22, and 0.20 in. for beams B-1, B-2, B-3, and B-4, respectively. Very similar deflections were observed when four or five diaphragms were used and the deflections in those cases were 0.25, 0.23, 0.22, and 0.21 in., and 0.24, 0.23, 0.21, and 0.21 in., respectively.

As anticipated, when the deck slab was partially cracked, larger deflections were observed compared to the uncracked stage, as shown in Figure 6.3-5 through Figure 6.3-8. For instance, in the cracked stage when beam B-1 was loaded and the TPT force of 80 kip was applied to three diaphragms, the deflections observed were 0.31, 0.30, 0.29, and 0.26 in. for beams B-1, B-2, B-3, and B-4, respectively. In the uncracked stage with the same TPT arrangment, the deflections observed were 0.26, 0.24, 0.22, and 0.20 in.

The case of "*No TPT"* in the cracked stage resulted in a larger differential deflection between the adjacent box-beams compared to other cases of number of diaphragms (three, four, and five). For example, the deflections for beams B-1, B-2, B-3, and B-4, when beam B-1 was loaded, were 0.41, 0.37, 0.26, and 0.21 in. in the case of "*No TPT*". However, the deflections observed were 0.31, 0.30, 0.29, and 0.26 in. for the case of three diaphragms, 0.32, 0.30, 0.29, and 0.25 in. for the case of four diaphragms, and 0.30, 0.29, 0.28, and 0.26 in. for the case of five diaphragms. The larger deflections observed in the cracked stage was partly due to the longitudinal cracks developed in deck slab and shear-keys as well as the flexueral cracks developed on the beams during the cracking process. This lead to the reduced stiffness of the bridge model.

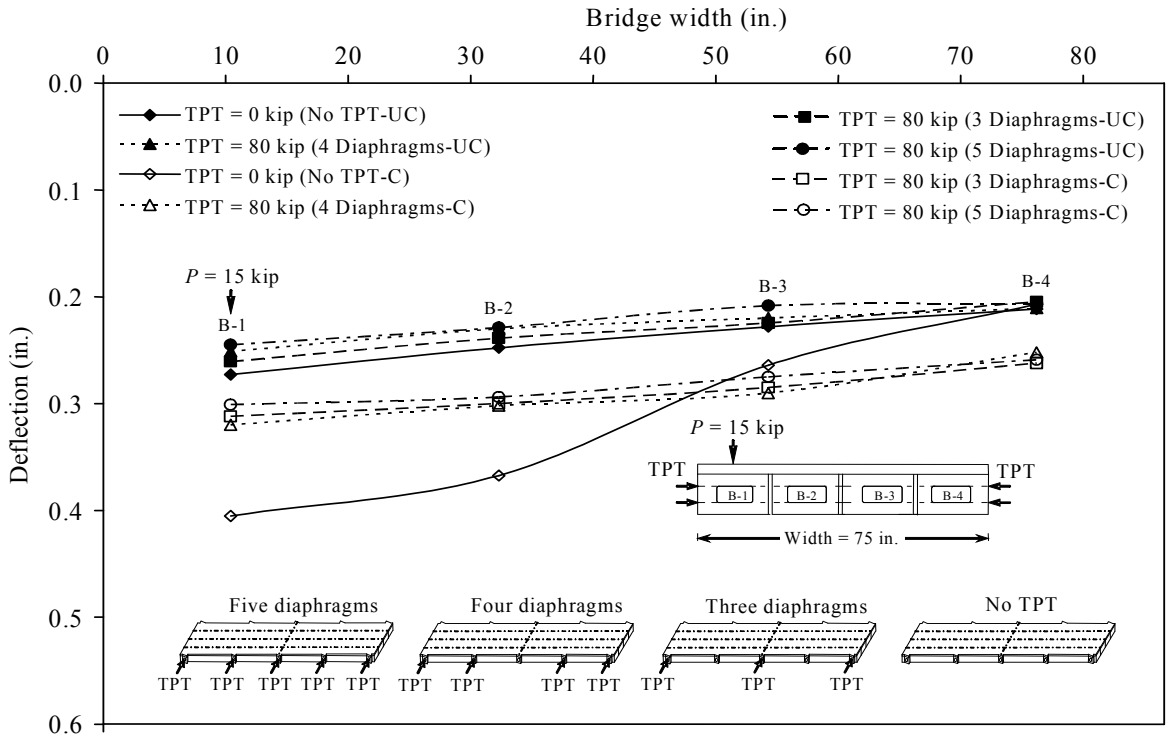

Figure 6.3-5 Load-deflection response of the bridge model while loading beam B-1.

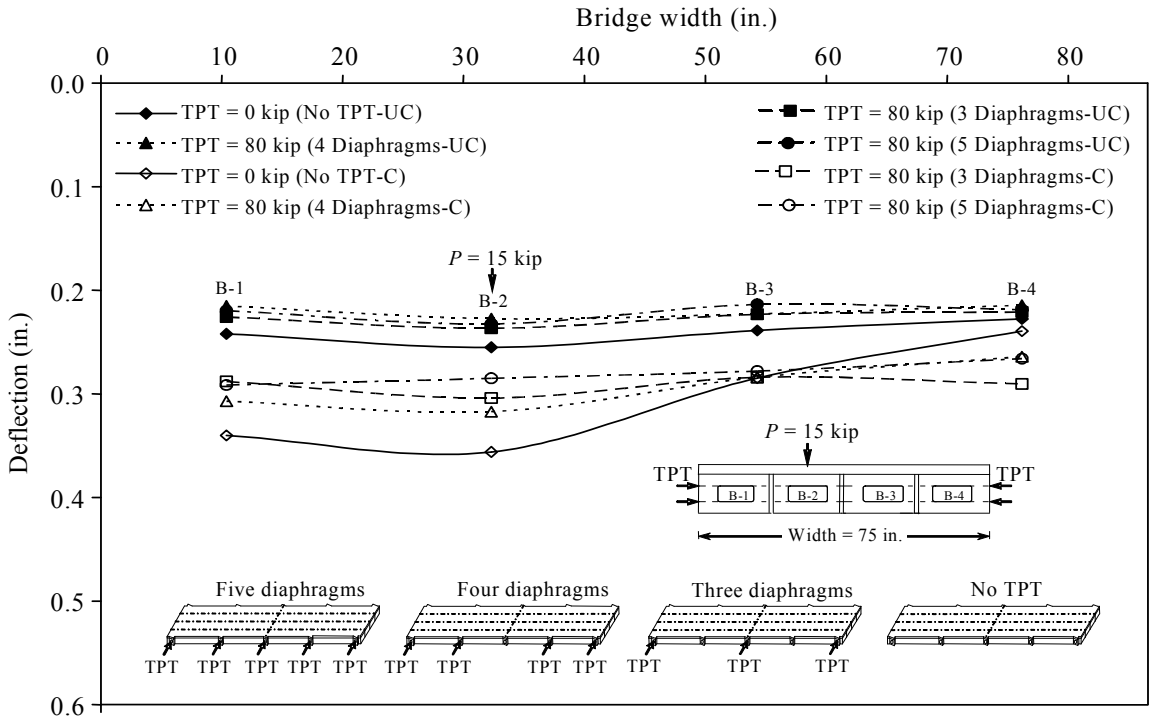

Figure 6.3-6 Load-deflection response of the bridge model while loading beam B-2.

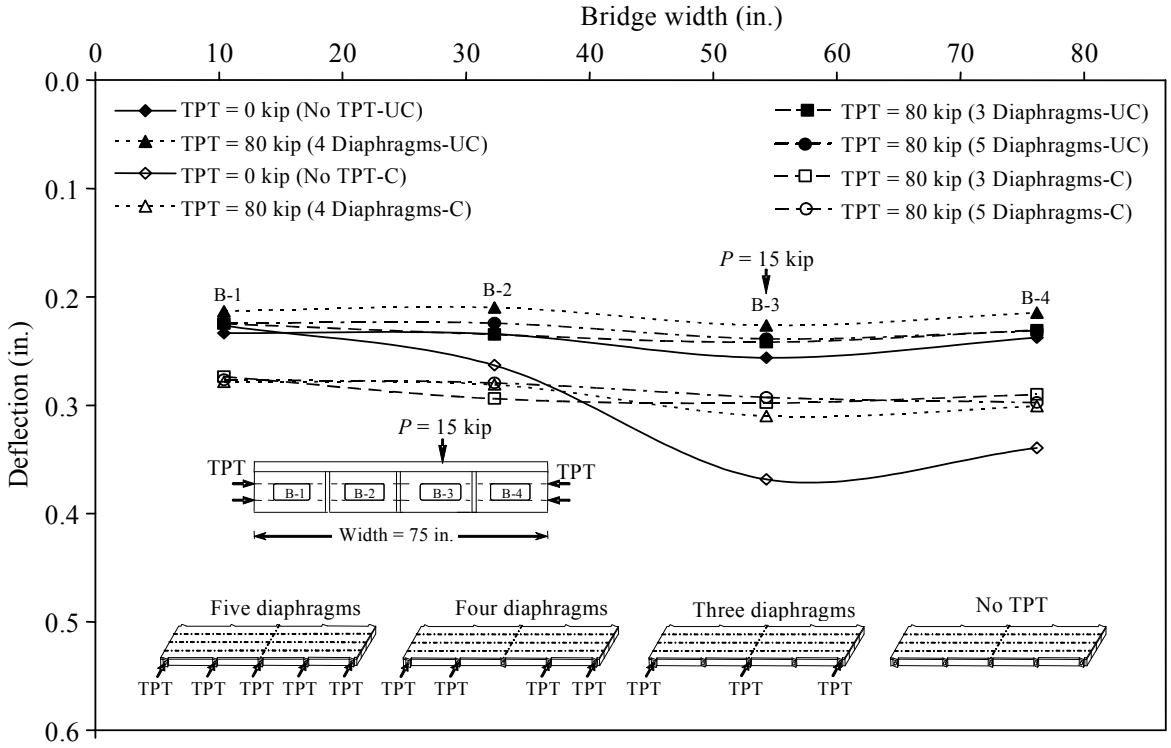

Figure 6.3-7 Load-deflection response of the bridge model while loading B-3.

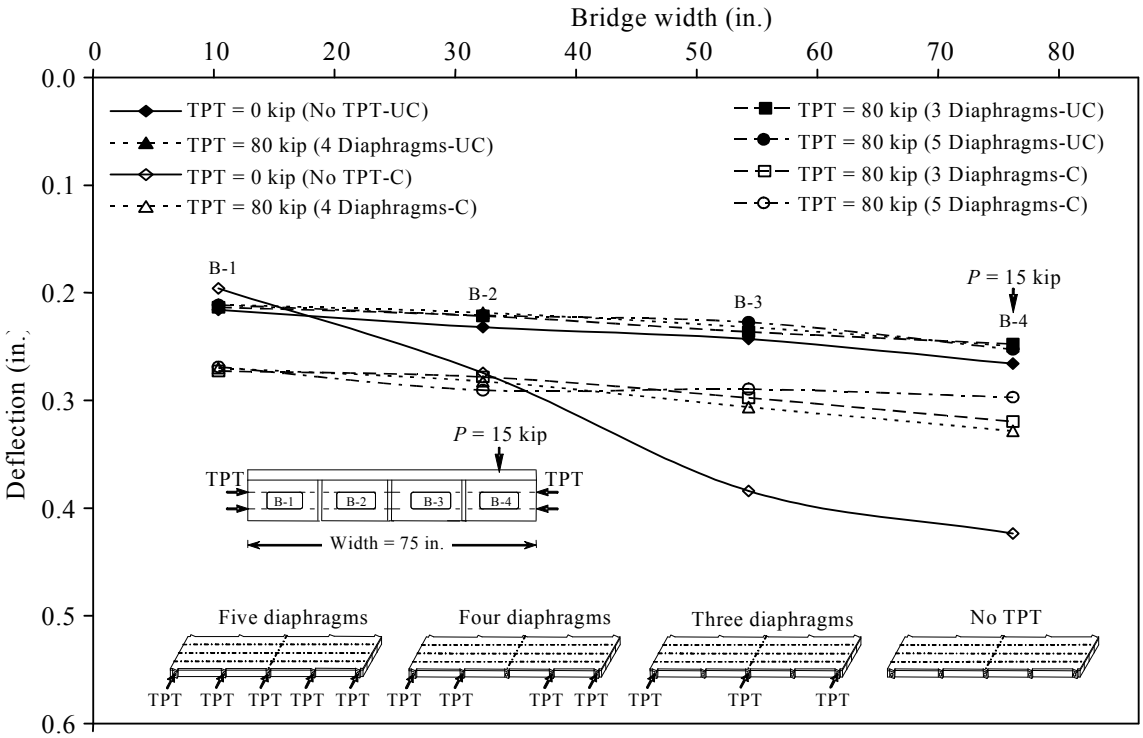

Figure 6.3-8 Load-deflection response of the bridge model while loading beam B-4.

As mentioned earlier, the repaired stage was simulated by replacing an exterior beam (B-4 with B-5) and repairing the adjacent shear-key and deck slab. The goal was to determine if the structural function could be restored. When the assumed damaged box-beam B-4 was replaced in the repaired stage, lower deflections were observed for beams B-3 and B-5 compared to the cracked stage. However, beams B-1 and B-2 experienced similar deflections in both stages, as shown in Figure 6.3-9 through Figure 6.3-12. Considering these results, it can be stated that the stiffness of the bridge model was restored. For example, the deflections observed when a TPT force of 80 kip was applied at three diaphragms and beam B-1 was loaded were 0.33, 0.30, 0.29, and 0.27 in. for B-1, B-2, B-3, and B-5, respectively. When compared to the cracked stage, the deflections recorded were 0.31, 0.30, 0.29, and 0.26 in. Furthermore, by increasing the number of transverse diaphragms to four, the deflections observed in the repaired stage were 0.34, 0.31, 0.29, and 0.27 in. for B-1, B-2, B-3, and B-5, respectively, while the deflections observed in the cracked stage were 0.32, 0.30, 0.29, and 0.25 in.

The *LF* was determined to evaluate the fraction of the load carried by each box-beam. When the *LF* of the box-beams was evaluated, it was generally noted that, the portion of the

load carried by the loaded box-beams is always greater than the other box-beams. For example, when the beam B-1 was loaded in the cracked stage with a TPT force of 80 kip applied to all five diaphragms, the *LF* observed were 27%, 26%, 24%, and 23% for beams B-1, B-2, B-3, and B-4, respectively**.** This trend in the *LF* was consistent regardless of the number of transverse diaphragms and the stage of the bridge model.

As the number of transverse diaphragms increased, the *LF* of the loaded beams decreased while the *LF* for the other beams increased in the cracked and repaired stages. For instance, when beam B-1 was loaded with TPT force of 80 kip applied to four diaphragms in the cracked stage, the *LF* for beams B-1, B-2, B-3, and B-4 were 27.5%, 25.9% 24.9%, and 21.4%, respectively. On the other hand, when the number of diaphragms was increased to five with the same level of TPT force, the *LF* noted were 26.7%, 26%, 24.4%, and 23.1%. Similarly, in the repaired stage, the *LF* for beams B-1, B-2, B-3, and B-5 were 28.1%, 25.6% 24.0%, and 21.8%, respectively, in the case of four diaphragms. Moreover, when the number of diaphragms was increased to five with the same level of TPT force, the *LF* observed were 27.7%, 25.0%, 24.1%, and 23.0%. This means that by increasing the number of diaphragms, the distribution of the applied load across the bridge width is improved. On the contrary, similar *LF* were observed in the uncracked stage irrespective of the number of diaphragms. The *LF* observed, when loading beam B-1 with TPT force of 80 kip, were 27.5%, 25.2%, 24.1%, and 23.2% for four diaphragms and 27.6%, 25.7%, 23.4%, and 23.2% for five diaphragms, respectively.

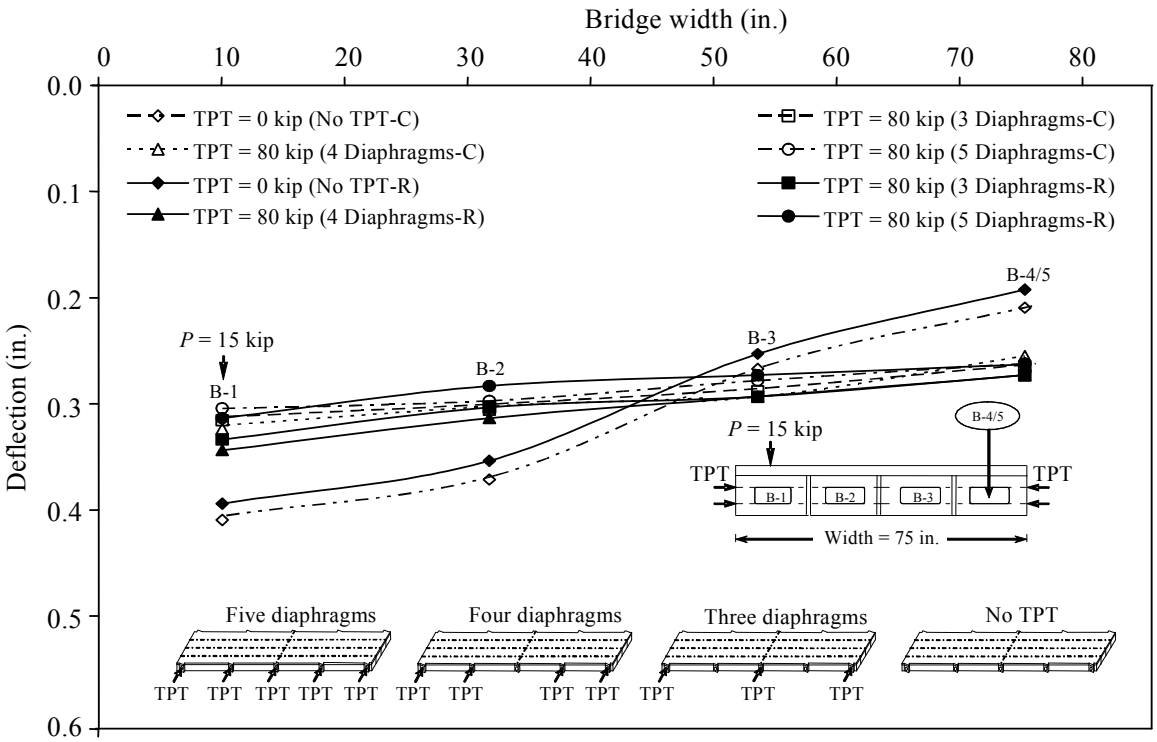

Figure 6.3-9 Load-deflection response for beam B-1 after repairs.

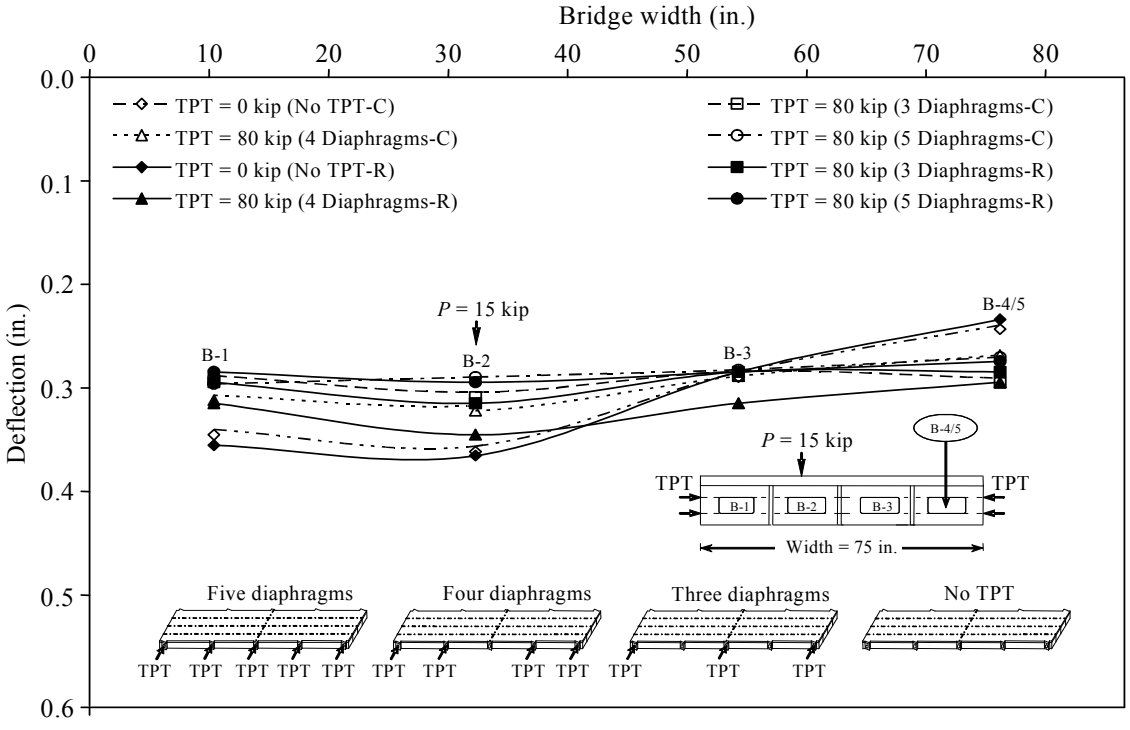

Figure 6.3-10 Load-deflection response for B-2 after repairs.

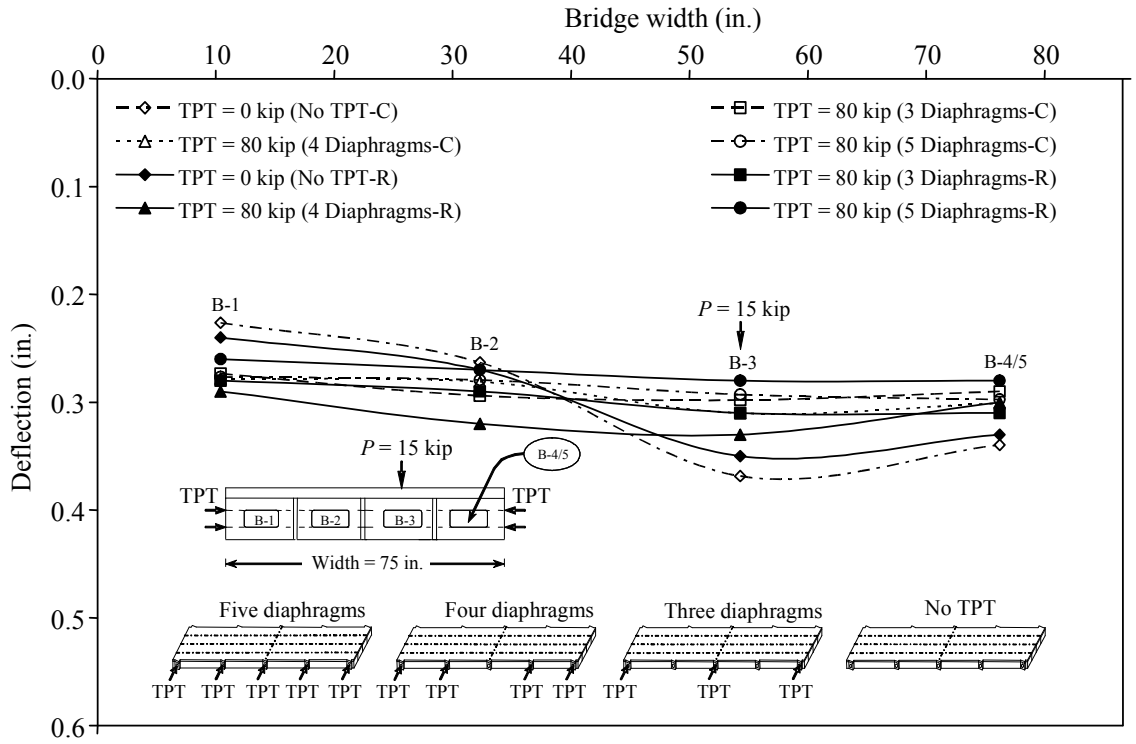

Figure 6.3-11 Load-deflection response for B-3 after repairs.

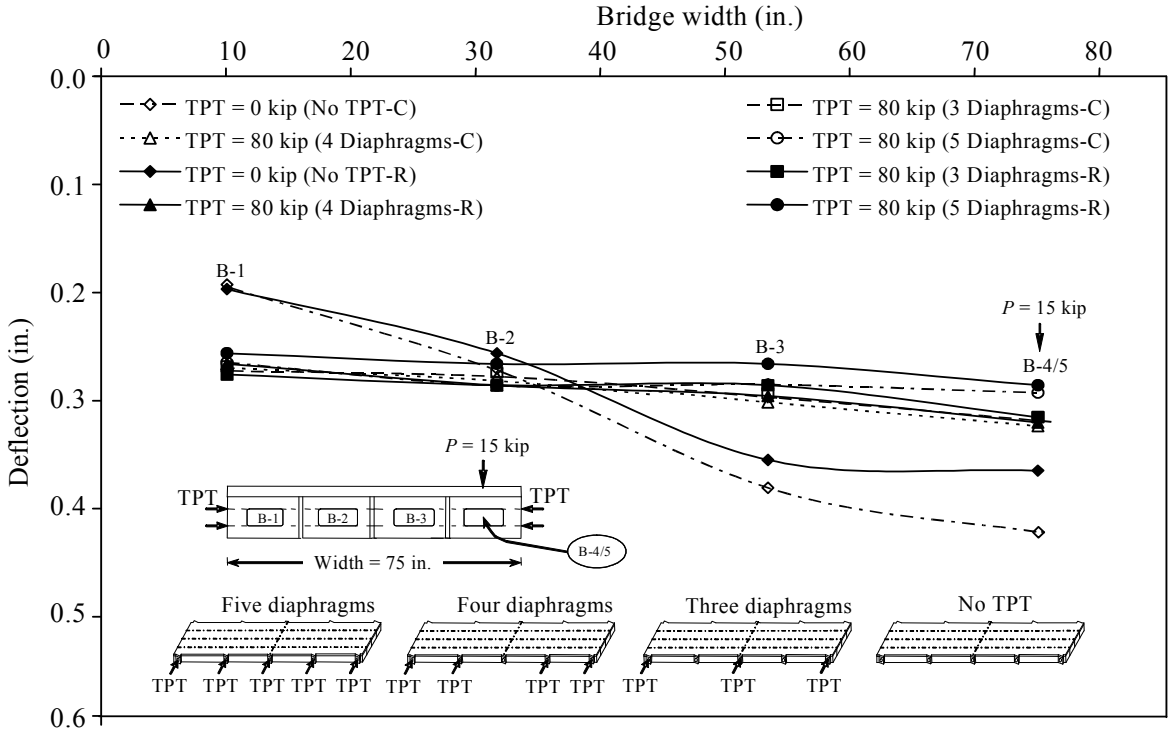

Figure 6.3-12 Load-deflection response for B-4 after repairs.

6.3.4.3 Improvement in the Behavior of the Bridge Model

This section presents the effect of the number of transverse diaphragms on improving the behavior of the bridge model in terms of *PI* in each stage of the bridge model. Varying the number of transverse diaphragms in the uncracked stage did not have significant impact on the *PI* of the bridge model with a maximum of 4% improvement observed when loading beam B-1. For instance, the *PI* in the uncracked stage when a TPT force of 80 kip was applied and B-1 was loaded were 1.2%, 3.1%, and 3.0% for three, four, and five diaphragms, respectively. The bridge model did not experience any definite trend in the *PI* at the uncracked stage, as shown in Figure 6.3-13 through Figure 6.3-16.

As the bridge deck experienced longitudinal cracks in the cracked stage, the effect of the number of transverse diaphragms was more pronounced as shown by an increase in the *PI* relative to the uncracked stage. For instance, the *PI* observed for three, four, and five diaphragms when loading beam B-1 in the cracked stage with TPT force of 80 kip were 17.4%, 15.6%, and 18.2%, respectively.

The rehabilitation of the "assumed damaged" beam B-4 and the shear-key resulted in an improvement in the stiffness of the bridge model and consequently led to a marginal reduction in the *PI* for beams B-3 and B-5 in the repaired stage relative to the cracked stage, as shown in Figure 6.3-13 through Figure 6.3-16. For instance, the *PI* observed for three, four, and five diaphragms when loading beam B-4 in the cracked stage with TPT force of 80 kip were 17.4%, 16.5%, and 21.85%, respectively. However, the *PI* observed for three, four, and five diaphragms when loading beam B-5 in the repaired stage with the same TPT force were 12.8%, 11.8%, and 14.4%, respectively. The reason is that the "*No TPT*" condition in the repaired stage performed better than the "*NO TPT*" condition of the cracked stage (see Figure 6.3-9 to Figure 6.3-12).

The *PI* for the interior box-beams was relatively lower than the exterior box-beams, as shown in Figure 6.3-13 and Figure 6.3-16. For example, the *PI*, when TPT forces of 20 and 40 kip are applied to all five diaphragms and beam B-1 was loaded in the cracked stage, were 14.3% and 15.2%, respectively. However, when beam B-2 was similarly loaded, the *PI* evaluated were only 9.5% and 10.2% for 20 and 40 kip, respectively. Furthermore, the *PI* observed for beam B-2 was lower than that of beam B-3, as shown in Figure 6.3-14 and Figure 6.3-15. As an example, the *PI*, when TPT forces of 20 and 40 kip were applied to all five

diaphragms in the cracked stage and beam B-2 was loaded, were 9.5% and 10.2%, respectively. However, when B-3 was loaded, the *PI* obtained were 14.5% and 15.7% for 20 and 40 kip, respectively. This was because the intensity of the cracks initiated during the cracked stage along the shear-key A-A (25% of the entire bridge span) was less than the intensity of the cracks initiated along the shear-key C-C (75% of the entire bridge span).

It was observed that the case of five diaphragms outperformed the three diaphragm case in terms of effectively distributing the applied vertical load especially in the cracked and the repaired stages of the bridge model. For instance, the *PI*, when loading beam B-2 with TPT force of 80 kip applied to three and five diaphragms, were 10.7% and 12.8% in the cracked stage while the *PI* were 9.4% and 12.3% in the repaired stage (see Figure 6.3-14). This was because the distance between the diaphragms increased from 7.5 ft in the case of five diaphragms to 15 ft in the case of three diaphragms. In addition, the case of four diaphragms resulted in a lower improvement in terms of load distribution compared to the three and five diaphragms. For example, the *PI* decreased to 7.3% and 7.8% in the cracked and repaired stages, respectively.

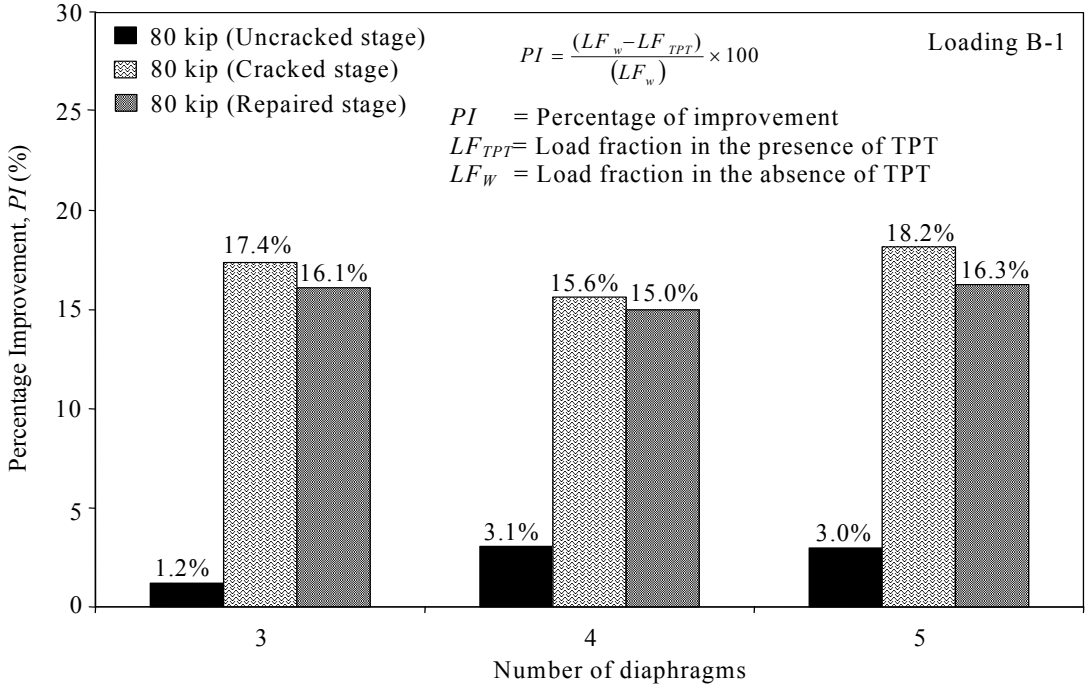

Figure 6.3-13 Effect of number of diaphragms on *PI* for loading beam B-1.

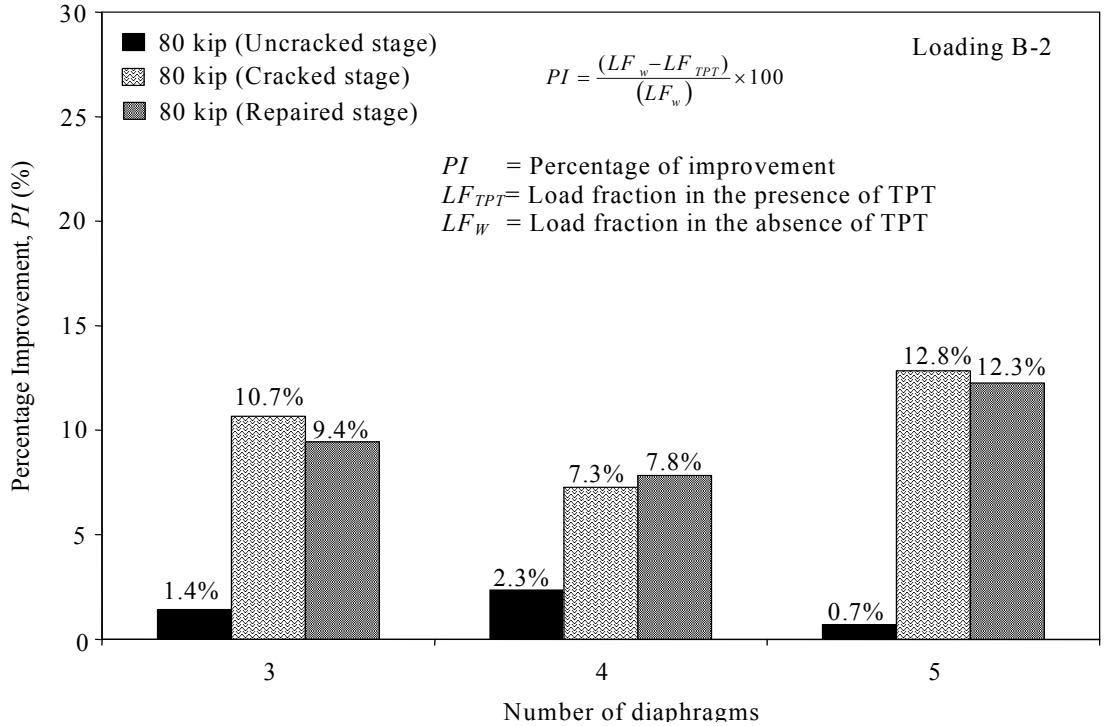

Figure 6.3-14 Effect of number of diaphragms on *PI* for loading beam B-2.

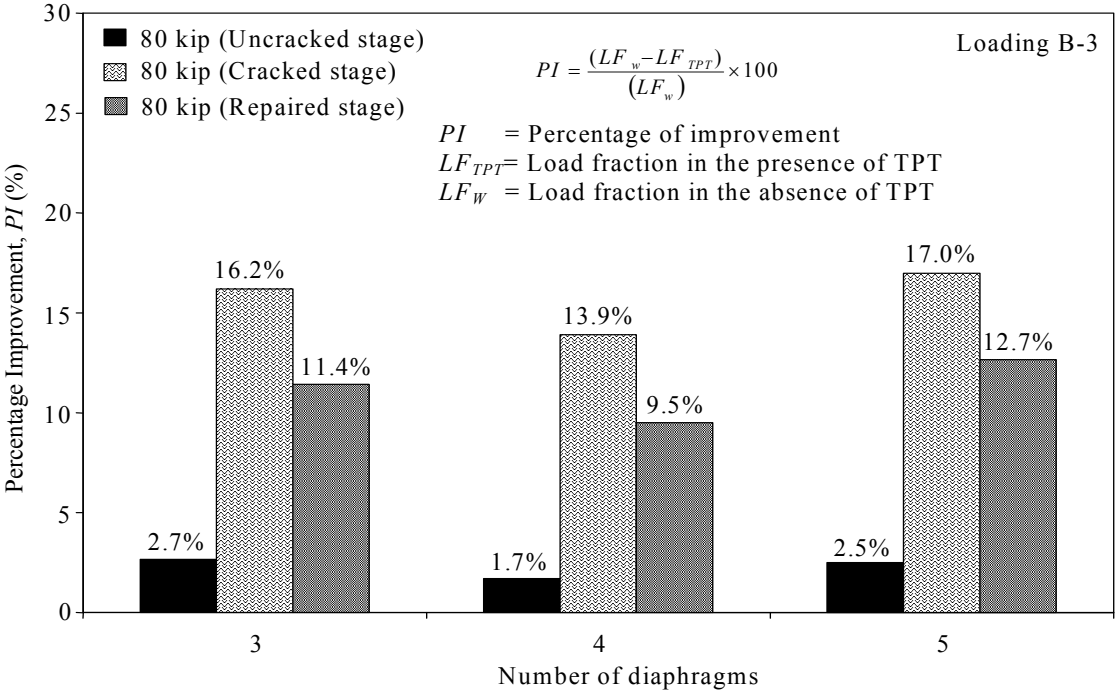

Figure 6.3-15 Effect of number of diaphragms on *PI* for loading beam B-3.

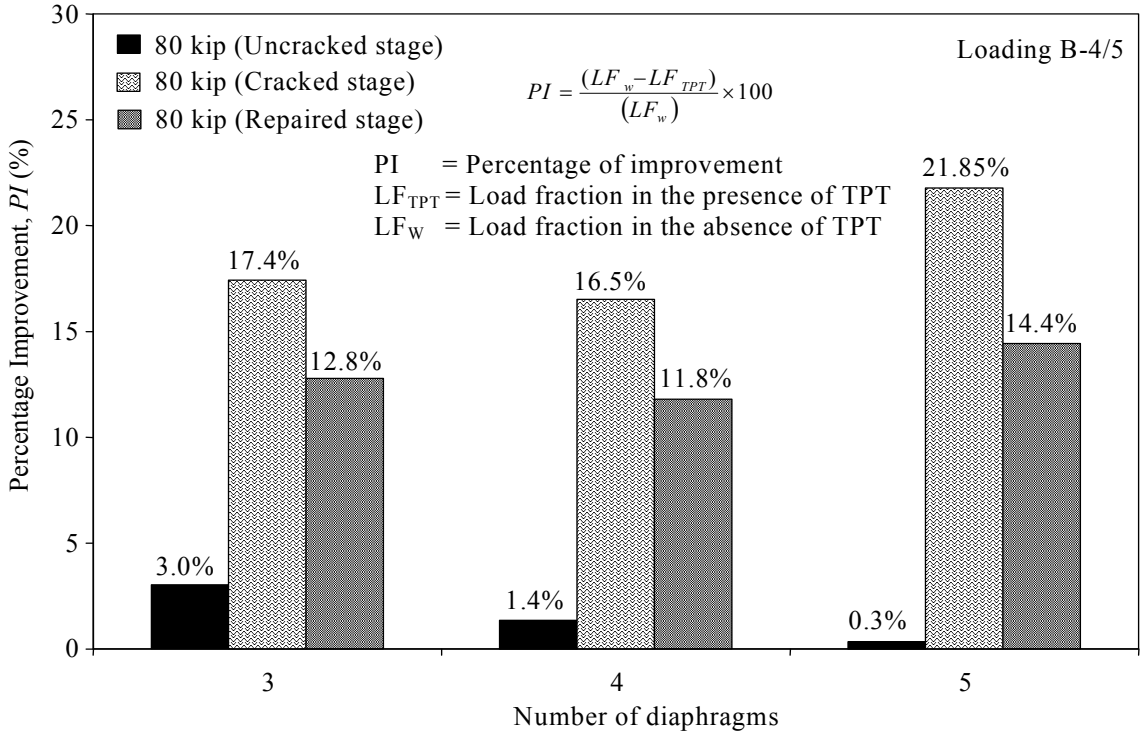

Figure 6.3-16 Effect of number of diaphragms on *PI* for loading beam B-4/5.

6.3.5 Effect of Levels of TPT Forces

6.3.5.1 Introduction

In this section, the effect of varying the level of TPT forces on the behavior of bridge model in the transverse direction is discussed. Three different levels of TPT forces were selected: 20, 40, and 80 kip while the number of transverse diaphragms remained constant. For each level of TPT force, the load distribution test was conducted and the corresponding deflections of the four beams were recorded. Similar to the previous section, the effect of level of TPT forces was evaluated in all the three stages of the bridge model; uncracked, cracked, and repaired stages. Comparative analyses were made on how different levels of TPT force affect the deflection, load fraction, and percentage improvement of the bridge model.

6.3.5.2 Deflection and Load Fraction of the Bridge Model

The deflections of the loaded interior beams were lower than the loaded exterior beam irrespective to the level of TPT force and the stage of the bridge model, as shown in Figure 6.3-18, Figure 6.3-19, Figure 6.3-22, and Figure 6.3-23. The deflections observed, when TPT

forces of 0, 20, 40, and 80 kip applied to five diaphragms, were 0.39, 0.34, 0.32, and 0.31 in. for the loaded exterior beam B-1 and 0.36, 0.32, 0.31, and 0.29 in. for the loaded interior beam B-2.

Similar deflections were observed for the loaded beam in the uncracked stage with different levels of TPT forces. The deflections recorded for the loaded beam B-1 were 0.27, 0.25, 0.25, and 0.24 in. for TPT force of 0, 20, 40, and 80 kip, respectively. Unlike the uncracked stage, the deflection of the loaded box-beam decreased as the level of the TPT forces increased in the cracked and the repaired stages of the bridge model. For example, the deflections observed for the loaded beam B-1 in the cracked stage were 0.41, 0.34, 0.33, and 0.30 in. corresponding to TPT force of 0, 20, 40, and 80 kip applied to all five diaphragms. Similarly, the deflections observed with the same beam loaded in the repaired stage were 0.39, 0.34, 0.32, and 0.31 in.

In the cracked and repaired stages, the deflections of the loaded beam B-1 was evaluated with different levels of TPT forces applied to three diaphragms. It was observed that the deflection reduced significantly as the level of TPT force increased from zero to 20 kip. However, only a slight reduction in deflections was observed as the level of TPT force increased from 20 to 80 kip. For example, the deflections in the cracked stage for beam B-1 with TPT forces of 0, 20, 40, and 80 kip applied to three diaphragms were 0.41, 0.35, 0.32, and 0.31 in., respectively. Also, the deflections in the repaired stage for beam B-1 with TPT forces of 0, 20, 40, and 80 kip applied to three diaphragms were 0.39, 0.34, 0.33, and 0.33 in., respectively. Relatively high difference in deflections was observed between 0 and 20 kip (0.06 in.) compared to 20 and 40 kip (0.03 in.) or 40 and 80 kip (0.01 in.). This shows that a significant improvement in the load distribution was observed as the level of TPT force increased from zero to 20 kip. However, the effect of level of TPT forces on the improvement in the load distribution of the bridge model was insignificant beyond TPT force of 40 kip.

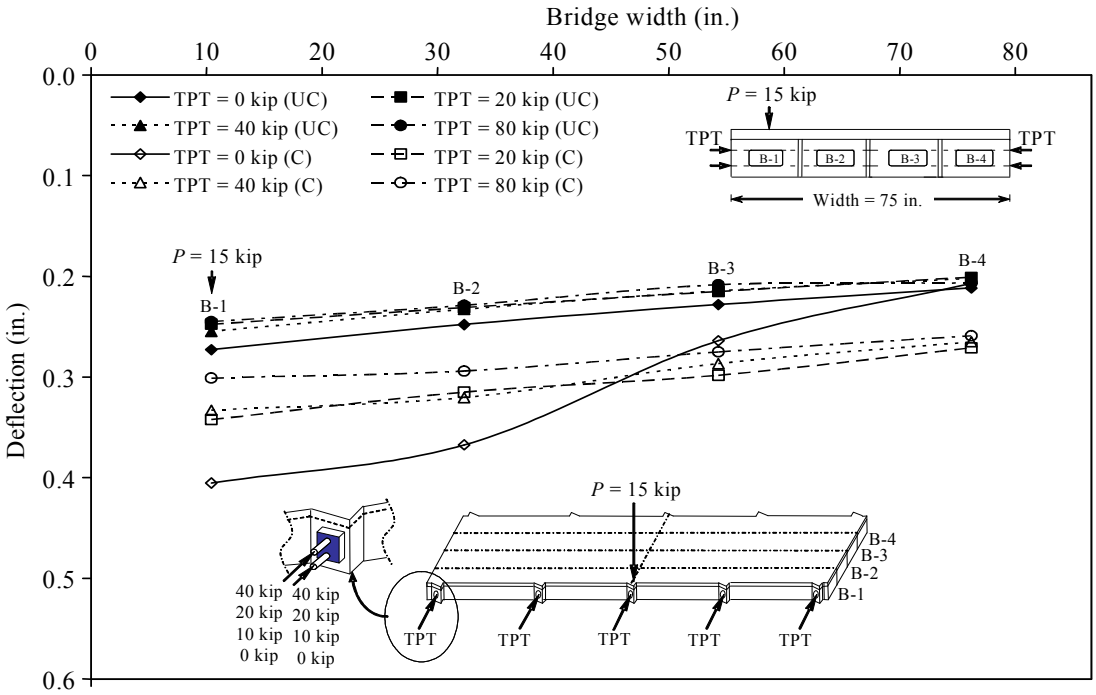

Figure 6.3-17 Load-deflection response for beam B-1 at different level TPT force.

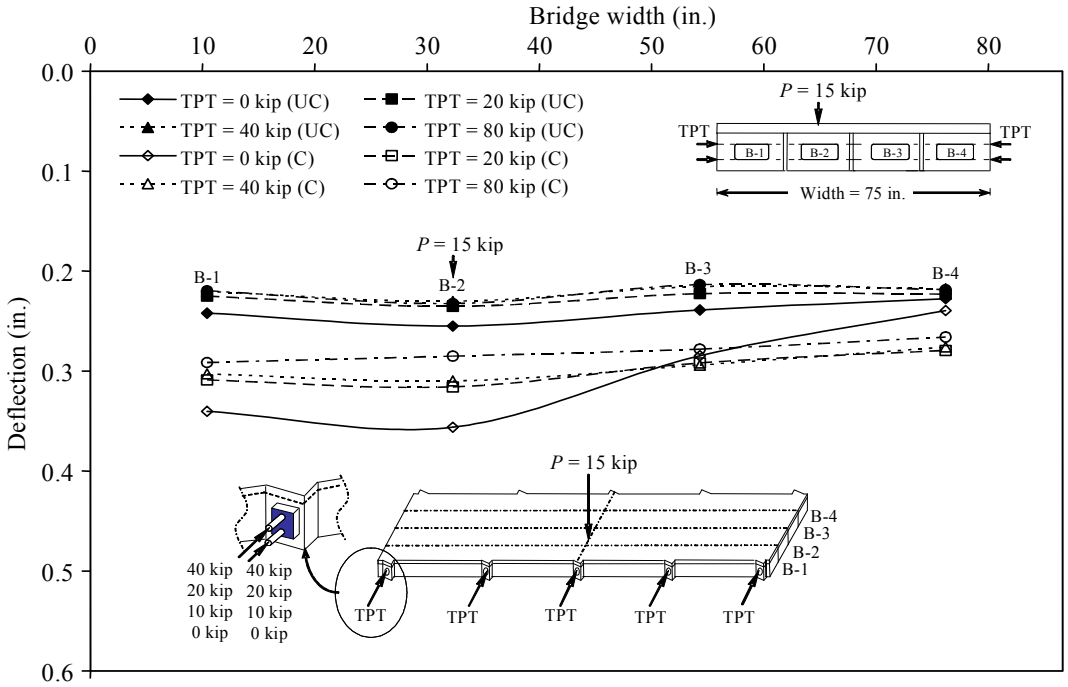

Figure 6.3-18 Load-deflection response for beam B-2 at different level TPT force.

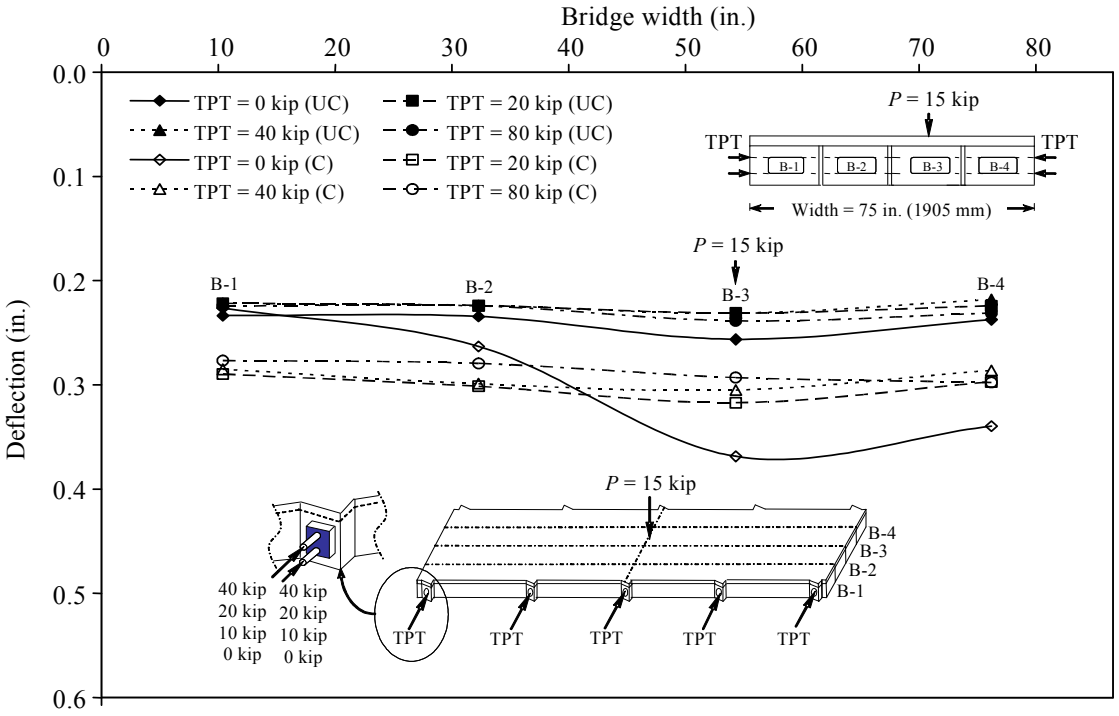

Figure 6.3-19 Load-deflection response for beam B-3 at different level TPT force.

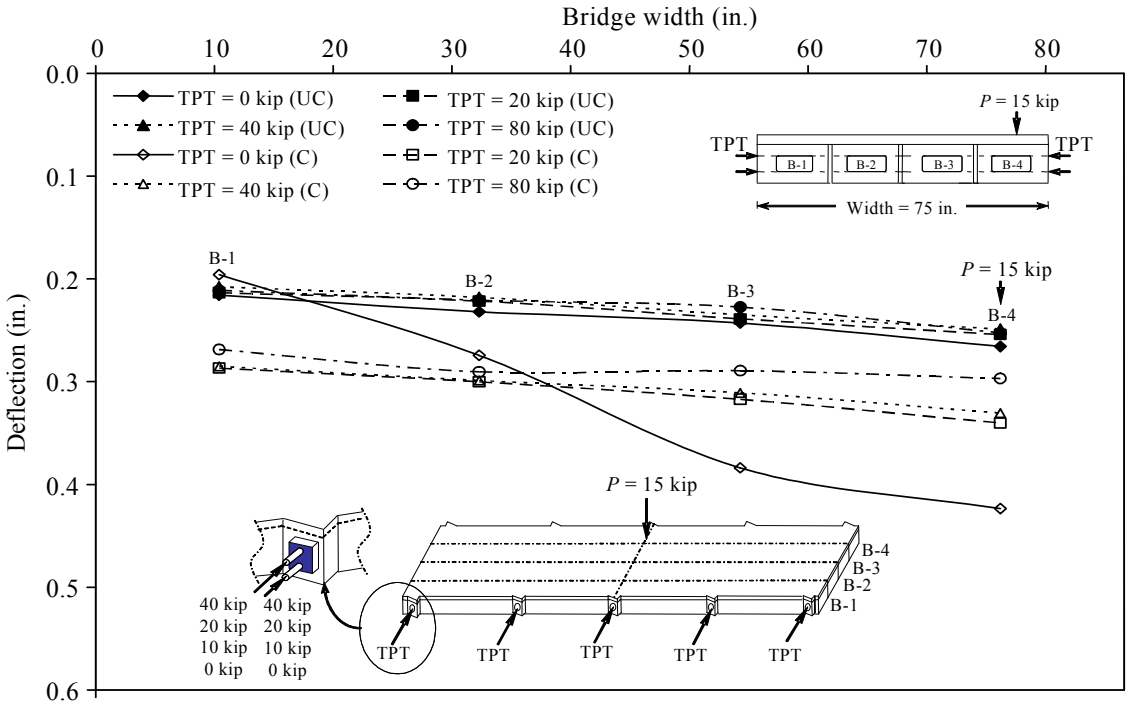

Figure 6.3-20 Load-deflection response for beam B-4 at different level TPT force.

When the *LF* was evaluated in each stage of the bridge model, it was generally observed that, applying different levels of TPT forces improved the distribution of the applied load. It was observed that the *LF* carried by the loaded beam decreased, while the *LF* carried by the other beams increased with increasing the level of TPT force. For instance, in the cracked stage, when beam B-1 was loaded in the absence of TPT forces, the *LF* of beam B-1 was 32.6% while that for beam B-4 was 16.8%. However, as the level of TPT force was increased to 20 kip at five diaphragms, the *LF* of beam B-1 decreased to 27.9% and that for beam B-4 increased to 22.1%. Similar trend in behavior was observed in the repaired stage when the levels of TPT forces were increased in a similar manner.

The *LF* for the loaded beam B-4/B-5 was monitored in the three stages of the bridge model with different levels of TPT forces applied to five diaphragms. In the case of *No TPT*, the *LF* for the loaded beam B-4 increased from 27.8% in the uncracked stage to 33.1% in the cracked stage due to the development of the longitudinal cracks in the deck slab and the shear-keys. However, the *LF* for the loaded beam B-5 with no TPT forces reduced to 31.0% in the repaired stage because of the repair of longitudinal deck crack and shear-key. Furthermore, similar *LF* was observed for beam B-4/B-5 in the three stages as the level of TPT forces was increased. For instance, in the case of five diaphragms, the *LF* observed for the loaded beam B-4/B-5 in the uncracked, cracked, and repaired stages were 27.7%, 27.0%, and 27.2% for TPT force of 20 kip and 27.4%, 27.3%, and 27.6% for TPT force of 40 kip. This clearly shows that, applying TPT forces improved the load distribution among the adjacent beams significantly.

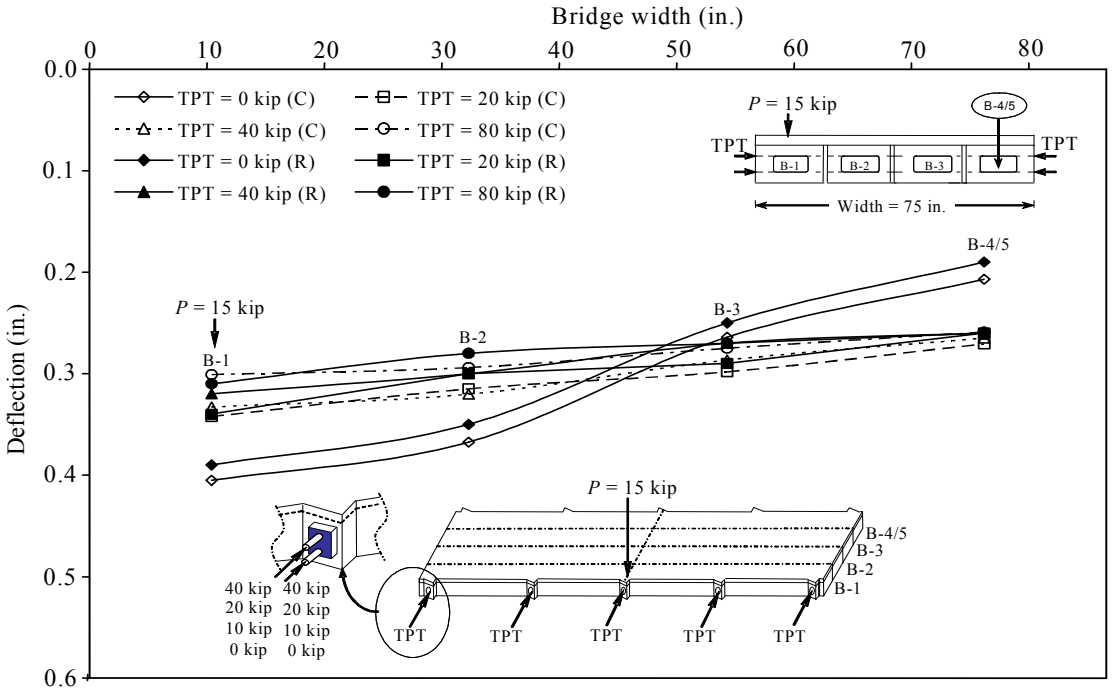

Figure 6.3-21 Load-deflection response for beam B-1 after repairs at different TPT forces.

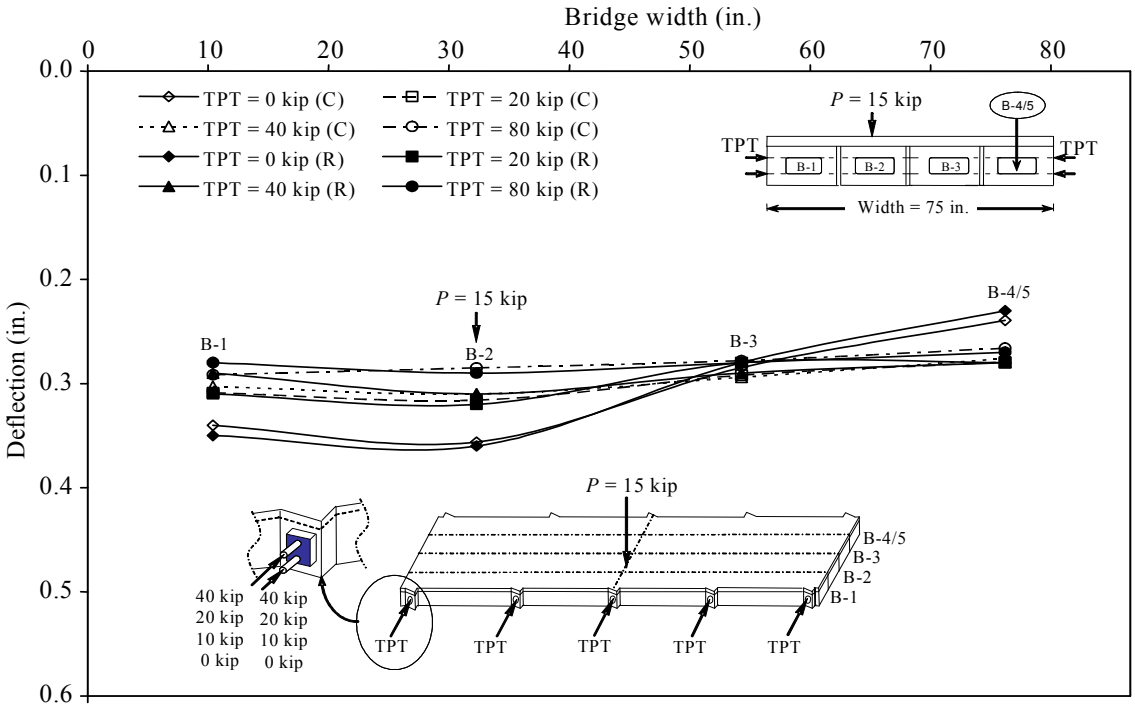

Figure 6.3-22 Load-deflection response for beam B-2 after repairs at different TPT forces.

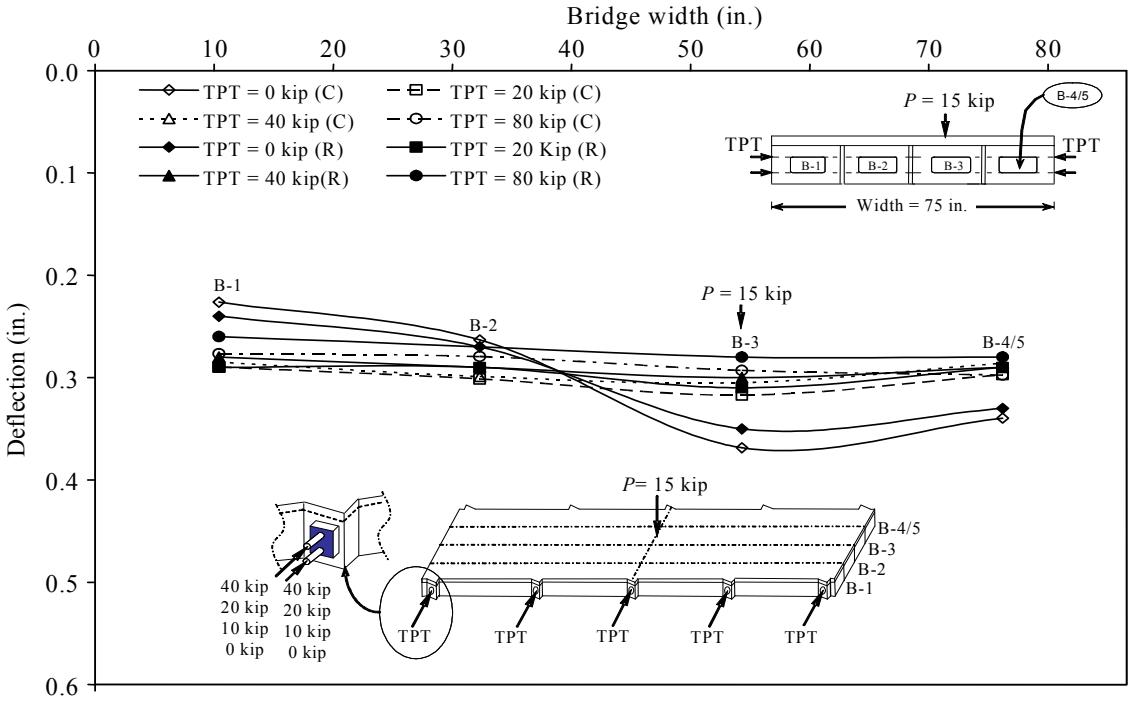

Figure 6.3-23 Load-deflection response for beam B-3 after repairs at different TPT forces.

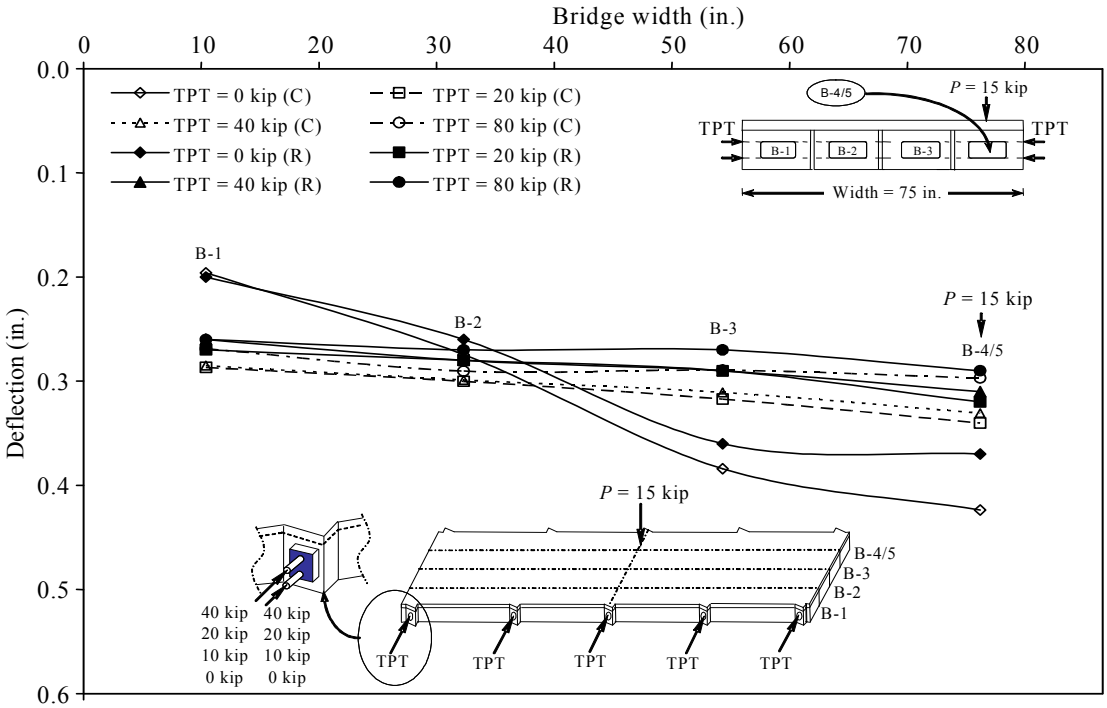

Figure 6.3-24 Load-deflection response for beam B-4 after repairs at different TPT forces.

6.3.5.3 Improvement in the Behavior of the Bridge Model

The *PI* was also determined to evaluate the effect of varying the level of TPT forces on the bridge model behavior. In the uncracked stage, *PI* was not affected by the level of the TPT force, as shown in Figure 6.3-25 through Figure 6.3-28. For instance, when beam B-1 was loaded, the *PI* for beam B-1 were 2.6%, 0.8%, and 3.0% corresponding to the TPT forces of 20, 40, and 80 kip applied to all five diaphragms, respectively.

In the cracked stage, the *PI* increased significantly relative to the uncracked stage. For example, in the cracked stage, when beam B-1 was loaded and the level of TPT forces were increased, the *PI* for beam B-1 were 14.3%, 15.2%, and 18.2% for TPT forces of 20, 40, and 80 kip applied to all five diaphragms, respectively.

No significant changes in the *PI* were observed in the repaired stage for the beams B-1 and B-2, as shown in Figure 6.3-25 through Figure 6.3-28. However, slight reduction was observed in the *PI* when beam B-3 and B-4/5 were loaded, as shown in Figure 6.3-27 and Figure 6.3-28. For example, in the cracked stage when beam B-3 was loaded, the *PI* was 14.5%, 15.7%, and 17.0% for TPT forces of 20, 40, and 80 kip at all five diaphragms, respectively. However, in the repaired stage and with the same TPT arrangments, the *PI* reduced slightly to 10.7%, 12.1%, and 12.7%.

Furthermore, it was noted that in the cracked and the repaired stages, the *PI* increased accordingly when the TPT increased from zero to 20 kip. However, insignificant improvement was observed in *PI* as the TPT force was increased to 40 and 80 kip, as shown in Figure 6.3-25 to 6.3-28. For example, the *PI* observed for beam B-3 due to TPT forces of 20, 40, and 80 kip were 14.3%, 15.1%, and 16.2% in the cracked stage and 8.6%, 10.7%, and 11.4% in the repaired stage. Based on this, it could be deduced that, applying TPT force of 40 kip is adequate to hold the adjacent beams to act as a one unit when the bridge model was subjected to the vertical load although it did not satisfy the AASHTO LRFD (2004) prestress limit of 250 psi.

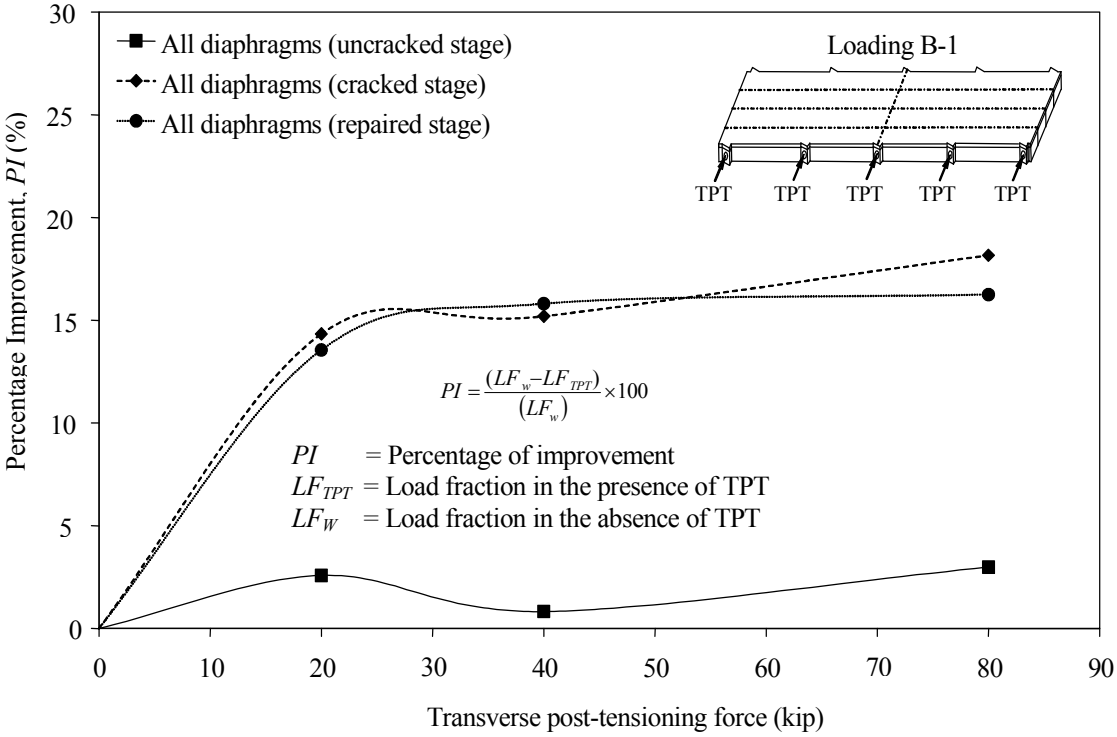

Figure 6.3-25 Effect of varying levels of TPT forces on *PI* for beam B-1.

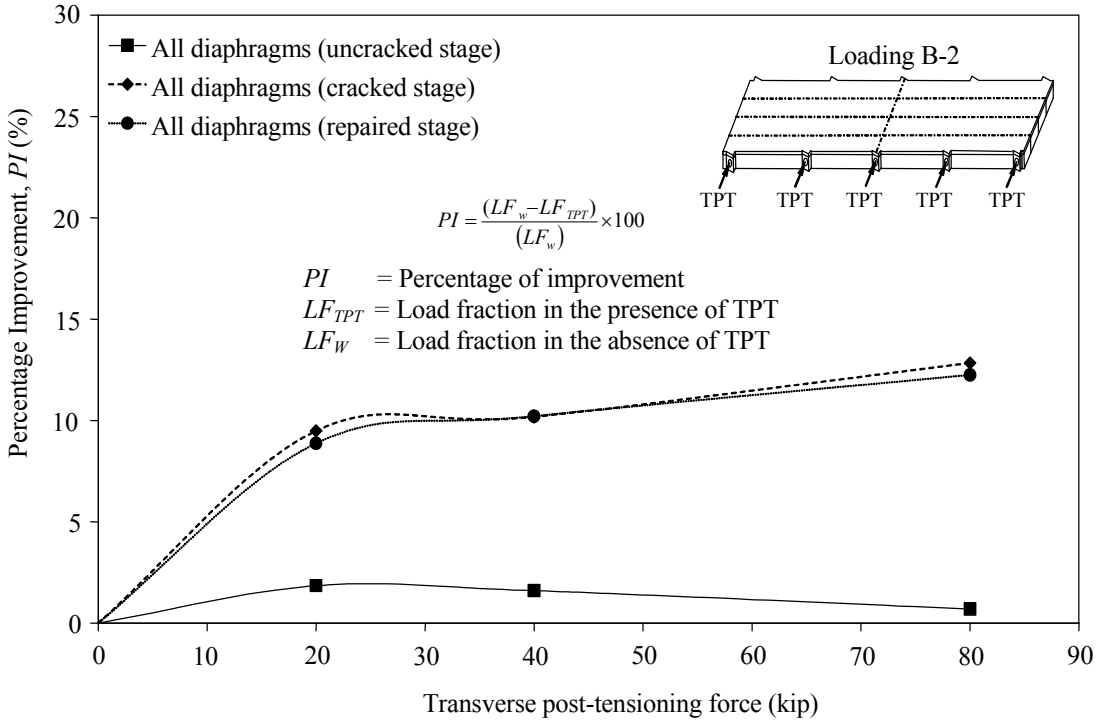

Figure 6.3-26 Effect of varying levels of TPT forces on *PI* for beam B-2.

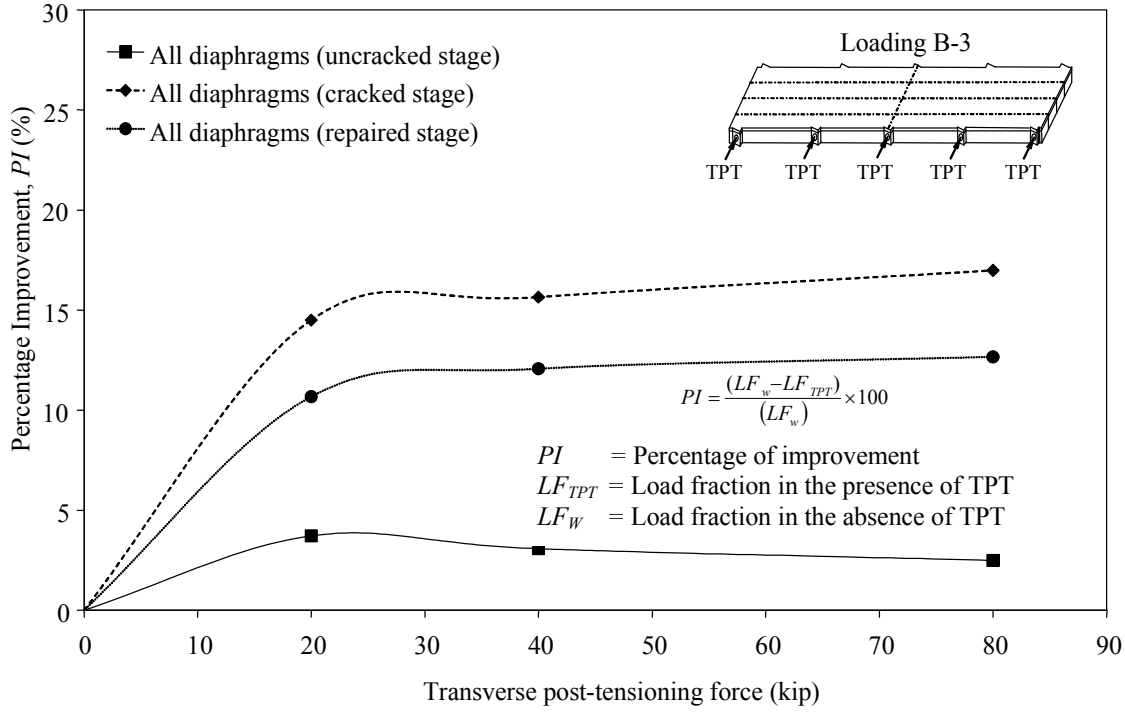

Figure 6.3-27 Effect of varying levels of TPT forces on *PI* for beam B-3.

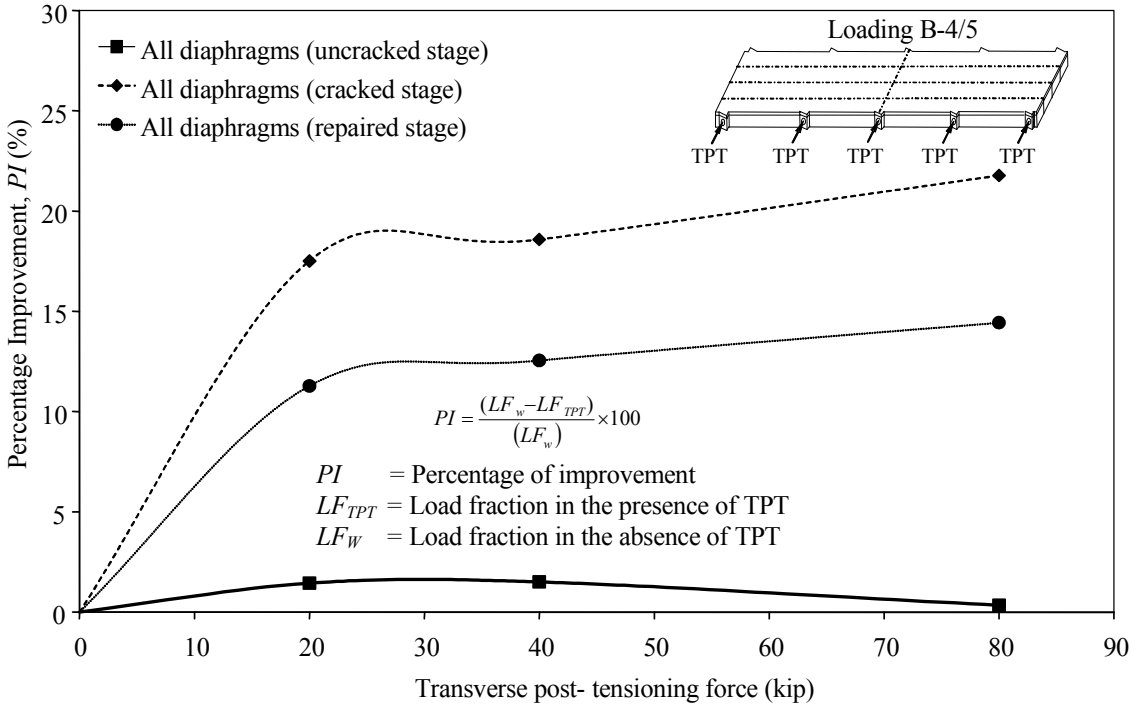

Figure 6.3-28 Effect of varying levels of TPT forces on *PI* for beam B-4/5.

6.4 Ultimate Load Test

6.4.1 Introduction

The function of TPT arrangement is to ensure that the bridge model acts as a monolithic system where the differential deflection between the adjacent box-beams are limited. The efficiency of the unbonded TPT arrangement has been demonstrated and discussed in the previous sections for the case of service and repair conditions. This section presents results on the evaluation of the efficiency of the unbonded TPT arrangement during failure as induced by an eccentric load. The bridge model was subjected to TPT forces of 80 kip at each of the five diaphrames during this test.

This prestressed bridge model reinforced with steel was designed according to the American Concrete Institute (ACI 318-05) as an under-reinforced bridge. Therefore, the three expected failure modes for the bridge model under the eccentric load were: 1) ductile flexural failure at maximum moment, 2) brittle shear failure between adjacent box-beams due to shear failure of the unbonded TPT CFCC, and 3) a combination between the first two failure modes.

The eccentric load was applied at the mid-span of the interior box-beam B-2. The load was applied using a symmetrical two-point loading frame. The distance between the two loading points was 7.5 ft, which was the same as the spacing between the diaphragms. Therefore, the two points of the loading frame were located exactly at the mid-distance between the mid-span and quarter-span diaphragms. The selected locations for the loading points experienced the lowest effect of TPT forces along the span as noticed in the transverse strain distribution test results. The load was applied on beam B-2 as the deck cracks were located evenly over the shear-keys whereas the deck cracking had propagated into the center of box-beam B-3. It was determined that the risk of local shear punchure failure would be less likely for box-beam B-2.

The eccentric load was applied in five different loading/unloading cycles with maximum load of 20, 40, 60, 80, and 100 kip before reaching the ultimate load. Throughout the test, the rates of loading and unloading were kept at an average of 15 kip/min. The following sections present details of the observed failure mode of the bridge model, load-deflection response for the four beams, concrete compressive strains at the extreme top fiber of the bridge deck, and the effect of the applied load on the TPT forces at the various diaphragms. Finally, comparison between the theoretical and experimental ultimate loads is also presented.

6.4.2 Load-Deflection Response

The deflection for each box-beam was measured using linear motion transducer attached at the mid-width of each beam. Figure 6.4-1 through Figure 6.4-4 show the load-deflection responses of the four beams for the various loading and unloading cycles. Prior to conducting the ultimate cycle, residual deflections of 2.07, 2.02, 2.02, and 1.97 in. were observed at the four box-beams B-1, B-2, B-3 and B-5, respectively. The residual deflections for the four box-beams were almost the same with a slight increase towards beam B-1. The bridge model acted as a single plate subjected to eccentric vertical load, which cause the plate to deflect with a slight rotation towards the location of the applied load.

During the ultimate load cycle, the deflection of the bridge model was proportional to the applied load up to about 100 kip, the deflection afterwards increased rapidly under constant vertical load. This was an indication of yielding of the bottom steel reinforcements. The deflections at 100 kip were 8.51, 8.30, 8.24, and 8.11 in. for beams B-1, B-2, B-3 and B-5, respectively. The ultimate load for the bridge model was 104 kip and the corresponding deflections were 10.76, 10.55, 10.46, and 10.34 in. The post-peak behavior of beam B-3 showed that the concrete around the deflection sensor crushed at level of 83 kip of the applied load. However, similar behavior of the deflections for beams B-1, B-2 and B-5 was observed till the complete failure of the bridge model. The maximum observed deflection for the bridge model was 27.07 in. and occurred at beam B-2.

Figure 6.4-5 shows the deflections of the four beams at different levels of the applied load during the last load cycle leading to failure. The deflections are shown for the four beams illustrating the transverse behavior of the bridge model at loads of 0, 20, 40, 60, 80, 100, 104, and 83 kip. As mentioned earlier, the deflections for the four box-beams at zero load were residual deflections from the previous loading and unloading cycles. It was also noticed that all box-beams deflected as one unit regardless of the level of the applied load, coupled with a slight rotation due to the eccentric load up to the ultimate load 104 kip.

6.4.3 Failure Mode

The expected failure modes for the bridge model were: flexural failure, transverse shear failure or a combination between them. The observed failure mode was a typical flexural ductile failure with localized failure at the location of maximum moment. The failure started by the

initiation and propagation of flexural tensile cracks at the soffit of the beams around the mid-span. This was followed by the yielding of the bottom reinforcements, resulting in increasing deformation of the bridge model at constant load. The yielding of the bottom reinforcement was followed by crushing of the deck slab concrete across the entire width of the bridge model near the mid-span, as shown in Figure 6.4-6. No rupture of the bottom reinforcement was observed. However, buckling of the top reinforcement was observed at the location of the concrete crushing. Failure of the shear-keys was observed at the mid-span only. Propagation of the existing longitudinal cracks in the deck slab was not observed.

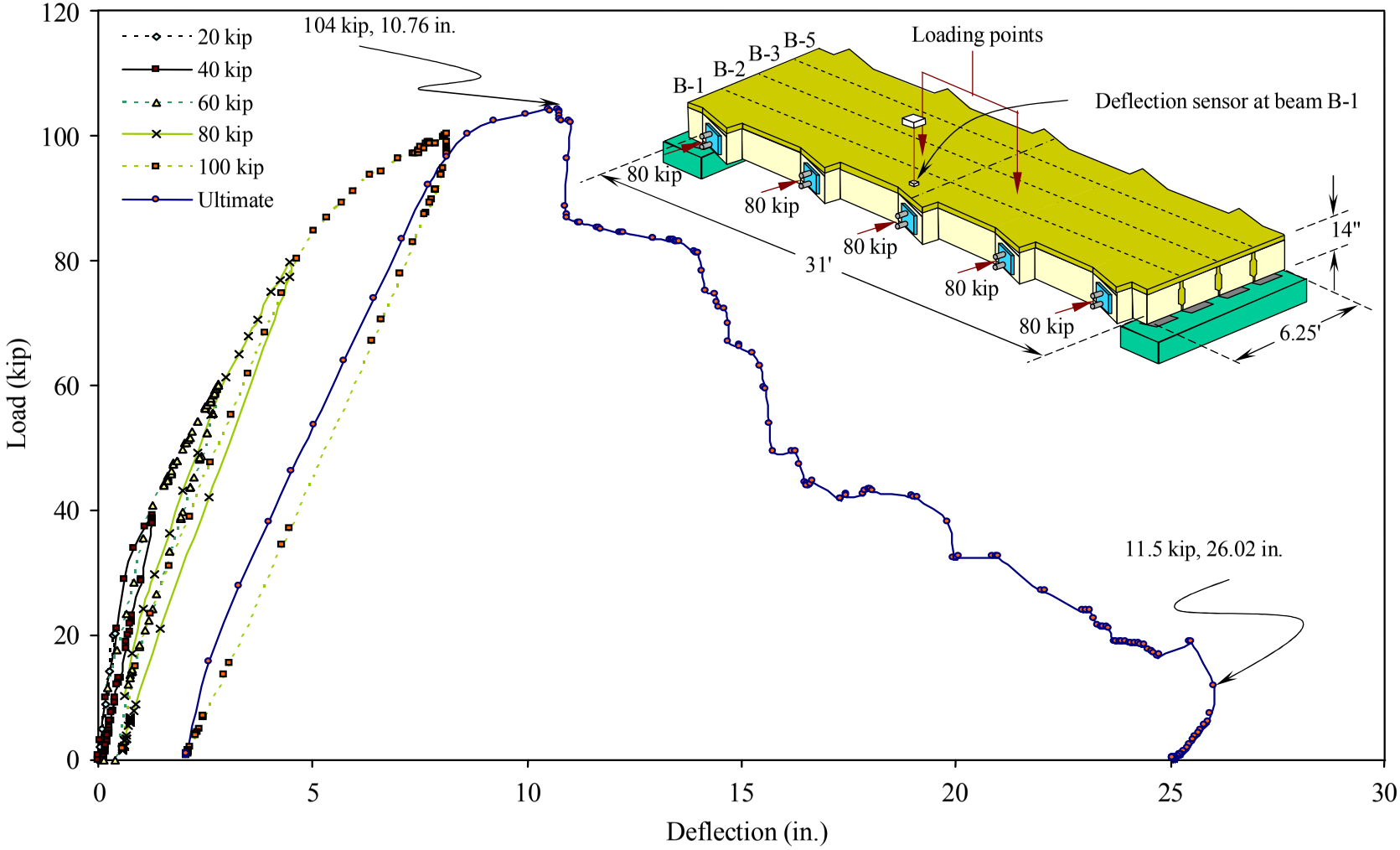

Figure 6.4-1Load-deflection response of box-beam B-1 for different loading/unloading cycles.

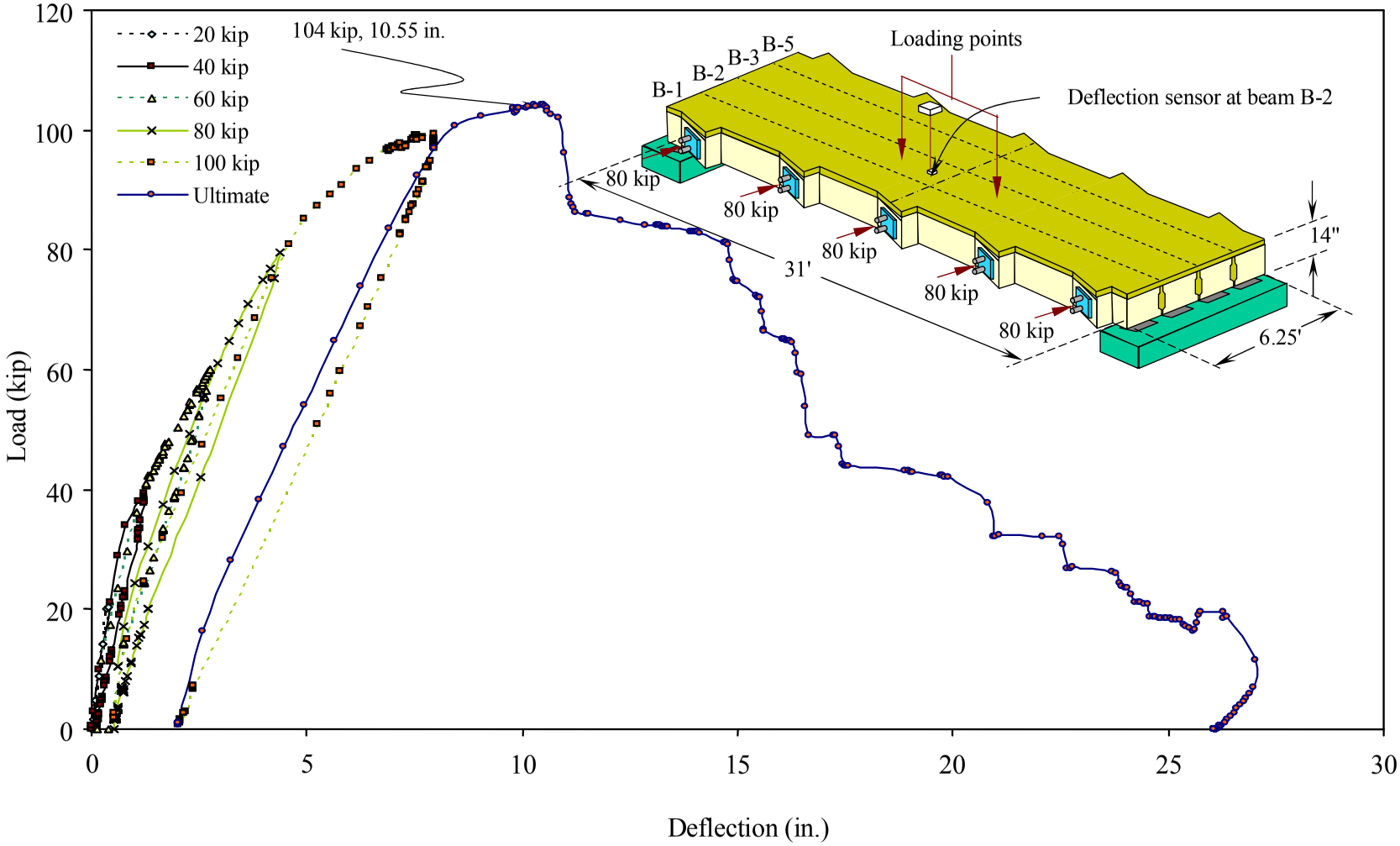

Figure 6.4-2 Load-deflection response of box-beam B-2 for different loading/unloading cycles.

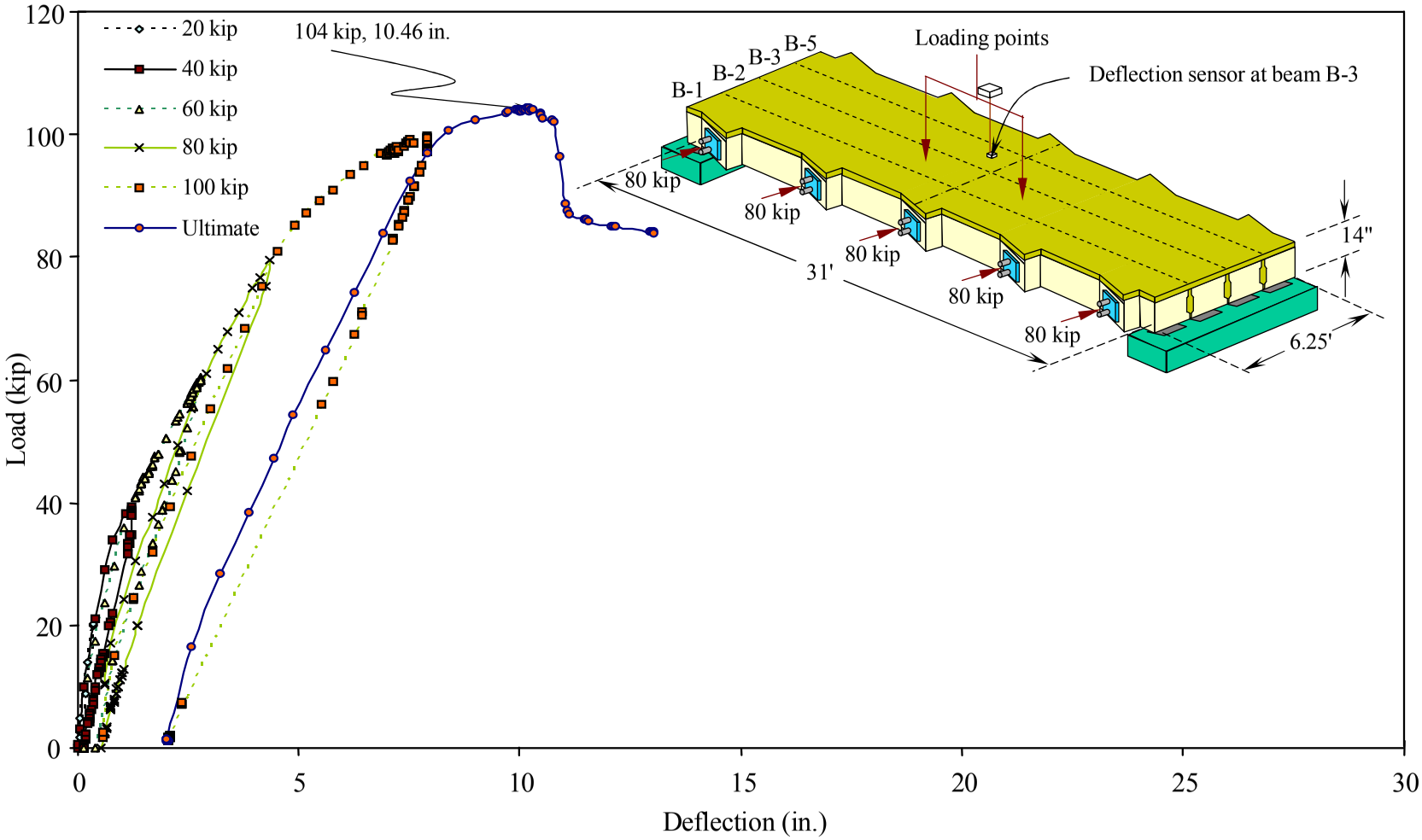

Figure 6.4-3 Load-deflection response of box-beam B-3 for different loading/unloading cycles.

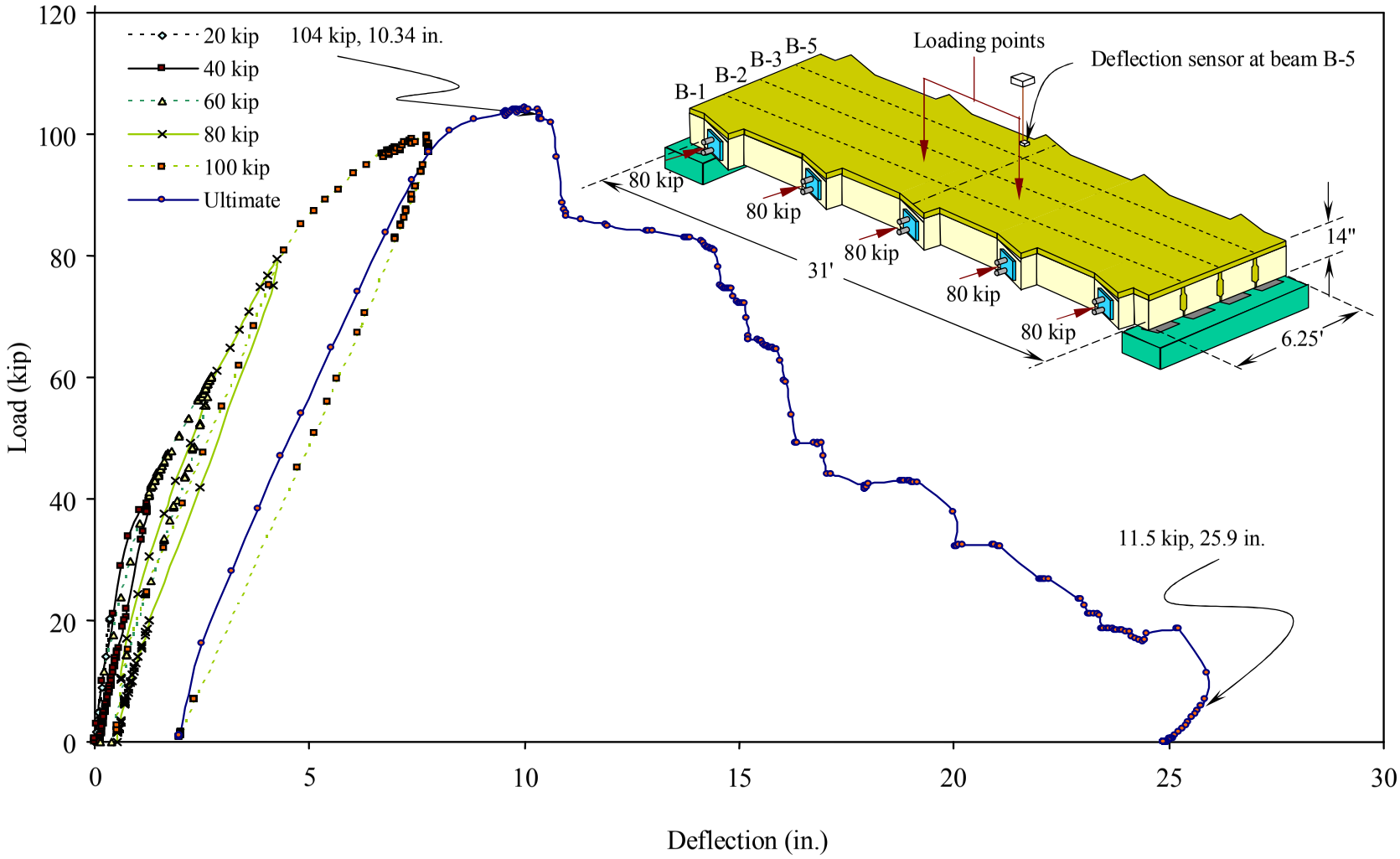

Figure 6.4-4 Load-deflection response of box-beam B-5 for different loading/unloading cycle.

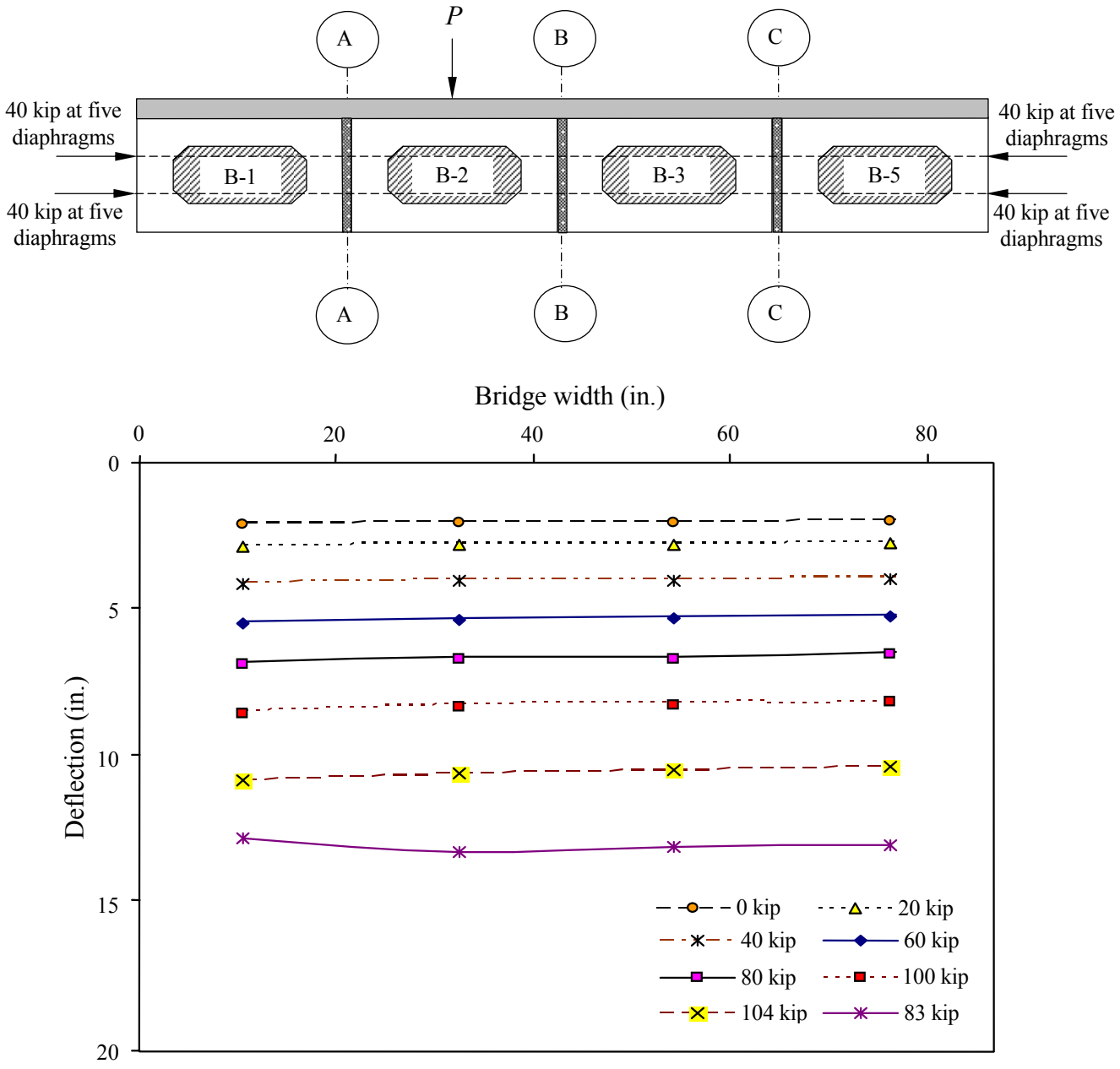

Figure 6.4-5 Deflection of the bridge model at different levels of applied load.

(a) Flexural cracks at mid-span

(b) Crushing of concrete

Figure 6.4-6 Failure of bridge model.

6.4.4 Concrete Compressive Strains

The concrete compressive strains at the top surface of the deck slab were monitored during the ultimate load cycle. Two longitudinal strain gages were attached to the deck slab and mounted exactly at mid-span directly over the box-beams B-2 and B-5, as shown in Figure 6.4-7. Figure 6.4-8 shows the variation of the compressive strains as a function of the applied load. Prior to the application of the load, both strain gages experienced residual strains resulted from the previous loading/unloading cycles (i.e. -379 and -226 με for beams B-2 and B-5, respectively). The compressive strains were proportional to the applied load during the ultimate load cycle up to 100 kip, after which the compressive strains increased at a constant level of applied load that corresponds to the yielding plateau experienced during the ductile failure of the bridge model. The final crushing of deck slab concrete occurred close to the location of the strain gages. The maximum compressive strains observed by the strain gages were -2,582 and -2,062 με for beams B-2 and B-5, respectively. These strain levels approaches the ACI recommendation for the maximum compressive strain at the concrete crushing of -3,000 με.

6.4.5 Variation of TPT Forces

Variations in the TPT forces were expected during loading as the transverse rotation would cause an elongation at the level of the TPT strands. As noted earlier, the bridge model had five transverse diaphragms located at equal spacing of 7.5 ft. The layout for the transverse diaphragms and the CFCC is shown in Figure 6.4-9. For instance, the top TPT CFCC located at the end diaphragm is designated as E(1)-T, the bottom strand at the mid-span diaphragm is designated as M(3)-B. The TPT forces were monitored continiously during the ultimate load cycle for six of the CFCC. Two strands were located at the end-diaphragm 1), two strands were located at the quarter-span diaphragms 2), and two strands were located at the mid-span diaphragms 3). The six CFCC represented one-half of the bridge model.

A slight increase in the TPT forces was observed prior to conducting the ultimate load test at each CFCC due to the residual deformations of the bridge model resulted from the previous loading/unloading cycles. It was observed that the strands located at the mid-span diaphragm experienced the largest increase in the TPT forces. Furthermore, the bottom strands experienced a larger increase in the TPT forces compared to the top strands for the same diaphragm. For example, an increase in the TPT forces observed at the top and bottom strands located at end-diaphragms (1) were 0.04 kip and 0.07 kip, respectively. For the quarter-spam diaphragms, the increase in the TPT forces observed at the top and bottom strands were 0.26 and 0.48 kip. Finally, for the mid-span diaphragm, the increase in the TPT forces observed at the top and bottom strands were 0.77 and 1.25 kip, respectively.

Figure 6.4-10 shows the variation of the TPT forces during the ultimate load cycle. The strands located at the end-diaphragms did not experience significant change in the TPT forces. The strands located at the mid-span diaphragms experienced the larger increase in the TPT forces. The largest increase of the TPT force was observed in the bottom strands located at the mid-span diaphragms, which increased by about 2.3 kip. This increase of about 9% above the TPT level corresponds to an elongation of 8%. However, the strand was still only stressed to 54% of its capacity. The top strand located at the mid-span diaphragms experienced an increase in the TPT force of 7% above the TPT level. The top and bottom strands located at the quarter-span diaphragms experienced increase in the TPT force of 1% and 2% of the TPT level, respectively. The strands located at the end diaphragms did not experience any increase in the TPT forces.

6.4.6 Theoretical and Experimental Load-Carrying Capacities

The load-deflection response of the bridge model show that the bottom reinforcement started to yield at a load of 100 kip and the ultimate load-carrying capacity was 104 kip. The deflections for all beams were similar at the ultimate load and the entire bridge was acting as a one unit when subjected to eccentric load. The theoretical load-carrying capacity was 88 kip and it was based on the strain compatibility approach (Appendix C). The failure of the bridge model in the theoretical calculations was assumed to be a ductile flexural failure for an under reinforced bridge model with a uniform distribution of the applied load in the transverse direction. The theoretical load-carrying capacity showed good agreement with the experimental capacity.

6.4.7 Ductility

The ductility is the ability of a structure to sustain load during increasing deformation. In this study, an energy based approach is used to quantify ductility (Grace et al., 1998). The energy based approach is based on the the area under the load-deflection curve where load and deflection are determined at the same points and in the same direction. A typical prestressed concrete bridge would experience two types of energies prior to the failure load. The first is the elastic energy ($E_{elastic}$) and second is the inelastic energy ($E_{inelastic}$). During increased loading, the structure creates new crack surfaces which create irreversible deformation upon unloading. Under several loading/unloading cycles of the vertical load, the structure stores the inelastic energy as newly formed cracks and releases the elastic energy. In the post-peak area, additional cracking and yielding cause additional inelastic energy which is denoted as $E_{in(add)}$. The total energy is the summation of the elastic and the inelastic energies. The ductility, based on these energies, can be expressed by the ductility index. The ductility index is the energy ratio between the absorbed inelastic energy and the total energy, as shown in equation 6.5 (Grace and Abdel-Sayed, 1998). The failure mode of a bridge could be classified as a ductile failure if the ductility index is greater than 75%. However, if the ductility index lies between 70 and 74%, the failure would be semi-ductile. The brittle failure is classified for those bridges which achieve ductility index less than 69%.

$$\text{Ductility Index} = \frac{E_{inelastic}}{E_{Total}} = \frac{E_{inelastic}}{E_{elastic} + E_{inelastic} + E_{in(add)}} \tag{6.5}$$

For the bridge model, several loading/unloading cycles were applied to separate the elastic and the inelastic energies. The loading cycles had maximum values of 20, 40, 60, 80, and 100 kip. The energy ratio was calculated based on the load-deflection curve of the loaded beam B-2, as shown in Figure 6.4-11. The inelastic energy observed by the bridge model prior to the ultimate load was 549 kip-in. and the elastic energy was 300 kip-in. The elastic energy was estimated by calculating the area under load-deflection curve for the unloading path of the fifth cycle 100 kip. The additional inelastic energy observed was 738 kip-in. and was estimated by calculating the area under the load-deflection curve subsequent to the ultimate load. The bridge model experienced ductility index of 81.1%, which lies within the range of the ductile failure.

6.4.8 Evaluation of TPT System

As mentioned earlier, the main objective of the ultimate load test was to evaluate the efficiency of the TPT system in distributing the eccentric load in the transverse direction. The TPT system consisted of five transverse diaphragms equally spaced each 7.5 ft. Each diaphragm contained two unbonded TPT CFCC placed in oval-shape ducts and prestressed with TPT force of 40 kip/strand. The following observations were made during the ultimate load test.

1. The failure mode for the bridge model was ductile flexural failure initiated by yielding of the bottom reinforcement and followed by crushing of concrete as a typical tension controlled prestressed concrete bridge.
2. No significant differential deflection was observed between the adjacent box-beams at any load levels prior to the ultimate load. The bridge was slightly rotating as a single unit subjected to an eccentric vertical load.
3. Furthermore, no new longitudinal cracks were initiated or propagated on the top surface of the deck slab between the adjacent box-beams.
4. No shear rupture of the TPT CFCC was observed during the ultimate load test and none of the transverse diaphragms failed even when complete failure occurred. The TPT strands located at the mid-span were able to transfer the vertical load in the transverse direction despite the failure of the shear-key and the deck slab at the mid-span.
5. The theoretical and experimental load-carrying capacity show good agreement. The theoretical load-carrying capacity was based on ductile flexural failure of the bridge

model. In addition, the energy ratio shows that the failure of the bridge model was ductile flexural failure.

Based on the previous observations, it could be noted that the TPT system was successful in distributing the eccentric vertical load to the adjacent box-beams, even after the failure of the shear-keys and the deck slab at the mid-span, which enabled the bridge model to act as a composite unit and not as individual beam elements.

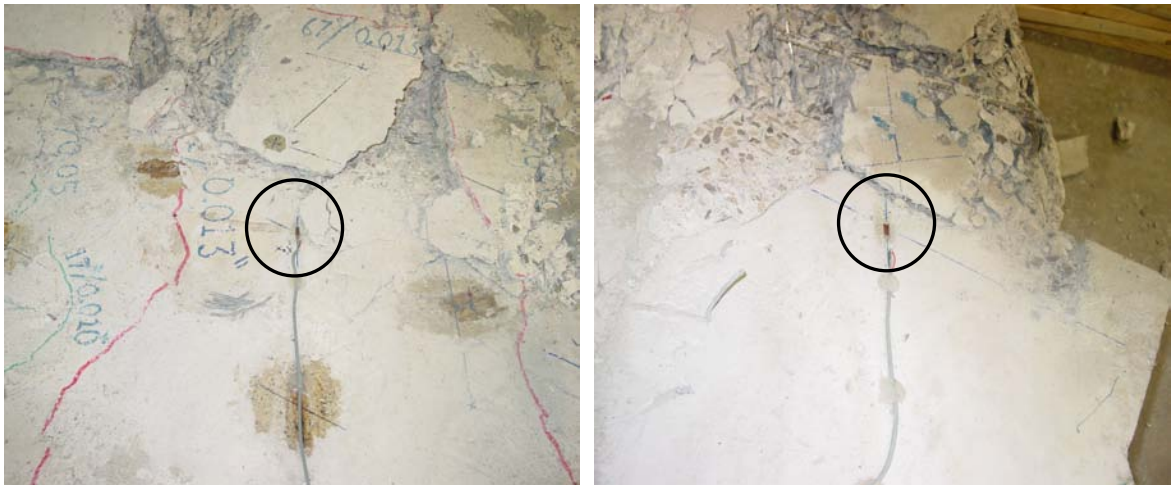

(a) Strain gage over beam B-2 (b) Strain gage over beam B-5

Figure 6.4-7 Crushing of concrete near the location of the strain gages.

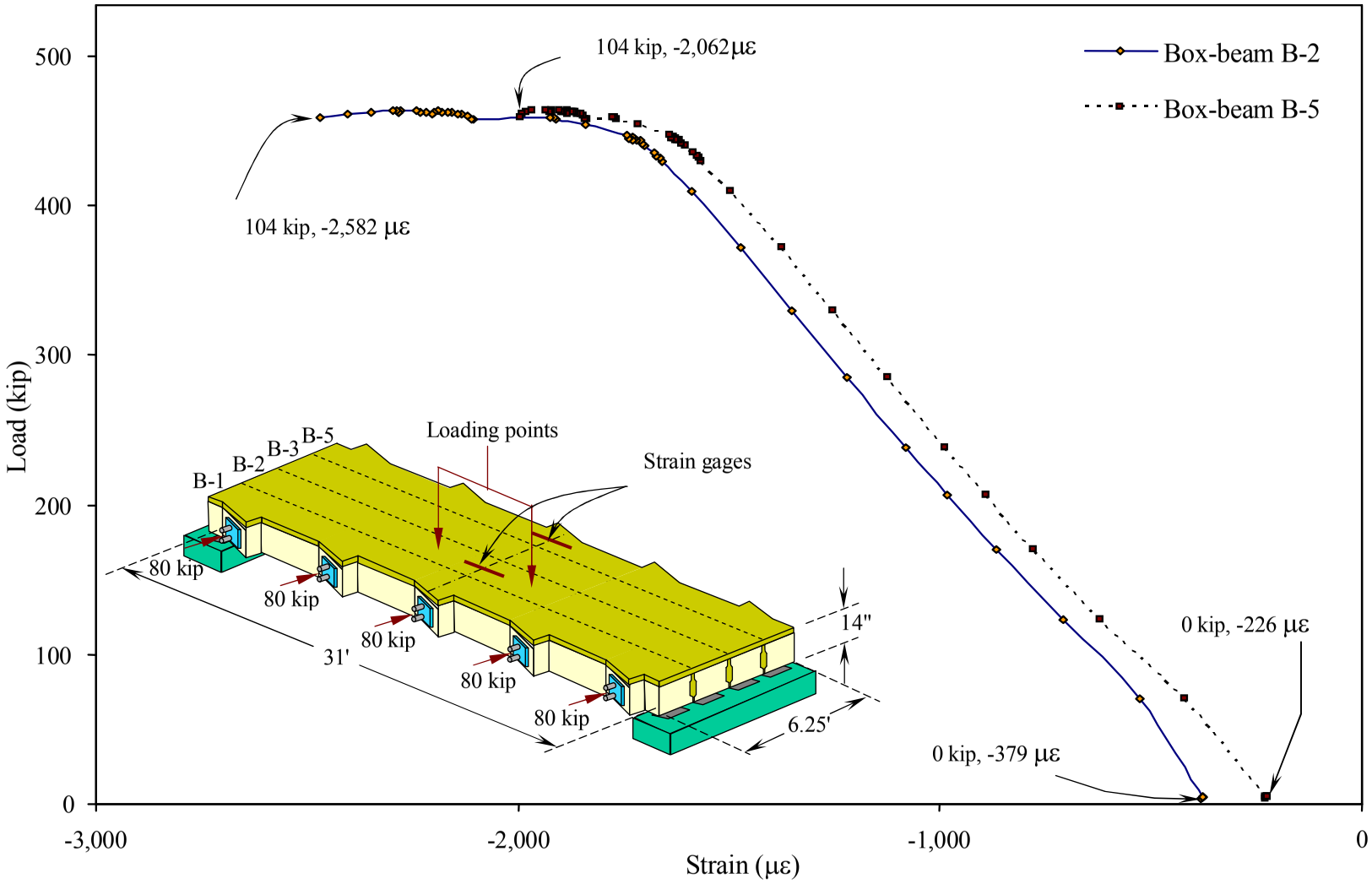

Figure 6.4-8 Concrete compressive strains at the top surface of deck slab during ultimate load cycle.

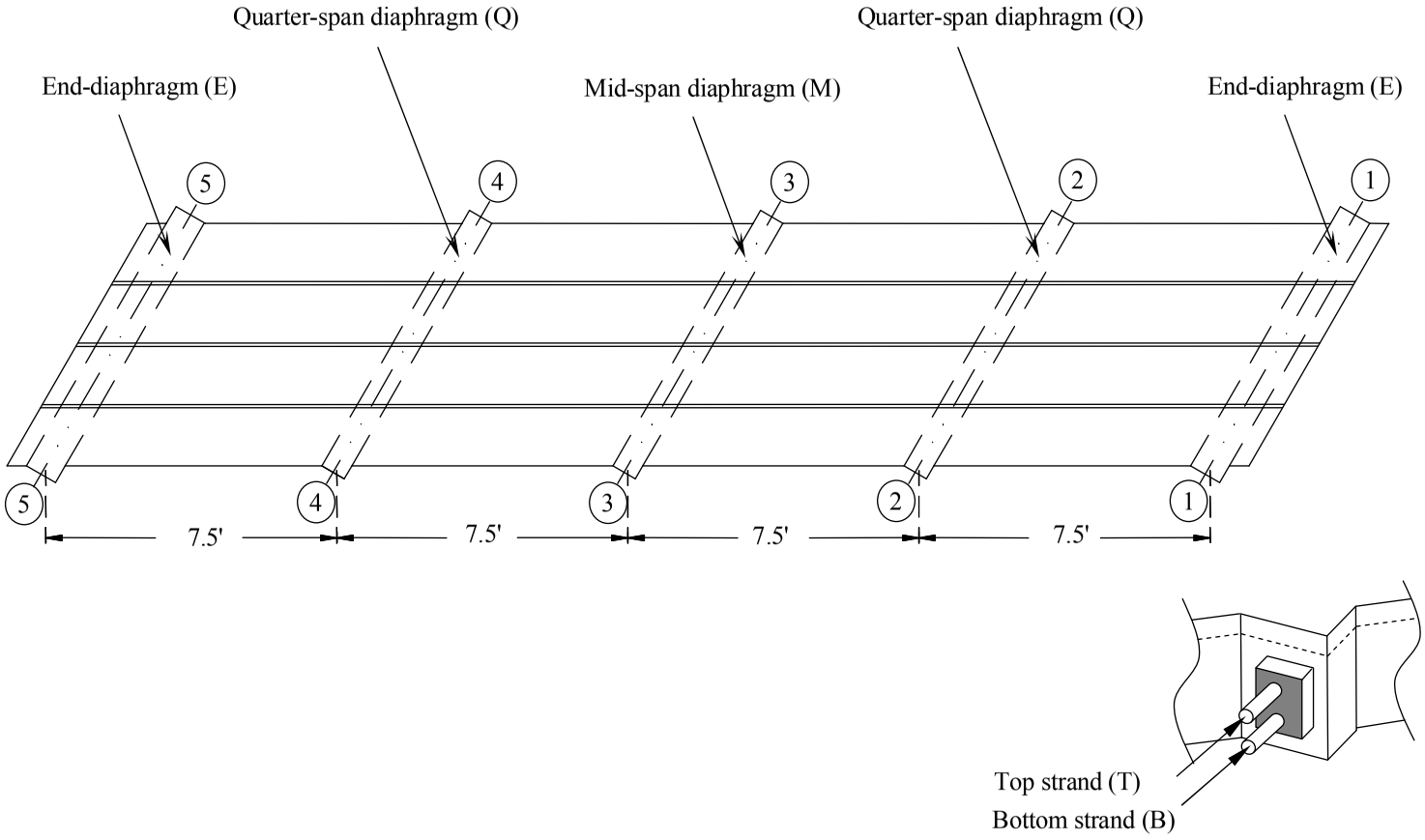

Figure 6.4-9 Layout of transverse diaphragms and CFCC.

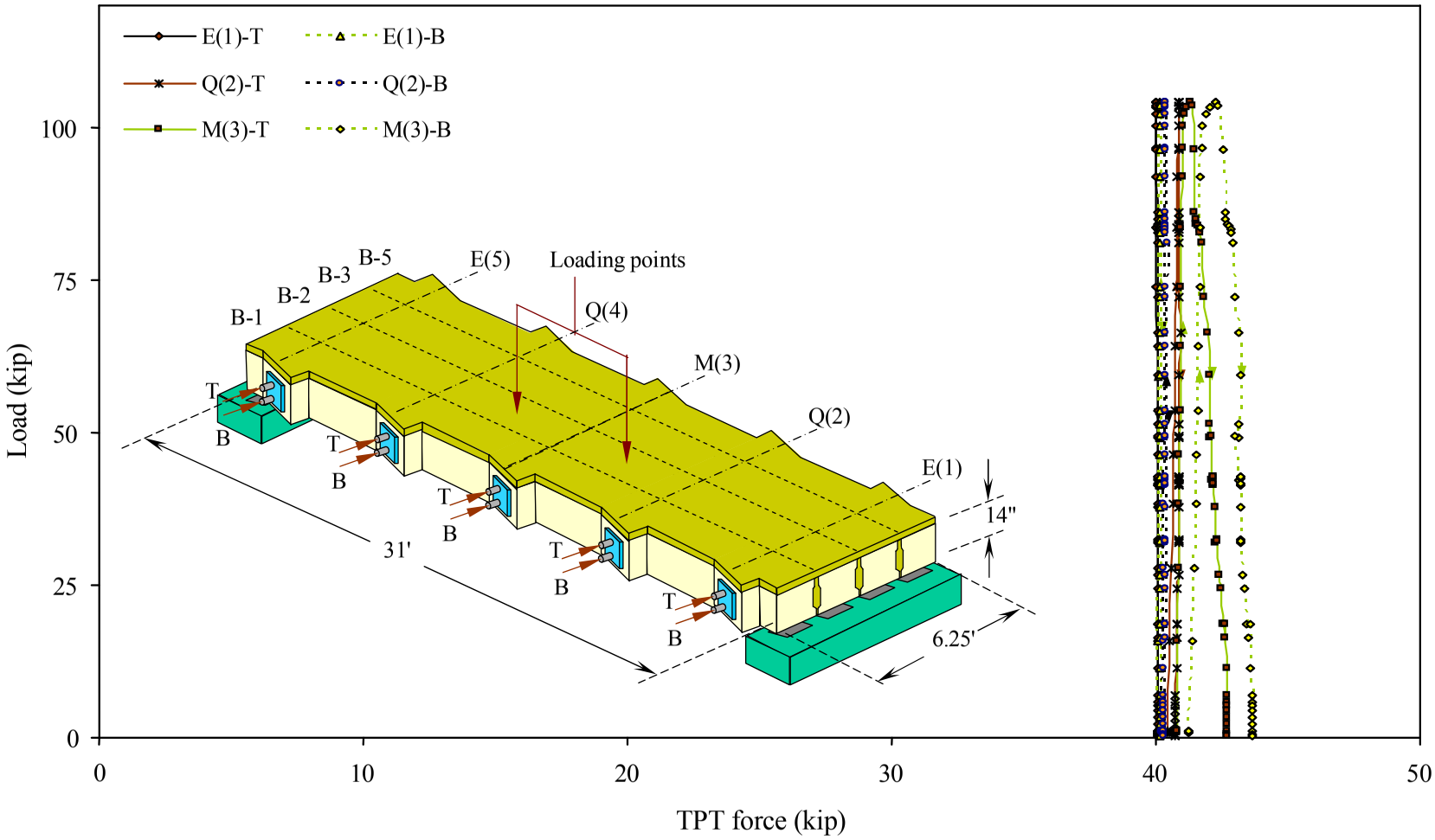

Figure 6.4-10 Variation of TPT forces for the ultimate load cycle.

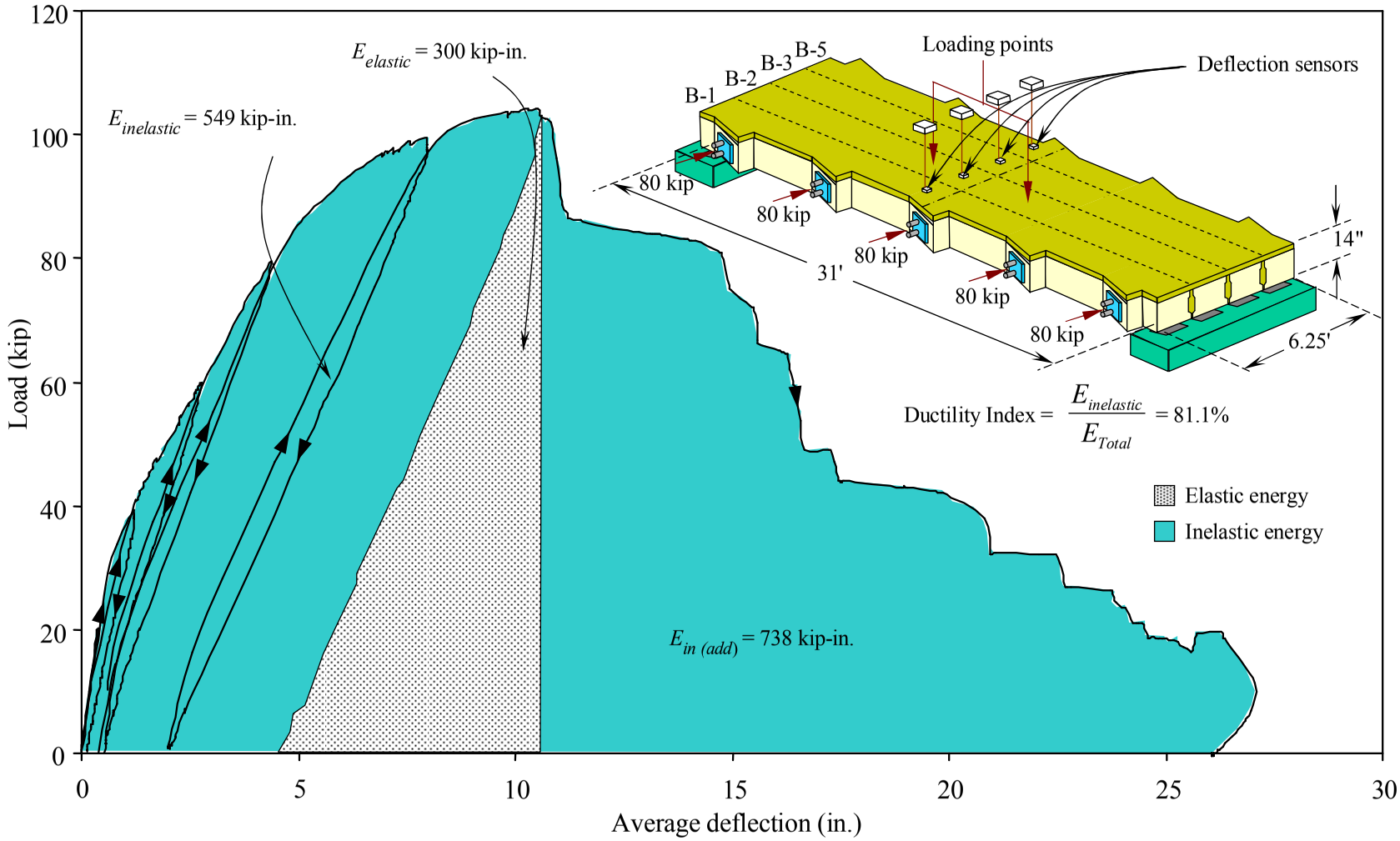

Figure 6.4-11 Elastic and inelastic energy bands of the bridge model during the ultimate load cycles.

CHAPTER 7: CONCLUSIONS AND RECOMMENDATIONS

Experimental and numerical studies were conducted to evaluate the number of transverse diaphragms and the level of transverse post-tensioning (TPT) forces in order to control the development of the longitudinal cracks in side-by-side box-beam bridges. This chapter is divided into two separate sections. The first section presents the conclusions and recommendations obtained from the experimental investigation while the second section provides the conclusions and the recommendations derived from the numerical investigations.

7.1 Findings and Conclusions from the Experimental Study

7.1.1 Introduction

A half-scale 30º skew bridge model was constructed, instrumented, and tested at the Center for Innovative Materials and Research (CIMR) at the Lawrence Technological University, Southfield, to investigate the effect of the number of the transverse diaphragms and the level of the TPT forces on the behavior of side-by-side box-beam bridge where unbonded TPT CFCC were used. Oval-shape ducts were used at each transverse diaphragm location to accommodate the unbonded TPT CFCC and to allow for the differential camber intensionally developed between the adjacent beams. Throughout the test program, three different types of transverse diaphragms configurations were used (three, four, and five diaphragms). Similarly, three different levels of TPT forces of 20 kip, 40 kip, and 80 kip were also used for each evaluated diaphragm configuration. The major tests conducted on the bridge model were 1) the transverse strain distribution test, 2) load distribution test, and 3) ultimate load test. The transverse strain distribution test primarily involved examining the transverse strains that developed on the top surface of the deck slab along the shear-key locations. Likewise, the load distribution test was also conducted to evaluate the efficiency of the different TPT arrangements in distributing the applied load across the width of bridge model. The purpose of the ultimate load test was to evaluate the response of the unbonded TPT CFCC in distributing the vertically applied load across the width of the bridge model.

7.1.2 Conclusions

7.1.2.1 General

The performance of the TPT system used in the experimental program was evaluated and the following conclusions are derived.

1. The use of unbonded CFCC is suitable for TPT application in side-by-side box-beam bridge system. The combination of TPT CFCC and ungrouted transverse diaphragms facilitates the replacement of damaged box-beam and allows restoration of the stiffness of the box-beam bridge. Furthermore, the flexueral capacity of the repaired bridge exceeded the design flexterual capacity (about 15%).
2. The use of oval-shape ducts to accommodate the unbonded TPT CFCC can overcome the construction problem observed when using the traditional circular ducts and the misalignment problem that arises as a results of differential camber between the adjacent box-beams.

7.1.2.2 Strain Distribution Test

Based on the results obtained from the strain distribution test conducted on the bridge model, the following conclusions are drawn.

1. Increasing the levels of TPT forces proportionally increases the transverse strains for all points located along the post-tensioned diaphragms. The linear relation between the level of the TPT forces and the corresponding transverse strains reflects the elastic behavior of the concrete when the TPT forces are applied.
2. Increasing the number of transverse diaphragms has insignificant influence on the transverse strain developed in the region between the diaphragms. The low transverse strains at these locations indicate a non-uniform distribution of the TPT forces along the entire span of the bridge model.
3. Regardless of the number of transverse diaphragms, and the levels of TPT forces experienced in this bridge model, the resulting transverse strain did not satisfy the transverse stresses limit of 250 psi in the deck slab recommended by the AASHTO LFRD (2004). However, 70% of the deck slab meets the criterion when TPT force of 80 kip was applied at five diaphragms.

7.1.2.3 Load Distribution Test

Based on the load distribution test, the following conclusions are drawn.

1. The level of TPT forces and the number of transverse diaphragms have no effect on the transverse behavior of the bridge model if the deck slab is uncracked.
2. The effect of TPT arrangements on the load distribution was significant when the deck slab experienced longitudinal cracks at the shear-key locations. Through the evaluation of the percentage improvement, it was observed that increasing the level of TPT forces improved the behavior of the bridge model.
3. The replacement of the damaged beam and reconstruction of the deck slab as well as the shear-key enhanced the behavior of the bridge model by reducing the deflection of the loaded new box-beam B-5 as well as the adjacent interior box-beam B-3. The effect increased with larger number of transverse diaphragms and higher levels of TPT forces.
4. The case of five diaphragms outperformed the case of three diaphragms in terms of percentage improvement of the load distribution for the cracked deck slab and the repaired stages. This was because, the spacing between the diaphragms increased from 7.5 ft (in case of five diaphragms) to 15 ft (in case of three diaphragms).
5. As the level of TPT force increased from zero to 20 kip, the behavior of the bridge model improved accordingly. However, at higher levels of the TPT force above 40 kip, the improvement in the behavior was reduced. This means that applying TPT force of 40 kip is adequate to hold the adjacent beams to act as a one unit when the bridge model was subjected to the vertical load although it did not satisfy the AASHTO LRFD (2004) prestress limit of 250 psi.

7.1.2.4 Ultimate Load Test

The failure mode experienced by the bridge model was ductile flexural failure. The failure started by yielding of the bottom steel reinforcements followed by crushing of deck slab concrete across the width of the bridge model. Failure of the shear-key and the crushing of the concrete were observed particularly at the mid-span of the bridge model. Prior and during the failure of the bridge model, no differential deflection was observed between the adjacent box-

beams, which substantiate the adequacy of the unbonded TPT CFCC along with the full-depth shear-keys in maintaining a composite behavior throughout the loading history.

None of the unbonded TPT CFCC ruptured and none of the transverse diaphragms failed during or after the complete failure of the bridge model. In addition, the TPT forces in the CFCC increased due to the deflection of the bridge model. The CFCC located at the mid-span of the bridge model experienced significant increase in the TPT forces (9% above the TPT level); whereas the TPT force in the CFCC located at the quarter-span diaphragms increased marginally (2% above the TPT level). Negligible increase in the TPT forces was observed in the strands located at the end-diaphragms. The used TPT system, coupled with the deck slab, jointly distributed the applied eccentric load in the transverse direction until the total collapse of the bridge model.

7.1.3 Recommendations for Field Implementations and Future Research

The results of this research project have yielded the following recommendations for field implementation and further consideration.

1. The oval-shape ducts, placed at the location of the transverse diaphragms, are successful in accommodating the differential camber between the adjacent beams in side-by-side box-beam bridges. The ducts were also useful to accommodate the two TPT strands at each diaphragm.

2. The unbonded CFCC were effective in the application of the TPT forces as they did not experience any rupture or permanent deformation during all tests conducted on the bridge model. Therefore, the CFCC can be implemented in the TPT system for side-by-side box-beam bridges since they have high corrosion resistance and higher tensile capacity than that of the conventional steel. In addition, the threaded anchorage system of the CFCC allowed for partial or full release of the TPT forces as needed.

The following issues require further investigations for a comprehensive evaluation of the box-beam bridge behavior:

1. It is recommended to examine the sensitivity of the vertical load to different locations along the entire span of the bridge model, since the applied load at the mid-span was sensitive to presence of the mid-span diaphragm.

2. In order to compare the load fraction determined from the AASHTO LRFD (2004) live load distribution factor equations, it is recommended to construct a bridge model of two lanes width and a larger number of beams (more than four) in order to examine the applicability range of these equations. Hence, the load distribution factors based on the experimental investigation cannot be directly compared with the predicted values obtained from the AASHTO equations.
3. The effect of different skew angles on the load and strain distribution of the bridge model was not investigated in this study. Thus, it is recommended that bridge models with different skew angles should be investigated.

7.2 Findings and Conclusions from the Numerical Study

7.2.1 Introduction

The numerical study presented herein was carried out in the Civil Engineering Computer Aided Design Laboratory at Lawrence Technological University and included generating and analyzing thirty-three extensive FE models for side-by-side box-beam bridges with spans of 50, 62, 100, and 124 ft and widths of 24, 45, 58, 70, and 78 ft. The FE study resulted in new recommendations for MDOT Specifications for the TPT arrangements for side-by-side box-beam bridges. The current specifications for TPT arrangements (MDOT Bridge Design Guide, 2006) were shown to be inadequate. All the FE bridge models with TPT arrangements following the current specifications experienced longitudinal deck slab cracking over the shear-key joints. It should be noted that the conclusions of this study is independent of the configuration of the shear-key and the TPT force was assumed to be applied in two stages: before and after pouring the deck slab. A summary of the results and recommendations are presented as follows:

1. With current layout of the TPT arrangements within the box-beams in side-by-side box-beam bridges, the AASHTO LRFD (2004) recommendation of 250 psi as minimum transverse prestress required throughout longitudinal joints in side-by-side box-beam bridges is impractical and unreachable. The stress level can be attained at the diaphragms. However, it can not be attained between the diaphragms.

2. Contrary to the findings of some previous studies (i.e. El-Remaily et al., 1996), live loads are not the major cause for developing longitudinal cracks in the slab.

3. The contributing factor of the positive temperature gradient, which had not been investigated in any of the previous studies, is the major contributing factor in the development of the longitudinal cracks in deck slabs of side-by-side box-beam bridges. When the bridge is exposed to a positive temperature gradient, the deck slab experiences compressive stresses in the longitudinal and transverse directions. However, the cracks do not develop because of the thermal stresses in the deck slab; instead, the cracks develop because of the relative movements of the box-beams when exposed to positive temperature gradient. The box-beams tend to separate from each other. This separation generates high tensile stresses in the deck slab bottom surface and consequently develops longitudinal cracks. This phenomenon is in agreement with observations made by Miller et al. (1999) when they conducted their experimental program to investigate the shear-key cracking problem in side-by-side box-beams bridges.

4. The positive temperature gradient combined with live loads develop longitudinal cracks in the deck slab if an adequate TPT arrangement is not provided. Thus, the design baseline for TPT arrangement is to ensure that maximum principal stresses developed in the deck slab when subjected to positive temperature gradient with live loads and Impact allowances are less than the cracking strength of the concrete.

5. Impact allowance of 75% recommended by AASHTO LRFD (2004) for the design of the transverse deck joints is appropriate for the design of the longitudinal joints as well.

6. The AASHTO LRFD (2004) should be updated to include the proper effect of the temperature gradient in the design of side-by-side box-beam bridge components.

7.2.2 Adequate Number of Diaphragms

Based on the analysis of 24 ft wide side-by-side box-beam bridge models of spans of 50, 62, 100, and 124 ft, using box-beams of widths of 36 and 48 in., the following conclusions are drawn:

1. The number of diaphragms specified in the MDOT Bridge Design Guide (2006) is not adequate to eliminate the longitudinal cracks in the deck slab over the shear-key joints.
2. In order to eliminate the longitudinal deck slab cracks in bridges constructed using side-by-side box-beams of a width of 48 in., the recommended number of diaphragms should be provided based on the bridge span as presented in Figure 4.2-41 Adequate number of diaphragms for bridges constructed using 48 in. wide beams.The Figure presents the *minimum* number of diaphragms required to prevent the longitudinal cracks. However, the research team recommends using one additional diaphragm over the minimum number to account for any unpredictable loads or concrete deterioration. The diaphragms should be equally spaced along the entire bridge span.
3. In the case of 36 in. wide side-by-side box-beams bridges, the number of diaphragms should be provided according to Figure 4.2-42. This Figure presents the *minimum* number of diaphragms required to prevent the longitudinal cracks.
4. Each number of diaphragms obtained from Figure 4.2-41 or Figure 4.2-42 is applicable for all bridges having the corresponding span regardless of their widths. However, to adjust for the effect of increasing the bridge width on the transverse tensile stresses, the TPT force should be adjusted as presented in the following section.

7.2.3 Appropriate TPT Force

The FE models for bridges of widths of 24, 45, 58, 70, and 78 ft and spans of 50, 62, and 100 ft were analyzed to investigate the influence of the bridge width on the proper level of the TPT force. The models in this phase of the analysis were provided with the minimum number of diaphragms as concluded from the preceding analysis phase using 24 ft wide bridges. Three classes of the deck slabs were investigated in the analysis; 1) deteriorated deck slabs (concrete of strength of 3,000 psi), 2) recently constructed deck slabs (concrete strength of 4,000 psi), and 3) higher strength deck slabs (concrete strength of 5,000 psi). The results can be summarized as follows:

1. The current TPT force recommended by MDOT Bridge Design Guide (2006) is not adequate in reducing and delaying the development of longitudinal cracks in the deck slab.

2. The TPT force per diaphragm is independent of the bridge span because the number of diaphragms increases with increasing the bridge span.
3. The analysis of the models composed of 48 in. wide box-beams and those composed of 36 in. wide box-beams yielded the same results for the appropriate level of the TPT force. In other words, the appropriate level of TPT force for a certain bridge width is independent of the width of an individual box-beam.
4. The appropriate level of the TPT force increases when increasing the bridge width and slightly decreases when increasing the concrete strength of the deck slab. The appropriate level of TPT force can be obtained from Figure 4.3-13.

REFERENCES

AASHTO (1996, 1998, 2004). "LRFD Bridge Design Specifications", American Association of State Highways and Transportation Officials, Washington D.C.

Abendroth, R. E., and Greimann L. F. (1989). "A Rational Design Approach for Integral-Abutment Bridge Piles", *Journal of the Transportation Research Board*, Transportation Research Record, 1223, pp. 12-23.

ACI Committee (2005). "Building Code Requirements for Structural Concrete (ACI 318-05) and Commentary (ACI 318R-05)", American Concrete Institute, Farmington Hills, Michigan.

Aktan, H., Ahlborn T. M., and Attanayaka U. (2004). "Condition Assessment and Methods of Abatement of Prestressed Concrete Box-Beam Deterioration", *First Quarterly Report*, Michigan Department of Transportation.

ASTM Standard (1997). "Annual Book of ASTM Standards", American Society for Testing Materials, Vol. 04. 02, ASTM International, West Conshohocken, PA.

Badwan, I., and Liang R. Y. (2007). "Transverse Post-Tensioning Design of Precast Concrete Multibeam Deck", *Prestressed Concrete Institute Journal*, 52 (4), pp. 84-92.

Bakht, B., Jaeger L. G., and Cheung M. S. (1983). "Transverse Shear in Multibeam Bridges", *Journal of Structural Engineering*, ASCE, 109 (4), pp. 936-949.

Bakis, C. E., Bank L. C., Brown V. L., Cosenza E., Davalos J. F., Lesko J. J., Machida A., Rizkalla S. H., and Triantafillou, T. C. (2002). "Fiber-Reinforced Polymer Composites for Construction State-of-the-Art Review", *Journal of Composites for Construction*, ASCE, 6 (2), pp. 73-87.

Barr, P. J., Eberhard M. O., and Stanton J. F. (2001). "Live-Load Distribution Factors in Prestressed Concrete Girder Bridges", *Journal of Bridge Engineering*, ASCE, 6 (5), pp. 298-306.

Bebawy, M. R. (2007). "Optimum Transverse Post-Tensioning Arrangement for Side-By-Side Box-Beam Bridges" M.Sc. Thesis, Lawrence Technological University, Michigan.

Bishara, A. G., Chuan-Liu M., and El-Ali N. D. (1993). "Wheel Load Distribution on Simply Supported Skew I-Beam Composite Bridges", *Journal of Structural Engineering*, ASCE, 119 (2), 399-419.

Braimah, A., Green M. F., and Soudki K. A. (1998). "Polypropylene FRC Bridge Deck slabs Transversely Prestressed with CFRP Tendons", *Journal of Composites for Construction*, ASCE, 2 (4), pp. 149-157.

Cai (2005). "Discussion on AASHTO LRFD Load Distribution Factors for Slab-on-Girder Bridges", Practice Periodical on Structural Design and Construction, ASCE, 10(3), pp. 171-176.

Cai, C. S., and Shahawy M. (2004). "Predicted and Measured Performance of Prestressed Concrete Bridges", *Journal of Bridge Engineering*, ASCE, 9 (1), pp. 4-13.

Chamberlain, C. M., and Kreger M. E. (1999). "Evaluation of Longitudinal Cracking in End Regions of Pre-tensioned Box-Beams", Project Report 96-0456, Texas Department of Transportation.

Csagoly, P. F. (1997). "Testing of a Composite Steel-Concrete Bridge Deck", *Concrete International*, 19 (2), pp. 47-53.

Ebeido, T., and Kennedy, J. B. (1996a). "Girder Moments in Continuous Skew Composite Bridges", *Journal of Bridge Engineering*, 1 (1), pp. 37-45.

Ebeido, T., and Kennedy, J. B. (1996b). "Shear and Reaction Distributions in Continuous Skew Composite Bridges", *Journal of Bridge Engineering*, 1 (4), pp. 155-165.

El-Ali, N. D. (1986). "Evaluation of Internal Forces in Skew Multistringer Simply Supported Steel Bridges", PhD Thesis, Ohio State University, Columbus, Ohio.

El-Esnawi, H. H., (1996). "Evaluation of Improved Shear-Key Designs for Multi-Beam Prestressed Concrete Box Girder Bridges", PhD Thesis, Case Western Reserve University, Cleveland, Ohio.

El-Remaily, A., Tadros M. K., Yamane T., and Krause G. (1996). "Transverse Design of Adjacent Precast Prestressed Concrete Box Girder Bridges", *Prestressed Concrete Institute Journal*, 41 (1), pp. 96-107.

Grace, N. F.; Jensen, E.; Till, R.; and Bebawy, M. R. (2007). "Optimal Transverse Post-tensioning Arrangement for Side-by-Side Box Beam Bridges, Part-I," *ACI Journal*, Submitted.

Grace, N. F. (2000). "Response of Continuous CFRP Prestressed Concrete Bridges Under Static and Repeated Loadings", *Prestressed Concrete Institute Journal*, November-December, pp. 84-102.

Grace, N. F., Nacey, R. B., Roller, J. J., Bonus, W., and Navarre, F. C. (2005). "Truck Load Distribution Behavior of the Bridge Street Bridge, Southfield, Michigan", *Prestressed Concrete Institute Journal*, pp. 76-89.

Grace, N. F., and Abdel-Sayed G. (1998). "Behavior of Externally Draped CFRP Tendons in Prestressed Concrete Bridges", *Prestressed Concrete Institute Journal*, pp. 88-101.

Grace, N. F., Navarre F. C., Nacey R. B., Bonus W., and Collavino L. (2002). "Design-Construction of Bridge Street Bridge - First CFRP Bridge in United States", *Prestressed Concrete Institute Journal*, 47 (5), pp. 20-35.

Green, T., Yazdani N., and Spainhour L. (2004). "Contribution of Intermediate Diaphragms in Enhancing Precast Bridge Girder Performance", *Journal of Performance of Constructed Facilities*, ASCE, 18 (3), pp. 142-146.

Greuel, A., Baseheart, T. M., Rogers, B. T., Miller, R. A., and Shahrooz, B. M. (2000). Evaluation of a high performance concrete box girder bridge, *Prestressed Concrete International Journal*, 45 (6), pp. 60-71.

Gulyas, R. J., Wirthlin G. J., and Champa J. T. (1995). "Evaluation of Keyway Grout Test Methods for Precast Concrete Bridges", *Prestressed Concrete International Journal*, 40 (1), pp. 44-57.

Hlavacs, G. M., Long, T., Miller, R. A., and Baseheart, T. M. (1996). "Nondestructive Determination of Response of Shear-Keys to Environmental and Structural Cyclic Loading", *Transportation Research Record*, 1574, pp. 18-24.

Huang, H., Shenton H. W., and Chajes M. J. (2004). "Load Distribution for a Highly Skewed Bridge: Testing and Analysis", *Journal of Bridge Engineering*, ASCE, 9 (6), pp. 558-562.

Huckelbridge, A. A. (1996). "Evaluation of Improved Shear-Key Designs for Multi-Beam Prestressed Concrete Box Girder Bridges", Final Report to ODOT/ FHWA, Research Contract No. 7679.

Huckelbridge, A. A., El-Esnawi H., and Moses F. (1995). "Shear-Key Performance in Multibeam Box Girder Bridges", *Journal of Performance of Constructed Facilities*, ASCE, 9 (4), pp. 271-285.

Issa, M. A., Yousif, A. A., Issa, M. A., Kaspar, I. I., Khayyat, S. Y. (1998). "Analysis of Full Depth Precast Concrete Bridge Deck Panels", *Prestressed Concrete Institute Journal*, 43 (1), pp. 74-85.

Issa, M. A., Ribeiro Do Valle, C. L., Abdalla, H. A., Islam, S., and Issa, M. A. (2003). "Performance of Transverse Joint Grout Materials in Full-Depth Precast Concrete Bridge Deck Systems", *Prestressed Concrete Institute Journal*, 48 (4), pp. 92-103.

Jones, H. L., and Boaz I. B. (1986). "Skewed Discretely Connected Multi-Beam Bridges", *Journal of Structural Engineering*, ASCE, 112 (2), pp. 257-272.

Kaneko, Y., Connor J. J., Triantafillou T. C., and Leung, C. K. (1993a). "Fracture Mechanics Approach for Failure of Concrete Shear-Key I: Theory", *Journal of Engineering Mechanics*, ASCE, 119 (4), pp. 681-700.

Kaneko, Y., Connor J. J., Triantafillou T. C., and Leung, C. K. (1993b). "Fracture Mechanics Approach for Failure of Concrete Shear-Key II: Verification", *Journal of Engineering Mechanics*, ASCE, 119 (4), pp. 701-719.

Khaloo, A. R., and Mirzabozorg, H. (2003). "Load Distribution Factors in Simply Supported Skew Bridges", *Journal of Bridge Engineering*, ASCE, 8 (4), pp. 241-244.

Klaiber, F. W., Wipf, T. J., Nahra, M. J., Ingersoll, J. S., Sardo, A. G., and Qin X. (2001). "Field and Laboratory Evaluation of Precast Concrete Bridges", The Iowa Department of Transportation, Highway Division and the Iowa Highway Research Board. Project TR-440.

Labib, M. L. (2007). "Effect Of Transverse Post-Tensioning on Load Distribution in Side-By-Side CFRP Prestressed Concrete Box Beam Bridges" M.Sc. Thesis, Lawrence Technological University, Michigan.

Lall, J., Alampalli S., and DiCocco E. F. (1998). "Performance of Full-Depth Shear-Keys in Adjacent Prestressed Box-Beam Bridges", *Prestressed Concrete Institute Journal*, 43 (2), pp. 72-79.

MacGregor, J. G., and Wight J. K. (2004). "Reinforced Concrete: Mechanics and Design", 4th Edition, Prentice Hall, ISBN 0-13-142994-9.

Marshe, S., and Green M. F. (1999). "Punching Behavior of Composite Bridge Decks Transversely Prestressed with Carbon Fiber Reinforced Polymer Tendons", *Canadian Journal of Civil Engineering*, 26 (5), 618-630.

Mahmoud, Z. I., Rizalla S. H., and Zaghloul E. R. (1999). "Transfer and Development Lengths of Carbon Fiber Reinforced Polymers Prestressing Reinforcement." *ACI Structural Journal*, 96 (4), pp. 594-602.

MDOT Design Manual (6.65.10A, 6.65.12, 6.65.13, and 7.02.18.B.6). (2006). "Prestressed Concrete Box-Beam and Post-Tensioning Details", Michigan Department of Transportation, Bureau of Highway Development, Michigan.

Miller, R. A., Hlavacs G. M., Long T., and Greuel A. (1999). "Full-Scale Testing of Shear-Keys for Adjacent Box Girder Bridges", *Prestressed Concrete Institute Journal*, 44 (6), pp. 80-90.

Miller, R. A., Weisgerber F. E., Zhang W., Dong X., Greuel A., and Long T. (1999). "Evaluation of the Cause of Cracking in Bridge # MEG - 124 - 6.78", Report No. FHWA/OH-99-014, Ohio Department of Transportation.

Moll, E. L. (1984). "Investigation of Transverse Stressing in Bridge Decks", M.Sc. Thesis, Department of Civil Engineering, McMaster University, Hamilton, Ontario, Canada.

Naaman, A. E. (2004). "Prestressed Concrete Analysis and Design", 2th Edition, Techno Press 3000, Ann Arbor, MI 48075, ISBN 0-9674939-1-9.

Nawy, E. G. (2003). "Prestressed Concrete. A Fundamental Approach", 4th Edition, Prentice Hall, Upper Saddle River, NJ 07458, ISBN 0-13-008391-7.

PCI (2003). "PCI Design Handbook", Precast/Prestressed Concrete Institute, 5th Edition, Chicago, Illinois.

Phipps, A. R., Almustafa R. A., Ralls M. L., Poston R. W., Breen J. E., and Carrasquillo R. L. (1985). "Structural Effects of Transverse Prestressing in Bridge Decks", Report No. FHWA/ TX-86/ 40-316-2, Texas State Department of Highways and Public Transportation.

Poston, R. W., Breen J. E., and Carrasquillo R. L. (1989). "Design of Transversely Prestressed Concrete Bridge Decks", *Prestressed Concrete International Journal*, 34 (5), 68-109.

Poston, R. W., Phipps A. R., Breen J. E., and Carrasquillo R. L. (1985). "Design Procedures for Prestressed Concrete Bridge Decks", Research Report 316-3F, Center for Transportation Research, University of Texas at Austin.

Ramey G. E., and Wright R. L. (1997a). "Bridge Deterioration Rates and Durability/Longevity Performance", *Practice Periodical on Structural Design and Construction*, 2 (3), pp. 98-104.

Ramey G. E., and Wright R. L. (1997b). "Results of Bridge Durability/Longevity Survey", *Practice Periodical on Structural Design and Construction*, 2 (3), pp. 105-117.

Ramey G. E., Wolff A. R., and Wright R. L. (1997a). "Structural Design Actions to Mitigate Bridge Deck Cracking", *Practice Periodical on Structural Design and Construction*, 2 (3), pp. 118-124.

Ramey G. E., Wolff A. R., and Wright R. L. (1997b). "DOT Management Actions to Enhance Bridge Durability/Longevity", *Practice Periodical on Structural Design and Construction*, 2 (3), pp. 125-130.

Roschke, P. N., and Pruski K. R. (2000). "Post-Tensioned Slab Bridge with Banded Transverse Tendons", *ACI Structural Journal*, American Concrete Institute, 97 (1), pp. 3-10.

Sithichaikasem, S., and Gamble W. L. (1972). "Effects of Diaphragms in Bridges with Prestressed Concrete I-Section Girders", Civil Engineering Studies, Structural Research Series No. 383, Department of Civil Engineering, University of Illinois, Urbana.

Stanton, J. F., and Mattock, A. H. (1986). "Load Distribution and Connection Design for Precast Stemmed Multi-Beam Bridge Superstructures", Transportation Research Board, Report No. 287, Washington, D.C.

Taly, N. (1998). "Design of Modern Highway Bridges", McGraw Hill Companies, Inc., New York, USA, pp. 382-487.

Thoman, S. J., Redfield C. M., and Hollenbeck R. E. (1984). "Load Test of Single-Cell Box Girder Bridge Cantilever Deck", *Journal of Structural Engineering*, ASCE, 110 (8), pp. 1773-1785.

Tokyo Rope. (1993). "Technical Data on CFCC." Tokyo Rope Mfg. Co. Ltd., Japan.

Yamane, T., Tadros M. K., Badie S. S., and Baishya M. C. (1998). "Full Depth Precast Prestressed Concrete Bridge Deck System", *Prestressed Concrete Institute Journal*, 43 (3), pp. 50-66.

Zou, P. X. W. (2003). "Long-Term Properties and Transfer Length of Fiber-Reinforced Polymers", *Journal of Composites for Construction*, ASCE, 7 (1), pp. 10-19.

APPENDIX A: TRANSFER LENGTHS, PRE-TENSIONING FORCES, AND DIFFERENTIAL CAMBER MONITORING

A.1 Introduction

The results related to the construction phase are presented in Appendix A. The appendix is divided into three sections. The first section involves a continous monitoring of the pre-tensioning forces in the four box-beams. The second demonstrates the transfer length of the pre-tensioning forces at the end-blocks. The continuous monitoring of the camber for the four individual box-beams is presented in the third section.

A.2 Monitoring Pre-Tensioning Forces During the Curing of Concrete

The pre-tensioning forces in the steel strands were monitored continuously during the first three days of curing the concrete to study the effect of the curing on the levels of pre-tensioning forces. As mentioned in Chapter 5, the two exterior box-beams had average pre-tensioning force of 20.6 kip/strand while, the interior box-beams had average pre-tensioning force of 25 kip/strand. The levels of pre-tensioning forces were measured for each pre-tensioning strand using the center-hole load cells attached to the dead-end between the face of the bulkhead and the sleeve. Figure A-1 shows the variation in the average pre-tensioning forces during the curing period of the four box-beams. For all strands, the levels of pre-tensioning forces decreased gradually to reach their minimum level after approximately 17 hours from the end of casting the box-beams. The reduction of the pre-tensioning forces could be attributed to the thermal effects of the hydration process, which led to a volumetric expansion in the concrete and elongation of the steel strands. The elongated steel strands counteracted the pressure on the load cells by reducing the reactive forces on the bulkhead. However, the thermal and shrinkage contraction of the concrete during the subsequent hydration led to close to complete recovery of the pre-tensioning forces. The difference between the average pre-tensioning forces for the exterior and the interior box-beams was 3.91 kip at the age of three days.

The pre-tensioning forces recorded at the time of casting (initial levels of pre-tensioning forces) for the exterior beams were 21.69, 20.26, and 20.47 kip for box-beam B-1 and 20.83, 20.64, and 21.57 kip for box-beam B-4. The minimum levels of pre-tensioning forces obtained after 17 hours were 20.33, 18.65, and 19.05 kip for box-beam B-1 with a reduction of 6%, 8%,

and 7% of the initial levels of the pre-tensioning forces. Also, the minimum levels of pre-tensioning forces obtained after 17 hours were 19.01, 19.39, and 20.24 kip for box-beam B-4 with a reduction of approximately 9%, 6%, and 6% of the initial levels of the pre-tensioning forces. The levels of pre-tensioning forces after three days were 21.64, 19.98, and 20.15 kip for box-beam B-1, which represent 100%, 99%, and 98% of the initial levels of the pre-tensioning forces. In addition, the levels of pre-tensioning forces after three days were 20.61, 20.51, and 21.39 kip for box-beam B-4, which represent approximately 99%, 99%, and 100% of the initial levels of the pre-tensioning forces.

For the interior box-beams, the initial pre-tensioning forces were 25.78, 24.82, and 25.02 kip for box-beam B-2, and 25.07, 24.43, and 25.37 kip for box-beam B-3. The minimum levels of pre-tensioning forces after 17 hours were 24.20, 23.50, and 23.00 kip for box-beam B-2 with a reduction of approximately 6%, 5%, and 8% of the initial levels of the pre-tensioning forces. Also, the minimum levels of pre-tensioning forces after 17 hours were 23.65, 22.86, and 23.90 kip for box-beam B-3 with a reduction of 6%, 6% and 6% of the initial levels of the pre-tensioning forces. The levels of pre-tensioning forces after three days were 25.46, 24.43, and 24.33 kip for box-beam B-2, which represent approximately 99%, 98%, and 97% of the initial levels of the pre-tensioning forces. In addition, the levels of pre-tensioning forces after three days were 24.76, 24.02, and 24.74 kip for box-beam B-3, which represent 99%, 98%, and 98% of the initial levels of the pre-tensioning forces.

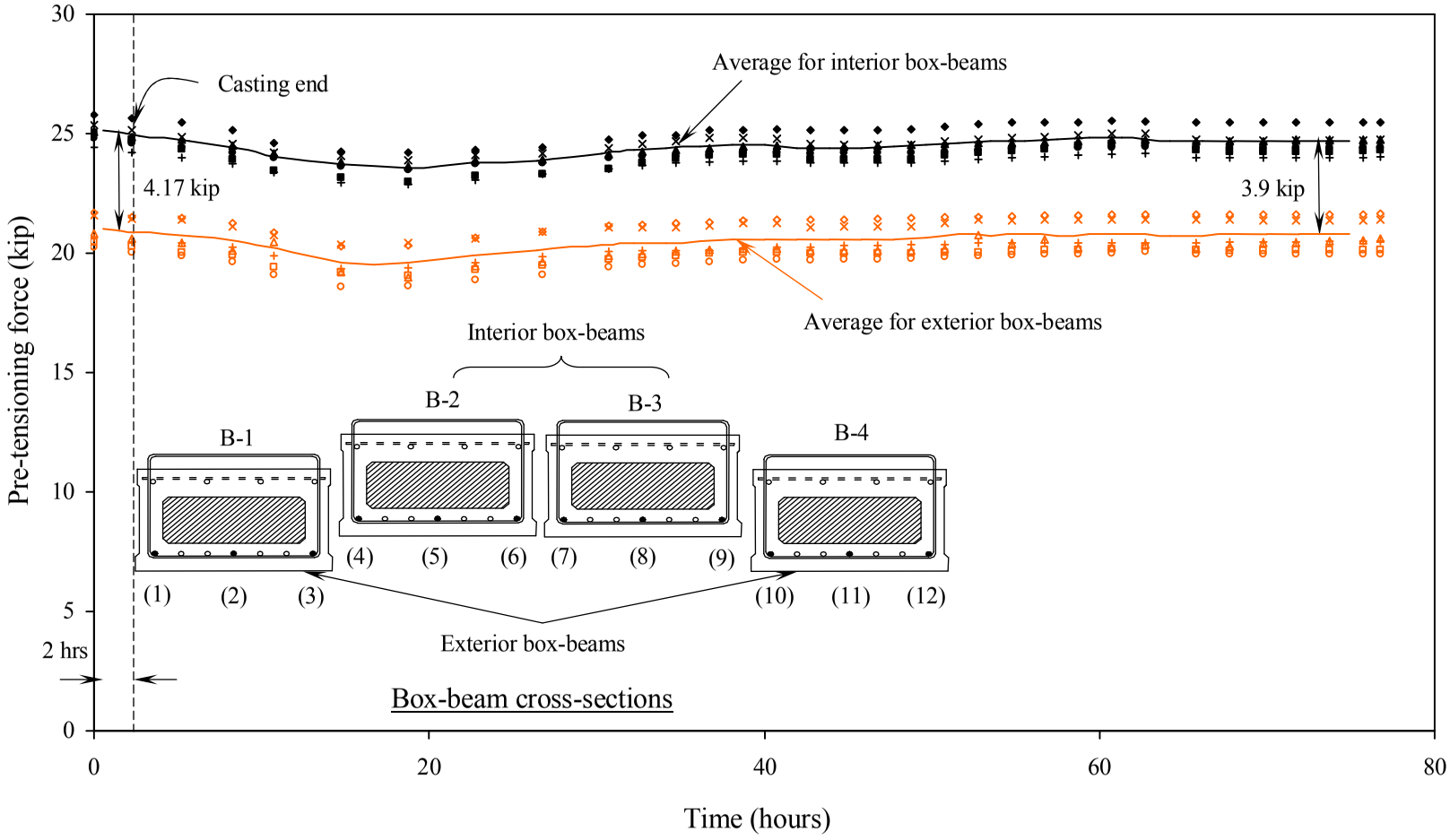

Figure A-1 Pre-tensioning forces in the steel strands for the exterior and the interior box-beams.

A.3 Transfer Length Evaluation

Transfer length (L_t) is defined as the length over which the applied prestressing force is transferred completely to the concrete (Mahmoud et al., 1999). In order to measure the transfer lengths in this bridge model, the demountable mechanical (DEMEC) points were installed on one side of the live and the dead-ends of the interior beams B-2 and B-3 along the location of the pre-tensioning strands, as shown in Figure A-2. Measurements between the successive DEMEC points were taken before and after the applied pre-tensioning force were released by cutting the prestressed steel strands. The computed compressive strains were plotted against the bridge span, as shown in Figure B-3 and B-4.

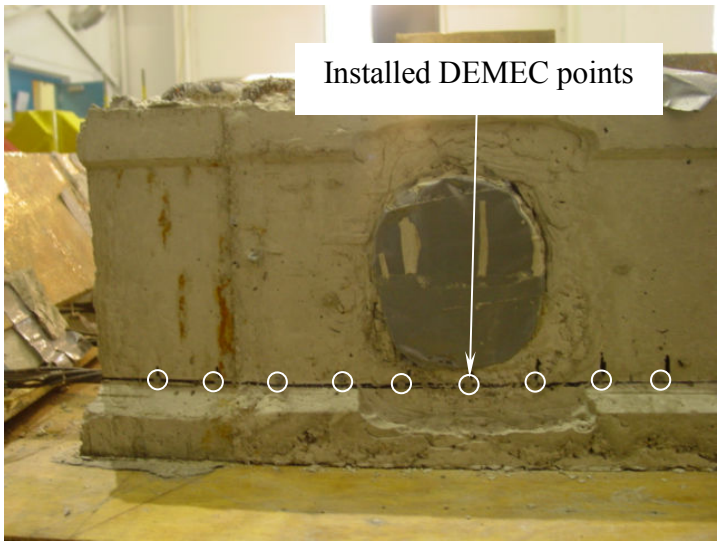

Figure A-2 Installation of DEMEC point at the live-end of beam B-2.

The transfer lengths were determined by using the 95% average maximum strain method which involved plotting a horizontal line at 95% of the maximum strain exerted by the prestressed strands on the concrete. The point of intercept between the horizontal line and the plotted measured strains represents the transfer length. Furthermore, the measured transfer lengths were compared with the theoretical using the following empirical equations.

$$L_t = \left(\frac{f_{se}}{3{,}000}\right) d_b \qquad \text{in inches (ACI 318, 2005)} \qquad \text{(A.1)}$$

where f_{se} is the prestress at transfer (psi) and d_b is the nominal diameter of the steel strand (in.).

$$L_t = \frac{480\, d_b}{\sqrt{f'_{ci}}} \qquad \text{in mm (Zou, 2003)} \qquad \text{(A.2)}$$

$$L_t = \frac{f_{pi} d_b}{\alpha_t f'^{\,0.67}_{ci}} \qquad \text{in mm (Mahmoud et al., 1999)} \qquad \text{(A.3)}$$

where f_{pi} is the prestress at transfer (MPa), d_b is the nominal diameter of the strand (mm), and α_t is transfer length coefficient (α_t = 2.4, for steel strands) and f'_{ci} is the concrete compressive strength at transfer (MPa).

The transfer lengths at the live and dead-ends of beam B-2 were 20 in. and 21 in., respectively. However, the beam B-3 resulted in a slightly higher transfer length relative to B-2 with 23 in. and 22 in. at the dead and live-ends, respectively, as shown in Figure A-4. A good conformity was observed between the values of transfer length at the live and dead-end for both beams which depicts the fact that the prestressed forces were effectively transferred equally at both ends of the beams.

The average values between the dead and live-ends obtained during the experimental transfer length were compared with the theoretical values, as shown in Table A-1. The transfer length determined by using the equation proposed by American Concrete Institute (ACI-318, 2005) and Zou et al. (2003) overestimated the transfer length by about 20 to 50%. However, good agreement was obtained with the transfer length predicted by the equation proposed by Mahmoud et al. (1999).

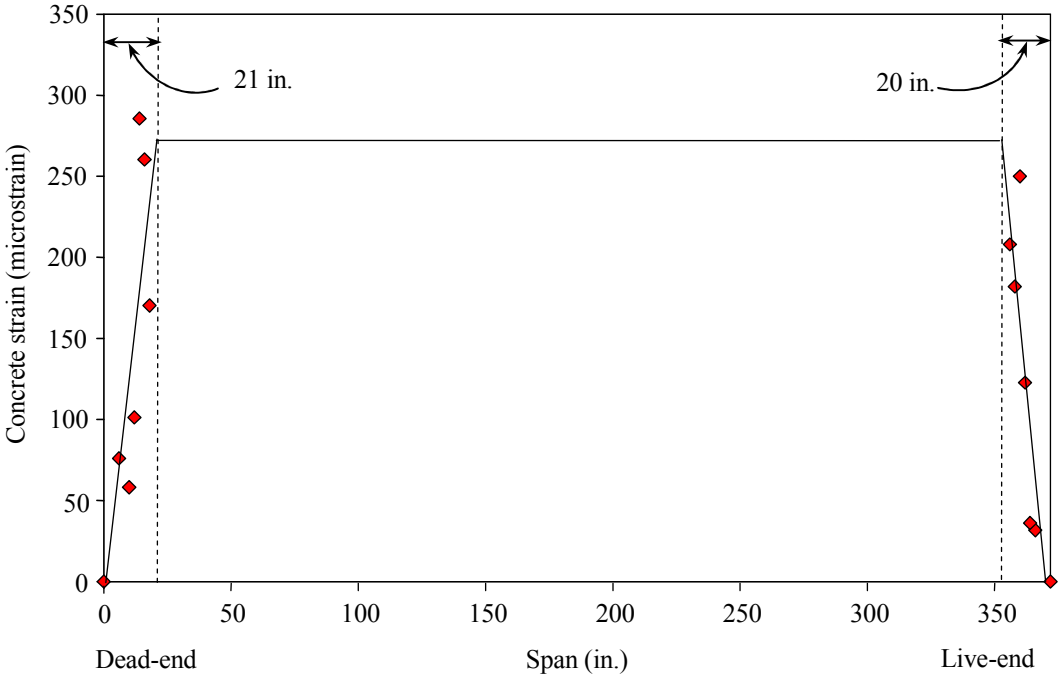

Figure A-3 Transfer length determination for beam B-2.

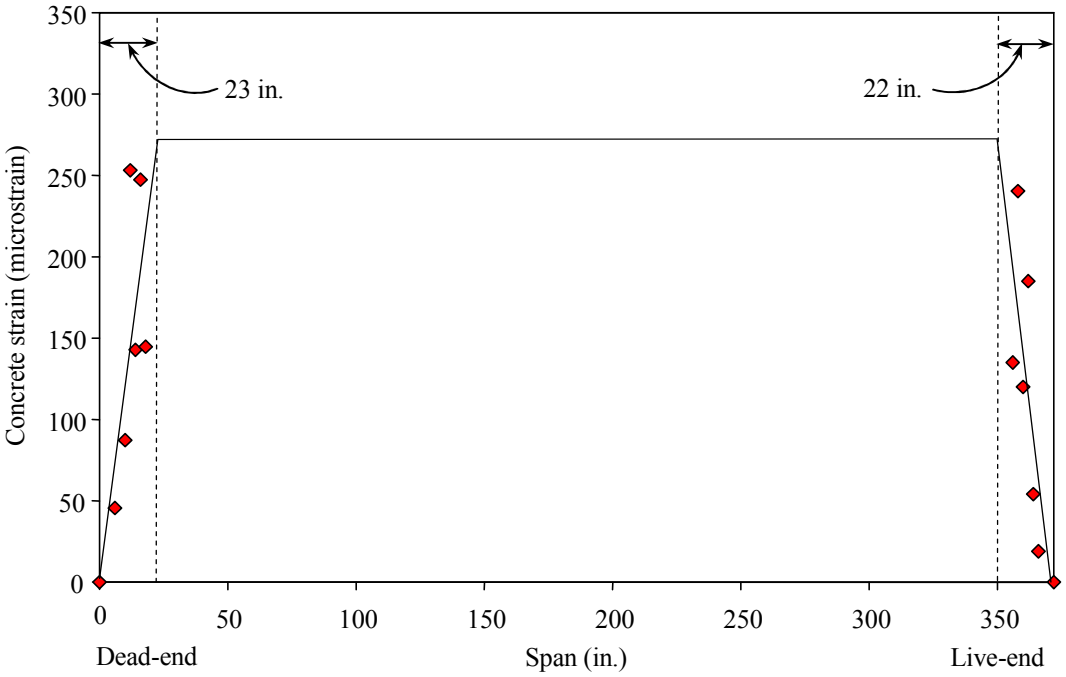

Figure A-4 Transfer length determination for beam B-3.

Table A-1 Transfer length of pre-tensioning steel strands of the box-beam bridge model.

Box-Beam	Average Prestress, ksi	Concrete Strength at Transfer, ksi	Measured Transfer Length, in.			Calculated Transfer Length, in.		
			Live-End	Dead-End	Average	Eq. (A.1) (ACI 318, 2005)	Eq. (A.2) (Zou, 2003)	Eq. (A.3) (Mahmoud, 1999)
B-2	130	6.1	20	2	20.5	27.2	37.1	19.2
B-3	130	6.1	22	23	22.5	27.2	37.1	19.2

A.4 Monitoring of Differential Camber

Camber is the upward deflection that results from applying eccentric pre-tensioning forces below the center of gravity of the cross-section in prestressed concrete beams. Cambers for identical beams casted on the same day with the same conditions may vary according to different factors such as exposure to air and humidity and/or the non-homogenous behavior of the concrete. Long-term camber is affected primarily by relaxation of steel strands, which leads to change in the levels of pre-tensioning forces and/or creep of concrete, which leads to change in deflections due to sustained loads. Unlike long-term camber, short-term camber does not change significantly.

One of the major objectives of the project was to study the adequacy of using oval- shape ducts that accommodates two TPT CFCC to adopt the uneven differential cambers between adjacent box-beams. In order to study that, different levels of pre-tensioning forces were applied to create different levels of cambers among the individual box-beams. In particular, the two exterior box-beams B-1 and B-4 were prestressed with an average pre-tensioning force of 60 kip/beam; while the two interior box-beams B-2 and B-3 were prestressed with an average pre-tensioning force of 75 kip/box-beam. The camber was monitored continuously over a period of 24 days for the individual box-beams and the values are plotted with time, as shown in Figure A-5.

In this study, the initial camber refers to the cambers measured directly after placing the individual box-beams on the supports (the cambers at the beginning of the monitoring period). The final camber refers to the cambers measured after 24 days from placing the individual box-beams on the supports (the cambers at the end of the monitoring period). From the results, the initial cambers developed in the exterior box-beams B-1 and B-4 were 0.23 and 0.16 in., respectively. However, the initial cambers developed for interior box-beams B-2 and B-3 were 0.48 and 0.53 in., respectively. The previous variation in the values of the cambers show clearly that the cambers for identical prestressed concrete beams may vary significantly. The average initial differential camber developed between exterior and interior box-beams was 0.31 in.

A superimposed dead load of 1,000 lb was added on each of the two exterior box-beams for one week in order to increase the average differential camber between the exterior and the interior box-beams. The cambers were monitored and the effect of the applied superimposed

dead loads on the cambers was evaluated. After one week, the superimposed dead loads were removed from the two exterior box-beams and the cambers were monitored further for two weeks.

In order to describe the camber-time relationship in details, seven points in time were selected to define the camber profiles for the exterior box-beams as follows.

1. Point A: Initial camber developed for each box-beam due to the effect of pre-tensioning forces and self-weight of the beam.
2. Point B: Camber after 0.6 days (15 hours) from the initial camber, just before adding the superimposed dead loads.
3. Point C: Camber after 0.66 days (15.84 hours) from the initial camber, immediately after adding the superimposed dead loads.
4. Point D: Camber after 6.8 days (163 hours) from the initial camber, just before removing the superimposed dead loads.
5. Point E: Camber after 6.9 days (166 hours) from the initial camber, immediately after removing the superimposed dead loads, at which the deflection due to the superimposed dead loads was partially recovered.
6. Point F: Camber after 9.2 days (220 hours) and 10.2 days (245 hours) from the initial camber for beams B-1 and B-4, respectively, at which the deflection due to the superimposed dead loads was totally recovered and the variation of the camber became approximately negligible.
7. Point G: Cambers after 24 days (576 hours) from the initial camber (final camber), the last point at the end of the monitoring period.

A.4.1 Exterior Box-Beams B-1 and B-4

The initial camber for the exterior box-beam B-1 was 0.23 in. Before adding the superimposed dead load, the camber decreased with relatively small rate of 0.005 in./day. The superimposed dead load was removed from the exterior beam B-1 after one week. A rapid decrease in the camber occurred after adding the superimposed dead load at a steep rate of 3.05 in./day. The rate of reduction in camber became approximately twice the initial one (-0.009 in./day). When the superimposed dead load was removed, a rapid increase in camber occurred with rate of 1.635 in./day. Only 60% of the total displacement was recovered immediately after removing

the superimposed dead load. The remaining 40% of the recovered displacement was achieved gradually through a period of 2.3 days (55 hours). The total recovered displacement was 0.113 in. and the total reduction in camber due to adding the superimposed dead loads was 0.128 in. The difference between the reduction in camber and the recovered camber is 0.015 in., which was 6.5% of the initial camber. That can be attributed to the effect of creep of the concrete under sustained superimposed dead load. After recovering all the displacement, the rate of reduction in camber was 0.002 in./day, which was close (slightly lower) to the initial rate of reduction in camber.

When the superimposed dead loads were placed on the exterior beams, the values of the reduced cambers were close (0.015 in. and 0.016 in. for beams B-1 and B-4, respectively). It clearly shows that, the reduction in the camber due to the superimposed dead load depended on the added load and/or the period of the addition of the load rather than the levels of the initial cambers.

A.4.2 Interior Beams B-2 and B-3

The camber was monitored for the interior box-beams continuously through 24 days. The interior beams experienced higher initial cambers than the exterior box-beams due to higher pre-tensioning forces. No superimposed dead loads were added on the interior box-beams. Therefore, the rate of change in camber was approximately constant and very small through the period of monitoring the cambers (e.g. -0.002 in./day and 0.001 in./day for beam B-2 and B-3, respectively).

A.4.3 Average and Differential Cambers

Figure A-5 shows the average cambers for exterior and interior box-beams. For the exterior box-beams, the average initial camber was 0.195 in., while the final camber after three weeks was 0.107 in. The reduction of the average camber due to creep of concrete under sustained superimposed dead loads and relaxation of steel strands with time was 0.088 in., which represented 45% from the initial camber. On the other hand, the average initial camber for the interior box-beams was 0.505 in., while the average final camber was 0.484 in. The reduction of the average camber for the interior box-beams due to creep of concrete and relaxation of steel was 4.16% only. This obviously shows the effect of creep of concrete under sustained

superimposed dead loads on the camber. The addition of superimposed dead loads on the exterior box-beams for one week increased the average differential camber between the exterior and the interior box-beams by 21.6%.

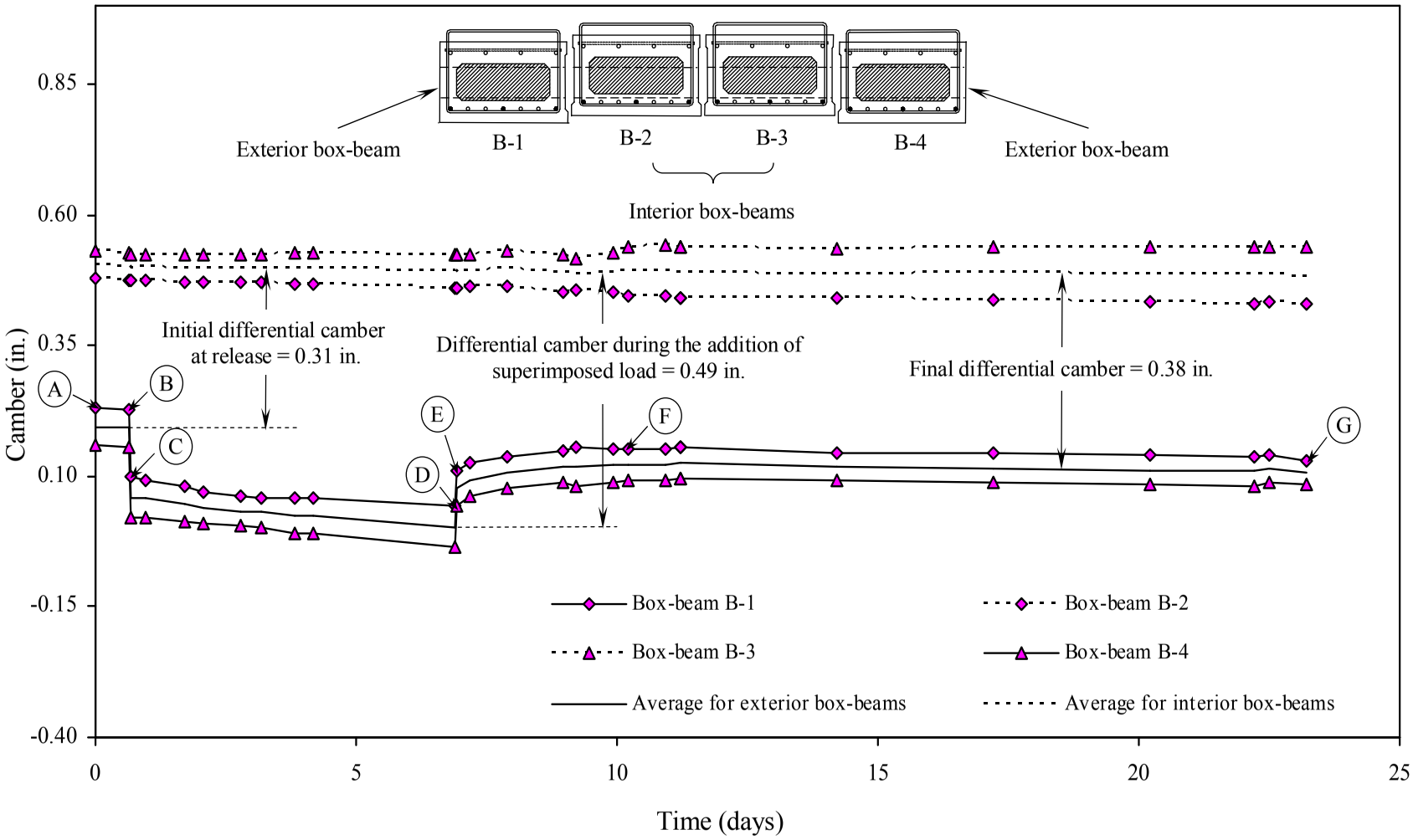

Figure A-5 Cambers for the exterior and the interior box-beams.

APPENDIX B: CRACKING OF DECK SLAB

B.1 Introduction

The bridge model was partially cracked at the shear-key joints between the adjacent box-beams. Additional structural boundary conditions were utilized to develop the required longitudinal cracks in the deck slab over the shear-keys. In general, these boundary conditions were based on applying a vertical load at the mid-span of one box-beam and partially supporting the other three beams from downward displacement and transverse rotation. This was to ensure that the difference in deflection (differential deflection) between the loaded beam and other box-beams would cause high shear stresses at the shear-key joints, and/or the rotation of the loaded beam would cause transverse moments that lead to the development of high transverse tensile stresses on the top surface of deck slab (extreme top fibers). The shear stresses developed at the shear-key joints caused partial shear failure while the transverse tensile stresses caused longitudinal cracks on the deck slab.

Cracking of the deck slab was carried out in three steps; each step was implemented in cracking one of the three longitudinal shear-keys A-A, B-B, and C-C. Two classes of cracks were initiated at this stage: shear-key cracks and other cracks. The shear-key cracks were the longitudinal cracks developed over the three shear-key locations, while the other cracks were the cracks developed on the top surface of deck slab at the locations of the application of the vertical load. In addition, cracking of the deck slab led to the development of transverse flexural cracks at the mid-span for the individual beams.

B.2 Cracking of Exterior Shear-Key C-C

The shear-key C-C was the first shear-key that was cracked in the bridge model. A vertical load was applied on the exterior box-beam B-4 and the other three box-beams were partially restrained from the vertical displacement and the transverse rotation using top and bottom steel supports, as shown in Figure B-1. A maximum vertical load of 89 kip was applied gradually at beam B-4 and the corresponding deflections for beams B-1, B-2, B-3, and B-4 were -0.17, 0.05, 0.3, and 0.6 in., respectively. Figure B-2 shows the deflections for the four box-beams

under different levels of the vertical load applied to beam B-3. It was noticed that beams B-4 and B-3 experienced downward displacement as well as transverse rotation, while beam B-2 experienced slight rotation only in the transverse direction. However, beam B-1 experienced upward displacement. This shows that the bridge model was rotating as a rigid structure around beam B-2 (maximum observed deflection for beam B-2 was 0.05 in.).

The shear-key cracks on axis C-C appeared first on the top surface of the deck slab near the supports and at mid-span. By increasing the vertical load, partial debonding between the shear-key and beam B-3 was observed starting from the bottom and propagating up towards the deck slab. The cracks on the top surface of deck slab propagated to cover approximately 75% of the entire length of the bridge and the maximum crack width observed on deck slab over the shear-key C-C during the loading of beam B-4 was 0.02 in. Figures B-3 and B-4 show the deformed shape of the bridge model due to the maximum vertical load and the cracks developed at the end of the shear-key C-C, respectively.

B.3 Cracking of Interior Shear-Key B-B

After cracking the exterior shear-key C-C, the interior shear-key B-B was cracked. The shear-key was cracked by applying the vertical load on the interior beam B-3 and partially restraining the other box-beams from the vertical displacement and the transverse rotation, as shown in Figure B-5. The exterior beam B-3 was loaded at the mid-span by a maximum vertical load of 123 kip. The cracks were developed due to the partial debonding between the shear-key and beam B-2. The behavior of the bridge model under different levels of vertical load applied to beam B-3 is shown in Figure B-6. By increasing the vertical load, the cracks propagated towards the top surface of deck slab. The deflections at the maximum applied vertical load (123 kip) for beams B-1, B-2, B-3, and B-4 were 0.06, 0.16, 0.23, and 0.12 in., respectively. The levels of deflection were relatively small compared to the applied vertical load. Figure B-7 shows the deformed shape of the bridge model due to applying the maximum load on beam B-3. The cracks reflected on the deck slab were approximately 60% of the entire length of the bridge model. The maximum crack width observed during loading beam B-3 was 0.013 in. Figure B-8 shows the cracks developed at the end of shear-key B-B.

B.4 Cracking of Exterior Shear-Key A-A

The exterior shear-key A-A was the last shear-key that was partially cracked. Similar procedure adopted in the preceding shear-keys (B-B and C-C) were followed to crack the shear-key A-A by applying the vertical load at beam B-1, and partially restraining the other three box-beams from the vertical displacement and the transverse rotation using top and bottom steel supports, as shown in Figure B-9. The maximum applied vertical load was 80 kip and the corresponding deflections for beams B-1, B-2, B-3, and B-4 were 0.28, 0.15, 0.06, and 0.02 in., respectively (see Figure B-10). The deformed shape of the bridge model under the applied vertical load on beam B-1 is shown in Figure B-11. Only 25% of the entire length of the bridge was cracked at that shear-key and no partial debonding of the shear-key was observed at either ends. The maximum cracks width observed over the shear-key A-A was 0.013 in.

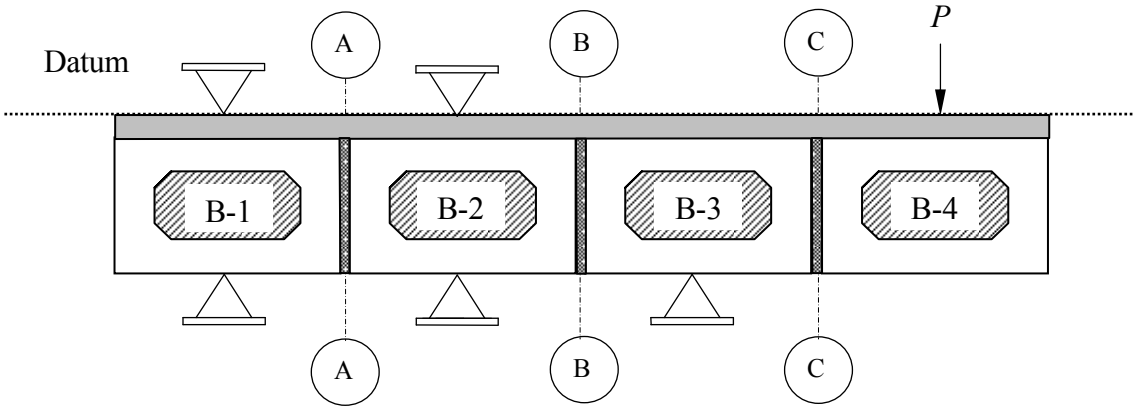

Figure B-1 Loading arrangements for cracking the exterior shear-key C-C.

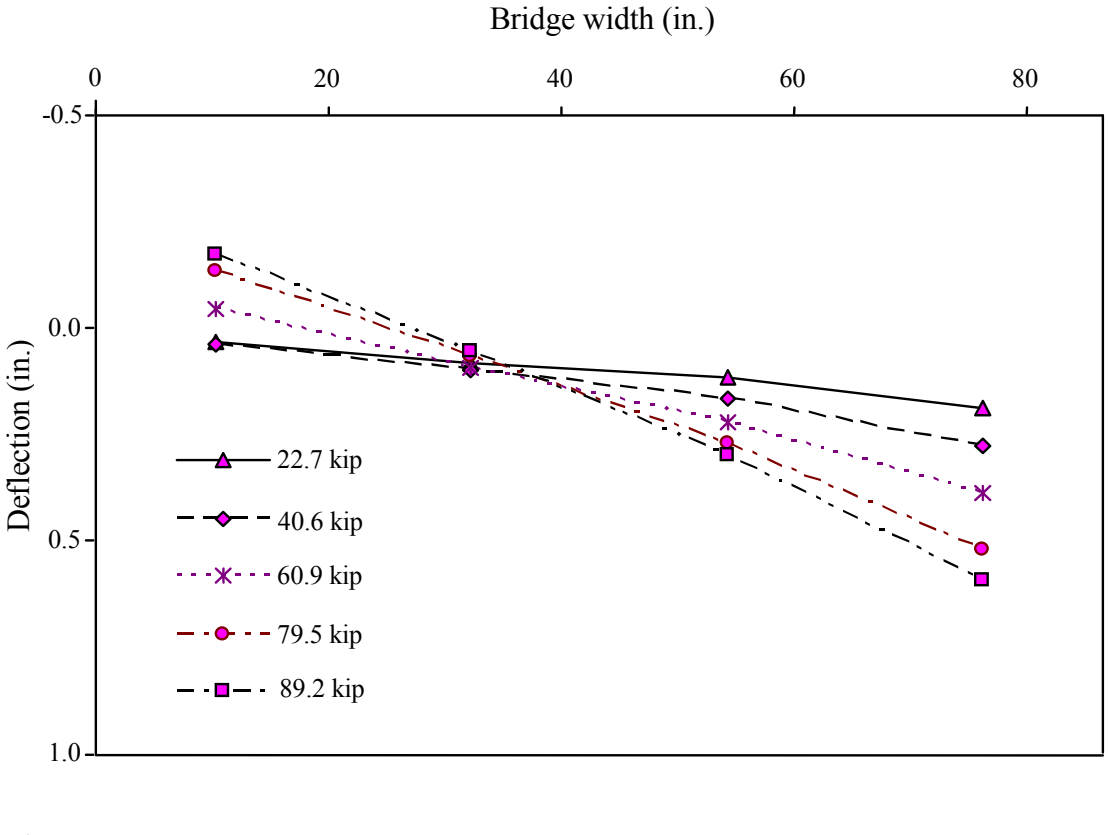

Figure B-2 Deflection of bridge model due to applying vertical load at box-beam B-4.

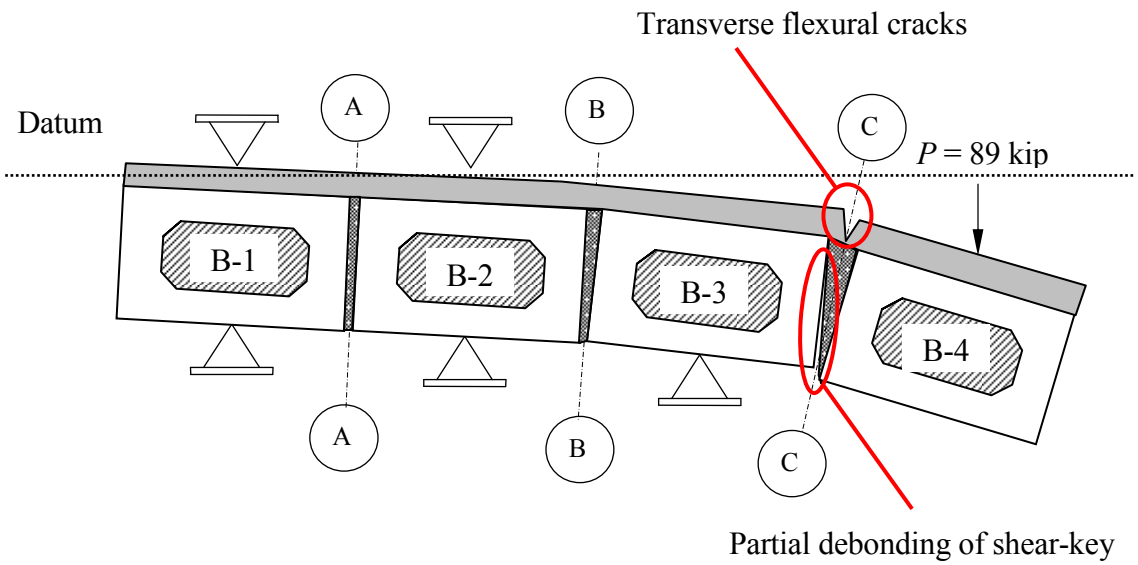

Figure B-3 Bridge deformed shape due to applying vertical load at beam B-4.

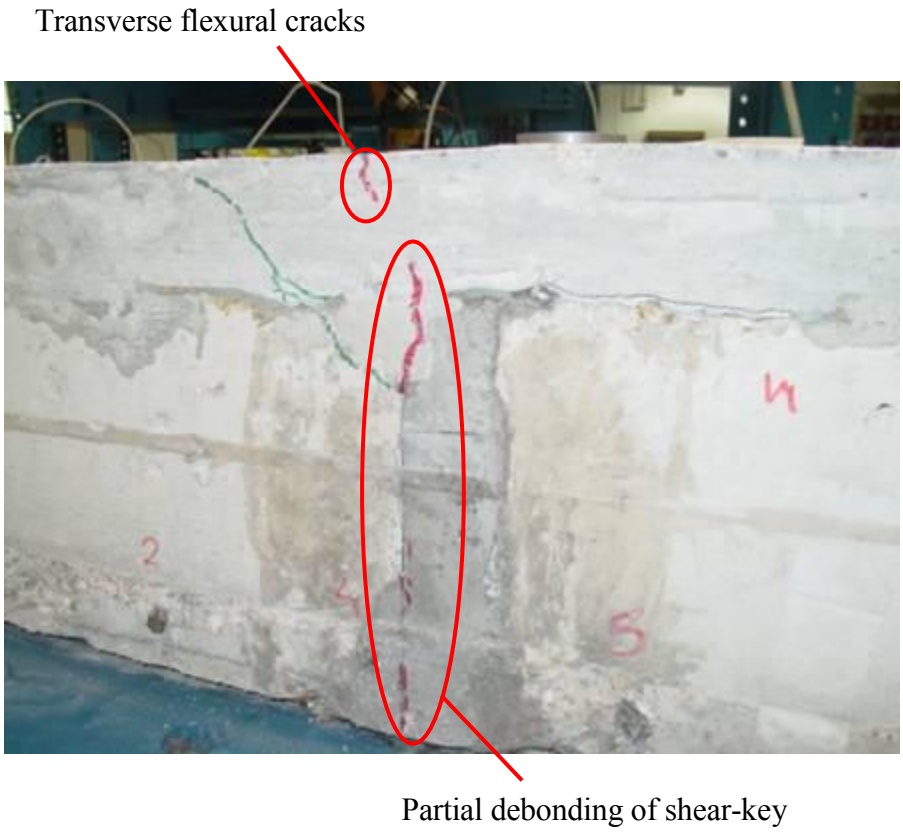

Figure B-4 Cracks of exterior shear-key C-C.

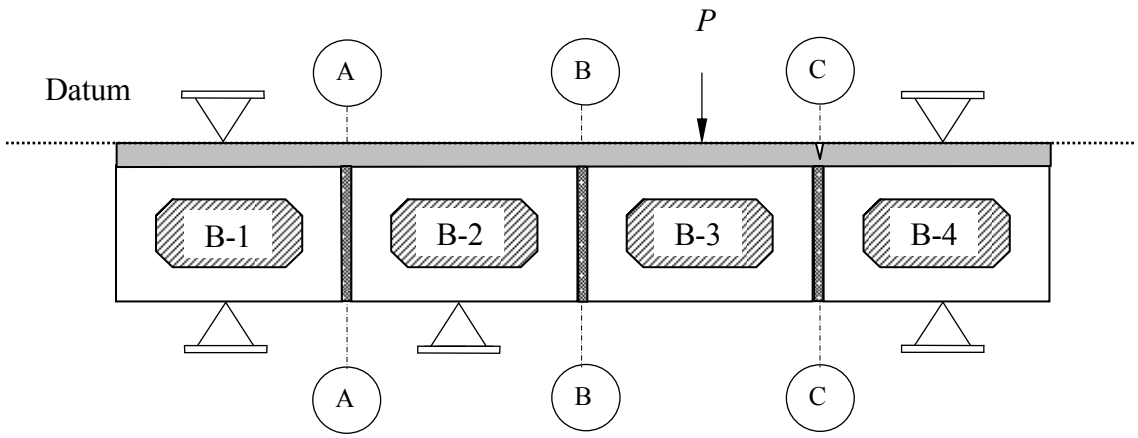

Figure B-5 Loading arrangements for cracking the exterior shear-key B-B.

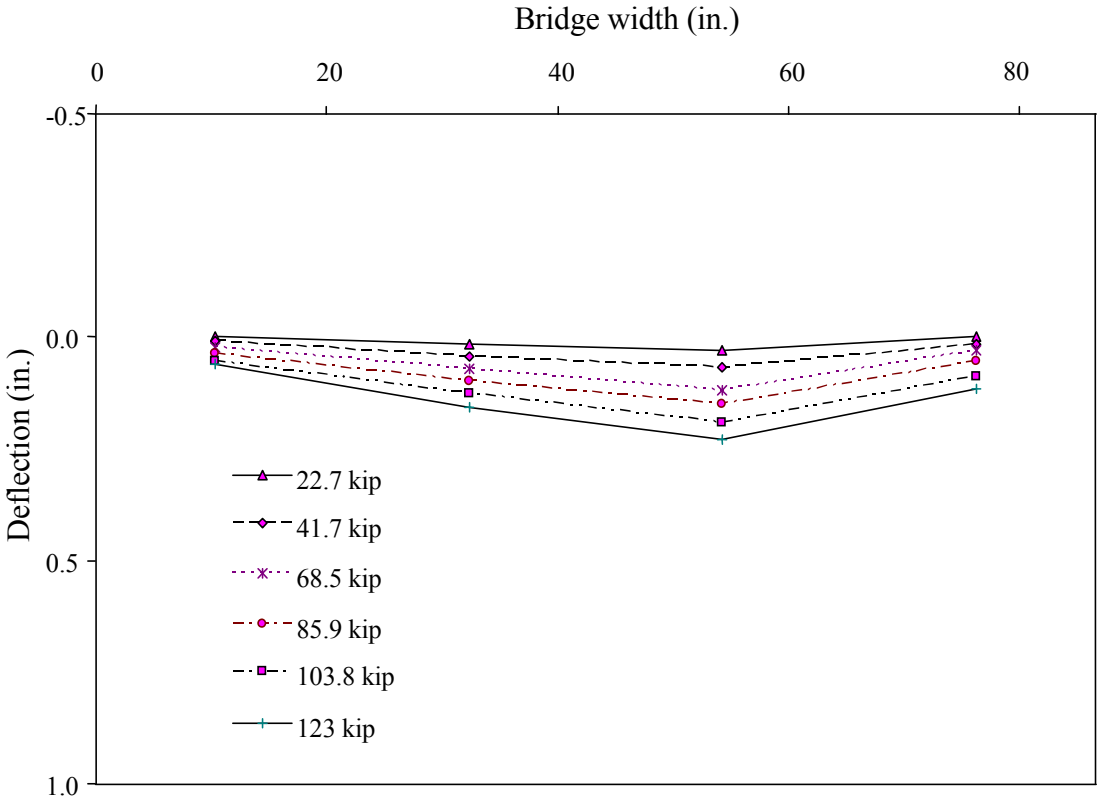

Figure B-6 Deflection of bridge model due to applying vertical load at box-beam B-3.

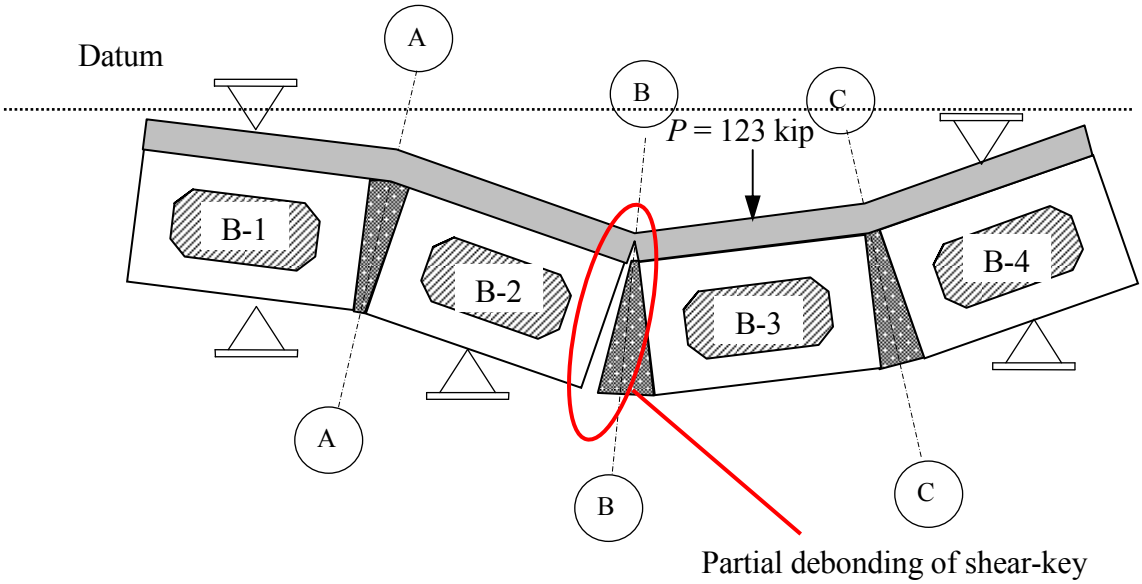

Figure B-7 Bridge deformed shape due to applying vertical load at beam B-4.

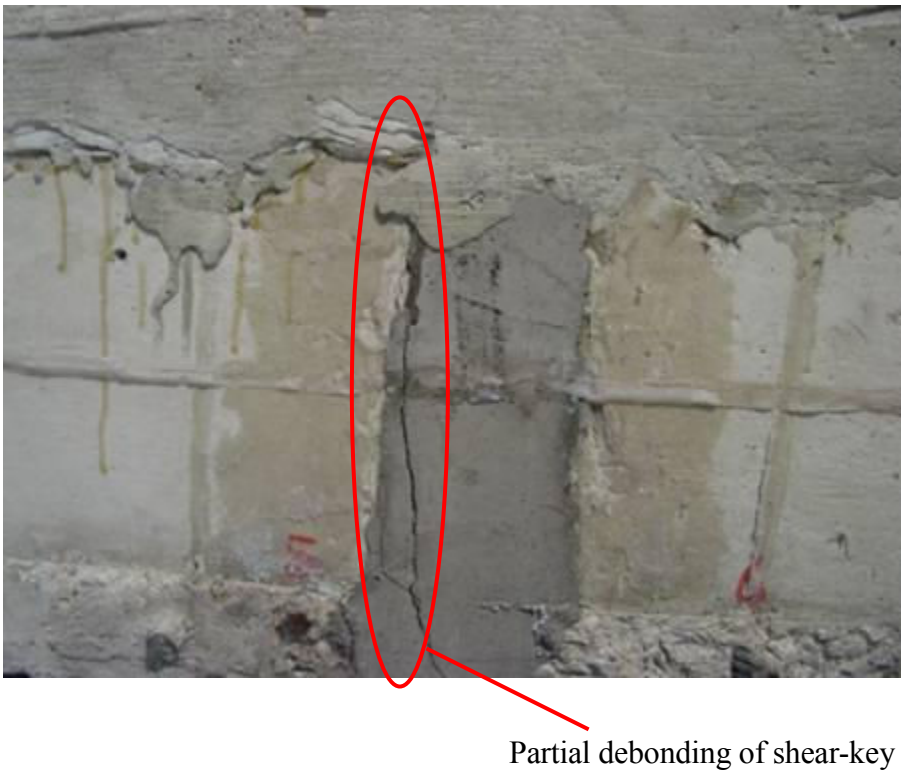

Figure B-8 Cracks of the interior shear-key B-B.

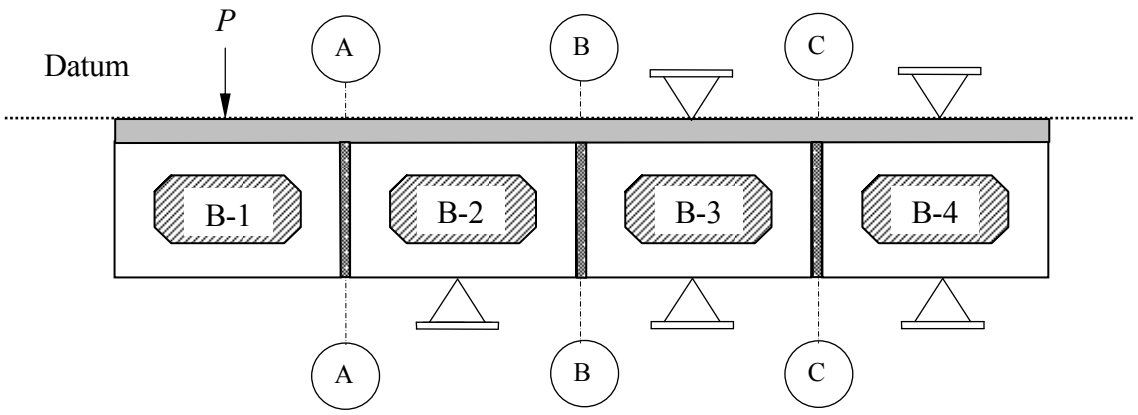

Figure B-9 Loading arrangements for cracking the exterior shear-key A-A.

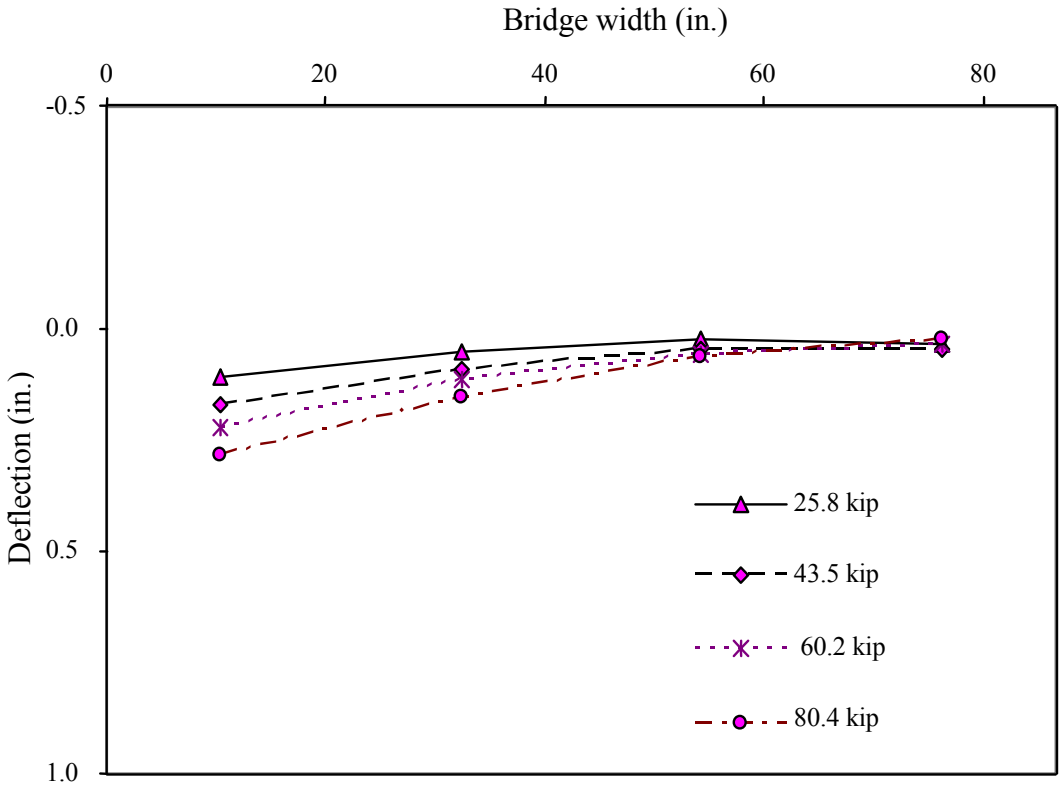

Figure B-10 Deflection of bridge model due to applying vertical load at box-beam B-1.

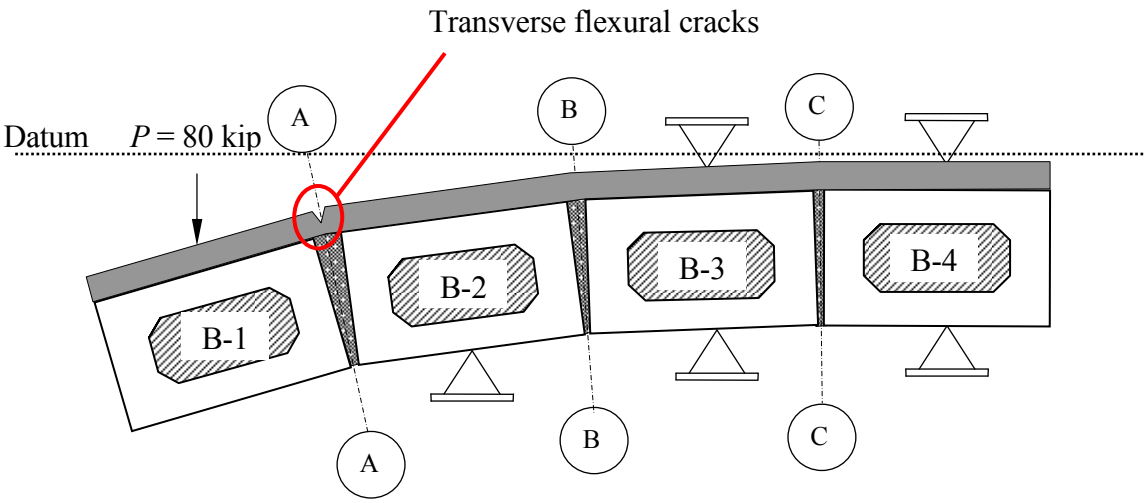

Figure B-11 Bridge deformed shape due to applying vertical load at beam B-1.

APPENDIX C: FLEXURAL DESIGN OF THE BRIDGE MODEL

Introduction

The bridge model was designed as under-reinforced structure with tension controlling the failure. The design was based on a uniform distribution of the vertical load in the transverse direction. The designed bridge model consisted of:

1. Four 30° skew box-beams, 18 in. wide and 11 in. deep, were placed side-by-side. The total span of the proposed one half scale 30° skew box-beam was 31 ft. Stirrups were extended 1.5 in. above the top flange of box-beams to provide a composite action with deck slab (Section 7.02.18.B.6 of MDOT Bridge Design Manual, 2006). Figure C-1 shows the cross-section of the individual box-beam.
2. The depth of the shear-key between box-beams was 8 in. and the maximum width was 2.5 in. A 3 in. thick reinforced concrete deck slab was cast over the individual box-beams and the shear-keys in between. Both the shear-key and the deck slab were provided to connect the individual box-beams.
3. Two strands were placed in each diaphragm to facilitate the transverse post- tensioning (TPT) process. Oval-shape aluminum ducts, 6 in. high and 4.5 in. wide, was used for the TPT to facilitate the proccess in the presence of differential camber in the bridge model as a part of the objectives.

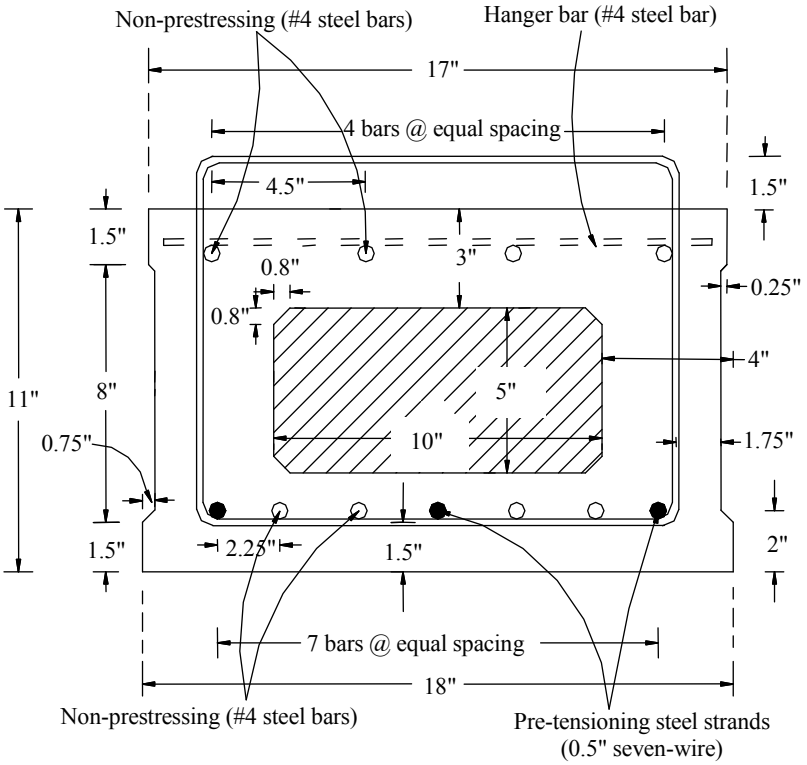

Figure C-1 Cross-sectional details of individual box-beam.

C-I Materials Properties

A. Concrete

1. Box-Beam

Compressive strength, $f'_{cb} = 6{,}268$ psi (uniaxial compression test of standard concrete cylinders after 28 days).

Initial compressive strength, $f'_{cbi} = 6{,}086$ psi (uniaxial compression test of standard concrete cylinders after 21 days).

Modulus of elasticity, $E_{cb} = 4{,}450$ ksi (uniaxial compression test of standard concrete cylinders after 28 days). Modulus of rupture, $f_r = -7.5\sqrt{f'_{cb}} = -7.5\sqrt{6{,}268} = -594$ psi [ACI 318-05, Section 9.5.2.3, equation (9-10)]

Unit weight of concrete, $\gamma_{cb} = 151.6$ lb/ft³

2. Deck slab

Compressive strength, $f'_{cs} = 4{,}600$ psi (uniaxial compression test of standard concrete cylinders after 28 days).

Modulus of elasticity, $E_{cs} = 57{,}000\sqrt{f'_{cs}} = 57{,}000\sqrt{4{,}600} = 3{,}866$ ksi (ACI 318-05, Section 8.5.1)

Modular ratio, $n = \dfrac{E_{cs}}{E_{cb}} = \dfrac{3{,}866}{4{,}450} = 0.87$

Unit weight of concrete, $\gamma_{cs} = 150$ lb/ft³

B. Steel Reinforcement

1. Non-Prestressing Steel Bars:

Yield strength, $f_y = 60$ ksi

Modulus of elasticity, $E_s = 29{,}000$ ksi

2. Prestressing Steel Strands:

Yield strength, $f_{py} = 229.5$ ksi

Ultimate tensile strength, $f_{pu} = 270$ ksi

Modulus of elasticity, $E_{ps} = 28{,}500$ ksi

C-II Properties of Cross-Section

A. ***Box-Beam***

Area of concrete, $A = 140$ in²

Moment of inertia, $I = 1{,}850$ in⁴

Distance from center of gravity to extreme top fiber, $y_t = 5.5$ in.

Distance from center of gravity to extreme bottom fiber, $y_b = -5.5$ in.

Bottom section modulus, $Z_b = \dfrac{I}{y_b} = \dfrac{1{,}850}{5.5} = 336.36$ in³

Top central kern, $k_t = -\dfrac{Z_b}{A} = -\dfrac{336.36}{140} = -2.4$ in.

Area of non-prestressing steel (#4 bar), $A_s = 0.2$ in²

Effective area of prestressing steel strands, $A_{ps} = 0.153$ in²

Eccentricity of prestressing steel strands, $e = 3.5$ in.

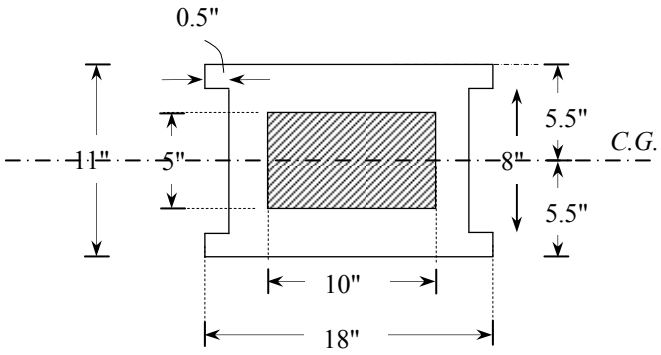

Figure C-2 Simplified cross-section.

B. ***Composite Section***

Composite area, $A_c = 194$ in²

Composite moment of inertia, $I_c = 3{,}435.88$ in⁴

Distance from center of gravity to extreme top fiber of slab, $y_{tc} = 5.41$ in.

Distance from center of gravity to extreme top fiber of beam, $\overline{y}_{tc} = 3.91$ in.

Distance from center of gravity to extreme top fiber of beam, $y_{bc} = -7.09$ in.

Bottom section modulus, $Z_{bc} = \dfrac{I_c}{y_{bc}} = \dfrac{3{,}435.88}{7.09} = 484.61$ in³

Transformed width of deck slab, $b_{tr} = nb = 0.87 \times 18 = 15.66$ in.

Eccentricity of prestressing steel strands, $e_c = 5.09$ in.

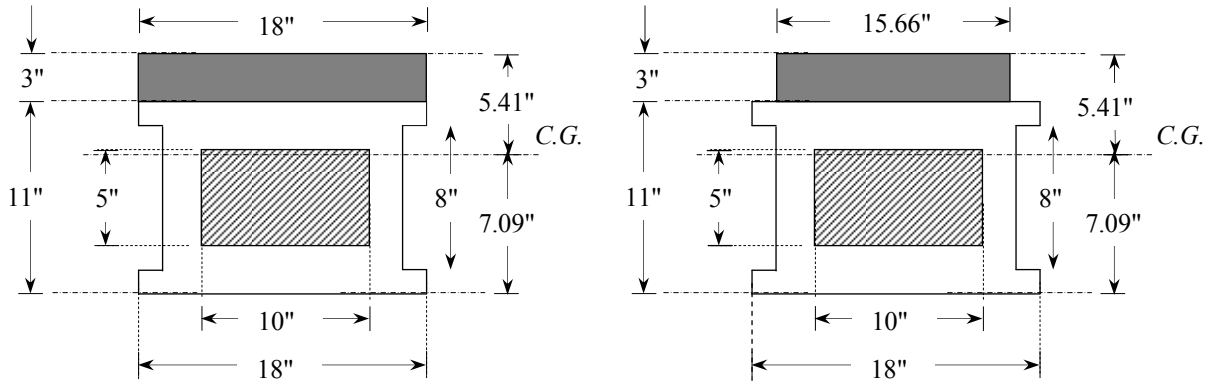

(a) Untransformed (b) Transformed

Figure C-3 Composite section.

C-III Loads

A. ***Self-Weight of Box-Beam***

$$w_b = A \times \gamma_{cb} = \frac{140 \times 151.6}{1{,}000 \times 12^2} = 0.147 \text{ kip/ft}$$

B. ***Self-Weight of Deck Slab***

$$w_s = (A_c - A) \times \gamma_{cs} = \frac{(194 - 140) \times 150}{1{,}000 \times 12^2} = 0.06 \text{ kip/ft}$$

Total dead load, $w_t = w_b + w_s = 0.147 + 0.06 = 0.207$ kip/ft

Effectice span, $l_e = 30$ ft

Total moment due to dead load, $M_{DL} = \frac{w_t l_e^{\,2}}{8} = \frac{0.207 \times 30^2}{8} = 23.29$ kip/ft

C. Prestressing Forces

1. Exterior Beam

Jacking prestressing force, $F_j =$ 20 kip/strand (60 kip/beam)

Assume instantaneous losses occurs in prestressing forces (friction, elastic shortening, and anchorage losses) $\cong 15\% F_j$

Initial prestressing force, $F_i =$ 17 kip/strand (51 kip/beam)

2. Interior Beam

Jacking prestressing force, $F_j = 25$ kip/strand (75 kip/beam)

Assume instantaneous losses occurs in prestressing forces (friction, elastic shortening, and anchorage losses) $\cong 15\% F_j$

Initial prestressing force, $F_i = 21.25$ kip/strand (63.75 kip/beam)

Average initial prestressing force, $F_i = 19.125$ kip/strand (57.375 kip/beam)

C-IV Check of Normal Stresses at Concrete (Unshored Action)

A. Allowable Stresses (at transfer)

Initial tensile stresses at mid-span, $f_{ti} = -3\sqrt{f'_{cbi}} = -3\sqrt{6{,}086} = -234$ psi (ACI 318-05, Section 18.4.1).

Initial tensile stresses at supports, $f_{ti} = -6\sqrt{f'_{cbi}} = -6\sqrt{6{,}086} = -468$ psi (ACI 318-05, Section 18.4.1).

Initial compressive stresses, $f_{ci} = 0.6 f'_{cbi} = 0.6 \times 6{,}086 = 3{,}652$ psi (ACI 318-05, Section 18.4.1).

B. Calculation of Stresses at Transfer (before placing deck slab)

1. At Supports

Top fiber stress, $f_t = \dfrac{F_i}{A} - \dfrac{F_i y_t e}{I} = \dfrac{57.375}{140} - \dfrac{57.375 \times 5.5 \times 3.5}{1{,}850} = -0.187$ ksi ≥ -0.468 ksi

Bottom fiber stress, $f_b = \dfrac{F_i}{A} - \dfrac{F_i y_b e}{I} = \dfrac{57.375}{140} - \dfrac{57.375 \times (-5.5) \times 3.5}{1{,}850} = 1.0$ ksi

$\leq 3{,}652$ ksi

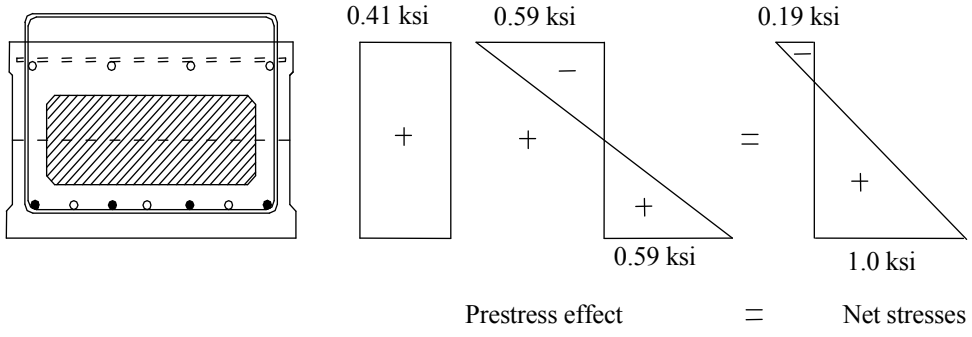

2. <u>At Mid-Span</u>

Top fiber stress,

$$f_t = \frac{F_i}{A} - \frac{F_i y_t e}{I} + \frac{w_b l_e^{\,2} y_t}{8I} = \frac{57.375}{140} - \frac{57.375 \times 5.5 \times 3.5}{1{,}850} + \frac{0.147 \times (30 \times 12)^2 \times 5.5}{12 \times 8 \times 1{,}850}$$

$$= 0.41 \text{ ksi} \le 3.625 \text{ ksi}$$

Bottom fiber stress,

$$f_b = \frac{F_i}{A} - \frac{F_i y_b e}{I} + \frac{w_b l_e^{\,2} y_b}{8I} = \frac{57.375}{140} - \frac{57.375 \times (-5.5) \times 3.5}{1{,}850}$$

$$+ \frac{0.147 \times (30 \times 12)^2 \times (-5.5)}{12 \times 8 \times 1{,}850} = 0.41 \text{ ksi} \le 3.625 \text{ ksi}$$

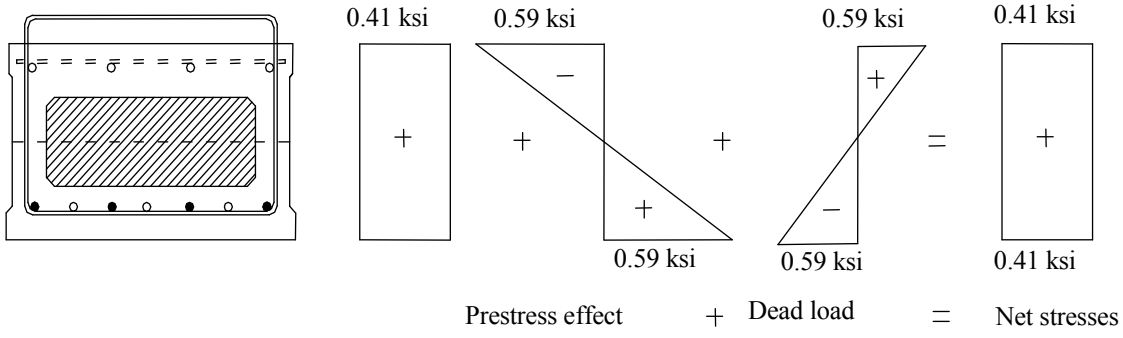

C. Calculation of Stresses (after placing deck slab)

1. <u>At Supports</u>

Top fiber stress, $f_t = \frac{F_i}{A} - \frac{F_i y_t e}{I} = \frac{57.375}{140} - \frac{57.375 \times 5.5 \times 3.5}{1{,}850} = -0.19 \text{ ksi} \ge -0.468 \text{ ksi}$

Bottom fiber stress, $f_b = \frac{F_i}{A} - \frac{F_i y_b e}{I} = \frac{57.375}{140} - \frac{57.375 \times (-5.5) \times 3.5}{1{,}850} = 1.0 \text{ ksi}$

$\leq 3.625 \text{ ksi}$

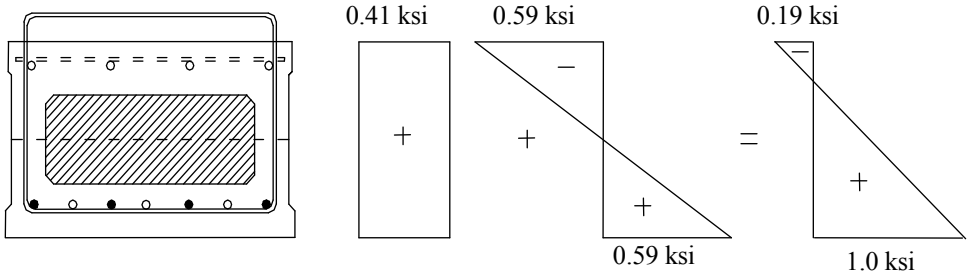

2. <u>At Mid-Span</u>

Top fiber stress,

$$f_t = \frac{F_i}{A} - \frac{F_i y_t e}{I} + \frac{w_t l_e^2 y_t}{8I} = \frac{57.375}{140} - \frac{57.375 \times 5.5 \times 3.5}{1{,}850} + \frac{0.207 \times (30 \times 12)^2 \times 5.5}{12 \times 8 \times 1{,}850}$$

$= 0.64 \text{ ksi} \leq 3.625 \text{ ksi}$

Bottom fiber stress,

$$f_b = \frac{F_i}{A} - \frac{F_i y_b e}{I} + \frac{w_t l_e^2 y_b}{8I} = \frac{57.375}{140} - \frac{57.375 \times (-5.5) \times 3.5}{1{,}850}$$

$$+ \frac{0.207 \times (30 \times 12)^2 \times (-5.5)}{12 \times 8 \times 1{,}850} = 0.18 \text{ ksi} \leq 3.625 \text{ ksi}$$

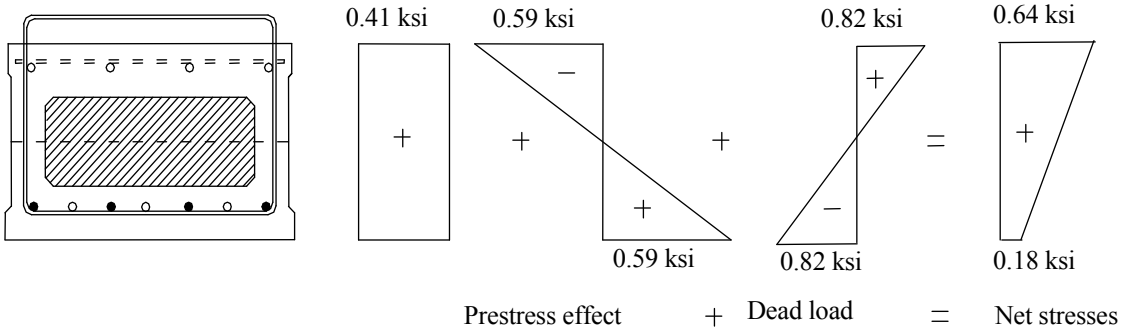

C-V <u>Elongation</u>

Effective cross-sectional area of strand, $A = 0.153$ in²

Modulus of elasticity, $E = 28{,}500$ ksi

Length of each strand, $L = 56$ ft $= 672$ in.

1. <u>For Interior Box-Beams (B-2 and B-3)</u>

Prestressing force, $P = 25$ kip

From the elasticity theory, $\frac{P}{A} = E\frac{\Delta L}{L} \longrightarrow \Delta L = \frac{PL}{EA}$

$$\Delta L = \frac{25 \times 672}{28{,}500 \times 0.153} = 3.85 \text{ in.}$$

2. <u>For Exterior Box-Beams (B-1 and B-4)</u>

Prestressing force, $P = 20$ kip

From the elasticity theory, $\frac{P}{A} = E\frac{\Delta L}{L} \longrightarrow \Delta L = \frac{PL}{EA}$

$$\Delta L = \frac{20 \times 672}{28{,}500 \times 0.153} = 3.08 \text{ in.}$$

C-VI <u>Cracking Moment (M_{cr})</u>

Cracking moment in axcess of the total self-weight, ΔM_{cr}

$$\Delta M_{cr} = \frac{Z_{bc}}{Z_b}\left[F_t(e - k_t) - M_{DL}\right] - f_r Z_{bc} \text{ (Naman 2004, equation 9.28)}$$

$$\Delta M_{cr} = \frac{484.61}{336.36}\left[57.375(3.5 + 2.4) - 23.39 \times 12\right] - \left(\frac{-594}{1000}\right)(484.61) = 371{,}18 \text{ kip-in.}$$

$= 30.93$ kip-ft

Total cracking moment for a single beam, M_{cr}

$M_{cr} = \Delta M_{cr} + M_{DL} = 30.93 + 23.39 = 54.3$ kip-ft (Naman 2004, equation 9.29)

Cracking load for load distribution test for single beam, $= \frac{4\Delta M_{cr}}{l} = \frac{4 \times 30.93}{31} = 4$ kip

Cracking load for the bridge model, $p_{cr} = 4 \times 4 = 16$ kip

C-VII <u>Nominal Moment Capacity (M_n) Using Strain Compatibility Approach</u>

A. First estimation of ultimate stresses in prestressing steel strands

$$f_{ps} = f_{pu}\left[1 - \frac{\gamma_p}{\beta_1}\left(\rho_p \frac{f_{pu}}{f_c'} + \frac{d}{d_p}\left(w - w'\right)\right)\right] \qquad \text{(ACI 318-05, equation 18-3)}$$

Specified tensile strength of prestressing steel, $f_{pu} = 270$ ksi

Factor for type of prestressing strands, $\gamma_p = 0.28$

Distance from extreme compression fiber to centroid of prestressing steel, $d_p = 12$ in.

Distance from extreme compression fiber to centroid of longitudinal tension non-prestressing reinforcement, $d = 8.25$ in.

Distance from extreme compression fiber to centroid of longitudinal compression non-prestressing reinforcement, $d' = 2$ in.

Prestressing reinforcement ratio, $\rho_p = \dfrac{A_{sp}}{bd_p} = \dfrac{3 \times 0.153}{15.66 \times 12} = 2.443 \times 10^{-3}$

Tension reinforcement index, $w = \dfrac{A_s}{bd}\dfrac{f_y}{f_c'} = \dfrac{8 \times 0.2}{15.66 \times 8.25}\dfrac{60}{4.6} = 0.1615$

Compression reinforcement index, $w' = \dfrac{A'_s}{bd}\dfrac{f_y}{f_c'} = \dfrac{3 \times 0.11}{15.66 \times 8.25}\dfrac{60}{4.6} = 0.03317$

Factor relating depth of equivalent rectangular compressive stress block to neutral axis depth,

$\beta_1 = 0.85 - 0.05(f_c' - 4) = 0.85 - 0.05(4.6 - 4) = 0.82$

$$\rho_p \frac{f_{pu}}{f_c'} + \frac{d}{d_p}\left(w - w'\right) = 2.443 \times 10^{-3}\,\frac{270}{4.6} + \frac{8.25}{12}\left(0.1615 - 0.033317\right)$$

$= 0.231 \geq 0.17$ (ACI 318-05, Section 18.7.2)

$$f_{ps} = 270\left[1 - \frac{0.28}{0.82}0.17\right] = 248.79 \text{ ksi}$$

B. First Estimation of the Depth of Neutral Axis (from equilibrium)

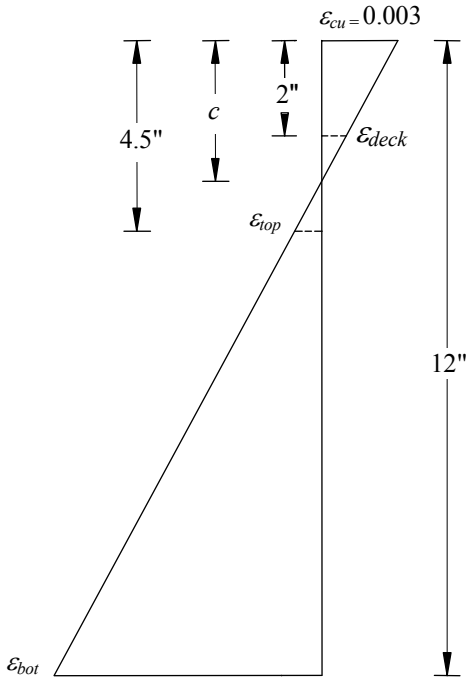

Strain distribution

Tension Force (T)

1. Prestressing Steel Strands ($d_p = 12$ in.)

Initial prestressing strain (locked in strain due to prestress),

$$\varepsilon_{pi} = \frac{F_i}{A_{ps} E_{ps}} = \frac{19.125}{0.153 \times 28{,}500} = 4.386 \times 10^{-3} \le 0.0086$$

Decompression strain,

$$\varepsilon_o = \frac{F_i}{A_c E_c}\left[1 + \frac{e^2}{r^2}\right] = \frac{19.125 \times 3}{194 \times 4{,}450}\left[1 + \frac{5.09^2}{4.208^2}\right] = 1.637 \times 10^{-4} \le 0.0086$$

Prestressing tension force, $T_{ps} = f_{ps} \times A_{ps} = 248.79 \times 3 \times 0.153 = 114.19$ kip

2. Non-Prestressing Bars

(a) First layer [top reinforcement] ($d = 4.5$ in.)

Strain, $\varepsilon_{top} = \left(\frac{4.5 - c}{c}\right) 0.003$ (from similar triangles)

Tension force, $T_1 = \varepsilon_{top} \times E_s \times A_s = \left(\frac{4.5-c}{c}\right) 0.003 \times 29{,}000 \times (4 \times 0.20) = 64.2\left(\frac{4.5-c}{c}\right)$

(b) Second layer [bottom reinforcement] ($d = 12$ in.), assume $f_s = f_y$

Tension force, $T_2 = f_y \times A_s = 60 \times (4 \times 0.20) = 48$ kip

Total tension force,

$$T = T_{ps} + T_1 + T_2 = 114.19 + 64.2\left(\frac{4.5-c}{c}\right) + 48 = 162.19 + 64.2\left(\frac{4.5-c}{c}\right)$$

Compression Force (C)

1. Concrete Compressive Stress Block

Assume the depth of neutral axis, $c < 3$ in. (neutral axis lies on the deck slab)

$C_c = 0.85 f_c' b \beta_1 c = 0.85 \times 4.6 \times 15.66 \times 0.82 \times c = 50.21c$

2. Deck Slab Steel Reinforcements

Strain, $\varepsilon_{deck} = \left(\frac{c-2}{c}\right) 0.003$ (from similar triangles)

Compression force, $C_s = \varepsilon_d \times E_s \times A_s = \left(\frac{c-2}{c}\right) 0.003 \times 29{,}000 \times (3 \times 0.11) = 28.71\left(\frac{c-2}{c}\right)$

Total compression force, $C = C_s + C_c = 50.21c + 28.71\left(\frac{c-2}{c}\right)$

Equilibrium

$T = C$

$50.21c^2 - 69.28c - 346.32 = 0$

$c = +3.41$ in. or $c = -2.71$ in.

$\therefore$ First depth of neutral axis, $c = +3.41$ in.

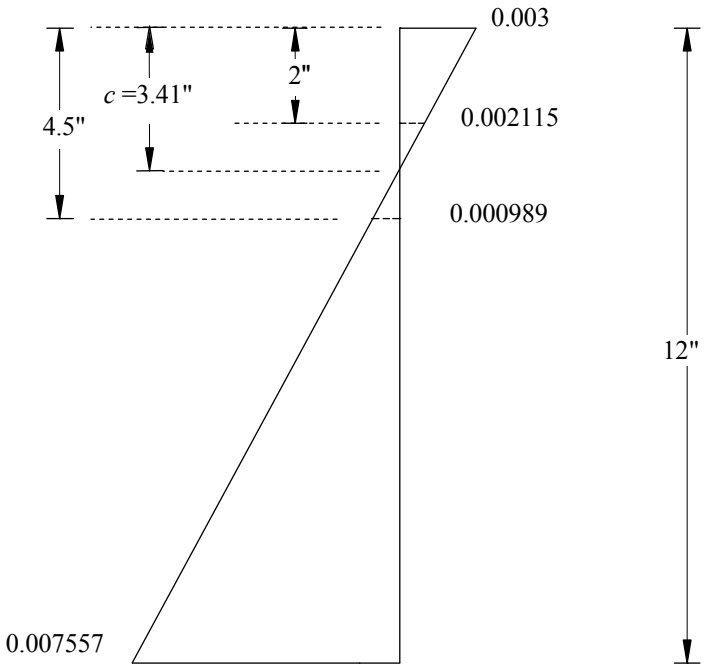

Strain distribution

C. Second Estimation of Ultimate Stresses in Prestressing Steel Strands

Total prestressing strain = Initial prestressing strain + Decompression strain + Ultimate strain at level of prestressing strands

$$\varepsilon_{ps} = \varepsilon_{pi} + \varepsilon_o + \varepsilon_{si}$$

$$\varepsilon_{ps} = 4.386\times10^{-3} + 1.637\times10^{-4} + 7.557\times10^{-3} = 0.01211 > 0.0086$$

$$f_{ps} = 270 - \frac{0.04}{\varepsilon_{ps} - 0.007}$$ (PCI Design Handbook (2003), Section 11.2.5)

$$f_{ps} = 270 - \frac{0.04}{0.01211 - 0.007} = 262.17 \text{ ksi}$$

D. Second Estimation of the Depth of Neutral Axis (from equilibrium)

By repeating the same procedures, we get

$$50.21c^2 - 75.43c - 346.62 = 0$$

$c = +3.48$ in. or $c = -1.98$ in.

$\therefore$ Depth of neutral axis, $c = +3.48$ in.

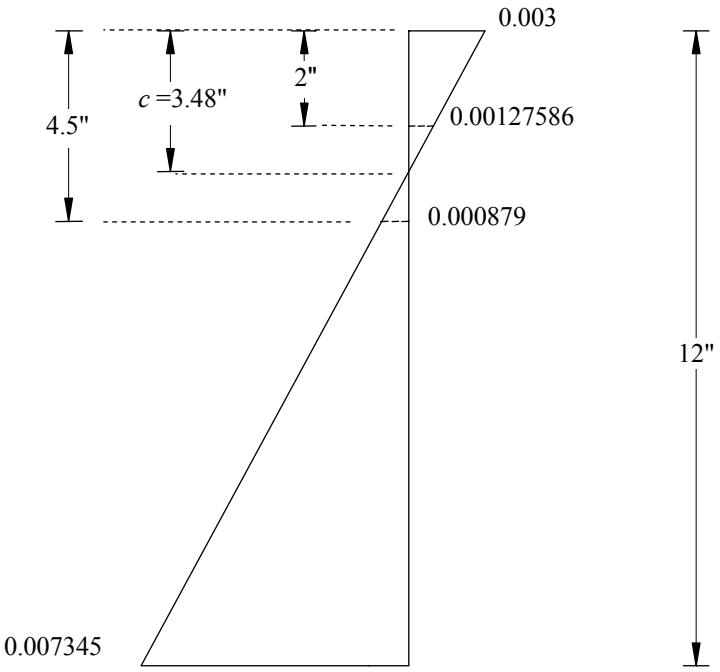

Strain distribution

D. Third Estimation of Ultimate Stresses in Prestressing Steel Strands

Total prestressing strain = Initial prestressing strain + Decompression strain + Ultimate strain at level of prestressing strands

$$\varepsilon_{ps} = \varepsilon_{pi} + \varepsilon_o + \varepsilon_{si}$$

$$\varepsilon_{ps} = 4.386\times10^{-3} + 1.637\times10^{-4} + 7.345\times10^{-3} = 0.0118947 > 0.0086$$

$$f_{ps} = 270 - \frac{0.04}{\varepsilon_{ps} - 0.007}$$

$$f_{ps} = 270 - \frac{0.04}{0.0118947 - 0.007} = 261.82 \text{ ksi (close enough to the previous iteration)}$$

E. Check of Forces Equilibrium

Total Tension Force

$$T = T_{top} + T_{bottom} = 168.17 + 18.8 = 186.97 \text{ kip}$$

Total Compression Force

$$C = C_c + C_s = 174.73 + 12.21 = 186.94 \text{ kip}$$

Total tension force ≈ Total compression force

E. Nominal Moment Capacity (M_n) [single box-beam]

By calculating the moment about the extreme top (compression) fiber,

Depth of compression stress block, $a = \beta_1 \times c = 0.82 \times 3.48 = 2.85$ in.

$$M_n = T_{bottom} \times 12 + T_{top} \times 4.5 - C_c \times 1.42 - C_s \times 2$$

$$M_n = 168.17 \times 12 + 18.82 \times 4.5 - 174.73 \times 1.42 - 12.21 \times 2 = 1{,}830 \text{ kip-in.}$$

$$= 152.52 \text{ kip-ft}$$

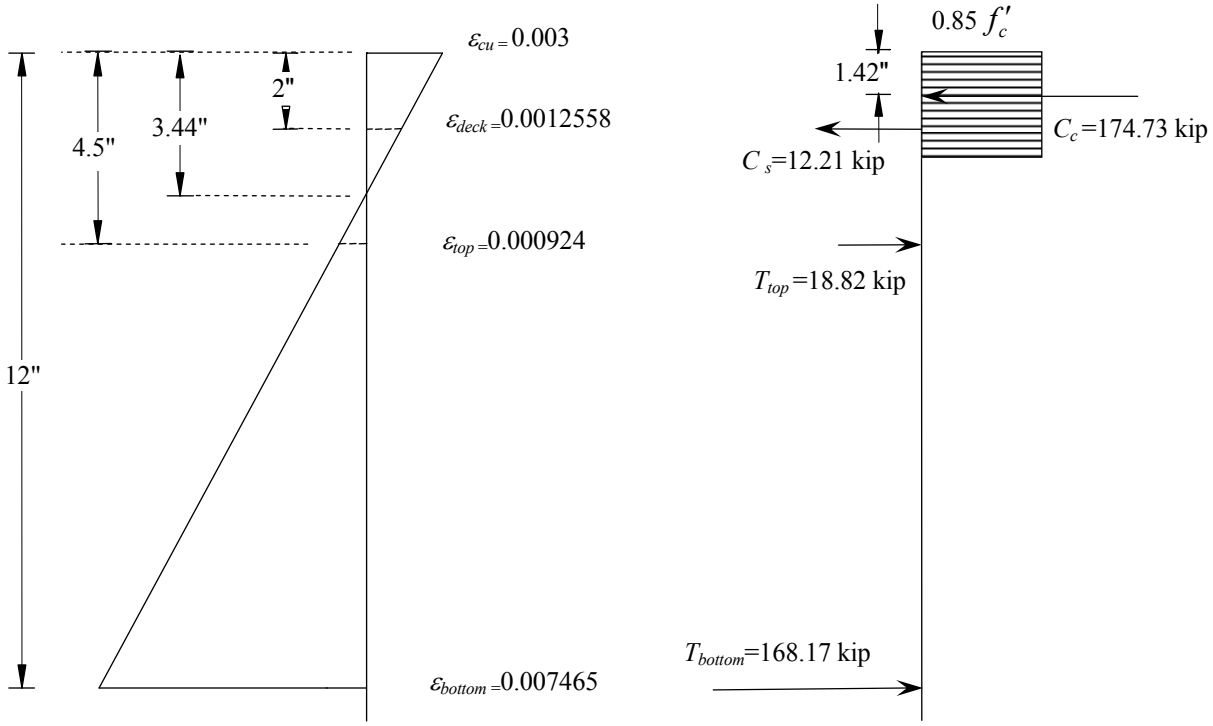

Strain Force

F. Ultimate vertical load (P_u)

$$M_{LL} = M_n - M_{DL} = 152.52 - 23.29 = 129.23 \text{ kip-ft}$$

By using two-point loading frame having a longitudinal spacing of 7.5 ft,

$$M_{LL} = \frac{P_u}{2}\left(\frac{L}{2} - \frac{l}{2}\right) \Rightarrow P_u = \frac{4M_{LL}}{(L-l)} = \frac{4 \times 129.23}{(31 - 7.5)} = 22 \text{ kip}$$

Load-carrying capacity of single box-beam, $P_u = 22$ kip

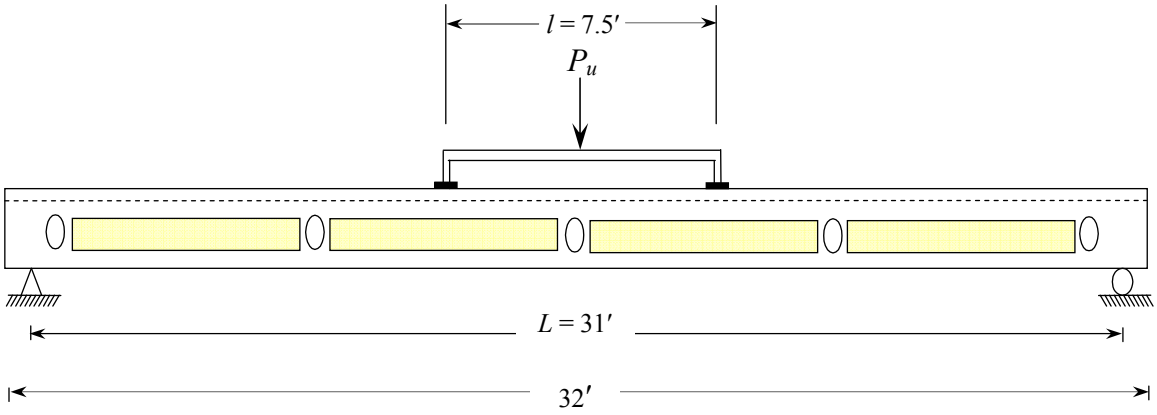

Figure C-4 Loading test setup.

By assuming equal distribution of the ultimate vertical load (P_u) in the transverse direction, the load-carrying capacity of the bridge model would be:

$P_u = 22 \times 4 = 88$ kip